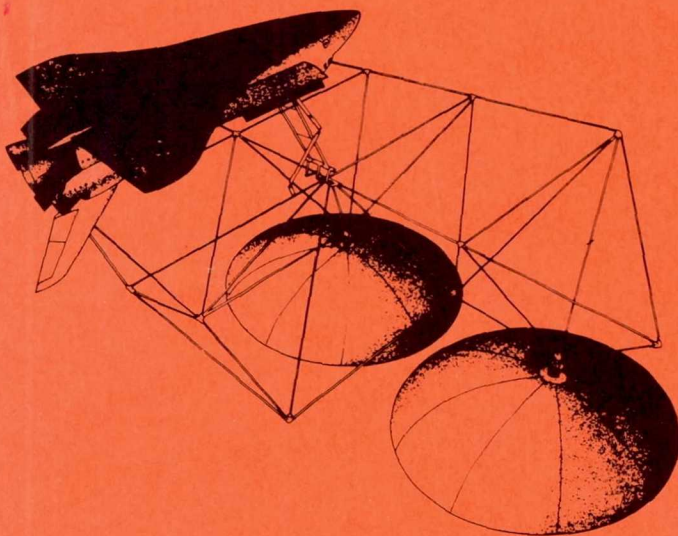


*NASA Conference Publication 2215
Part 2*

Large Space Systems Technology - 1981



FL 2827
WSMC/PMET TECHNICAL LIBRARY
VANDENBERG AFB, CA 93437-6021

*Third Annual Technical Review
held at NASA Langley Research Center
Hampton, Virginia
November 16-19, 1981*

NASA

*NASA Conference Publication 2215
Part 2*

Large Space Systems Technology - 1981

*Compiled by
William J. Boyer
NASA Langley Research Center
Hampton, Virginia*

Third Annual Technical Review
held at NASA Langley Research Center
Hampton, Virginia
November 16-19, 1981

NASA

National Aeronautics
and Space Administration

**Scientific and Technical
Information Branch**

1982

The use of trade names or manufacturers' names in this publication does not constitute endorsement, either expressed or implied, by the National Aeronautics and Space Administration.

PREFACE

This publication is a compilation of the papers presented at the Third Annual Large Space Systems Technology (LSST) Technical Review conducted at NASA Langley Research Center on November 16-19, 1981. The Review provided personnel of government, university, and industry with an opportunity to exchange information, to assess the present status of technology developments in the Large Space Systems Program, and to influence the course of development of new technology for large space systems.

The papers describe technological or developmental efforts that were accomplished during Fiscal Year 1981 in support of the LSST Program and were prepared by those in government, university, and industry who performed the work. These papers were divided into four major areas of interest: (1) technology pertinent to large antenna systems, (2) technology related to the control of large space systems, (3) basic technology concerning structures, materials, and analyses, and (4) flight technology experiments.

This publication is divided into two parts. Part 1 contains information on program status; structures, materials, and analyses; and control of large space systems. Part 2 covers large antenna systems and flight technology experiments.

This compilation provides the participants and their organizations with the papers presented at the Review in a referenceable format. Also, users of large space systems technology can follow the development progress with this document along with proceedings of previous and future LSST Technical Reviews. (See NASA CP-2168, 1981.) The LSST Program Office, Langley Research Center, which hosted the Review, provides this information as an aid in measuring performance and in planning future tasks.

This publication was expedited and enhanced through the efforts of the staff of the Research Information and Applications Division, Langley Research Center.

William J. Boyer
Manager, LSST Program Office
NASA Langley Research Center

Page intentionally left blank

CONTENTS

PREFACE	iii
THIRD ANNUAL TECHNICAL REVIEW ATTENDEES	xi

PART 1*

PROGRAM STATUS

MATURING LSST ROLE IN NASA PLANNING	1
Richard F. Carlisle	
LSST: BEYOND THE GROUND PROGRAM	11
William T. Tumulty	

STRUCTURES, MATERIALS, AND ANALYSES

THE EFFECTS OF ELECTRON AND GAMMA RADIATION ON EPOXY-BASED MATERIALS	27
R. E. Fornes, J. D. Memory, R. D. Gilbert, and E. R. Long, Jr.	
BASIC PHYSICAL AND CHEMICAL PROCESSES IN SPACE RADIATION EFFECTS ON POLYMERS	37
E. Kamaratos, J. W. Wilson, C. K. Chang, and Y. J. Xu	
PULSED RADIOLYSIS OF MODEL AROMATIC POLYMERS AND EPOXY BASED MATRIX MATERIALS	59
Amitava Gupta, Jovan Moacanin, Ranty Liang, and Dan Coulter	
THE EFFECTS OF MICROCRACKING ON THE THERMAL EXPANSION OF GRAPHITE-EPOXY COMPOSITES	67
D. E. Bowles	
THERMAL EXPANSION OF GRAPHITE-EPOXY BETWEEN 116 K AND 366 K	81
John S. Short, Michael W. Hyer, David E. Bowles, and Stephen S. Tompkins	
FINITE ELEMENT THERMAL-STRUCTURAL MODELING OF ORBITING TRUSS STRUCTURES	93
Earl A. Thornton, Jack Mahaney, and Pramote Dechaumphai	
VIBRATION AND BUCKLING STUDIES OF PRETENSIONED STRUCTURES	109
W. Keith Belvin	
VIBRATION DAMPING CHARACTERISTICS OF GRAPHITE/EPOXY COMPOSITES FOR LARGE SPACE STRUCTURES	123
R. F. Gibson	

*Part 1 is presented under a separate cover.

THE POTENTIAL OF NONPERIODIC TRUSS STRUCTURES FOR SPACE APPLICATIONS	133
K. C. Park and J. M. Winget	
IAC LEVEL "0" PROGRAM DEVELOPMENT	145
R. G. Vos	
IAC CONTROL SYSTEM ANALYSIS DEVELOPMENT	159
Harold P. Frisch	
LARGE ADVANCED SPACE SYSTEMS (LASS) COMPUTER-AIDED DESIGN PROGRAM ADDITIONS	169
C. E. Farrell	
SEQUENTIAL DEPLOYMENT OF TRUSS STRUCTURES	179
John M. Hedgepeth	
MOBILE WORK STATION CONCEPT FOR ASSEMBLY OF LARGE SPACE STRUCTURES (ZERO-GRAVITY SIMULATION TESTS)	193
Walter L. Heard, Jr., Harold G. Bush, Richard E. Wallson, and J. Kermit Jensen	
ORBITER BASED CONSTRUCTION EQUIPMENT	205
C. J. Goodwin	
DEPLOYABLE PLATFORM SYSTEMS DEVELOPMENT	219
R. E. Jewell	
TECHNOLOGICAL NEEDS OF ADVANCED EARTH-OBSERVATION SPACECRAFT (Slides only)	235
A. L. Brook	

CONTROLS

LSS CONTROL TECHNOLOGY	241
A. F. Tolivar	
CONTROL OF LARGE SPACE ANTENNAS: WRAP-RIB - HOOP/COLUMN	249
Yu-Hwan Lin	
SPATIAL, HIGH-ACCURACY, POSITIONING-ENCODING SENSOR (SHAPES) FOR LARGE SPACE SYSTEM CONTROL APPLICATIONS	283
J. M. McLaughlan	
CONTROL TECHNOLOGY DEVELOPMENT	297
David B. Schaechter	
LSS REFERENCE PLATFORM CONTROL	313
Rance S. Edmunds	
A STUDY OF AUTONOMOUS RENDEZVOUS AND DOCKING SYSTEMS	335
J. D. Micheal	
A DISTURBANCE ISOLATION CONTROLLER FOR THE SOLAR ELECTRIC PROPULSION SYSTEM FLIGHT EXPERIMENT	345
H. B. Waites	

MODULAR ATTITUDE CONTROL OF A LARGE SPACE PLATFORM	363
F. D. Chichester	
SYSTEMS IDENTIFICATION TECHNOLOGY DEVELOPMENT FOR LARGE SPACE SYSTEMS	371
E. S. Armstrong	
CONFIGURATIONAL AND SYSTEM REQUIREMENTS FOR CONTROL OF LARGE SPACE SYSTEMS	375
L. W. Taylor, Jr.	
INTEGRATED CONTROLS/STRUCTURES STUDY OF ADVANCED SPACE SYSTEMS	389
C. S. Greene and T. B. Cunningham	
ACTIVE CONTROL OF SPACE STRUCTURES: PROOF OF CONCEPT EXPERIMENT	413
J. A. Breakwell	

PART 2

ANTENNAS

JPL ANTENNA TECHNOLOGY DEVELOPMENT	429
R. E. Freeland	
OFFSET WRAP RIB ANTENNA CONCEPT DEVELOPMENT	439
A. A. Woods, Jr., and N. F. Garcia	
ANALYTICAL PERFORMANCE PREDICTION FOR LARGE ANTENNAS	471
M. El-Raheb	
SURFACE MEASUREMENT SYSTEM DEVELOPMENT	479
Martin Berdahl	
SUMMARY OF ANTENNA TECHNOLOGY DEVELOPMENT AT THE LANGLEY RESEARCH CENTER	491
Thomas G. Campbell	
MAYPOLE (HOOP/COLUMN) CONCEPT DEVELOPMENT PROGRAM	503
M. R. Sullivan	
RADIO FREQUENCY VERIFICATION TASKS RELATED TO A MULTIPLE APERTURE REFLECTOR SYSTEM	551
Thomas G. Campbell	
PRELIMINARY EXPERIMENTAL TEST RESULTS USING 35 GHz OFFSET FED REFLECTOR SIMULATING SURFACE PILLOWS AND APERTURE CABLES	557
Thomas G. Campbell and W. Robert Young	
PRELIMINARY ANALYTICAL RESULTS USING SURFACE CURRENT INTEGRATION FOR PREDICTING EFFECTS OF SURFACE PILLOWS ON RF PERFORMANCE	583
C. E. Farrell and D. A. Strange	

RF VERIFICATION TASKS UNDERWAY AT THE HARRIS CORPORATION FOR MULTIPLE APERTURE REFLECTOR SYSTEM	591
T. A. Gutwein	
DISTORTED REFLECTOR ANTENNA PERFORMANCE PREDICTION TECHNIQUE	605
M. C. Bailey	
MEASUREMENT OF LOSSES OF MESH MEMBRANE MATERIAL FOR REFLECTOR APPLICATIONS WITH AN S-BAND RADIOMETER	611
Hans-Juergen C. Blume	
THE SUITABILITY OF MESH MEMBRANE MATERIAL FOR RADIOMETER REFLECTOR APPLICATIONS	621
W. F. Croswell	
CONCEPTUAL DESIGN OF A SURFACE MEASUREMENT SYSTEM FOR LARGE DEPLOYABLE SPACE ANTENNAS	631
R. S. Neiswander	
ELECTRO-OPTICAL SYSTEM FOR REMOTE POSITION MEASUREMENTS IN REAL TIME	641
P. W. Collyer, S. C. Spielberger, and K. A. Ward	
NEAR-FIELD TESTING OF LaRC MULTIPLE-BEAM ANTENNA	657
G. J. Lang	
PROGRESS REPORT ON THE ELECTROSTATIC MEMBRANE ANTENNA CONCEPT TESTING	681
J. W. Goslee	
CONCEPTUAL DESIGN OF ELECTROSTATIC ANTENNA	689
J. V. Coyner	
ANTENNA SUBSYSTEM REQUIREMENTS	707
R. E. Freeland	
CONFIGURATION DEVELOPMENT OF THE LAND MOBILE SATELLITE SYSTEM (LMSS) SPACECRAFT	711
C. T. Golden, J. A. Lackey, and E. E. Spear	
CONFIGURATION DEVELOPMENT OF THE LAND MOBILE SATELLITE SYSTEM (LMSS) SPACECRAFT - CONCLUSIONS	761
C. T. Golden, J. A. Lackey, and E. E. Spear	
LAND MOBILE SATELLITE SYSTEM (LMSS) - SINGLE APERTURE SYSTEM DESIGN	767
W. J. Weber III	
QUAD APERTURE RF DEFINITION	781
P. Foldes	
ATTITUDE CONTROL SUBSYSTEM STUDY FOR THE LAND MOBILE SATELLITE SYSTEM SPACECRAFT	821
A. F. Tolivar	

FLIGHT TECHNOLOGY EXPERIMENTS

STRUCTURAL ASSEMBLY DEMONSTRATION EXPERIMENT	841
Jack W. Stokes	
STRUCTURAL ASSEMBLY DEMONSTRATION EXPERIMENT (SADE) -	
EXPERIMENT DESIGN	859
D. L. Akin and M. L. Bowden	
SOLAR ARRAY FLIGHT EXPERIMENT (SAFE)	881
R. W. Schock	
LARGE SPACE STRUCTURES SHUTTLE FLIGHT EXPERIMENT	893
Lyle M. Jenkins	

JPL ANTENNA TECHNOLOGY
DEVELOPMENT

R. E. Freeland
Jet Propulsion Laboratory
Pasadena, California

Large Space Systems Technology - 1981
Third Annual Technical Review
November 16-19, 1981

LONG TERM OBJECTIVE

The basic objective of the LSST Program is to provide systems-level technology for evolving cost-effective, STS compatible antennas that will be automatically deployed in orbit to perform a variety of missions in the 1985 to 2000 time period. For large space-based antenna systems, the LSST Program has selected deployable antennas for development. The maturity of this class of antenna, demonstrated by the success of smaller size apertures, provides a potential capability for satisfying a significant number of near-term, space-based applications. The offset wrap-rib concept development is the basis of the JPL LSST Antenna Technology Development Program. Supporting technology to the antenna concept development include analytical performance prediction, the capability for measuring and evaluating mechanical antenna performance in the intended service environment, and the development of candidate system-level configurations for potential applications utilizing the offset wrap-rib antenna concept.

TO DEVELOP THE TECHNOLOGY NEEDED TO EVALUATE,
DESIGN, FABRICATE, PACKAGE, TRANSPORT, AND DEPLOY
COST EFFECTIVE AND STS COMPATIBLE ANTENNA
SYSTEMS UP TO 300 meters IN DIAMETER FOR CLASSES OF
POTENTIAL APPLICATIONS

- COMMUNICATIONS
- EARTH RESOURCES
- ORBITING VLBI

JPL PROGRAM ELEMENTS

The offset wrap-rib antenna conceptual development program at LMSC is intended to result in technology that will accommodate the application of reflectives up to 100 meters in diameter and larger. The program benefits from an extensive heritage of demonstrated technology for axisymmetric reflector structures that is directly applicable to the offset reflector. The offset deployable feed support structure development is expected to be a new configuration design for the large antennas.

Analytical estimates of antenna performance are essentially estimates of reflector surface precision and feed structure alignment in the intended service environment. Such analyses are under development at JPL to (a) understand the fundamental wrap-rib antenna, (b) accomplish an independent assessment of potential antenna performance, and (c) determine the applicability of this concept for a number of different applications.

The determination of antenna interface requirements and constraints as a consequence of specific applications is under development at the Boeing Company. These interfaces will result from the development of system level configuration designs for classes of applications. The interface characterizations will then be used to guide the conceptual antenna development.

Remote measurement of antenna reflector surfaces and feed structure alignments in space is needed to (a) validate the mechanical design of precision surfaces, (b) characterize dynamic and thermal performance for verification of analytical performance prediction models, and (c) accommodate active control basic structural elements. Such a system is currently under development at JPL.

- OFFSET WRAP-RIB ANTENNA CONCEPT DEVELOPMENT
- ANALYTICAL PERFORMANCE PREDICTION FOR LARGE ANTENNAS
- ANTENNA SUBSYSTEM REQUIREMENTS
- SURFACE MEASUREMENT SYSTEM DEVELOPMENT

OFFSET WRAP-RIB ANTENNA-CONCEPT DEVELOPMENT

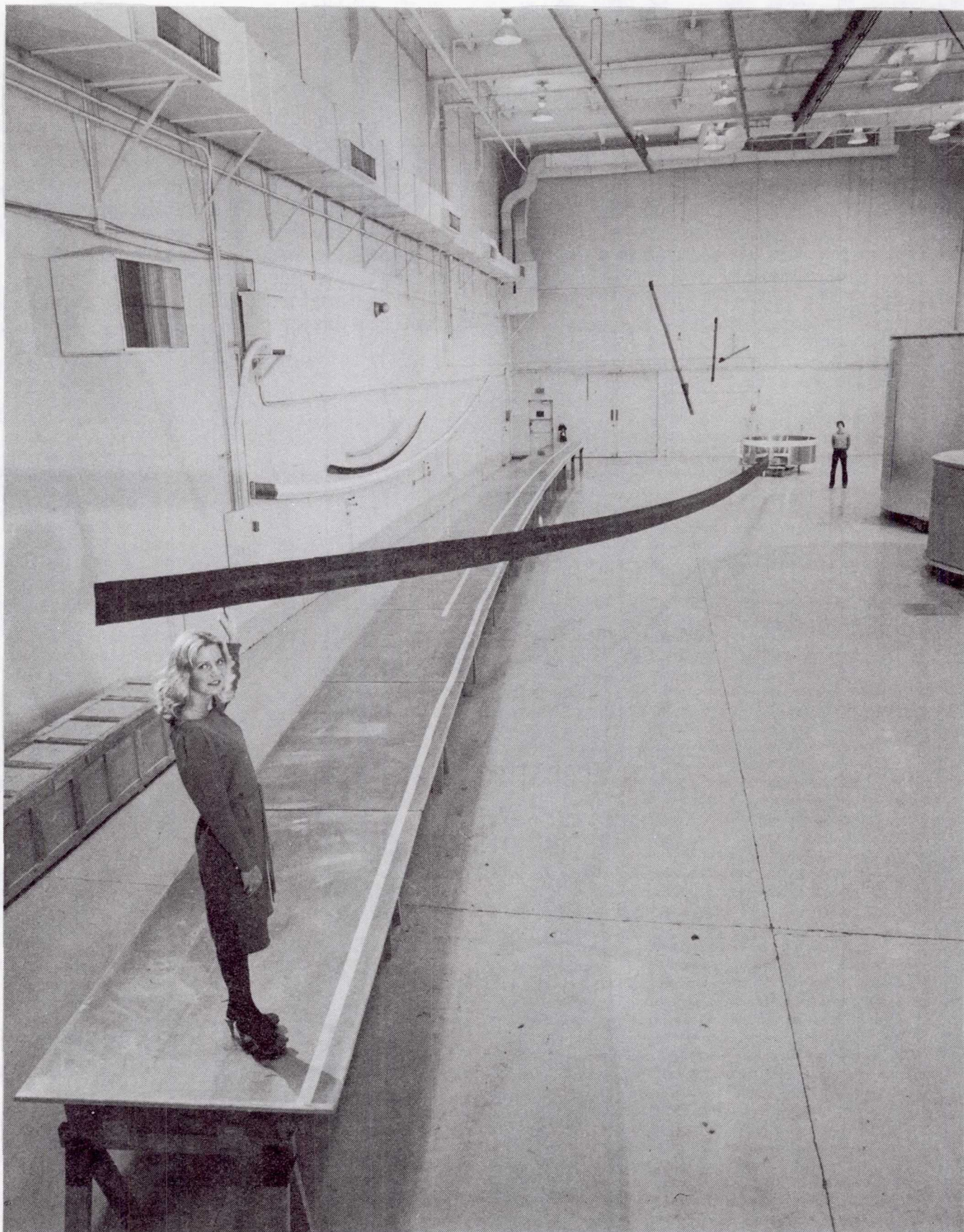
The demonstration of technology for the offset wrap-rib antenna concept will be based on functional deployment tests of the proof of concept hardware and analytical projections of full scale antenna performance. The demonstration hardware consists of a partial 55 meter diameter offset reflector structure and two bays of a deployable feed support structure. The partial reflector is composed of four graphite epoxy ribs, three RF reflective mesh gores and hub structure with deployment mechanism. The ground based deployment test will demonstrate rib structure deployment, mesh management, and partial verification of analytical performance prediction models. Ground based evaluation of the two-bay feed support boom will focus on deployment characteristics, deployed stillness, dimensional repeatability, and analytical model verification. Results of the proof of concept hardware evaluation will be used to refine the analytic performance prediction models and update the detail design used to support fabrication of the test hardware. The test validated, 55 meter hardware design, will be the basis of the preliminary design for the 100 meter diameter antenna, which represents the focus for the concept development. Additionally, the fabrication cost associated with test hardware will be used to update the antenna cost models. The results of the offset wrap-rib antenna technology development will include a) high confidence structural designs for antennas up to 100 meters, b) high confidence estimates of functional performance and cost, c) risk assessment for the fabrication of large size antennas, and d) 55 meter diameter flight type hardware that can be cost effectively completed to accommodate a flight experiment and/or application.

- PROOF OF CONCEPT HARDWARE
 - RIBS
 - MESH GORES
 - HUB
 - FEED BOOM
- GROUND TEST PROGRAM
 - RIB DEPLOYMENT
 - FEED BOOM DEPLOYMENT
 - MESH MANAGEMENT
 - MODEL VERIFICATION
- PRELIMINARY ANTENNA DESIGN
 - FULL SCALE ANTENNA
 - PERFORMANCE MODELS
 - COST MODELS

ANALYTICAL PERFORMANCE PREDICTION FOR LARGE ANTENNAS

The analytical characterization of the antenna structure is based on finite element models of the reflector and feed support designs. These models have sufficient detail to accommodate the determination of structural modes involving reflector mesh as well as other structural members. These models provide the antenna dynamic characteristics used to support control technology development and are used with the temperature distributions resulting from the finite difference models to provide the antenna thermal distortions. The reflector distortions are characterized by the coordinates and slopes of a large number of points on the finite element model. A spline fit routine was developed that defines the thermally distorted surface mathematically to accommodate RF analysis. The antenna far field patterns are then determined using a ray tracing technique to determine the adequacy of the mechanical design.

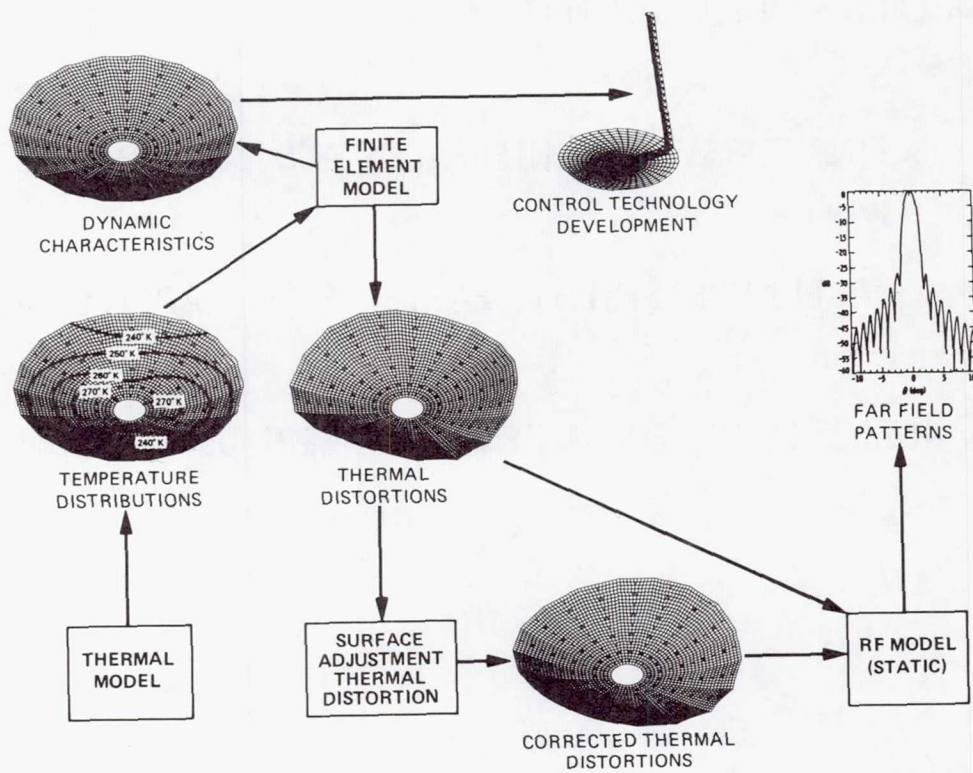
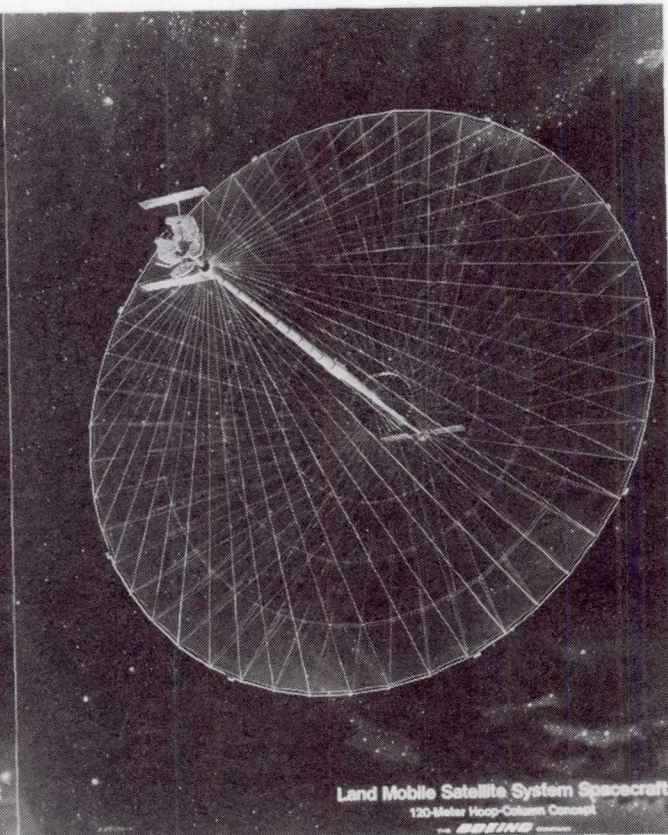
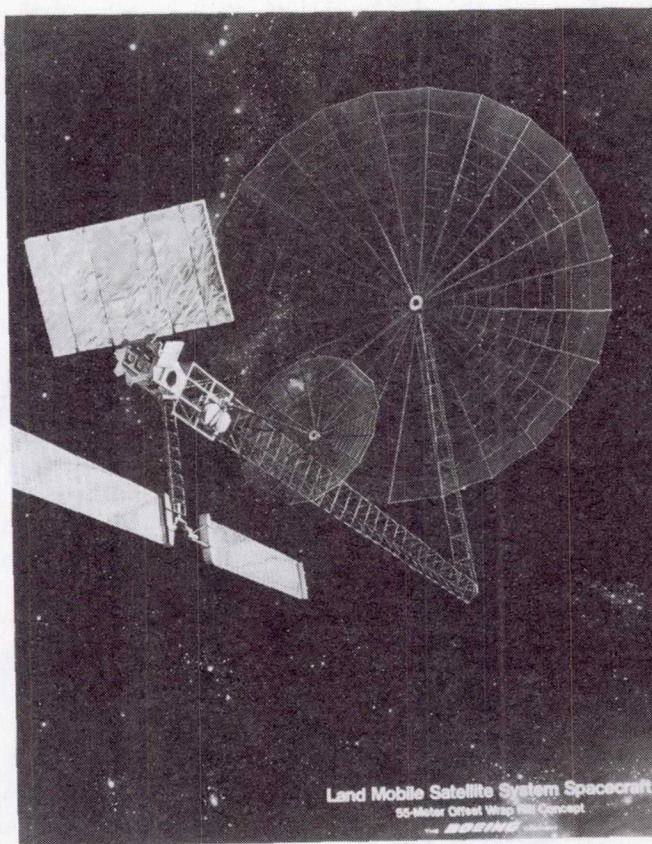
- FINITE ELEMENT MODELS
- DYNAMIC CHARACTERISTICS
- FINITE DIFFERENCE MODELS
- TEMPERATURE DISTRIBUTIONS
- THERMAL DISTORTIONS
- FAR FIELD PATTERNS
- SURFACE CORRECTION



ANTENNA SUBSYSTEM REQUIREMENTS

The subsystem requirements study is intended to develop candidate, system level configurations to the degree necessary to identify and characterize the necessary subsystems. These subsystem definitions and constraints can significantly contribute to the refinement of the current focus which is driving the two LSST conceptual antenna developments. The Land Mobile Satellite Service (LMSS) was selected as an example of a potential communications application. System level mechanical configurations were developed by the Boeing Company for both the LMSS offset wrap-rib antenna and the Harris Hoop/column antenna based on LMSS system requirements. The resulting subsystem requirements have been accounted for by the two LSST antenna conceptual developments. The impact of the subsystem constraints is covered under LSST system studies.

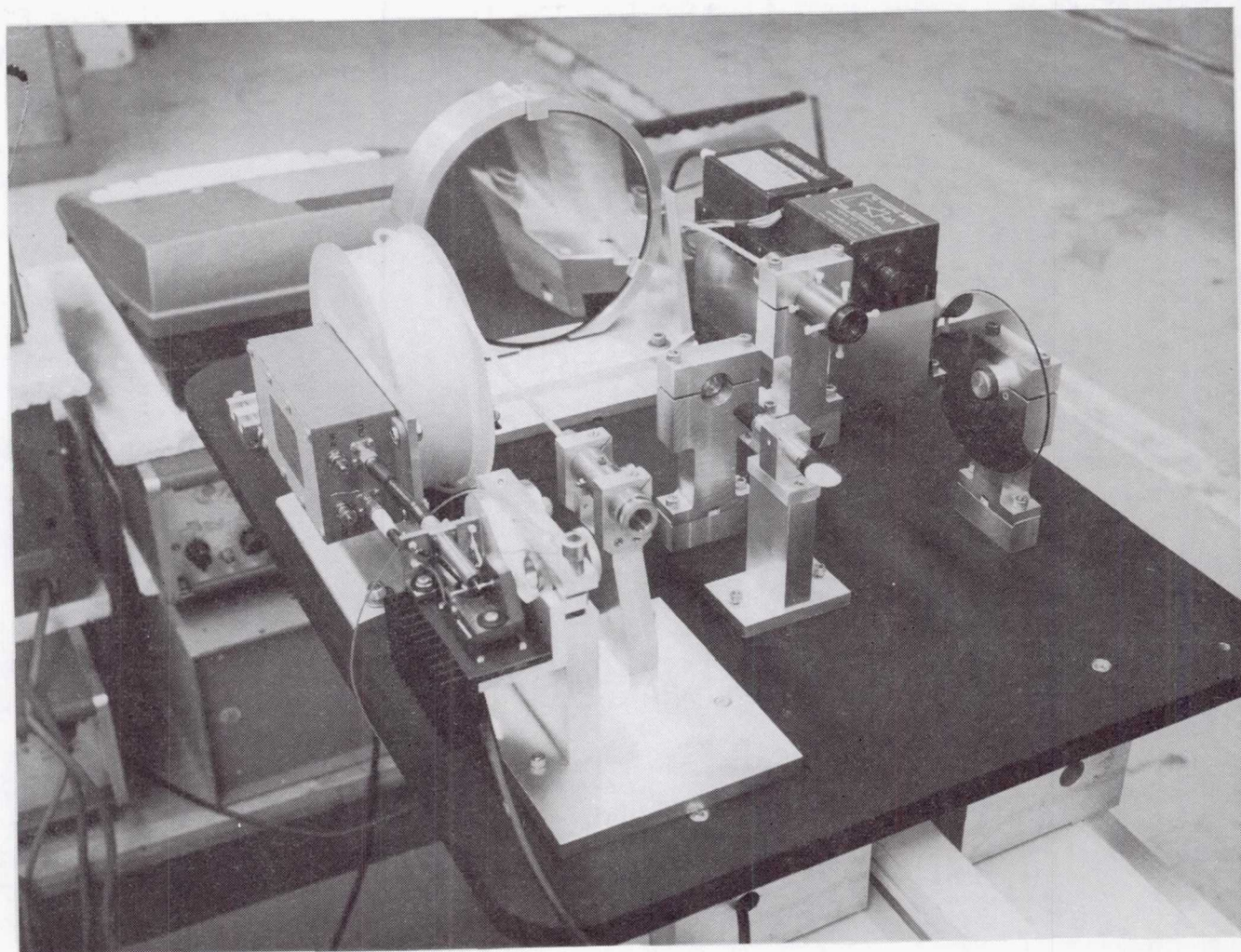
- DEVELOP CANDIDATE SYSTEM LEVEL CONFIGURATIONS
- LAND MOBILE SATELLITE SYSTEM
- DEFINE SUBSYSTEM INTERFACES AND CONSTRAINTS
- ESTABLISH FEASIBILITY FOR POTENTIAL APPLICATIONS
- REFINE FOCUS FOR ANTENNA CONCEPT DEVELOPMENT



SURFACE MEASUREMENT SYSTEM DEVELOPMENT

The breadboard surface sensing system, built and evaluated during FY 80, represents the functional demonstration of a) the principals of the concept, b) displacement measurement resolution on the order of 0.5 mm, and c) measurement repeatability on the order of 3 mm. The breadboard system was completely redesigned for the engineering model demonstration with goals for improving measurement resolution by a factor of 5 and measurement repeatability by an order magnitude. The detail design for the engineering model has been completed and all major subsystems and components have been purchased. However, a reduction of FY 81 funding precluded completing the assembly, performing the alignment and system calibration, and evaluating a functional engineering system. The completion of FY 81 objectives for evaluating an improved functional system and projecting performance for a flight type system would require an additional 9 months of engineering support plus some shop time.

- BREADBOARD MODEL REDESIGNED
- ENGINEERING MODEL 50% COMPLETE
- SIMULATED 200 meter RANGE COMPLETE
- ADDITIONAL EFFORT REQUIRED TO COMPLETE AND EVALUATE ENGINEERING MODEL



OFFSET WRAP RIB ANTENNA
CONCEPT DEVELOPMENT

A. A. Woods, Jr.
N. F. Garcia
Lockheed Missiles and Space Company
Sunnyvale, California

Large Space Systems Technology - 1981
Third Annual Technical Review
Langley Research Center
Hampton, VA

November 16-19, 1981

STUDY OBJECTIVES

A multi-year large offset antenna technology proof-of-concept program was initiated in 1980 between The Jet Propulsion Laboratory and Lockheed Missiles and Space Company. This contract, which extends through 1984, has as its primary objective the demonstration of 50 to 150 m, STS compatible, offset antenna technology readiness. This objective is intended to be satisfied through fabrication of a ground and flight testable partial 55 m reflector section and feed support structure. Reduction to practice through ground test verification is presently contained in the program. Figure 1 presents an overview of key objectives for the program.

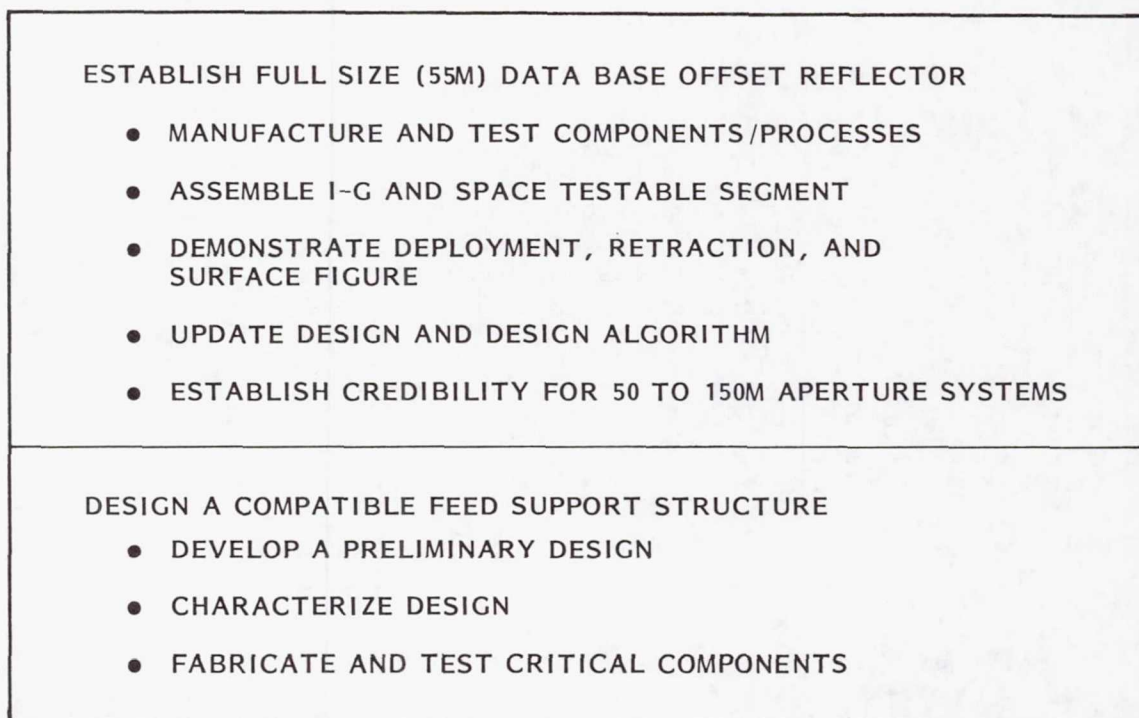


Figure 1

STUDY TASKS

The specific study tasks are described in Figure 2 in the program schedule. This schedule presents the full program activity segmented by the four funding phases of the contract. Phase III which is the subject of this report has yielded a fully assembled hub, deployment control device and rib. These units have been integrated and rib automatic deployment and re-stowage has been accomplished. In addition, the major structural element and mechanism in the feed support structure, the longeron, has been fabricated and assembled and limited structural and functional testing accomplished.

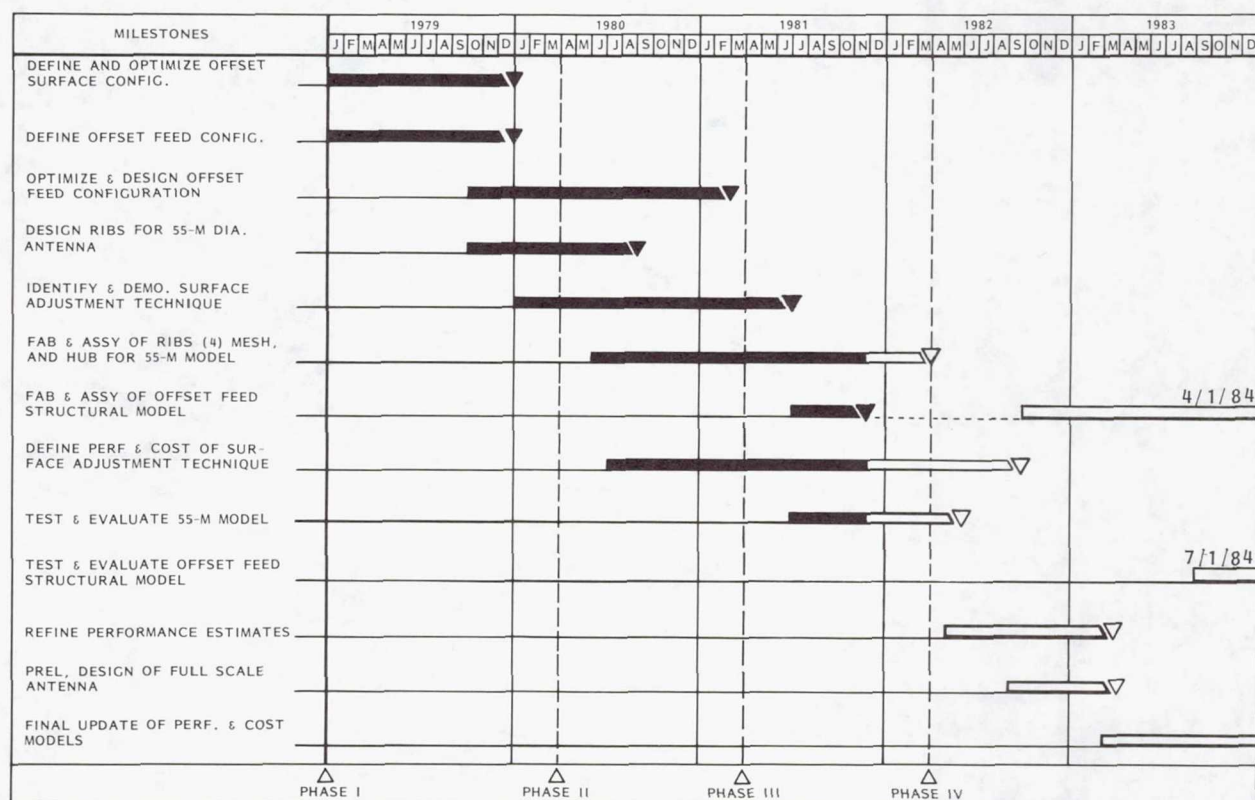


Figure 2

OFFSET ANTENNA SYSTEM OVERVIEW

The system under study is presented in Figure 3 which depicts a 100 m diameter communication antenna. The reflector is of the offset Wrap Rib design with the hub structure located at the center of the offset section. The cantilevered rib surface support structure can be seen radiating from this central hub. The spacecraft, which contains the control, communications, and power subsystems, is located in the focal point area but out of the microwave aperture to assure optimum performance. A deployable truss mast connects the reflector to the spacecraft and maintains system alignment. The mast is also configured to remain outside of the microwave path.

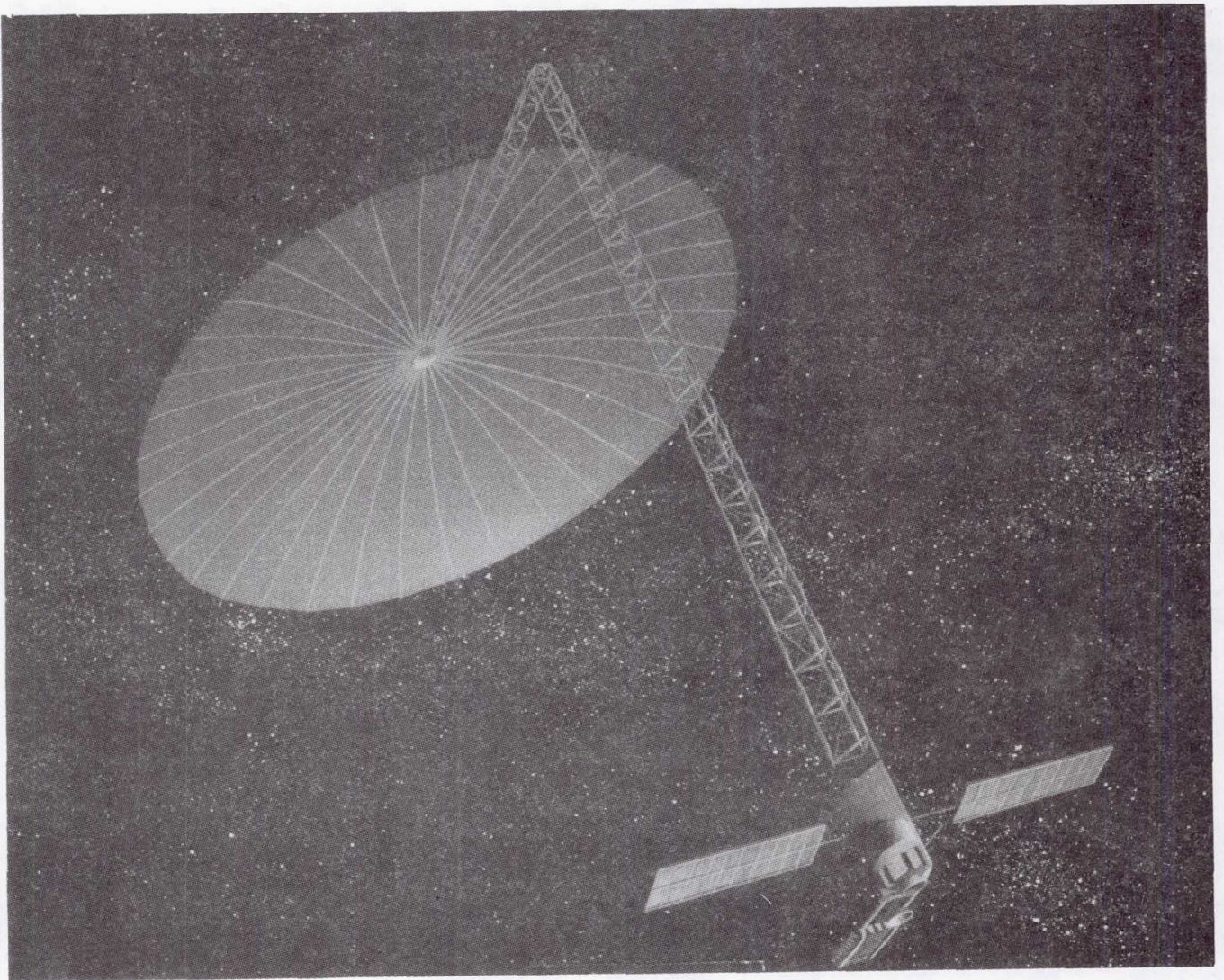


Figure 3

OPERATIONAL DEPLOYMENT SEQUENCE

Figure 4 presents the stowed spacecraft configuration as it is being deployed from the shuttle. The stowed reflector seen as a flat cylinder is shown at one end of the spacecraft and the IUS, used for orbit transfer, on the opposite end. The spacecraft segment is depicted next to the IUS with the feed system and solar array panels folded forward toward the reflector. In this configuration the mast is stowed in the triangular section hidden by the spacecraft equipment.

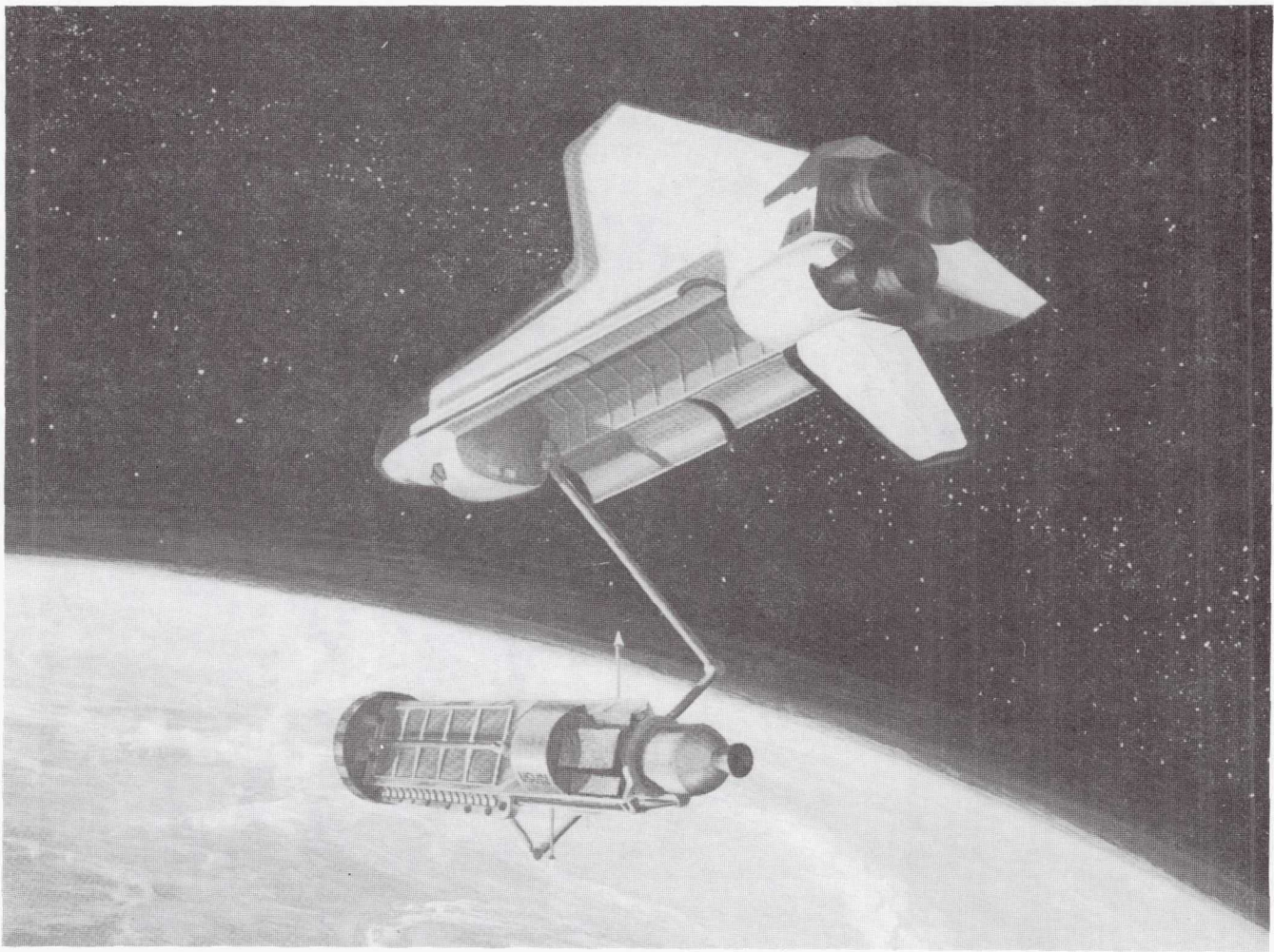


Figure 4

After the spacecraft has achieved operational orbit (Figure 5), the IUS is separated and the deployment sequence initiated. The first deployment is that of the mast. This activity can be seen in the figure as the reflector is being moved away from the spacecraft segment.

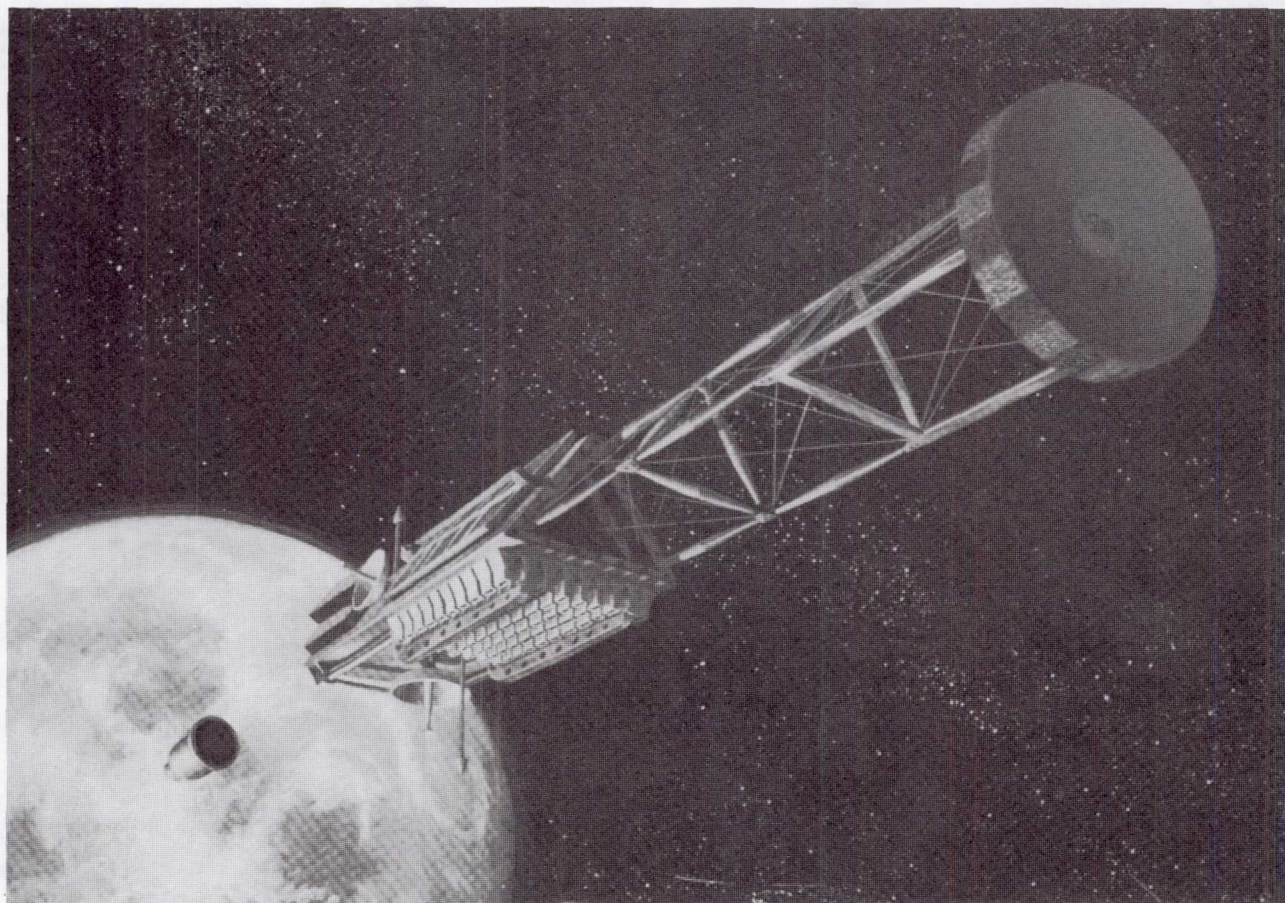


Figure 5

The final operation is that of reflector deployment. Figure 6 depicts this event at about the one-third point. The reflective surface and ribs can be seen unwrapping off the hub at the end of the fully deployed mast.

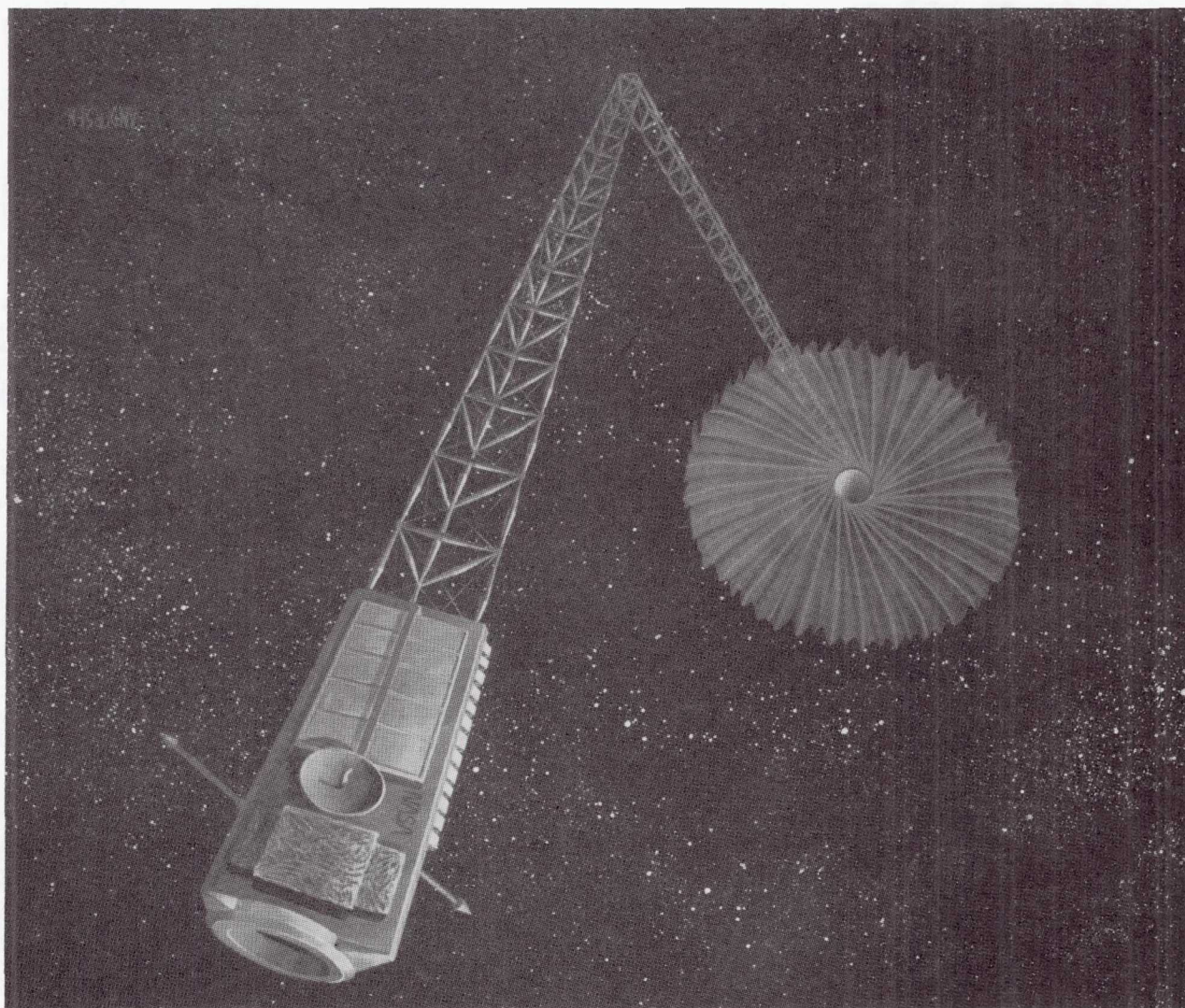


Figure 6

DESIGN/MISSION COMPATIBILITY

Previous study activities have identified the growth limits of the offset Wrap Rib design. These limits are presented in Figure 7 along with the data point which locates the 55 m data base design. The three major mission regions of interest are also presented to provide an appreciation for the projected design capability with respect to the defined mission models. The results show that the design potential comfortably envelops the defined near term mission zones as well as the projected far term missions (dotted projections).

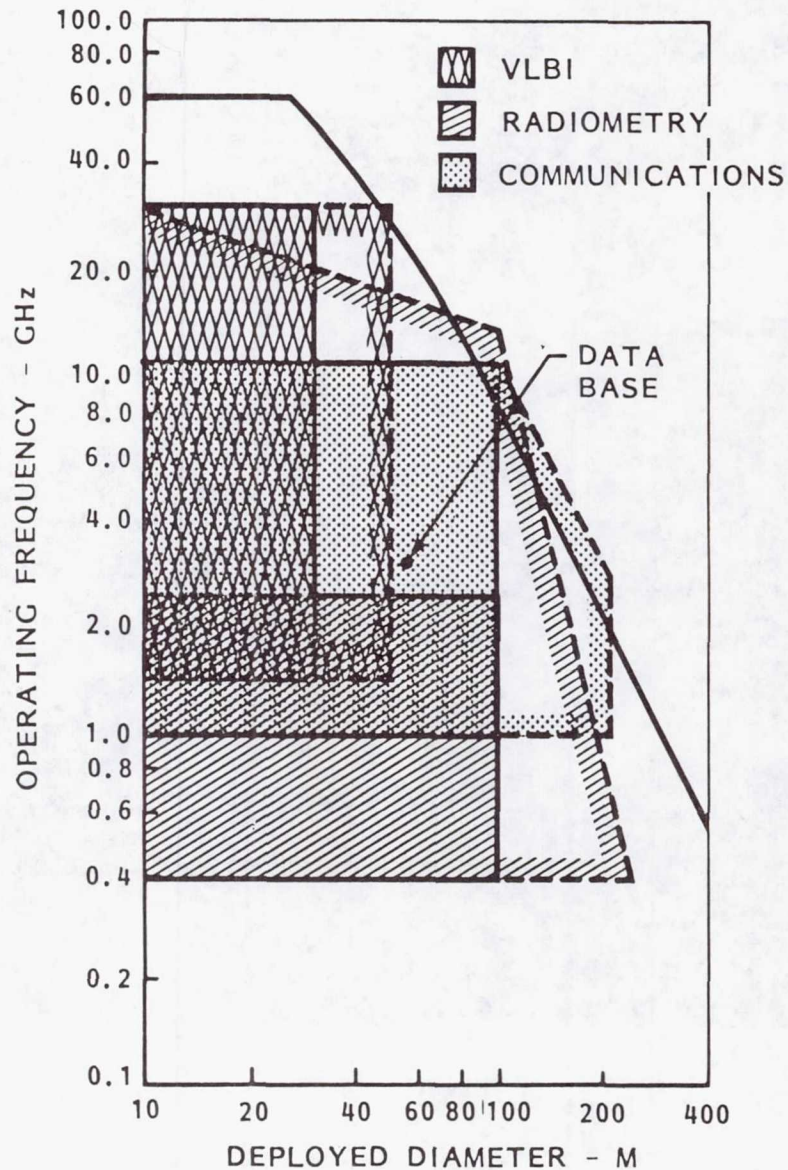


Figure 7

PROGRESS AGAINST OBJECTIVES

Significant progress was made this year in the fabrication of the 55 m proof-of-concept reflector hardware. The completion of the first full rib structure validated the fabrication and assembly processes. Assembly of the hub and deployment control device and integration of these components into the single rib deployment test article allowed for initial functional testing of the integrated reflector design which was successfully accomplished. The design activity on the feed support structure continued and a significant characterization data base was assembled. In parallel, the key structural element, the longeron, was assembled and evaluated. Figure 8 presents an overview of this progress.

<p>55M DATA BASE OFFSET REFLECTOR</p> <ul style="list-style-type: none">● COMPONENT /PROCESSES EVALUATION COMPLETE● HUB /DEPLOYMENT /RIB ASSEMBLY COMPLETE● SINGLE RIB AUTOMATICALLY DEPLOYED AND RESTOWED
<p>FEED SUPPORT STRUCTURE</p> <ul style="list-style-type: none">● PRELIMINARY DESIGN COMPLETE● CHARACTERIZATION COMPLETE● LONGERON AND HINGE FABRICATED AND ASSEMBLED

Figure 8

RIB TOOL DESIGN AND DEFINITION

The rib layup tool design, engineering and manufacturing definition was accomplished using CADAM (Computer Graphics Augmented Design And Manufacturing System). Engineering tool definition (reflector shape, three-dimensional tool contour and tool segments) was created on CADAM. CADAM then produced numerical control (N/C) tapes which defined the flat pattern part to be scribed, contour templates to be used in bump forming and bump forming guidelines.

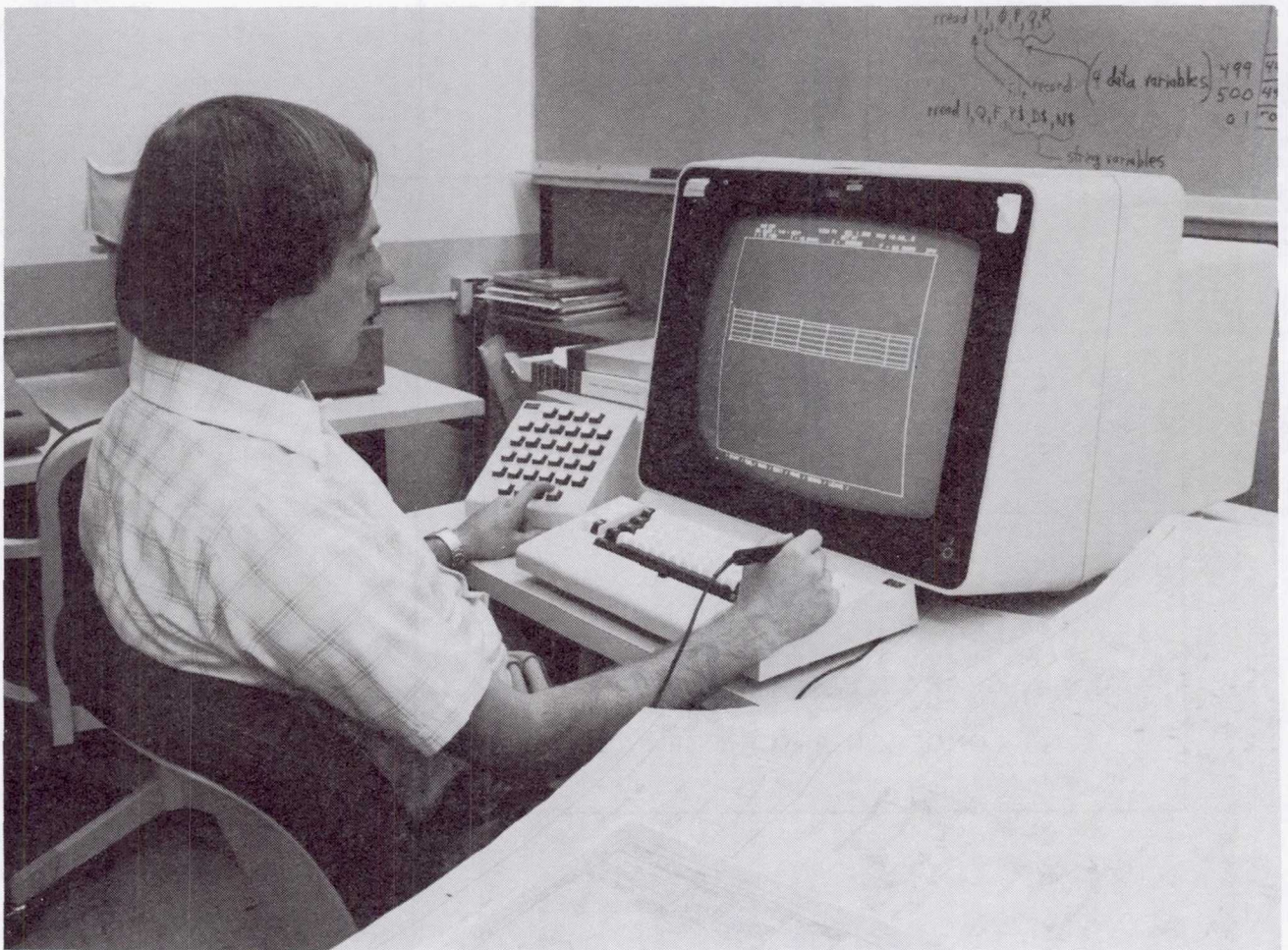


Figure 9

SHAPE CONTROL

Scribed invar sheets were bump formed in a hydraulic brake using steel dies against a hard rubber reactor. The three dimensional variation of tool layup surface was maintained using the bump forming guidelines for reflector curvature and cross-sectional rib contour templates at intervals along the length of the tool.

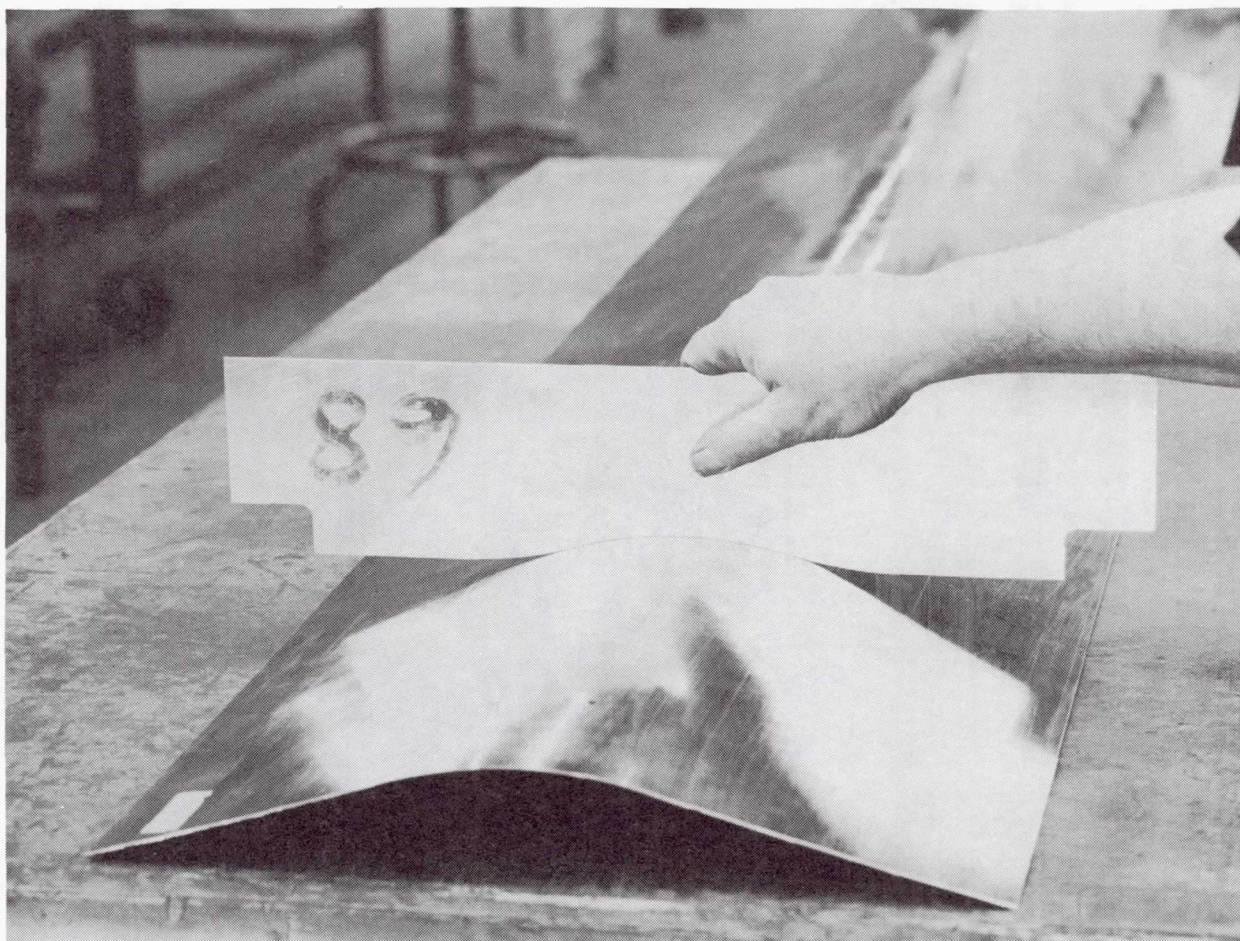


Figure 10

TOOL ASSEMBLY

The bump formed semi-lenticular top is mated to the base, the final contour checked, and the assembly clamped. Spot welding along the edges holds the assembly together. Seam welding the edges completes the tool.



Figure 11

GRAPHITE LAYUP

Epoxy impregnated graphite is placed on the layup tool in three layers. The first and third layers are graphite fabric while the second layer is unidirectional graphite tape.



Figure 12

CURE PREPARATION

Completed graphite-epoxy layups are prepared for curing by placing over the layup release cloth, a bleeder sheet, and breather cloth. A vacuum bag is then placed over the assembly and thermocouples installed.



Figure 13

CURING

Temperature and pressure are applied in an autoclave to cure the assembly.

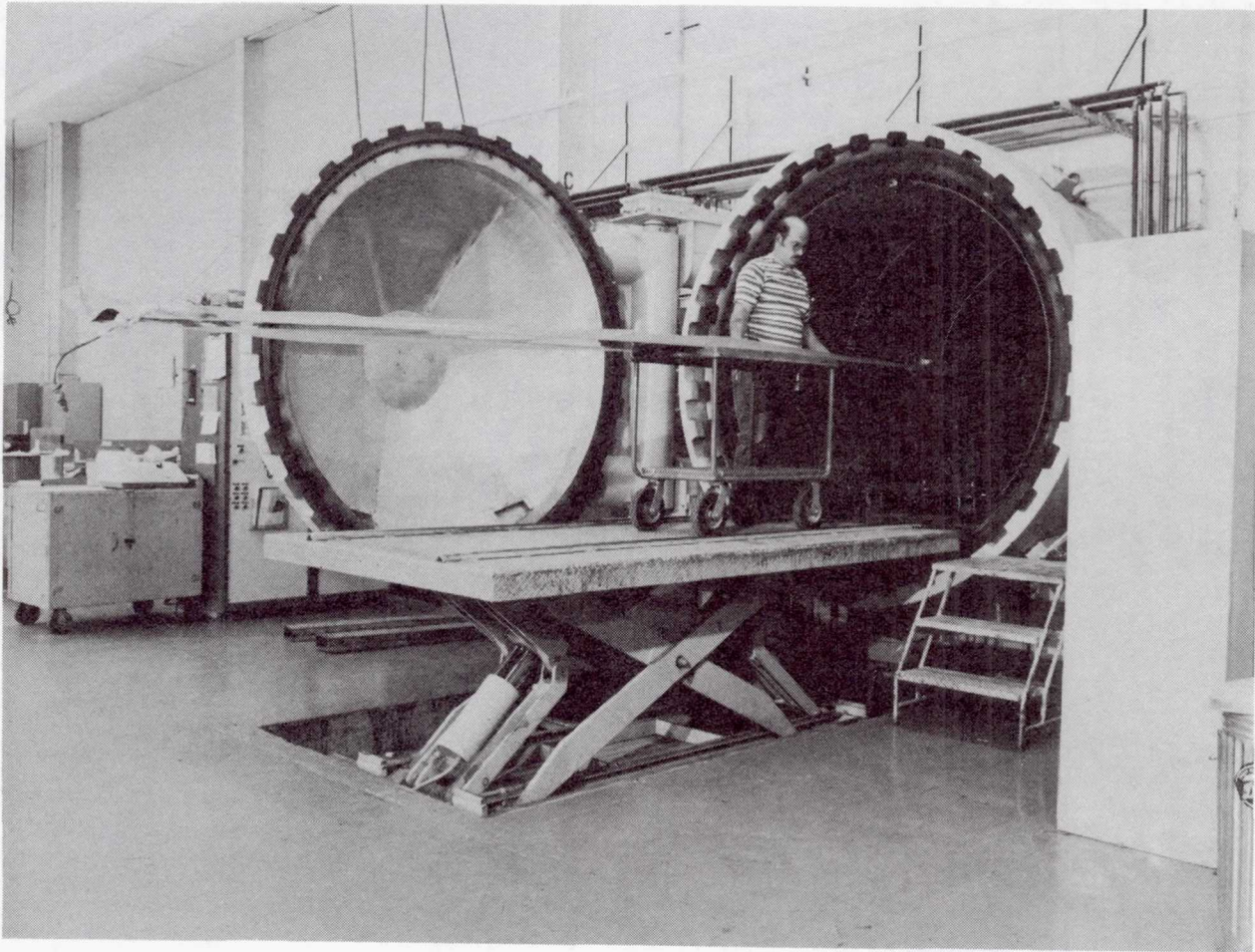


Figure 14

COMPLETED RIB SEGMENT

A cured part is removed from the autoclave and stripped of the vacuum bag assembly. The exposed cured rib segment is then easily removed from the tool.

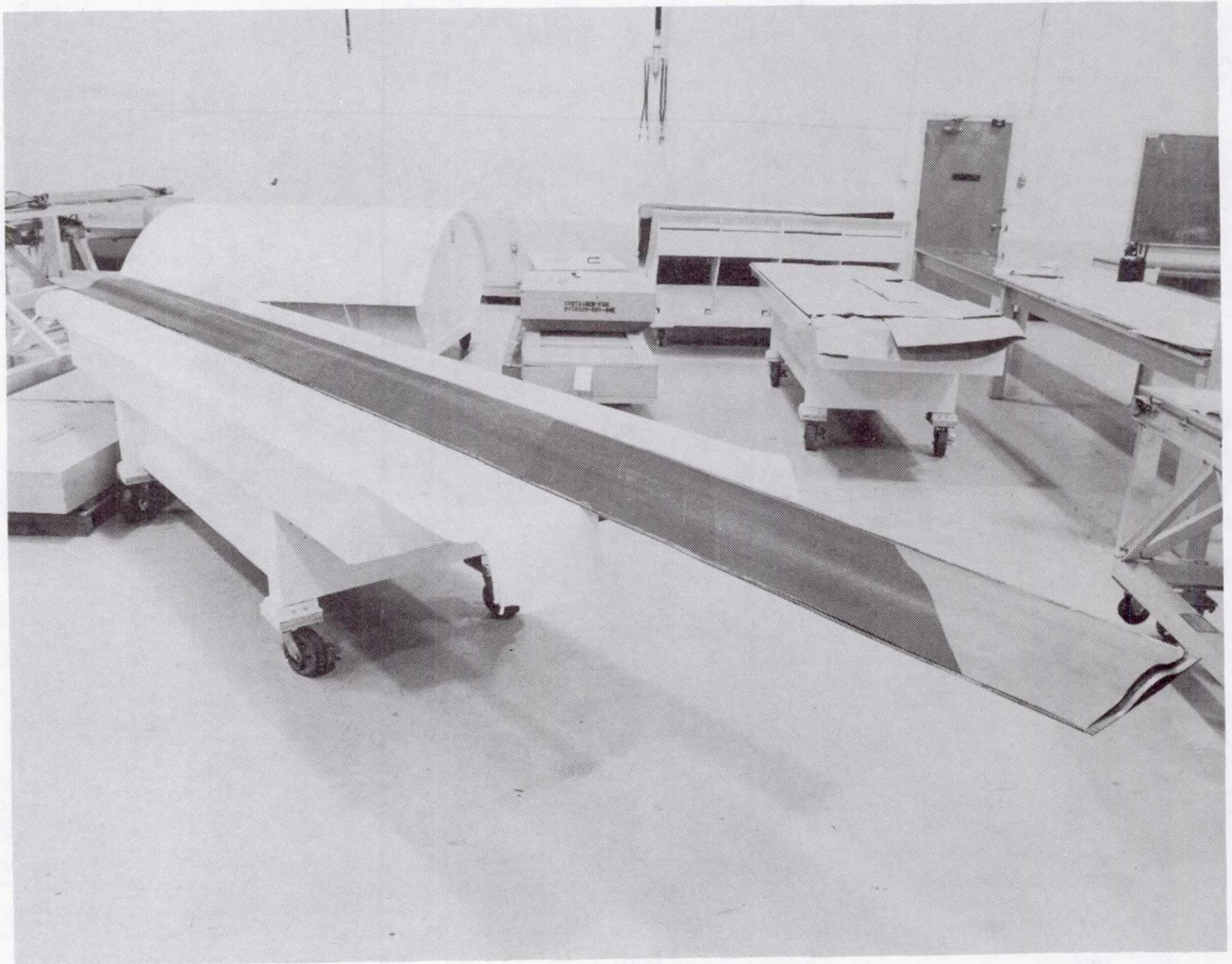


Figure 15

SPLICE BOND PREPARATION

Rib segments are placed end to end and marked for the trim operation. Pins protruding from the table mate with locating holes in the segments insuring accurate alignment of the parts.

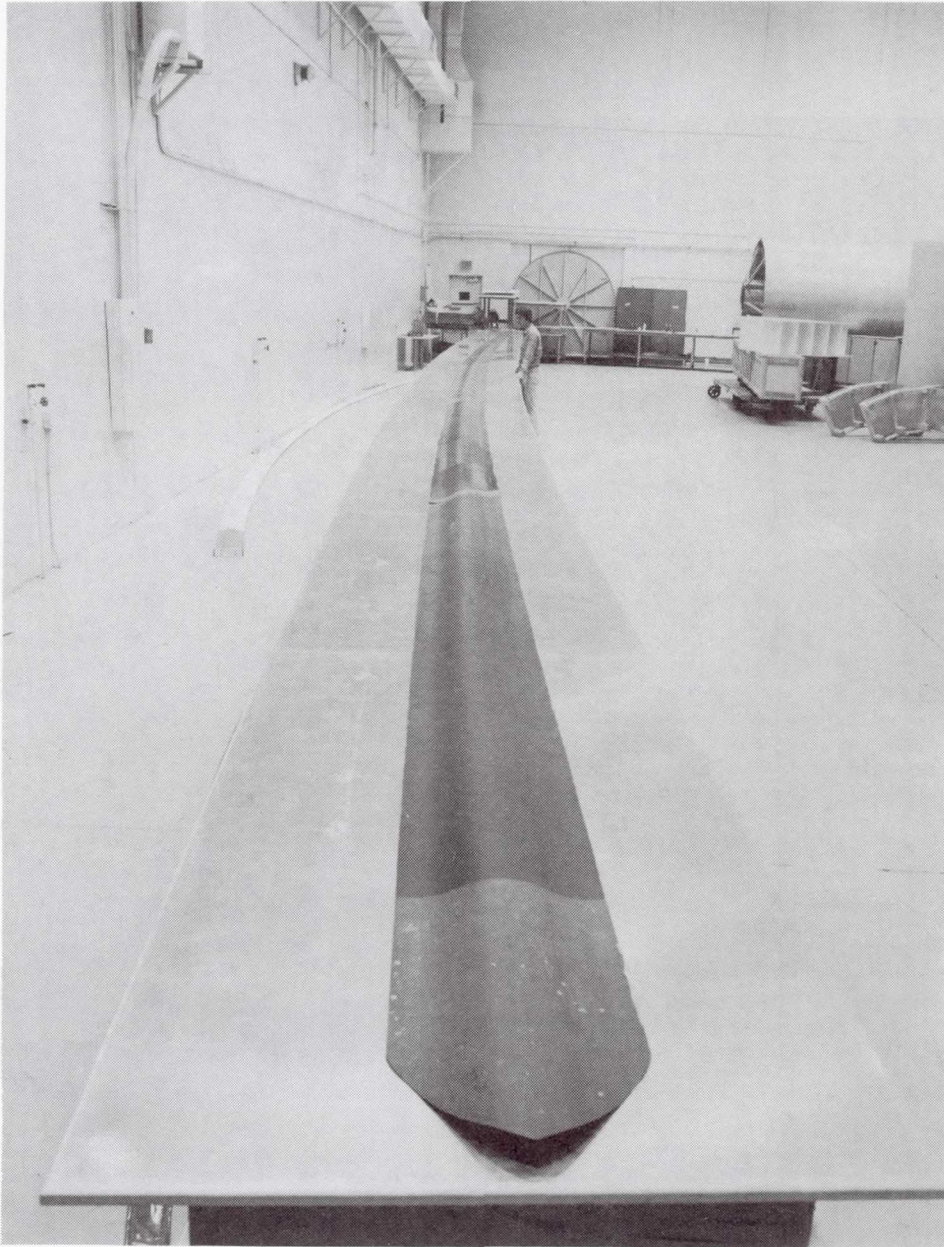


Figure 16

SPLICE BONDING

Adhesive is applied to the surface of butted segments and a splice strap positioned over the joint.

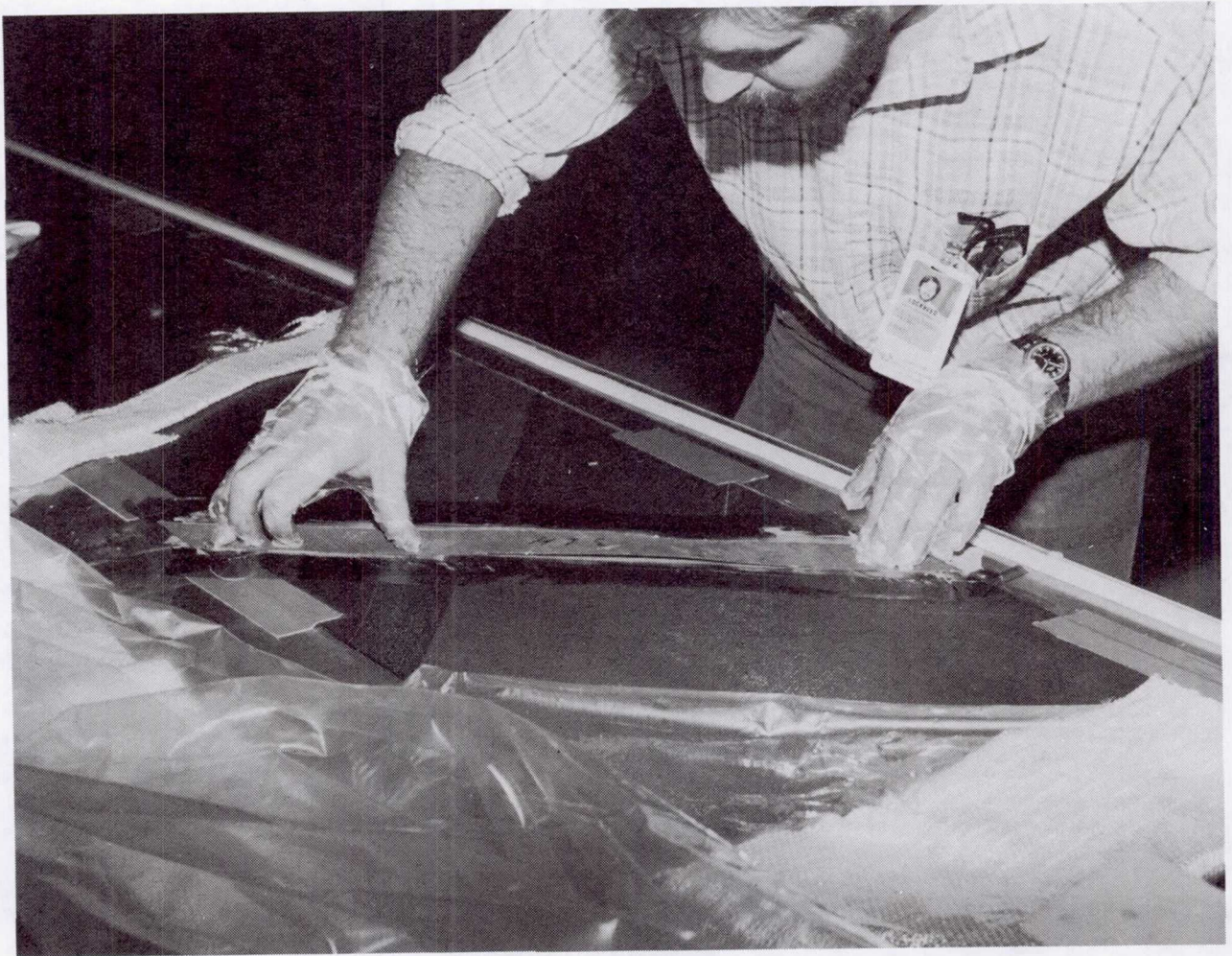


Figure 17

ROOT SECTION BONDING

Adhesive is applied to the surface of the graphite epoxy root segment and the root section placed over the bond area. A vacuum bag is placed over the assembly and drawn down during the splice and root section cure of the 1/2 lenticular rib.

Spliced rib halves are bonded together at the upper and lower edges generating a full lenticular cross-section. The root portion of the rib is seam welded rather than bonded. The rib is completed with a trim operation to the desired reflector contour.

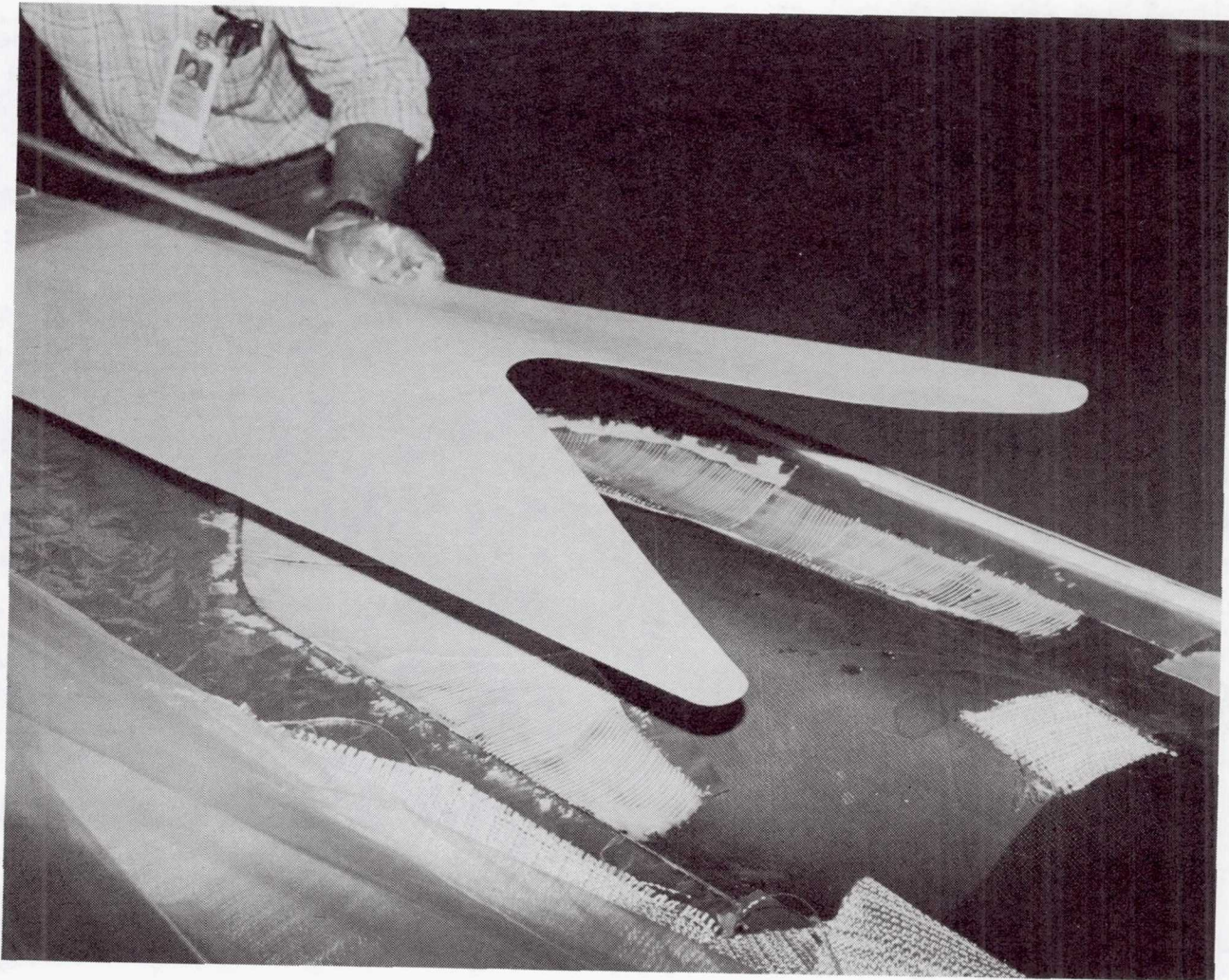


Figure 18

SINGLE RIB DEPLOYMENT TEST

The single rib deployment test involved the deployment and re-wrap of a single rib (Figures 19, 20 and 21).

The rib is stored coiled about the hub in the flattened configuration, regaining the lenticular cross-section when deployed.

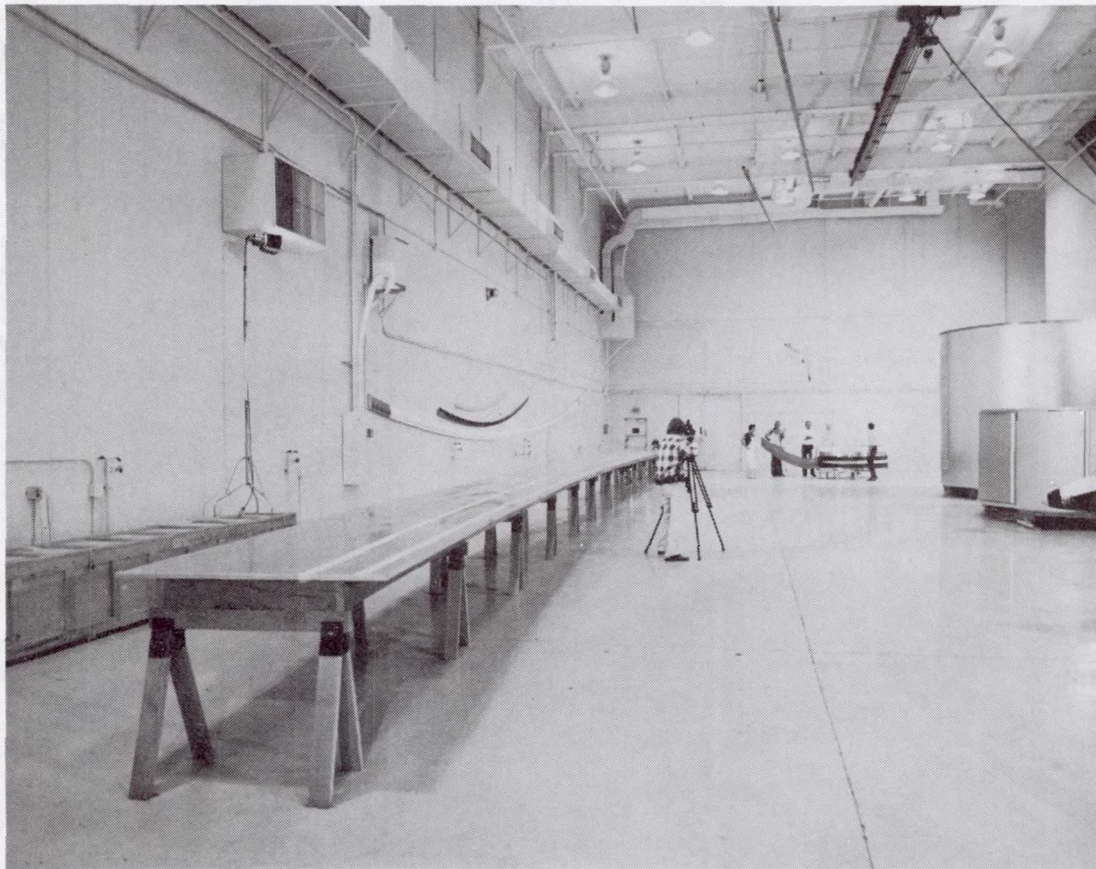


Figure 19

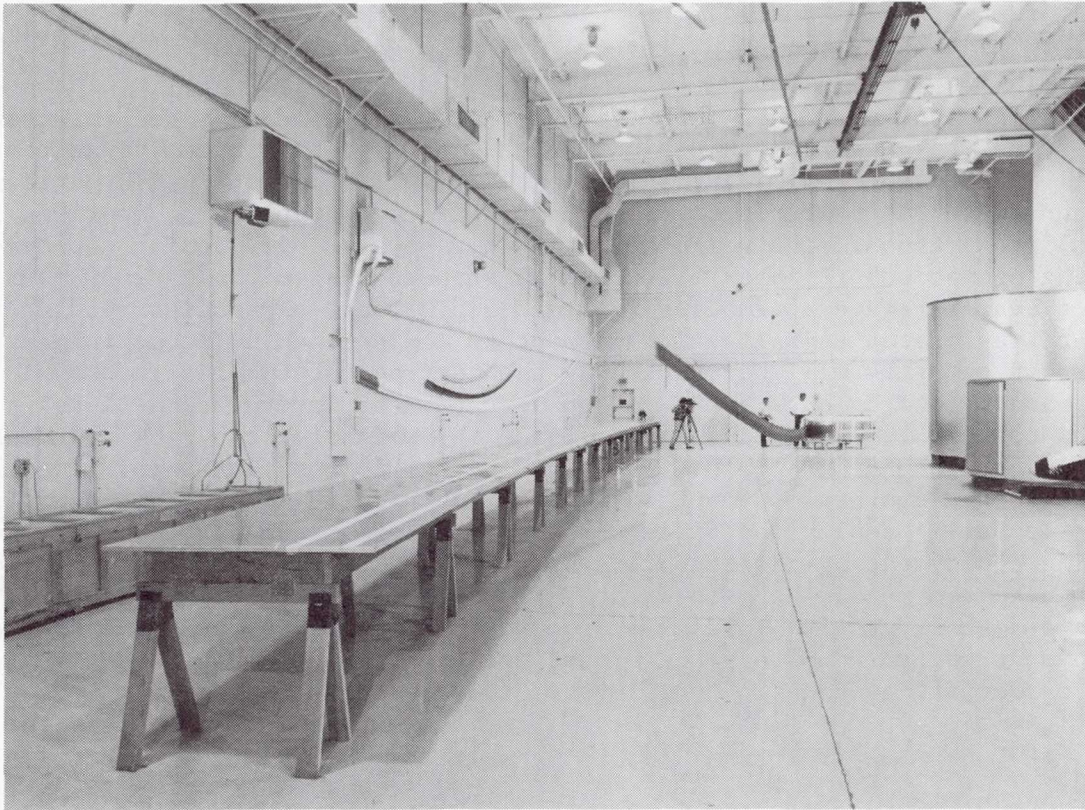


Figure 20

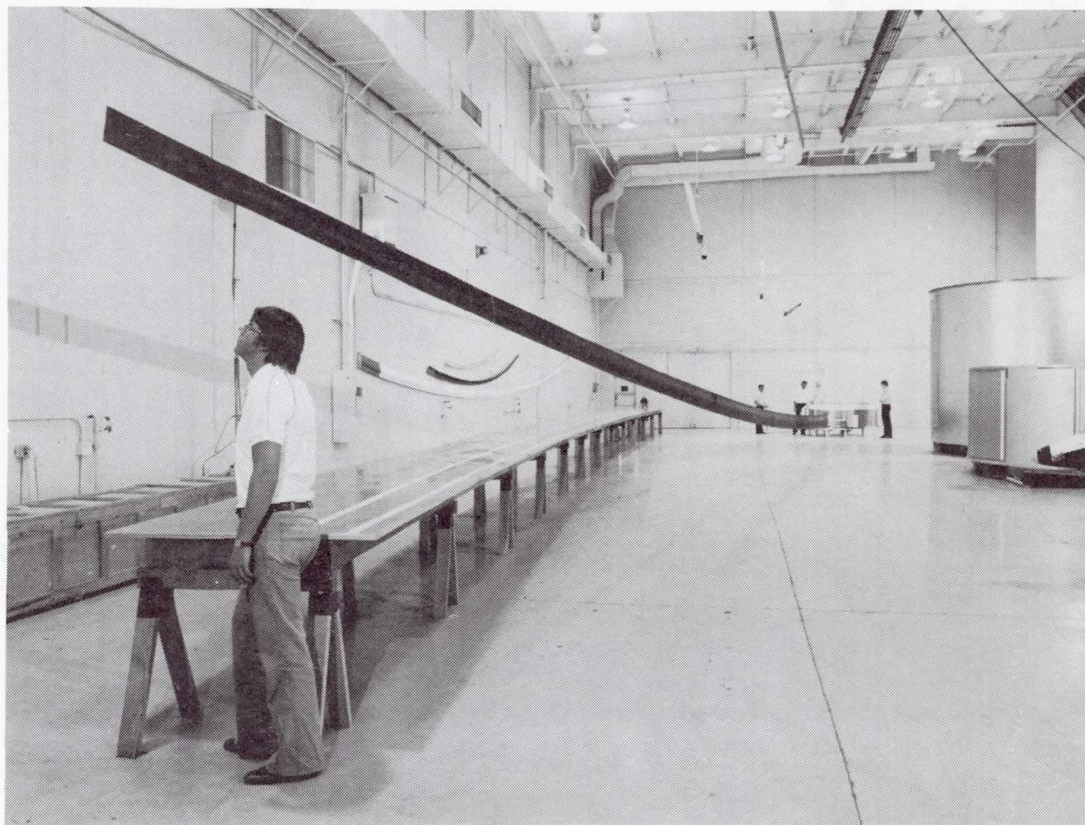


Figure 21

GROUND TEST OF DATA BASE MODEL

The ground test of the 55-meter diameter proof-of-concept model represents the largest ground-based demonstration for this concept. Further ground test programs will include the deployment and repeated refurling of the 4-rib partial antenna and measurement of rib stiffness and surface contour for comparison with analytical predictions. The reflector ribs will be supported during deployment and furling operations (Figure 22). The rib support system consists of four sets of balance beam/carriage assemblies for each rib. These assemblies ride on fixed rails that are located radially with respect to the antenna. The deployment displacements of the ribs will be tracked by the carriage assemblies in the radial direction and by the balance beams in the vertical and lateral directions. This passive support system progressively offloads the weight of the ribs and mesh as they unfold from the central hub. To maintain the rib positions approximately colinear with the overhead support rails, the hub will be mounted on a platform that rotates during deployment. The three degrees of freedom accommodated to the ribs during deployment by the support system results in a controlled deployment sequence where the unfolding mesh is not affected by the rib support system. Since the effect of gravity loading on the mesh will tend to force the mesh against the deployment control devices, the ground demonstration of mesh management with respect to identifying snagging problems is considered conservative.

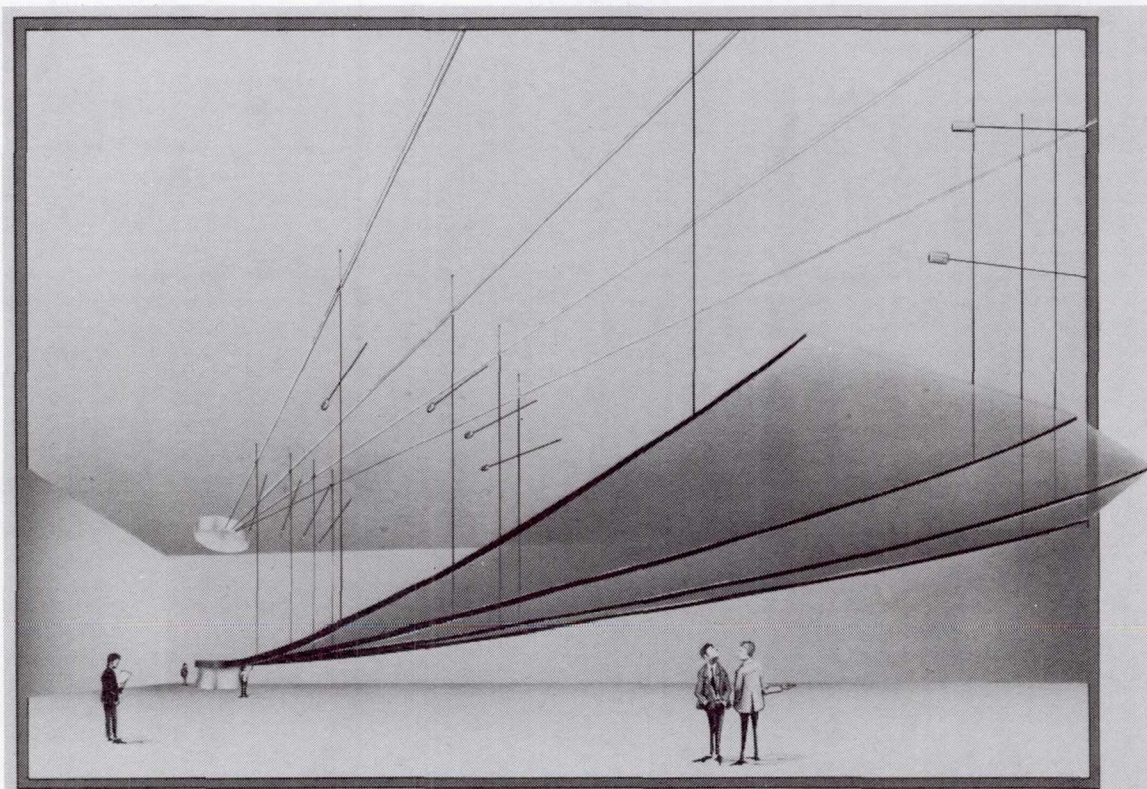


Figure 22

FEED SUPPORT STRUCTURE DESIGN APPROACH

The tapered tube mast design, as implied in the name, is constructed with tapered graphite epoxy tubes as the major structural elements. These tubes are used as both longeron and batten members as shown in Figure 23. The longerons are hinged with a prestressed joint in the center which allows them to be folded so that the battens can be stowed next to each other for ascent. In the folding operation the longerons fold adjacent to the battens so that a maximum length can be used and the central area of the stowed package is open and available for equipment. The diagonal stiffeners are small diagonal high modulus graphite epoxy rods. The stowed package is completely contained within a rigid deployment cage which houses the deployment control device and can be used to mount spacecraft components. Deployment is accomplished one bay at a time so that stiffness is maintained throughout the event.

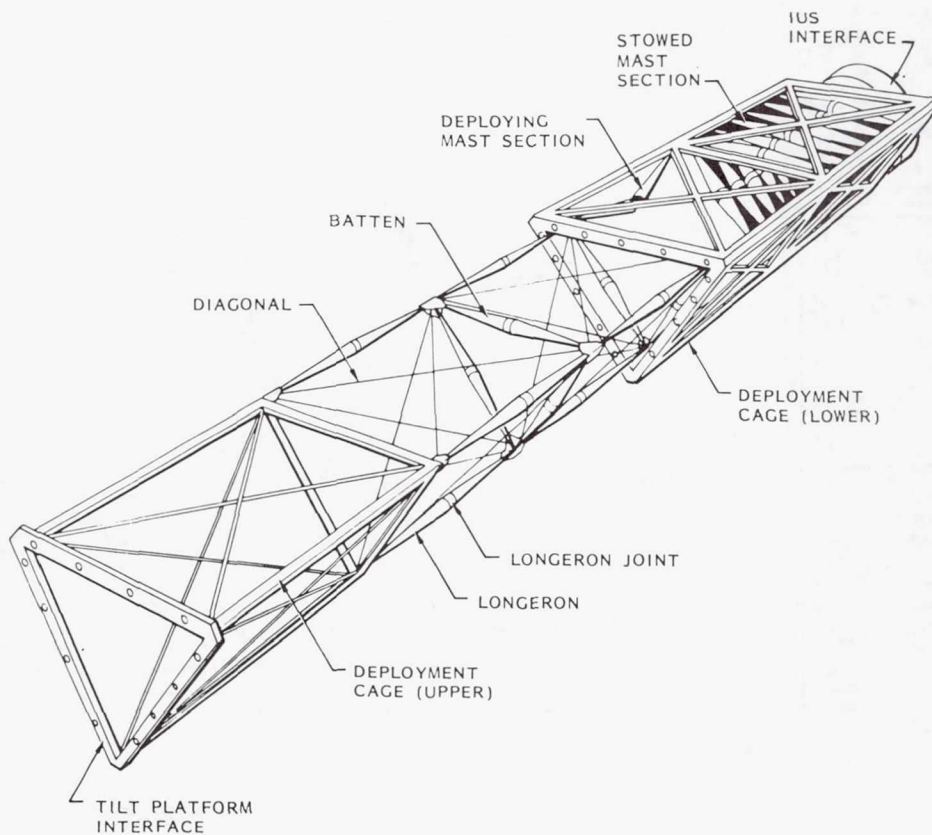


Figure 23

EXTENSION/RETRACTION PRINCIPLE

The mast elements are stacked and compressed into a lower compartment of the container; the stack is slowly raised toward the upper compartment of the container by the mechanism; the mechanism in the upper compartment rapidly lifts a single batten to the point where a single bay is formed within the upper compartment; and then this fully formed bay is extruded from the container through the formation of the next bay. This is illustrated in Figure 24.

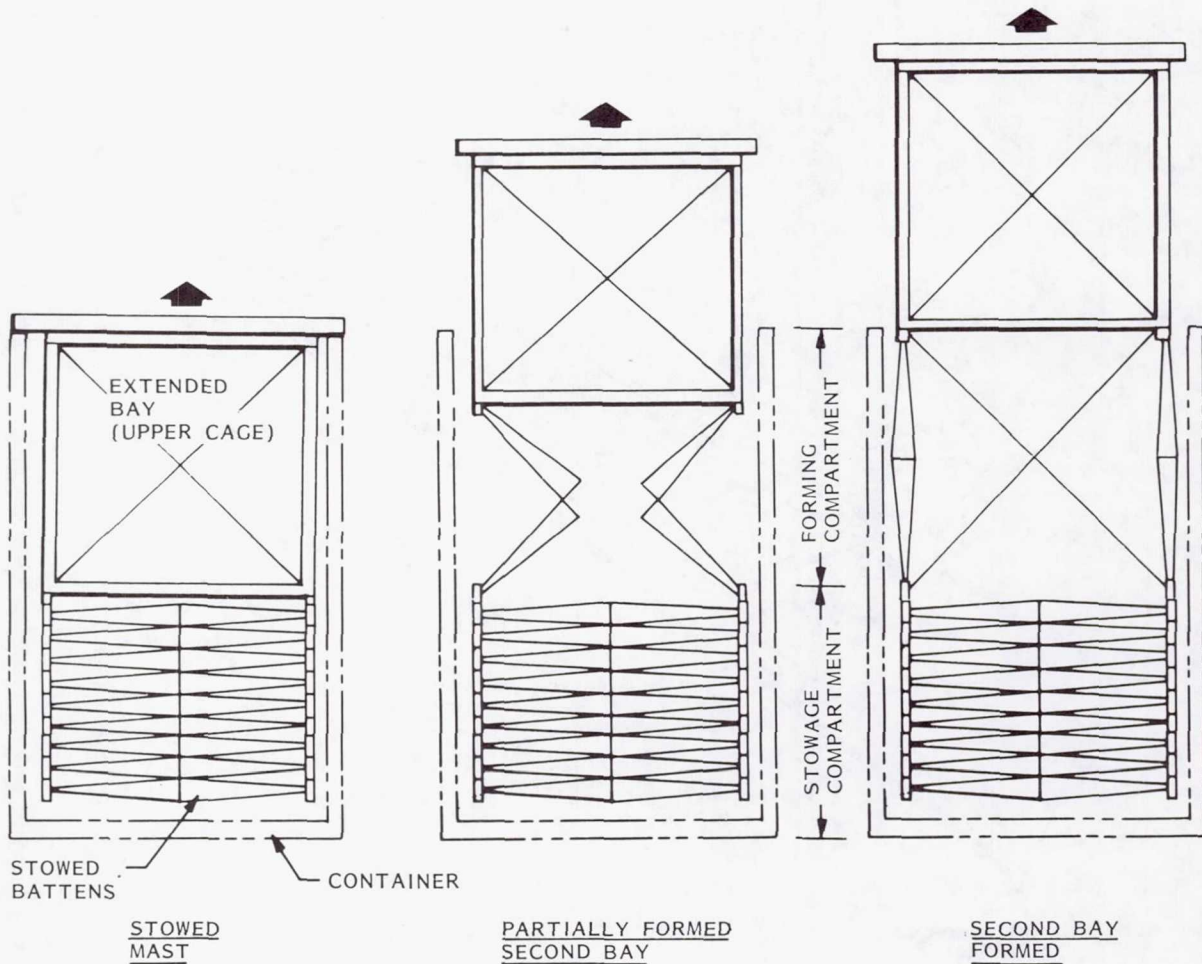


Figure 24

FEED SUPPORT STRUCTURE CHARACTERIZATION

Figures 25 through 28 present the results of a design parametric study illustrating the essential tradeoffs that may be made within the constraints of the given design requirements using various structure member sizes and material thicknesses.

Figures 25 and 26 are graphs of bending and torsional stiffness per bay vs bay aspect ratio (longeron length divided by batten length). By way of example, we select a design case of a structure consisting of 10, 3.6 x 3.6 m bays with 7.62 - 2.54 cm diameter longerons.

DEPENDENCE OF NORMALIZED BENDING STIFFNESS ON
MAST LENGTH, ASPECT RATIO, AND LONGERON DIAMETER

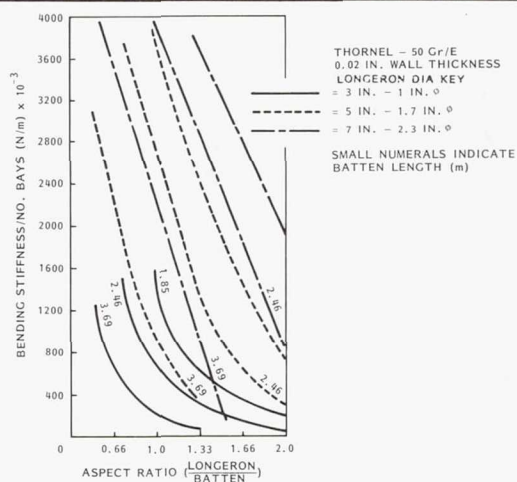


Figure 25

DEPENDENCE OF NORMALIZED TORSIONAL STIFFNESS ON
MAST LENGTH, ASPECT RATIO, AND LONGERON DIAMETER

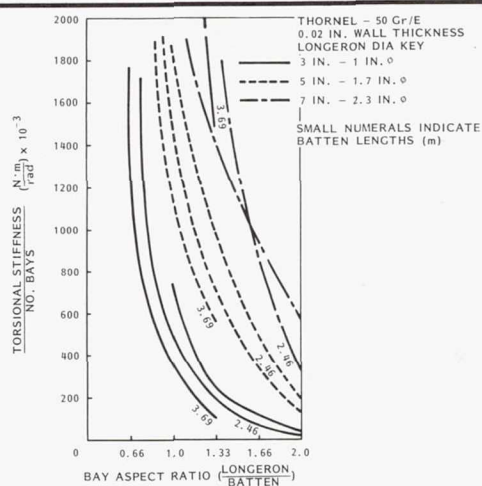


Figure 26

The next set of graphs, Figures 27 and 28 are presented on a per length basis. That is, to obtain a value for the stowed length of a 115 m mast containing bays with an aspect ratio of one, we would enter Figure 27 at the point corresponding to the first curve on the left and an aspect ratio of 1. This gives a stowed length of approximately 2.66 when 0.23 is multiplied by 115 m.

STOWED LENGTH AS A FUNCTION OF MAST LENGTH,
ASPECT RATIO, AND LONGERON DIAMETER

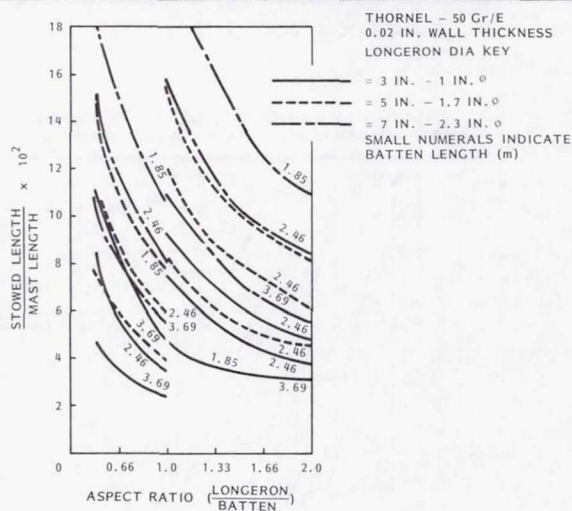


Figure 27

DEPENDENCE OF STRUCTURAL MAST WEIGHT ON
LENGTH, ASPECT RATIO, AND LONGERON DIAMETER

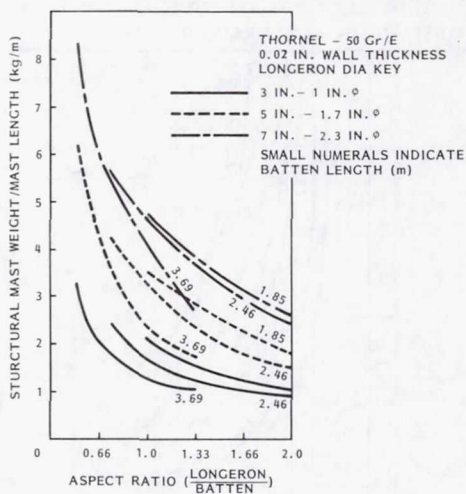


Figure 28

LONGERON FABRICATION

The fabrication of a longeron is shown in Figure 29. Four layers of epoxy impregnated graphite are used, two angled at 45 degrees to the longeron center-line and two at zero degrees.

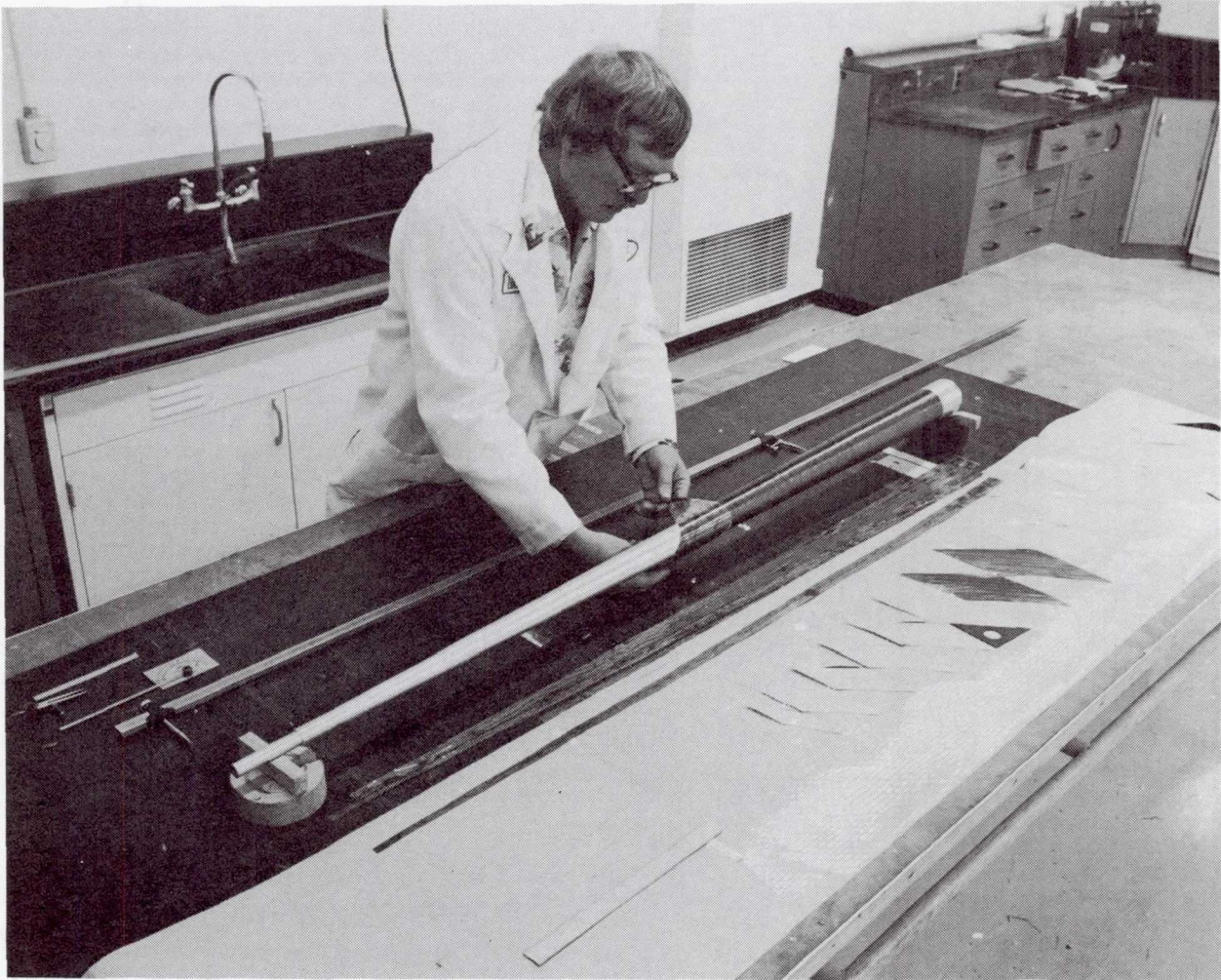


Figure 29

LONGERON JOINT

The longeron center joint is shown in schematic in Figure 30. It consists of a crossed four-bar linkage with a toggle link added to lock the joint at full deployment. A torsion spring at the end of one of the toggle links provides the deployment and locking force. The joint is designed to provide a balanced load path for tension and compression loads, and can be adjusted to display no back-lash over a range of loads.

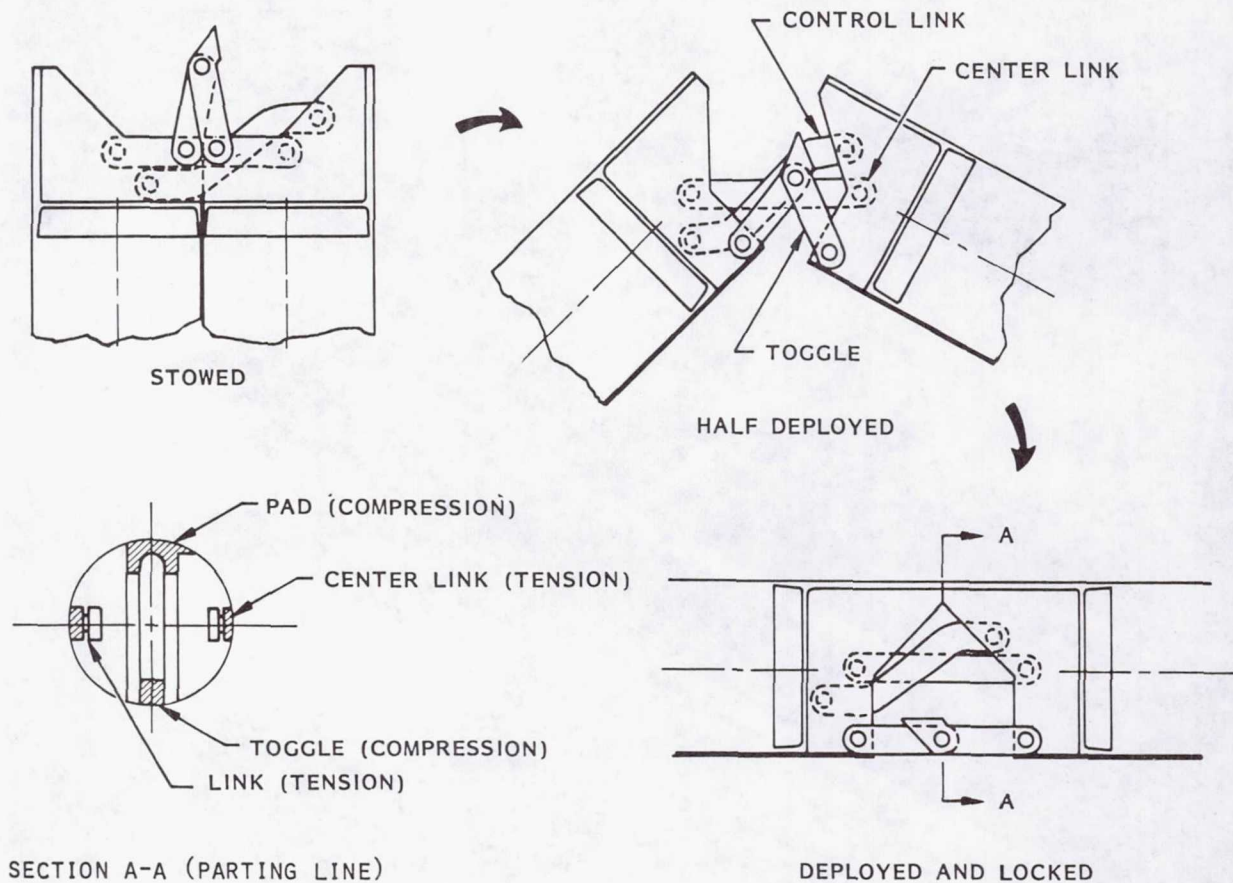


Figure 30

HINGE FITTINGS

The fittings for the longeron joint are bonded in place after the tubes are fully cured and trimmed to the proper length. Correct alignment of the fittings is assured through the use of a bonding jig. Figure 31 presents this process.

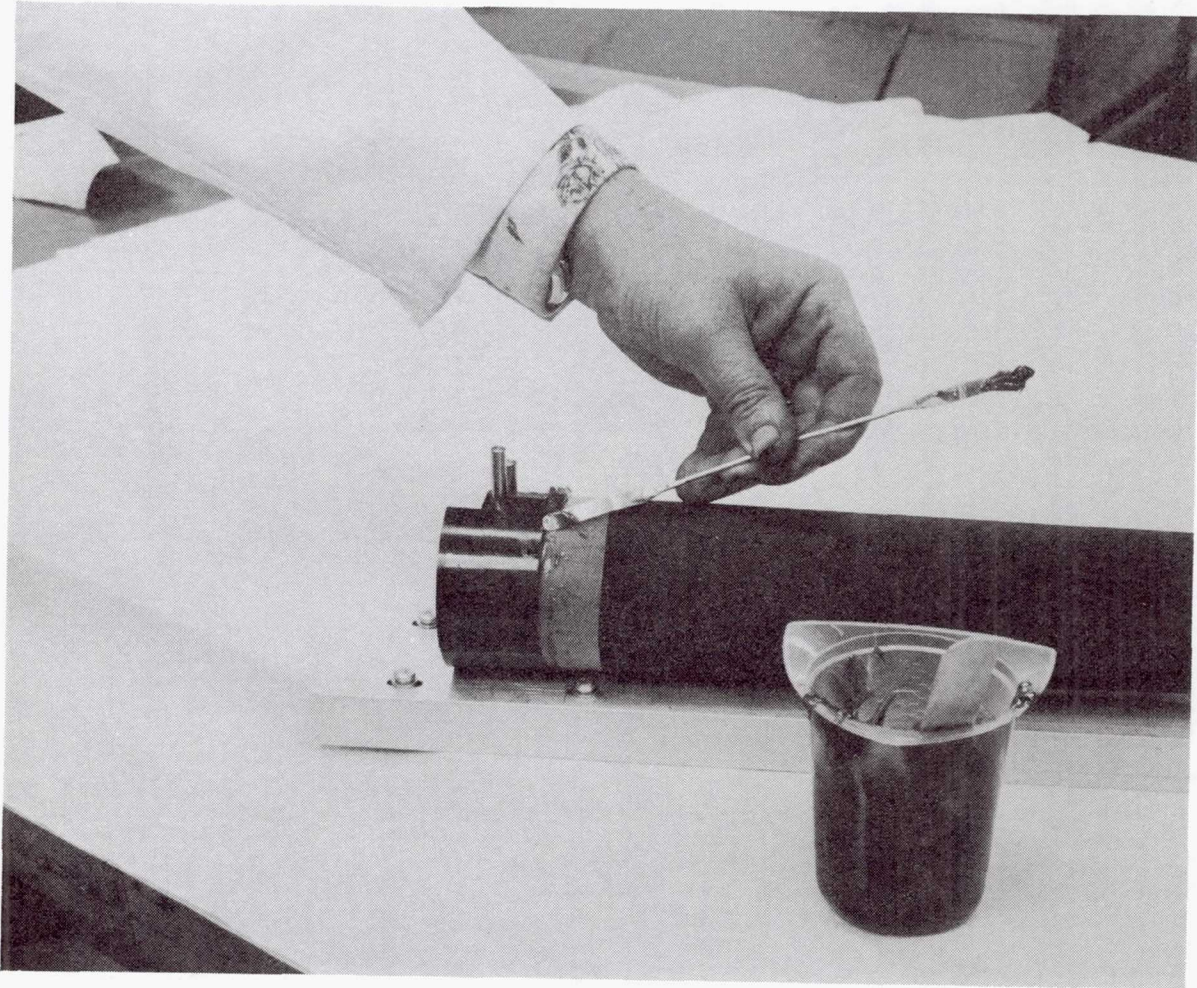


Figure 31

LONGERON ASSEMBLY

The complete longeron is shown in two positions in Figures 32 and 33. It is 10 feet long when extended and weighs less than two pounds.



Figure 32



Figure 33

PROGRAM PLAN

The success of the current program indicates continuation will yield substantial technological and cost benefits. The success in the reflector development should encourage definition of a similar activity in the deployable mast design and proof-of-concept development.

CONTINUE 55M REFLECTOR DATA BASE PROGRAM

- ASSEMBLE TESTABLE SEGMENT
- DEMONSTRATE DEPLOYMENT AND RETRACTION
- MEASURE DEPLOYED CONTOUR WITH OFFLOADING TEST AID
- UPDATE DESIGN AND DESIGN ALGORITHM

ESTABLISH A DEPLOYABLE MAST DATA BASE PROGRAM

- DEVELOP DEPLOYMENT/RETRACTION SYSTEM
- MANUFACTURE AND TEST COMPONENTS/PROCESSES
- ASSEMBLE TESTABLE SEGMENT
- DEMONSTRATE DEPLOYMENT AND RETRACTION
- MEASURE DEPLOYMENT REPEATABILITY
- UPDATE DESIGN AND DESIGN ALGORITHM

Figure 34

Page intentionally left blank

ANALYTICAL PERFORMANCE PREDICTION FOR LARGE ANTENNAS

M. El-Raheb
Jet Propulsion Laboratory
Pasadena, California

Large Space Systems Technology - 1981
Third Annual Technical Review
November 16-19, 1981

COUPLED REFLECTOR-FEED SUPPORT STRUCTURE MODES

The coupled free-free modes of the 55M LMSS antenna configuration 4A shown in Figure 1 were determined using modal synthesis. Reflector modes clamped at the hub are calculated adopting the efficient cyclic symmetry technique. Similarly, clamped hub modes of the offset boom structure are calculated. The modes of the two sub-structures are then combined through the process of modal synthesis on the assumption that the interface at the hub structure is rigid thus satisfying statically determinate matching conditions. For attitude control purposes, only modes associated with symmetric components zero and one involve net motions of the center of gravity of the reflector. This condition restricts the set of admissible eigenfunctions for modal synthesis. Modes with symmetric components higher than one are excited only by forces acting on the ribs. These modes are totally uncoupled from the boom dynamics. There exists two mechanisms through which these latter modes couple to the boom modes.

The first mechanism depends on hub elasticity while the second mechanism relates to imperfection of reflector geometry from the hypothetical ideal axisymmetric shape. The generalized coordinates that couple these modes to the boom are functions of relative rib to hub bending stiffness and normalized imperfection parameter. In the present application, these effects are small and therefore neglected to a first approximation.

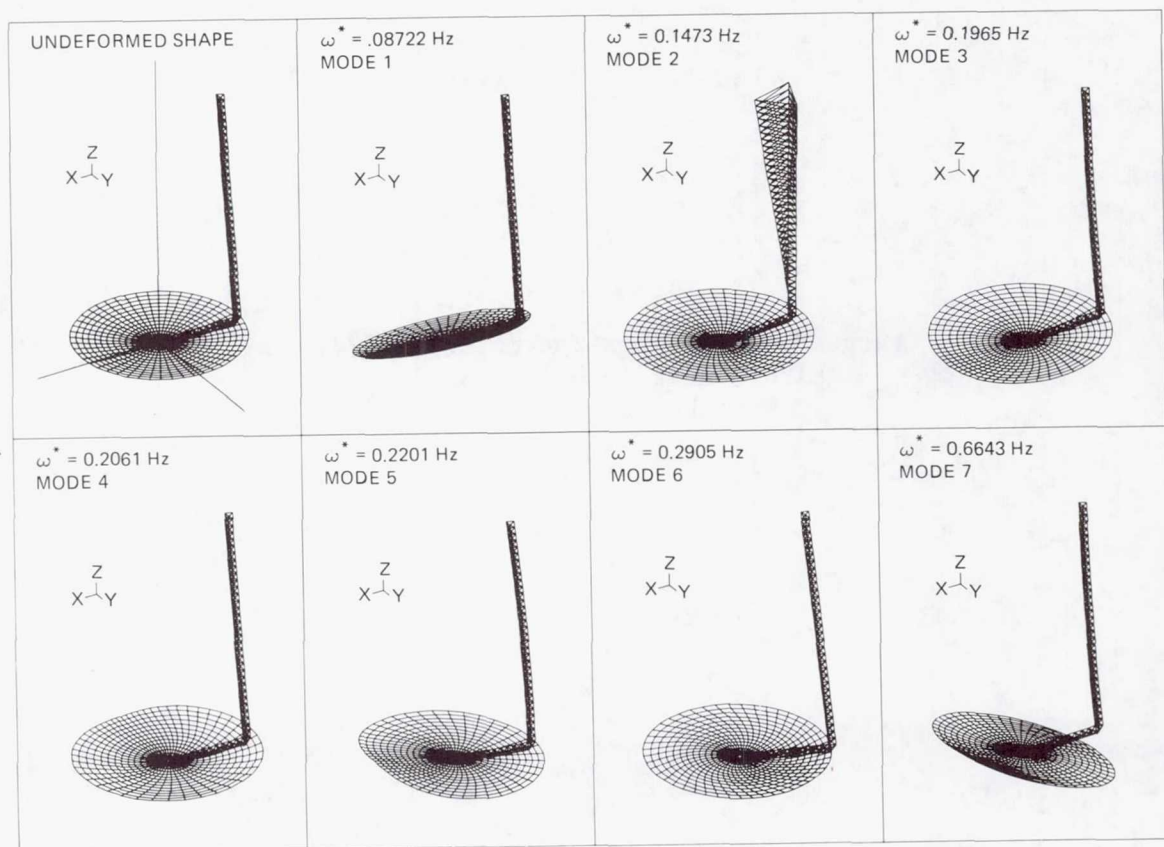


Figure 1. Combined free modes of LMSS configuration 4A

A structural dynamic requirement of the antenna is the coalescence of the fundamental bending resonance of the clamped reflector and the fundamental coupled system resonance. The reasons behind the requirement are now explained. As illustrated in Figure 1, the fundamental resonance at $\omega_{c1} = 0.0872$ Hz involves torsion of the short boom arm and rocking of the reflector about that arm. The rocking excites bending motions of the ribs about their weak axis (torsional mode of reflector with a circumferential dependence described by one full wave, $n = 1$). This elastic mode is identified as the fundamental mode of the clamped reflector and resonates at $\omega_{r1} = 0.18$ Hz. In the present situation, $\omega_{c1} < 1/2 \omega_{r1}$ and the elastic reflector mode is in phase with the torsional mode of the short arm resulting in a coupled system with the reflector moving mostly as a rigid inertial mass. As ω_{c1} approaches ω_{r1} from below, the excitation energy is consumed by rigid body motions and strain energy followed by a decrease in relative amplitude of the ribs. For ω_{c1} slightly higher than ω_{r1} , the reflector resonance is crossed, followed by a change in phase between the short arm torsional vibrations and the elastic torsional mode of the reflector. Consequently destructive interference of rigid body rocking and elastic effects abates the response.

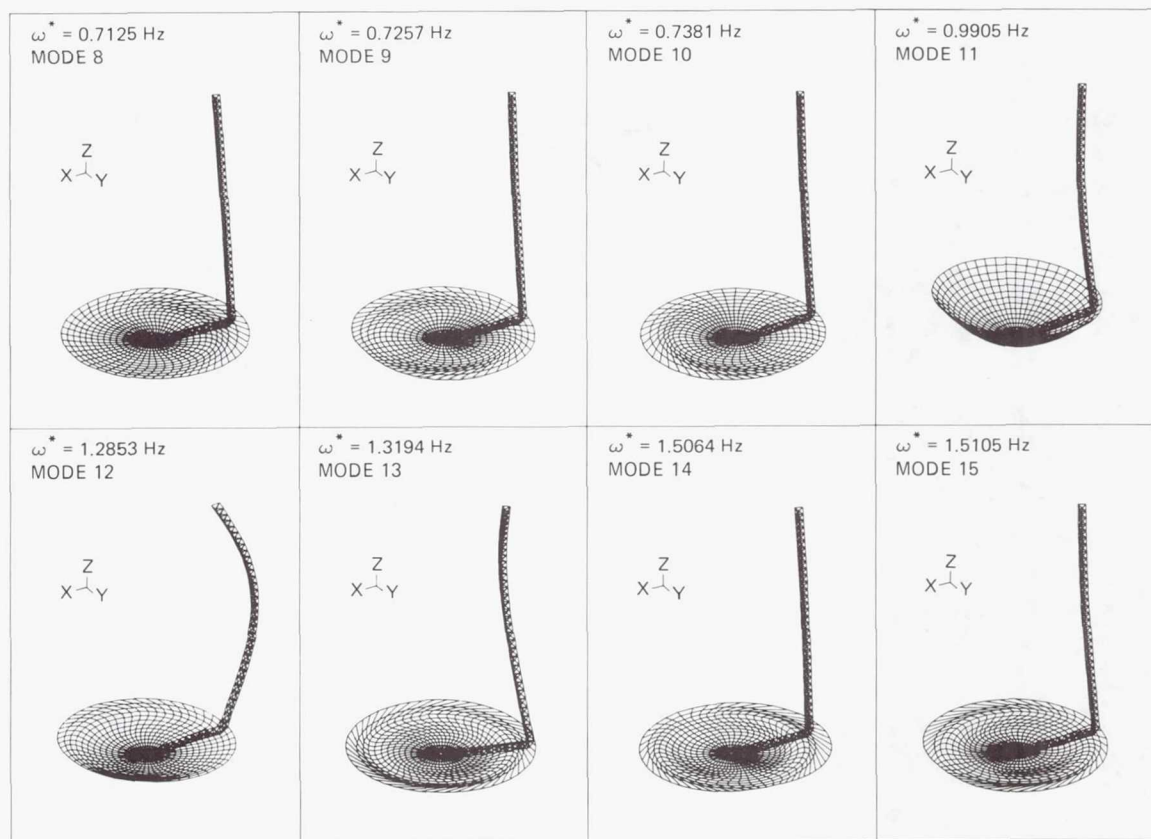


Figure 1. Combined free modes of LMSS configuration 4A (contd)

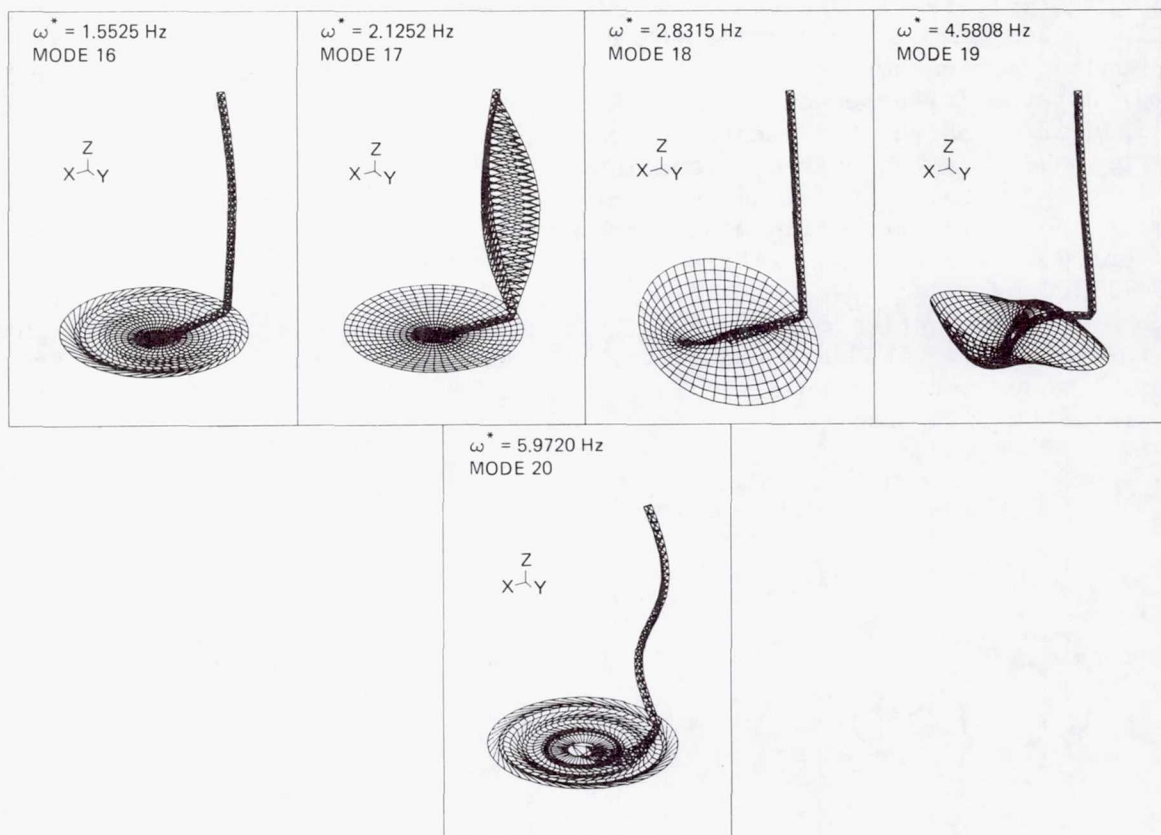


Figure 1. Combined free modes of LMSS configuration 4A (contd)

SPLINE FITTING OF RESPONSE MODES

Due to the discretized nature of the solution method, displacements and slopes are given at finite locations of the mesh surface. Since the objective of the study is to evaluate the deterioration of the radio frequency performance resulting from elastic distortions, a continuous mathematical definition of the deformed surface is necessary. An efficient numerical method is constructed for the spline interpolation on a two-dimensional non-rectangular domain with non-rectangular partitions representing the gore. The physical domain is mapped onto a rectangular domain, on which the spline interpolation is to be performed. A new boundary condition is derived for domains with mesh lines having at least four nodes, resulting in an almost tridiagonal linear system of equations for the spline coefficients. A numerical algorithm is developed for the solution of this system. Results are shown in Figures 2 and 3 when the method is applied to the interpolation of the normal displacement on a segment of the 55m wrap-rib reflector gore.

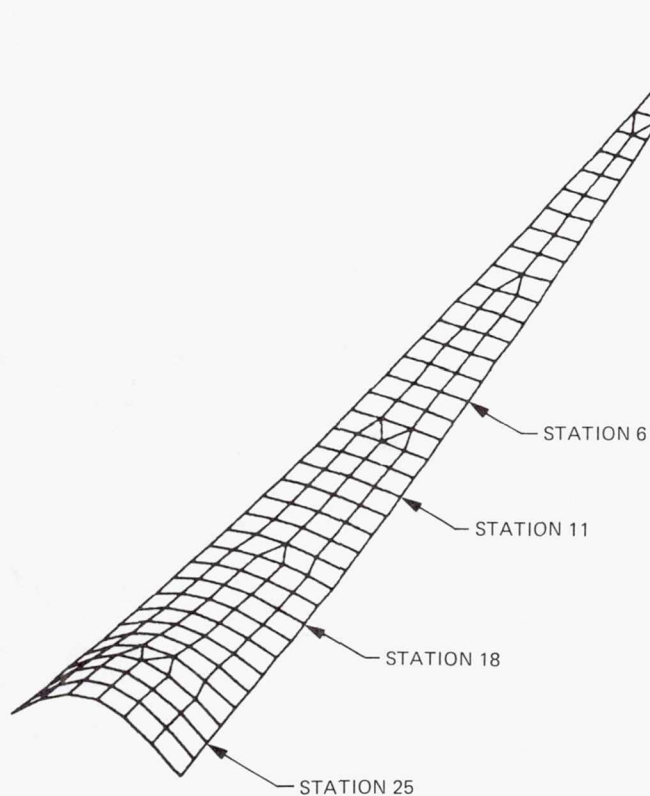


Figure 2a. Finite element model
of deformed 55m gore

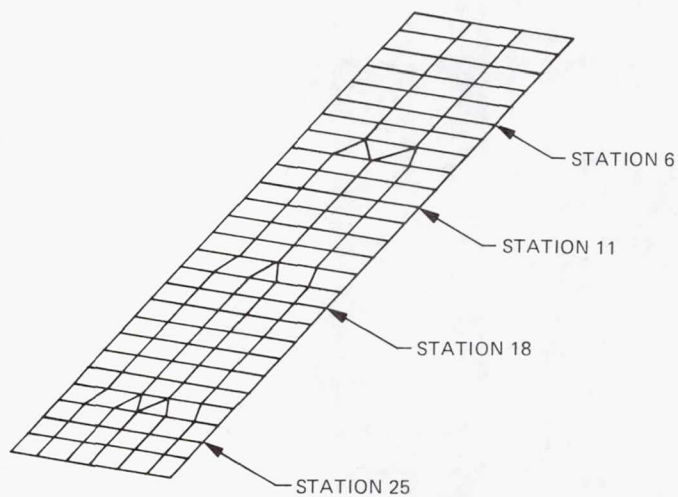


Figure 2b. Transformed plane

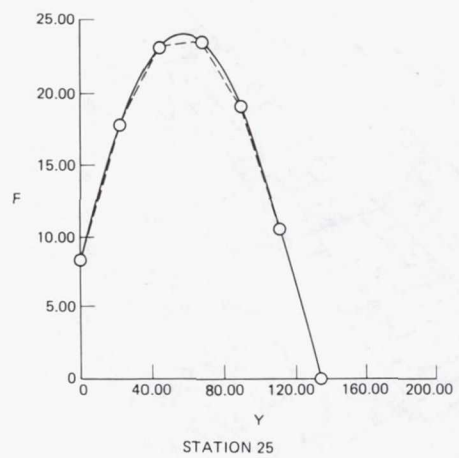
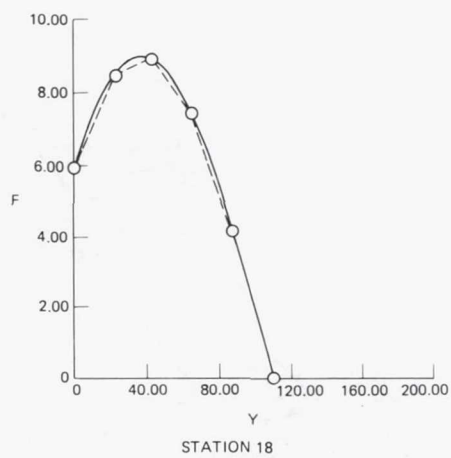
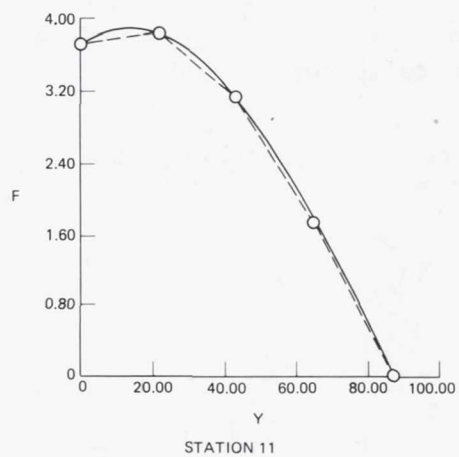
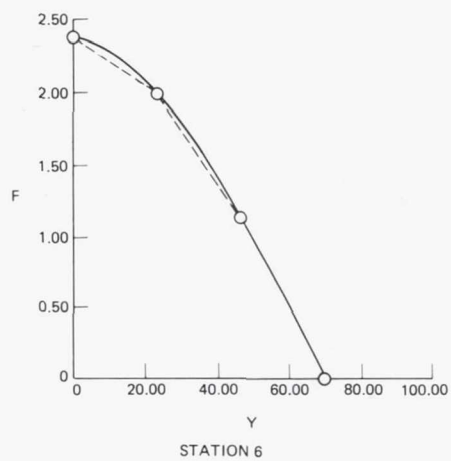


Figure 3. Comparison of spline interpolation — with finite element distribution —○—○—○

ANTENNA THERMAL DISTORTION ANALYSIS

Temperature distributions in the antenna structure are determined with the use of a finite difference numerical code. The model takes into consideration solar, albedo, and planet shine thermal loads on the structure throughout half the orbit. Thermal nodes are connected by conduction and radiation. Transient rib node temperatures so calculated are interpolated to match the nodal points on the finite element structural model, since the structural model has significantly more nodal resolution. The temperature distribution is essentially the forcing function for the structural model and results in thermal strain distributions, which produce the thermal distortions in the structural model.

Page intentionally left blank

SURFACE MEASUREMENT SYSTEM
DEVELOPMENT

Martin Berdahl
Jet Propulsion Laboratory
Pasadena, California

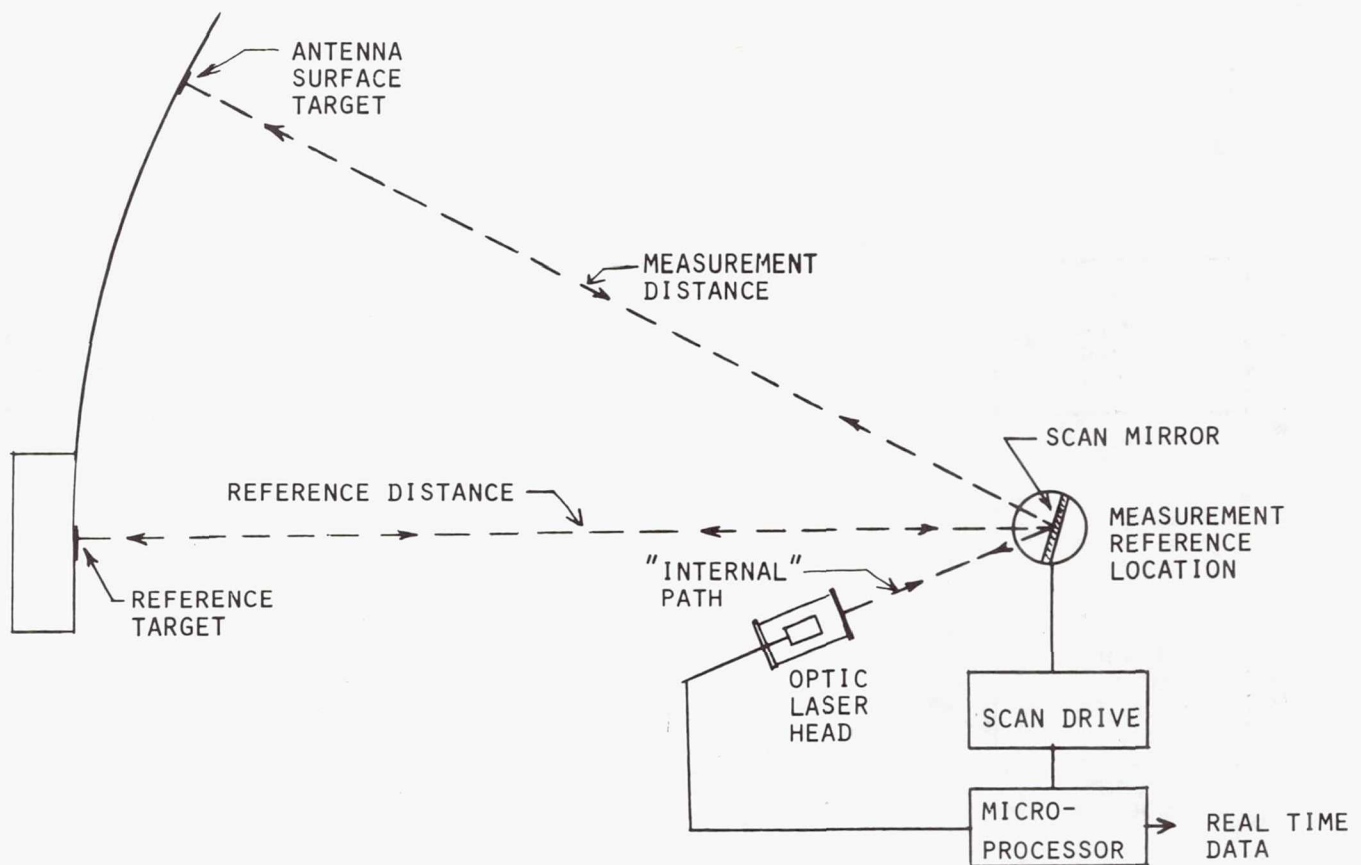
Large Space Systems Technology - 1981
Third Annual Technical Review
November 16-19, 1981

INTRODUCTION AND BACKGROUND

JPL recently made a study of several methods and systems for measurement of antenna surface curvature. The investigation covered the use of methods varying from comparatively simple to extremely complex, high resolution systems using phase comparison and optic interferometry. A system of intermediate complexity which is of suitable capability for measuring early deployed antennas was demonstrated by Lockheed Missiles and Space Corp. under Contract No. 955130 to JPL. Most of the systems investigated could not demonstrate the ability to unambiguously measure absolute distance to a target. Some systems used angular measurement techniques rather than distance measurement to determine surface distortion. Most of the promising systems are presently in the development stage. Some have the projected capability of satisfying the requirements of future conceptual designs. An optical system designed to satisfy the requirements of early deployable concepts such as the LMSC offset wrap rib antenna is under development at JPL. The system is relatively lightweight, will measure distance to several targets, and provide data in engineering units in real time. Accuracy of measurement is such that use of the system will permit evaluation of surface quality of large parabolic antenna dishes. Operation of the system has been conceptually proven and is now in the stage of hardware development.

BREADBOARD SYSTEM DESCRIPTION

A very short pulse of light energy is emitted from a laser transmitter and is directed toward a mirror called a scan mirror. The scan mirror position is programmed by a microprocessor to reflect the light pulse to one of several target retro reflectors located on the surface of the antenna to be measured. The retro reflector returns the light pulse to the scan mirror and back toward the transmitter. The returned pulse is collected by telescopic optics, detected by a solid state sensor, amplified, and caused to initiate another light pulse. Self-initiation of a light pulse in this manner results in a continuous string of pulses being sent to the target, each pulse being successively initiated by the return of the previous pulse. Since the travel time is determined by the speed of light a pulse repetition rate, or frequency, is established which is uniquely determined by the distance to the target. Dividing the speed of light by the frequency provides a distance which is equivalent to the total air path and electrical path traveled by the pulse on each round trip to the target. If the pulse is reflected directly back to the detector from the scan mirror, an "internal path" distance will be given. The "internal path" distance includes the effect of electronic time delays as well as the optical path time required for a pulse to make the round trip to the scan mirror. Subtracting this distance from the total round trip distance to a target provides the precise distance from the scan mirror to the target.



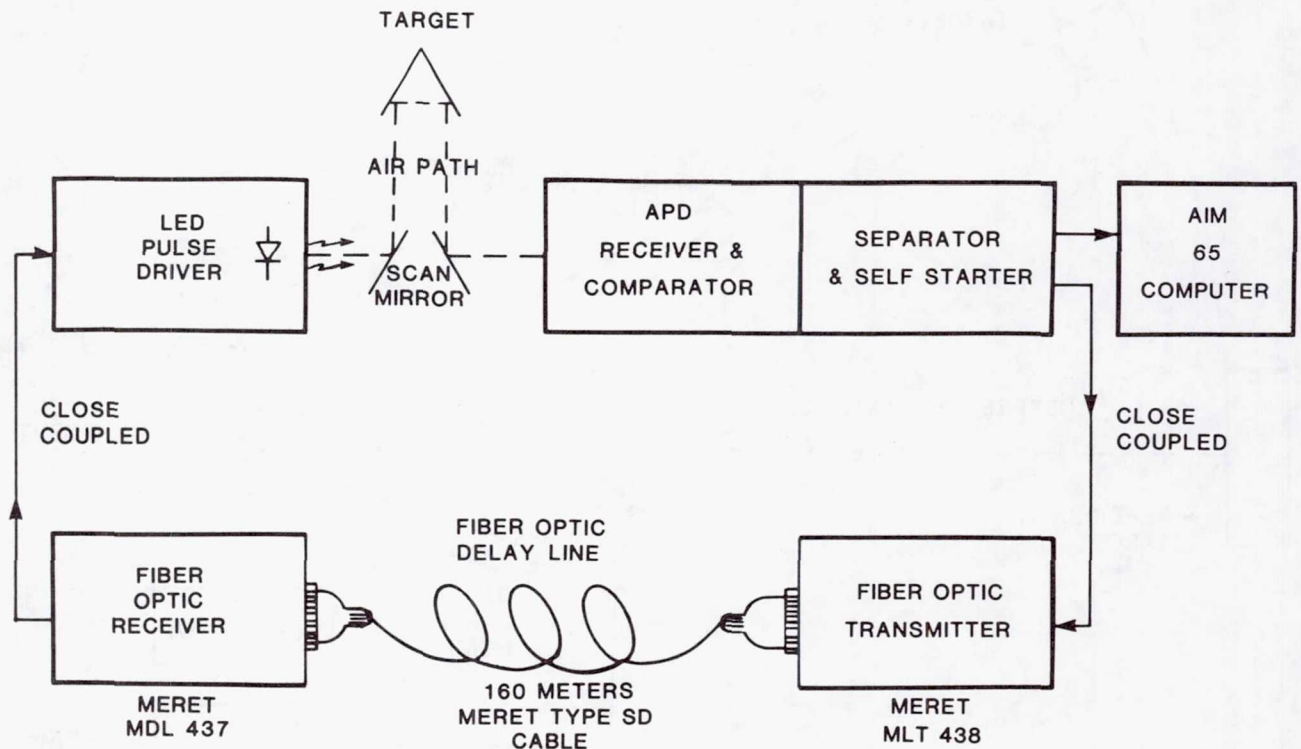
JPL SELF-PULSED LASER RANGING SYSTEM

BREADBOARD SYSTEM OPERATION

An automatic start signal is transmitted to the fiber optic delay line until a target is acquired. Acquisition of a target causes self-pulsed operation and inhibits the self-start signal. Output of the delay line is sent directly to the LED driver amplifier in the optic head. Here it initiates a new pulse from the LED.

After being received and detected the signal is again sent to the fiber optic delay line. At the same time it is sent to the microprocessor which is a Rockwell AIM65. Here the frequency is processed into distance and printed out directly in meters. The microprocessor has been altered and programmed only for signal processing at this time. It is capable of eventually being programmed to scan a set of targets and transmit the resulting data for analysis of antenna figure. With the exception of programming and controlling the scan mirror the entire system is operative. Once the scan mirror has been adjusted to acquire a target, pressing a button on the microprocessor keyboard will initiate the sampling, computing, and readout of the target distance.

SYSTEM BLOCK DIAGRAM



BREADBOARD SYSTEM PERFORMANCE

An optical bench setup was made in which the actual air path from the optic head to targets ranged from approximately three to seven meters. Since the scan mirror was placed at three meters from the optic head the computed target distances ranged from one to four meters. Several scans of the four in line targets were made returning to the zero range (scan mirror reflecting transmitted signal back to the optic head) between each scan. A single one inch retro reflector was placed at twenty meters from the scan mirror for a range test. The following performance characteristics were derived:

BREADBOARD SYSTEM PERFORMANCE

ERROR IN ABSOLUTE MEASUREMENT	~ 2 CM
PRECISION (REPEATABILITY)	~ 3 MM
RESOLUTION (DIGITAL LIMIT 0.1 MM)	~ 0.5 MM
DRIFT RATE	~ 1 MM/MINUTE
AIR PATH RANGE LIMIT (1" RETRO)	30 METERS
MEASURING TIME	0.5 SECONDS
CALCULATION AND PRINT TIME	2 SECONDS
TARGET SCAN TIME	NOT DETERMINED

FY'81 OBJECTIVES

Test results of the FY'80 Self-Pulsed Ranging System indicated several areas where improvement could be made. The system's air path range capability was on the order of thirty meters instead of the two hundred meters required by the contemplated antenna which the system was intended to measure. The precision was on the order of three millimeters, the absolute distance measurement accuracy on the order of two centimeters and the drift rate on the order of one millimeter per minute. In order to meet the requirements of a useable measuring system the following set of objectives was established for the FY'81 measuring system:

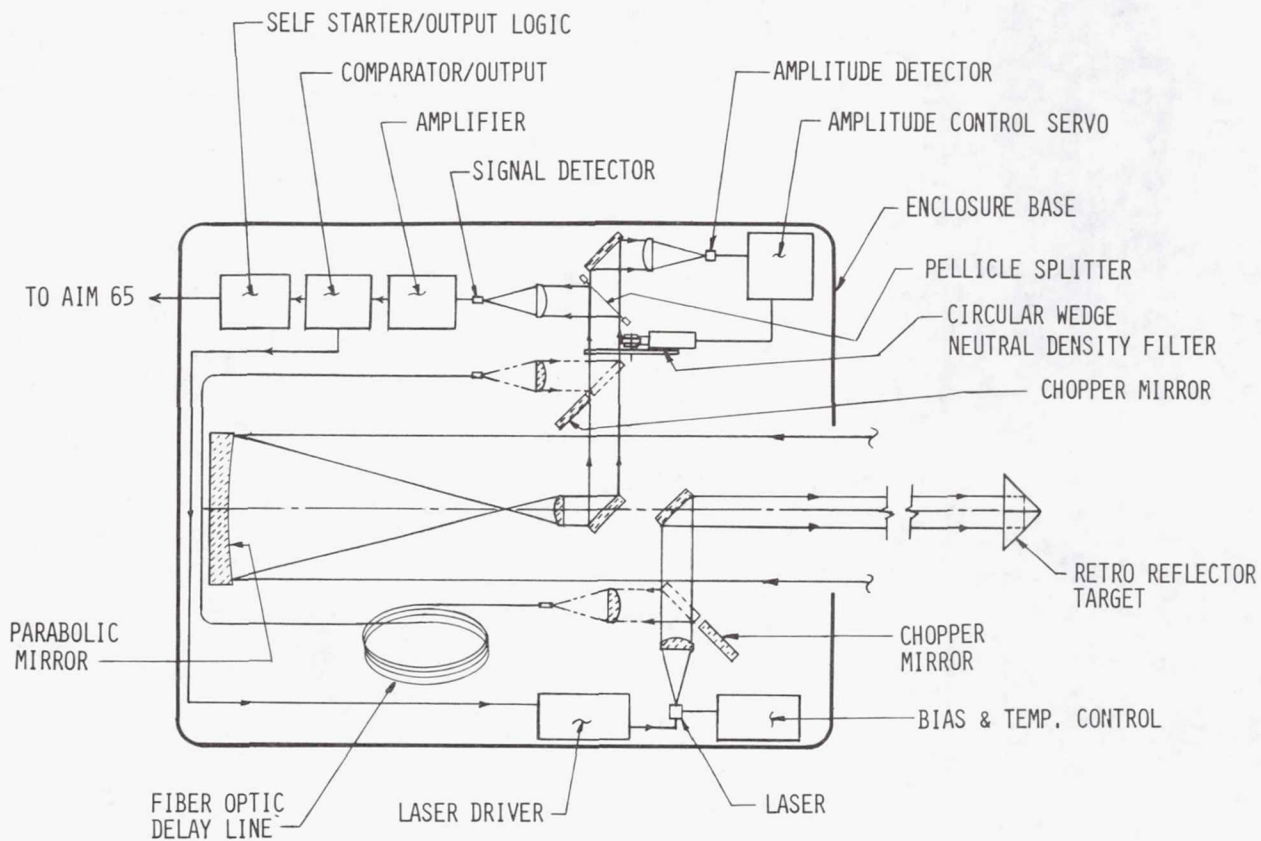
- IMPROVE RESOLUTION TO 0.1 MM
- IMPROVE PRECISION TO 0.5 MM
- REDUCE EFFECTIVE DRIFT RATE TO ZERO
- INCREASE RANGE CAPABILITY TO >200 METERS
- APPROACH AND ENGINEERING MODEL DESIGN
- TEST AND EVALUATE SYSTEM PERFORMANCE

APPROACH

The approach taken for making the necessary improvements included changes in several parts of the system and a basic change of using a fixed, passive, fiber optic internal reference path to which each target distance is compared while scanning to the next target. This short time (less than two seconds) for comparison to a reference distance should suffice to reduce the effect of any drift to less than one tenth millimeter.

A new layout in the form of an engineering model was necessary to accomplish the optical chopping to an internal reference. The need for additional range capability as well as a faster rise rate pulse dictated the use of a laser diode transmitter rather than the light emitting diode (LED) previously used. At least a ten to one improvement in rise time is to be expected from the LED to laser change. The laser beam also has the advantage of better optical collimation as well as power and therefore is expected to increase range capability. Receiving optics were changed to incorporate a large (six inch diameter) collecting mirror and a fast detector and amplifier for compatibility with the fast rise pulse. The laser diode was built into a special cooled and temperature controlled mount and supplied with constant controlled bias power to minimize drift. The signals to the receiver are to be monitored and optically servo controlled so that their rise signature is preserved and all signals are at the same peak amplitude.

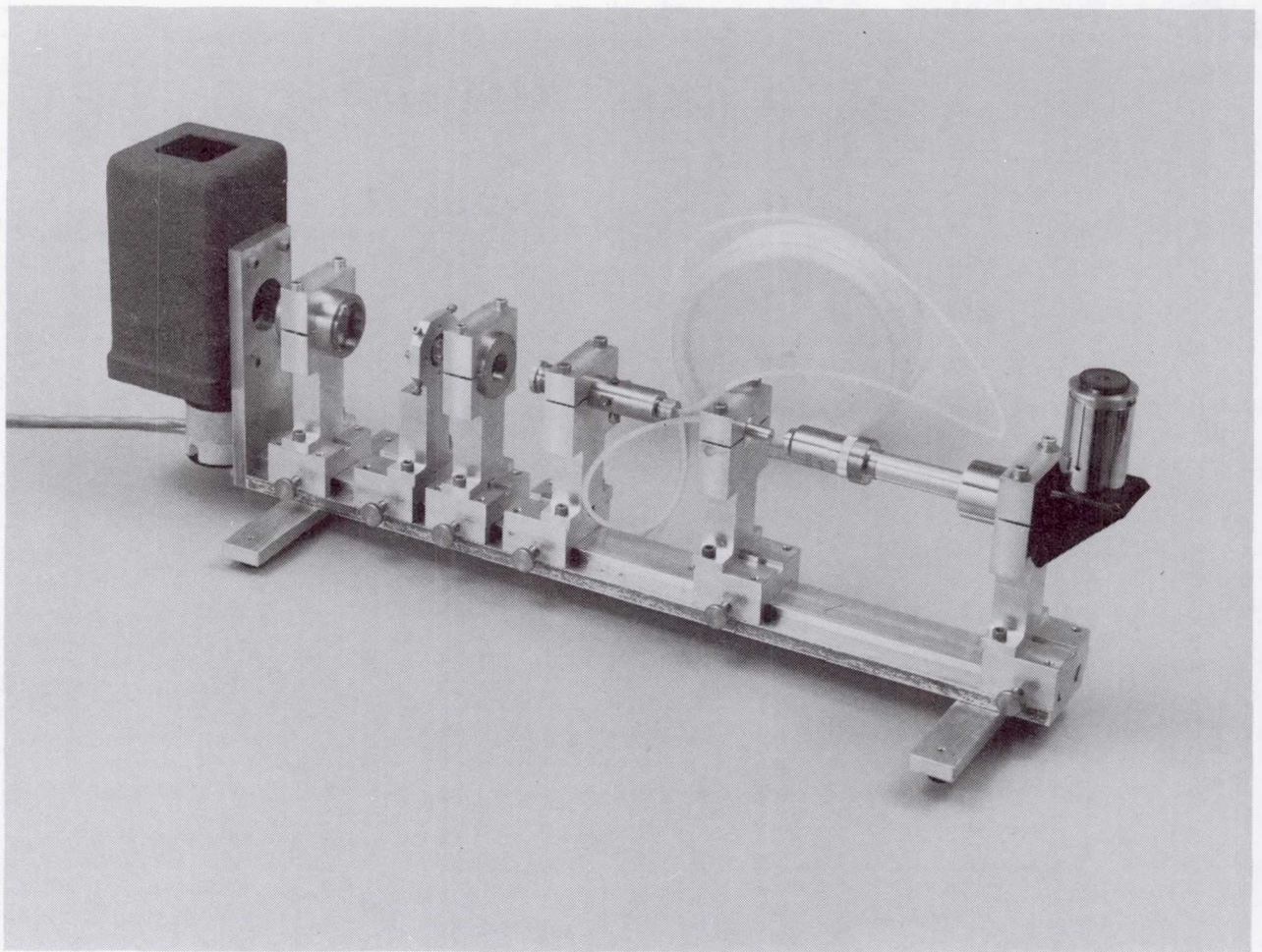
MODIFIED OPTIC HEAD LAYOUT



FY'81 HARDWARE DEVELOPMENT IMPROVED OPTIC COMPONENTS

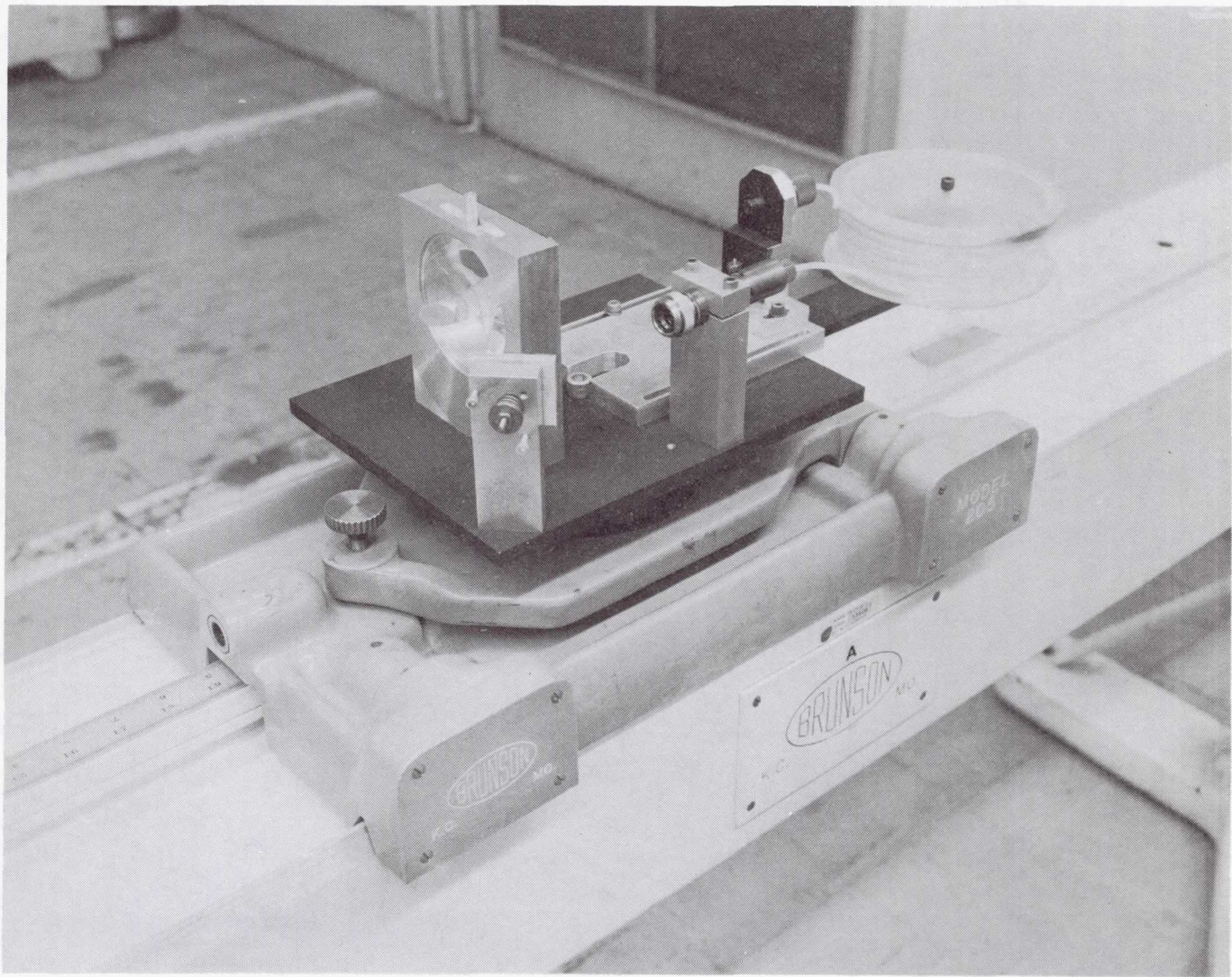
Special care has been taken with optic components to minimize signal losses. The signal transmitted by the laser to the target has been collimated by the use of an optimized lens. The number of optic components in the path to the target and return to the sensor has been minimized. Special lenses were designed and fabricated to focus as much as possible of the energy from the switched laser beam into an optical fiber for the internal reference path. Special three-axis micropositioners were designed and fabricated to assure accurate beam to fiber alignment.

Shown below is a precision optic bench which was fabricated for use in testing coupling efficiency of an optic beam into a fiber. The light source is a bright ribbon filament lamp which was focussed on to a 0.002 inch diameter (50 micrometers) pin hole to establish a source size. The source is subsequently collimated at approximately twelve millimeters diameter and refocussed on to the end of a fiber whose central core is also fifty micrometers in diameter. Prior to running the beam through the fiber, the image size and intensity are observed and later compared with the emerging beam. With the use of the bench, single element optimized lenses with two different curvature radii were satisfactorily tested. Another use of the same lens is in the two hundred meter simulated range.



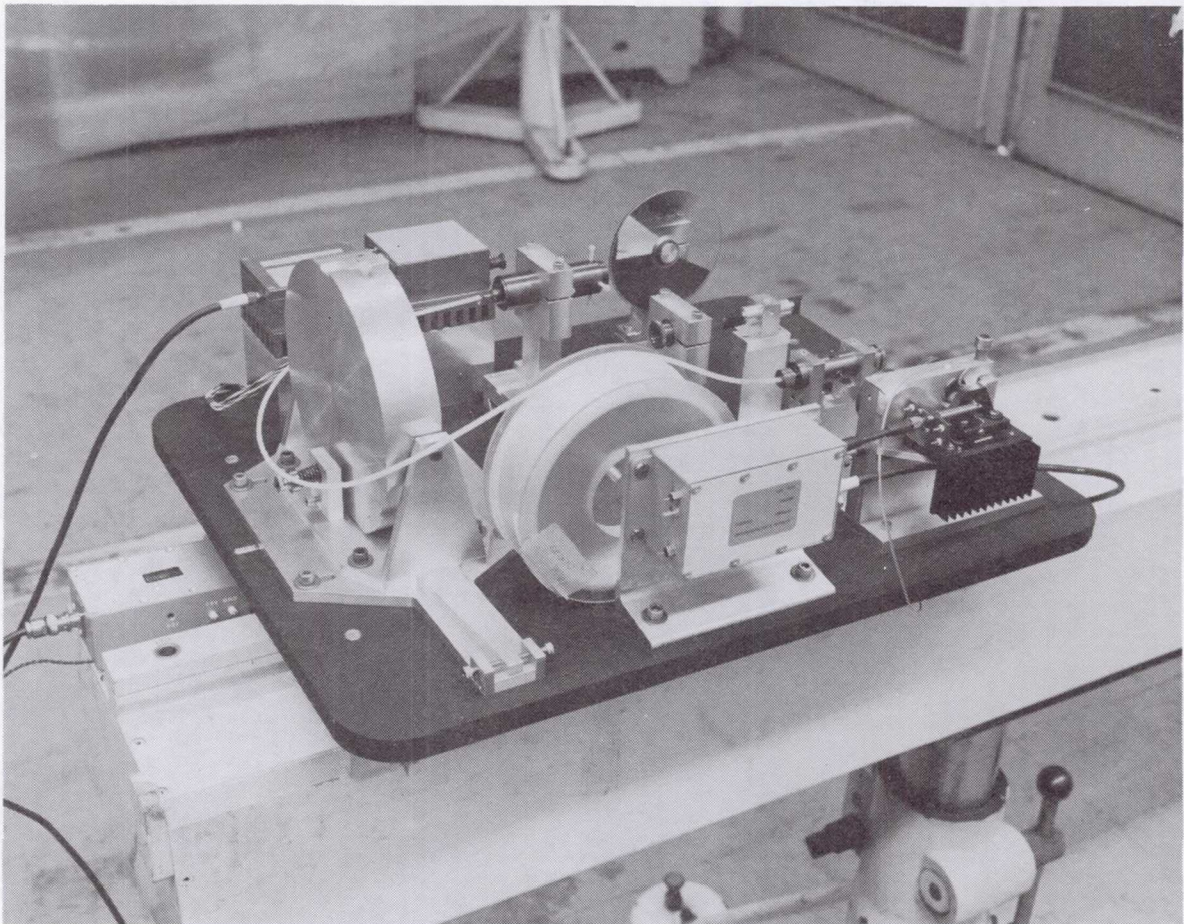
200 METER RANGE SIMULATOR

The same optical test equipment served to make possible the construction of a synthetic two hundred meter range. This is a device which receives the twelve millimeter collimated beam from the laser transmitter at a short distance from the optic head and focusses it into an equivalent four hundred meter length of optical fiber. After passing through the optic fiber the emerging diverging beam is collected by a three inch collimating lens and returned to the optic head some twelve hundred nanoseconds later. This device is used on the same bench as the optic head and allows the equivalent of testing at a range of two hundred meters with a measureable target motion resolution of one tenth of one millimeter. Both the signal attenuation and the size of the return beam are nearly equivalent to that of a signal from a target at the full range. The simulated range device has been used and tested with the FY'80 optic head.



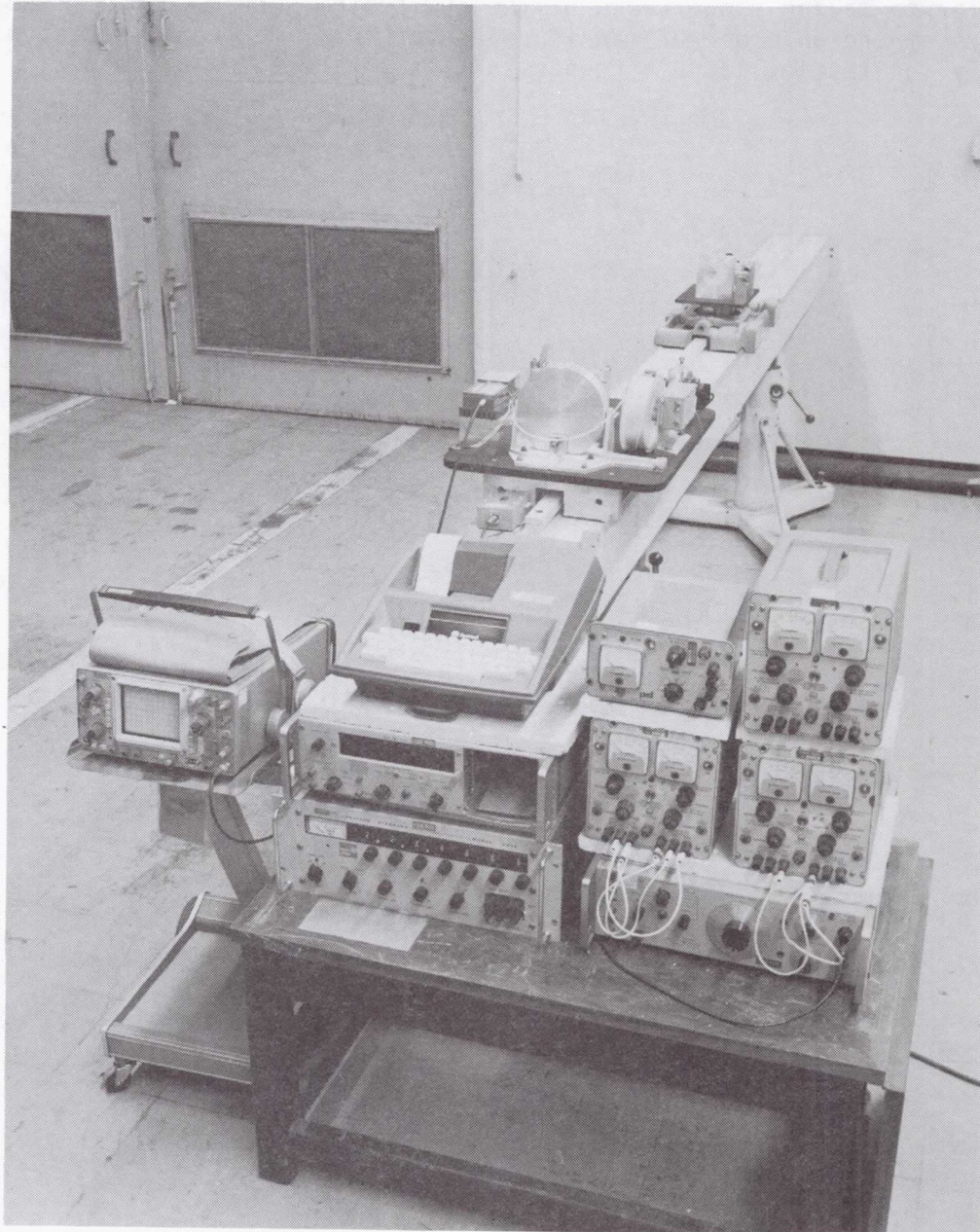
FY'81 DESIGNED OPTIC HEAD

The optic head, the principal unit of the system, is shown in a partial state of completion. It is larger than a flight unit; however, it will contain all of the unit components to be included in the final design. At the left center of the unit is a six inch diameter parabolic mirror used for receiving the return signal. At the lower center is the laser pulse driver coupled to the laser transmitter. The transmitter is Peltier cooled. After leaving the laser diode, the optic beam is collimated to twelve millimeters diameter and transmitted in the direction of a target by a small diagonal mirror. This beam may be intercepted prior to being sent down range by a chopper mirror (not shown) and directed into the four hundred meter reference optic fiber shown on the spool. After passing through the fiber the reference signal is again directed to the receiver after passing through another chopper mirror (also not shown). All return signals pass through a variable density filter, at upper right, which is servo driven by a portion of the received signal to provide constant signal signature and amplitude at the receiver shown at the upper left. The receiver is a fast avalanche photodiode with a two hundred picosecond rise time to match the laser pulse. After detection, the signal is returned to the laser driver to initiate another pulse. The comparator detector unit is a state-of-the-art solid state electronic package which is yet in fabrication. The signal received from a target is focussed by the six inch mirror, recollimated and directed to the receiver. The external signal is chopped out of the path during internal path measurement.



FY'81 SYSTEM TEST SETUP

Shown in the foreground is the AIM65 microprocessor computer which controls operation of the optic head, calculates target range and provides data in real time on printed paper tape. Surrounding the AIM65 are various temporary power supplies and diagnostic equipment not associated with a deployable system. On the optic bench and directly behind the AIM65 is the FY'81 revised optic head. When completed it will transmit a pulsed laser beam along the bench to the simulated range device. Measurements of one tenth millimeter resolution at the equivalent distance of two hundred meters may be made within the approximate three meter length of the bench.



SUMMARY

During FY'81, a new physical design of the optic head was undertaken in order to improve the performance of the previously designed unit. The improvements included freedom from drift, greater resolution, extended range capability and higher precision. An attempt was also made to design toward an engineering model including state-of-the-art components and a configuration which might conceivably be used in a flight model. All of the necessary purchases were made, the new design was successfully completed and several of the components, fabricated, tested and assembled. Optimized lenses were designed and tested and a two hundred meter simulated range was completed. Several components remain to be fabricated and assembled prior to making range tests of the new system. Predictions of performance of the new system are an order of magnitude better than the previous system and should qualify for testing large antennas such as the Lockheed wrapped rib and other structures.

FY'81 ACCOMPLISHMENTS

- ④ ENGINEERING MODEL DESIGN COMPLETED
- ④ OPTIMIZED LENSES FABRICATED AND TESTED
- ④ 200 METER SIMULATED RANGE COMPLETED
- ④ ENGINEERING MODEL FIFTY PERCENT COMPLETE

SUMMARY OF ANTENNA TECHNOLOGY DEVELOPMENT
AT THE LANGLEY RESEARCH CENTER

Thomas G. Campbell
NASA Langley Research Center
Hampton, Virginia

Large Space Systems Technology - 1981
Third Annual Technical Review
November 16-19, 1981

FOREWORD

The purpose of this presentation (fig. 1) is to describe antenna-technology-development work conducted through FY-81 as funded through the LSST Program. As a point of introduction, it must be stated that the following papers presented in this compilation were directed from the LSST efforts at LaRC toward antenna development:

Bailey, M. C.: Distorted Reflector Antenna Performance Prediction Technique . . .	605
Blume, Hans-Juergen C.: Measurement of Losses of Mesh Membrane Material for Reflector Applications With an S-Band Radiometer	611
Croswell, W. F.: The Suitability of Mesh Membrane Material for Radiometer Reflector Applications	621
Farrell, C. E.; and Strange, D. A.: Preliminary Analytical Results Using Surface Current Integration for Predicting Effects of Surface Pillows on RF Performance	583
Lang, G. J.: Near-Field Testing of LaRC Multiple-Beam Antenna	657

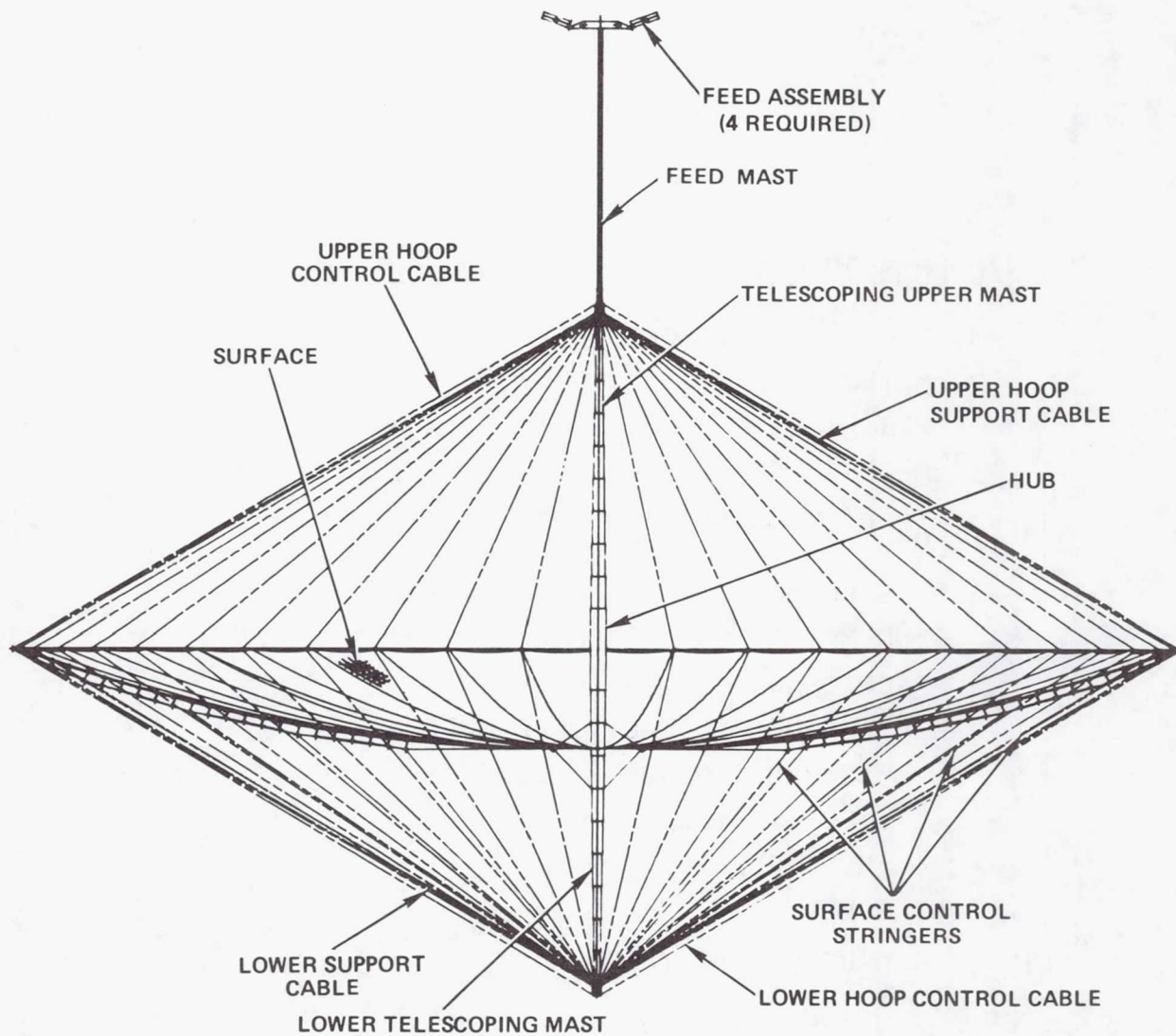
ANTENNA DEVELOPMENT OBJECTIVE: TO DEVELOP THE TECHNOLOGY
NEEDED TO EVALUATE, DESIGN, FABRICATE, PACKAGE, TRANSPORT,
AND DEPLOY COST-EFFECTIVE, STS-COMPATIBLE ANTENNA SYSTEMS
(UP TO 300 METERS IN DIAMETER) FOR POTENTIAL APPLICATIONS.

- COMMUNICATIONS
- RADIOMETRY/EARTH RESOURCES
- RADIO ASTRONOMY

Figure 1

MAYPOLE (HOOP/COLUMN) 100-METER POINT DESIGN

The thrust of the LSST antenna development work has been focused on the development of a multiple aperture, maypole, Hoop/Column antenna concept. This concept is shown in figure 2.



MAYPOLE (HOOP/COLUMN) 100-METER POINT DESIGN.

Figure 2

LARC HOOP/COLUMN PROGRAM ELEMENTS

The elements of the LSST Hoop/Column Program are shown in figure 3, and each element will be discussed in detail by subsequent speakers.

A brief overview of several program elements will now be presented.

HOOP/COLUMN ANTENNA CONCEPT DEVELOPMENT

- MESH MANAGEMENT MODEL

- 50-METER MODEL

- RF VERIFICATION MODELS

- 15-METER MODEL

ANALYTICAL PERFORMANCE PREDICTIONS

- FINITE ELEMENT STRUCTURAL DYNAMIC
(100-METER, 64M, 122M DIAMETER)

- SURFACE CHARACTERIZATION

- RADIO FREQUENCY ANALYTICAL MODELS

 - SURFACE GEOMETRY EFFECTS

 - SCATTERING EFFECTS

 - MULTIPLE APERTURES

- COST MODEL

MATERIALS DEVELOPMENT (CABLES)

ANTENNA REQUIREMENTS (ARD)

EVALUATION OF FACILITIES FOR LARGE-SCALE TESTING

DEVELOPMENT OF SURFACE ACCURACY MEASUREMENT SYSTEM

Figure 3

MESH MANAGEMENT DEVELOPMENT MODEL

Shown in figure 4 is a 1/20-scale model of a mesh management model that was tested at LaRC in FY-81. The results of these tests indicated that mesh stowage can indeed be accomplished within the volume constraints imposed. Restow operations using the restow cable and skewer design appear to be acceptable.

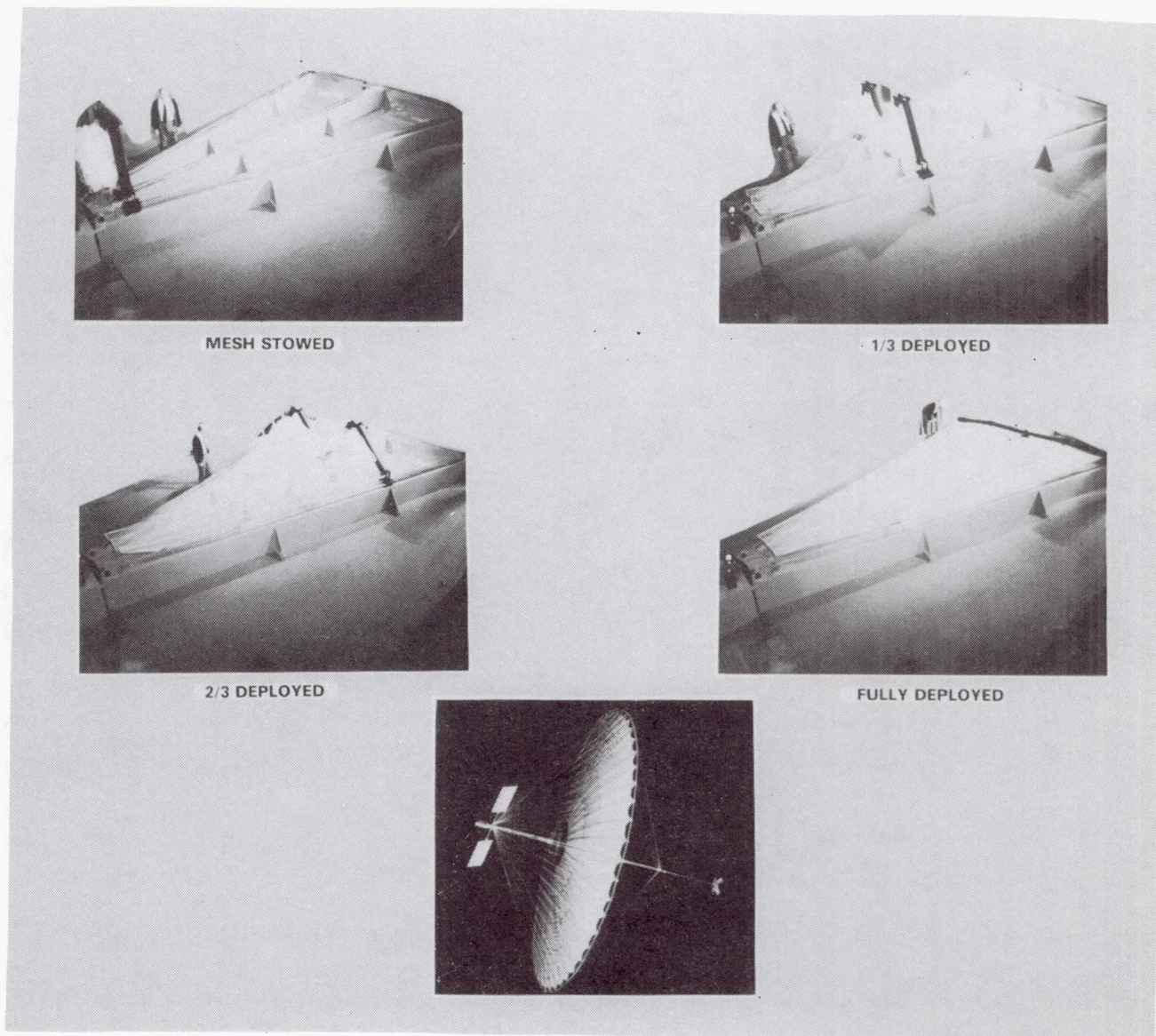


Figure 4

50-METER REFLECTOR MODEL

A significant hardware development presently underway is the 50-meter reflector model (see figure 5) at the Harris Corporation. This surface breadboard model is nearing completion, and testing should begin in early 1982. This model will be used in verifying the analytical surface model as well as establishing the effect of manufacturing tolerances on the resulting surface tolerance. This model will also be used in testing the (LED) Surface Accuracy Measurement System in March 1982.

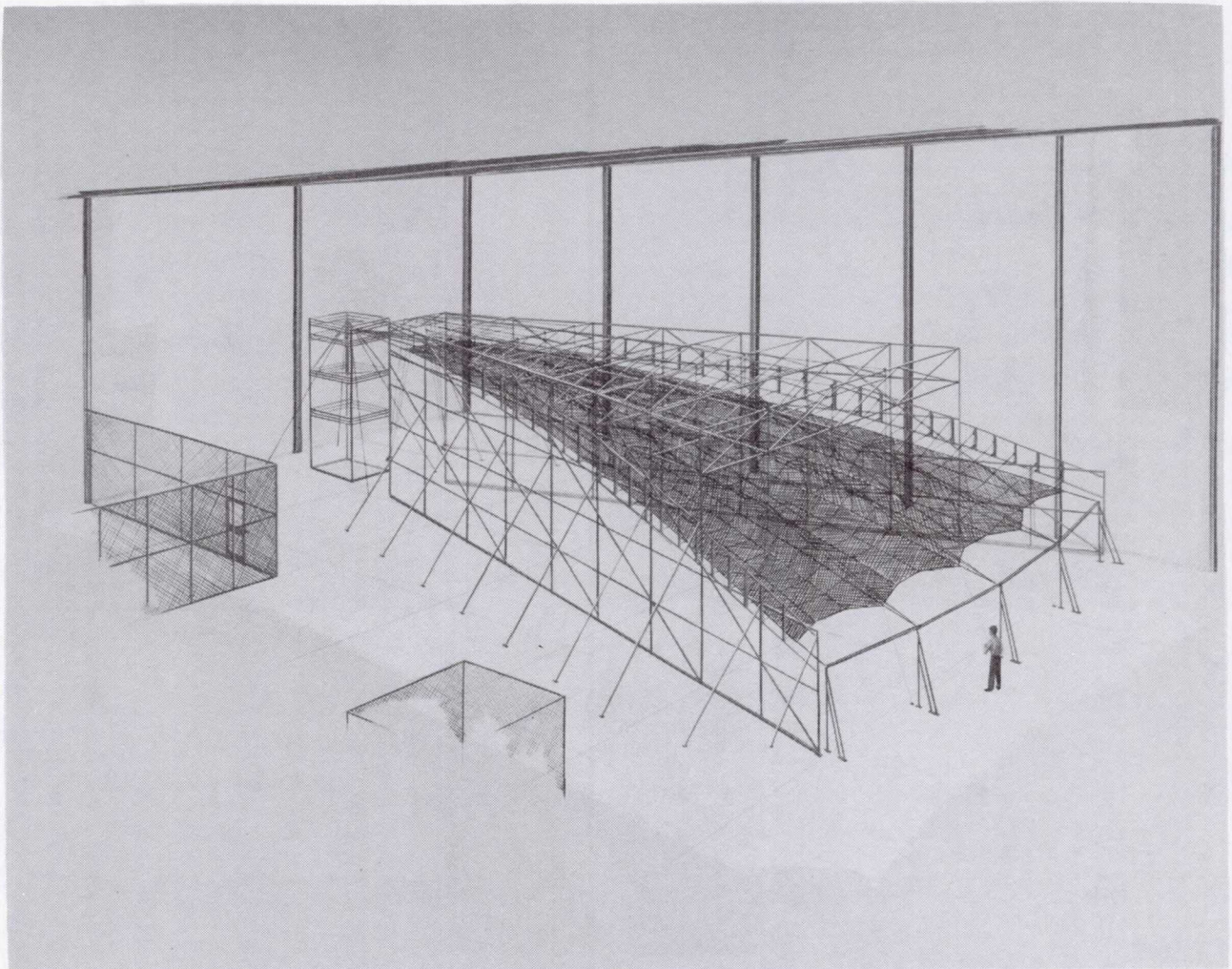


Figure 5

15-METER MODEL

Shown in figure 6 is an artist's conception of the 15-meter model that is planned for FY-84. This will be a kinematic model as well as a surface characterization model. The mesh surface will be suitable for Ku-band operation.

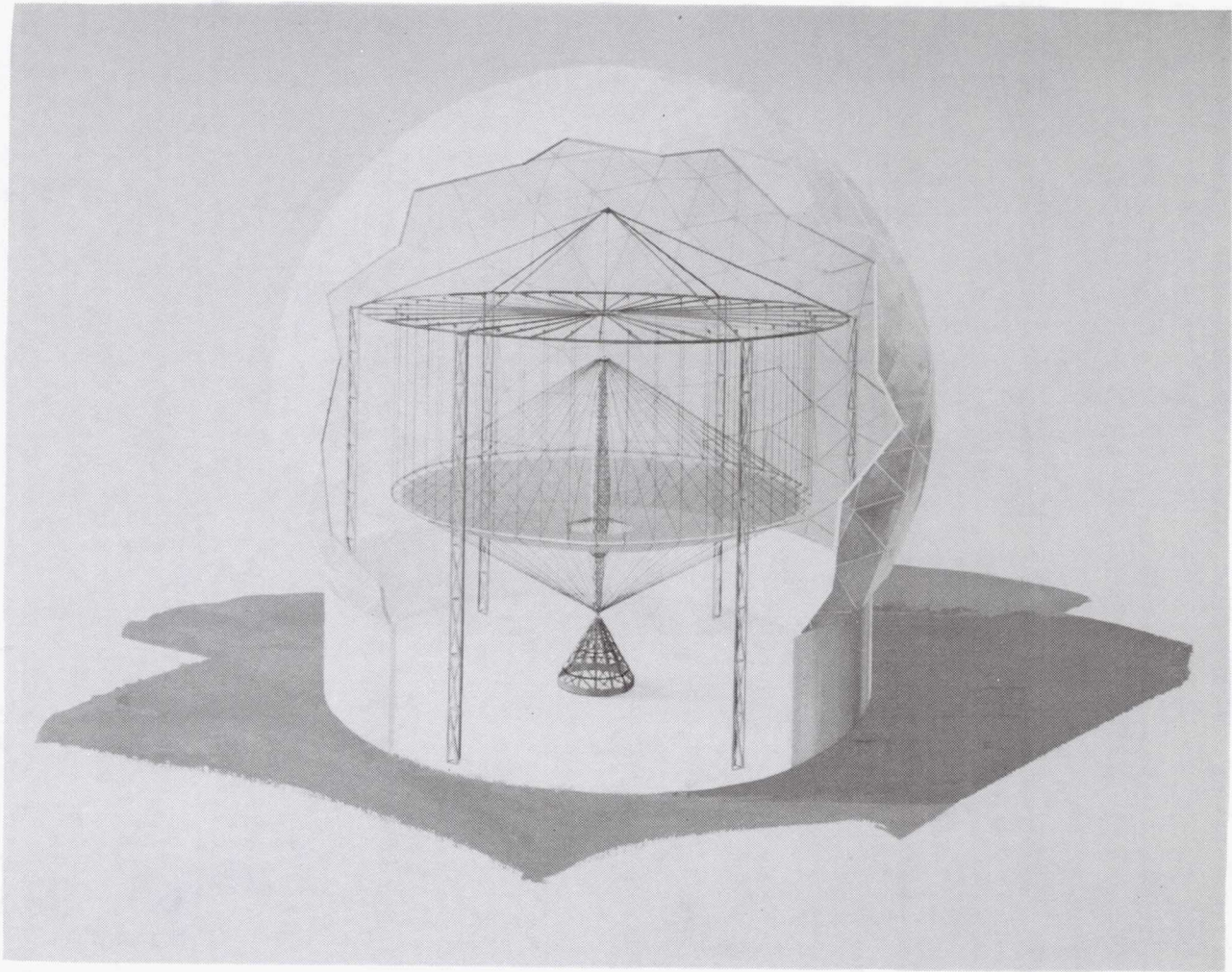


Figure 6

RADIO-FREQUENCY (R.F.) PERFORMANCE EVALUATION
(SIMULATED SURFACE AND CABLE EFFECTS)

In addition to the large-scale hardware models at the Harris Corporation, there has been the fabrication and testing of subscale radio-frequency models for assessing the RF performance of antennas such as the Hoop/Column. (See figure 7) The purpose of these models is to simulate the surface pillows and hoop-control cables in a precise nature so that radiation-pattern effects can be determined. The results of these tests shall be presented in subsequent papers describing the 35 GHz RF tests. These models were machined from solid-aluminum sections by using the equation for the offset, multiple-aperture geometry.

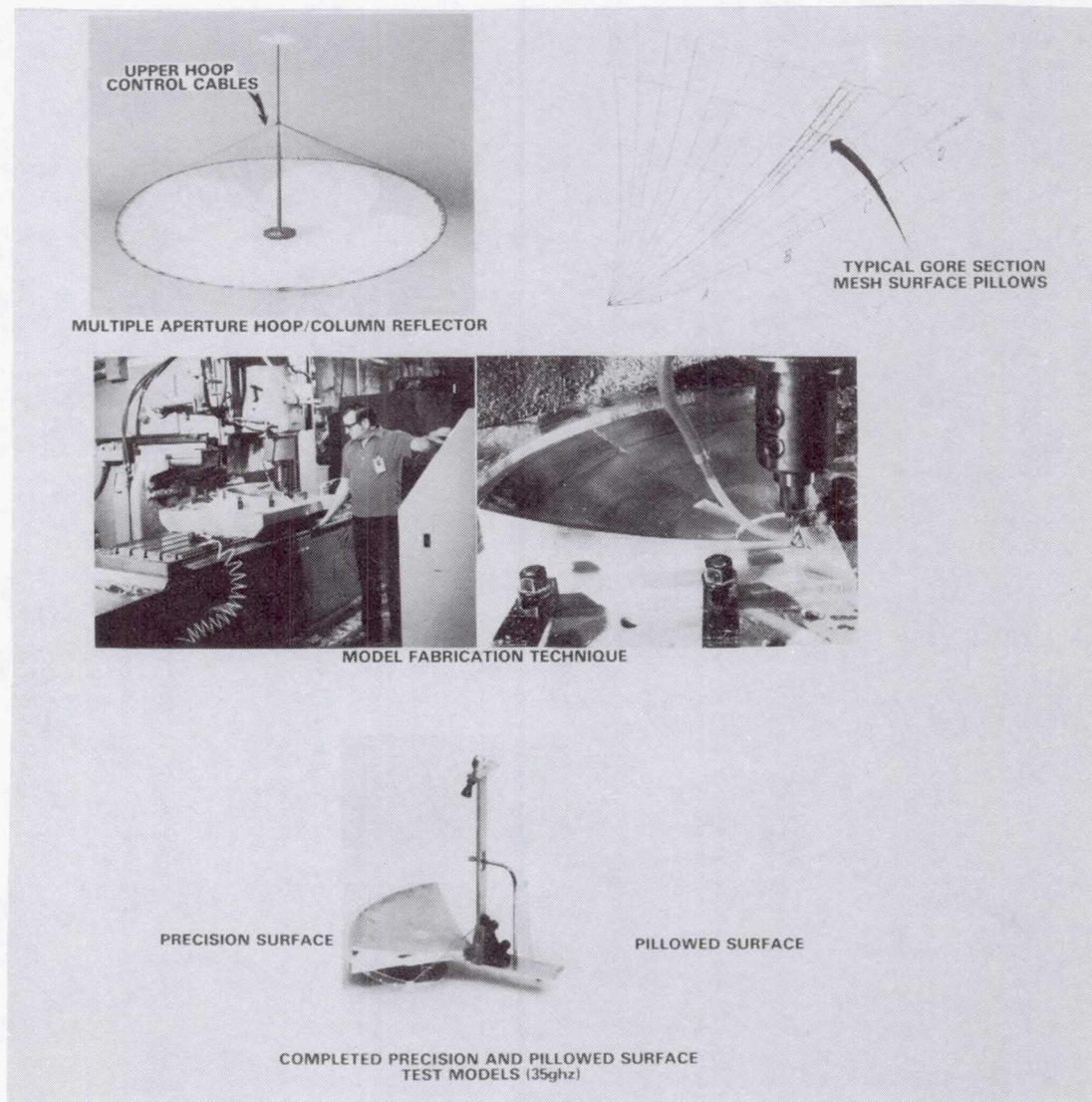


Figure 7

EVALUATION OF NEAR-FIELD MEASUREMENT TECHNIQUE FOR LARGE-APERTURE, MULTIPLE-BEAM ANTENNAS

In an effort to identify possible test facilities for future large-aperture antenna tests, the question of RF testing has been of concern. The utilization of a near-field facility has been discussed, but whether such a facility can, indeed, accommodate a large aperture is unresolved. Therefore, in an effort of assuming the capability of a candidate near-field facility (Martin Marietta), a test using a precision multiple-beam antenna was conducted. (See figure 8) The test results indicated that near-field testing is, indeed, a possible method of testing (for apertures up to 15 meters) for intermediate-scale testing.

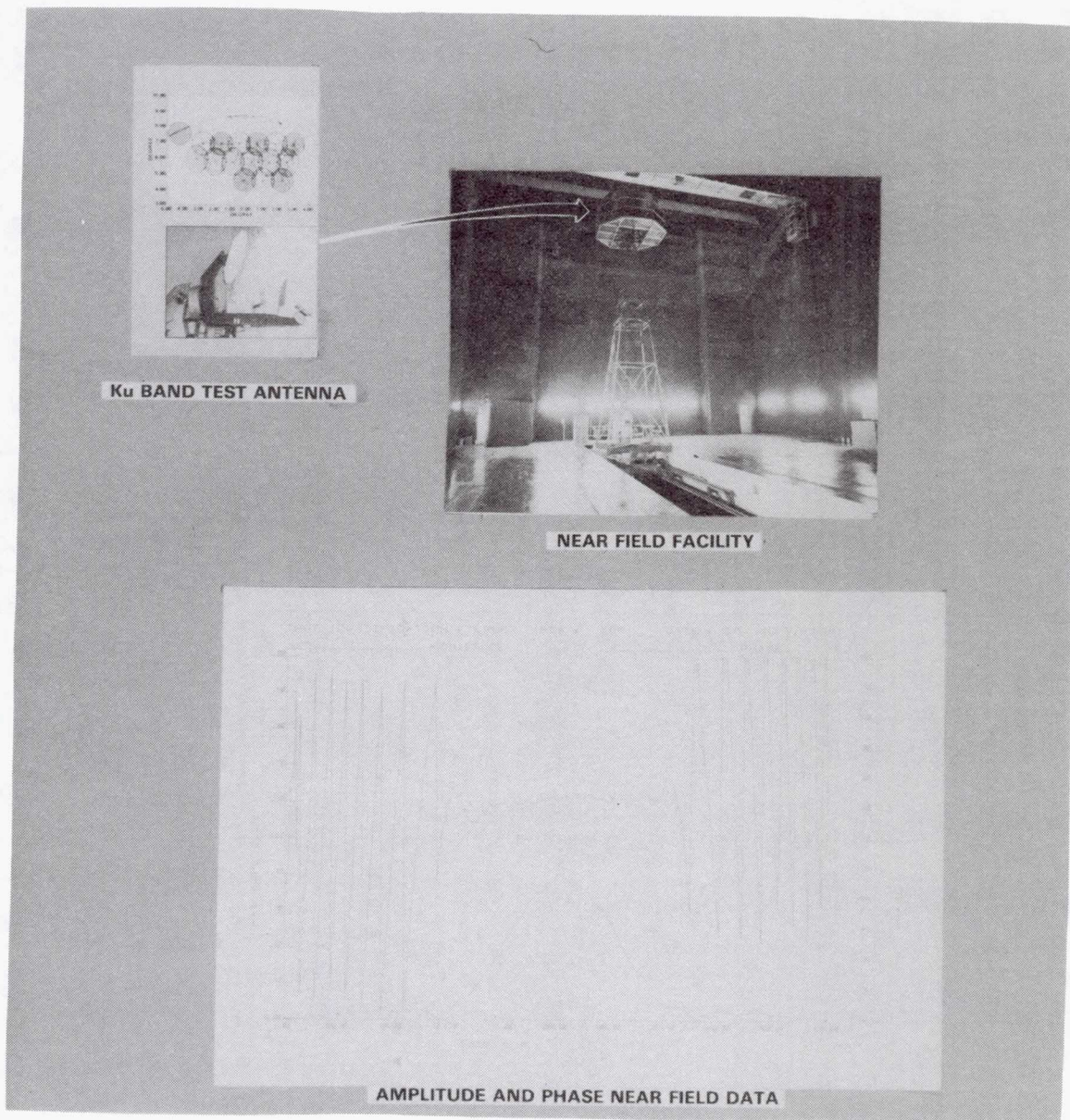


Figure 8

SURFACE-ACCURACY MEASUREMENT-SYSTEM DEVELOPMENT

Another element of the LaRC antenna development program is the development of a surface-accuracy measurement system using the infrared emitting diode concept. Figure 9 shows portions of the system and test configuration. This system will be used in tests at Harris using the 50-meter model.

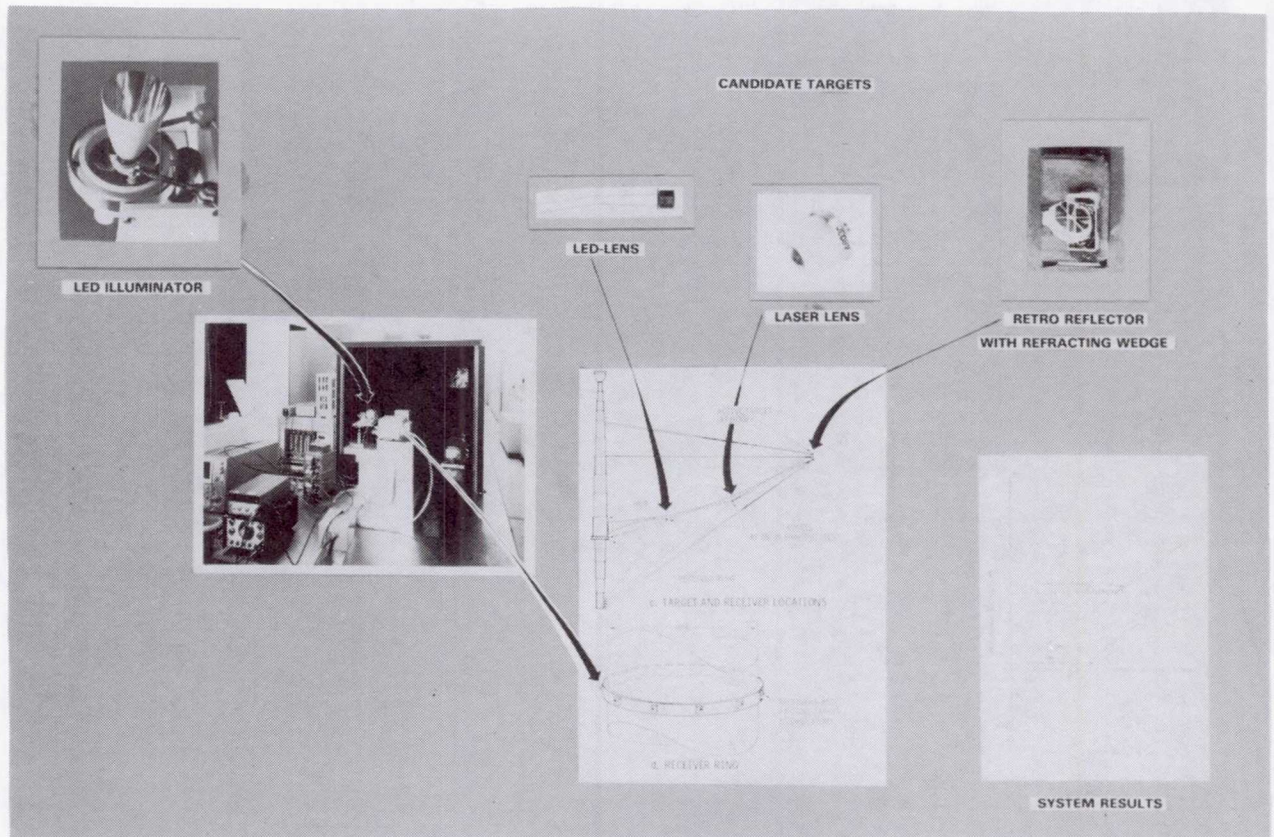


Figure 9

HOOP/COLUMN ANTENNA DEVELOPMENT PROGRAM

Due to the funding constraints imposed, the Hoop/Column development program has been extended through FY-84 after the completion of abbreviated testing of the 15-meter model. The present development plan is shown in figure 10.

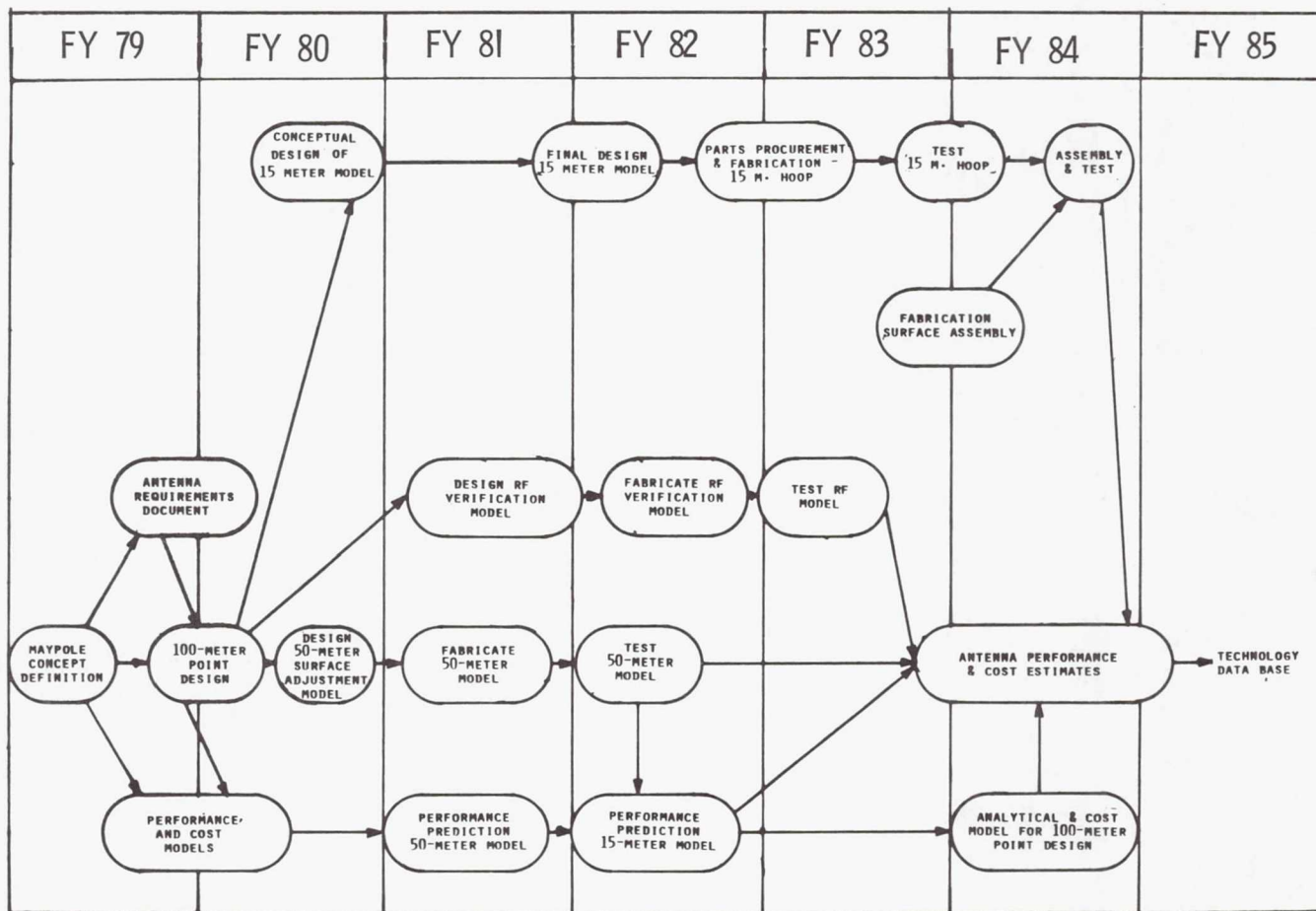


Figure 10

Page intentionally left blank

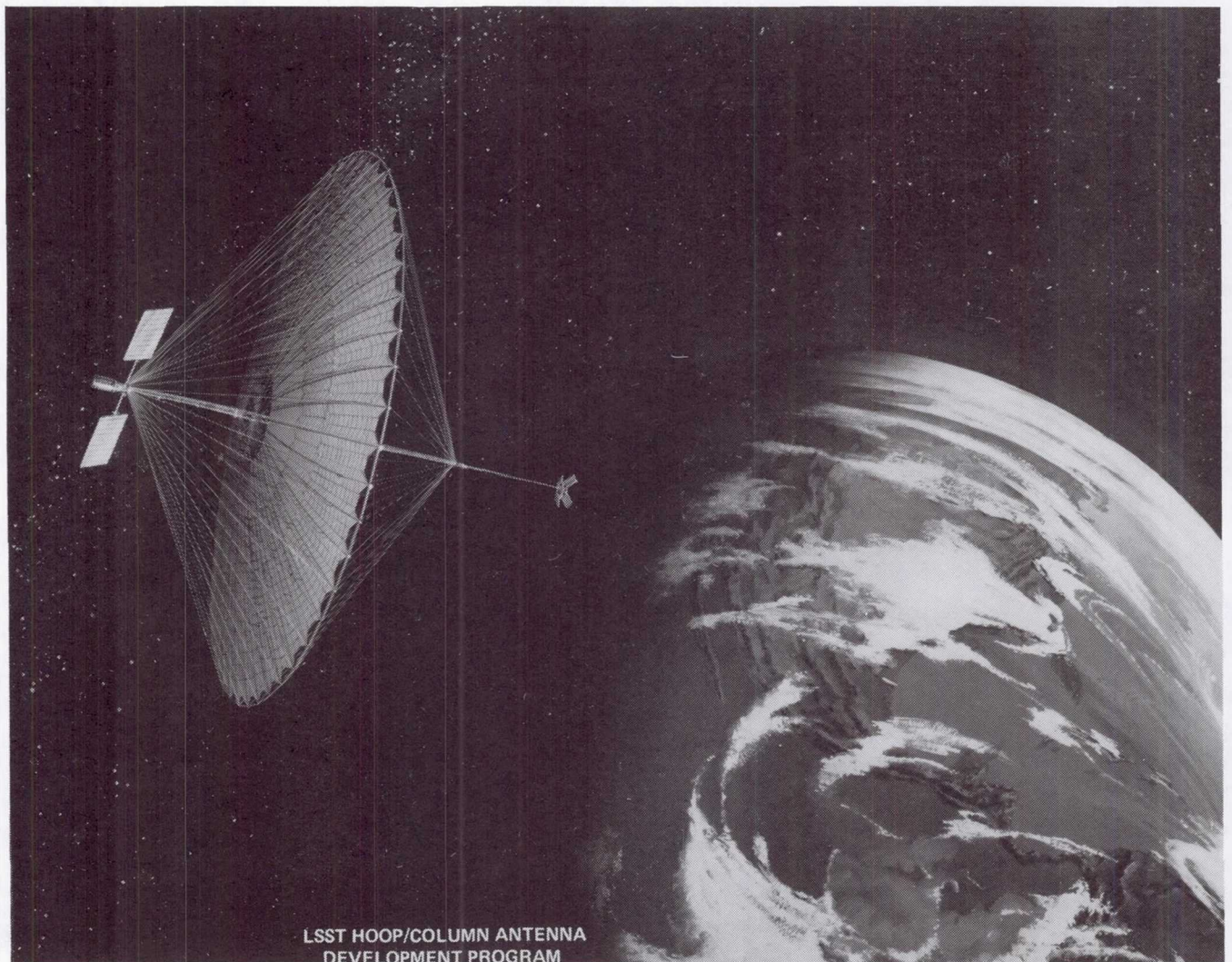
**MAYPOLE (HOOP/COLUMN) CONCEPT
DEVELOPMENT PROGRAM**

**M. R. Sullivan
Harris Corporation
Melbourne, Florida**

**Large Space Systems Technology - 1981
Third Annual Technical Review
November 16-19, 1981**

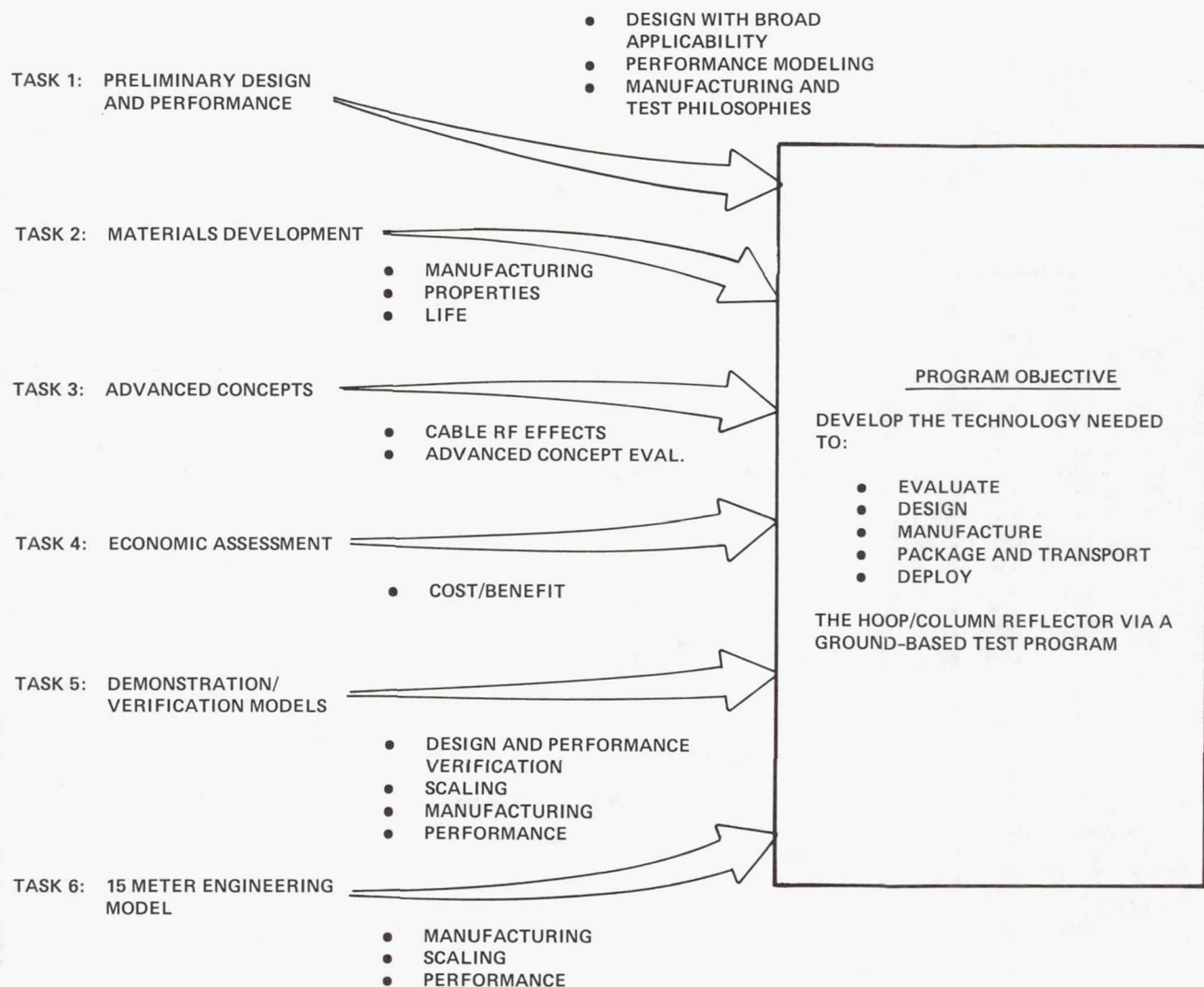
LSST HOOP/COLUMN ANTENNA DEVELOPMENT PROGRAM

The results of the development program to date indicate the versatility of the generic concept. Performance evaluations of the Hoop/Column concept have determined that it is capable of meeting the requirements of future identified large antenna missions.



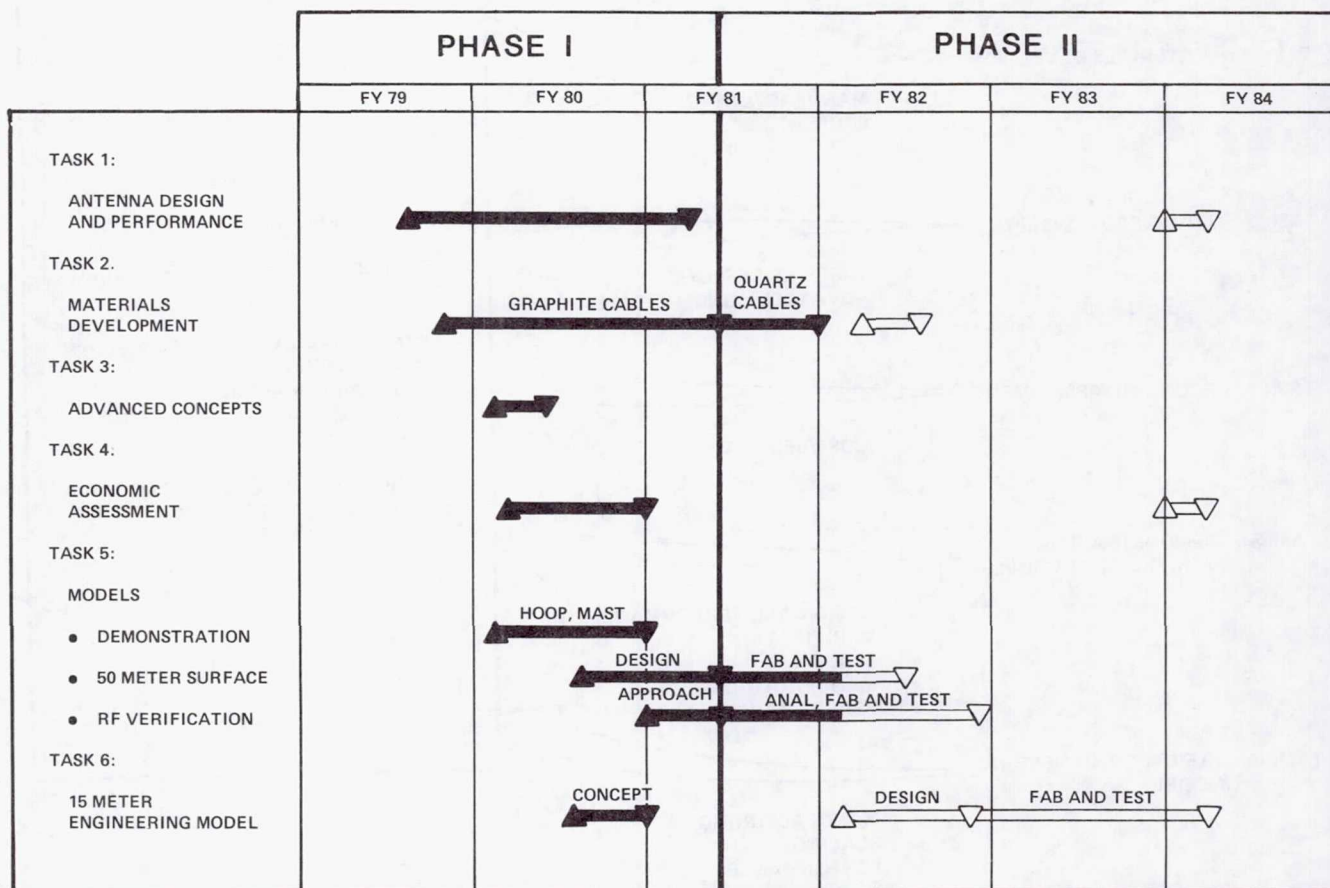
TASK DESCRIPTIONS AND PROGRAM OBJECTIVES

The Hoop/Column antenna development program is divided into six Tasks. All support the main objective of the program which is the technology development necessary to evaluate, design, manufacture, package, transport and deploy the Hoop/Column reflector by means of a ground-based test program.



SCHEDULE SUMMARY

The Hoop/Column Phase I Development Program is now complete. Phase II is underway and continues through FY 84. Each of the tasks are discussed on the following pages.



POINT DESIGN SELECTION

The program was initiated with a review of the NASA supplied mission scenarios for the communications, radiometry and radio astronomy missions. The study of these mission scenarios led to specific Hoop/Column antenna configurations for each mission. The mission configurations were then evaluated to identify specific technology items requiring further development. The compilation of these technology drivers resulted in a specification of a point design. All design and performance estimates for the program were made for the point design.

REVIEW MISSION SCENARIOS:

COMMUNICATIONS

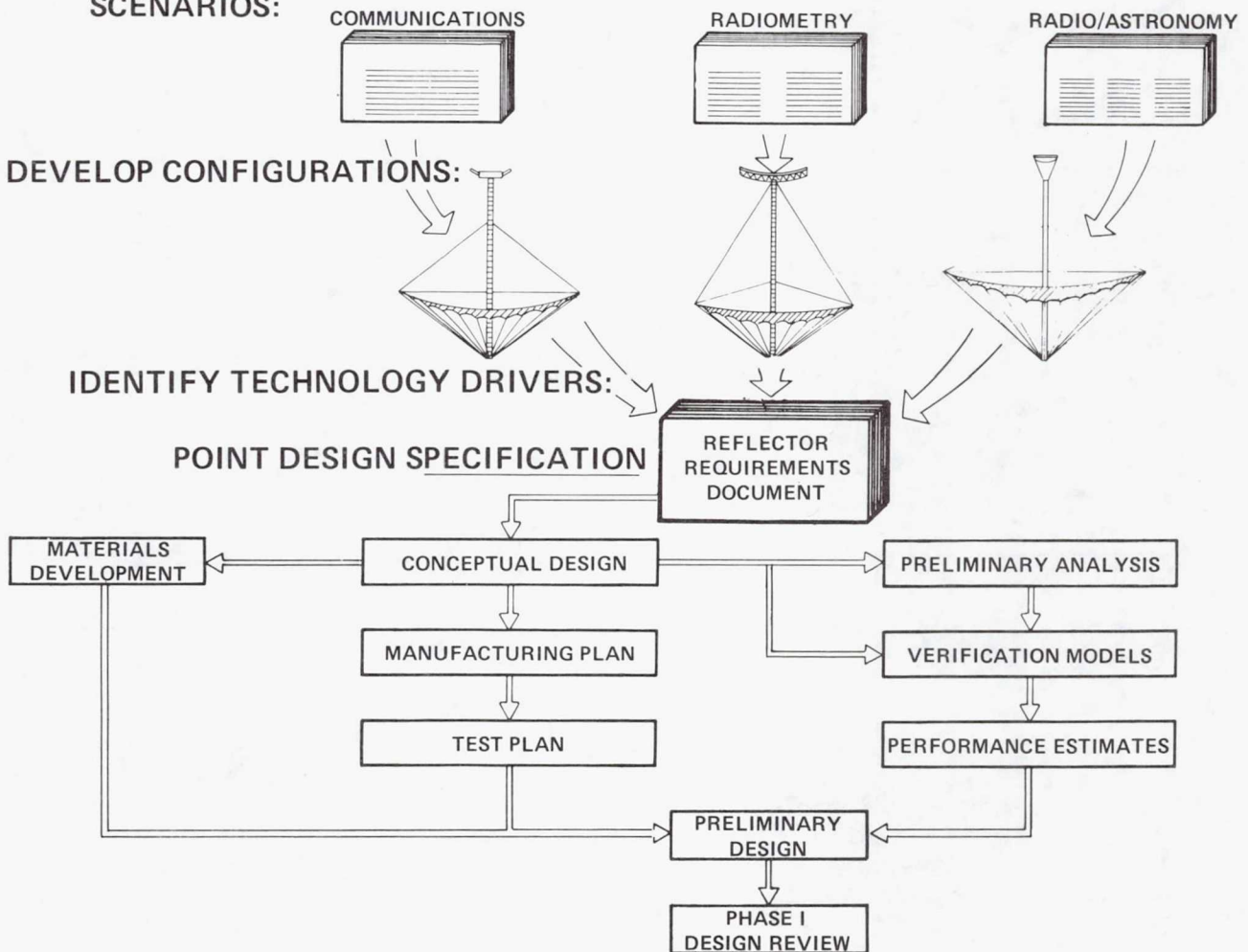
RADIOMETRY

RADIO/ASTRONOMY

DEVELOP CONFIGURATIONS:

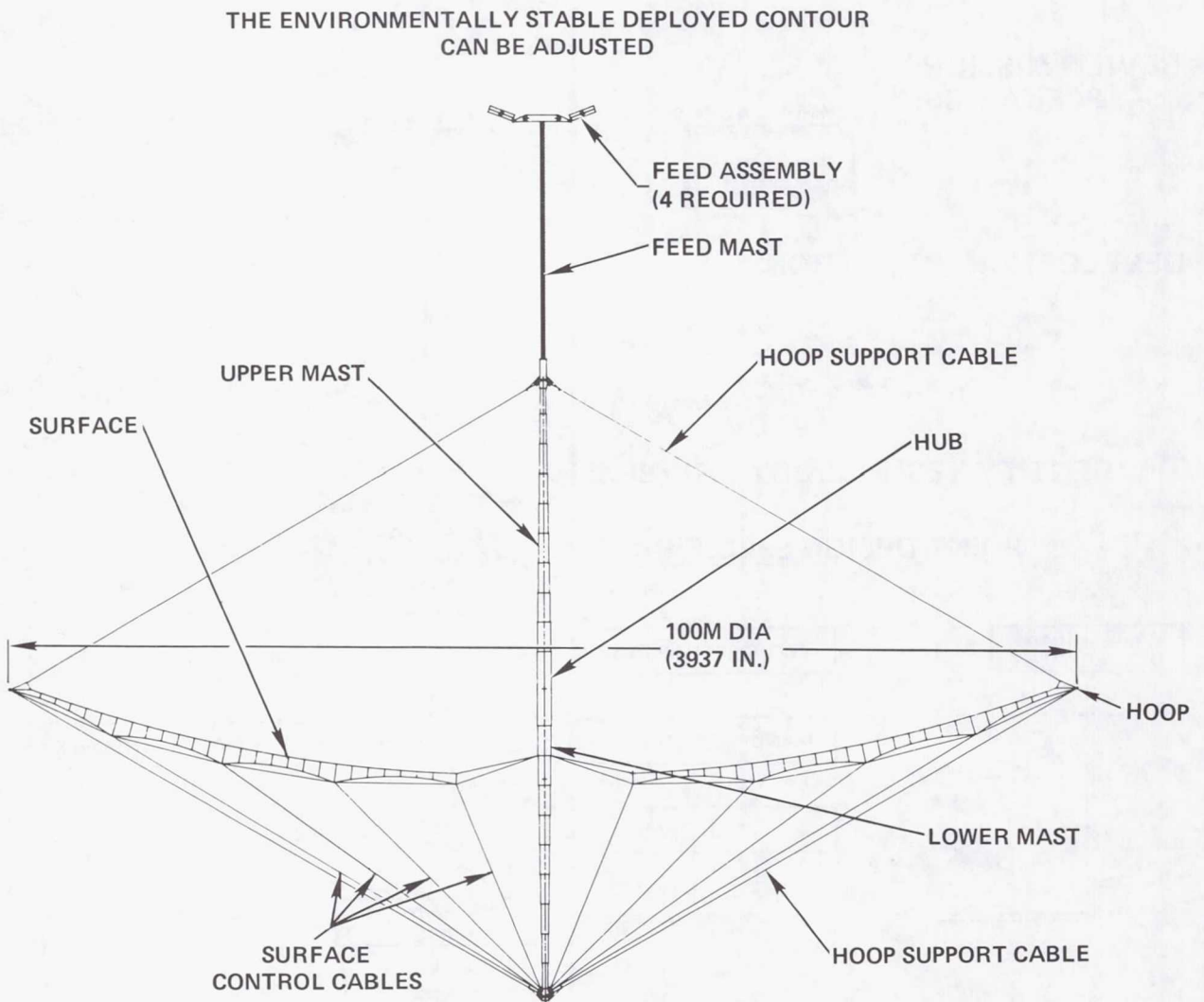
IDENTIFY TECHNOLOGY DRIVERS:

POINT DESIGN SPECIFICATION



CONFIGURATION OF HOOP/COLUMN POINT DESIGN – DEPLOYED CONFIGURATION

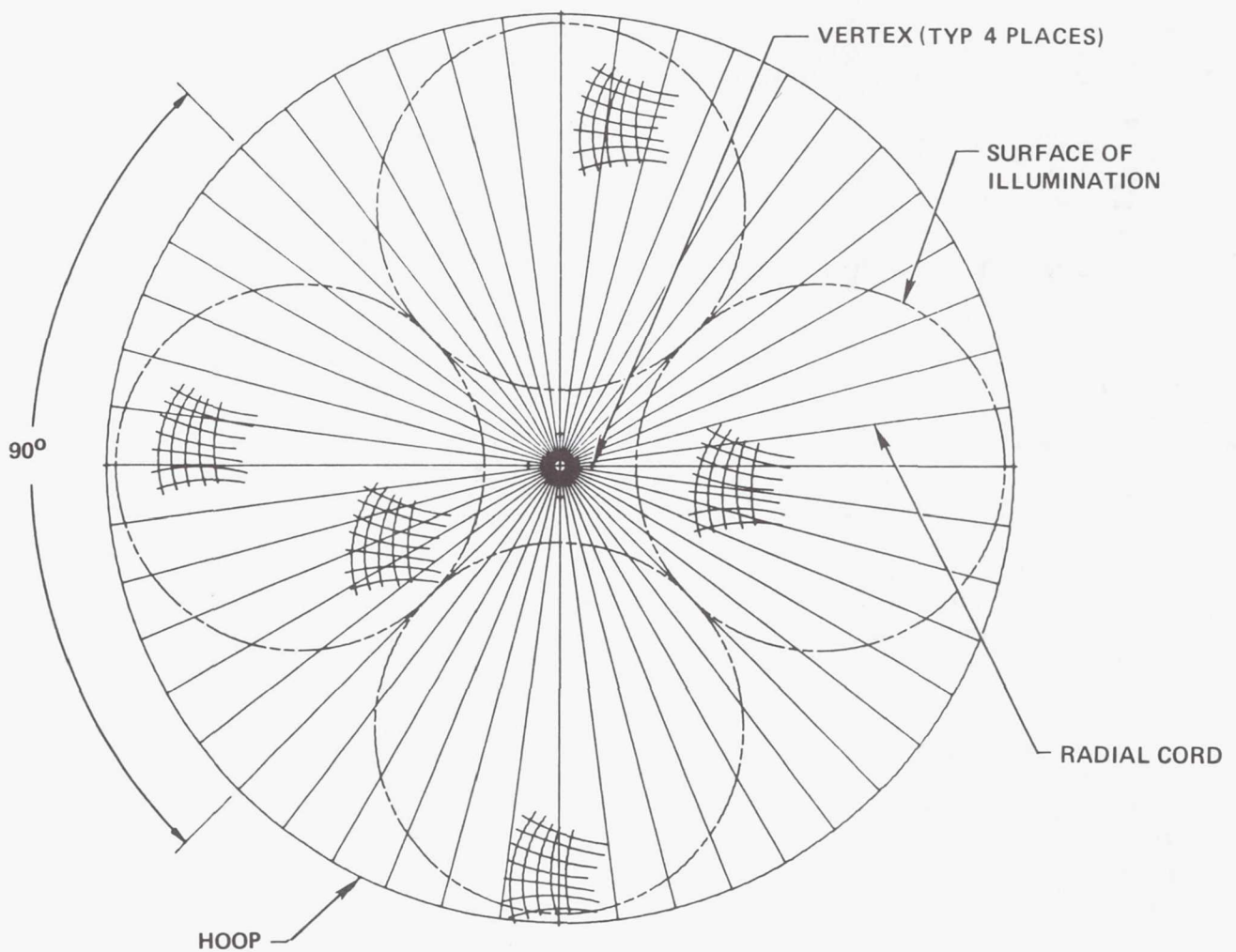
The deployed configuration of the Hoop/Column point design is shown below. A 100-meter point design has been selected that provides the quad aperture reflector system.



REFLECTOR SURFACE

The point design is a multiple beam/multiple quadrant offset reflector system. Four separate areas of illumination or aperture areas on the parent reflector are shown by imaginary lines. The surface is shaped as if it were four offsets; thus the parent reflector is cusped.

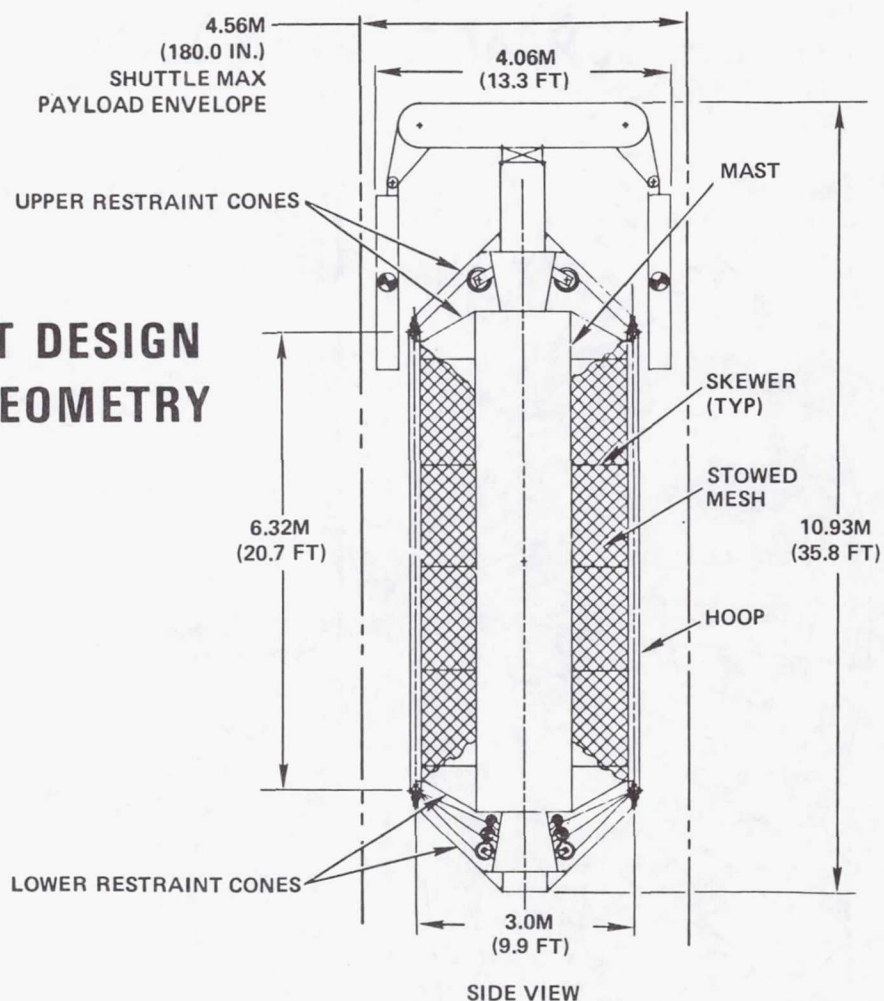
SURFACE - PLAN VIEW



POINT DESIGN STOWED CONFIGURATION

The stowed Hoop/Column antenna packages vary efficiently within the constraints of the Shuttle bay. The configuration selected for the point design, which is a 100-meter diameter deployed reflector, utilizes 48 articulating hoop segments. This dictates the aspect ratio of length to diameter of the stowed package. The aspect ratio can be modified for any given deployed diameter by changing the number of hoop segments.

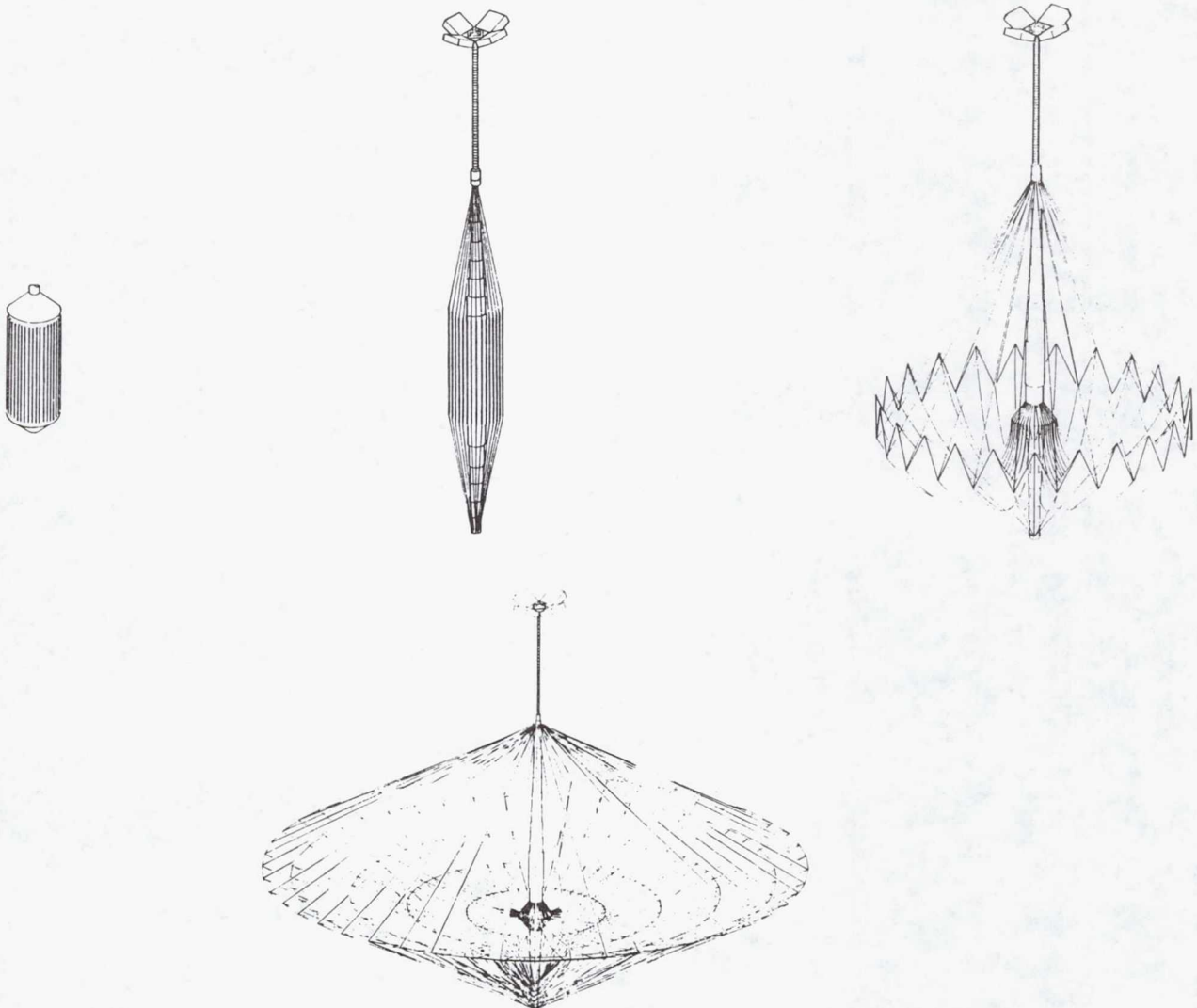
LSST POINT DESIGN - STOWED GEOMETRY



HOOP/COLUMN ANTENNA DEPLOYMENT SEQUENCE

The deployment sequence of the Hoop/Column antenna is initiated by the extension of both the feed mast and the main structural mast. Once this mast extension is completed, the hoop begins to deploy outward. The energy for deployment is provided by four separate drive units located on joints 90° apart around the hoop. Once the hoop is deployed to its full circular approximation, a separate section of the mast called the preload section is deployed. This motion tensions all of the hoop support cables and thus preloads the system.

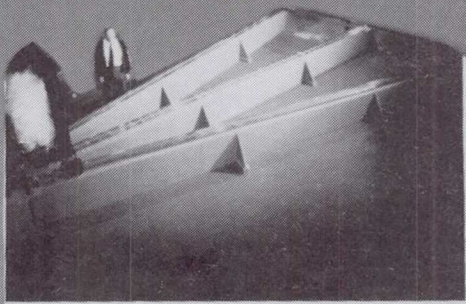
LSST DEPLOYMENT SEQUENCE



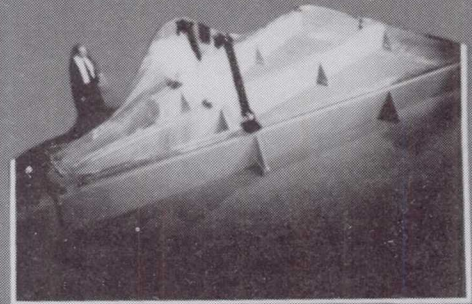
MESH MANAGEMENT DEVELOPMENT MODEL

A method of stowing and deploying the mesh in an organized and unobstructed manner has been preliminarily confirmed by a NASA developed mesh management model. Various stages of deployment are shown below.

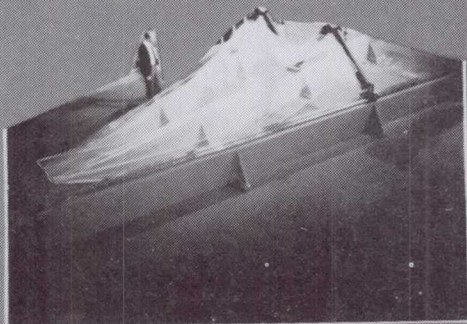
MESH MANAGEMENT DEVELOPMENT MODEL (1/20 SCALE - SIMULATED MESH)



MESH STOWED



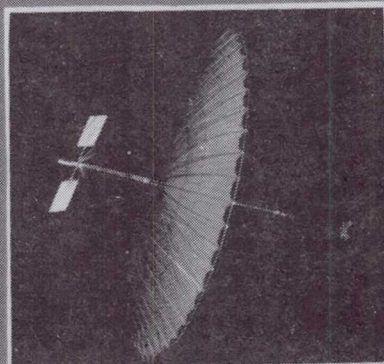
1/3 DEPLOYED



2/3 DEPLOYED

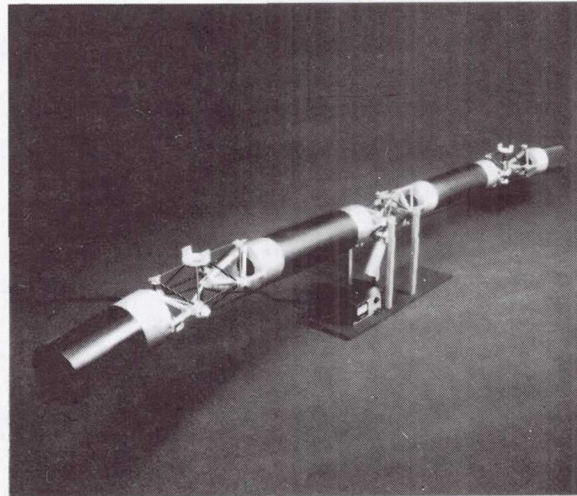
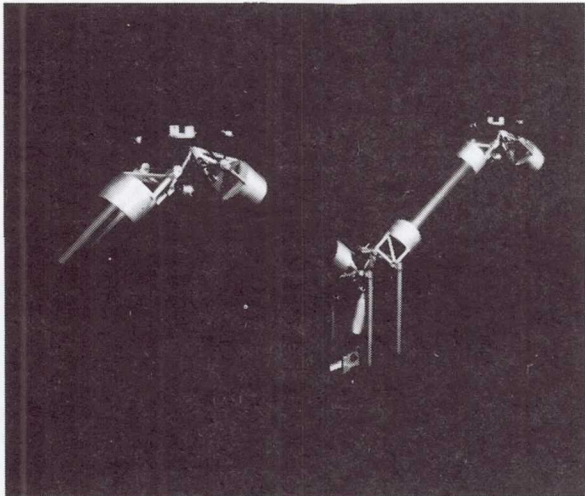
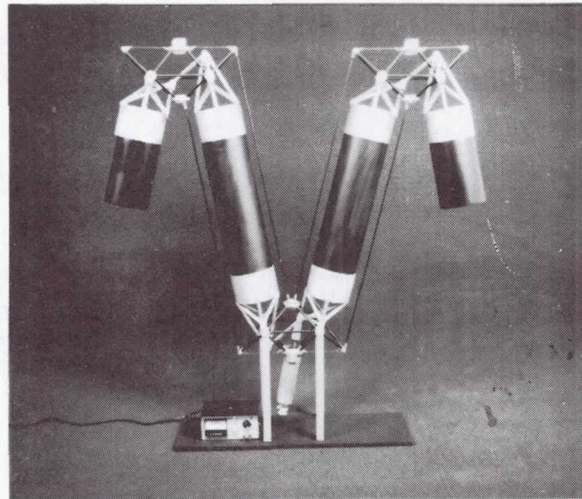
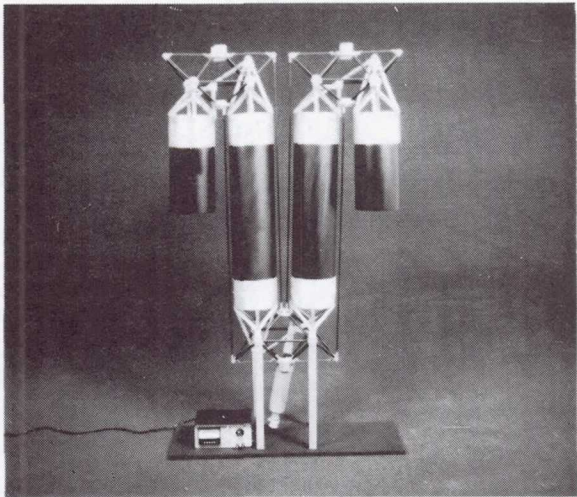


FULLY DEPLOYED



HOOP HINGE JOINT MODEL

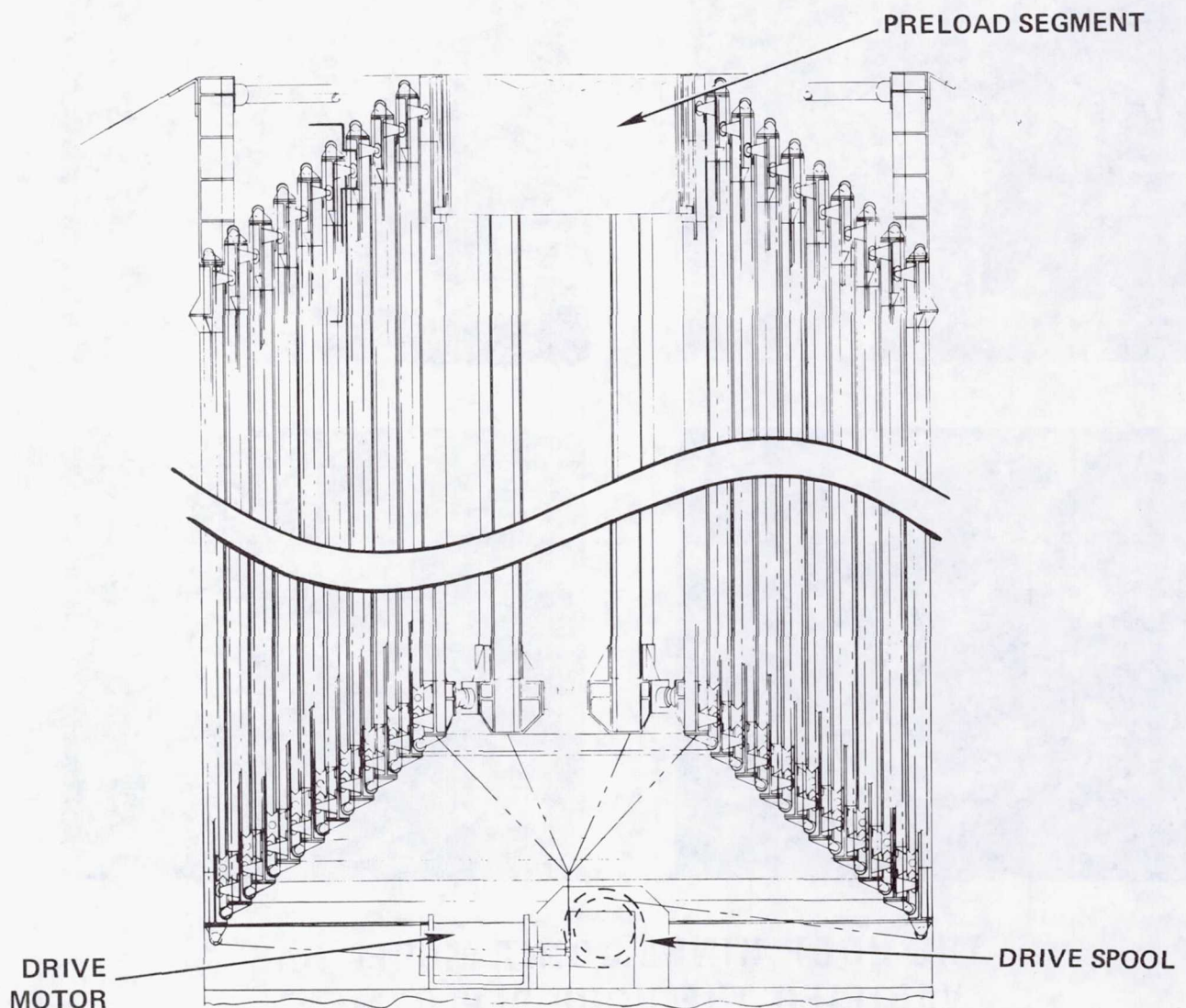
One critical element of the design is the hoop and its deployment method. A model of three full-scale hinge joints with truncated hoop segments was fabricated to evaluate the hoop's deployment, synchronization, and repeatability. A single drive unit deploys the model with synchronization being accomplished by means of synchronizing strips connecting adjacent hinge platforms and drive motion accomplished by means of a push rod link.



**THE HOOP HINGE JOINT MODEL HAS
VERIFIED THE HOOP DEPLOYMENT
MECHANISM DESIGN**

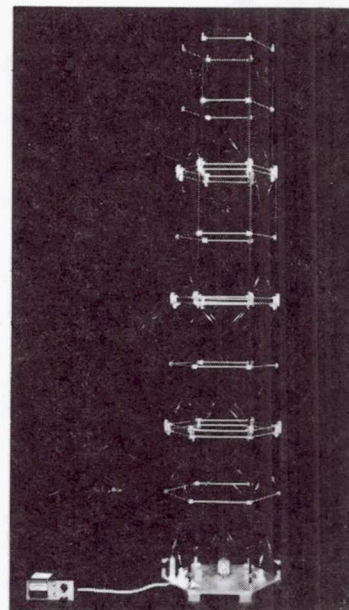
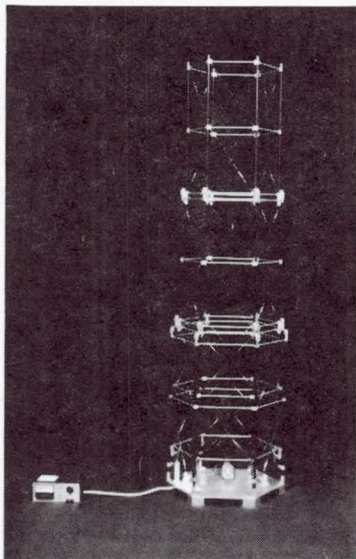
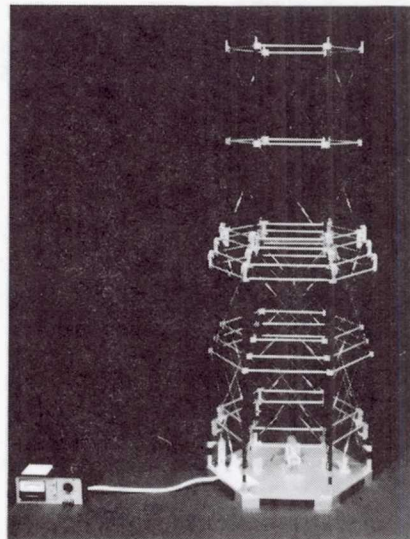
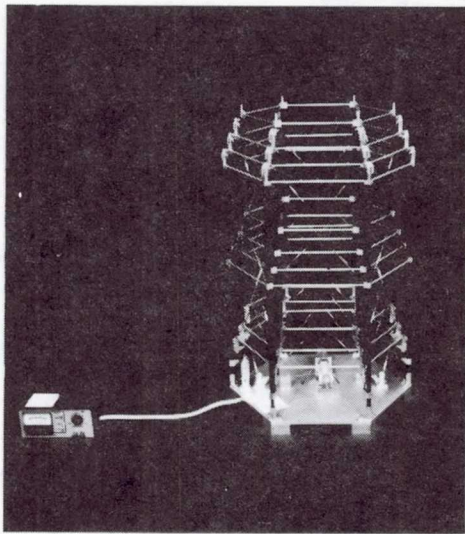
TELESCOPIC MAST

After many trade-off exercises, the cable driven telescopic mast was selected as the candidate approach which offered the most advantages. The deployment mechanism design consists of a cable that emanates from a drive spool and extends to the outermost section of the mast. The cable runs over a pulley at the outermost section, up the full length of the section, over a pulley at the top of that section and back down the adjacent section. It continues this path until it reaches the innermost section, at which time the cable crosses over to the opposite side and returns to the drive spool by an identical circuit to that just described. Deployment is initiated by activating the drive spool which takes up the cable and thus forces the sections to expand outward.



DEPLOYABLE MAST MODEL

Design verification of the mast was accomplished by means of a deployment model. This model represents an approximate 1/5-scale of the point design.



THE MAST MODEL HAS VERIFIED MAST DEPLOYMENT

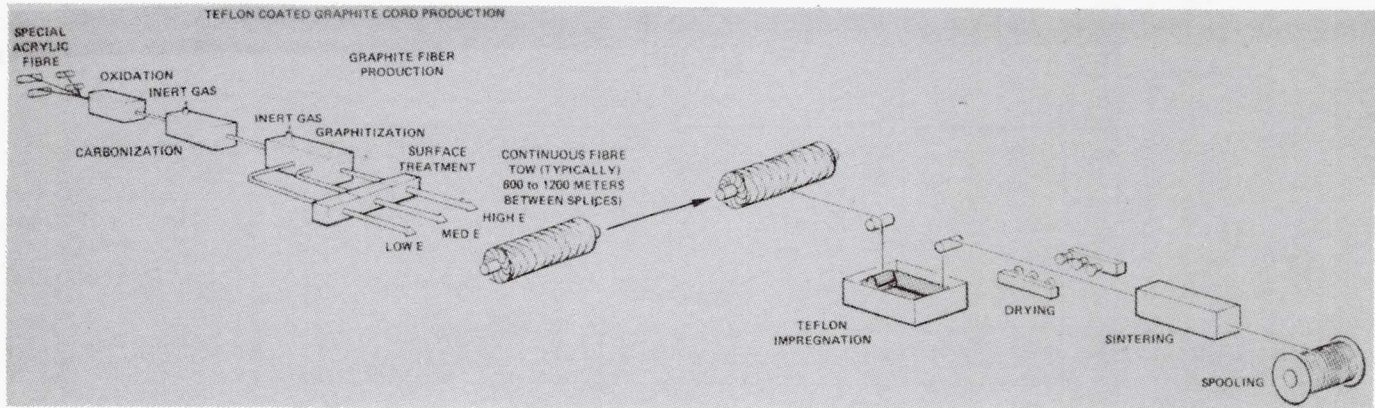
MATERIALS DEVELOPMENT TASK

Because of the large number of cable elements in the Hoop/Column concept, this task was devoted entirely to the development of cable materials that meets the reflector design requirements. The primary objectives of the task are listed below.

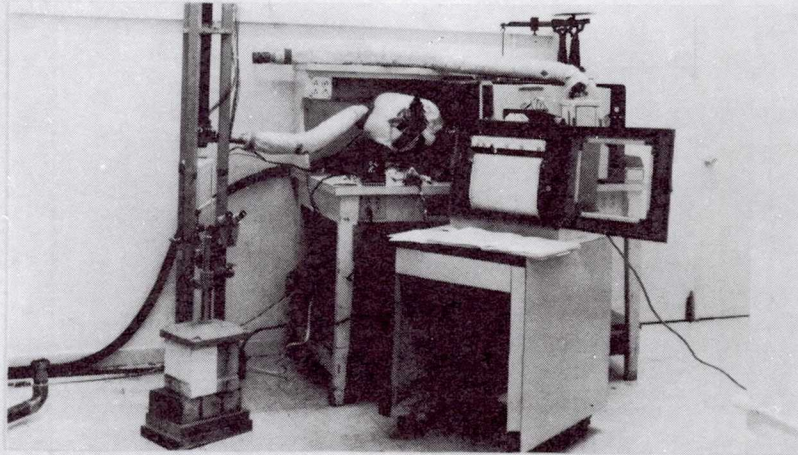
- **DEVELOP CABLE MATERIAL**
- **DETERMINE CABLE PROPERTIES THROUGH TESTING**
- **DEVELOP CABLE JOINT DESIGNS FOR THE HOOP/COLUMN ANTENNA**

CABLE DEVELOPMENT

Extensive research of cable materials and constructions lead to the selection of continuous graphite fiber cables that are impregnated with teflon while under load to improve fiber load sharing and handling toughness. Cable properties were verified by testing.



CABLE MANUFACTURE IS VERIFIED



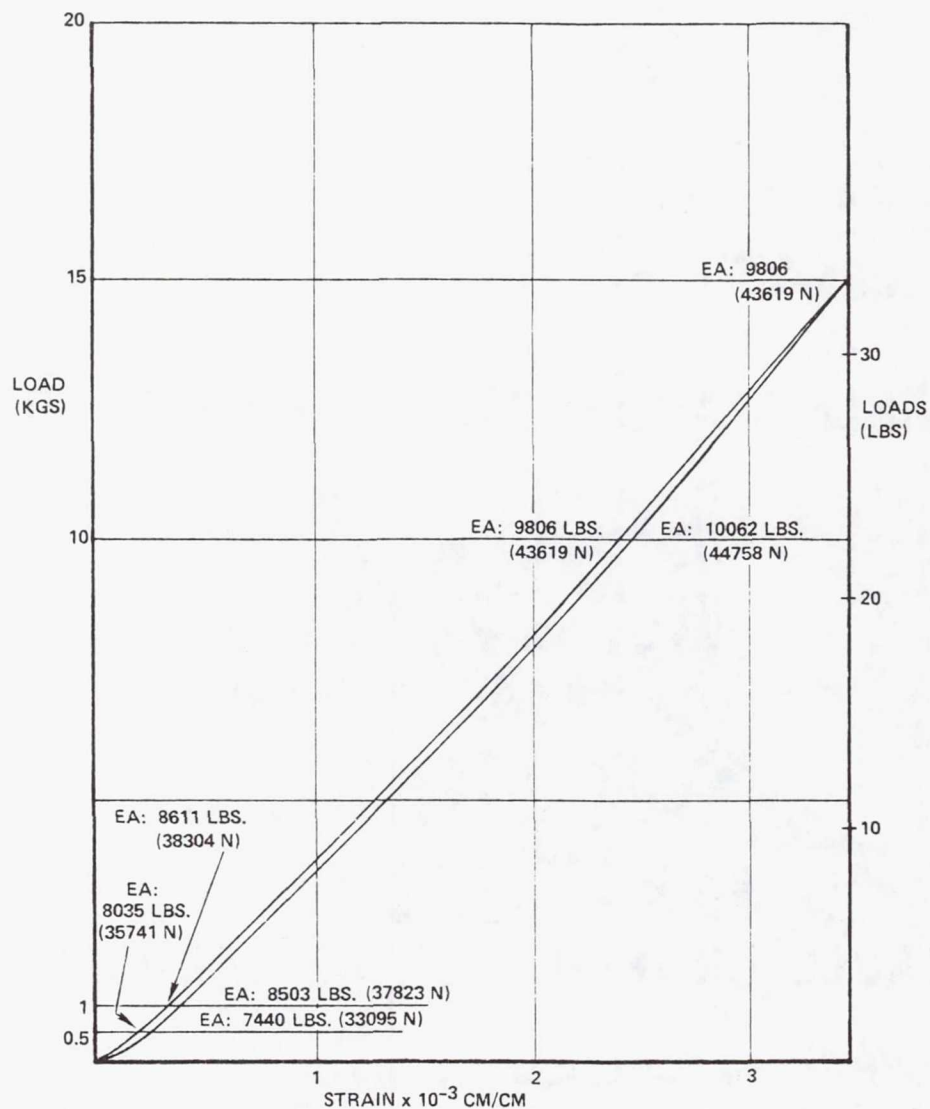
CABLE PROPERTIES ARE VERIFIED

- STRENGTH
- STIFFNESS
- RESIDUAL STRAIN
- COEFFICIENT OF THERMAL EXPANSION (CTE)

GRAPHITE CABLE STIFFNESS

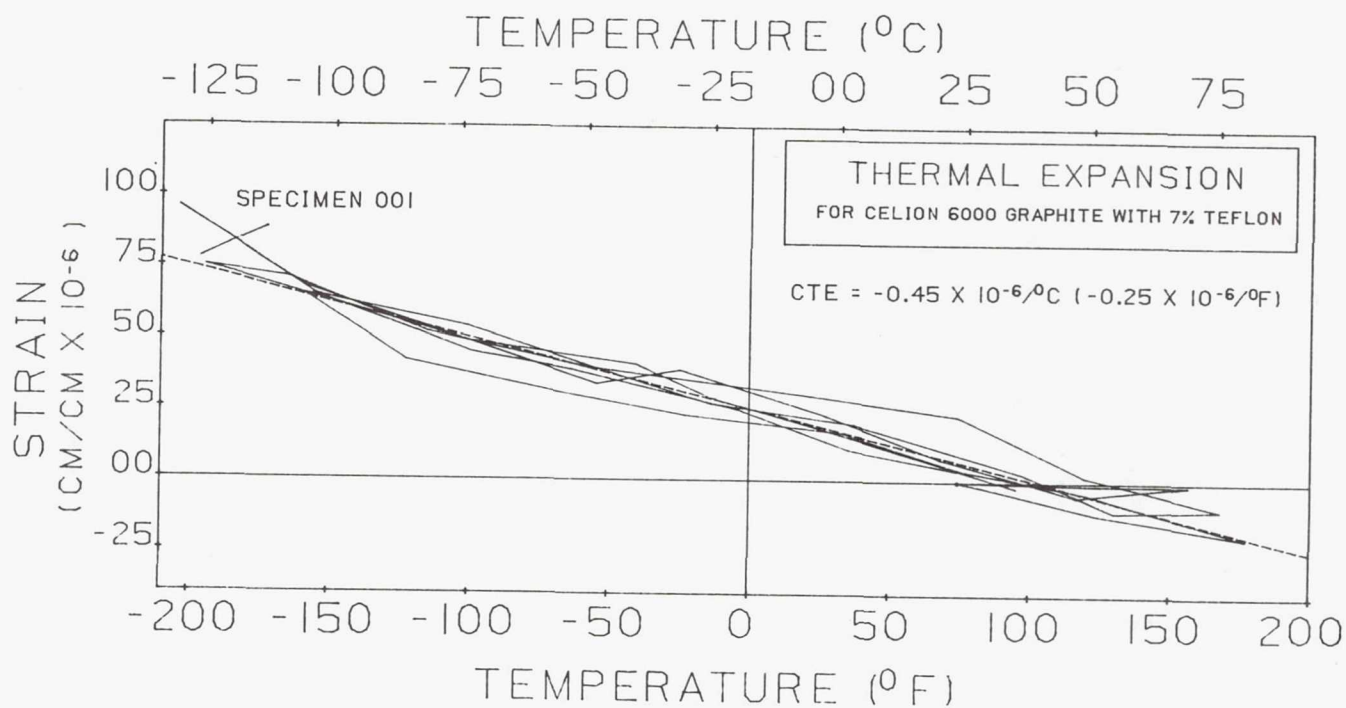
The figure below shows the results of load/strain tests for a number two cord (Celion 6000 graphite fiber) with a 7 percent teflon coating. The curve shows the relatively linear characteristics of the graphite material over the load range indicated. The cable has an EA (Modulus of Elasticity x Area) of approximately 40,000 N (9000 pounds) over the load range of interest.

LOAD VS. STRAIN FOR CELION 6000 GRAPHITE WITH 7 % TEFLON
(NO. 2 CORD)



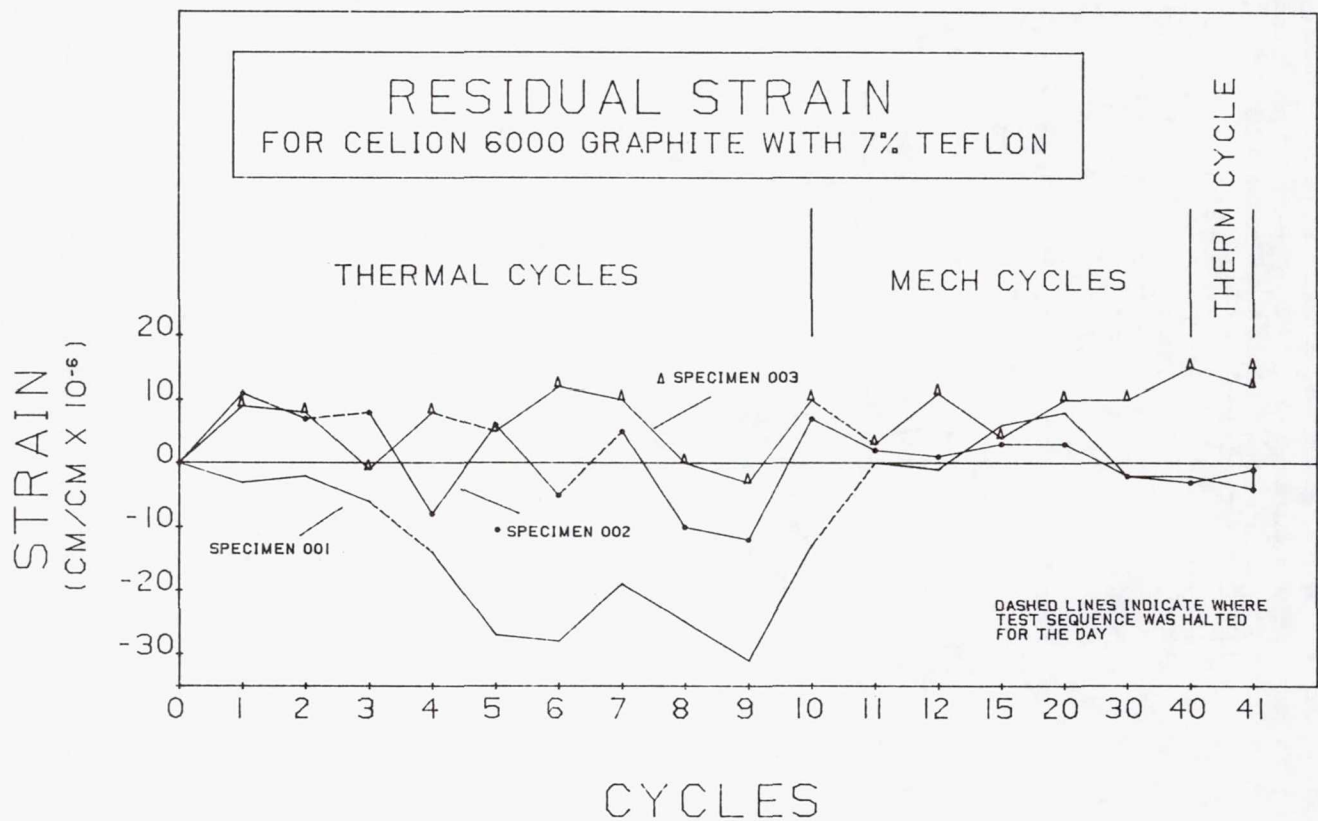
GRAPHITE CABLE COEFFICIENT OF THERMAL EXPANSION

The coefficient of thermal expansion is determined by means of a deflection test setup using a long cord specimen which is heated and cooled over the appropriate temperature range. Deflection is measured at various temperature increments. It can be seen by the curve below that good repeatability of strain versus temperature occurs and the resulting CTE is very low (approximately $-0.4 \times 10^{-6} \text{ cm/cm/}^{\circ}\text{C}$).



RESIDUAL STRAIN RESULTS

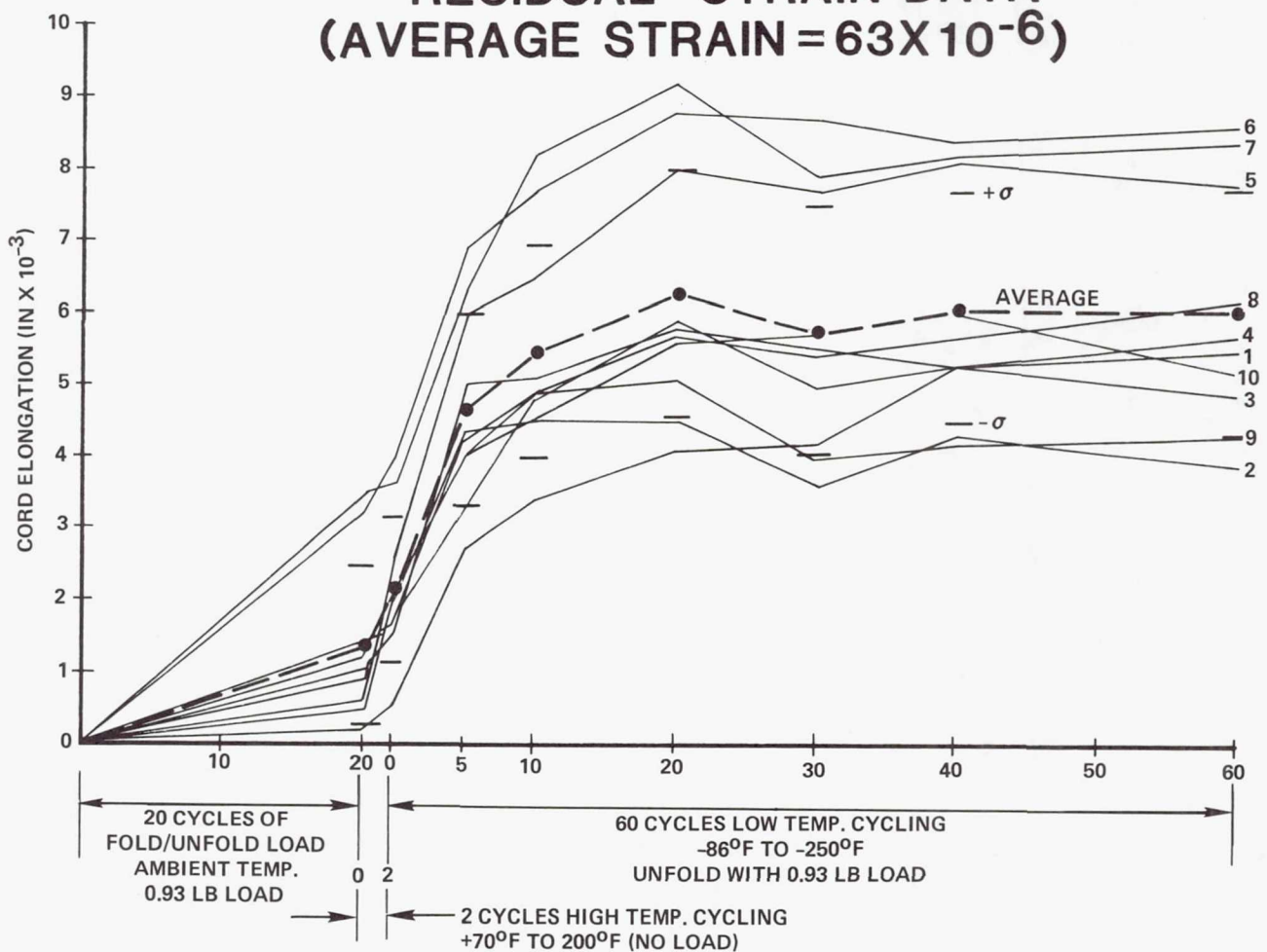
The following residual strain data indicate that the average strain is approximately zero for graphite cables with 7 percent teflon. This is a very significant result because all other cable types previously tested showed a residual strain (or stretch caused by initial load and/or thermal cycles) of 60 or more micro strains. For comparison the next page shows the residual strain data for the x-wrapped quartz cord used on the TDRSS antenna program.



TDRSS RESIDUAL STRAIN CORD DATA

The residual strain data shown below is for the x-wrapped cables used on the TDRSS antenna program. It is shown here for comparison to the new cords being developed.

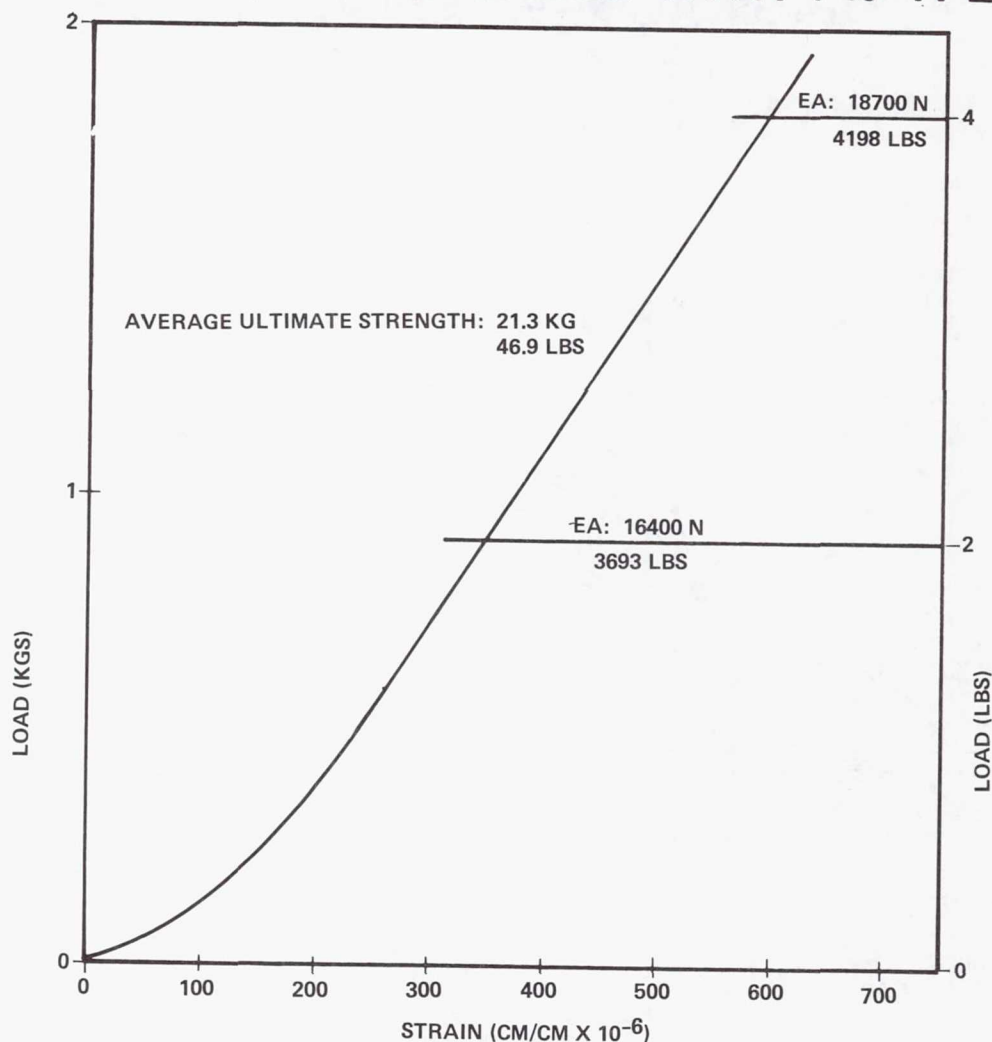
ORIGINAL X-WRAPPED QUARTZ CORD RESIDUAL STRAIN DATA (AVERAGE STRAIN = 63×10^{-6})



DIELECTRIC QUARTZ CABLE DEVELOPMENT

The teflon impregnated cables previously described are used for 80 percent of the cables in the Hoop/Column reflector design that are located in or below the RF reflective surface. An additional set of 48 cables are located above the reflective surface and interfere with the RF illumination. It is required that these cables be made of a low-loss dielectric material. Quartz cables impregnated with teflon have been developed for this application. The EA of the quartz cable is approximately one third that of the graphite cables, however, quartz meets the requirements for the upper hoop control cable set.

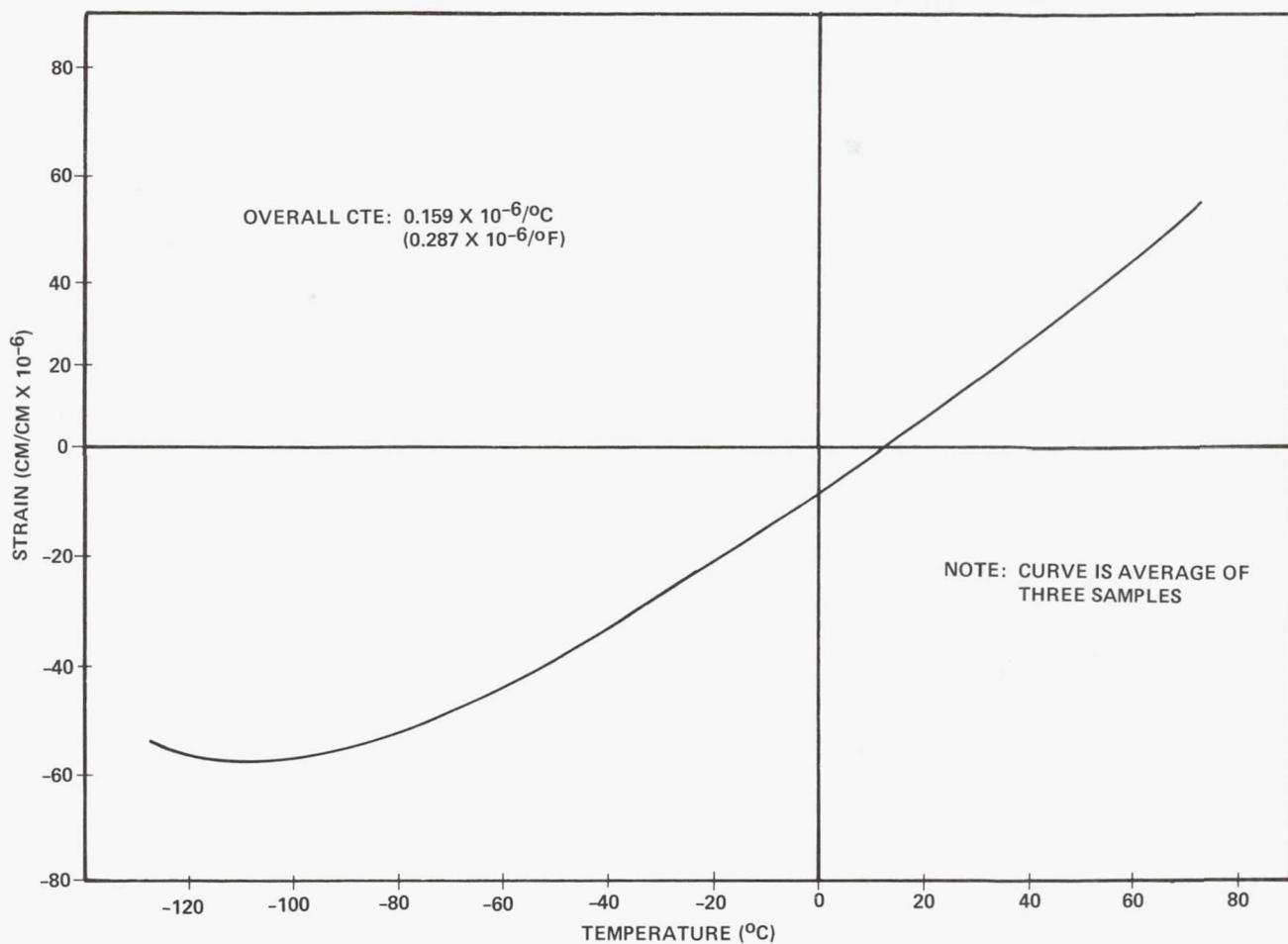
EA #2 QUARTZ CABLE WITH 7% TFE



QUARTZ CABLE THERMAL EXPANSION

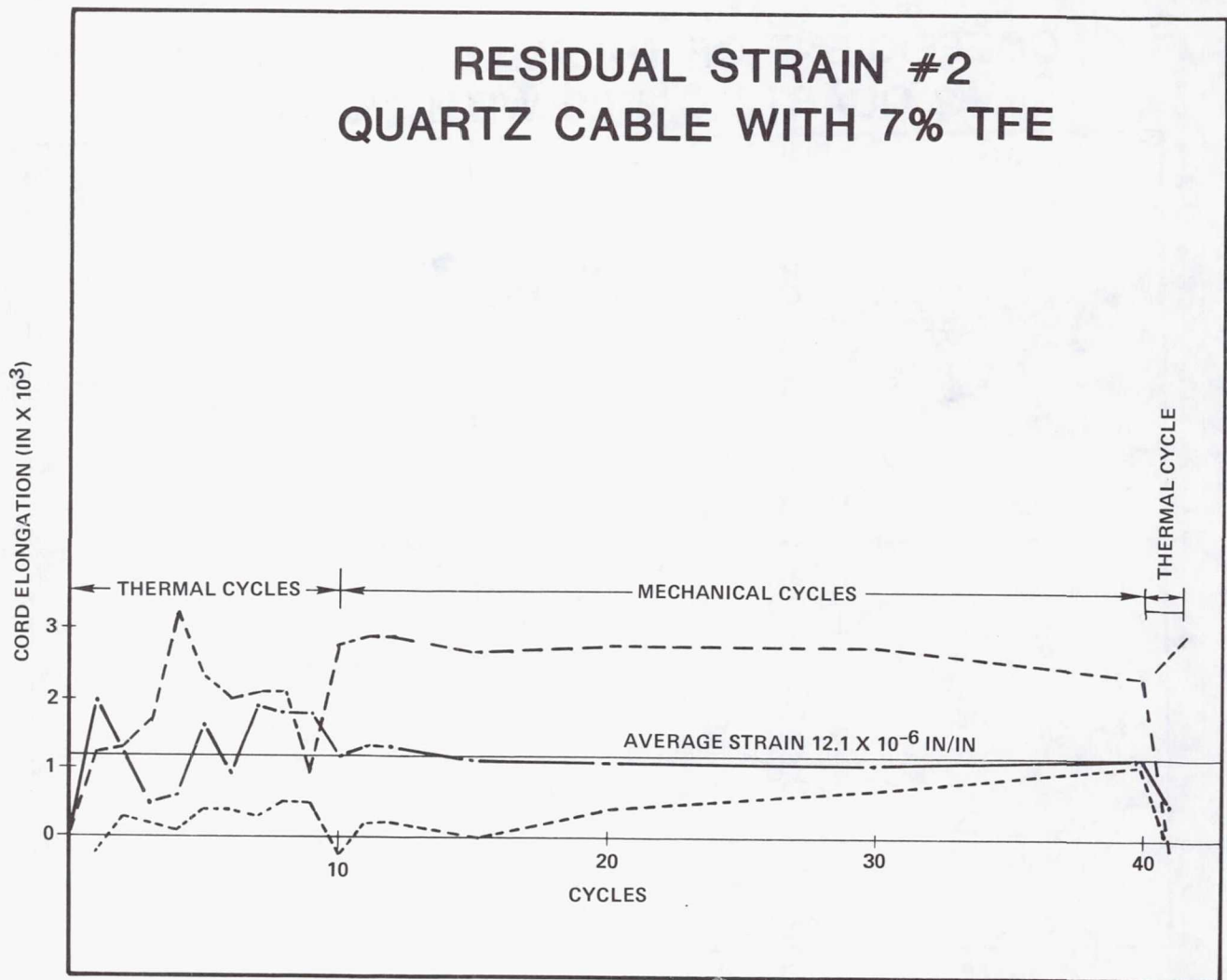
The coefficient of thermal expansion of quartz cables varies from approximately $0.3/^{\circ}\text{F}$ at high temperatures to $-0.3/^{\circ}\text{F}$ at low temperatures.

COEFFICIENT OF THERMAL EXPANSION #2 QUARTZ CABLE WITH 7% TFE



QUARTZ CABLE RESIDUAL STRAIN

The average residual strain of quartz cable with teflon impregnation is approximately 12 micro strains. This compares to cables without teflon of 63 micro strains.



CABLE TEST RESULT SUMMARY

The table below summarizes the graphite and quartz cable test data presented on the previous pages.

DESCRIPTION	EA (LBS)	ULTIMATE (LBS)	CTE (/°F X 10 ⁻⁶)	RS (X 10 ⁻⁶ IN/IN)
NO. 2 QUARTZ TFE COATED	4200	47	0.29	12
NO. 2 QUARTZ TFE X-WRAP	3100	30	0.20	63
NO. 2 GRAPHITE TFE COATED	8100	80	-0.24	0.22

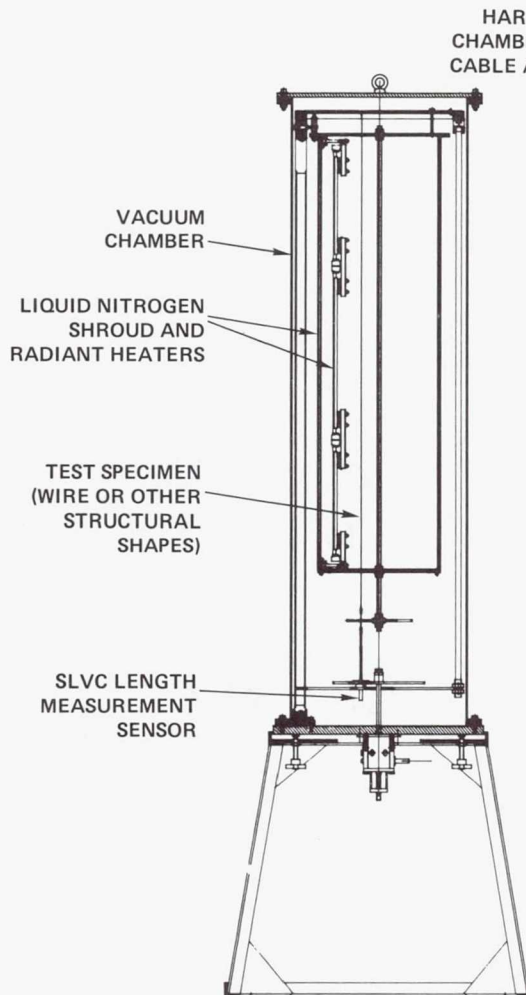
CABLE TECHNOLOGY ACHIEVEMENTS

The chart below lists some of the achievement highlights of the cable development program.

- **RESEARCH HAS DEVELOPED A HIGH PERFORMANCE CABLE MATERIAL WITH:**
 - **NEAR ZERO THERMAL EXPANSION**
 - **NEAR ZERO CREEP**
- **IN ADDITION, THE CABLE HAS THE FOLLOWING PROPERTIES:**
 - **FLEXIBILITY**
 - **RESILIENCY**
 - **IMMUNITY TO SPACE RADIATION AND TEMPERATURE EXTREMES**
- **THESE CABLE COMPONENTS MEET AND EXCEED THE REQUIREMENTS FOR THE MAYPOLE HOOP/COLUMN ANTENNA DESIGN**
- **THE RESULT PROVIDES AN OPPORTUNITY FOR THE DEVELOPMENT OF LARGE SPACE STRUCTURES WITH DIMENSIONAL STABILITY NEVER BEFORE OBTAINABLE**
- **DEVELOPED CABLE JOINT DESIGNS FOR THE HOOP/COLUMN ANTENNA (DESCRIBED IN 50 METER MODEL DESCRIPTION)**

THERMAL CYCLE CHAMBER

A Harris built thermal cycle chamber is scheduled for completion in January of 1982. It is to be used for future cord CTE and creep testing. The chamber is a Harris capital expenditure that will greatly reduce the cost and increase accuracy of future cable testing.



SPECIFICATIONS

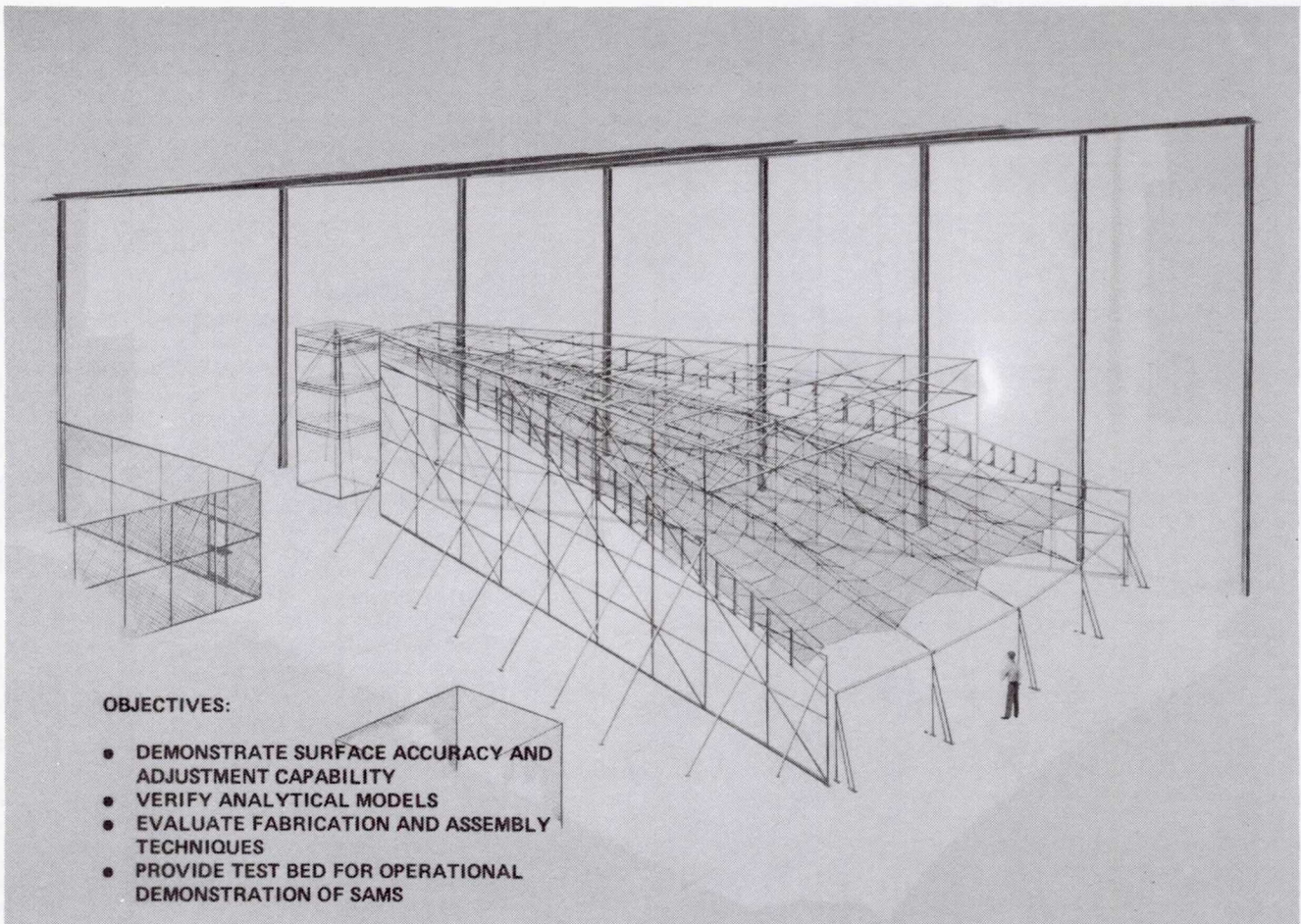
- TEMPERATURE RANGE: -185°C TO 150°C
(-300°F TO 300°F)
- PROGRAMMED TEMPERATURE PROFILES
- CYCLE TIME: 40 MINUTES
- NUMBER OF SPECIMEN PER TEST: 12
- STRAIN MEASUREMENT ACCURACY: ± 1
- TEMPERATURE ACCURACY CONTROL: $\pm 3^{\circ}\text{C}$ (5°F)
- SPECIMEN MAXIMUM LENGTH: 127 cm (50 IN)

OUTPUTS

- CONTINUOUS PLOTS OF TEMPERATURE AND LENGTHS
- COEFFICIENT OF THERMAL EXPANSION
- STRAIN VERSUS NUMBER CYCLES
- CREEP VERSUS TEMPERATURE AND/OR TIME

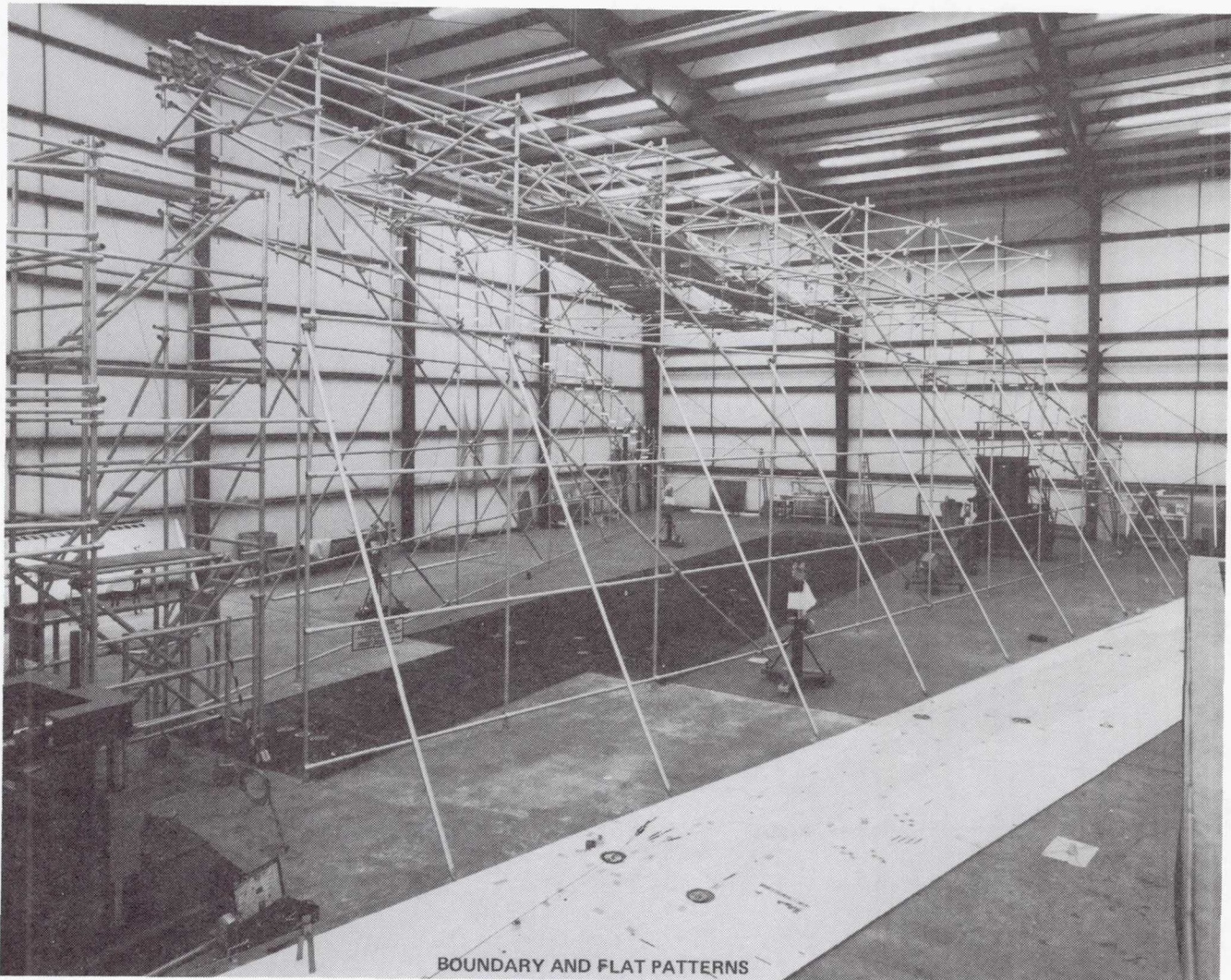
50-METER SURFACE MODEL

Harris is nearing completion of a 50-Meter Surface Model. This model represents a logical step towards the eventual goal of fabrication of very large antenna surfaces. The objectives of the task are defined in the figure below.



BOUNDARY AND FLAT PATTERNS

The 50-Meter Surface Model is fabricated from flat patterns which were developed by means of analytical models. The boundary structure, which simulates the hoop, column and adjacent gores, is a fixed boundary to which the surface attaches. An overall view of the structure and flat patterns is shown below.

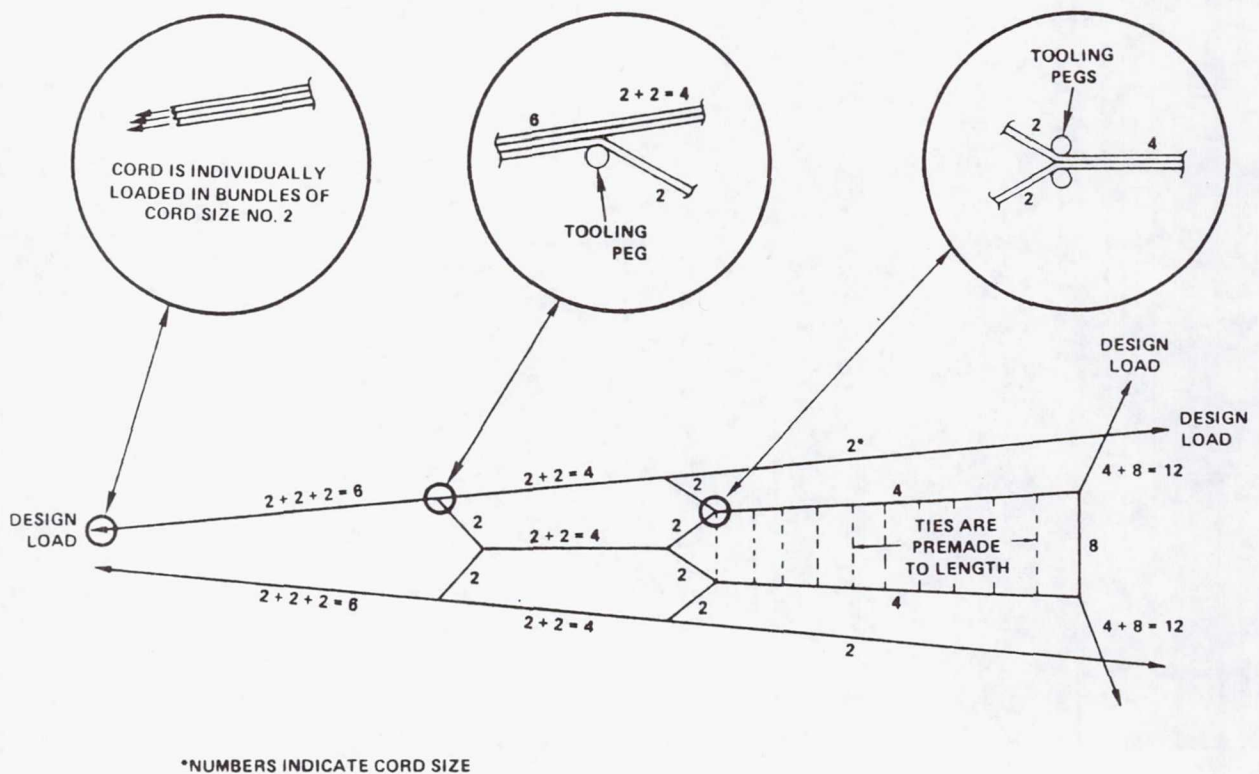


BOUNDARY AND FLAT PATTERNS

CABLES JOINT MANUFACTURING

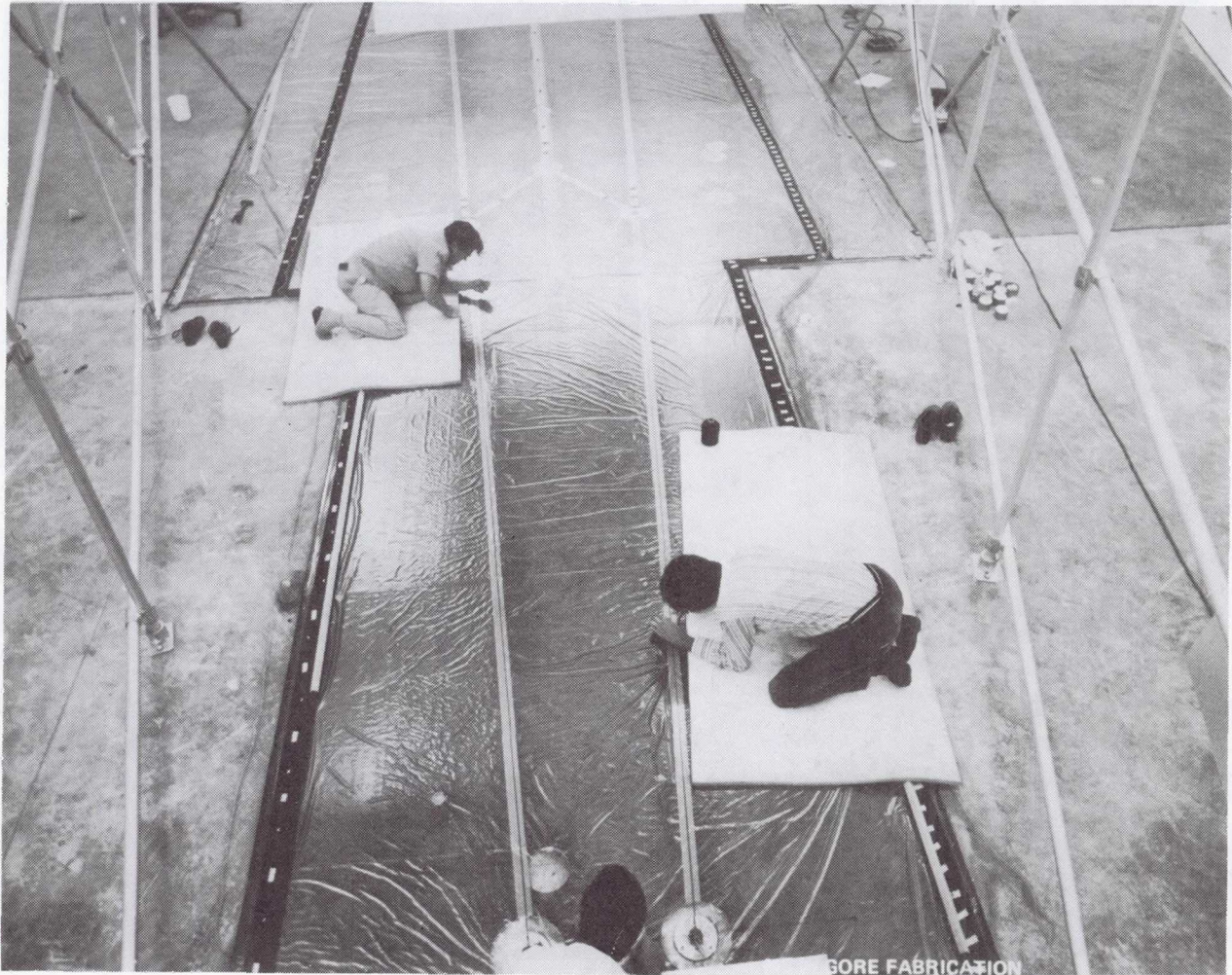
The unique configurations of cable junctions presented problems in joining techniques. After various trade studies were completed, the following joint concept was selected as being the most readily implementable and providing uniform structural properties. To meet the primary goal of build to dimension for the point design, an assembly method was devised which would yield the lowest manufacturing tolerances. The method selected involves maintaining control of both geometry and preload during the manufacturing process. Individual cords are loaded and positioned over accurately placed tooling pegs at each cable junction. The appropriate regions of teflon coating on the cords are stripped off and adhesive applied. A graphite epoxy board fitting is placed over the tool pegs and bonded to the cords. The result is a very high strength joint for transitioning load around angles in the cables while still maintaining full cable properties. The various joints and cord quantities per panel are shown in the following three figures.

FRONT CORD ASSEMBLY



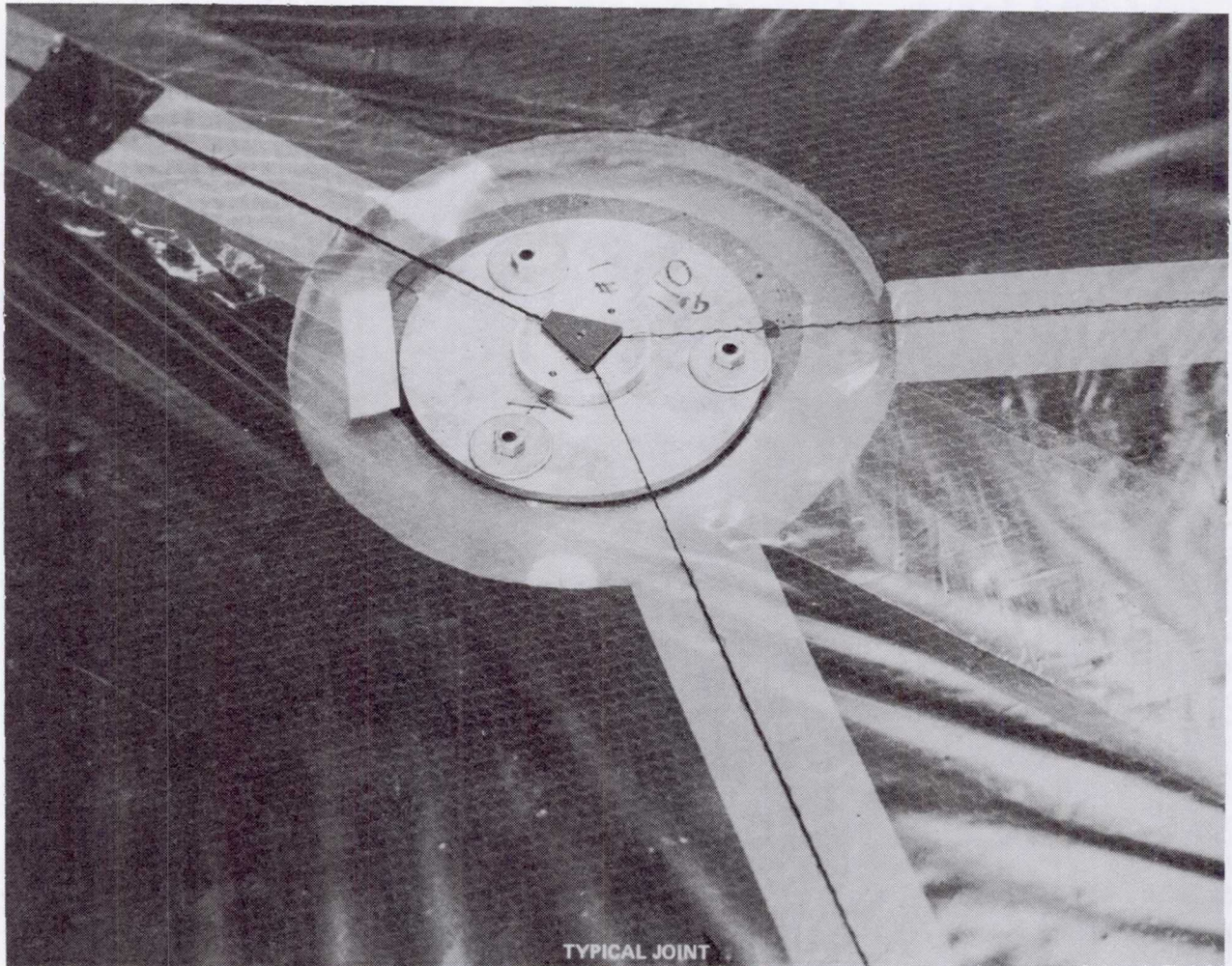
MESH GORE FABRICATION

After the front cord system has been final bonded, the mesh is stretched over the cords to a predesignated tension field. It is then laced to the front cords and trimmed. The figure below shows this activity in progress.



TYPICAL JOINT

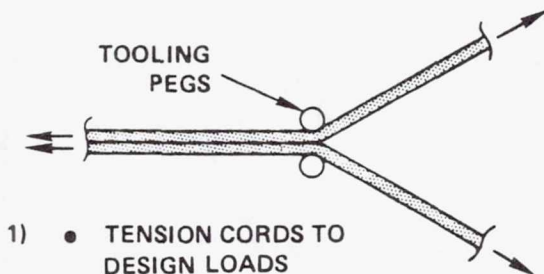
This illustration shows a typical front cord joint consisting of two fiberglass plates which sandwich and bond the graphite front cords. This joint is located with pegs to an accuracy of ± 0.020 inch. The steps of this joint fabrication are explained on the following page.



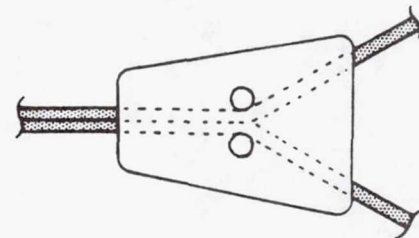
CORD JOINT MANUFACTURING PROCESS

Illustrated below is a sequential representation of a typical surface junction manufacturing process.

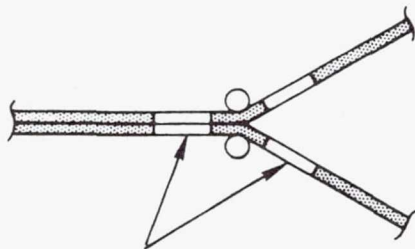
CORD JOINT MANUFACTURING PROCESS



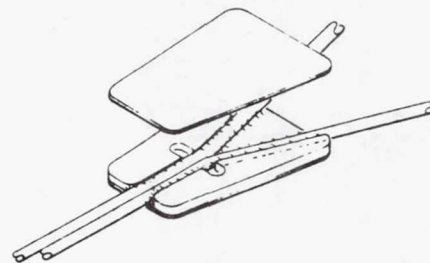
- 1) • TENSION CORDS TO DESIGN LOADS



- 3) • TO APPLY EPOXY ADHESIVE TO GRAPHITE/EPOXY FITTING
- PLACE FITTING OVER TOOLING PEGS WITH ADHESIVE IN CONTACT WITH CORDS
- ALLOW 24 HOURS FOR ADHESIVE CURE



- 2) • REMOVE TEFLON WITH MINIATURE BUTANE TORCH
- APPLY EPOXY ADHESIVE TO CORD AREAS

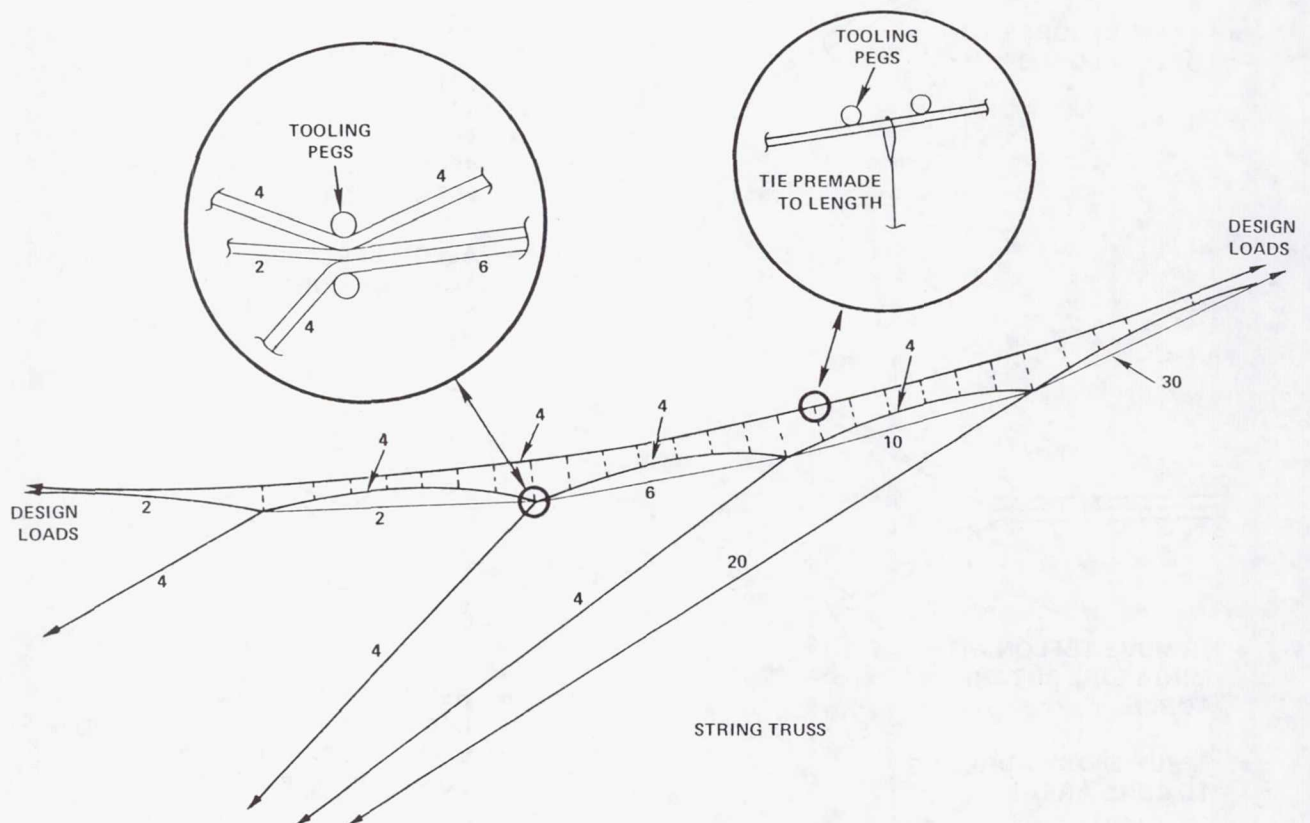


- 4) • REMOVE FITTING AND CORDS FROM TOOLING PEGS AND BOND LAMINATE CAP TO EXPOSED CORD SIZE OF FITTING

STRING TRUSS ASSEMBLY

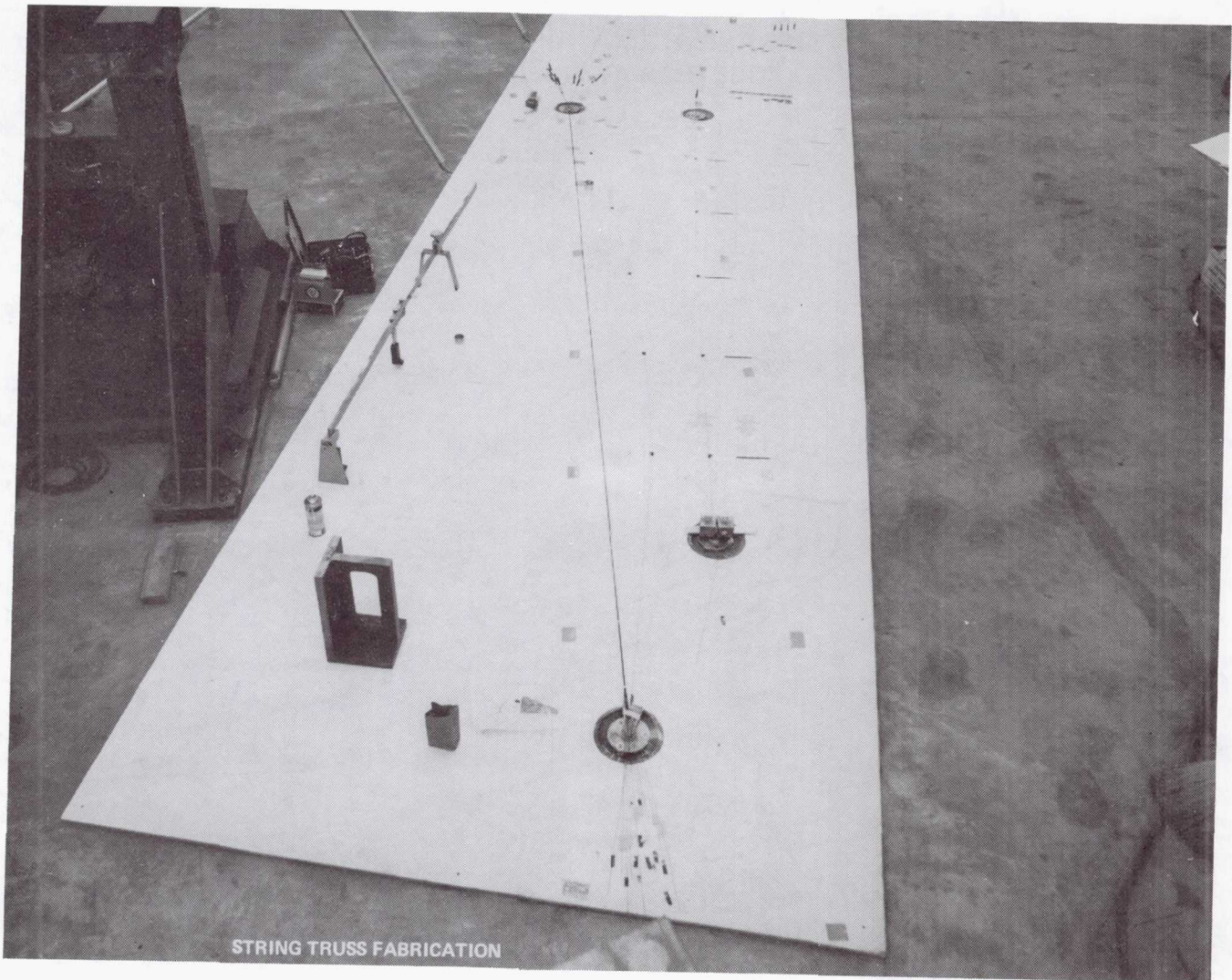
The string truss assembly is manufactured in the same manner as the front cord system. The string truss dictates the contour of the surface. It also provides the hard point interfaces to the surface control cables.

STRING TRUSS ASSEMBLY



STRING TRUSS FABRICATION

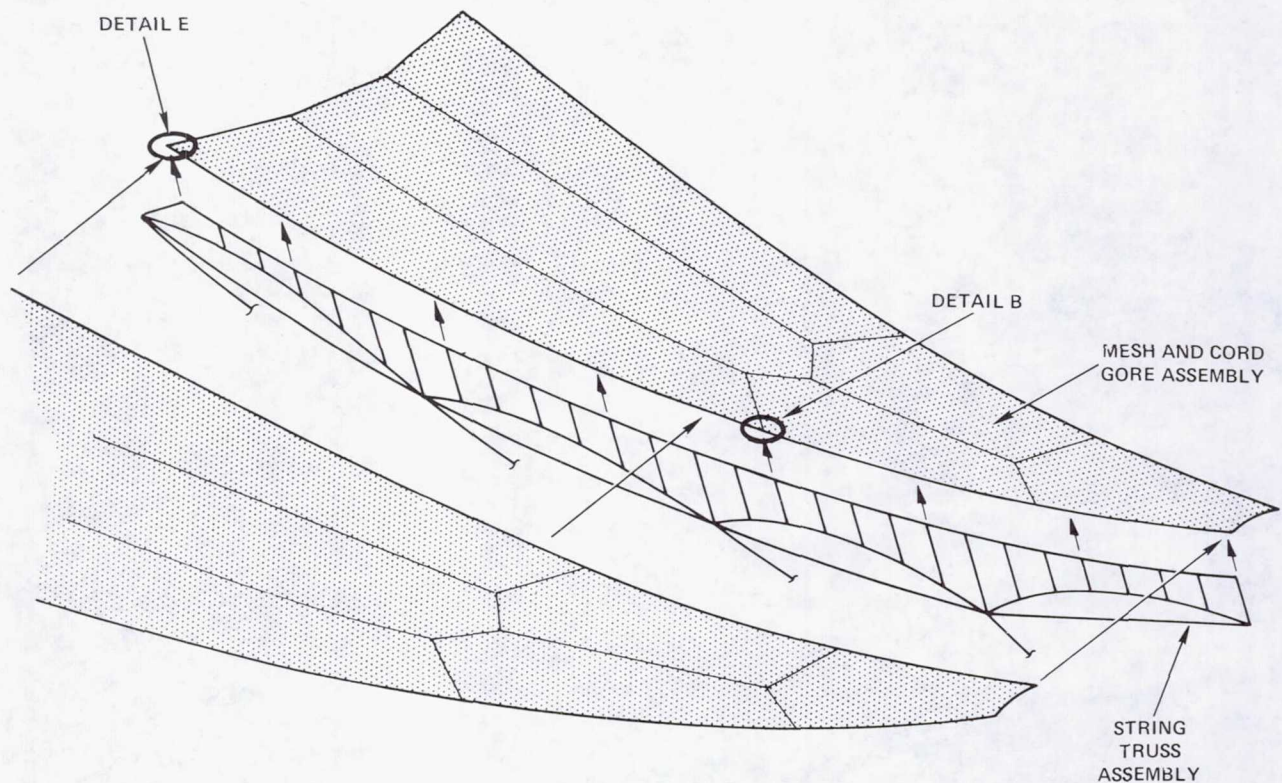
The string truss system is fabricated on a flat pattern surface located on the floor. Plywood provides an adequate surface; however, the major node points are anchored directly to the concrete floor for dimensional stability.



MAJOR SUBASSEMBLY

Two adjacent front cord assemblies and a string truss assembly are laced together at their common front cord interface line.

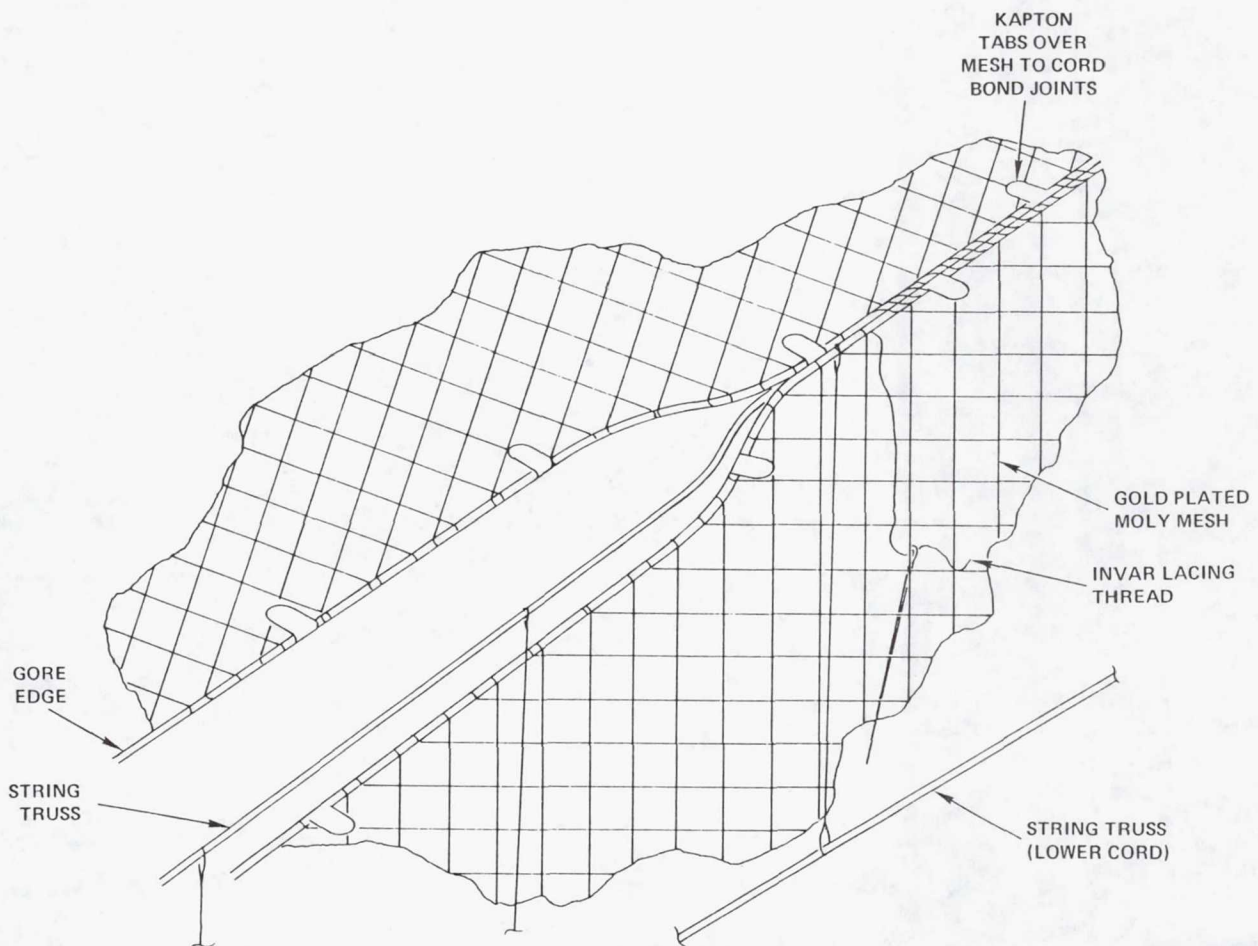
GORE ASSEMBLIES AND STRING TRUSS ASSEMBLIES ARE LACED TOGETHER AT TOP ASSEMBLY



ADJACENT GORE AND STRING TRUSS LACING

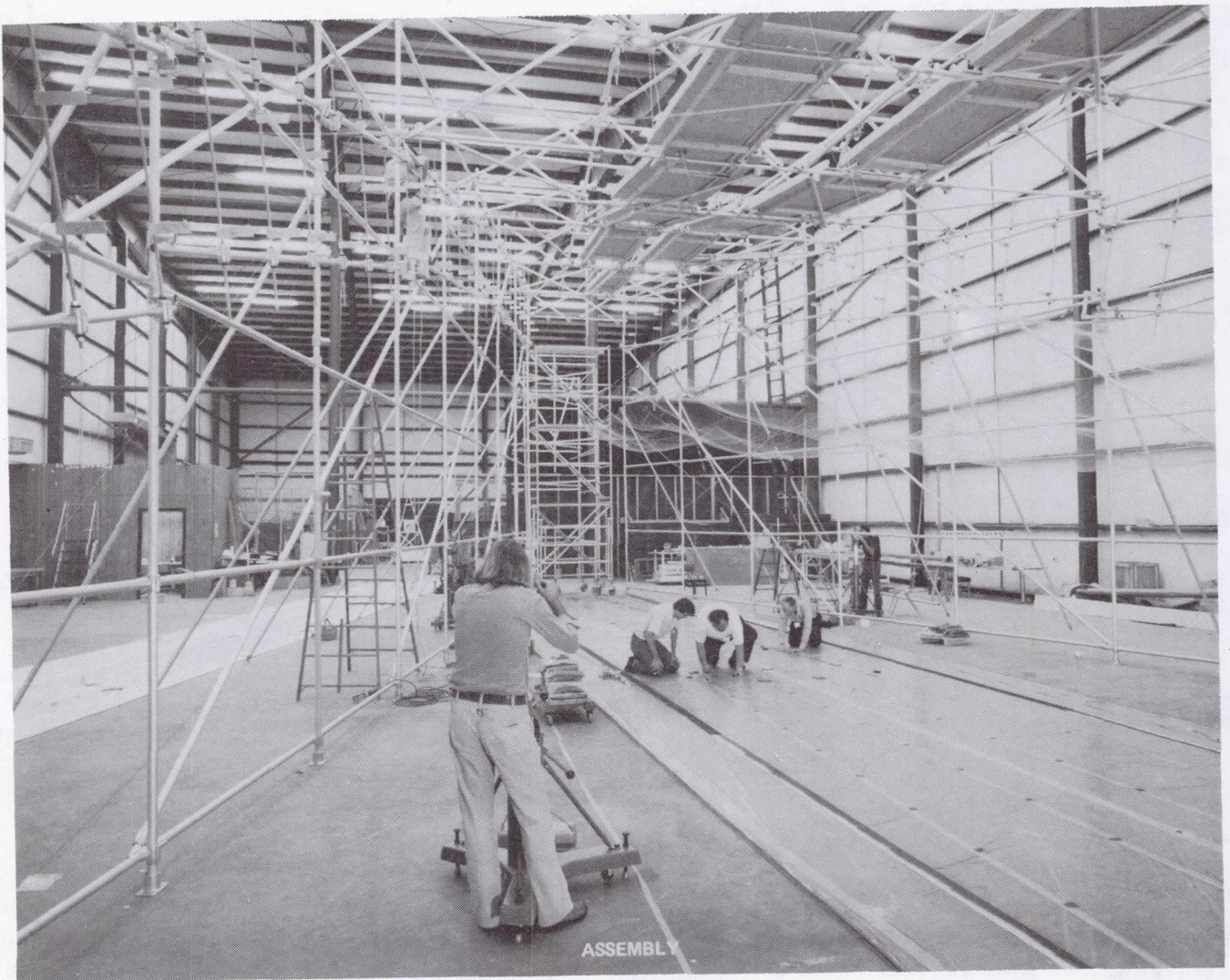
The adjacent gores and associated string truss are laced together by a 49-strand invar thread material. Spot bond joints are accomplished every $\frac{1}{3}$ meter to prevent mesh/cord motion subsequent to removing them from tooling.

ADJACENT GORES AND STRING TRUSS ARE LACED TOGETHER



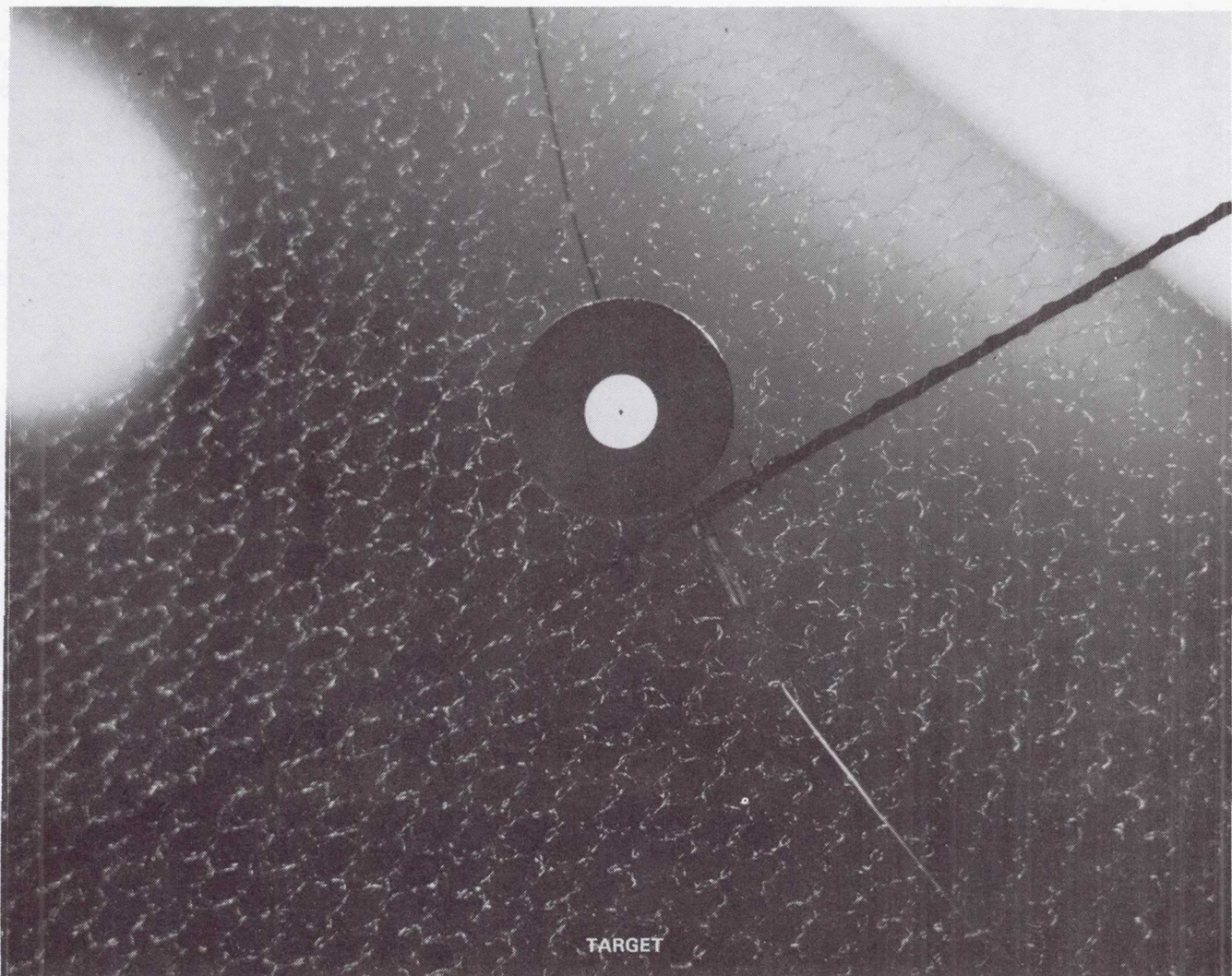
ASSEMBLY

This is a photo looking from the hoop toward the simulated mast of the model. Workers are shown in the process of fabricating the front cord system. Two completed gores may be seen temporarily hung from the boundary structure. Theodolites are strategically placed around the model for measurements and verification of major geometry points.



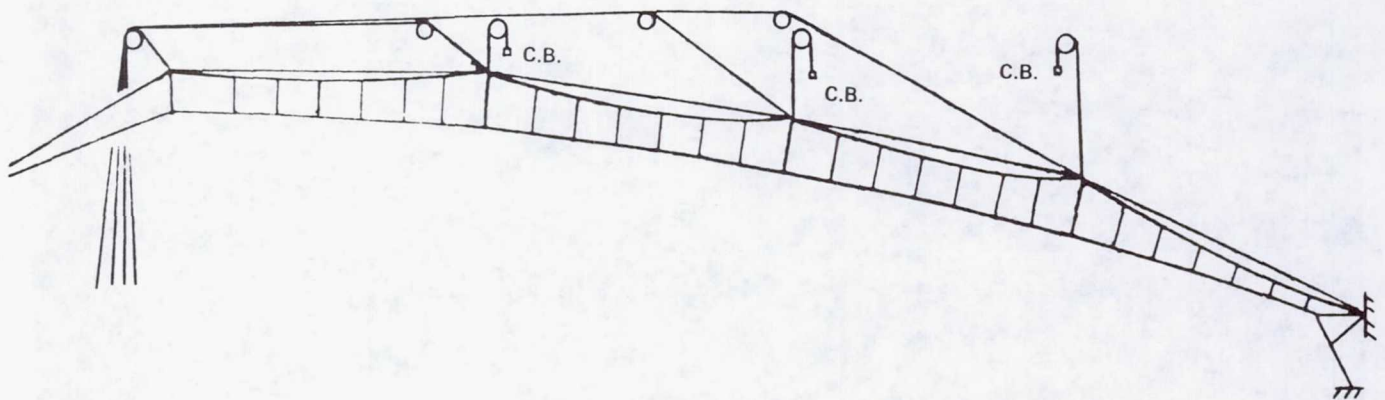
TARGET

Targets are located in predesignated areas on the surface to characterize the contour. They are constructed of printed thin film which sandwiches the mesh.



CONTROL CABLE ADJUSTMENT

The surface of the model may be enhanced by adjustment of the surface control cables. Also shown in the figure below are the counter balance cables which aid in the simulation of a zero gravity contour.

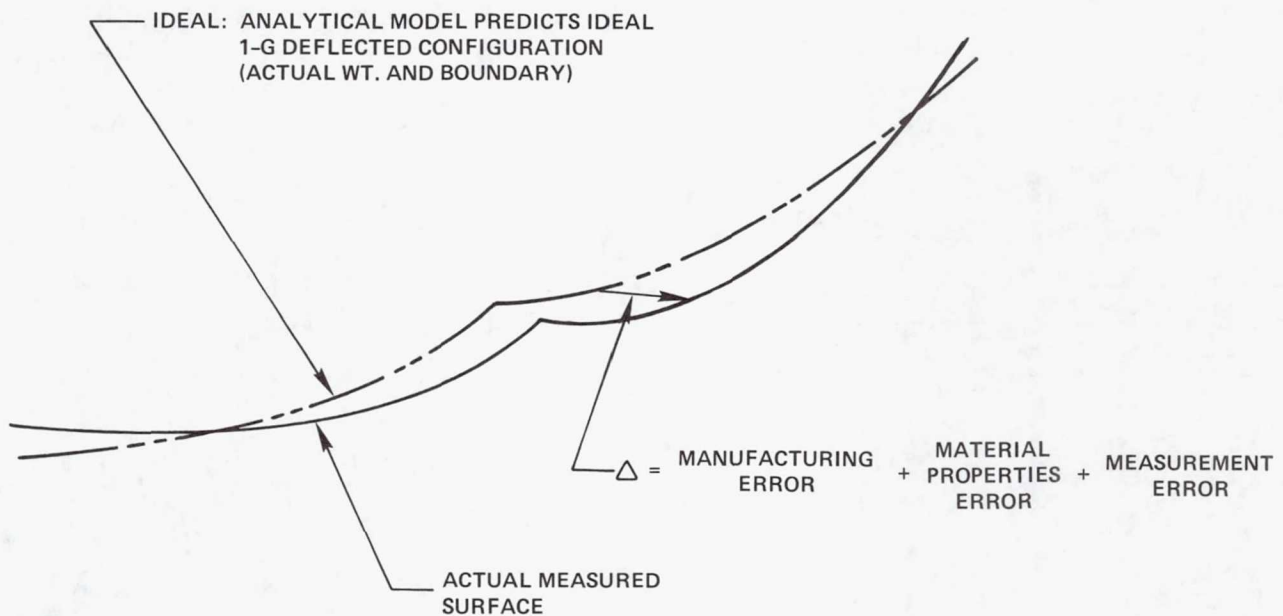


C.B. = COUNTERBALANCE POINTS

SURFACE VERIFICATION

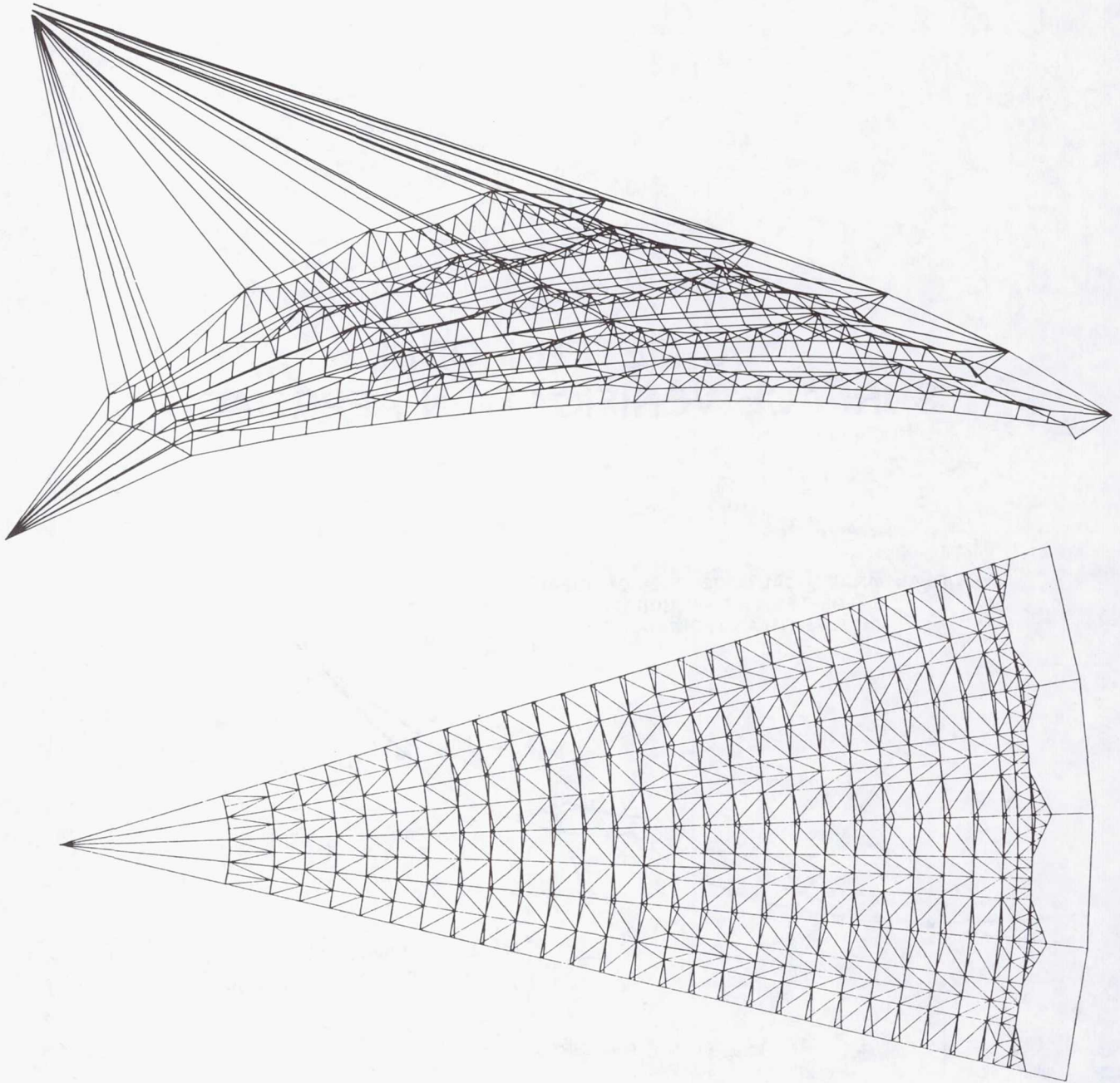
Harris has generated an analytical model which takes into account gravity and actual boundary conditions. This analytically generated contour is compared to the as-measured contour to ascertain the actual as-built error.

50-METER MODEL SURFACE VERIFICATION APPROACH



SURFACE MODEL FINITE-ELEMENT MODEL

Detailed analytical models were made to assess the performance of the 50-Meter Surface Model. The figures below are graphic representations of the four-gore finite-element model used in the analysis. Artificial displacements were induced in each control cord to determine the resulting surface perturbation. This data then permitted an evaluation of the overall adjustment capability of the entire model. The next figure displays the results of this analysis.

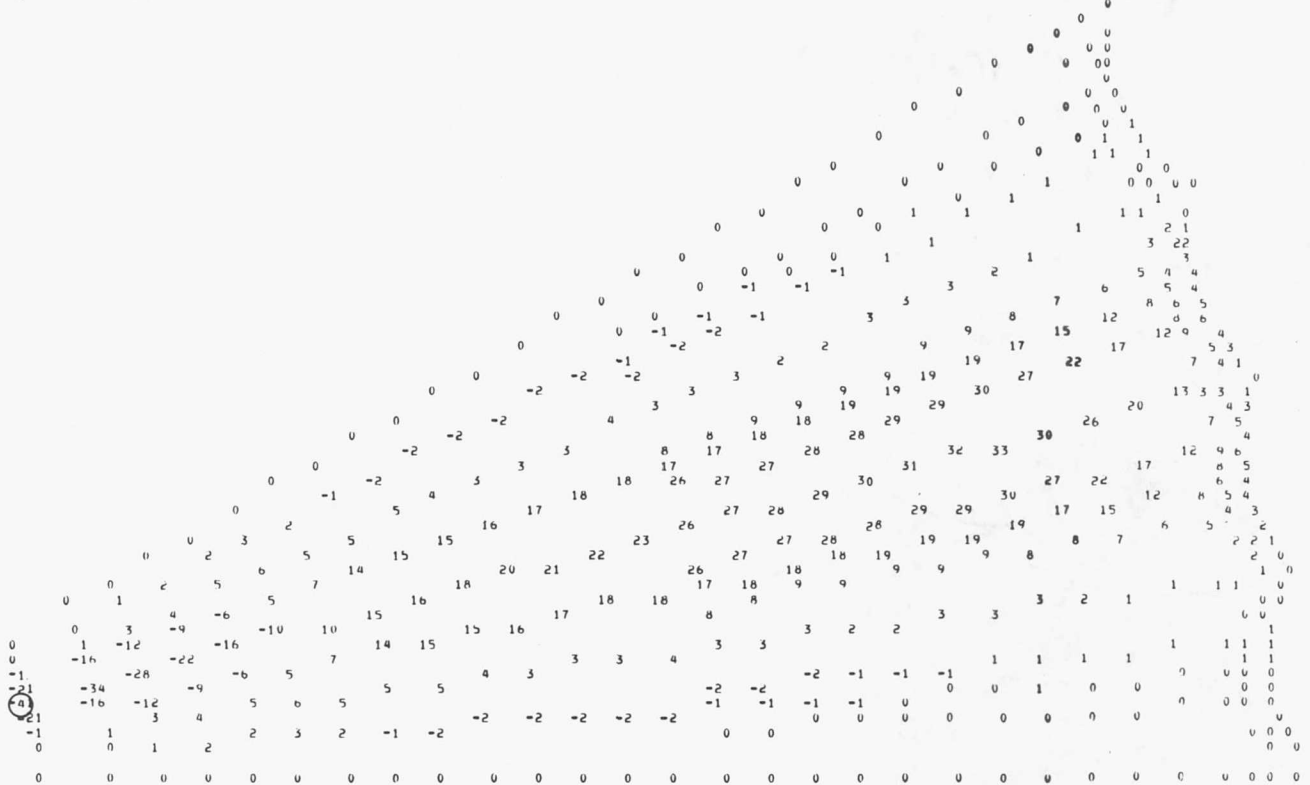


FIRST CONTROL CORD

After the surface is adjusted by means of control cable adjustments, the contour is measured and the results are compared with those predicted by an analytical interaction model. Relative node displacements are shown below as a result of the adjustment of the in-board control cord.

LSST FIRST CONTROL CORD
DOF 1 BEING PLOTTED

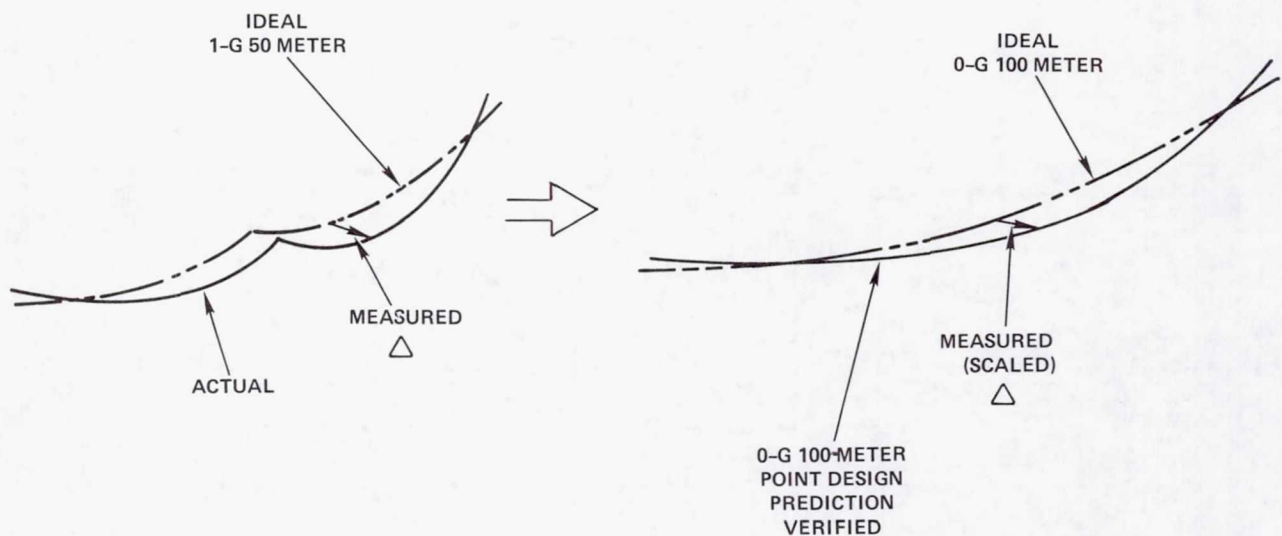
LSST FIRST CONTROL CORD
DOF 1 BEING PLOTTED



100-METER VERIFICATION

Measured deviations from the 1-G Ideal 50-Meter surface will be extrapolated and used to verify the predicted deviations related to the 0-G 100-Meter point design surface.

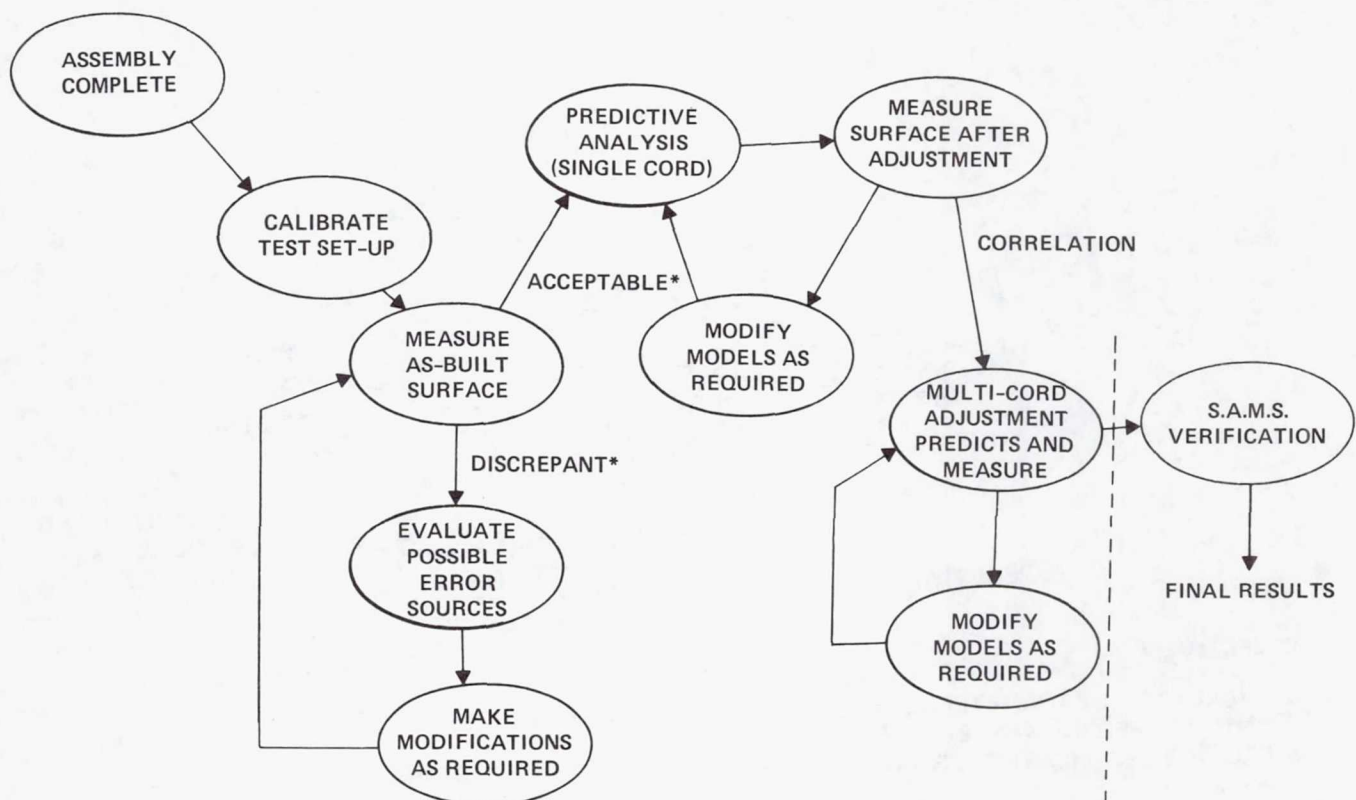
50-METER MODEL VERIFIES 100-METER POINT DESIGN



50-M SURFACE ADJUSTMENT BREADBOARD TEST FLOW

The test flow for the surface adjustment breadboard involves iterative measurements and adjustments of either the model or analytical software. The influence coefficients of each adjustment will be determined analytically and correlated by test. This method will result in a full interaction model capable of predicting cable displacements required to enhance the surface in orbit.

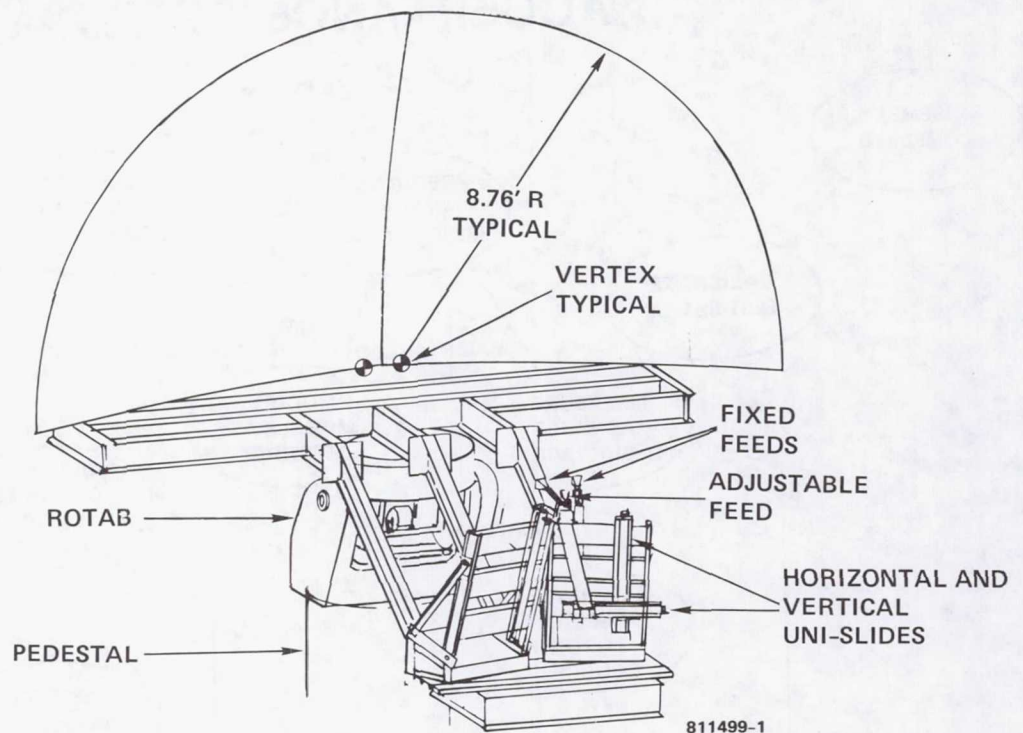
50-METER MODEL TEST FLOW AND ACCEPTANCE CRITERIA



*ACCEPTANCE CRITERIA:
DEFocus ≤ 3.95 CM (1.55 IN)
RMS ≤ 0.212 CM (0.083 IN)

RF VERIFICATION MODEL

Fabrication of the RF Verification Model is underway and will be in operation by March 1982. Shown below is a perspective of the model.



OBJECTIVES:

- EVALUATE RF PARAMETERS CRITICAL TO THE MULTIBEAM QUAD-APERTURE ANTENNA PERFORMANCE
- PROVIDE VERIFICATION OF CRITICAL PARAMETERS THROUGH TEST AND ANALYSIS
- VERIFY ANALYTICAL METHODS

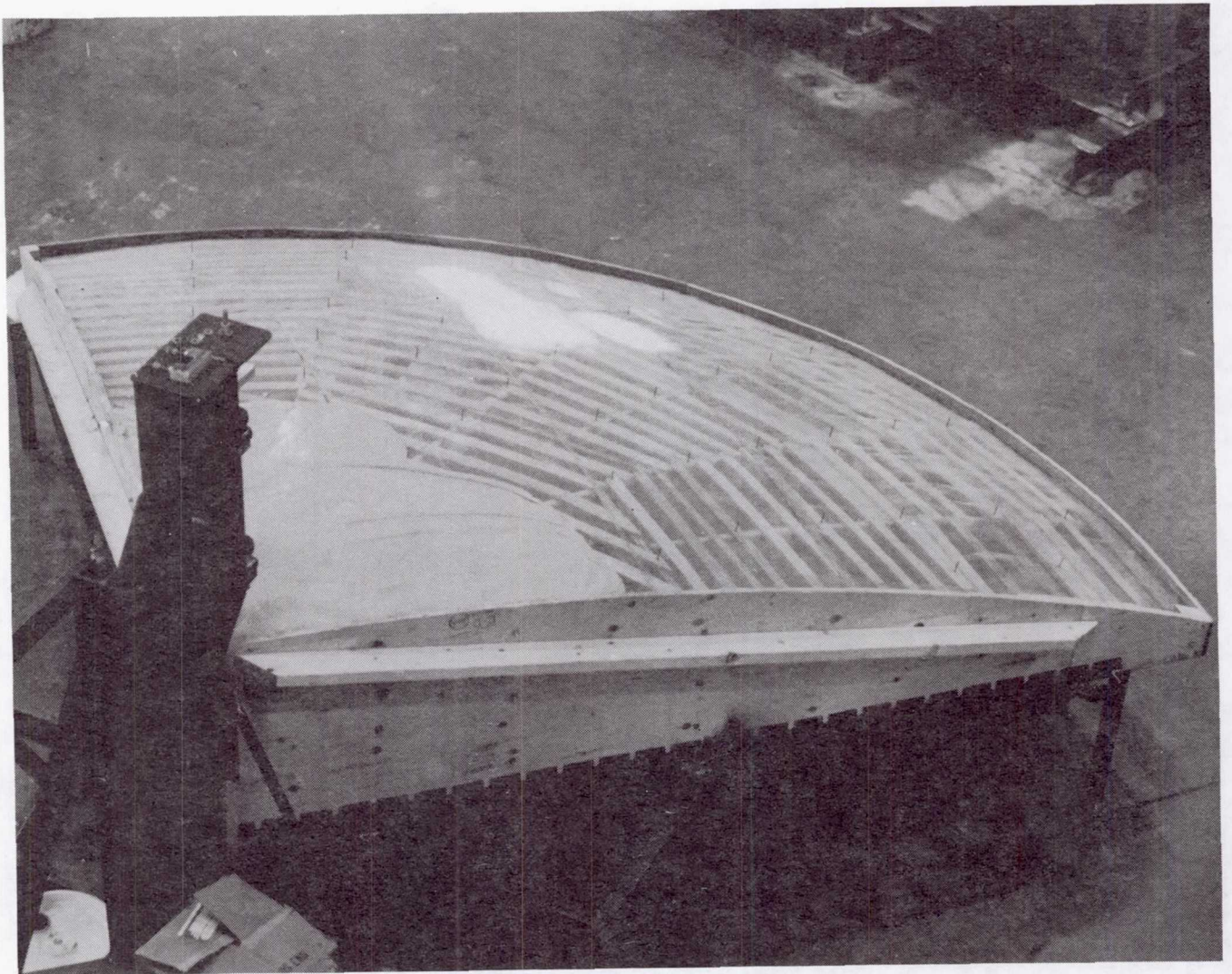
ANTENNA RANGE

Below is a view of the Harris antenna far field range from the roof mounted pedestals. The various source towers give Harris the capability to check many different parameters of antennas. The tower on the extreme right is set up for the LSST Model RF Verification testing.



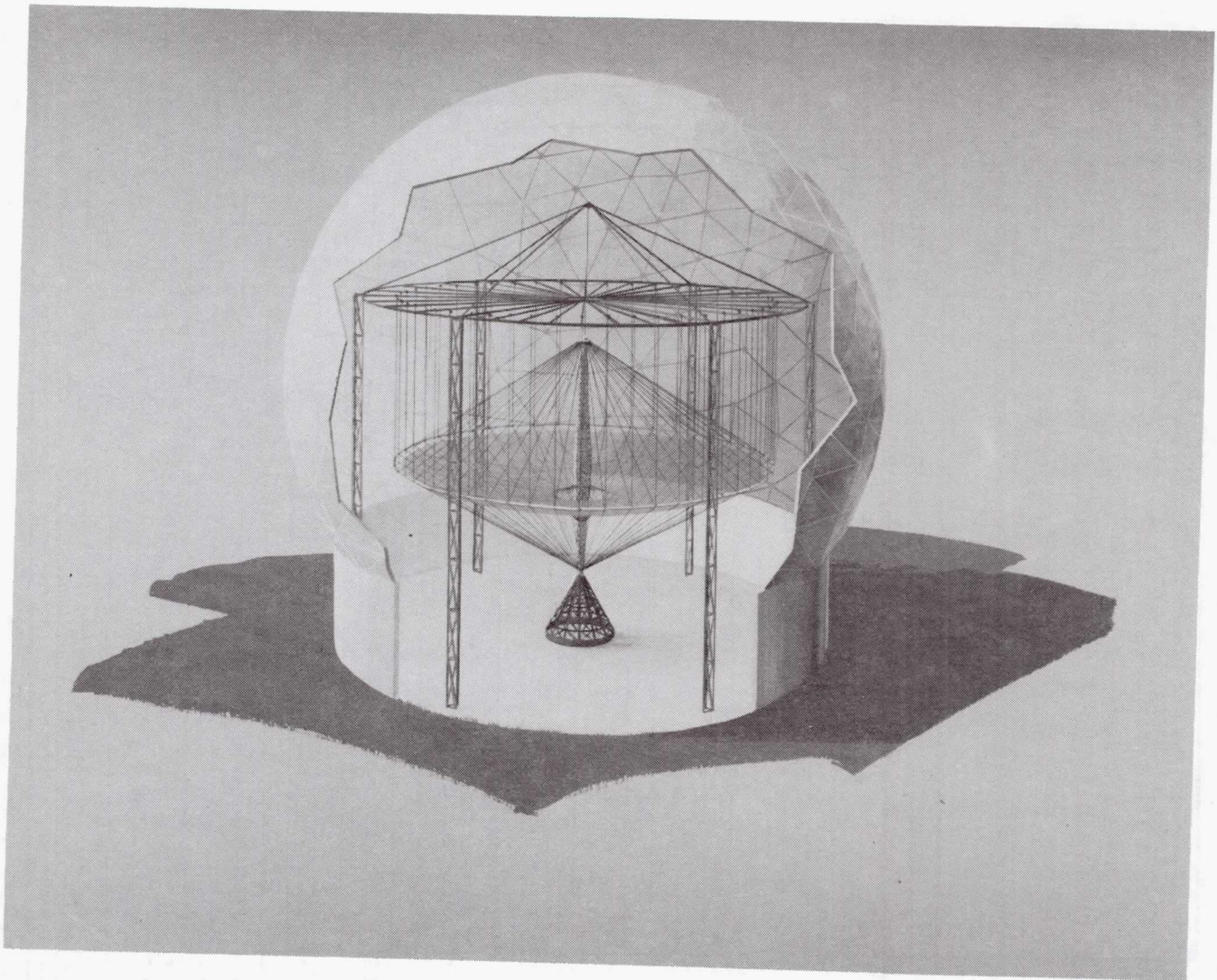
MOLD

Pictured below is the partially finished mold for fabrication of the LSST RF Verification Model antenna reflector. The accuracy of the mold along with the rigidity of the backup structure and surface adjustment capability will allow the accuracy of the reflector to be better than 0.010-inch rms. The reflectors and backup structure are scheduled for delivery by February 1982.



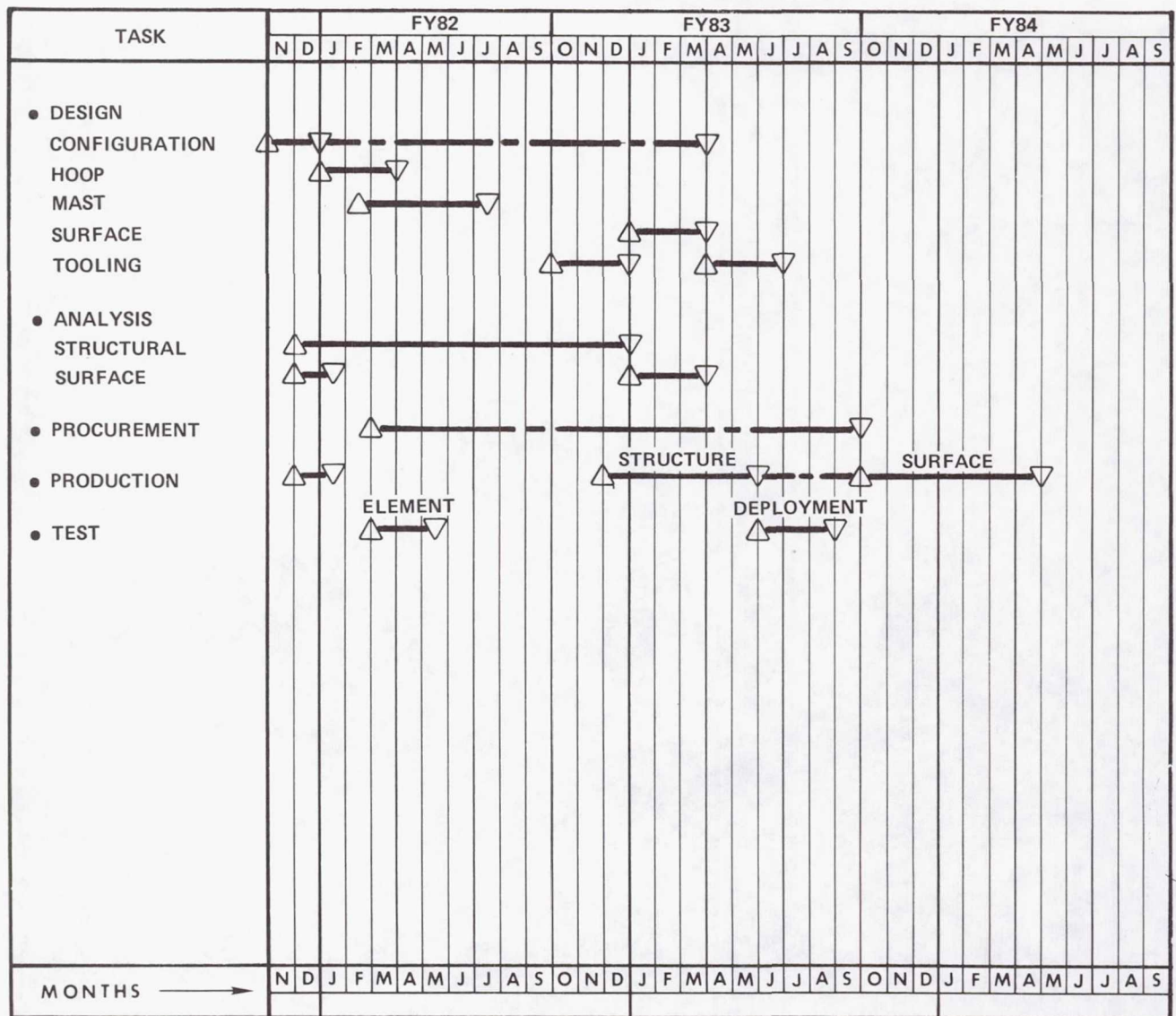
15-METER MODEL

The 15-Meter Kinematic Model will verify the overall deployment scheme of the Hoop/Column antenna. The model will be capable of deployment and stow cycles, repeatability measurements, cup-up/cup-down measurements and a series of deployment and failure modes testing. It is anticipated that the model will be fabricated in the Harris radome as shown below.



Activities associated with the 15-Meter Model are anticipated to run into FY 84. Below is an overall schedule with time lines for the major tasks.

15-METER ENGINEERING MODULE SCHEDULE



RADIO FREQUENCY VERIFICATION TASKS RELATED TO A
MULTIPLE APERTURE REFLECTOR SYSTEM

Thomas G. Campbell
NASA Langley Research Center
Hampton, Virginia

Large Space Systems Technology - 1981
Third Annual Technical Review
November 16-19, 1981

OBJECTIVES

A significant program element associated with the technology development of the Hoop/Column antenna concept is the radio frequency verification task. This task is believed to be of the utmost importance since it must be shown that these large space concepts will indeed be suitable for large aperture, high gain, multiple beam antenna systems. The objectives of this task are presented in figure 1. The multiple aperture multiple-beam configuration is the baseline configuration for this effort.

- TO ESTABLISH ANALYTICAL METHODS FOR PREDICTING THE ELECTROMAGNETIC PERFORMANCE OF MULTIPLE OFFSET FED APERTURES FOR MULTIPLE BEAM LARGE SPACE ANTENNA SYSTEMS.
- TO DEVELOP EXPERIMENTAL MODELING TECHNIQUES FOR VERIFYING THE ANALYTICAL METHODS USED IN PREDICTING THE EFFECTS OF SURFACE ROUGHNESS (PILLOWS), SCATTERING, AND APERTURE COUPLING ON RF PERFORMANCE.

Figure 1

DISCUSSION OF QUAD-APERTURE REFLECTOR CONFIGURATION

The configuration of a quad-aperture, multiple aperture reflector using the Hoop/Column configuration is shown in figure 2. The light colored regions of each quadrant simply indicate the illuminated regions depending upon the feed illumination tapers assumed. Actually, mesh will be attached to the cable truss system throughout the quad area.

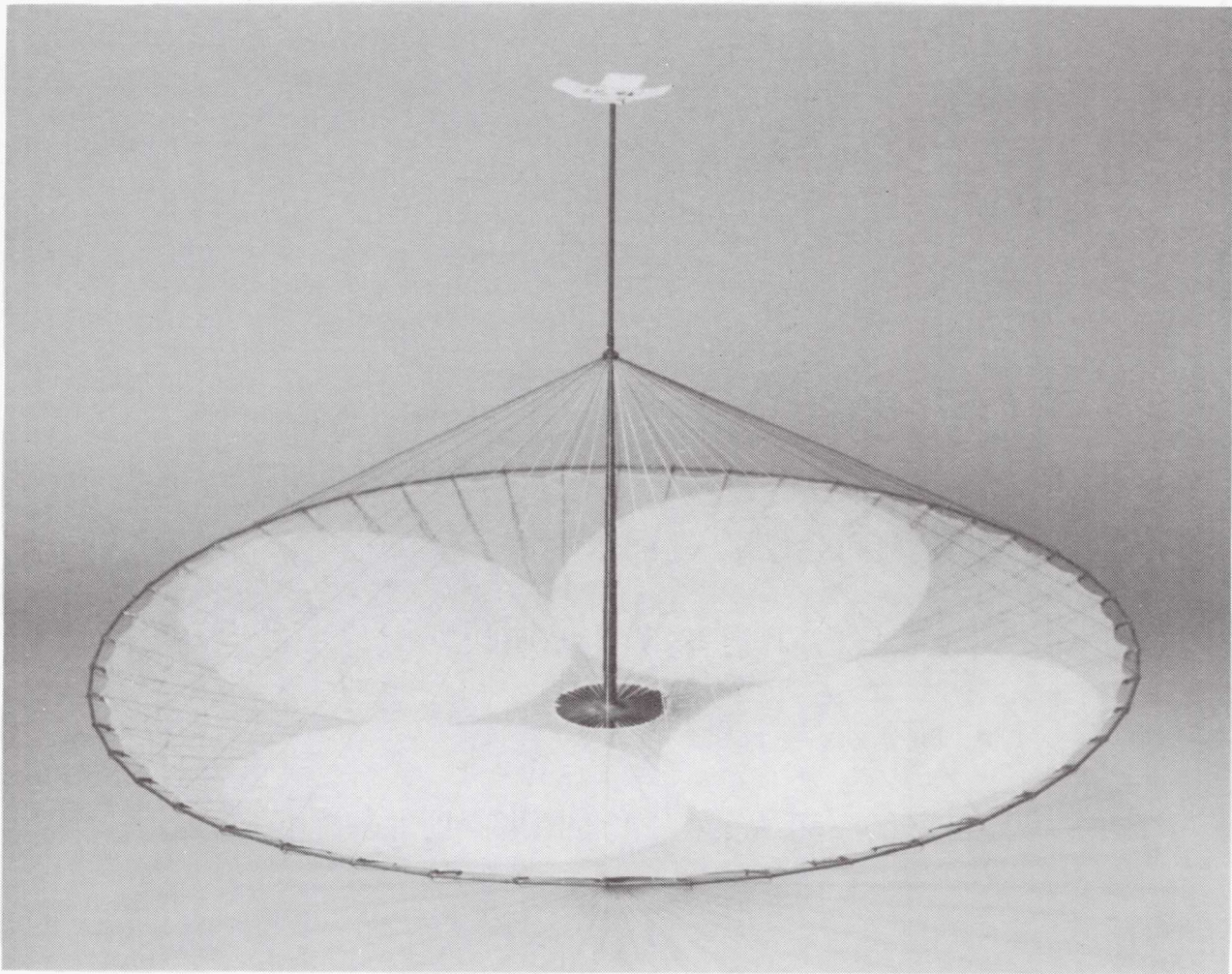


Figure 2

ATTRIBUTES OF A MULTIPLE APERTURE APPROACH FOR MULTIPLE BEAM APPLICATIONS

The expected attributes of a multiple aperture system are listed in figure 3. The primary advantage will be to reduce the complexity of a given feed system as the apertures (uplink, downlink, etc.) can be separated. The capability for using multiple apertures in achieving a required spot or contiguous beam topology plan will indeed enhance the RF design as attempts are made in meeting the stringent multiple beam requirements projected for future systems.

- REDUCE DEPLOYMENT MECHANISMS
- PROVIDE EFFICIENT STOWED VOLUME
- IMPROVED BEAM ISOLATION
- IMPROVED FEED ARRAY PACKAGING, DEPLOYMENT, ETC.

Figure 3

MULTIPLE APERTURE ANTENNA SYSTEM USING THE HOOP/COLUMN CONCEPT

A paper was presented during the LSST Second Annual Technical Review by Mr. Peter Foldes on the utilization of a multiple-aperture Hoop/Column approach for multiple-beam systems. This reference is listed in figure 4.

NOTE: THE MULTIPLE APERTURE ANTENNA SYSTEM USING THE HOOP/COLUMN CONCEPT IS DISCUSSED IN PAPER PRESENTED AT SECOND ANNUAL TECHNICAL REVIEW, LSST-1980 BY PETER FOLDES, GENERAL ELECTRIC COMPANY.

REF: OFFSET FED UTILIZATION OF FOUR QUADRANTS OF AN AXIALLY SYMMETRICAL ANTENNA STRUCTURE.

Figure 4

REFLECTOR PARAMETER DESIGN VERIFICATION TASKS

In addressing the radio frequency verification tasks, it was necessary to coordinate the activities between the contractual (Harris) efforts and the in-house (LaRC) antenna pattern tests. Also, most of the key antenna parameters will be addressed analytically and experimentally (for analysis verification). The breakdown of the test and analysis activities are presented in figure 5. The mesh surface (construction) technique is the only area that will not be tested as well as analyzed.

KEY PARAMETERS	VERIFICATION TECHNIQUE	
	TEST	ANALYSIS
MULTIBEAM INTERLEAVING	X	X
BEAM-TO-BEAM ISOLATION	X	X
BEAM PARAMETERS		
GAIN	(X)	X
BEAMWIDTH*	(X)	X
SIDELOBES*	(X)	X
POLARIZATION EFFECTS	(X)	X
EDGE-OF-SCAN EFFECTS	X	X
DUAL-BAND EFFECTS	X	X
SURFACE EFFECTS		X
MESH CONSTRUCTION		X
● HARD AND SOFT		X
● REFLECTIVITY		X
ROUGHNESS		X
● PILLOWS	(X)	(X)
● CONTOURING		(X)
RIM		X
CABLE EFFECTS	(X)	(X)

X HARRIS TASKS, (X) HARRIS, LARC TASKS

*SOLID ANGLE COVERAGE

Figure 5

PRELIMINARY EXPERIMENTAL TEST RESULTS USING
35 GHz OFFSET FED REFLECTOR SIMULATING
SURFACE PILLOWS AND APERTURE CABLES

Thomas G. Campbell and W. Robert Young
NASA Langley Research Center
Hampton, Virginia

Large Space Systems Technology - 1981
Third Annual Technical Review
November 16-19, 1981

TEST OBJECTIVE

The subject of this presentation is to present the preliminary experimental results of the 35 GHz pattern tests that were conducted in the Antenna Test Facility at LaRC. The objective of these tests is listed in figure 1. The effect of surface pillows and aperture cables has been of concern throughout the technology development activities for the Hoop/Column antenna. The effect of aperture cables was reported on briefly during the Second Annual Technical Review but that test was conducted using available hardware at a $F/D \approx 1.0$. This test uses models that have been designed to be replicas of a quad aperture at the proper $F/D=1.50$ as provided in the LSST point design. Separate pillow models were machined from solid aluminum sections that simulated the surface contour pillows but on an exaggerated basis. The worse case pillow heights $\lambda/20$ and $\lambda/5$ were machined onto the precision reflector. The exact pillow geometry will be described later. In addition to the pillow effects, the scattering effects of aperture (Hoop/Column cables) cables were determined. Therefore, simulated quartz and graphite cables were tested with the smooth, $\lambda/20$, and $\lambda/5$ reflector models.

TO PROVIDE EARLY ASSESSMENT OF THE EFFECTS CAUSED
BY REFLECTOR SURFACE PILLOWS AND APERTURE CABLES
ON RF PERFORMANCE OF OFFSET FED REFLECTOR SYSTEMS.

Figure 1

CLASSES OF REFLECTOR SURFACE IRREGULARITIES

The categories of errors that will degrade reflector performance are listed in figure 2. Obviously, the periodic errors will include the effect of contour surface pillows, facets, and surface roughness.

SYSTEMATIC ERRORS: CAUSED BY THERMAL EXPANSION OR MECHANICAL STRESS. CAUSES BEAM BROADENING, HIGH SIDELobe LEVELS.

RANDOM ERRORS: MANUFACTURING IMPERFECTIONS WHICH FORM IRREGULAR BUMPS ON REFLECTOR. CAUSES INCREASE IN FAR OUT SIDELOBES.

PERIODIC ERRORS: SURFACE ROUGHNESS, PILLOWS, AND FACETS PRODUCED BY PARTICULAR DESIGN. (EFFECTS BEING DETERMINED)

Figure 2

The method used in constructing the 35 GHz precision reflector models is shown in figure 3. A quad reflector was machined from a solid aluminum section using a numerically controlled milling machine. This machine was programmed in accordance with the surface equation and pillow distribution provided with the Hoop/Column design. The pillow heights were exaggerated in order to show "worst case" effects and sensitivity.

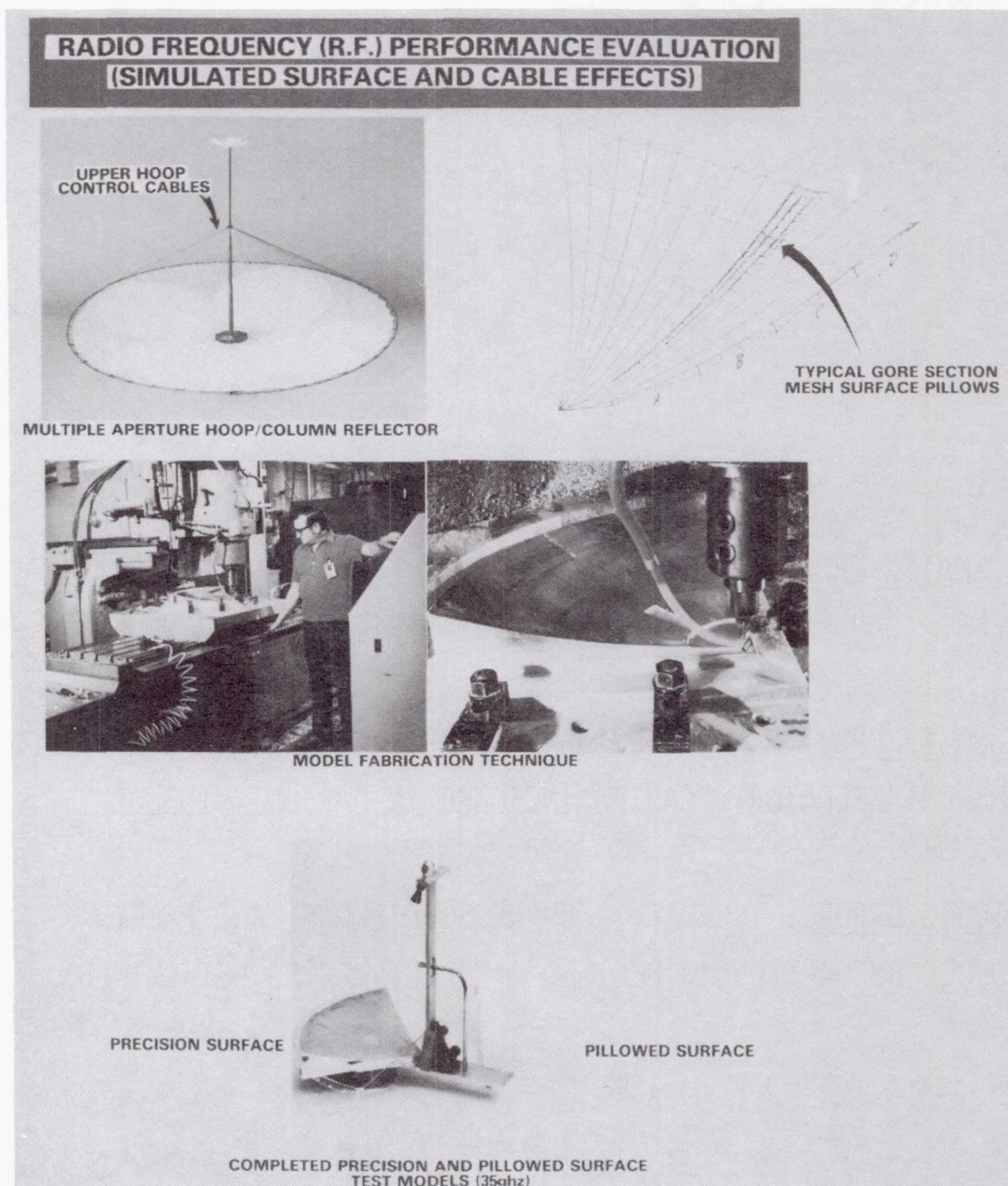


Figure 3

FEED HORN SUPPORT ARRANGEMENT AND THE 35 GHz PRECISION REFLECTOR MODEL

Figure 4 shows the feed horn support arrangement and the 35 GHz precision reflector model (with maximum pillow heights of $\lambda/20$) in the anechoic chamber for antenna pattern tests. A partial hoop is also shown for positioning the simulated hoop support cables at the proper location and angle with respect to the feed horn.

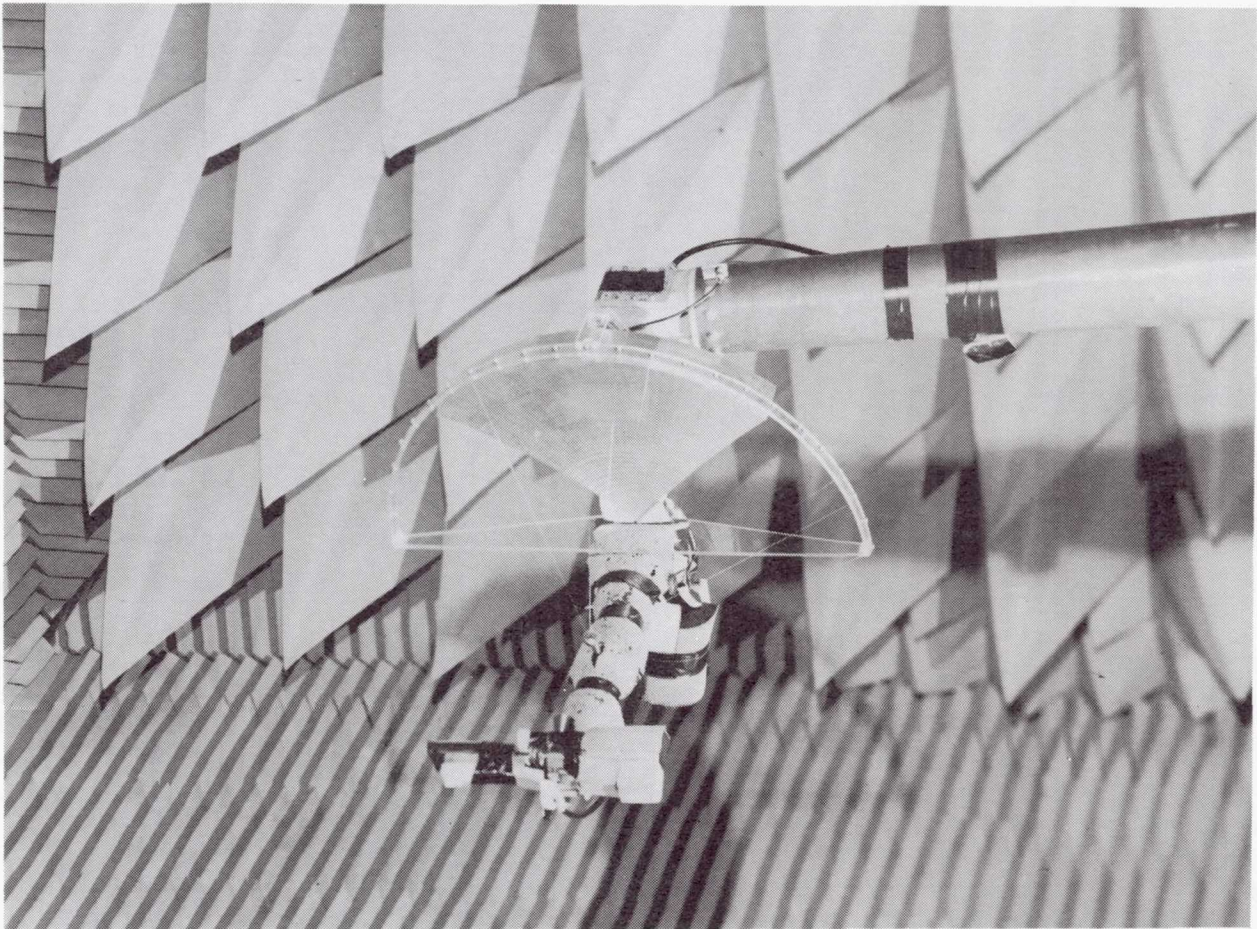


Figure 4

REFLECTOR REQUIREMENTS

This table shows the relative size of the radio frequency test models in diameter in wavelengths. These sizes can then be compared with the LSST Hoop/Column point design ($D_{\lambda} \approx 250$). It can be seen that achieving an adequate scale factor of the aperture size is a difficult task for antenna tests. Therefore, analysis will be needed in extrapolating performance for the larger aperture sizes.

	LSST HOOP/COLUMN POINT DESIGN	LARC 35 GHz TEST MODEL	HARRIS TEST MODEL
D_{λ}	250 (OFFSET)	35	118
F/D	1.5	1.5	1.5
G (dB)	55	38	49
HPBW	0.25°	1.9°	0.5°
BEAMS	55/APERTURE	SCAN TESTS	SCAN TESTS
BEAM ISOLATION (dB)	30	TBD	TBD

Figure 5

REFLECTOR/FEED GEOMETRY FOR MAST INTERACTION TESTS

Before antenna pattern tests were started, it was necessary to insure proper focus for the feed horn using the ($D_\lambda = 35$) precision offset reflector. The F/D was selected to be 1.5 as in the LSST point design. During the initial pattern runs, it was detected that significant pattern effects (reflection) were caused by the feed mast. This multipath effect caused a high sidelobe at 8 degrees from the main beam. This reflection was controlled by repositioning the feed mast and thereby moving the reflected rays out of the field of view of the feed horn. This could indeed be a significant problem as further discussions concerning mast designs are held.

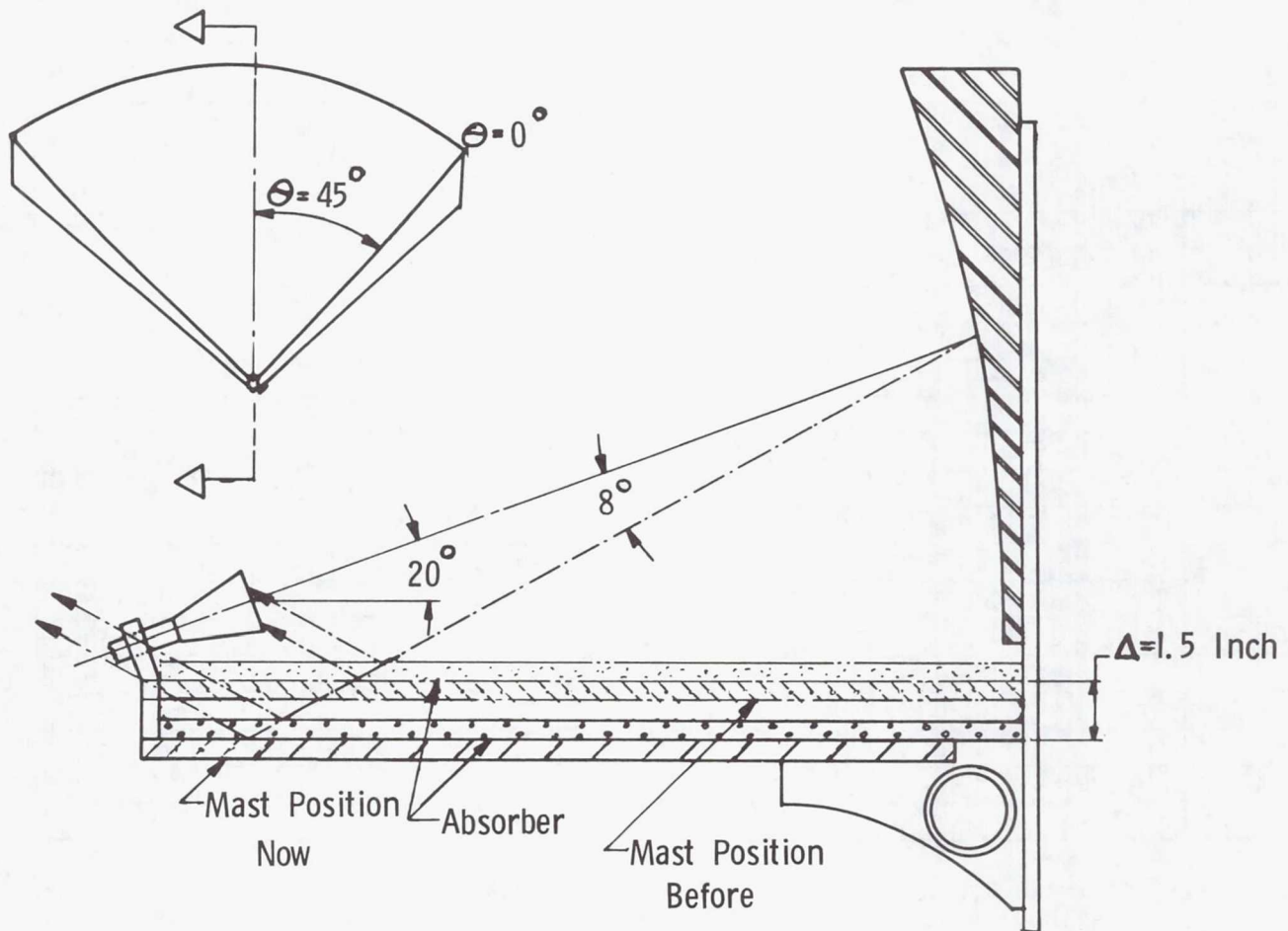
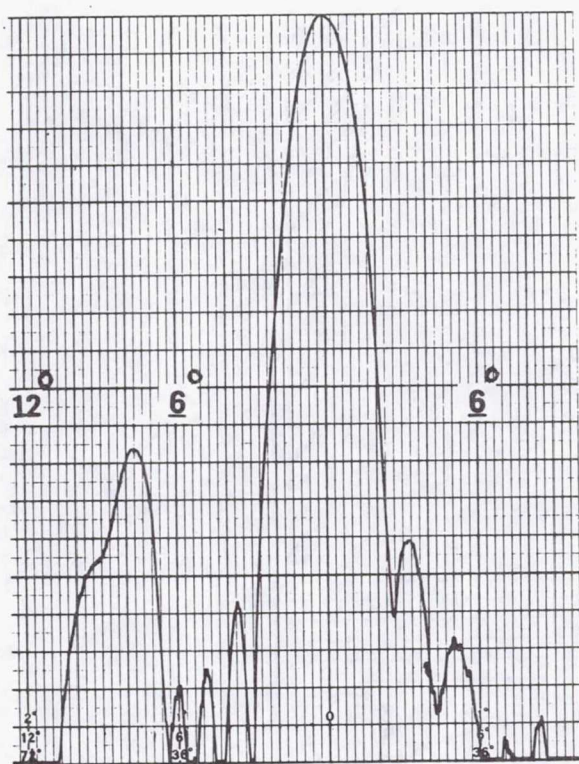


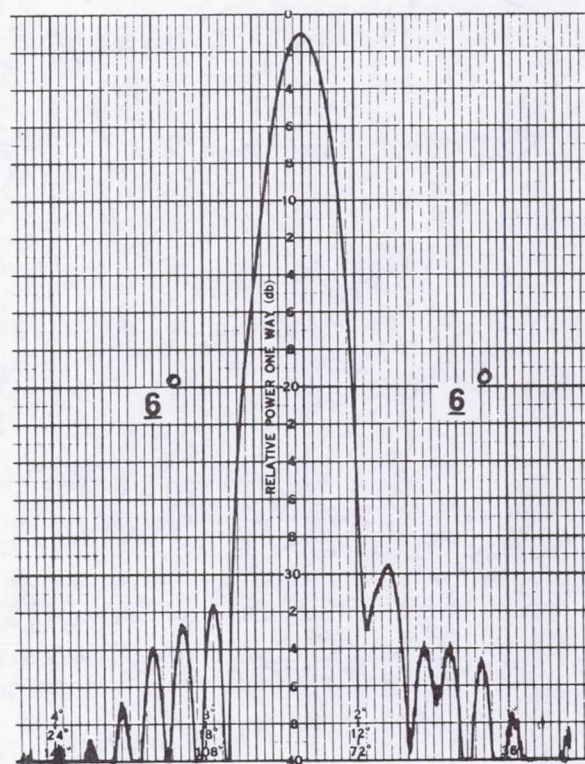
Figure 6

RADIATION PATTERN - 35 GHz OFFSET FED REFLECTOR MODEL (SMOOTH SURFACE)
ASYMMETRIC PLANE (E PLANE), PRINCIPAL POLARIZATION,
SHOWING FEED MAST INTERFERENCE EFFECTS

These radiation patterns show the effect of the feed mast. For example, the feed mast produced a sidelobe at 8 degrees from the main beam as shown in chart a. The mast was initially positioned in accordance with the LSST point design. In order to reduce the reflective effects, the mast had to be repositioned but still maintain the feed in the proper focused position. Absorber did not eliminate the reflection effect in the original mast portion. The pattern after relocating the mast is shown in chart b.



(A) FEED MAST IN ORIGINAL POSITION
WITHOUT ABSORBER



(B) FEED MAST ADJUSTED TO NEW POSITION
WITHOUT ABSORBER

$$F/D = 1.5 \quad D/\lambda = 35$$

Figure 7

POSSIBLE REFLECTOR RE-CONFIGURATION CAUSED BY
FEED/MAST INTERACTION EFFECTS

A possible effect of mast reflection is shown in this figure. If nonmetallic materials for mast design cannot be utilized, then proper separation distances between feed and mast will be required. This operation could cause an increase in the overall diameter of the space frame structure for the offset geometries. The effect on the Hoop/Column design is shown in this figure.

(100 METER POINT DESIGN)

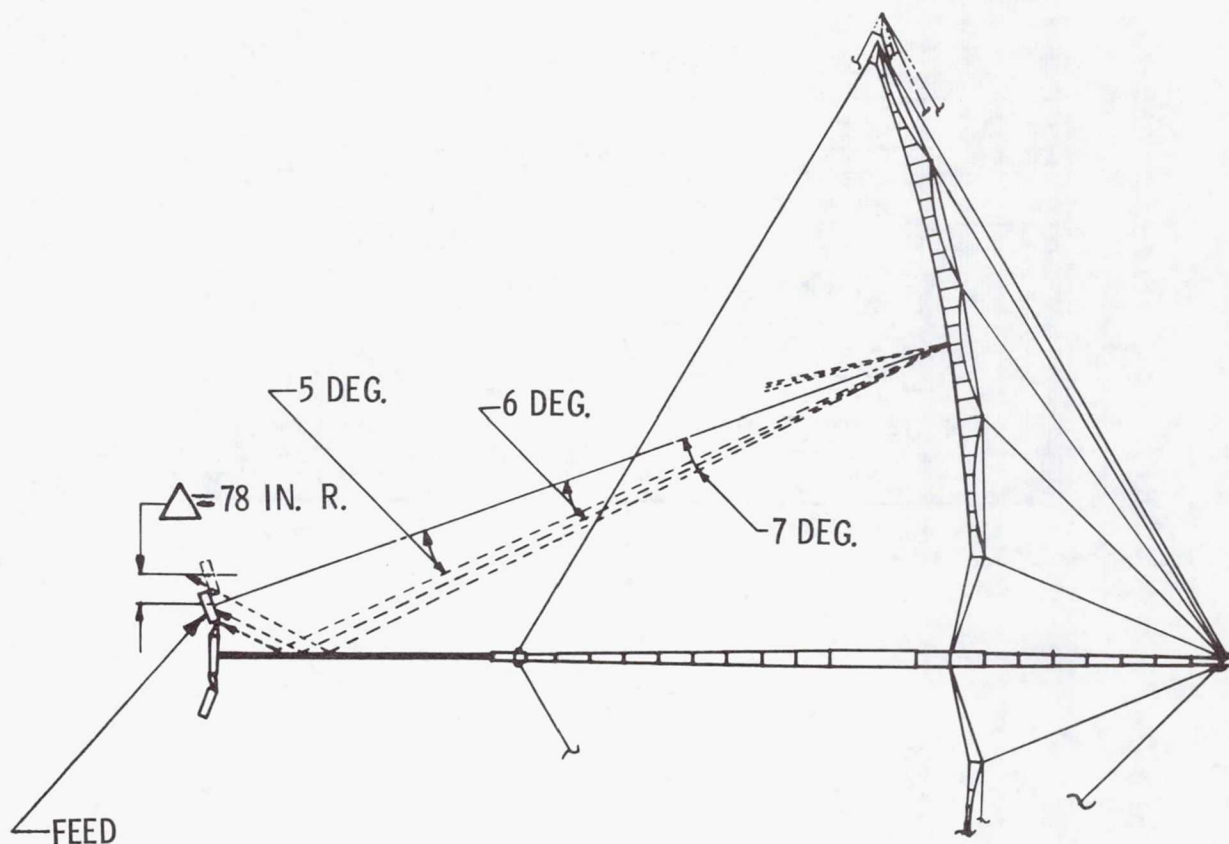


Figure 8

RADIATION PATTERN - 35 GHz OFFSET FED REFLECTOR MODEL IN THE
SYMMETRIC PLANE (H PLANE) - PRINCIPAL POLARIZATION

The preliminary results of the radiation pattern tests using the smooth, $\lambda/20$, and $\lambda/5$ pillow reflector models. A 40-dB dynamic range is provided, but in the future an improved dynamic range will be utilized. The effect of surface pillows is shown in figures 9a, 9b, and 9c.

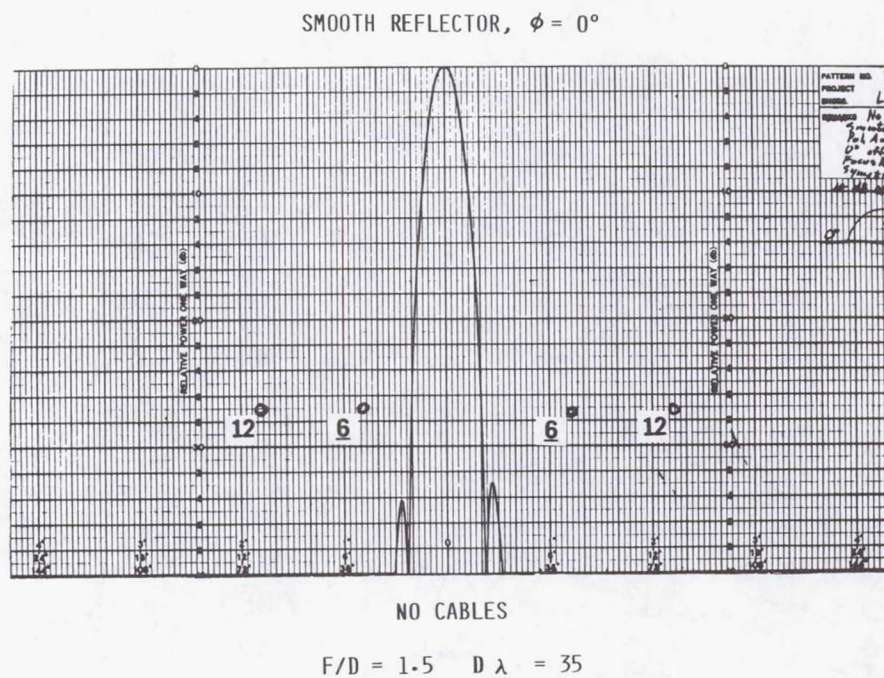
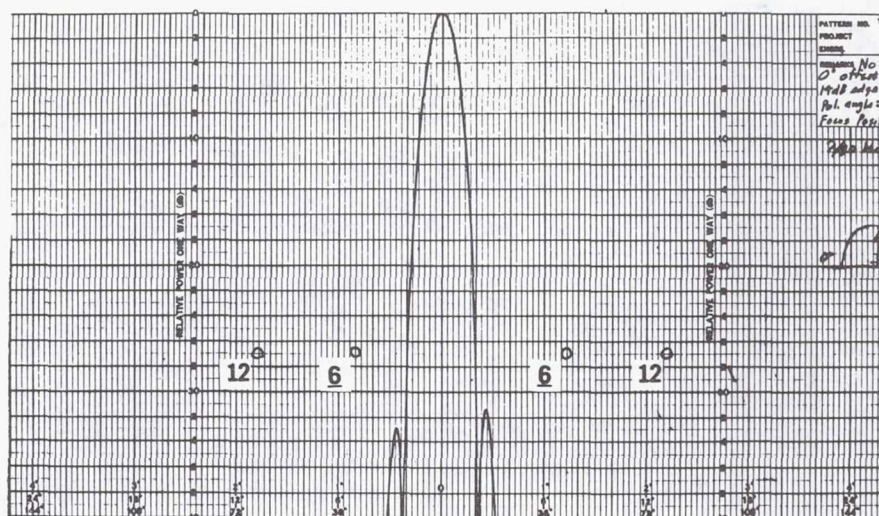


Figure 9a (Smooth Reflector)

RADIATION PATTERN - 35 GHz OFFSET-FED REFLECTOR MODEL IN THE SYMMETRIC
PLANE (H PLANE) - PRINCIPAL POLARIZATION

$\lambda/20$ PILLOWED REFLECTOR, $\phi = 0$

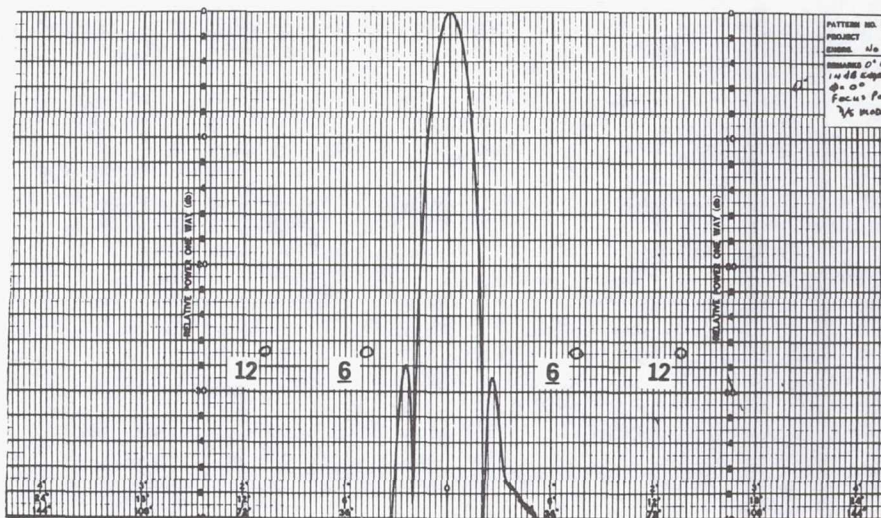


NO CABLES

$F/D = 1.5 \quad D \lambda = 35$

Figure 9b ($\lambda/20$ Reflector)

$\lambda/5$ PILLOWED REFLECTOR, $\phi = 0^\circ$



NO CABLES

$F/D = 1.5 \quad D \lambda = 35$

Figure 9c ($\lambda/5$ Reflector)

RADIATION PATTERN - 35 GHz OFFSET FED REFLECTOR MODEL IN THE
SYMMETRIC PLANE (H PLANE) - PRINCIPAL POLARIZATION

The scattering effects (or lack of effects) on the radiation pattern using quartz cables are shown in figures 10a, 10b, and 10c for the smooth, $\lambda/20$, and $\lambda/5$ reflector respectively.

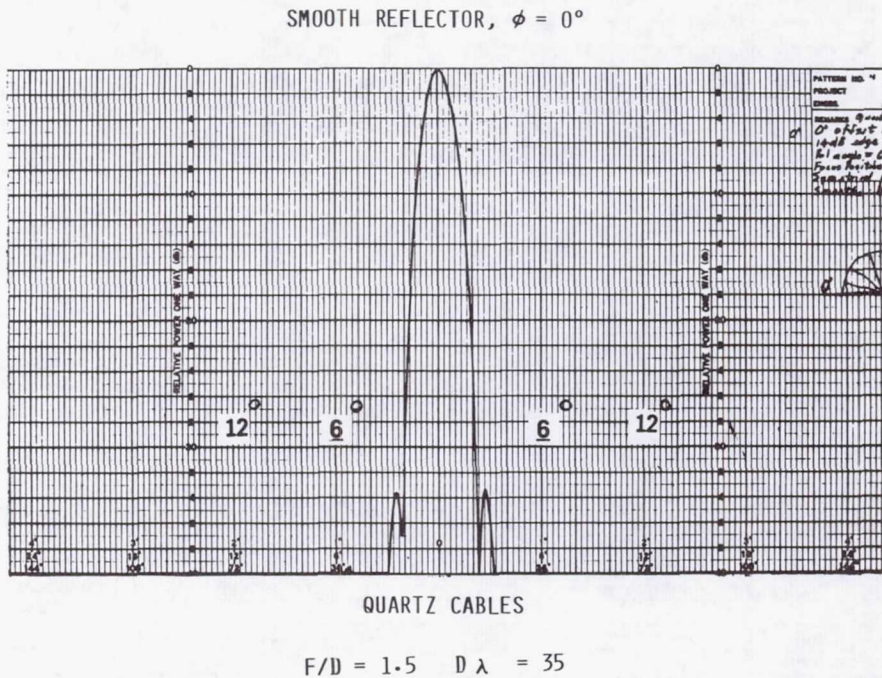
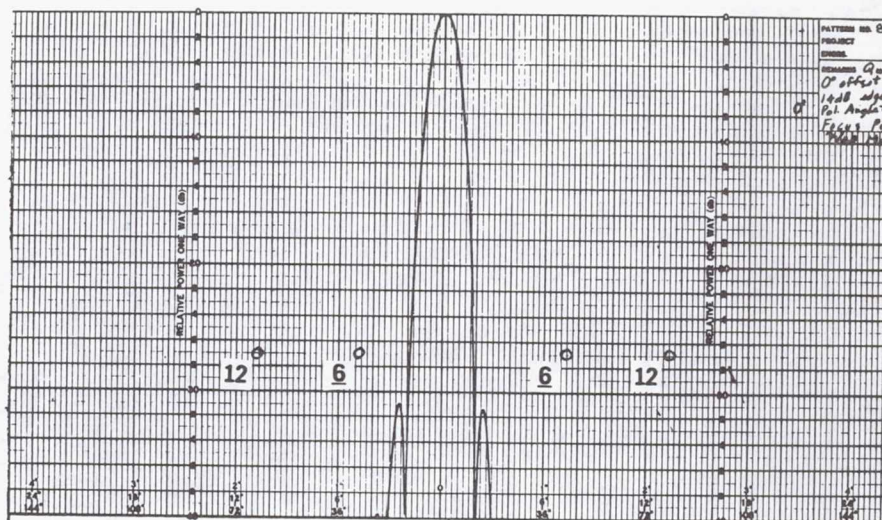


Figure 10a (Smooth Reflector)

RADIATION PATTERN - 35 GHz OFFSET-FED REFLECTOR MODEL IN THE SYMMETRIC
PLANE (H PLANE) - PRINCIPAL POLARIZATION

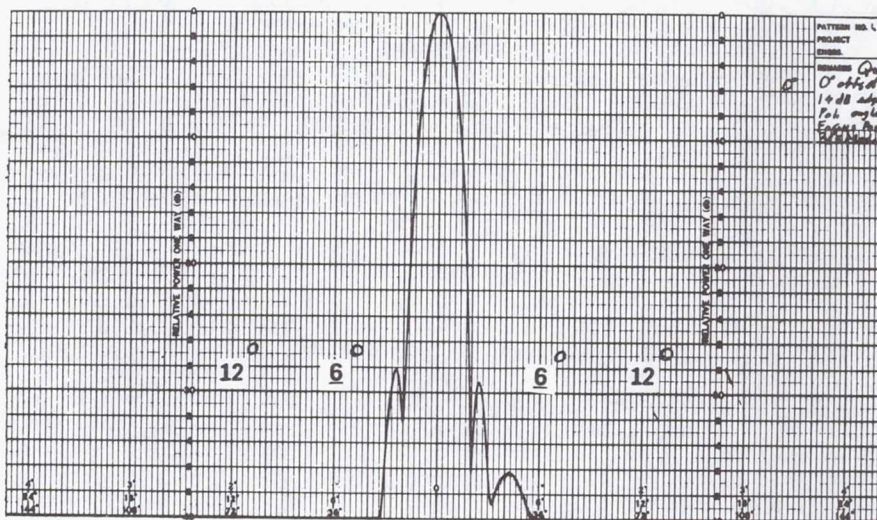
$\lambda/20$ PILLOWED REFLECTOR, $\phi = 0$



$F/D = 1.5 \quad D/\lambda = 35$

Figure 10b ($\lambda/20$ Reflector)

$\lambda/5$ PILLOWED REFLECTOR, $\phi = 0^\circ$

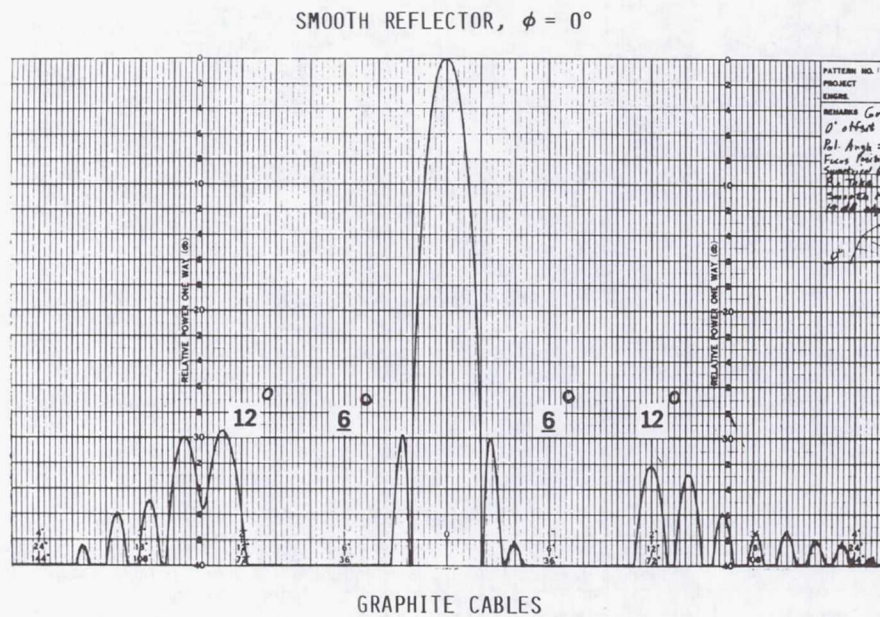


$F/D = 1.5 \quad D/\lambda = 35$

Figure 10c ($\lambda/5$ Reflector)

RADIATION PATTERN - 35 GHz OFFSET FED REFLECTOR MODEL IN THE
SYMMETRIC PLANE (H PLANE) - PRINCIPAL POLARIZATION

The scattering effects on the radiation patterns using graphite hoop support cables are shown in figures 11a, 11b, and 11c for the smooth, $\lambda/20$, and $\lambda/5$ reflector respectively.

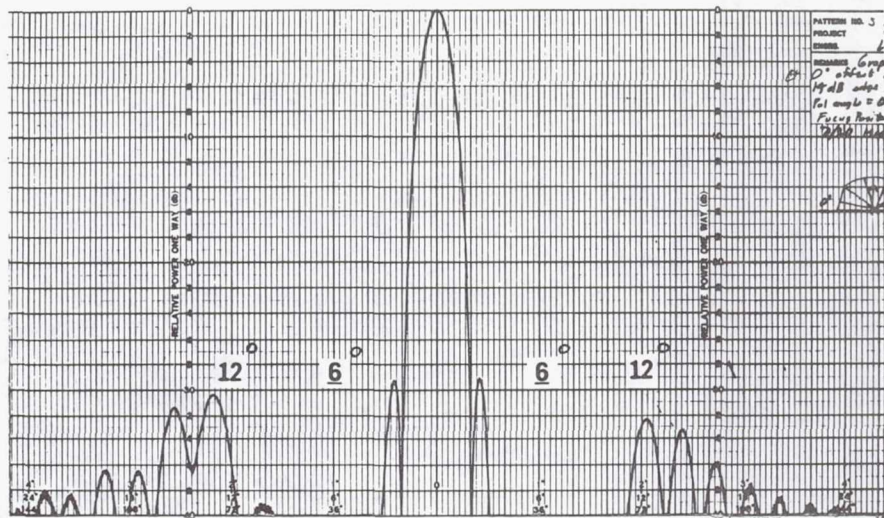


$$F/D = 1.5 \quad D/\lambda = 35$$

Figure 11a (Smooth Reflector)

RADIATION PATTERN - 35 GHz OFFSET-FED REFLECTOR MODEL IN THE SYMMETRIC
PLANE (H PLANE) - PRINCIPAL POLARIZATION

$\lambda/20$ PILLOWED REFLECTOR, $\phi = 0^\circ$

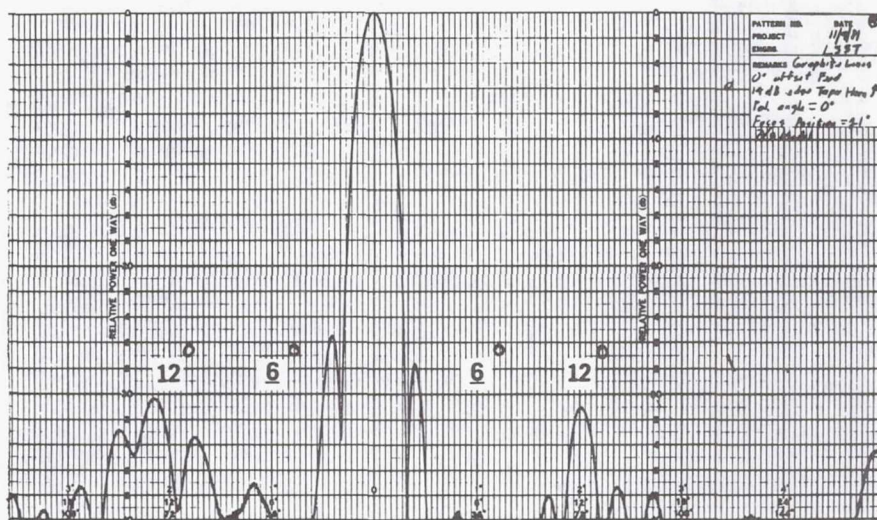


GRAPHITE CABLES

$F/D = 1.5$ $D \lambda = 35$

Figure 11b ($\lambda/20$ Reflector)

$\lambda/5$ PILLOWED REFLECTOR, $\phi = 0^\circ$



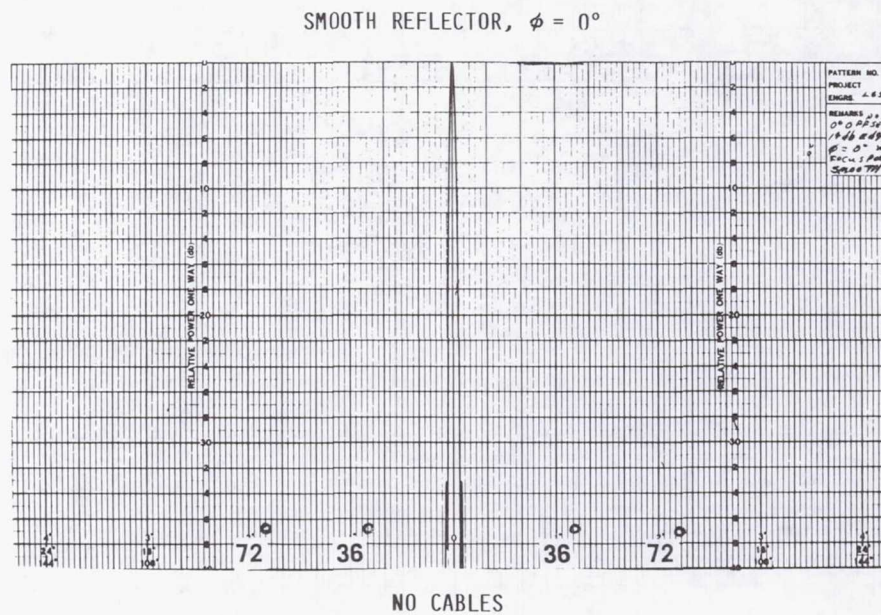
GRAPHITE CABLES

$F/D = 1.5$ $D \lambda = 35$

Figure 11c ($\lambda/5$ Reflector)

RADIATION PATTERN - 35 GHz OFFSET FED REFLECTOR MODEL IN THE SYMMETRIC PLANE (H PLANE) - PRINCIPAL POLARIZATION

In order to show the various parametric effects of the pillowed reflector models and the hoop cables, it was necessary to repeat some of the pattern cuts to determine the presence of far out sidelobes. Therefore, these patterns are presented using an expanded azimuth scale. This compresses the main beam (1.8 degree HPBW) as shown in the following figures. Basically, no surprises were found in the far out angular regions where sidelobes could occur. No aperture cables are used for figures 12a, 12b, and 12c.

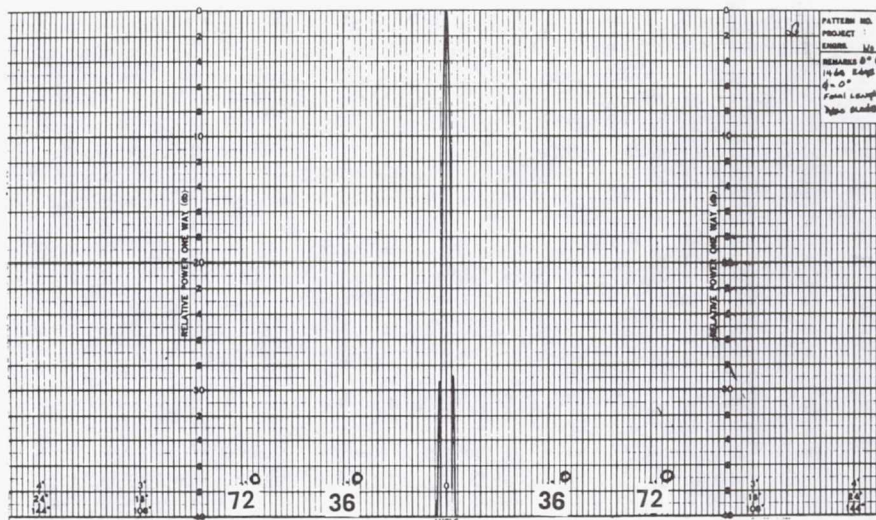


$$F/D = 1.5 \quad D/\lambda = 35$$

Figure 12a (Smooth Reflector)

RADIATION PATTERN - 35 GHz OFFSET-FED REFLECTOR MODEL IN THE SYMMETRIC
PLANE (H PLANE) - PRINCIPAL POLARIZATION

$\lambda/20$ PILLOWED REFLECTOR, $\phi = 0^\circ$

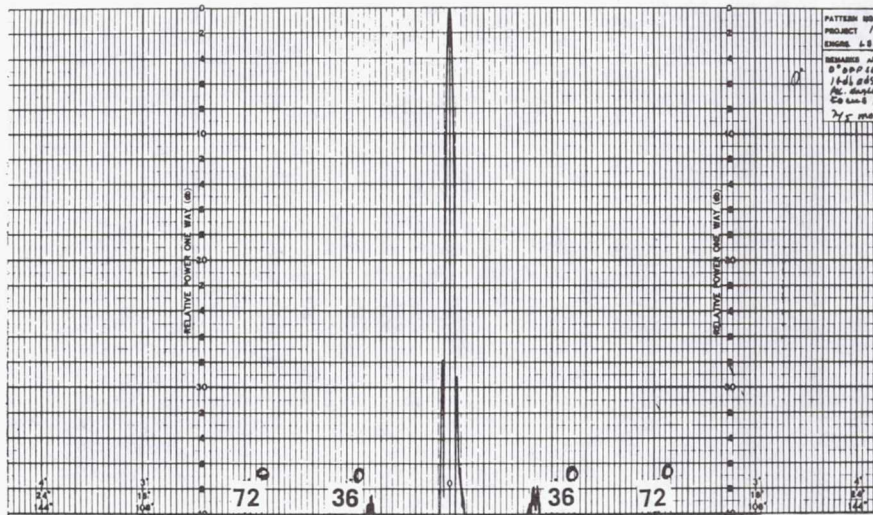


NO CABLES

$$F/D = 1.5 \quad D \lambda = 35$$

Figure 12b ($\lambda/20$ Reflector)

$\lambda/5$ PILLOWED REFLECTOR, $\phi = 0^\circ$



NO CABLES

$$F/D = 1.5 \quad D \lambda = 35$$

Figure 12c ($\lambda/5$ Reflector)

RADIATION PATTERN - 35 GHz OFFSET FED REFLECTOR MODEL IN THE SYMMETRIC PLANE (H PLANE) - PRINCIPAL POLARIZATION

The expanded angular plots were repeated using the quartz aperture cables. These results are presented in figures 13a, 13b, and 13c for the smooth, $\lambda/20$, and $\lambda/5$ reflector respectively.

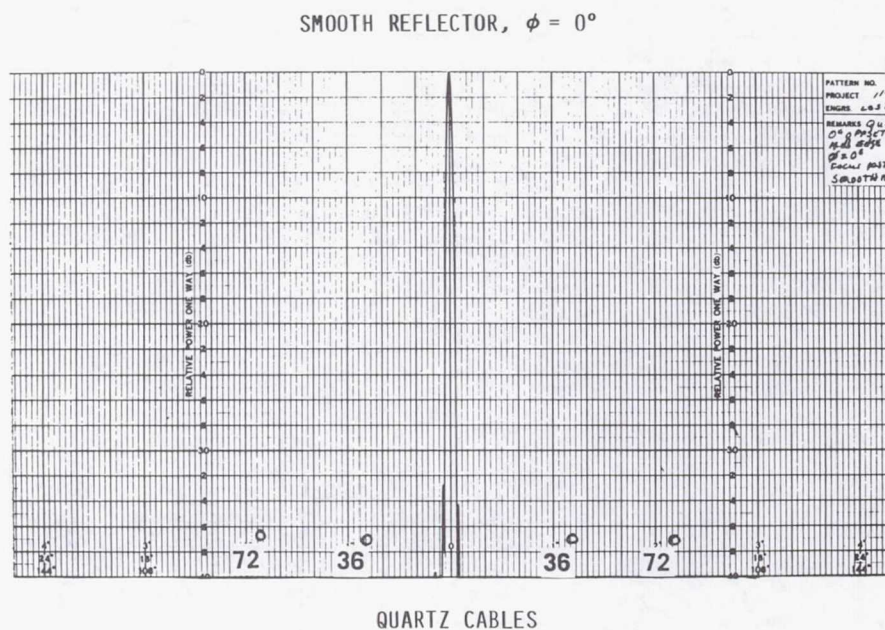
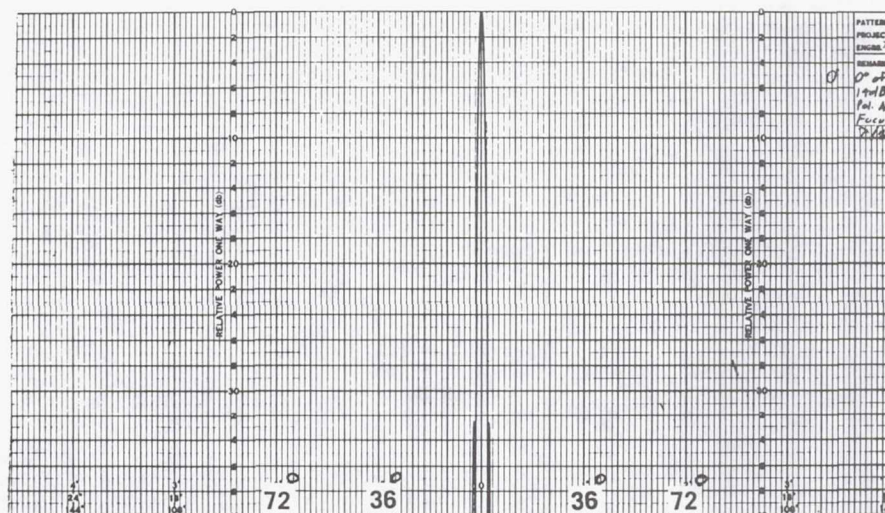


Figure 13a (Smooth Reflector)

RADIATION PATTERN - 35 GHz OFFSET-FED REFLECTOR MODEL IN THE SYMMETRIC
PLANE (H PLANE) - PRINCIPAL POLARIZATION

$\lambda/20$ PILLOWED REFLECTOR, $\phi = 0^\circ$

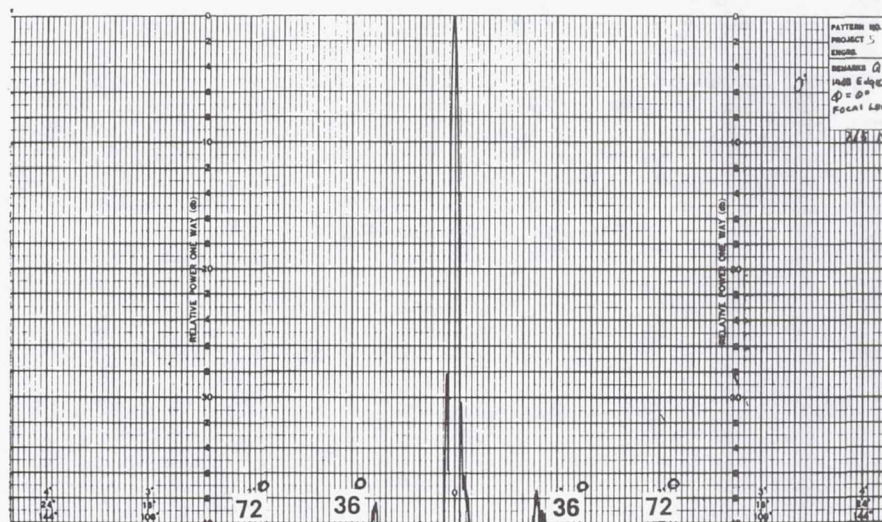


QUARTZ CABLES

$$F/D = 1.5 \quad D \lambda = 35$$

Figure 13b ($\lambda/20$ Reflector)

$\lambda/5$ PILLOWED REFLECTOR, $\phi = 0^\circ$



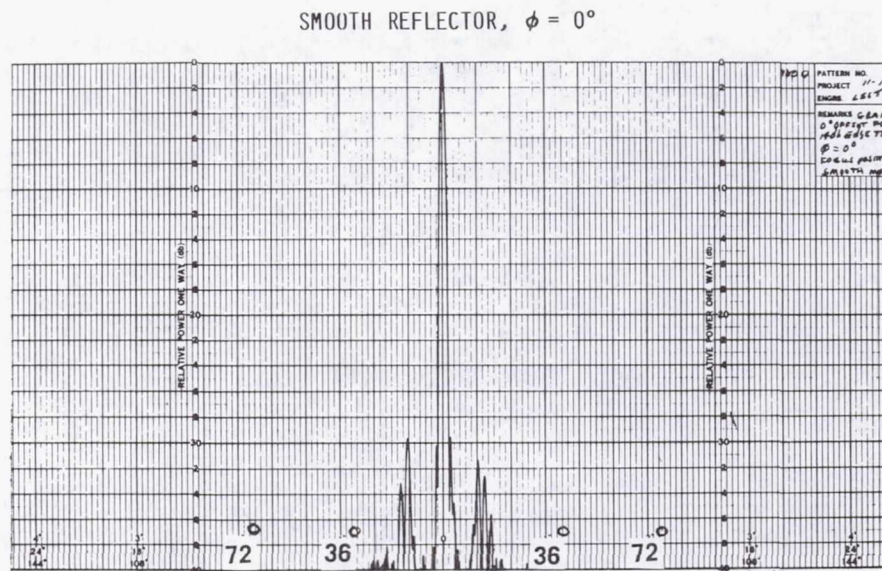
QUARTZ CABLES

$$F/D = 1.5 \quad D \lambda = 35$$

Figure 13c ($\lambda/5$ Reflector)

RADIATION PATTERN - 35 GHz OFFSET FED REFLECTOR MODEL IN THE
SYMMETRIC PLANE (H PLANE) - PRINCIPAL POLARIZATION

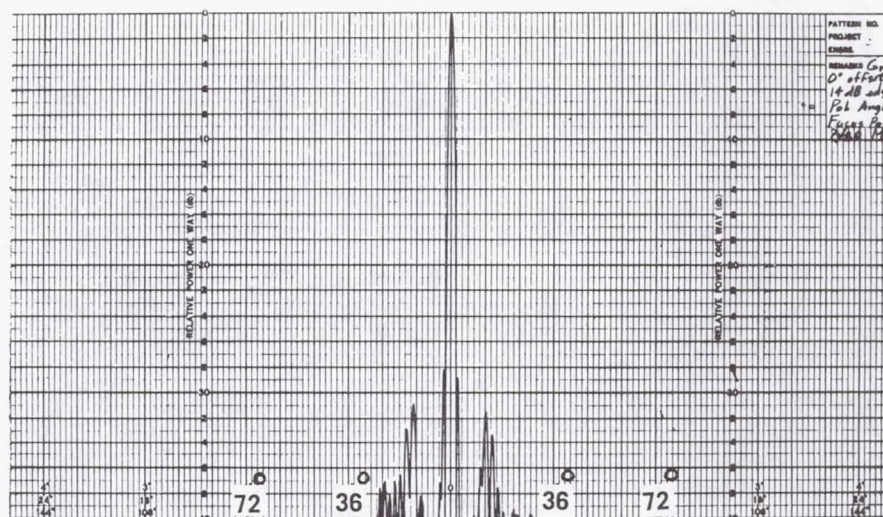
The expended angular plots were repeated using the graphite aperture cables.
These results are presented in figures 14a, 14b, and 14c for the smooth, $\lambda/20$, and
 $\lambda/5$ reflectors respectively.



GRAPHITE CABLES

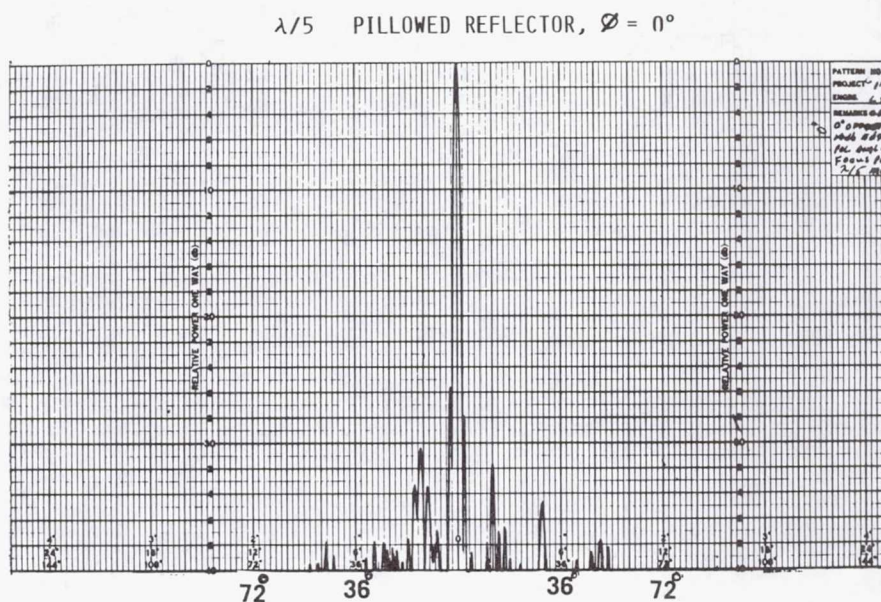
$$F/D = 1.5 \quad D/\lambda = 35$$

Figure 14a (Smooth Reflector)

$\lambda/20$ PILLOWED REFLECTOR, $\phi = 0^\circ$ 

GRAPHITE CABLES

$$F/D = 1.5 \quad D \lambda = 35$$

Figure 14b ($\lambda/20$ Reflector)

GRAPHITE CABLES

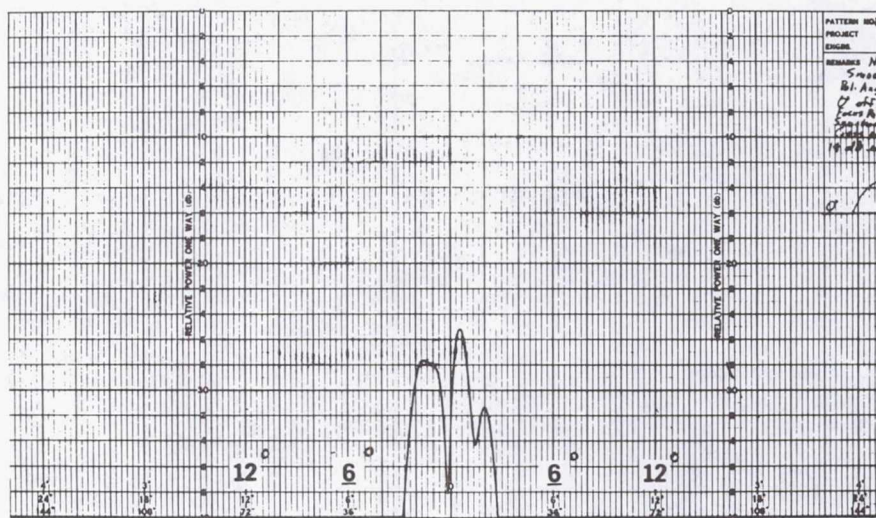
$$F/D = 1.5 \quad D \lambda = 35$$

Figure 14c ($\lambda/5$ Reflector)

RADIATION PATTERN - 35 GHz OFFSET FED REFLECTOR MODEL IN THE SYMMETRIC PLANE (H PLANE) - CROSS POLARIZATION

Typical examples of the effect of surface pillows on cross polarization levels are presented in figures 15a, 15b, and 15c for the smooth, $\lambda/20$, and $\lambda/5$ reflectors respectively. Basically, no substantial increase in cross polarization for this ($F/D = 1.5$) reflector case occurred. All of these preliminary results are under review. Basically, the cross polarization levels did not increase substantially using the aperture cables.

SMOOTH REFLECTOR, $\phi = 0^\circ$



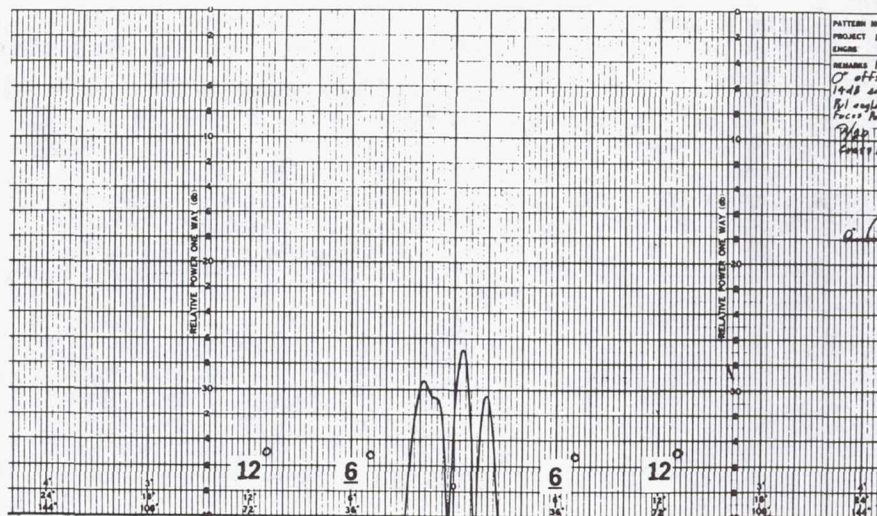
NO CABLES

$$F/D = 1.5 \quad D/\lambda = 35$$

Figure 15a (Smooth Reflector)

RADIATION PATTERN - 35 GHz OFFSET-FED REFLECTOR MODEL IN THE
SYMMETRIC PLANE (H PLANE) - CROSS POLARIZATION

$\lambda/20$ PILLOWED REFLECTOR, $\phi = 0^\circ$

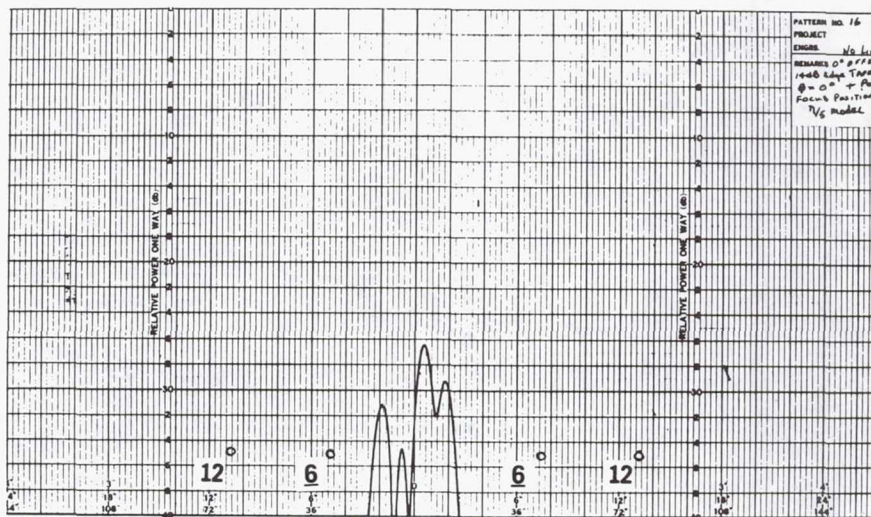


NO CABLES

$F/D = 1.5 \quad D\lambda = 35$

Figure 15b ($\lambda/20$ Reflector)

$\lambda/5$ PILLOWED REFLECTOR, $\phi = 0^\circ$



NO CABLES

$F/D = 1.5 \quad D\lambda = 35$

Figure 15c ($\lambda/5$ Reflector)

35 GHz REFLECTOR TEST RESULTS

The preliminary results of the 35 GHz test model are presented in the figure shown below. It can be seen that a ≈ 6 dB increase in sidelobe levels occurred for the $\lambda/5$ reflector without aperture cables. The utilization of quartz support cables had a minor effect (0.7 dB) on first order sidelobes. No far out scattering lobes were observed. It must be noted that these experimental results are preliminary and further testing and evaluation are underway.

	NEAR IN SIDELOBE LEVELS			CROSS POL. LEVELS			FAR OUT SIDELOBE LEVELS		
	SMOOTH	$\lambda/20$	$\lambda/5$	SMOOTH	$\lambda/20$	$\lambda/5$	SMOOTH	$\lambda/20$	$\lambda/5$
NO CABLES	-34.5, -33	-33, -31.5	-28, -29	-25.5	-27	-26.5	NONE	NONE	-30, -32
QUARTZ	-33.8, 33.5	-31, -31.5	-28, -29	-26	-26.5	-21.8	-40	NONE	-37.5
GRAPHITE	-30, -30	-29.5, 29.5	-25.5, -28	-22	-21.5	-21	-38	-38	-35

Figure 16

PRELIMINARY RESULTS

Based on these preliminary test results using the 35 GHz precision offset reflector models the following conclusions are presented. As stated earlier, further tests and evaluations are underway and these conclusions could indeed be changed.

- BASIC EFFECT OF PILLOWS WAS TO INCREASE NEAR IN SIDELOBES
- PILLOWED SURFACE HAD MINIMAL EFFECT ON GAIN
- CROSS POLARIZATION AMPLITUDE DECREASED WITH PILLOWED SURFACE
- BASICALLY NO SCATTERING EFFECTS FOR QUARTZ CABLES AT -40 dB
- INCREASED FOCAL LENGTH ($F/D = 1.5$) CAUSED INCREASE IN FAR OUT SCATTERING LOBES USING GRAPHITE CABLES
- MAJOR REFLECTIONS COULD CAUSE INCREASE IN EFFECTIVE DIAMETER OF REFLECTOR

Figure 17

Page intentionally left blank

PRELIMINARY ANALYTICAL RESULTS
USING SURFACE CURRENT INTEGRATION
FOR PREDICTING EFFECTS OF SURFACE
PILLOWS ON RF PERFORMANCE

C. E. Farrell
D. A. Strange
Martin Marietta Corporation
Denver, Colorado

Large Space Systems Technology - 1981
Third Annual Technical Review
November 16-19, 1981

FIRE PROGRAM

Figure 1 presents an overview of the Fast Integral rf Evaluation (FIRE) program under development by the Martin Marietta Corporation, Denver Division. This program uses surface current integration to evaluate rf performance of antenna systems. It requires modeling of surfaces in X, Y, Z coordinates along equally spaced X and Y grids with Z in the focal direction. The far field contribution of each surface point includes the effects of the Z-component of surface current which is not included in the aperture integration technique. Because of this, surface current integration is the most effective and inclusive technique for predicting rf performance of non-ideal reflectors. This paper presents some results that were obtained from use of the FIRE program and an aperture integration program to predict rf performance of a LSS antenna concept. The FIRE program is proprietary to Martin Marietta.

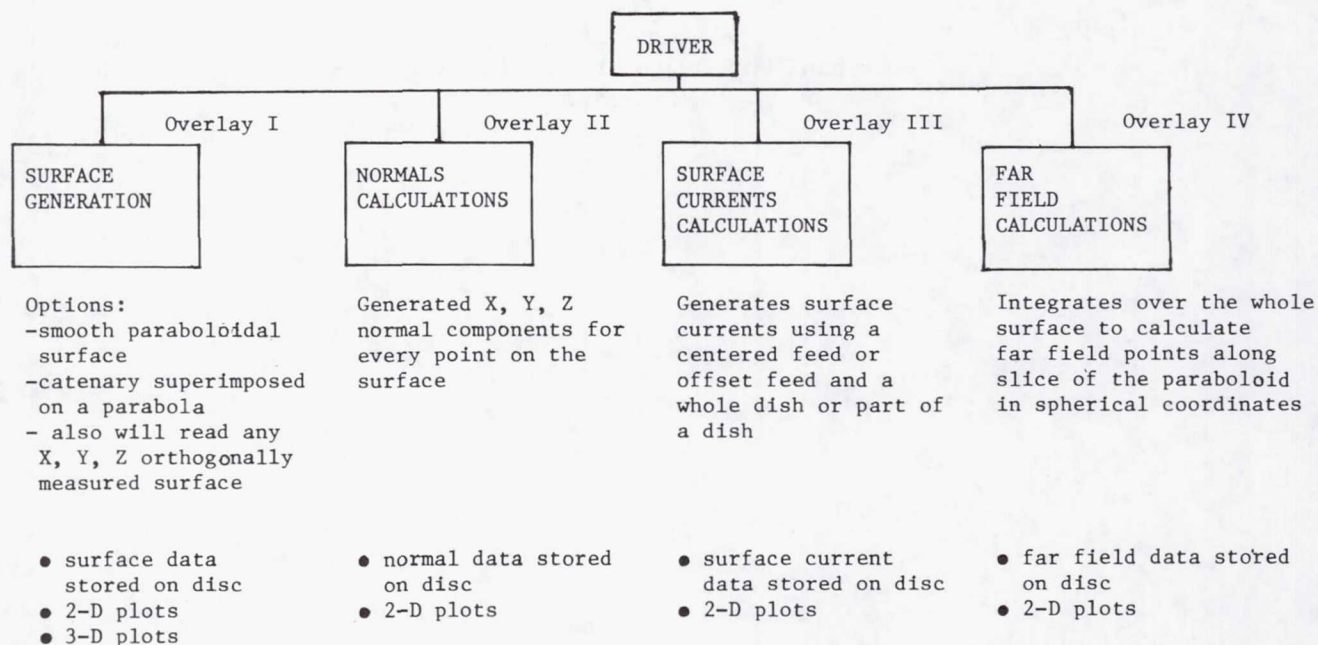


Figure 1

FIRE SAMPLE SURFACE PLOTS

Figures 2 and 3 show plots of faceted reflector surface models used in test runs with the FIRE program. In each case the Z-displacements are scaled up by a factor of 10 for ease of viewing. Such faceted surfaces are of particular interest for LSS antenna systems that typically will use a reflective surface tied down or restrained at distinct points.

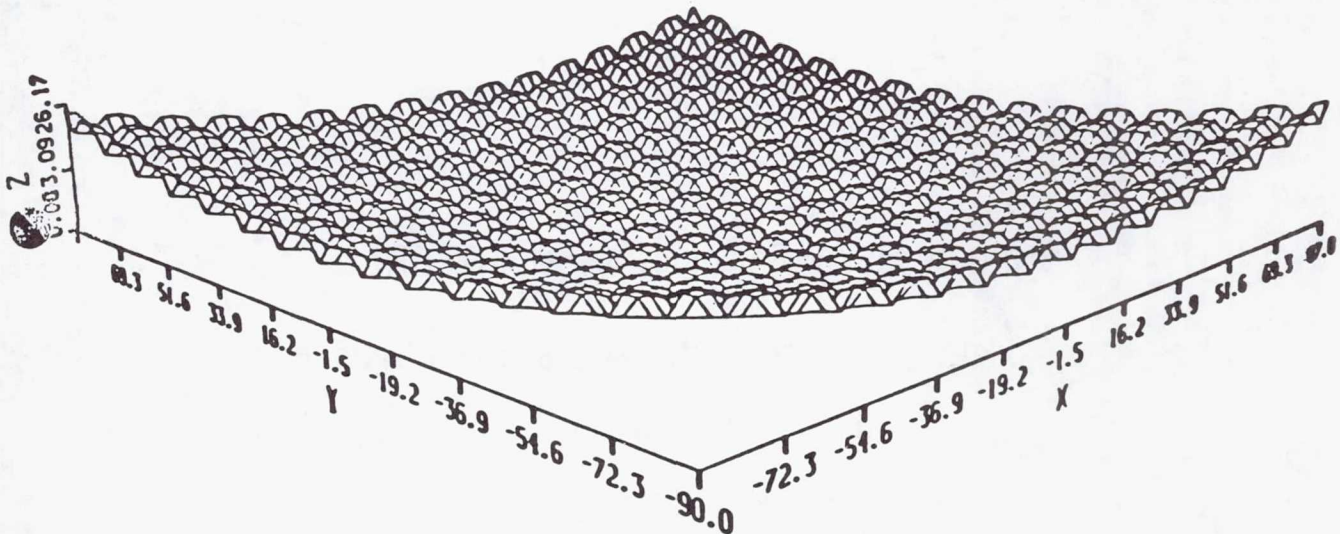


Figure 2

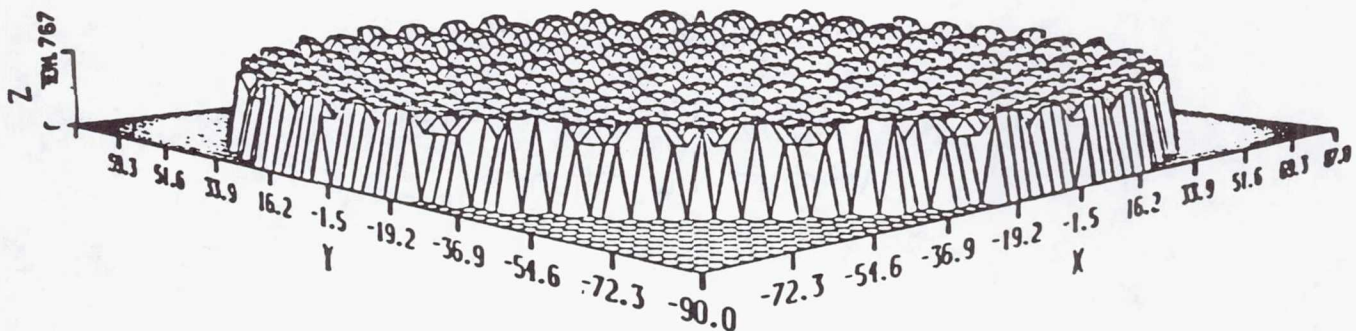


Figure 3

RF ANALYSIS - APPROACH

The FIRE program and an aperture integration program were used to analyze the performance of a distorted Kapton reflector surface. The frequency of interest was 4.95 GHz. The objectives were to determine the radiation pattern, including "grating" lobes that might result from the surface shape control subsystem and reflector material seams. In addition, the two analytical techniques would be compared for consistency and validity.

- Evaluate ECMM Performance at 4.95 GHz
- Model Worst Case Systematic Surface Distortion
 - Electrode Spacing
 - Tie Spacing
 - Seam Spacing
- Determine Radiation Pattern
- Evaluate Side Lobes
- Evaluate "Grating Lobes"
- Compare Results from Analytical Programs
 - Surface Current Integration
 - Aperture Integration

Figure 4

ECMM ANTENNA SURFACE MODEL

Figure 5 shows a top view of the ECMM antenna with the hexagonal surface shape control electrodes. Figure 6 shows a side view of part of the reflector surface. The final design modeled had electrode spacing of 5 meters rather than the 4.5 meters shown. The effects of seams in the surface were included in the modeling equation to give a "worst case" surface model. The rms distortion was less than $\lambda/50$ at 4.95 GHz.

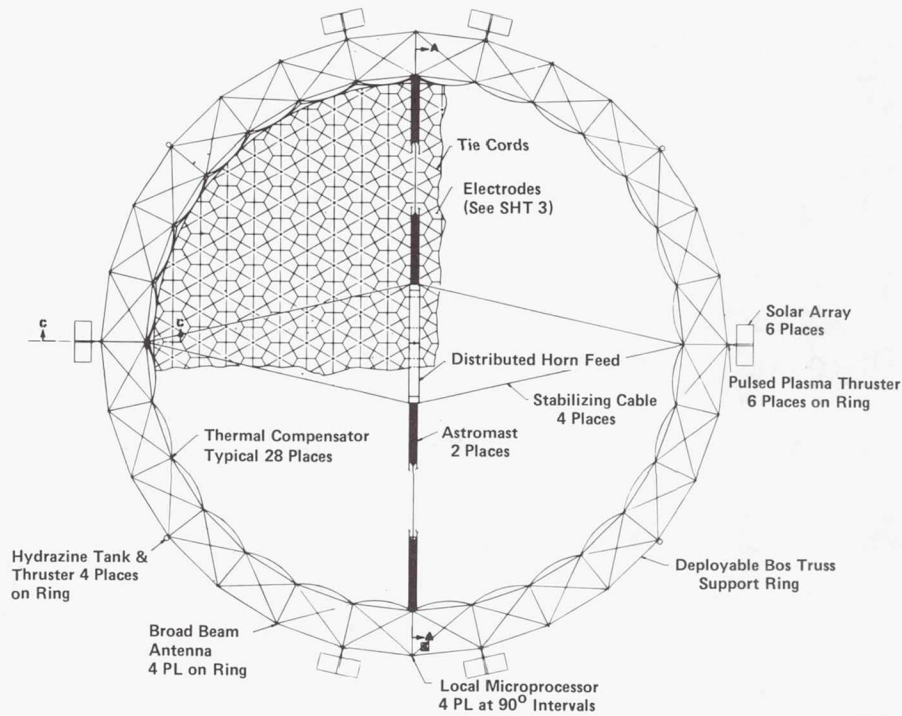


Figure 5

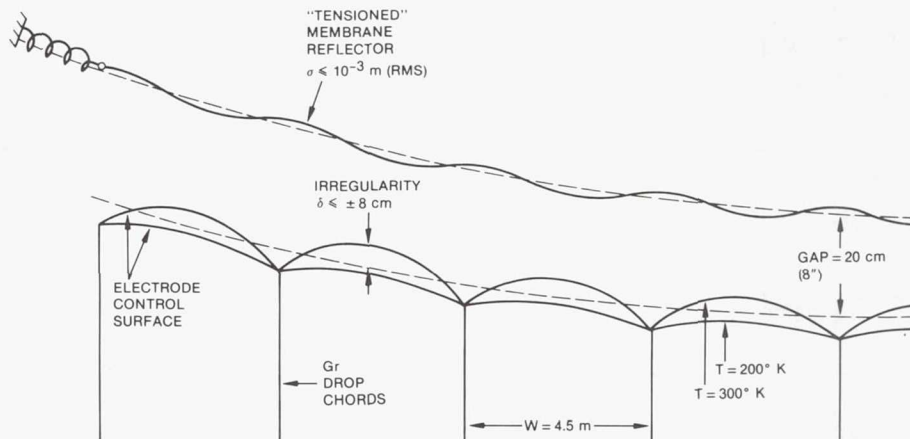


Figure 6

RF ANALYSIS - RESULTS AND CONCLUSION

The results and conclusion of this analysis are summarized below. The overall conclusion was that the ECMM reflector will perform well at the frequency of interest (4.95 GHz) if its surface maintains its shape as described previously. The results from the two analytical techniques show similar radiation patterns with respect to location of the main beam axis. The gains differ for the sidelobes.

Results

- Radiation Patterns Consistent between Models
- Loss in Gain Due to Surface Irregularities 0.164 dB
- Sidelobe Levels Higher with Surface Current Integration
- First Grating Lobe Identified by Surface Current Model is 10 dB above Level for Ideal Surface
- First Grating Lobe Gain 39 dB below Main Beam Gain

Conclusion

- At 4.95 GHz Surface Distortion of 1mm Will Not Significantly Degrade ECMM Antenna Performance

Figure 7

RF PERFORMANCE - RESULTS (Cont.)

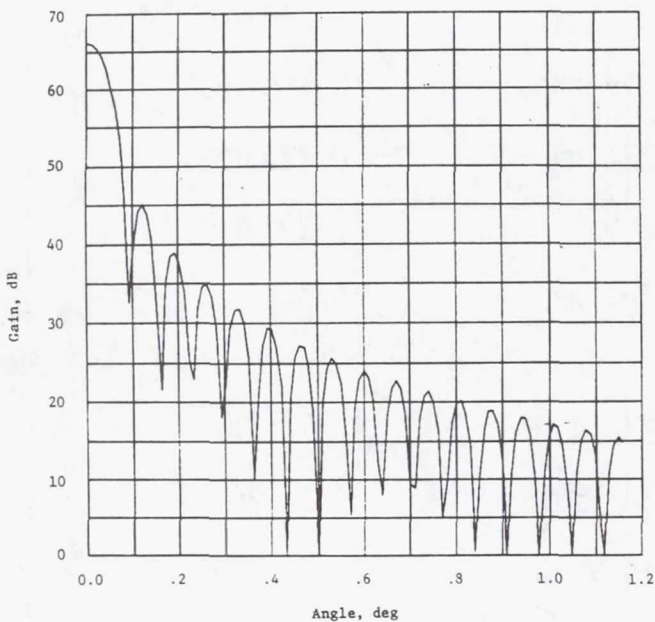
The table below shows the results obtained from the 2 analytical models for the ideal reflector operating at 4.95 GHz. The position of the 3dB point for the primary beams and the position of the first 5 nulls are the same for both techniques. There are differences in the primary and sidelobe peak gains which increase as the angle from the primary beam axis increases. These differences in gain need to be resolved.

Parameter	Aperture Integration	Surface Current Integration
3 dB Beamwidth	0.073 deg	0.074 deg
Position of First Null	0.092 deg	0.090 deg
Position of Second Null	0.159 deg	0.159 deg
Position of Third Null	0.227 deg	0.225 deg
Position of Fourth Null	0.290 deg	0.293 deg
Position of Fifth Null	0.363 deg	0.363 deg
First Sidelobe Level	-21.32 dB	-21.09 dB
Second Sidelobe Level	-27.74 dB	-27.11 dB
Third Sidelobe Level	-34.15 dB	-31.24 dB
Fourth Sidelobe Level	-36.99 dB	-34.43 dB
Fifth Sidelobe Level	-45.01 dB	-36.93 dB
Peak Gain	66.78 dB	66.18 dB

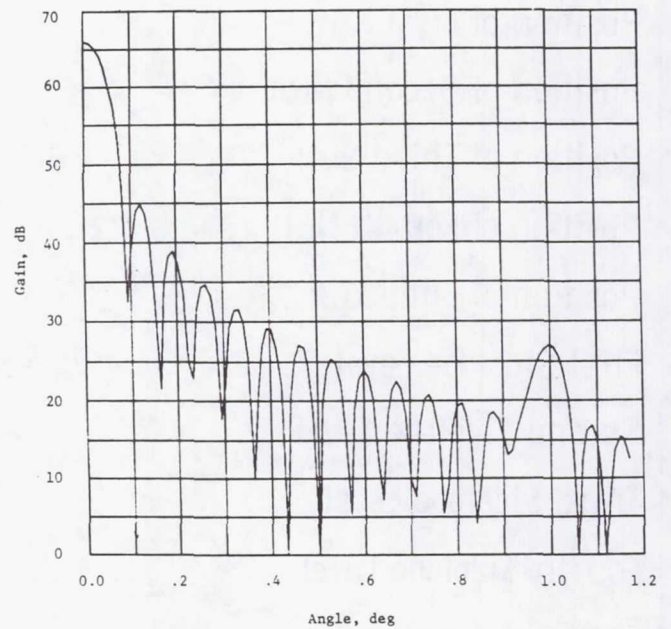
Table 1

RF PERFORMANCE - RESULTS (Concl.)

Figure 8 compares the antenna performance for the ECMM surface and the ideal reflector predicted by the FIRE program. The primary beam does not show significant loss. The sidelobes are the same with the only difference being the appearance of a "grating" lobe at 1 degree. This lobe location was predicted from the surface model which had grid spacing of 5 meters. It should be noted that the aperture integration technique inherently does not predict "grating" lobes. For LSS reflector surfaces these lobes may result dependent upon the manner in which the surface is constrained. It seems that surface current integration analysis will be necessary for LSS antenna rf performance analyses.



Radiation pattern, surface current integration,
ideal surface.



Radiation pattern, surface current integration,
modulated surface.

Figure 8

**RF VERIFICATION TASKS UNDERWAY
AT THE
HARRIS CORPORATION
FOR
MULTIPLE APERTURE REFLECTOR SYSTEM**

**T. A. Gutwein
Harris Corporation
Melbourne, Florida**

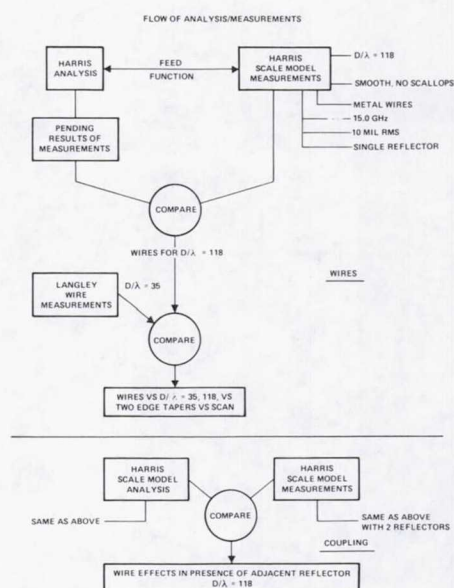
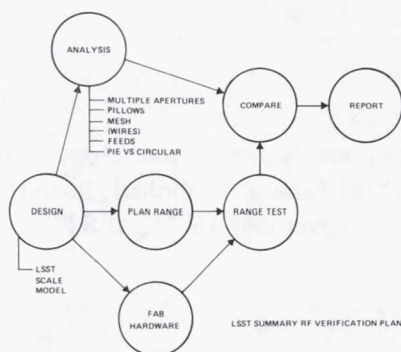
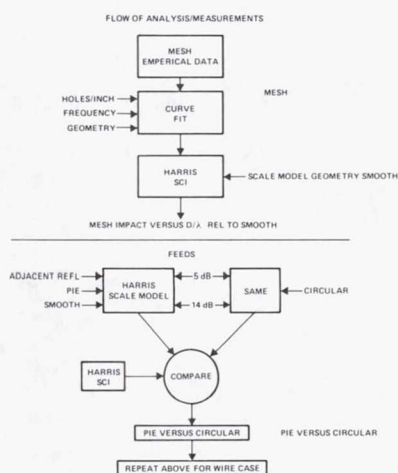
**Large Space Systems Technology — 1981
Third Annual Technical Review
November 16-19, 1981**

OVERALL LSST RF VERIFICATION PLAN

Both experimental scale model and analysis activities are underway at Harris Corporation. Scale model experiments on a 17.75:1 scale model of the 100-meter hoop-column/quad-aperture point design will verify analysis software. Two out of the four apertures will be scaled.

Major areas of study are:

1. Mesh effects on gain and patterns
2. Adjacent aperture coupling effects for "pie" and circular apertures
3. Wire effects for Harris model with Langley scale model results included for assessing D/λ effects.
4. Wire effects with adjacent aperture coupling
5. Reflector surface distortion effects (pillows and manufacturing roughness)

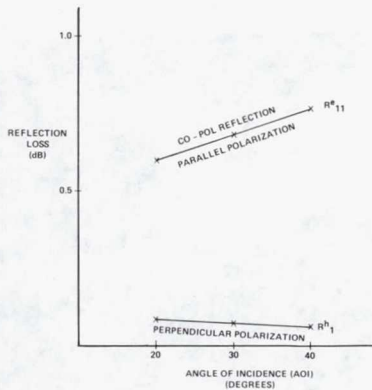


MESH MODELS

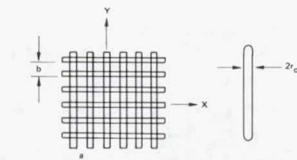
The mesh model for the analysis is based on the characterization of the mesh reflection coefficients given holes per inch, wire size, and other physical parameters. Both perpendicular and parallel reflection coefficients are characterized in the model for eventual use in the surface current integral program. Cross polarization of the mesh is accounted for in the model.

Both 15 GHz and 35 GHz mesh has been characterized to obtain frequency trend data.

MESH REFLECTANCE FOR ANALYSIS
(15 GHz)



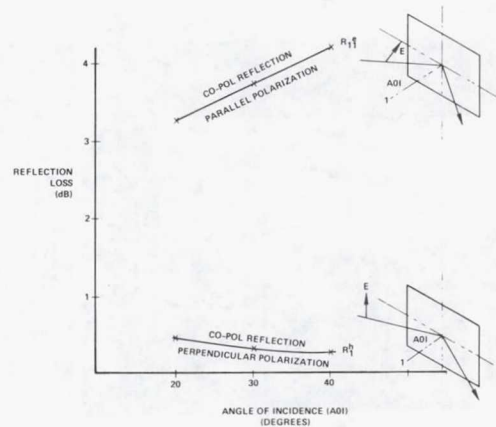
MESH REFLECTANCE GEOMETRY
AND
PARAMETERS OF MODEL



- COMBINATION OF EMPIRICAL DATA AND ANALYTICAL MODEL.
- THE REFLECTION COEFFICIENTS AT EACH DISH POINT CAN BE DETERMINED USING THE FORMULAS FROM THE RUSSIAN PAPERS ON WIRE GRID REFLECTION.
- THE INPUTS NEEDED ARE:
 - $\frac{a}{\lambda}, \frac{b}{\lambda}, \frac{r_0}{\lambda}$ - MESH DIMENSION (DEFINED ABOVE)
 - σ - CONDUCTIVITY OF MESH
 - μr - RELATIVE PERMEABILITY OF MESH
 - $\frac{a}{\lambda}, \frac{b}{\lambda}$ - COMPLEX IMPEDANCE BETWEEN MESH AT GRID INTERSECTIONS
 - ω - FREQUENCY, AND INCIDENT ANGLE ϕ

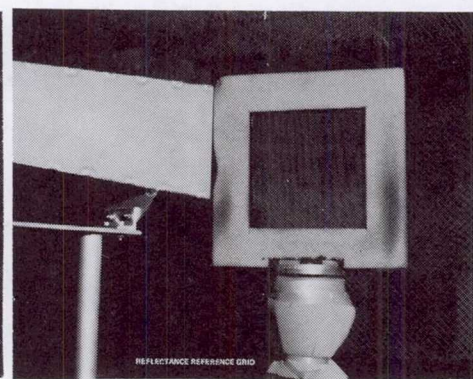
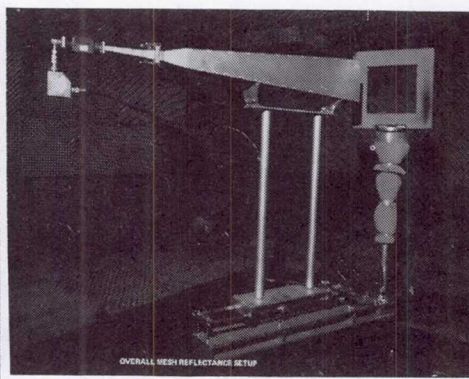
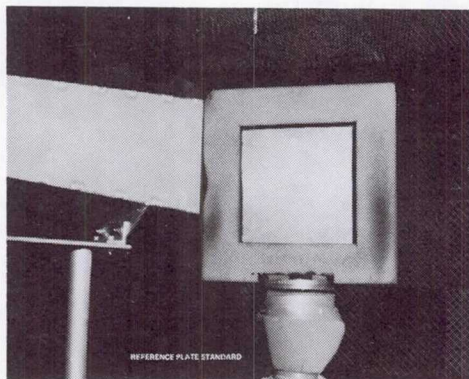
- R^h_{11} - CO-POL REFLECTION FOR HORIZONTALLY POLARIZED INCIDENT FIELD
- R^h_{12} - CROSS-POL REFLECTION FOR HORIZONTALLY POLARIZED INCIDENT FIELD
- R^v_{11} - CO-POL REFLECTION FOR VERTICALLY POLARIZED INCIDENT FIELD
- R^v_{12} - CROSS-POL REFLECTION FOR VERTICALLY POLARIZED INCIDENT FIELD

MESH REFLECTANCE FOR ANALYSIS (35 GHz)



MESH MEASUREMENT SYSTEM

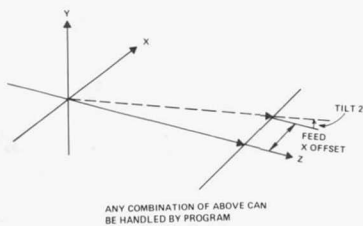
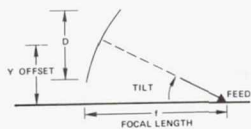
Electrical characterization of the mesh material and correlation to the mesh model is obtained by using a "near field" horn illuminating an unknown mesh sample in an anechoic chamber. Measurements are obtained relative to a conducting aluminum plate. Calibration of the system is obtained by parallel wire gratings of known reflection coefficient amplitude and phase.



MESH ANALYSIS MODEL

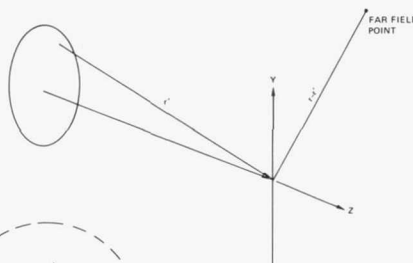
The mesh reflection coefficients are combined in the surface current integral program to obtain mesh import results. The SCI can handle feed tilt, scan, and all polarizations. A triangular grid structure is used for the surface grid. The number of integration points is selected based on frequency, size, and surface distortions.

SCAN AND TILT CORRECTION



ANY COMBINATION OF ABOVE CAN BE HANDLED BY PROGRAM

INTEGRATION OF ELECTRIC AND MAGNETIC CURRENTS IS TAKEN INTO ACCOUNT FOR MESH

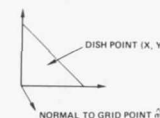
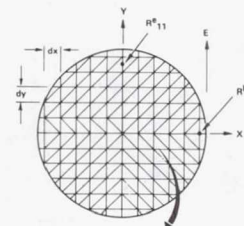
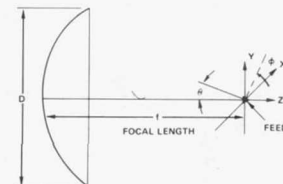


$$\begin{aligned} \vec{J} &= \hat{n} \times \vec{H} \quad (\text{ELECTRIC}) \\ \vec{M} &= \vec{E} \times \hat{n} \quad (\text{MAGNETIC}) \\ \vec{A} &= \frac{1}{4\pi} \iint \frac{\vec{J}(\vec{r}') e^{-jk|\vec{r}-\vec{r}'|}}{|\vec{r}-\vec{r}'|} d\vec{r}' \\ \vec{F} &= \frac{1}{4\pi} \iint \frac{\vec{M}(\vec{r}') e^{-jk|\vec{r}-\vec{r}'|}}{|\vec{r}-\vec{r}'|} d\vec{r}' \end{aligned}$$

$$\text{SIMPLIFYING } \vec{A} = \frac{e^{-jk|\vec{r}|}}{4\pi r} \left[\int \vec{J}(\vec{r}') \phi(\vec{r}, \vec{r}') d\vec{r}' \right]$$

$$\vec{F} = \frac{e^{-jk|\vec{r}|}}{4\pi r} \left[\int \vec{M}(\vec{r}') \phi(\vec{r}, \vec{r}') d\vec{r}' \right]$$

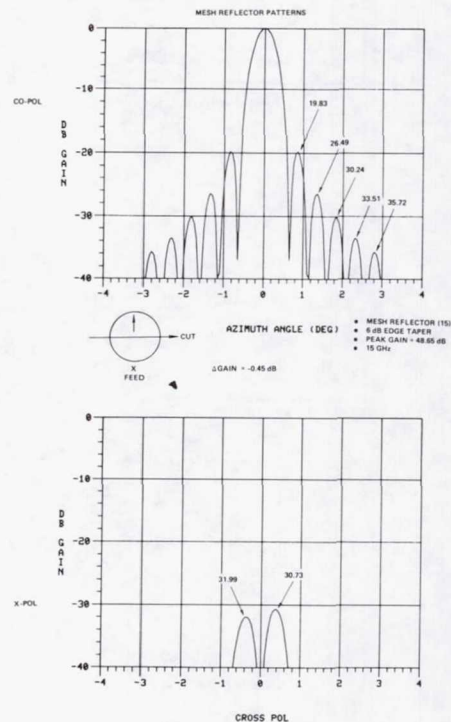
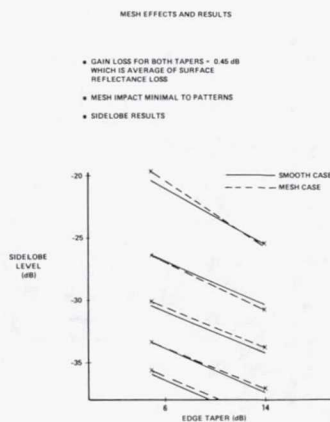
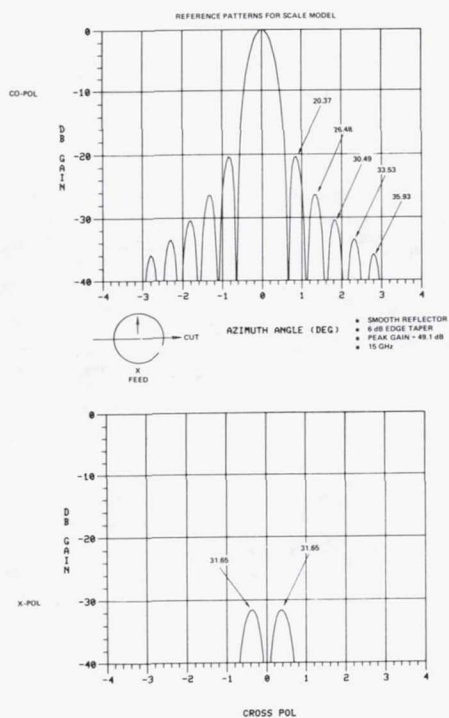
MESH REFLECTION COEFFICIENTS IN THE ANALYSIS GRID



- NORMAL AT DISH POINT IS NORMAL TO TRIANGULAR PLANE
- AREA IS AREA OF TRIANGULAR PATCH
- USING APERTURE (X, Y) COORDINATES THE CORRESPONDING POINT ON REFLECTOR IS DETERMINED FROM POLYNOMIAL EQUATION.

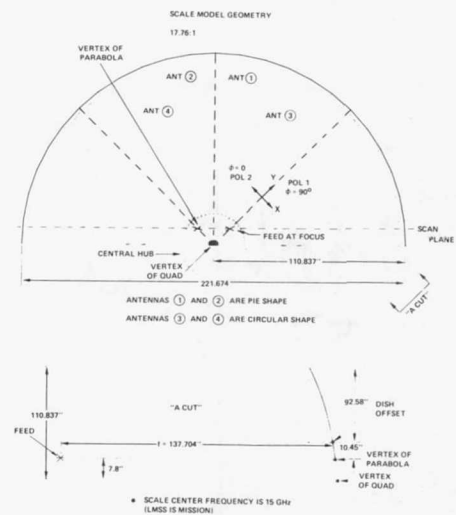
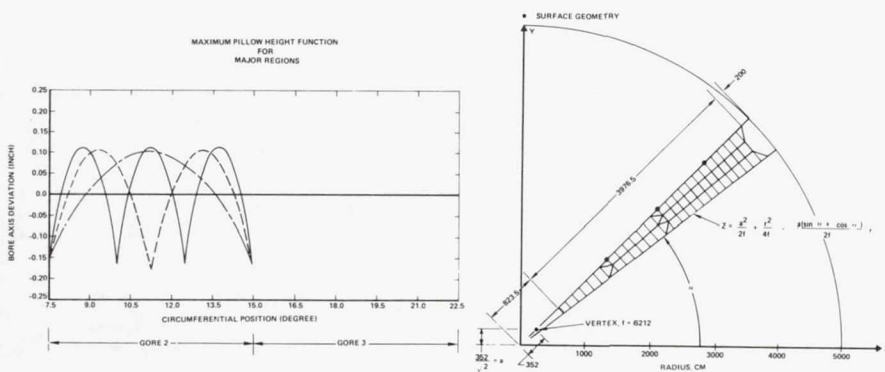
MESH EFFECT RESULTS

The impact to performance for a single offset aperture due to mesh is minor. Results at 15 GHz show that the gain impact is on the order of the average of the reflection coefficient versus angle of incidence curve. Side lobes are altered approximately 1 dB relative to a smooth reflector. Edge taper does not significantly effect side lobe levels.



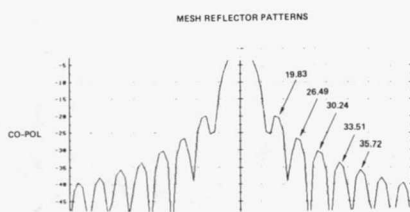
PILLOW MODELS

A worst-case pillow model was obtained for the point design. The pillow model is different for three major sectors of the reflector in the radial direction. A gore model is repeated every 7.5 degrees in the analysis. The rms of the pillow model is 80 mils for the full scale 100-meter point design. The scale model rms is 4.5 mils. The pillows are biased about the average of the pillow function.

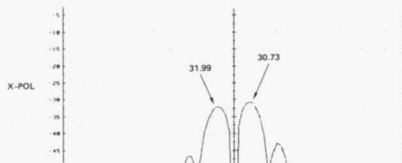


SCALE MODEL MESH PREDICTIONS

Mesh reflector patterns were calculated for the scale model showing the impact due to mesh effects and roughness. Mesh impact is minimal. Roughness effects reduce gain an amount comparable to a "Ruze" curve for the 12.4-mil total roughness. Roughness is $\lambda/63.5$.

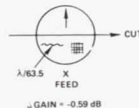
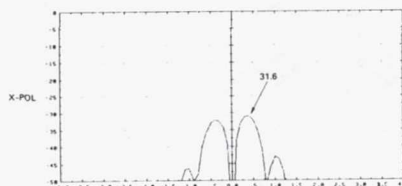
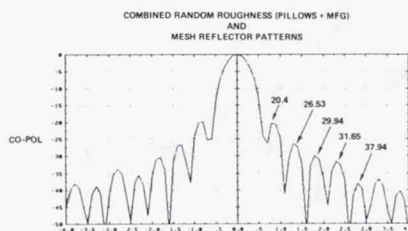


• NO SIGNIFICANT PATTERN DISTORTION



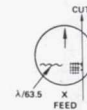
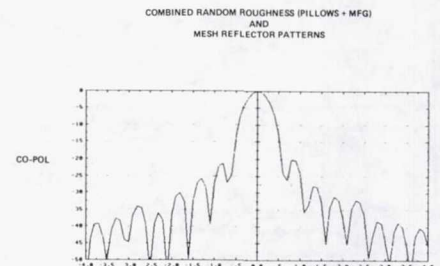
Δ GAIN = -0.45 dB

- MESH REFLECTOR (15)
- 6 dB EDGE TAPER
- PEAK GAIN = 48.65 dB
- 15 GHz



Δ GAIN = -0.59 dB

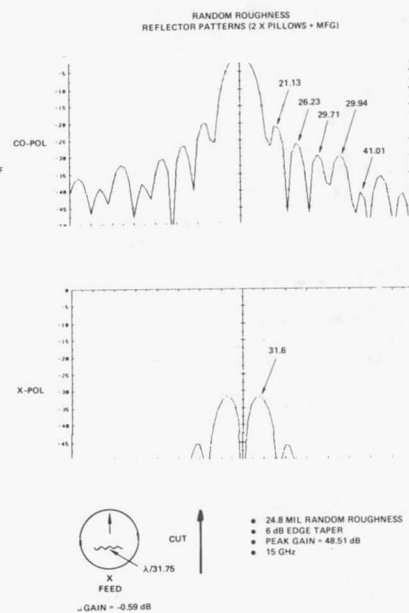
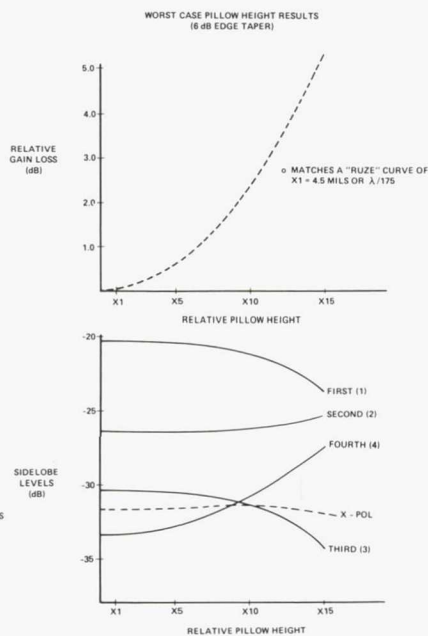
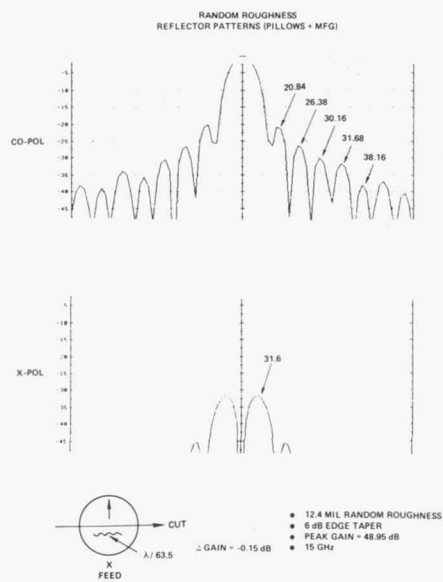
- 12.4 MIL RANDOM ROUGHNESS
- MESH AT 15 GHz
- 6 dB EDGE TAPER
- PEAK GAIN = 48.51 dB
- 15 GHz



- 12.4 MIL RANDOM ROUGHNESS
- MESH AT 15 GHz
- 6 dB EDGE TAPER
- PEAK GAIN = 48.51 dB
- 15 GHz

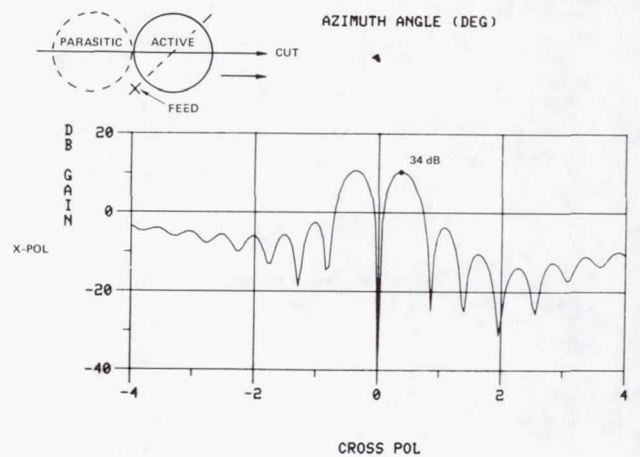
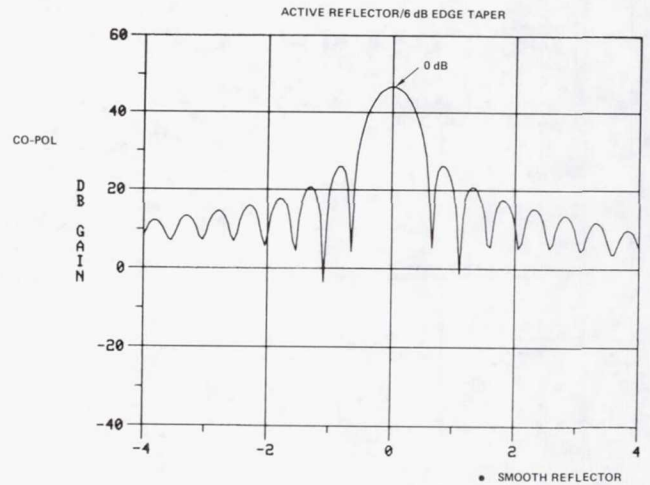
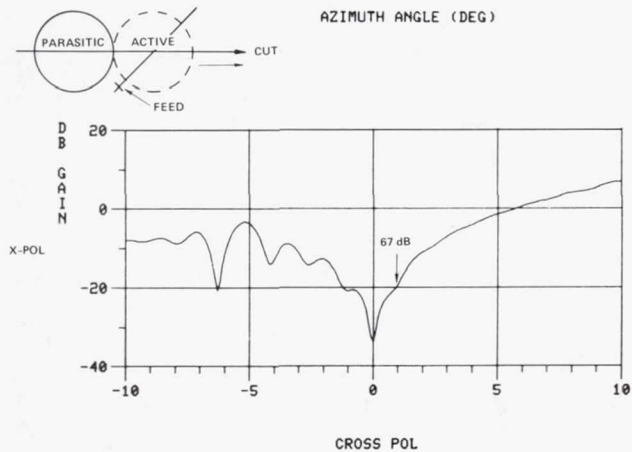
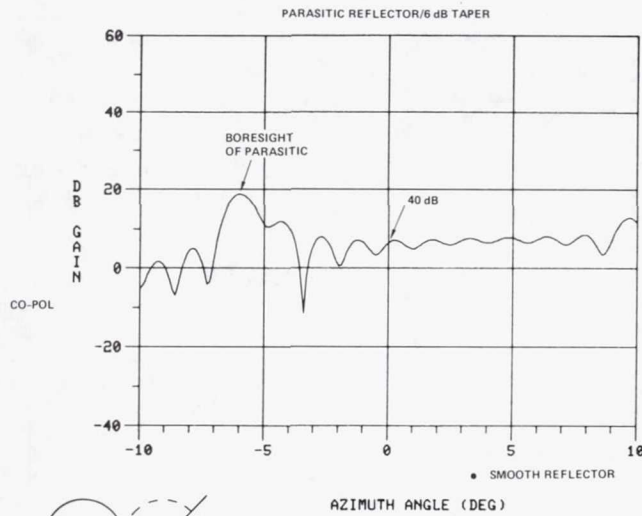
PILLOW RESULTS

The pillow model (rms = 4.5 mils) follows a Ruze roughness curve. The pillow rms is approximately $\lambda/175$. The curve shows the effect of increasing pillow height by factors which begin to effect pattern side lobe levels. A 6 dB edge taper case is shown. No significant change in performance occurs for a 14 dB edge taper.



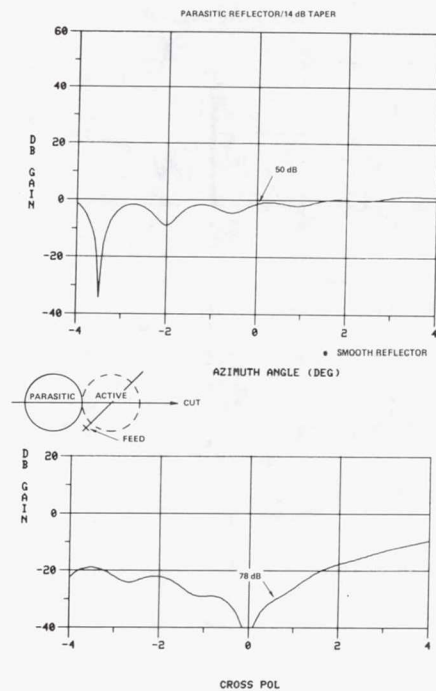
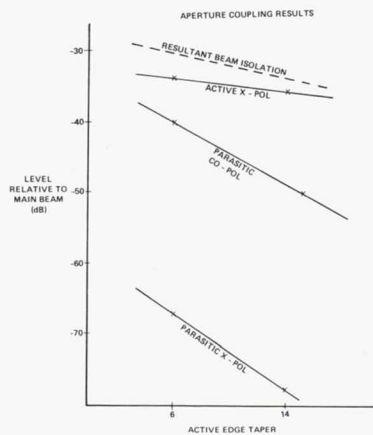
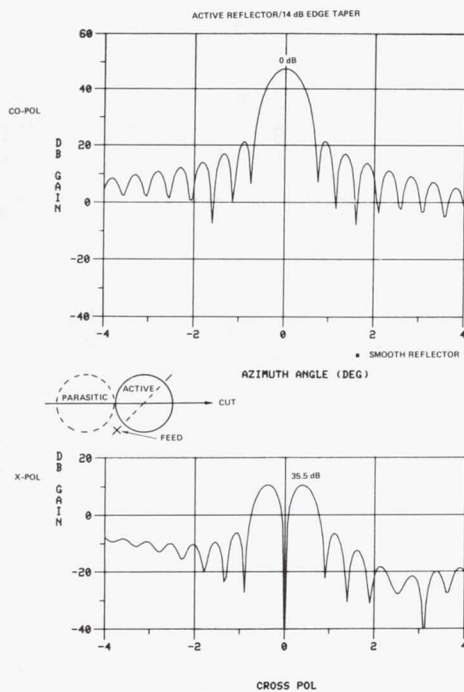
COUPLING ANALYSIS RESULTS

Several cases for the RF verification model were run to predict effects of adjacent aperture coupling. The active reflector was illuminated with a 6 dB and 14 dB edge taper and the pattern calculated in the Surface Current Integral (SCI) program. The pattern for the adjacent aperture was calculated to determine coupling effects. The patterns are shown below.



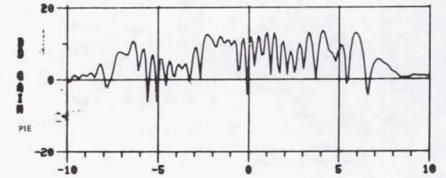
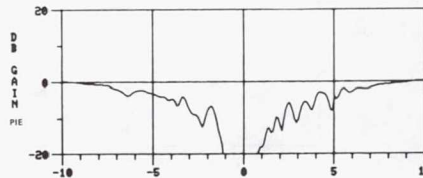
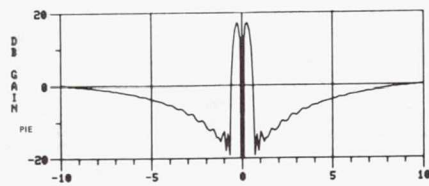
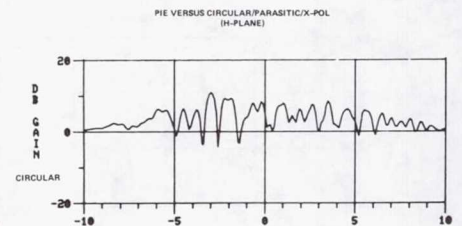
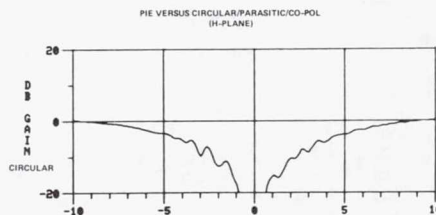
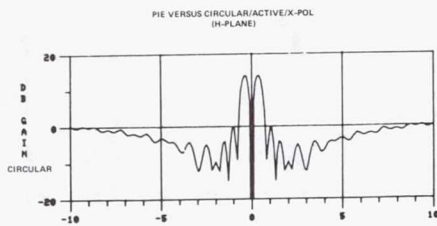
COUPLING ANALYSIS RESULTS (CONTINUED)

The effect of edge taper on resultant beam isolation is shown. Parasitic aperture coupling for the cases analyzed to date show that isolation is better than 30 dB for a 6 dB edge taper and improves by 2 dB for a 14 dB edge taper. The 14 dB edge taper patterns are shown for reference.



CIRCULAR VERSUS PIE ANALYSIS

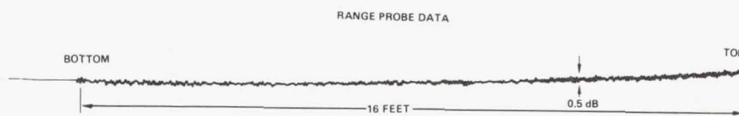
The effect of a pie shape aperture relative to a circular aperture was analyzed relative to coupling effects. Degradation of coupling was less than 1 dB for the pie case relative to the circular case. Gain increase was 1.5 dB for the "pie" relative to the circular. This increase correlates with the expected 100 percent gain increase.



WORK IN PROGRESS FOR THE RF VERIFICATION TASK

The scale model range tests for the two aperture pie reflectors is planned for late February 1982. The range has been designed and probe data obtained of the incident field. The testing hardware is designed to allow investigation of aperture coupling, wire, and feed illumination effects on performance of the quad aperture.

The analysis effort will continue with correlation to the measurement as the primary goal for the verification of the software. Wire effects will be analyzed pending results of the measurements.



HARRIS SCALE MODEL CHARACTERISTICS

TWO 7.5 FEET REFLECTORS: SEPARATION PER 0.87 GHz POINT DESIGN: FREQUENCY OF TEST 15.0 GHz

ROUGHNESS OF AT LEAST ONE REFL 10 MILS ($\lambda/80$)

TWO FEEDS PER REFLECTOR AT 5 dB EACH

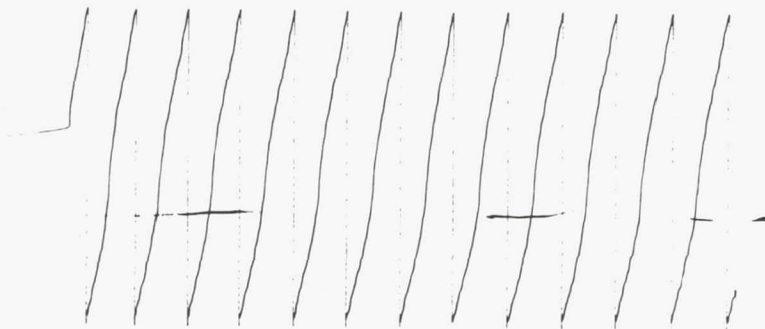
TWO FEEDS PER REFLECTOR AT 14 dB EACH

(F/D)' OF EACH REFLECTOR IS 1.5

MEASUREMENT VERIFICATION SHALL INCLUDE CONTOUR MAP

"PIE" CAPABILITY

FEED SCAN OF ONE FEED TO EXTREME CASE FOR DESIGN



- MULTIPATH SATISFACTORY
- NO EXTRANEOUS

Page intentionally left blank

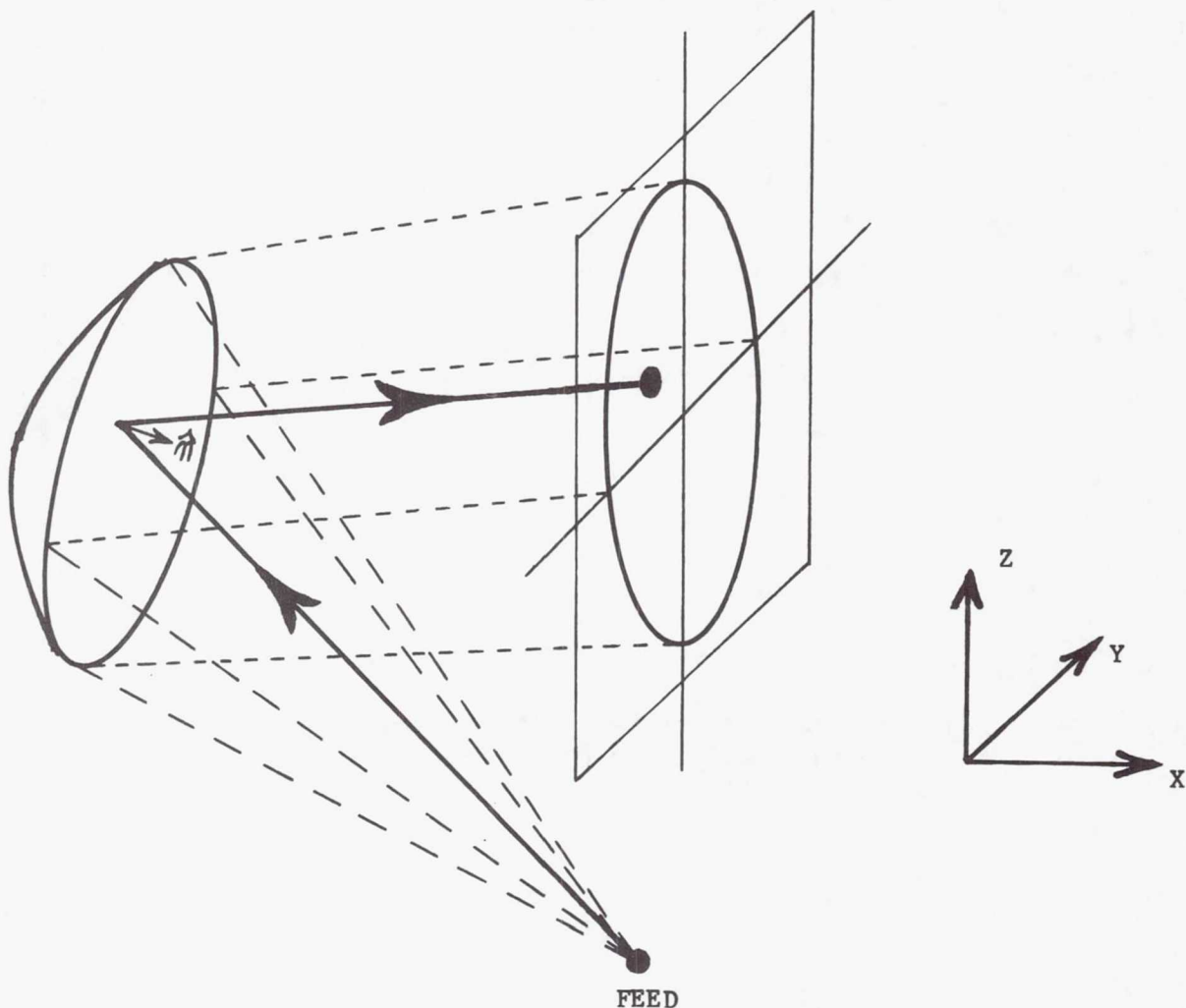
DISTORTED REFLECTOR ANTENNA
PERFORMANCE PREDICTION TECHNIQUE

M. C. Bailey
NASA, Langley Research Center
Hampton, Virginia

Large Space Systems Technology - 1981
Third Annual Technical Review
November 16-19, 1981

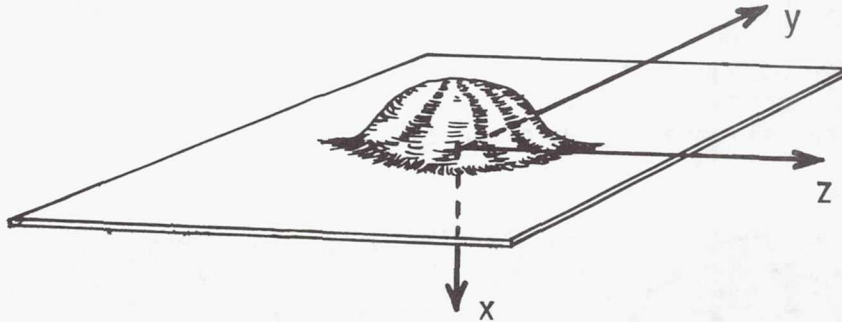
REFLECTOR ANTENNA GEOMETRY

All reflector antenna analysis methods have one thing in common. At any point on the surface (e.g. the sampling point for surface-current-integration or the point of reflection for geometric-optics techniques), the coordinate location and the unit normal vector must be known. For a reflector antenna whose surface can be described mathematically (paraboloid, sphere, ellipsoid, etc.), this information is obtained from the equation of the surface and its derivatives. When an antenna becomes distorted a mathematical description of the surface will, most likely, not be available. In such cases, one must resort to a discrete point definition of the surface and the utilization of approximate or 3-D curve-fit techniques for the surface at other points of interest. Various techniques are available; however, there are restrictions on the initial measured data points used to define the reflector surface (e.g. requiring the measured points to be located in a prearranged regular grid and requiring that the slope of the surface be known at the measured points). The purpose of the present effort is to demonstrate the application of a 3-D curve-fit technique (ref. 1) to the electromagnetic analysis of reflector antennas, which are only described by the coordinates of an irregular distribution of measured points on the reflector surface. The reflector antenna analysis method used here to calculate radiation patterns is geometric-optics with aperture-integration since an efficient and accurate computer code (ref. 2) was readily available for modification.



SURFACE INTERPOLATION FUNCTION

The interpolation function (ref. 1) for the surface defined by the measured (x_i, y_i, z_i) coordinates of the points is summarized in this chart. This interpolation function is continuous everywhere and its first derivatives are continuous, thus allowing the determination of points of reflection and the normal to the surface at the points of reflection.



Interpolation function for surface characterized by N points

$$x = a_0 + a_1 y + a_2 z + \sum_{i=1}^N F_i r_i^2 \ln r_i^2$$

$$r_i^2 = (y - y_i)^2 + (z - z_i)^2$$

Coefficients obtained by solving $(N+3)$ by $(N+3)$ matrix equation

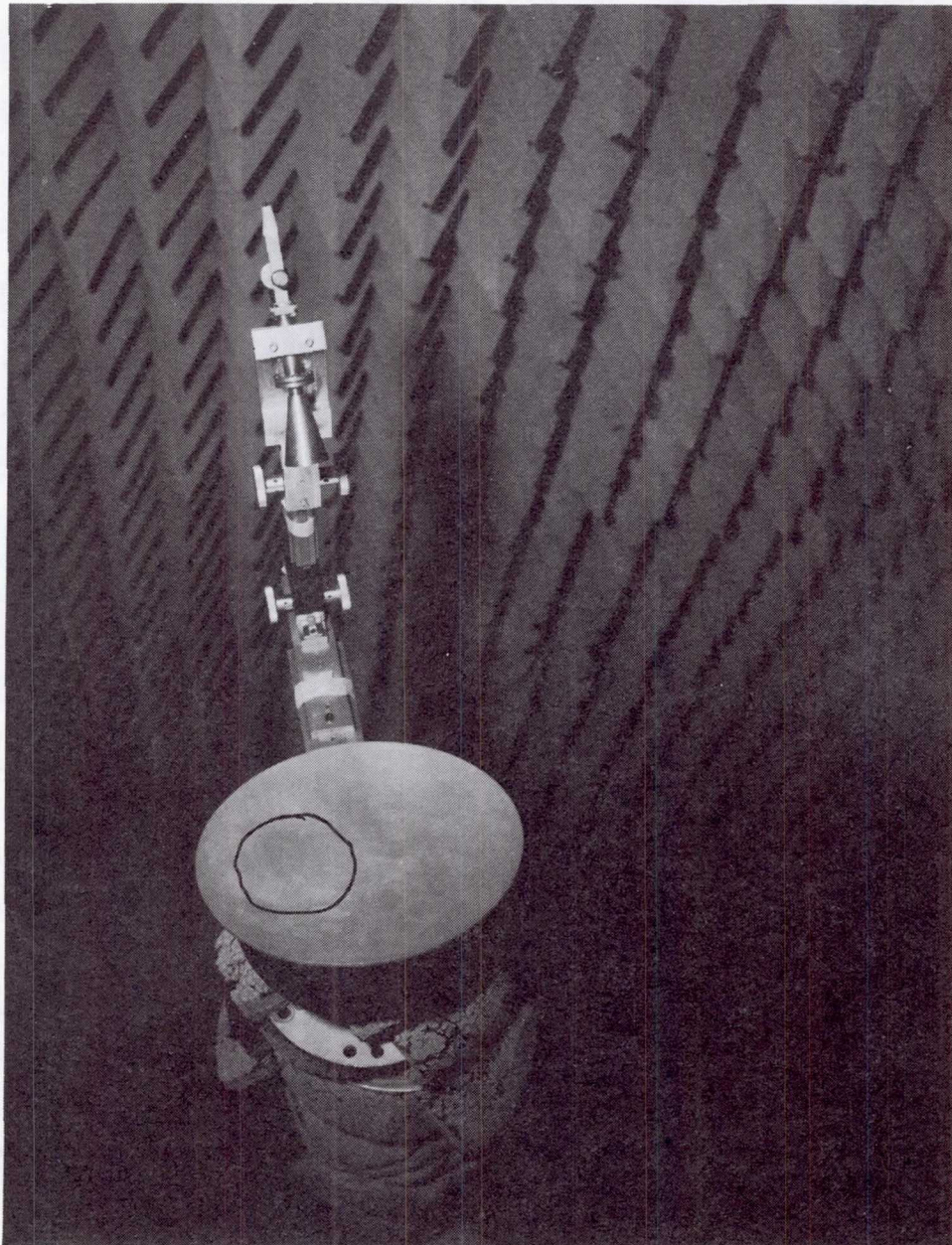
$$x_j = a_0 + a_1 y_j + a_2 z_j + \sum_{i=1}^N F_i r_{ij}^2 \ln r_{ij}^2 \quad (j=1, N)$$

$$\sum_{i=1}^N F_i = \sum_{i=1}^N y_i F_i = \sum_{i=1}^N z_i F_i = 0$$

$$r_{ij}^2 = (y_j - y_i)^2 + (z_j - z_i)^2$$

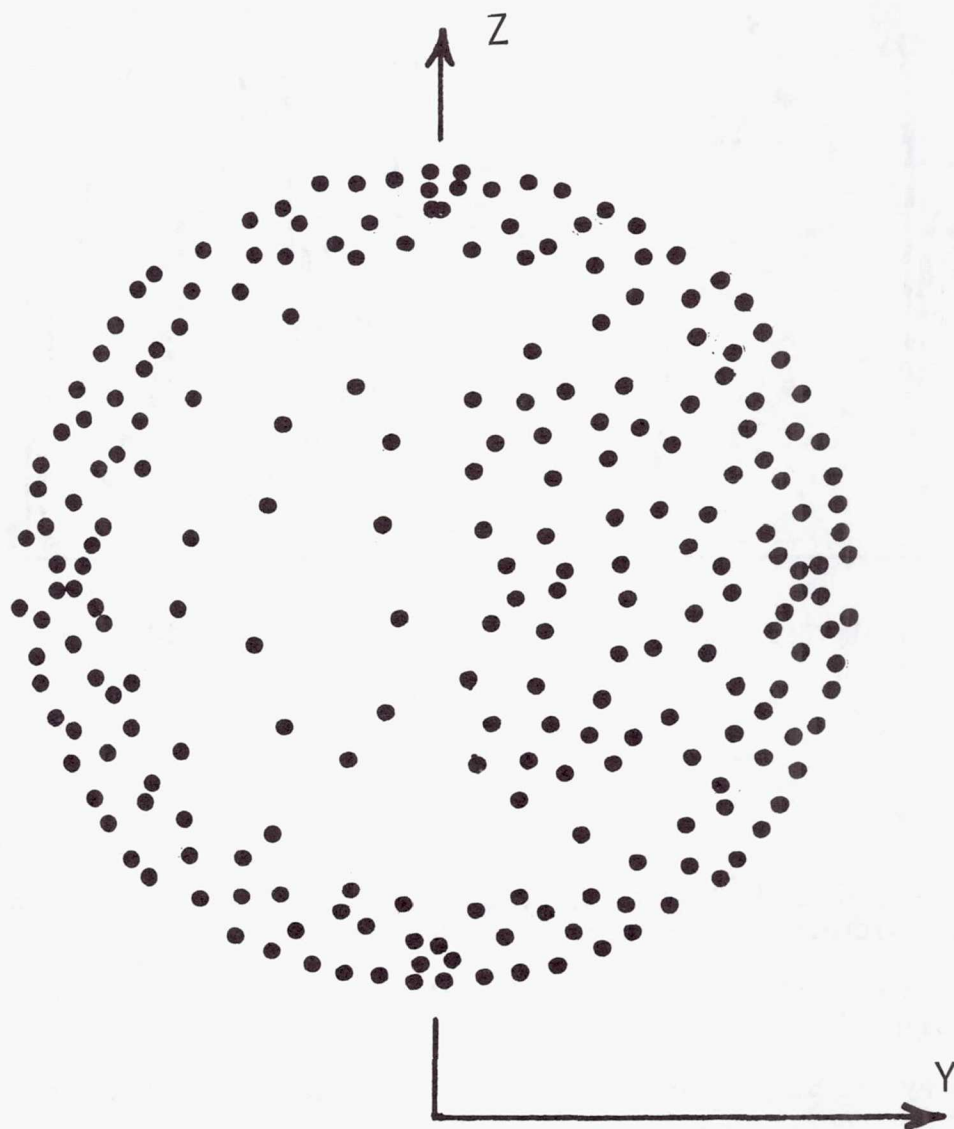
DISTORTED REFLECTOR

A distorted reflector was fabricated for experimental verification of the technique. The experimental antenna is an offset-fed spherical reflector (radius of curvature of 61 centimeters and reflector diameter of 26 centimeters) with an unknown distortion created by a glob of putty placed on the reflector surface in the region indicated in the photograph. The putty was smoothed by hand such that a gradual distortion was formed (thus the contour of the hump is not visible in the photograph) with a maximum height of approximately 0.16 centimeters and a somewhat irregular diameter of approximately 18 centimeters. The entire front surface of the reflector was then coated with conductive paint. The antenna patterns were measured at 35 GHz with the reflector illuminated by a dual-mode horn and with an edge taper of about 14 dB.



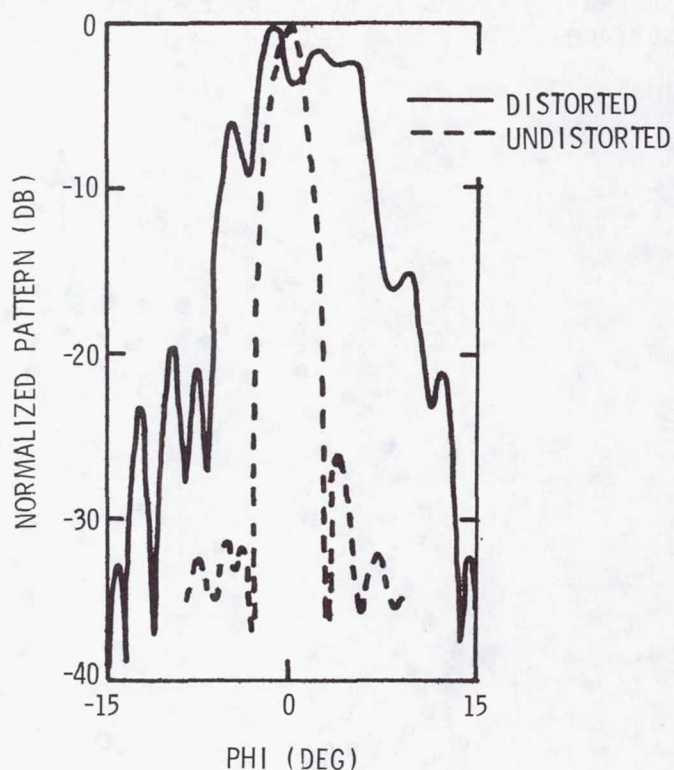
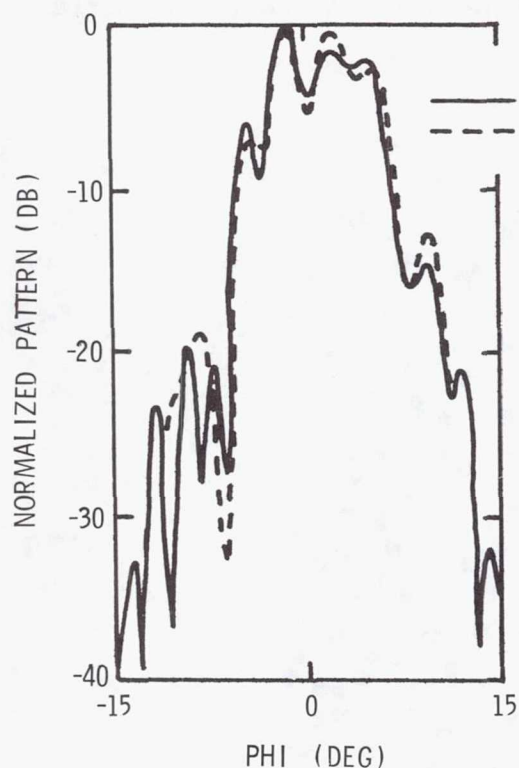
DISTRIBUTION OF MEASURED POINTS USED FOR CHARACTERIZING DISTORTED REFLECTOR SURFACE

The surface of the distorted reflector was measured at a large number of points and 234 of these points, distributed as shown in this chart, were used in the interpolation function to describe the reflector. It had been determined earlier (ref. 3) that 200 points, with a heavy concentration near the reflector rim, was adequate for describing an offset-fed paraboloidal reflector; however, an additional 34 points were concentrated in the distorted region for the present calculations. It has since been determined that an increase in the density of measured points in the vicinity of the distortion is not necessary and that a pseudo-uniform distribution with some increase in density near the reflector edge is also sufficient for the distorted surface.



RADIATION PATTERN FOR DISTORTED SPHERICAL REFLECTOR

The technique was verified by comparison of the calculated and measured radiation patterns in the plane perpendicular to the feed offset plane. The measured pattern for the undistorted reflector (taken before the distortion was created) is shown to indicate that the effect of the distortion is not a trivial one; however, the present technique predicts the radiation pattern quite well.



REFERENCES

1. R. L. Harder and R. N. Desmarais, "Interpolation Using Surface Splines," *Journal of Aircraft*, Vol. 9, Feb. 1972, pp. 189-191.
2. J. F. Kauffman, "Calculation of the Radiation Patterns of Reflector Antennas," North Carolina State Univ. Tech. Report, May 21, 1976.
3. M. C. Bailey and S. M. Moskowitz, "Radiation Pattern Prediction for Arbitrary Reflector Antennas," *IEEE AP-S International Symposium Digest*, Los Angeles, Cal., June 16-19, 1981, pp. 492-495.

MEASUREMENT OF LOSSES OF MESH MEMBRANE MATERIAL
FOR REFLECTOR APPLICATIONS WITH AN S-BAND RADIOMETER

Hans-Juergen C. Blume
NASA Langley Research Center
Hampton, Virginia

Large Space Systems Technology - 1981
Third Annual Technical Review
November 16-19, 1981

THE SUITABILITY OF MESH MEMBRANE MATERIAL
FOR RADIOMETER REFLECTOR APPLICATIONS

The spacial resolution, the frequency of revisits, and the accuracy requirements for the detection of Earth surface parameters from space (such as sea surface temperature, salinity, soil moisture, rain rate, and wind speed requested by the user communities) force the satellite designers to consider large space structures (such as large reflectors) for microwaves. Some Earth surface parameters are only detectable with radiometers. Because the large reflectors should be much lighter than solid and deployable reflectors, mesh membrane material is considered to be used as the reflector. It is essential to determine the emissivity of the reflecting material even when close to zero to estimate the accuracy of the radiometer measurement. Therefore, the objectives of this task are to define appropriate test set-ups and to evaluate the measurement results. An existing S-band radiometer was used to determine the loss of a 1 m^2 pretensioned mesh supplied by the Harris Corporation first in a field experiment and later in a well shielded laboratory set-up. The models for retrieving the emissivity of the mesh are described in detail and the equivalent losses for different mesh positions are calculated.

S-BAND RADIOMETER SYSTEM

The S-band (2.65 GHz) radiometer is a third-generation, advanced, switched radiometer. The design of the radiometer is based on the application of two concepts to the switched-input-type receiver introduced by Dicke. The first concept is to equalize the temperature of the reference noise source at the circulator switch with the temperature of the lossy microwave components between the antenna terminal and the receiver input. This temperature is maintained extremely constant (± 0.03 K). The second concept is to use a feedback loop to inject pulsed portions of a constant noise source (avalanche diode) into the received noise power at the antenna terminals to equalize the noise power at both inputs of the circulator switch. The pulse frequency, which determines the average value of injected noise power, is a measure of the noise power (radiation) received by the antenna. As a result of these two design improvements, the radiometer is nearly independent of gain variations and errors that are contributed by front-end losses. The radiometer, therefore, exhibits the long-term stability that is necessary to achieve absolute brightness temperature measurements to within a few tenths kelvin.

A simplified block diagram of the radiometer system is shown in figure 1. The radiation received by the antenna has the injected noise added to it. The circulator switch then switches between this sum of noise power and that of the matched termination which is at the reference temperature. The circulator switch output is amplified by the receiver's slow noise amplifier and detected by a square-law detector. The detector is demodulated in synchronisms with the circulator switch to produce a voltage driving the voltage-to-frequency converter. The output signal from the voltage-to-frequency converter is used to gate the noise injection pulse driver which adjusts the injected noise power level to achieve a null at the output. Gating the noise source with constant-width pulses produces a linear relationship between the pulse frequency and the averaged injected noise. It is this linearity that allows accurate measurement over a wide range of brightness temperatures (typically 303 K). Finally, output data are plotted in analogue form on a strip-chart recorder. The S-band radiometer resolutions are ± 0.08 K and, with suitable calibration, has an absolute accuracy of better than ± 0.2 K.

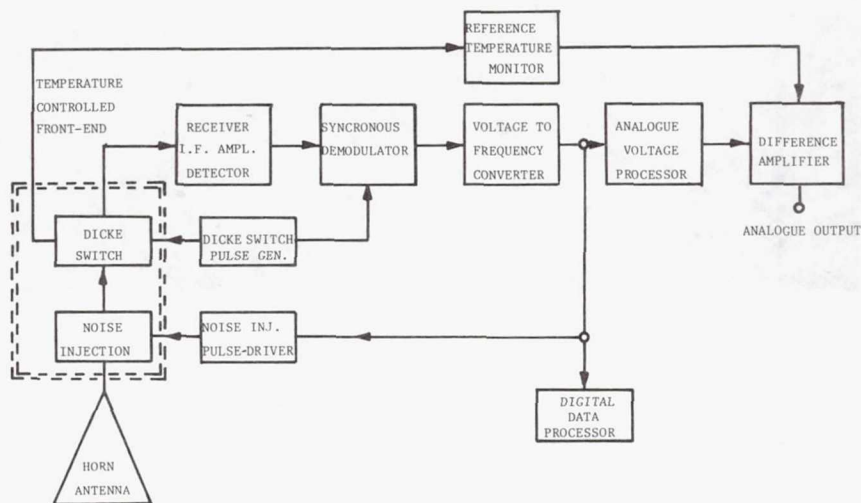


Figure 1.- Block diagram of S-band radiometer system.

MESH MEMBRANE MATERIAL

An enlarged photograph of the Harris mesh designed for deployable antennas is shown in figure 2. The mesh is fabricated with gold-plated molybdenum wires with $25\text{ }\mu\text{m}$ diameter and approximately 15 mesh openings per cm^2 . The penetration or skin depth at 2.65 GHz frequency for gold is $2\text{ }\mu\text{m}$ and the molybdenum has a relative resistivity of 3.3 to soft copper. The mesh area was 1 m^2 and pretensioned to the deployment specifications determined by the Harris Corporation.

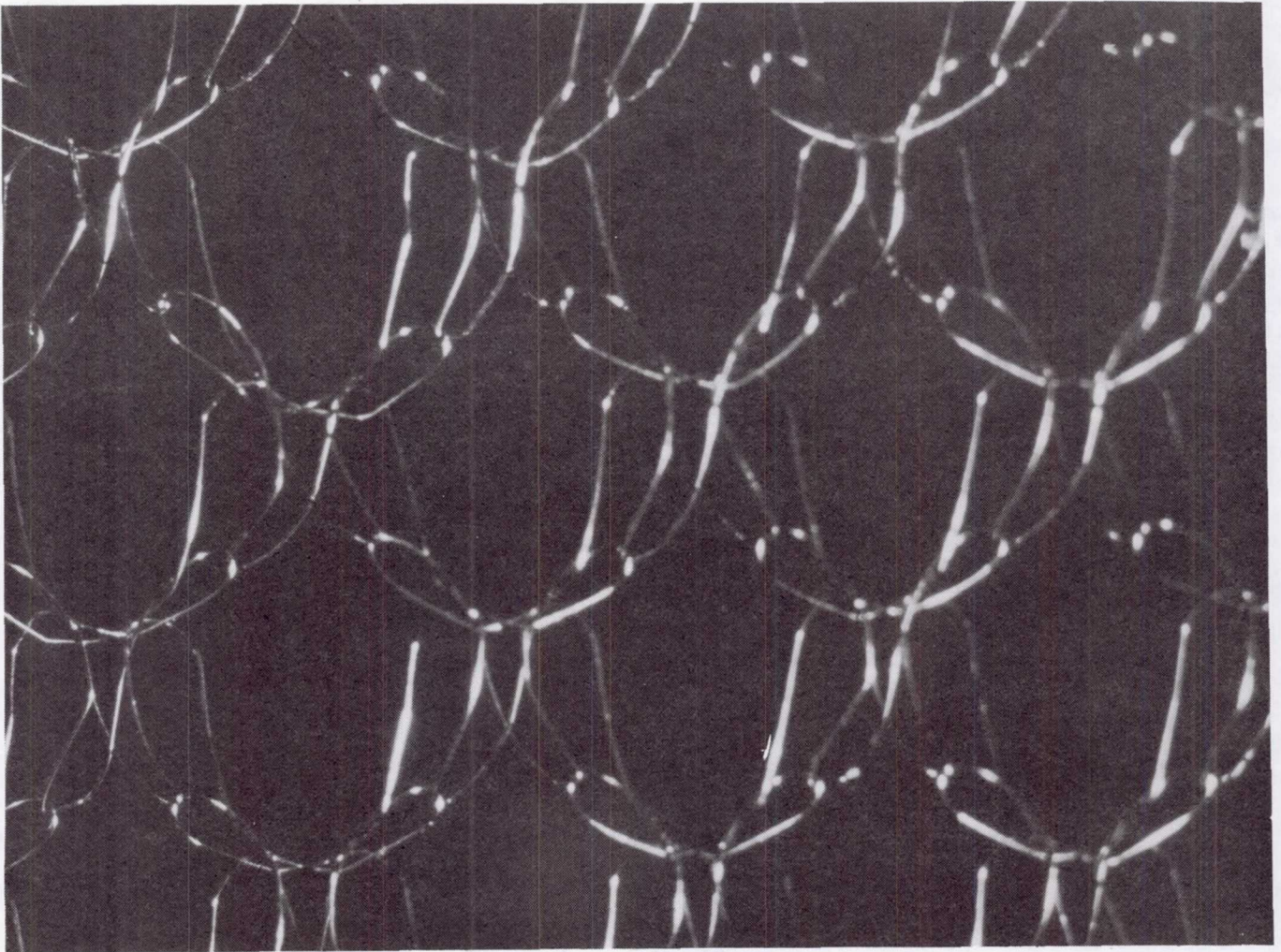


Figure 2.- Harris mesh designed for deployable antennas.

FIELD EXPERIMENT

The location, where the experiment was conducted, and the time were selected carefully to prevent radio frequency interference (RFI) and unnecessary thermal microwave radiation from surrounding structures. The experiment consisted of six different measurements.

1. The radiometer horn antenna was directed toward the Sun and the equivalent temperature of the Sun's radiation and the down-welling radiation of other sources, such as the galactic and absorption radiation of the oxygen resonance, was measured.

2. The aluminum plate (Alu-plate) of 1 m^2 was set up to reflect the Sun's radiation into the horn antenna of the radiometer. The geometry of the positioning of the plate in relation to the aperture of the horn antenna and the Sun's radiation direction was chosen carefully to avoid spillover into the background of the set-up. Because the aluminum plate was 1 cm thick, the transmissivity was considered to be zero. The equivalent temperature of the received radiation is

$$T_{R1} = T_{\text{sun}} \cdot r_p + T_o \cdot e_p + T_k \quad (1)$$

where T_{sun} is the equivalent temperature of the down-welling of all radiations being reflected off the plate including the Sun, the galactic, and the oxygen absorption effects. The Alu-plate reflectivity is r_p and its emissivity is e_p . T_o is the physical temperature of the plate. T_k represents the radiometer front-end effects such as sidelobes of the antenna, the antenna losses, and the side effects of the reflector supports.

3. The next arrangement is shown in figure 3. The antenna was positioned in a westerly direction away from the Sun's radiation. The reflector was positioned in front of the antenna aperture to receive the sky radiation together with the other down-welling radiations mentioned above. For the Alu-plate alone, the equivalent temperature of the received radiation is

$$T_{R2} = T_{\text{sky}} \cdot r_p + T_o \cdot e_p + T_k \quad (2)$$

where T_{sky} includes the big-bang residual radiation and the aforementioned down-welling.

4. The fourth measurement was carried out by placing the mesh in front of the Alu-plate, and the equivalent temperature of this set-up is approximately

$$T_{R3} = T_{\text{sky}} \cdot r_s + T_o \cdot e_s + T_k \quad (3)$$

where r_s is the reflectivity and e_s the emissivity of the mesh.

5. The fifth experiment consisted of using the mesh alone as a reflector, and we obtained the equivalent temperature

$$T_{R4} = T_{\text{sky}} \cdot r_s + T_o \cdot e_s + T_{\text{back}} \cdot t_s + T_k \quad (4)$$

where T_{back} is the equivalent temperature of the background radiation and t_s is the transmissivity of the mesh.

6. The last measurement consisted of the determination of T_{back} by removing the reflector completely but leaving the support equipment in place.

Assuming $r_p + e_p = 1$ (transmissivity = 0) and subtracting equation (2) from equation (1) results in obtaining r_p and e_p . Then $T_{R3} - T_{R2}$ gives approximately r_s and e_s . Using $T_{R4} - T_{R3}$ and applying the result from experiment 6 gives the transmissivity t_s . The results are $e_s = 0.105$, $r_s = 0.866$ and $t_s = 0.029$ or in power terms $L_s = 0.4812$ dB and $T_s = 0.128$ dB where L_s is the ohmic loss and T_s the transmission loss of the mesh membrane material.

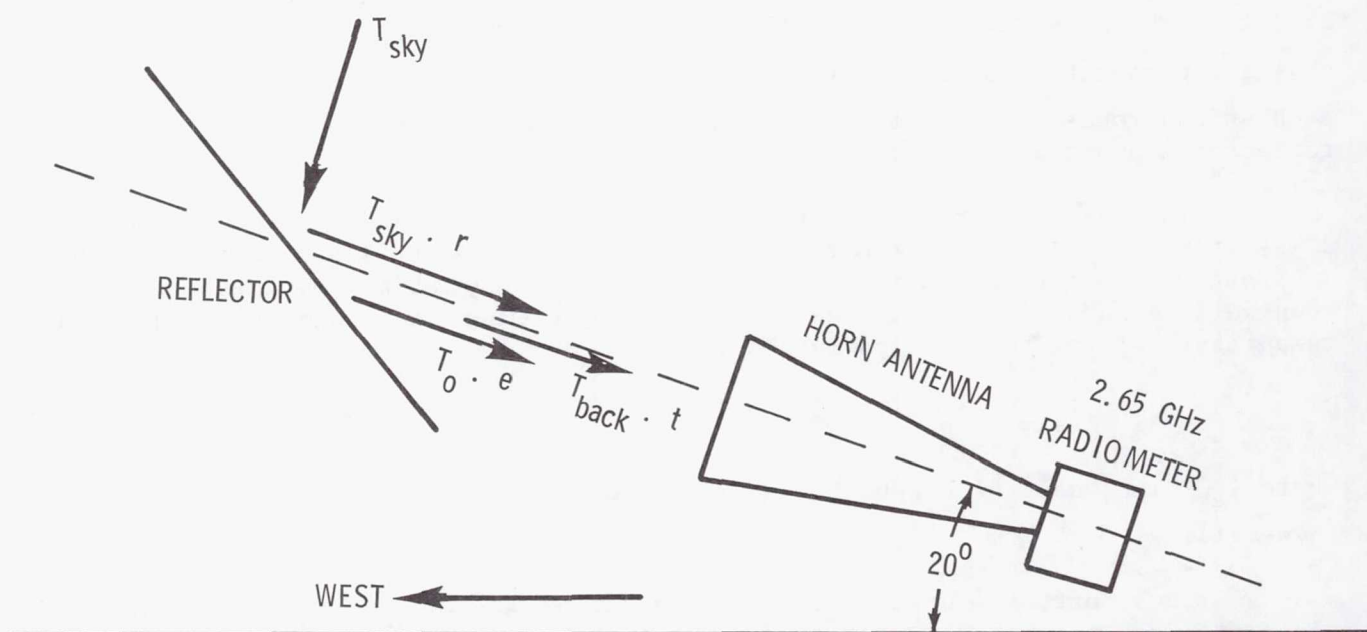


Figure 3.- Field experiment to determine mesh emissivity and transmissivity.

LABORATORY EXPERIMENT

The results of the field experiments appeared to be not accurate enough, i.e., the ohmic losses seemed to be too high and the reflectivity too low. Therefore, a more controlled experiment set-up in the laboratory was planned and constructed. The set-up is shown in figure 4. The 2.65 GHz radiometer is mounted horizontally with its horn antenna. A horn extension is reaching over a cryoload. The cryoload is a matched load filled with liquid nitrogen. The cryoload is used to calibrate radiometers. It consists of a box containing microwave-absorbing material with pyramidal absorption facets that were cooled with liquid nitrogen. The horn extension is terminated with the Alu-plate as the reflector with a 45 degree inclination angle over the cryoload. Provisions have been built into the set-up for the insertion of the mesh in front of and close to the Alu-plate. With this set-up two measurements were conducted.

The first measurement excluded the mesh, and the radiation condition of the enlarged section is shown in figure 5. The measured equivalent temperature of this condition is

$$T_{R5} = T_N \cdot r_p + T_p \cdot e_p + T_c \quad (5)$$

where T_N is the cryoload temperature, T_p is the physical temperature of the Alu-plate, and T_c represents the front-end contribution for this set-up. The plate emissivity is e_p and the reflectivity r_p . The radiation loss $T_N \cdot e_p$ is directed away from the radiometer input because this radiation loss is converted into heat (not measurable) and does not enter into the measuring process.

The next measurement was performed with the mesh inserted into the system as shown in figure 4. The radiation component composition and condition is indicated in figure 6. In this reflector combination all components including multireflection and transmissivity are considered. The measured temperature is

$$T_{R6} = T_N \cdot r_s + T_N \cdot t_s^2 \cdot r_p + T_s \cdot e_s + T_s \cdot e_s \cdot r_p \cdot t_s + T_p \cdot e_p \cdot t_s + T_c \quad (6)$$

The index s relates to the mesh and the index p relates to the Alu-plate as far as the temperature T , emissivity e , reflectivity r , and transmissivity t are concerned. Subtracting equation (5) from equation (6), i.e., $T_{R6} - T_{R5}$, and solving for e_s gives the emissivity of the mesh. The mesh was positioned in different orientations to detect any polarization effects. The results are presented in table I.

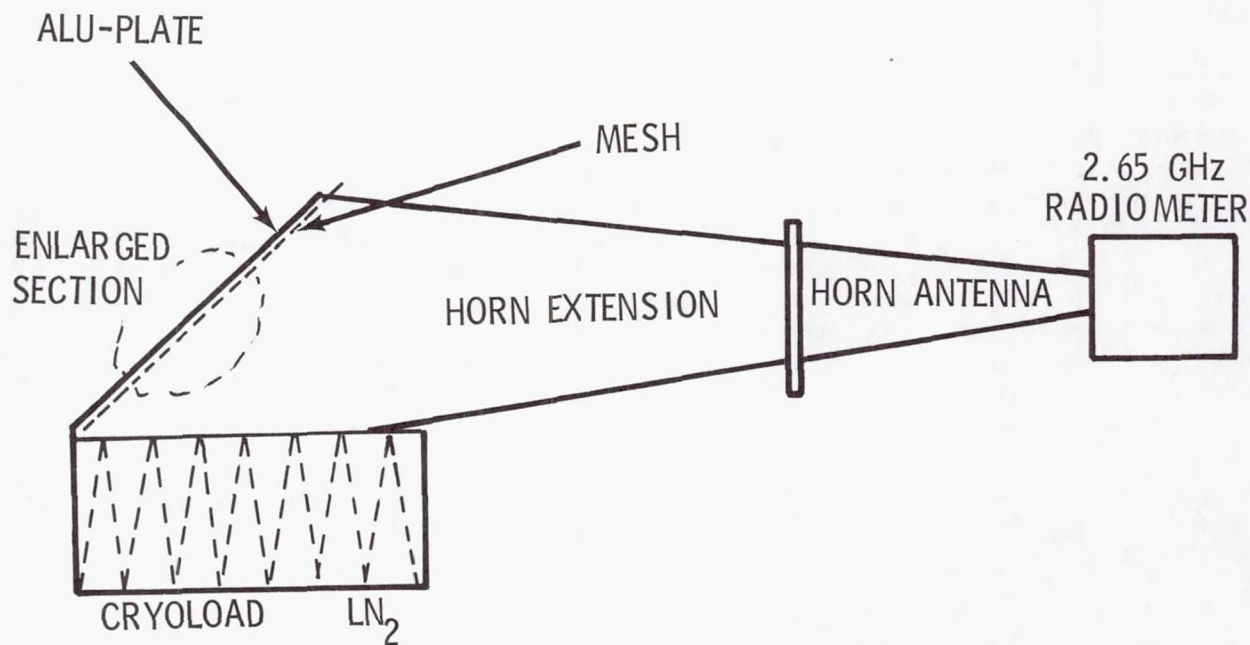


Figure 4.- Laboratory set-up.

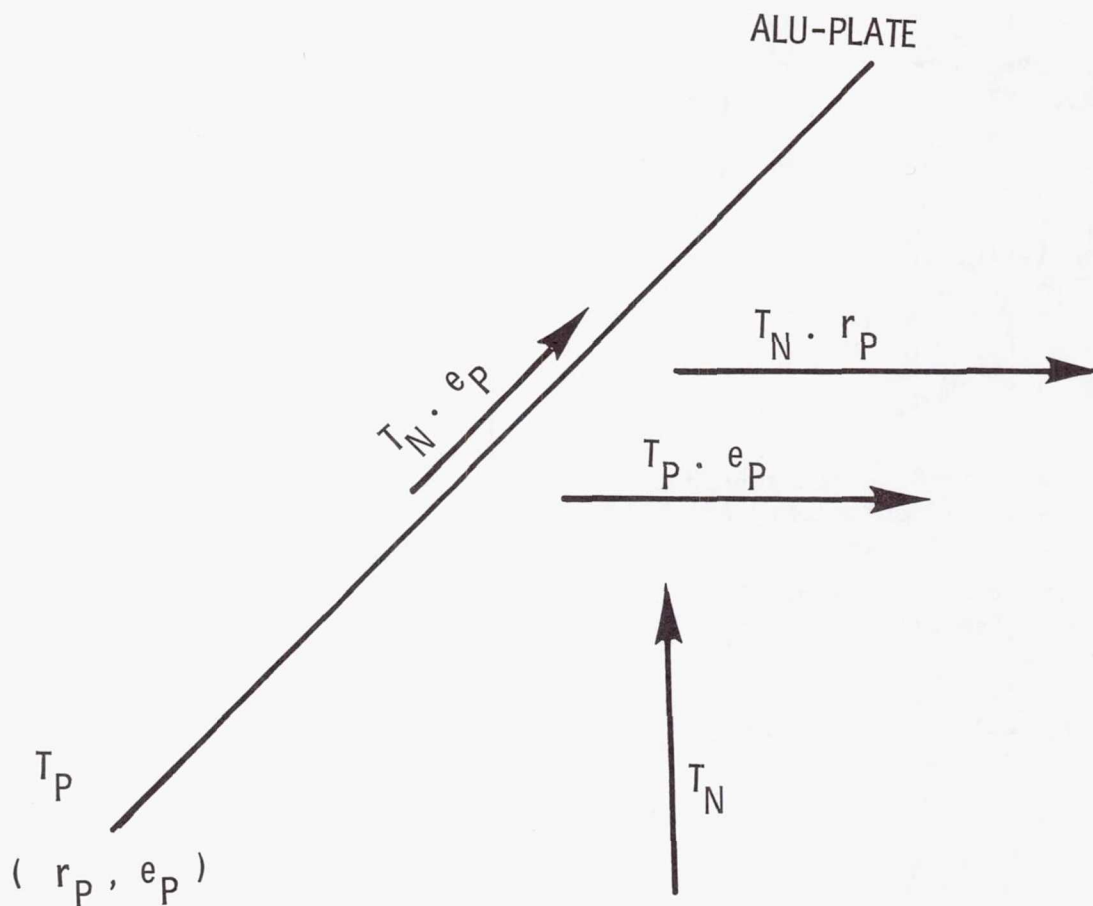


Figure 5.- Radiation components at Alu-plate of enlarged section.

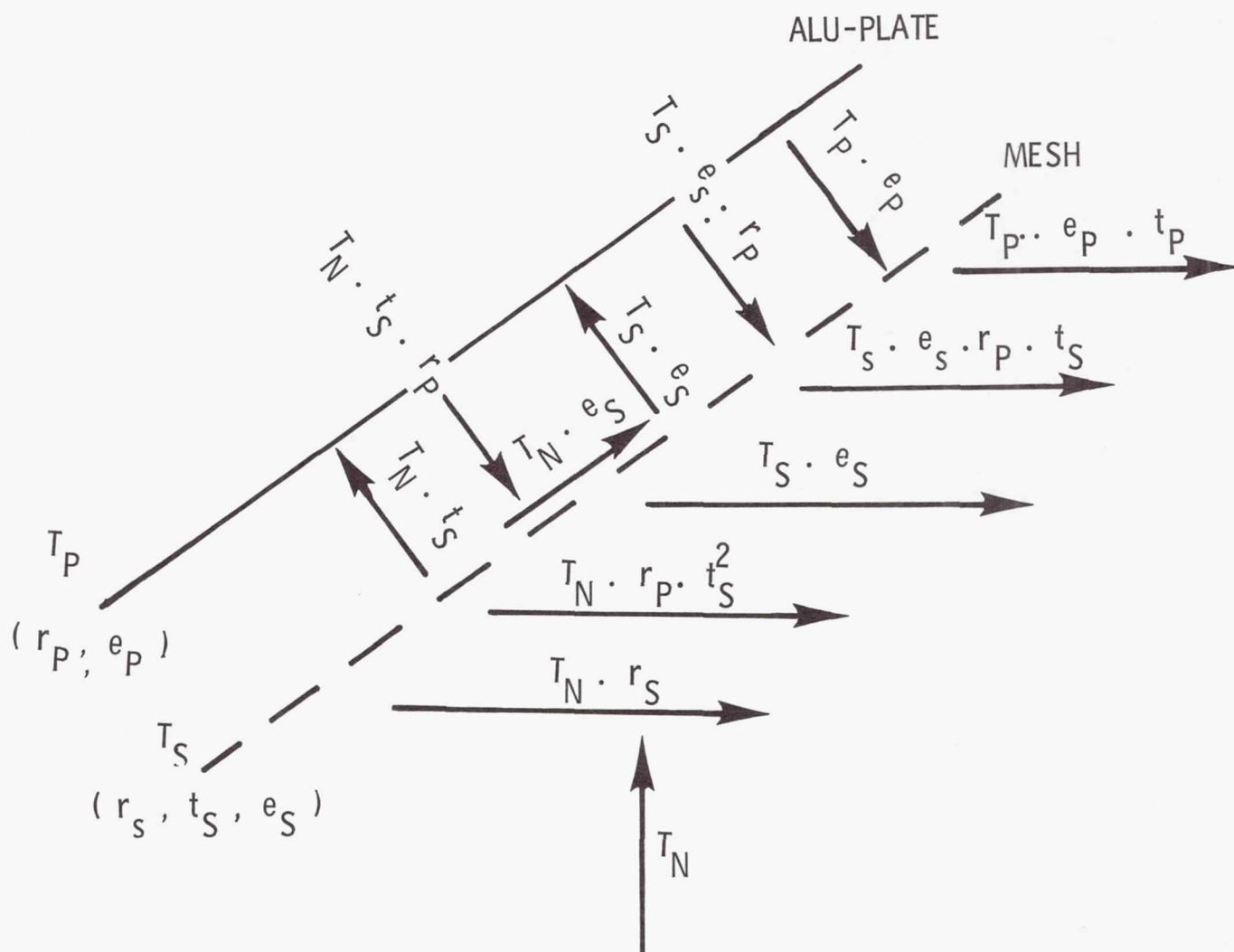


Figure 6.- Radiation components at the Alu-plate and mesh combination of enlarged section.

TABLE I.- RESULTS OF MEASUREMENTS

DIRECTION	EMISSIVITY e_s	L_s (dB)
↑	0.07775	0.35
→	0.07945	0.36
↓	0.07877	0.356
←	0.07775	0.352

CONCLUSIONS

A polarization effect was not detected. The mesh membrane material designed for frequencies up to 15 GHz has a loss of 0.35 dB measured with a radiometer at 2.65 GHz. A knowledge of ± 2 Kelvin of the temperature of the mesh would be required for a radiometer accuracy of 0.1 Kelvin. A mesh technology development program is needed to improve the suitability for radiometer applications over a wide frequency range.

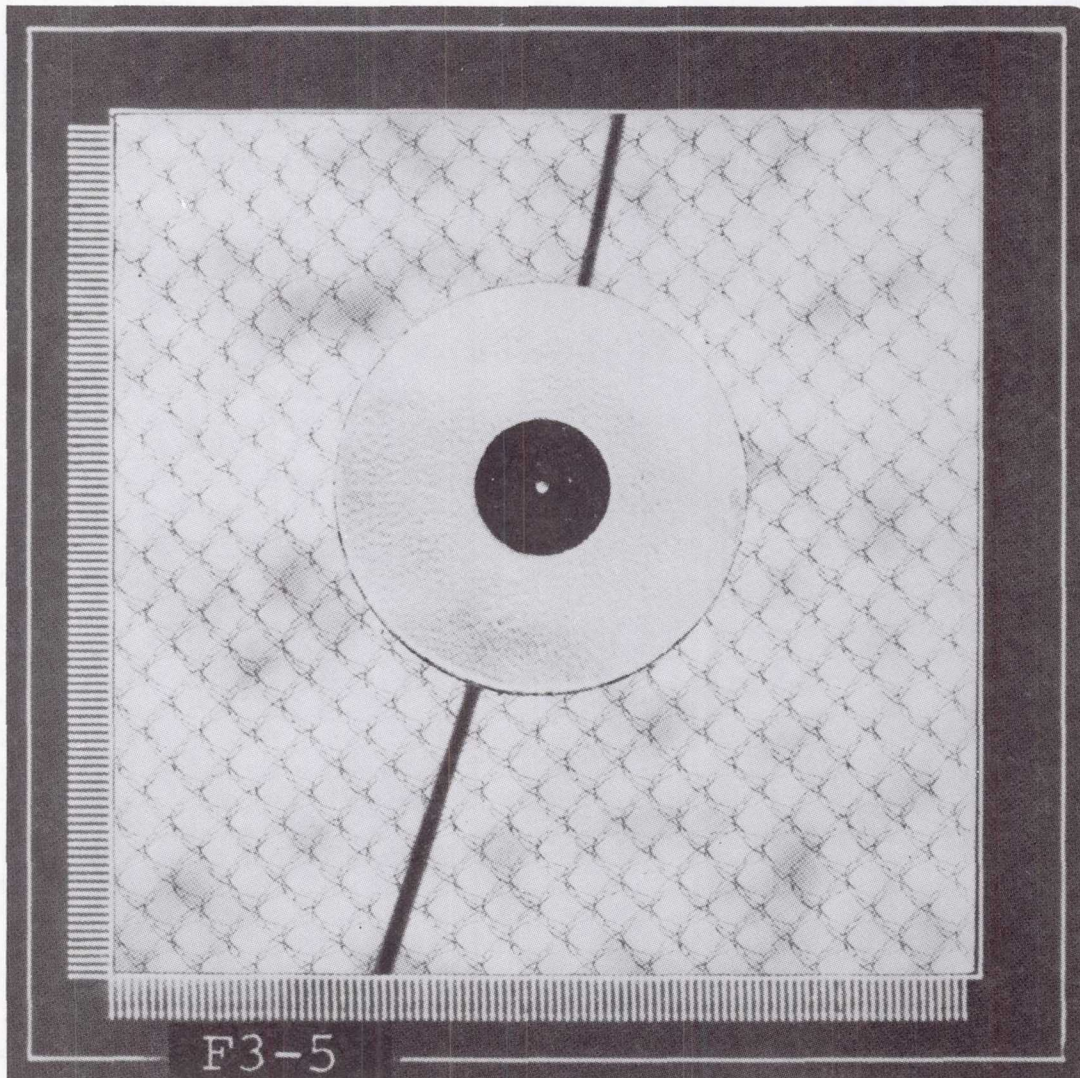
THE SUITABILITY OF MESH MEMBRANE MATERIAL
FOR RADIOMETER REFLECTOR APPLICATIONS

W. F. Croswell
Harris Corporation
Melbourne, Florida

Large Space Systems Technology - 1981
Third Annual Technical Review
November 16-19, 1981

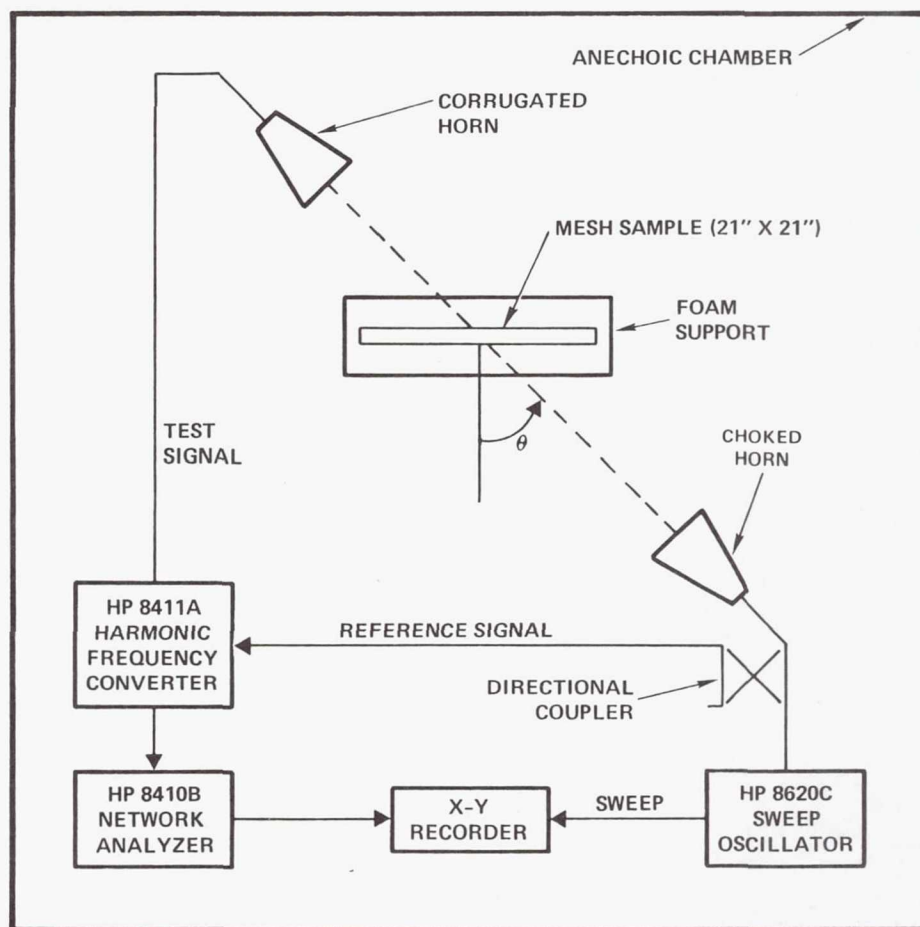
TYPICAL ANTENNA MESH

A detailed photograph of the typical mesh used in Harris deployable antennas is given here. The wires which make up the mesh are gold plated molybdenum approximately 1 mil in diameter.



FREE SPACE TRANSMISSIVITY MEASUREMENT SYSTEM

The standard measurement system used at Harris for evaluating the transmission properties of mesh used in deployable antennas is shown schematically in this figure. The system allows the rapid measurement of the transmissivity of mesh samples at a given incidence angle. Low density foam fixtures are configured to hold mesh samples in such a way as to minimize extraneous scattering. It is important to note that this measurement does not separate leakage through the mesh from the I^2R loss.



THEORETICAL MODEL OF MESH

The theoretical model used to compute the EM properties of antenna mesh is given in this figure. The model is based upon two papers in Radio Engineering and Electronic Physics:

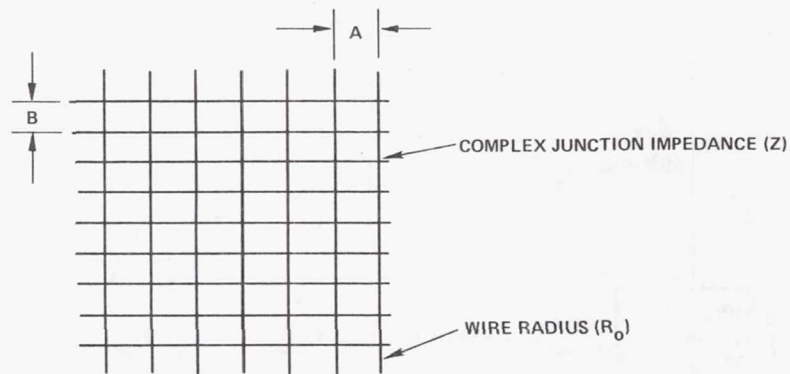
"Average Boundary Conditions on a Grid Surface with Square Cells," Sept. 1963

by M.I. Kontorovich

"Averaged Boundary Conditions on the Surface of Lattice with Rectangular Cells," Aug. 1964

by M.I. Astrakhan

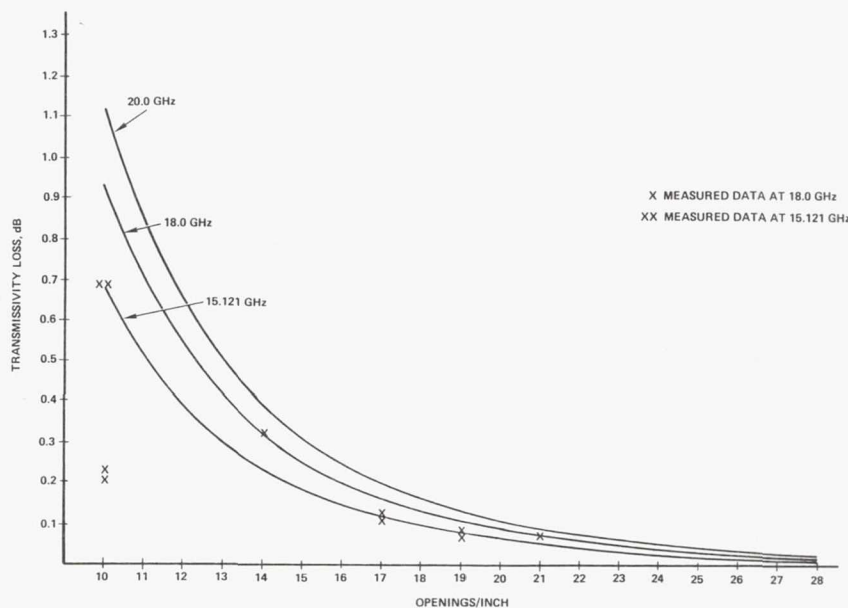
The analysis has the advantage in that the effects of conductivity loss, junction impedance, and cross polarization can be treated. The mesh effects are now incorporated in the Harris reflector SCI programs.



- AVERAGE BOUNDARY CONDITIONS
- INCLUDES CONDUCTIVITY LOSS
- JUNCTION IMPEDANCE CAN BE CAPACITIVE OR INDUCTIVE
- CALCULATES CROSS POLARIZATION TERMS DUE TO SURFACE IMPEDANCE

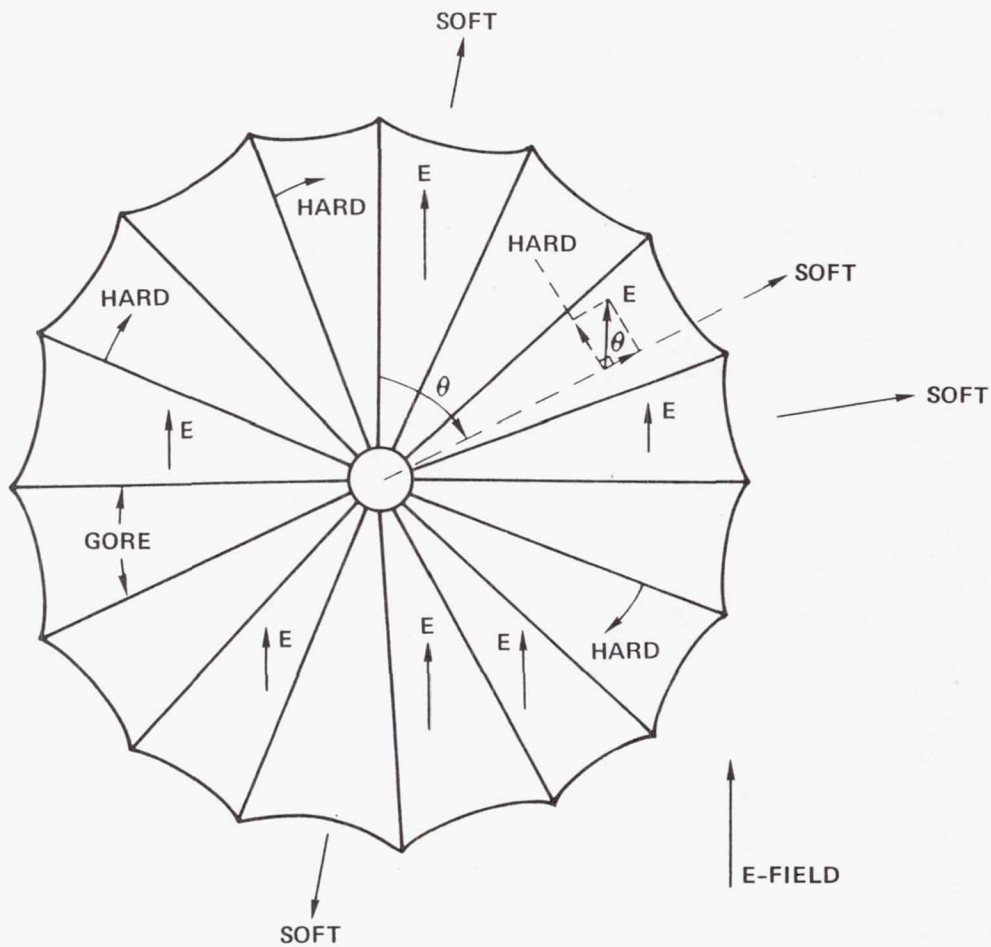
TRANSMISSIVITY LOSS PROPERTIES OF MESH AT MICROWAVE FREQUENCIES

The purpose of this figure is to present the design data used at Harris for predicting mesh transmissivity loss at microwave frequencies. The theoretical curves were obtained using the numerical model described previously; the experimental data was obtained with the free space transmissivity measurement system. The measured data agrees well with the experimental data until the openings per inch are approximately 0.1 wavelengths. For these sizes the details of mesh construction, not accounted for in the theoretical model, began to dominate. Note that the transmissivity loss numbers include energy leaked through the mesh plus the I^2R loss.



MESH REFLECTOR POLARIZATION AVERAGING DIAGRAM

The TDRSS antenna is composed of 10 openings per inch mesh which is a very complex structure. Basically the mesh is manufactured so that it has a continuous strand direction (hard) and an orthogonal knit direction (soft). The mesh is stretched between ribs in the approximately hard direction. Due to the very open nature of the mesh the scattering and transmission properties are direction and polarization dependent. This figure presents a description of these properties for the TDRSS antenna.

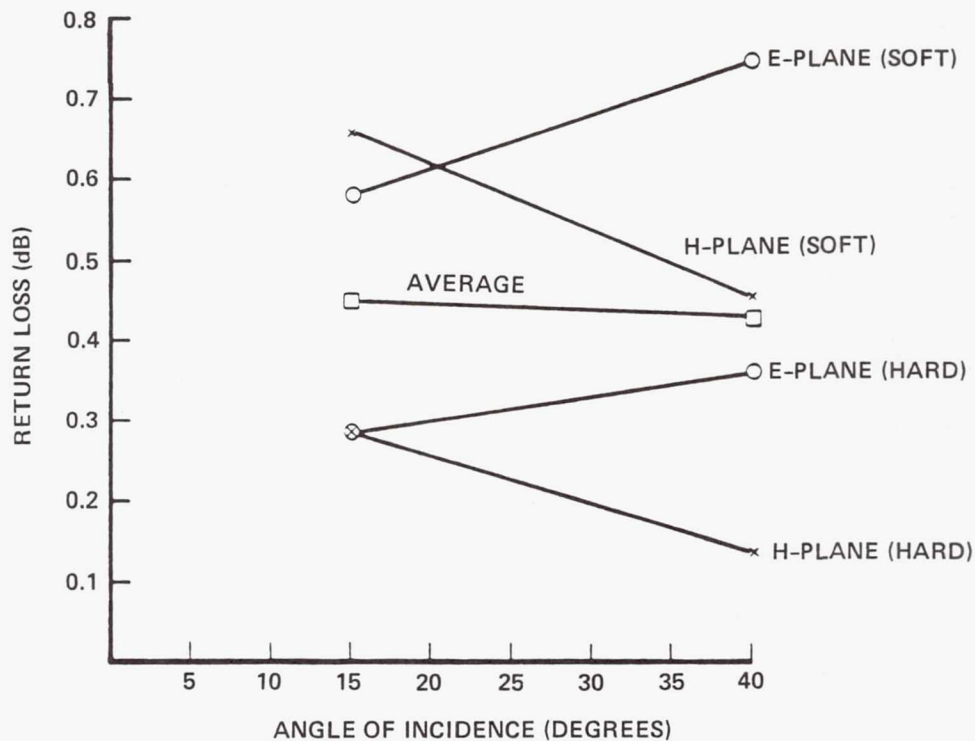


MESH RETURN LOSS VS ANGLE OF INCIDENCE

AT 15 GHz

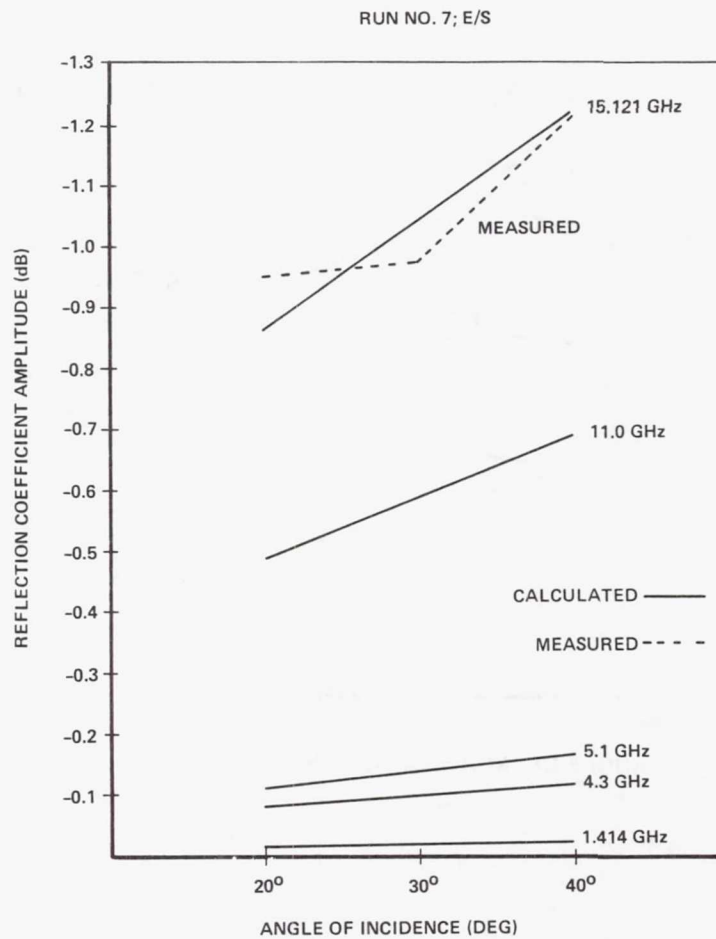
This figure presents the computed reflection properties of the TDRSS mesh for the different directions of mesh and polarization.

The average value of the reflective loss is approximately 0.5 dB. This value combines both energy leaked through the mesh and the I^2R loss.



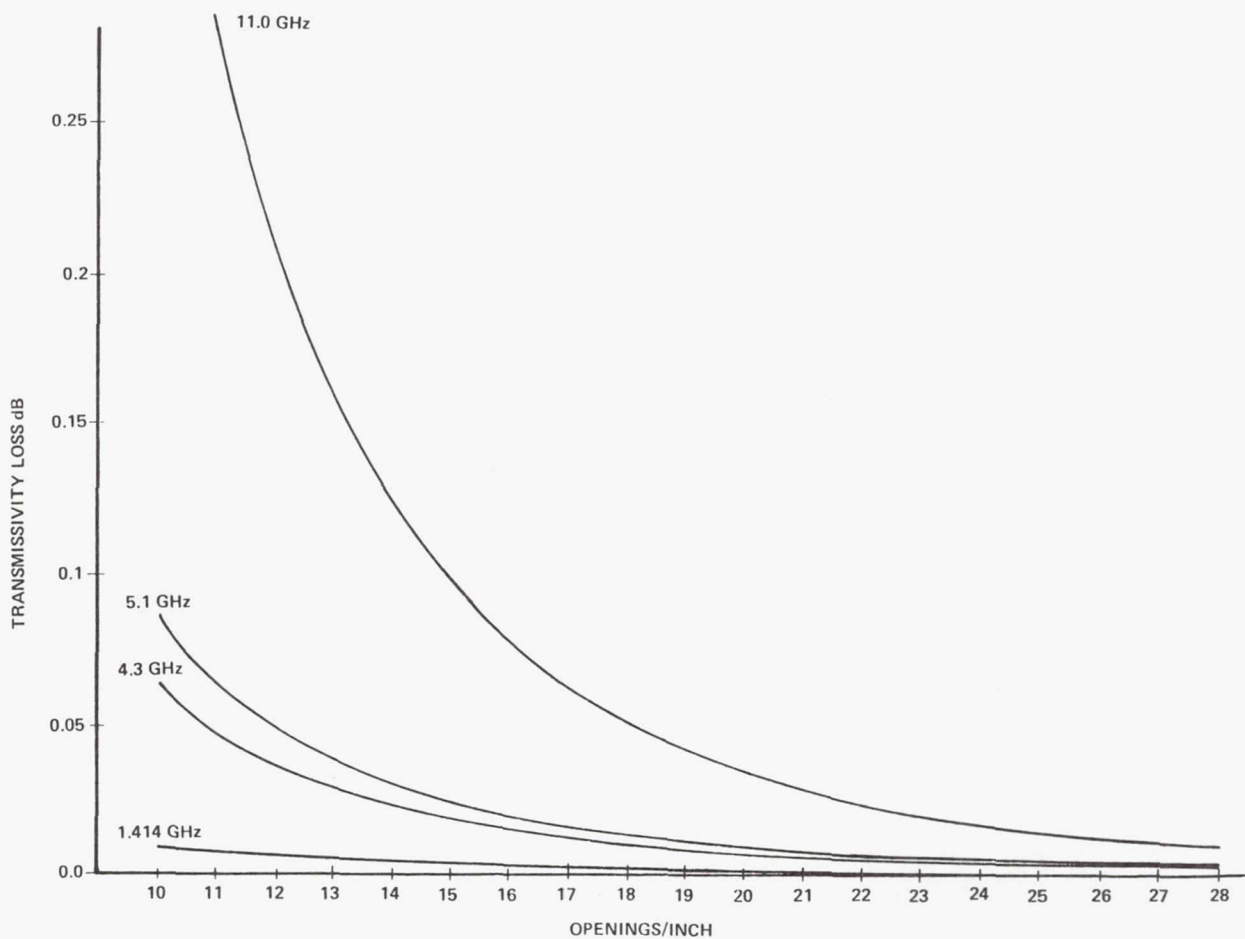
TDRSS MESH REFLECTION PROPERTIES
AT RADIOMETRIC FREQUENCIES

The worst case reflection properties of the TDRSS 10 openings per inch mesh are given in this figure along with measured data. Using the analysis presented earlier, calculations of reflective loss of the TDRSS mesh are given for the typical radio-meter frequencies of 11.0, 5.1, 4.3, and 1.414 GHz.



TRANSMISSIVITY PROPERTIES OF MESH
AT RADIOMETER FREQUENCIES

This figure presents transmissivity loss of mesh as a function of opening size for typical radiometer frequencies. It should be noted that the TDRSS mesh is approximately 10 openings/inch.



Page intentionally left blank

CONCEPTUAL DESIGN OF A SURFACE MEASUREMENT SYSTEM
FOR LARGE DEPLOYABLE SPACE ANTENNAS

R. S. Neiswander
TRW Defense and Space Systems Group
Redondo Beach, California

Large Space Systems Technology - 1981
Third Annual Technical Review
November 16-19, 1981

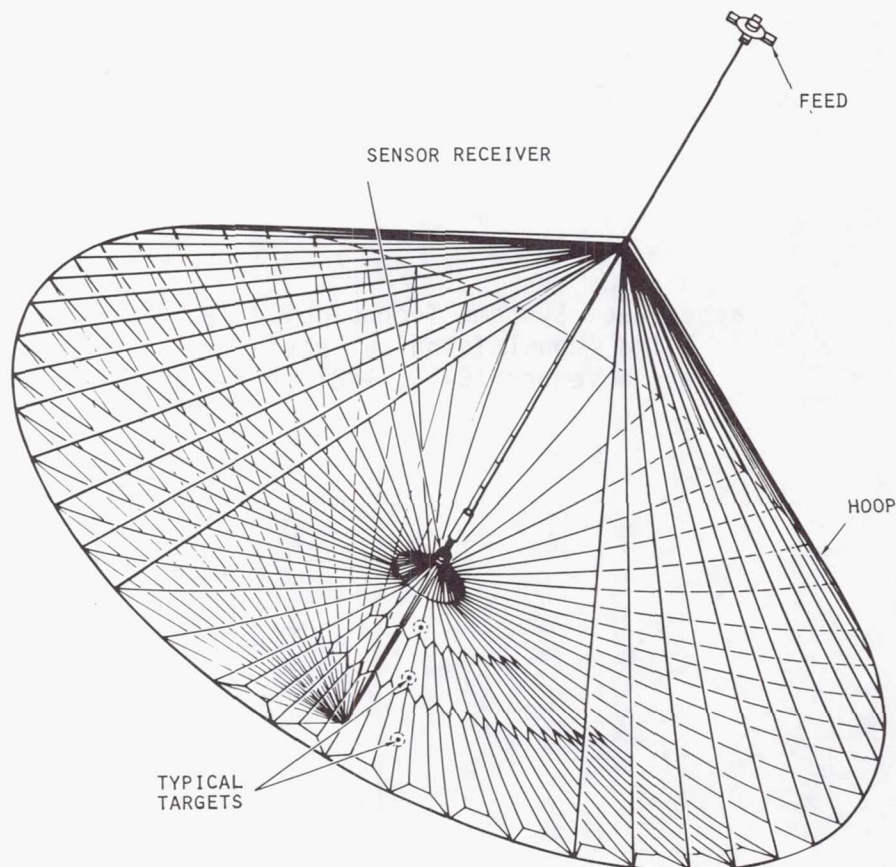
MEASUREMENT SYSTEM CONCEPTUAL DESIGN

The effort reviewed here has been conducted under Contract NAS1-16461 for NASA Langley Research Center. Technical monitor at NASA is Mr. Robert B. Spiers, Jr.

A major portion of this program has been the development of a flight design sensor system to a level where its performance and interface characteristics can be established. This sensor system is in essence a point design, specifically interfacing with the Harris, Inc., 100-meter deployable mesh communication antenna. It is to be noted, however, that the design can, without large modification, be adapted to other large deployable antennas such as the Lockheed Wrap-rib, the General Dynamics Precision Erectable Truss and the TRW Advanced Sunflower antennas.

Measurements are optical displacements. As shown in the figure, the elements of the system are 1) a central cluster of receivers near the apex of the antenna and 2) active "bright" targets at the antenna. The cluster defines a single coordinate frame from which all surface positions are referenced. The receivers continuously observe an extended array of sample points located throughout the reflecting surface and its supporting structure. For the Harris antenna, the surface samples are at the mesh gore lines and at the supporting hoop.

Output data is in real-time, compatible with on-board processing and active control of antenna figure. Lifetime of the system is at least 10 years continuous operation in space.

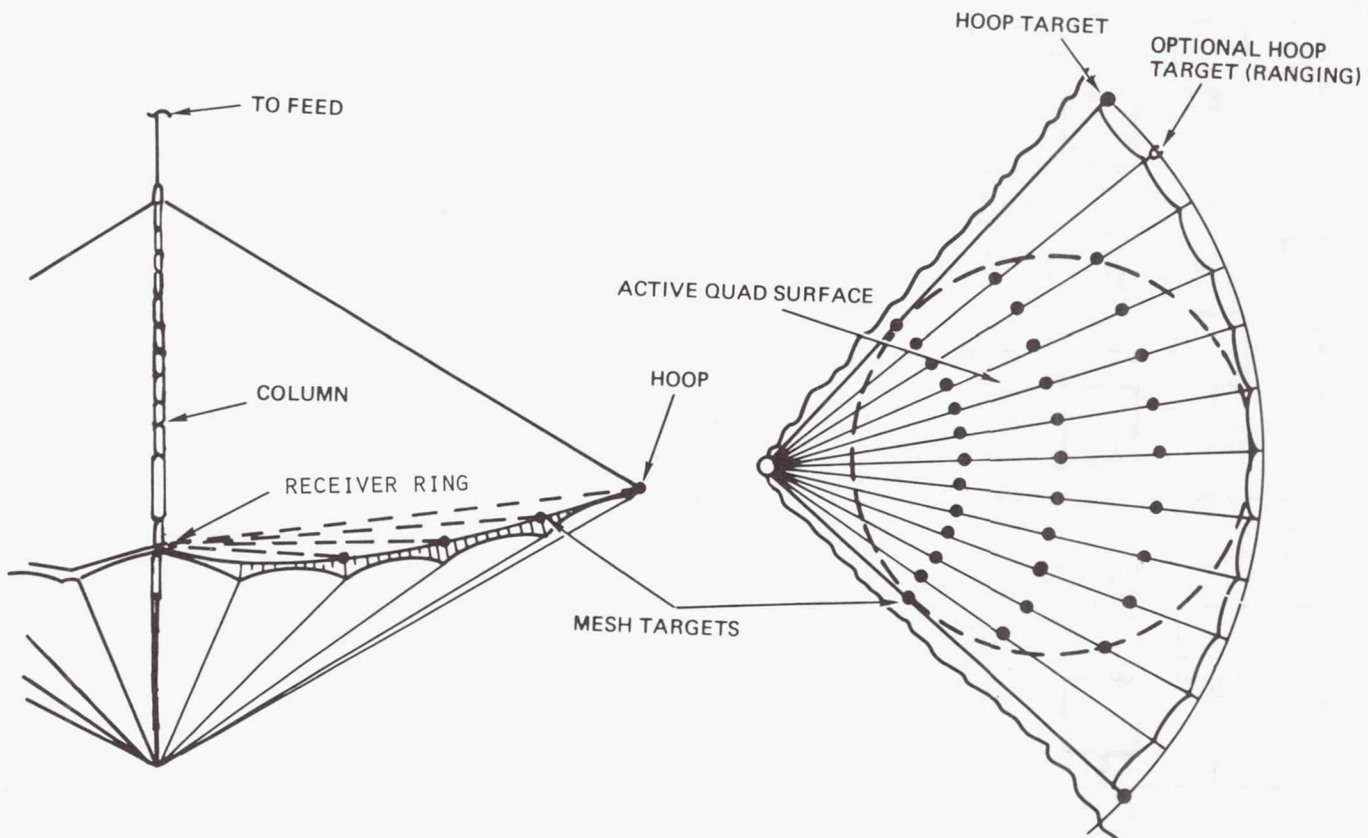


SURFACE SAMPLE COVERAGE FOR THE HARRIS POINT DESIGN ANTENNA

The Harris Maypole, or Hoop and Column, is a deployable mesh antenna that offers light weight and Shuttle compatibility. It consists of a central dual ended telescoping column, a segmented hoop, and an intervening mesh held to figure by secondary ties and by tensioning stringers. Deployment is primarily controlled by payout of the central control stringers.

The baseline antenna is a 48-gore, 100-meter diameter configuration. Its mission is geosynchronous coverage of continent-wide areas, providing multi-frequency, multi-beam communication. For this application, the antenna has a multiple feed at the tip of the column and a reflecting surface containing four sub-reflectors. Each sub-reflector, or quad surface, is approximately circular with an offset center of curvature.

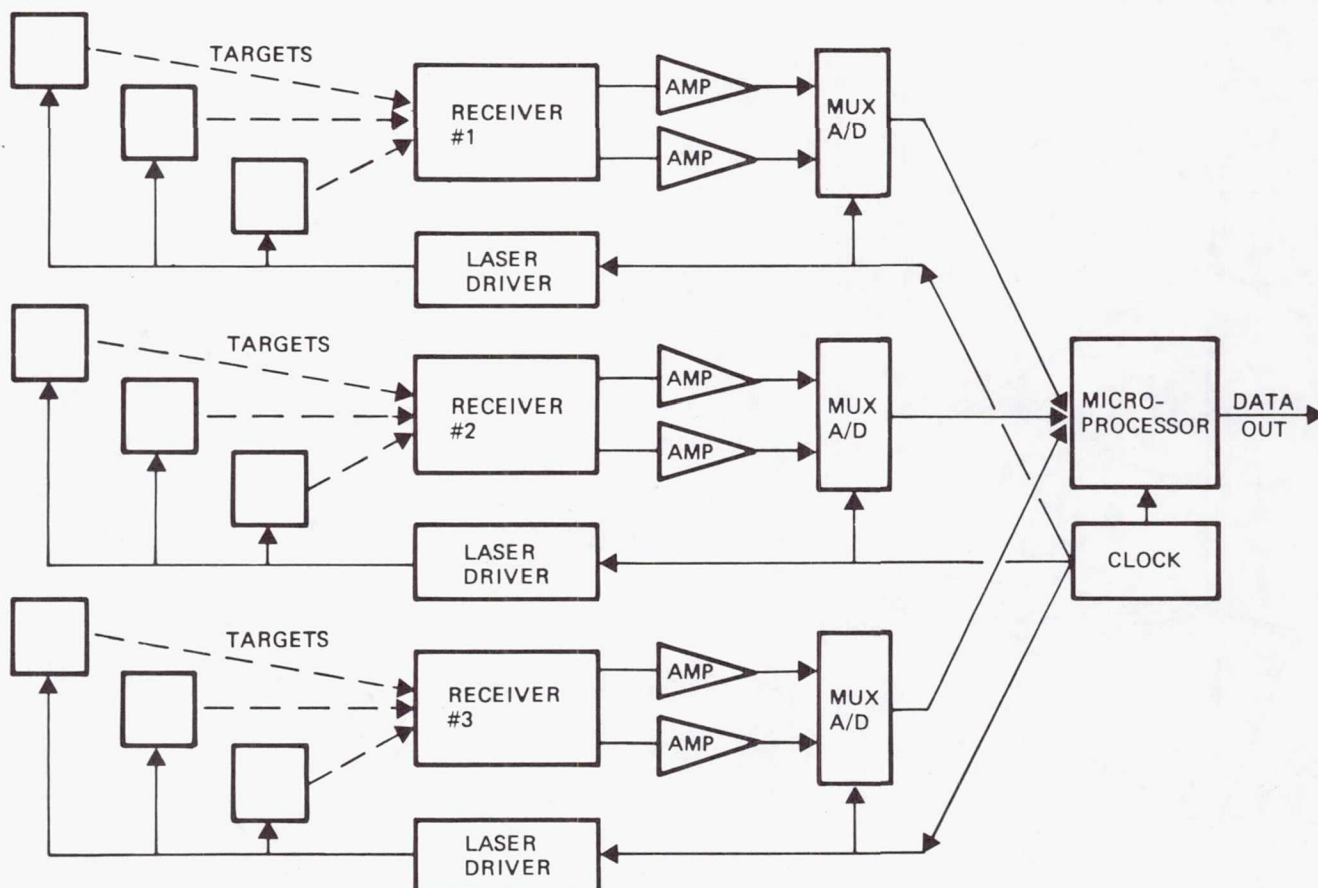
To define the reflecting surface shape, sampling is required at the intersections of the ribs and the tensioning stringers and at the hoop. As shown in the figure, sampling is only within the active area of the reflector. Disallowing the innermost tie points, 33 sample points at the mesh of each sub-reflector are required. Since the outer targets are shared with adjacent reflectors, the total number of mesh targets is 128. The segmented hoop forms a somewhat rigid perimeter than can be located by as few as 4 sample points. At these points both axial and tangential (i.e., twist) displacements of the hoop are to be measured.



FLIGHT SENSOR SYSTEM FUNCTIONS SCHEMATIC

Illustrated are the functions of the sensor system. Three of the receiver channels are shown, each containing three targets observed simultaneously by the assigned receiver. Synchronously controlled by the master clock, the targets are turned on in sequence so that only one target is active within a sub-frame interval. As each target is imaged at the receiver detector, its angular position relative to an expected or ideal position is evidenced as an image offset at the receiver detector. This image offset is transduced at the detector to differential current signals that are amplified, multiplexed to common analog-to-digital converters and fed to the central microprocessor. At the processor, the image coordinate is computed, from which the target angular dislocation and its surface normal deformation are calculated.

If this system is part of an actively controlled antenna, the resultant set of deformations are then entered into a dynamic model of the antenna that computes the corrective actions to be taken by the network of surface adjustment actuators. For passive antennas, the measurement set can be either recorded or directly transmitted to a manned station. For either passive or active type of operation, a complete deformation data frame is available up to four times a second.

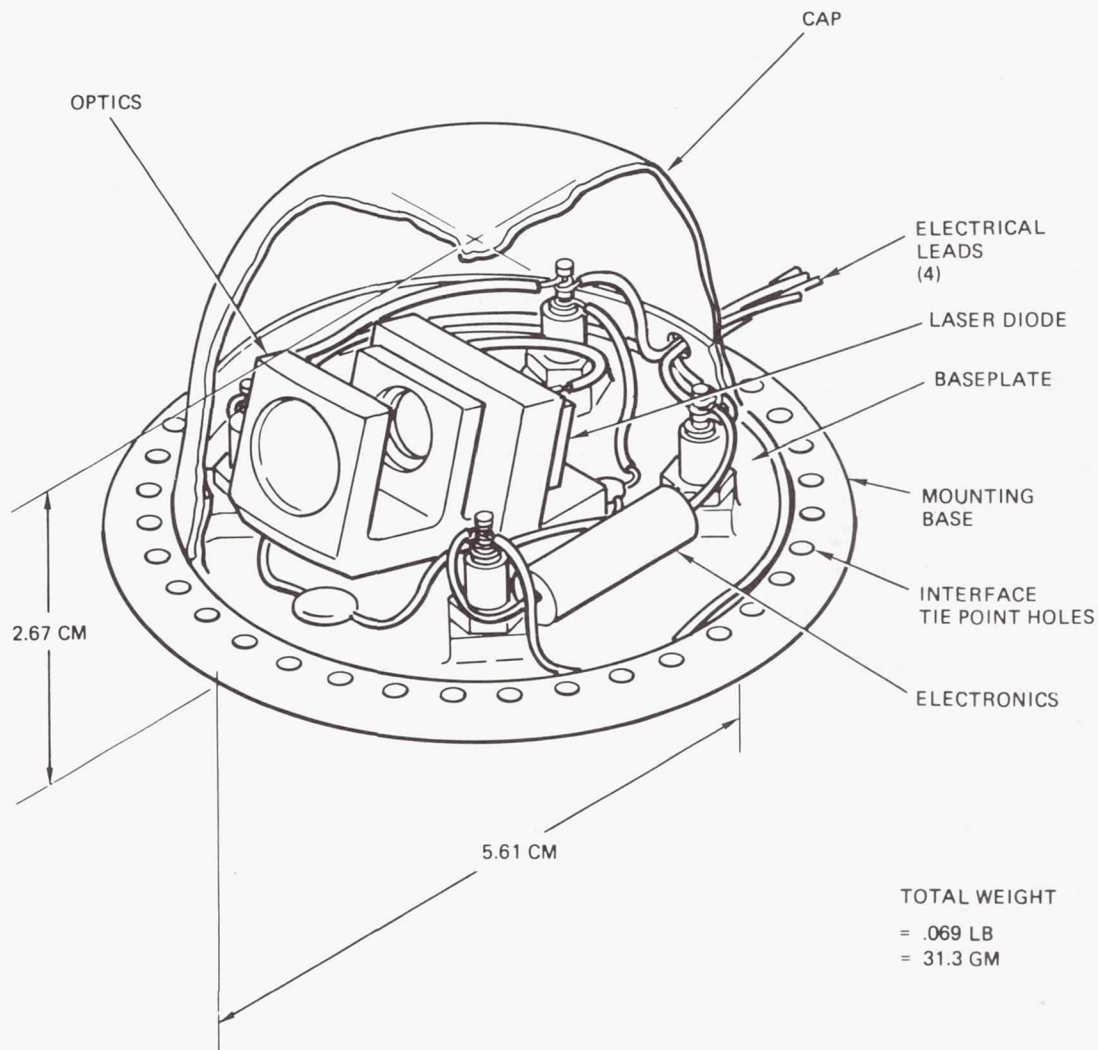


TYPICAL MESH-MOUNTED TARGET

A closeup view of the target is shown in the figure. Each target is a miniature source consisting of a laser diode, beam shaping optics, and passive/active thermal control. At the mesh sites, the targets are mounted upon pads or bases integrally fabricated with the antenna and connected to small supply lines laced to the gore tensioning cords. At the hoop, the targets are attached to similar bases fixed to the rigid hoop segments.

Orientation of the source is such that the narrow beamwidth (i.e., 2°) is in elevation. At maximum elevation tilt error of 5 milliradians this amounts to a reduction of 6% in beam power at the receiver. In azimuth, the beam is wider; a pointing error of $\pm 1^\circ$ in azimuth is acceptable.

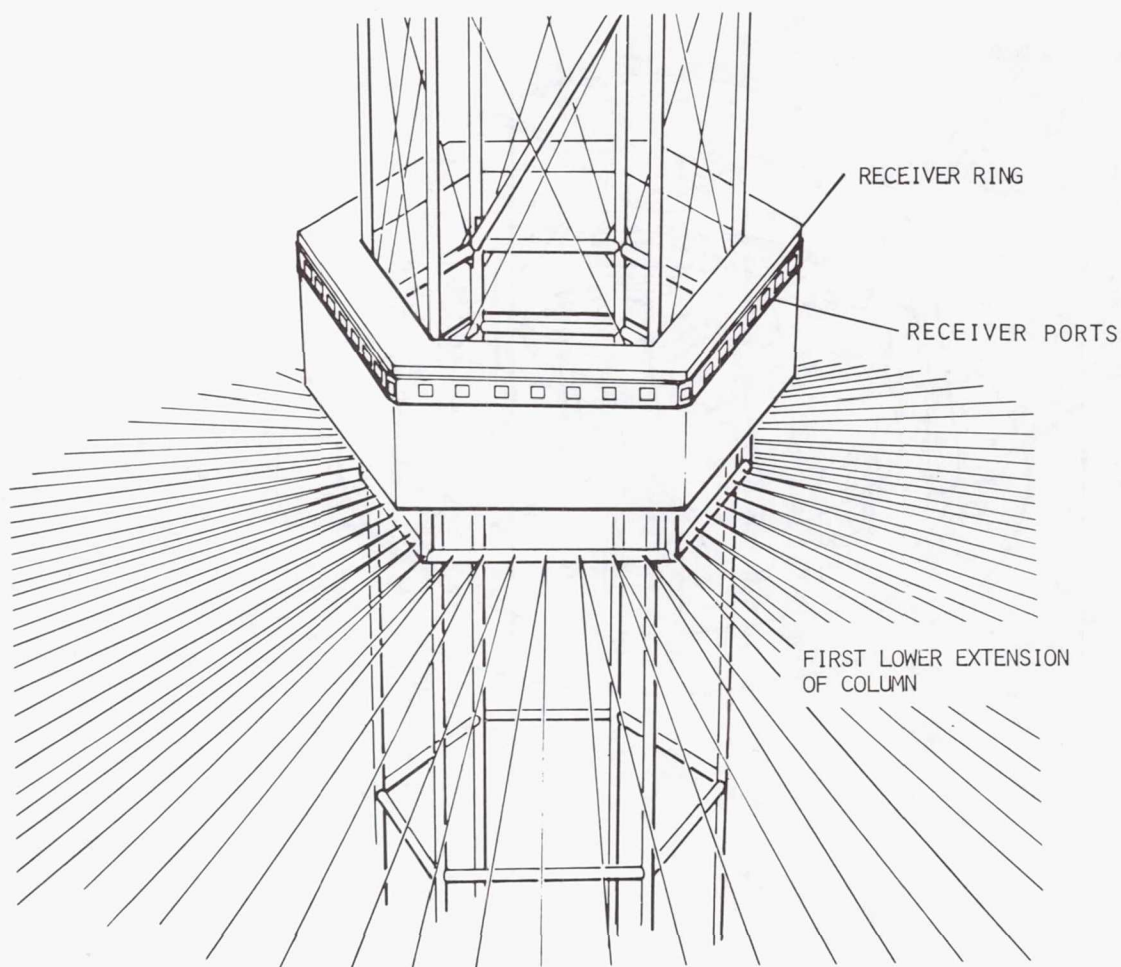
The target source is a gallium aluminum arsenide solid state laser diode producing approximately 5 milliwatts radiant power out. Each target is square wave driven at 200 Hz, 25% duty cycle. Lifetime at which 2% of the components have suffered 3 db loss in radiant power output is estimated to be 10^6 hours.



RECEIVER RING AT ANTENNA COLUMN

As shown in the figure, the receiver cluster is supported by a hexagonal ring carried by the first lower extension of the column. Within this support ring, 48 receivers are dedicated to observing targets along the 48 gore lines (or false ribs) of the antenna. Forty-four receivers measure the surface normal deformations at the assigned targets, and four additional receivers measure the peripheral motion or twist of targets at the hoop and at the mesh.

Within the hexagonal support ring, the 48 receivers are mounted, each approximately at the root of the gore intersection line carrying the receiver's designated targets. All of the receivers are identical simple telescopes, mounted with their axes parallel to the ring (and antenna) centerline. Immediately ahead of the objective lens at each receiver, a view splitter prism divides its view into two or three superimposed subfield. Each subfield is folded in elevation by the prism to center the field at its designated target. At the receiver's detector, thus, are superimposed images of the targets. When the antenna geometry is ideal, these targets all lie at the detector center.

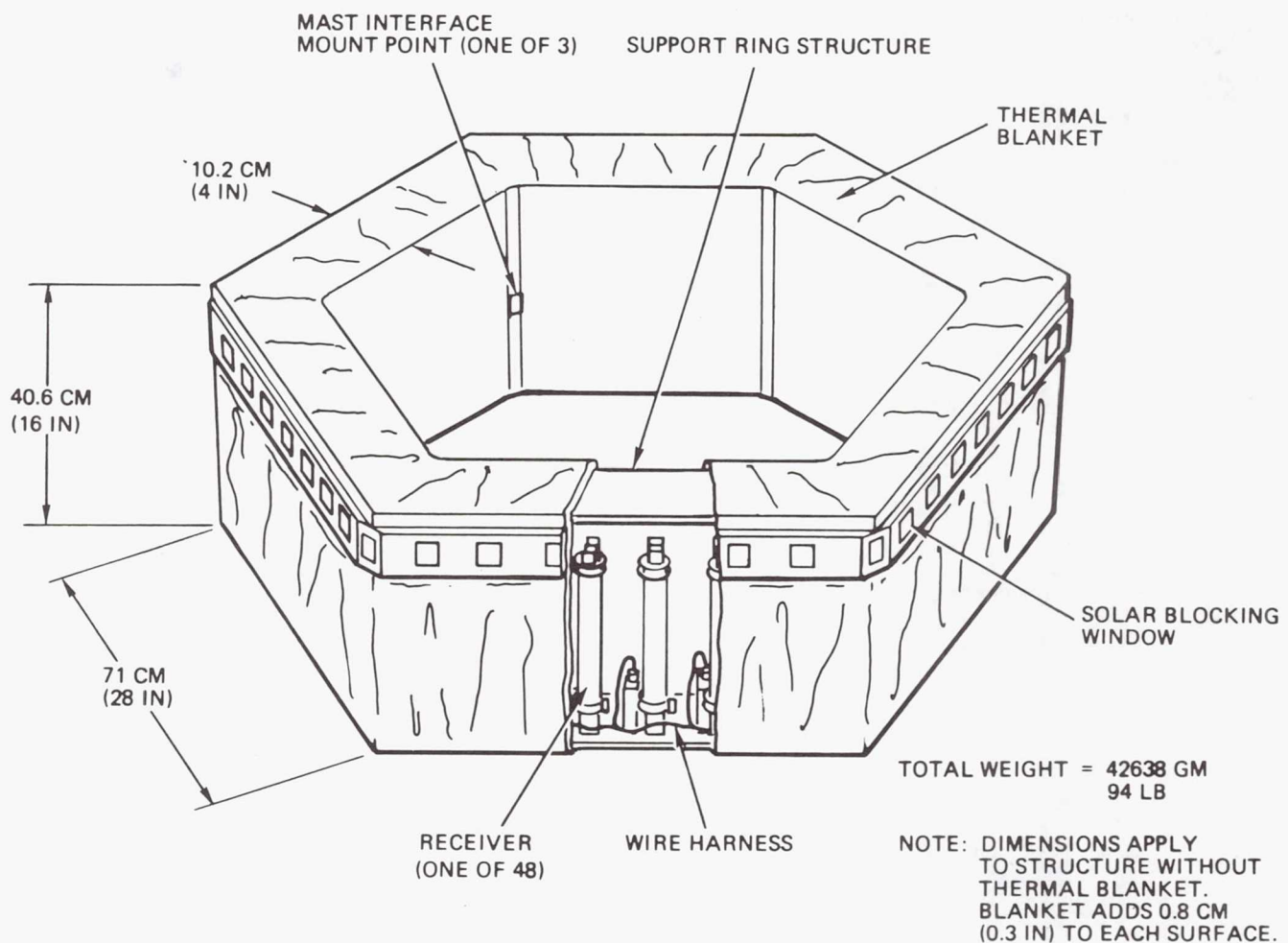


RECEIVER AND SUPPORT RING SUBSYSTEM

The subsystem shape is derived from the hexagonal cross section of the antenna mast to which the subsystem mounts. The structural dimensions are 40.6 cm (16 in) high by 142 cm (56 in) maximum across the points. These dimensions do not include the thermal blanket, which will add approximately 0.8 cm (0.3 in) to each surface. The structure is supported by three kinematic mount assemblies on the inner ring surface. These mate with three interfaces at the antenna mast.

The baseline ring design is constructed from graphite-epoxy to provide environmental compatibility with the Invar receivers and graphite antenna mast. The 48 receivers are positioned around the ring perimeter at 7.5° intervals, coincident with the antenna gore edge cord lines.

Solar blocking windows attached to the ring reduce the quantity of sunlight entering the receiver optical systems. This reduces thermal deformations and attendant pointing error. A wire harness surrounds the ring immediately below the receivers and links them to a central connector. The connector is located near one of the three main ring support points.

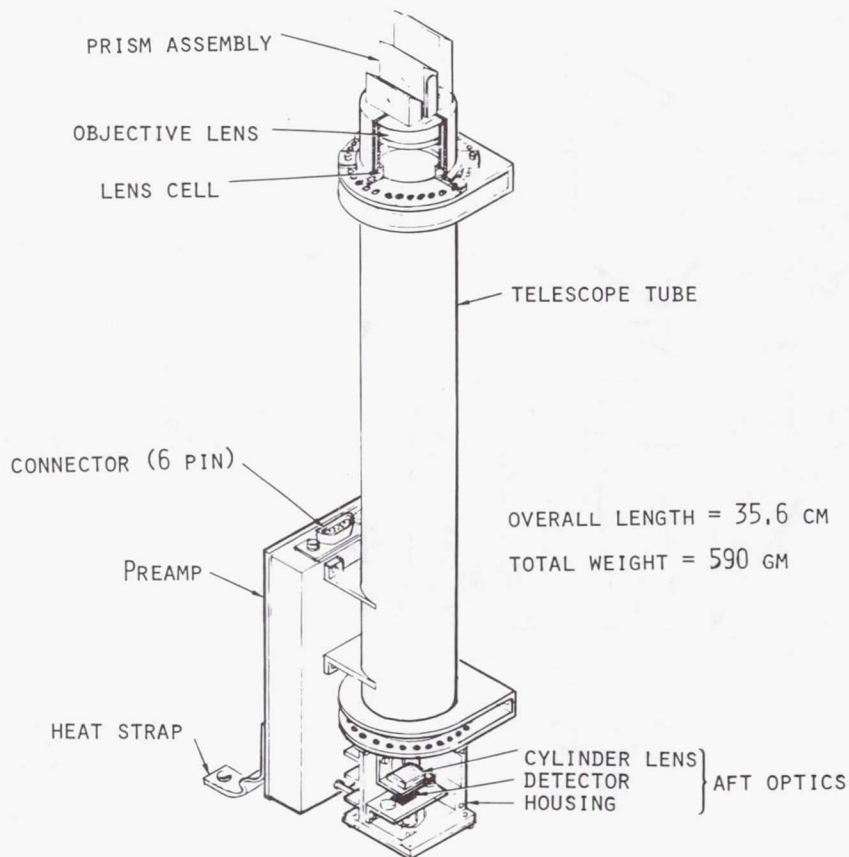


RECEIVER CONFIGURATION

The optical configuration for the receiver is simple. It consists of a prism beam splitter, a single element objective, a single element cylindrical field lens, and a single axis image position detector.

Although the target can move both normal to the antenna reflecting surface and tangentially in the surface plane, the deformation sensor system is concerned primarily with the surface normal displacements. Here, the combination optical train and detector are sensitive in the surface normal direction but totally insensitive to other motions. This is accomplished by the use of the cylindrical field lens. In the sensitive direction the cylinder exerts no influence upon the image motion; image displacement at the detector is the angular movement of the target times the lens-detector separation distance. In the cross-axis, the cylinder lens images the exit pupil at the aperture. The resultant image at the detector is immobile regardless of the target motion along the cross-axis.

Throughout the flight design effort, compatibility of the hardware with predicted environmental effects has been stressed. For example, the receiving telescope bodies are of stabilized Invar, electrically discharge machined for minimum weight. These receivers are imbedded within a lightweight composite material supporting ring that is kinematically isolated from the antenna mast. Temperature of the telescopes and their alignment mounts is controlled both by isolating thermal paths within the structure and by active heater and a thermal blanket.



FLIGHT SENSOR SYSTEM MEASUREMENT CAPABILITIES VS REQUIREMENTS

While the sensor system point design has been simplified for minimum complexity and interference with the antenna handling and operating functions, the system does meet or exceed the required performances. These capabilities vs. requirements are compared in the table. It is to be noted that the accuracy estimate includes a complete budget of error contributions including those arising from environmental influences.

Although not considered in this design study, the full-up flight configuration will also include coordinate referencing the antenna feed and the antenna support module. These additional measurements provide the sensor system with the capability of defining the feed position relative to the antenna surface and of transferring its entire antenna map to an attitude reference.

In addition to the performance and mechanical interfacing, requirements are introduced by the assumed operating scenario for the mission:

Boost survival: Precise receiver coalignment is maintained through the shock and vibration environment of shuttle boost and orbit injection.

Thermal: For the communication mission, the antenna can be diurnally cycled through the earth's shadow. During this cutoff of solar influx, the thermally isolated targets rely upon auxilliary heating.

EMI-RFI: The laser diode targets cannot tolerate overvoltage or overcurrent; and, therefore, contain protection from spurious pickup at their feed lines.

PARAMETERS	REQUIREMENTS	CAPABILITIES
ANTENNA CONFIGURATION	<div style="display: flex; justify-content: space-between; align-items: center;"> <div style="width: 45%;"> <p>———— MESH DEPLOYABLE</p> <p>———— 100 METER DIAMETER</p> <p>———— FOUR ACTIVE SURFACES</p> <p>———— 48</p> </div> <div style="width: 45%; text-align: right;"> <p>HOOP-AND-COLUMN</p> </div> </div>	
TYPE		
SIZE		
SURFACE GEOMETRY		
NO. OF GORE		
NO. OF SAMPLING POINTS		
AT MESH	128 SAMPLES	128 TARGETS
AT HOOP	4 SAMPLES	4 NORMAL DEFLECTION 4 TWIST DEFLECTION
MEASUREMENT RANGE		
MAXIMUM EXCURSION AT HOOP	± 25 CM	± 48 CM
MAXIMUM EXCURSION AT MESH	SCALED WITH RADIAL DISTANCE	SCALED WITH RADIAL DISTANCE
HIGH ACCURACY RANGE AT HOOP	± 7.5 CM	± 9.6 CM
HIGH ACCURACY RANGE AT MESH	SCALED WITH RADIAL DISTANCE	SCALED WITH RADIAL DISTANCE
MEASUREMENT ACCURACY	1.5 MM (3 σ)	1.3 MM (3 σ)
DATA RATE	1 HZ RESPONSE	4 FRAMES/SECOND

Page intentionally left blank

ELECTRO-OPTICAL SYSTEM FOR
REMOTE POSITION MEASUREMENTS
IN REAL TIME

P. W. Collyer, S. C. Spielberger, K. A. Ward
Barnes Engineering Company
Stamford, Connecticut

Large Space Systems Technology-1981
Third Annual Technical Review
November 16-19, 1981

LARGE SPACE SYSTEM SENSOR REQUIREMENTS

Barnes Engineering Company has been conducting a company-funded research and development project on a position sensing system usable for Large Space System (LSS) applications. In the course of the project, a brassboard model of the system was fabricated, tested and evaluated. This paper discusses both the general design problem of sensors for LSS and the background and rationale for development of the brassboard sensor. Laboratory test results for the sensor are also presented.

The need for making accurate position measurements of LSS structures has been well recognized for some time. In some LSS, such as space-deployed antennas, it is critical as the figure of such antennas is determined after deployment and, because of structural gravity restrictions, may only be measured in space. In other LSS of an experimental nature, where it is planned to mechanically excite the structure on orbit to observe its dynamics, real time orbital position measurements are necessary to evaluate system response. The active control of LSS is also being considered, a function which requires sensors to become a part of the feedback network and close the control loop. It is for satisfying these general types of LSS applications, and others, that a sensor approach will be described based upon currently available technology. General purpose LSS position sensors should be capable of meeting the requirements noted in Table 1 below. Although there are demanding missions where measuring accuracy in the micron range may be necessary, the majority of projected LSS missions can be satisfied by a sensor meeting these specification criteria.

0 MULTIPLE POINT SENSING CAPABILITY

0 PROVISIONS FOR WIDE ANGULAR COVERAGE WITH NO MOVING PARTS

0 OPERATIONAL RANGE - FROM 4 METERS TO GREATER THAN 100 METERS

0 REJECTION OF SPURIOUS SIGNALS - SUN, MOON, OTHER SATELLITE SOURCES

0 MEET SPACE ENVIRONMENT CRITERIA INCLUDING RELIABILITY

0 REAL TIME PERFORMANCE FOR LSS CONTROL APPLICATIONS

0 SUFFICIENT ACCURACY - TYPICALLY, 0.5 MM AT 100 METER RANGE

TABLE 1

TECHNOLOGY BACKGROUND

Various active type sensing technologies were assessed to determine the one best suited for LSS applications. Ranging approaches utilizing modulated lasers or LED sources were first considered. Although this technology is in some ways the most straightforward approach, the need for reliable mechanical scanners and a precise read-out of their instantaneous position posed significant development problems. We have long considered other specialty types of electro-optical systems employing polarized light, Bragg cells, etc. These technologies rely on the development or use of specialty components with unknown developmental risk factors. It is difficult to establish that such approaches have the potential to meet all sensor requirements. A form of autocollimation was finally selected as the best overall technology. In autocollimation, a target reflector is placed at infinity. Angular deviation of collimated light from the reflector is measured as a lateral movement of a refocused image at the detector focal plane. A variant of autocollimation, autoreflection, measures translation of the remote target, which for LSS applications is the parameter of interest. In autoreflection, the target reflector is placed in a converging bundle at the remote focal point. Since a corner cube is used as a retro-reflector, the returned light beam is insensitive to angular rotation, and its deviation in the image plane is a measure only of translation (position) of the cube. Barnes' experience with autocollimation is extensive with design and manufacture of arcsecond precision sensing systems for Polaris and Trident submarines and the recent Magsat satellite. There are various advantages in using an autocollimation approach, which are noted in Table 2. The most significant advantage is that by marrying an old technology, autocollimation, to a new semiconductor technology, the Charge-Coupled Detector, substantially all LSS sensor requirements can be met.

0 SENSING TECHNOLOGIES

RANGING

SPECIALTY SYSTEMS

AUTOCOLLIMATION

0 BARNES SELECTED TECHNOLOGY - AUTOCOLLIMATION

PRIOR EXPERIENCE ON U.S. NAVY AND MAGSAT PROGRAMS

SAME TECHNOLOGY PROVIDES ANGLE OR POSITION

0 AUTOCOLLIMATION ADVANTAGES

PROVEN TECHNOLOGY - RELIABLE COMPONENTS ARE AVAILABLE

EMPLOYS PASSIVE TARGETS (RETROREFLECTORS)

TARGETS CAN BE SMALL SIZE

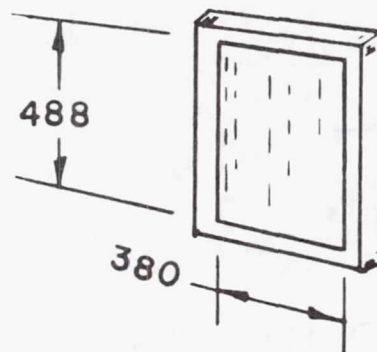
TABLE 2

LSS SENSOR DESIGN

A design study was conducted to evolve an instrument concept which could satisfy all major LSS sensor performance requirements. The auto-reflection technique, with retroreflector corner cubes providing the target returns, was chosen for the baseline sensor. Light-emitting diodes (LED's) were selected as the illumination sources. Previous usage had already proven their reliability and effectiveness in this type of application. The position of images resulting from returned LED light from the corner cubes was to be sensed by a Charge-Coupled Device (CCD) area detector. This type of detector array (Figure 1) provides thousands of silicon photodetector elements (pixels) with known locations, established by highly precise microlithography. If the returned light from a number of monitoring corner cubes is imaged onto the array, the resulting electrical signals along with their positions can be sequentially clocked out of the array at television rates of 30 frames per second. With the location of each image on the array a direct measure of position coordinates of a specific corner cube, further electronic processing of the CCD data can produce the desired sensor positional outputs.

MULTIPLE POINT SENSOR

AREA TYPE CHARGE-COUPLED DEVICE (CCD)



- 185,000 PHOTO-OPTICAL MEASURING SITES (PIXELS)
- MEASUREMENT DATA OUTPUTS AT 30HZ FRAME RATE
- MEASUREMENT ACCURACY IS BETTER THAN 1/5 PIXEL THROUGH USE OF CENTROID ALGORITHM

FIGURE 1

LSS SENSOR DESIGN

In the actual instrument design, a single 488 x 380 pixel element CCD detector was used. Each monitored point was assigned a sensing "window", i.e., a square area of a specific number of pixels, depending on the allowable deviation of the LSS structure. Although all cubes were imaged onto the same detector, problems relating to image point identification and overlap of images on the CCD array were eliminated by using multiple LED's and time sharing the array as described later. While the CCD array device has some 185,000 pixels available for measurement purposes, the tradeoffs between field of view size and the number of monitored points requires resolution capability better than that available from the array. Therefore, a centroid algorithm was employed to determine the x, y array coordinates of each returned image. This technique improved accuracy of the array from the granularity of a single pixel to about one-fifth of a pixel. An attractive feature achieved by the use of the centroid concept is that the retroreflector can have almost any shape without altering system accuracy. For certain applications, particularly membrane antennas, the use of a low-mass, long, thin reflector could have great advantages.

Operation of the sensor is shown in Figure 2 and Table 3.

MULTIPLE POINT SENSOR

SIMPLIFIED BLOCK DIAGRAM

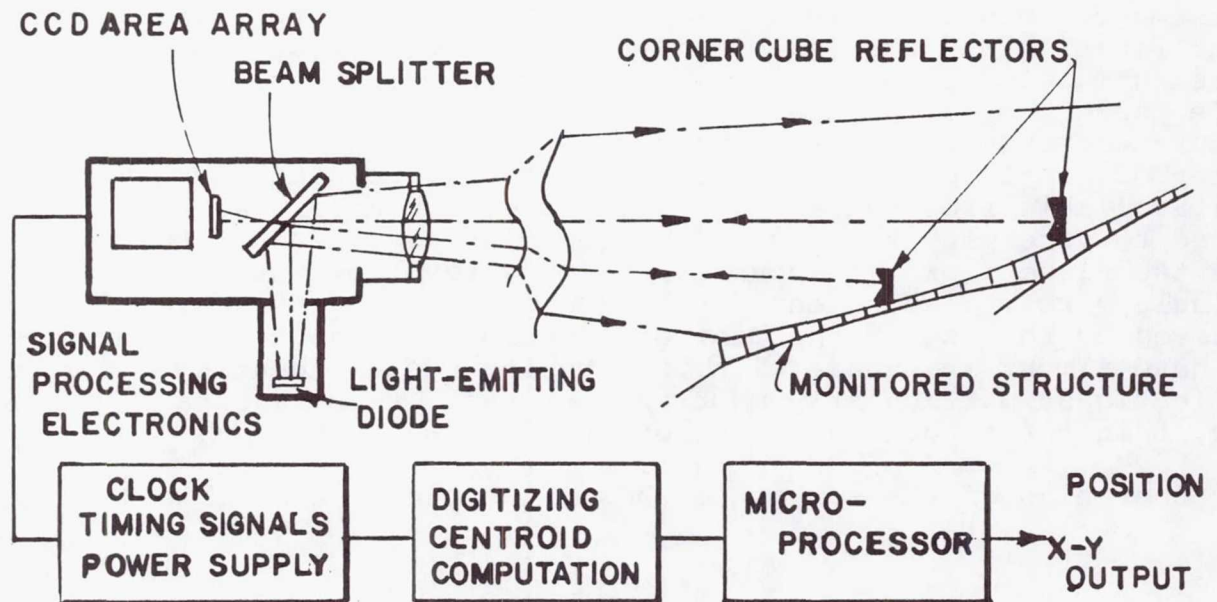


FIGURE 2

BASIC OPERATION

- o CORNER CUBE REFLECTORS ARE LOCATED ON MONITORED LSS
- o LED ILLUMINATES SCENE
- o OPTICAL SYSTEM ROUTES RETURNED SIGNALS FROM CORNER CUBES TO PRESELECTED AREAS ON CCD AREA TYPE DETECTOR
- o DATA IS CLOCKED OUT OF CCD ARRAY AT A RATE OF 30 FRAMES PER SECOND AND PROCESSED TO DETERMINE CENTROID OF EACH CORNER CUBE IMAGE
- o CENTROID (IMAGE) COORDINATES ARE TRANSFORMED BY MICROPROCESSOR INTO X, Y, POSITIONS OF LSS

TABLE 3

LSS SENSOR DESIGN

An important objective of the program was to achieve a no-moving-parts instrument design and still provide angular coverage of many widely distributed LSS points. This was accomplished by providing an optical system comprising a number of LED illuminators and fields of view. By combining various focal lengths and fields of view in a single optical head, it was possible to monitor close-range and far-range points. Multiple LED illuminators made it possible to time-multiplex the use of the CCD array and thereby considerably increase its monitoring capability.

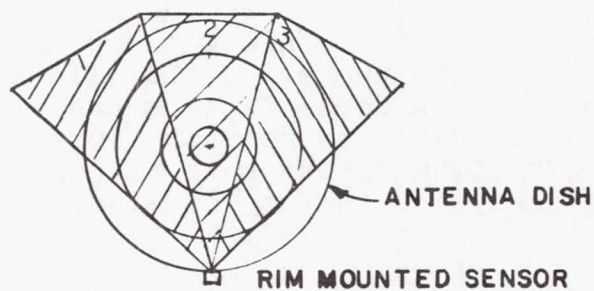
Typical examples of how the optical system could be implemented are shown in Figures 3 and 4. To monitor the figure of the large antenna disc shown in Figure 3, small retroreflectors are installed on the antenna surface facing the sensor which is located on the rim. The monitoring zones for this configuration are defined as 1, 2, 3 in azimuth and A, B, C in elevation. Figure 4 shows the optical concept to provide this broad monitoring capability. A single CCD array detector images all returned retroreflector signals, from the three azimuth fields of view as well as from elevation fields of view. The number of monitored points and the range of allowable deviations determine how the LED's serving each field of view should be commutated. The multiple field concept affords many system advantages as shown in Table 4. However, the most significant advantage is the elimination of moving parts, which eliminates the need for precision encoders and their associated errors and generally enhances system reliability.

ADVANTAGES OF MULTIPLE FIELD CONCEPT

- O NO-MOVING-PARTS DESIGN
- O ALL RANGE CAPABILITY - NO FOCUSING PROBLEM
- O TIME MULTIPLEXING OF LED'S - AIDS IN IMAGE
IDENTIFICATION - INCREASES MONITORING CAPABILITY
- O ACCURACY CAN BE ESTABLISHED INDEPENDENT OF RANGE

TABLE 4

MULTIPLE FIELDS OF VIEW IN AZIMUTH



MULTIPLE FIELDS OF VIEW IN ELEVATION

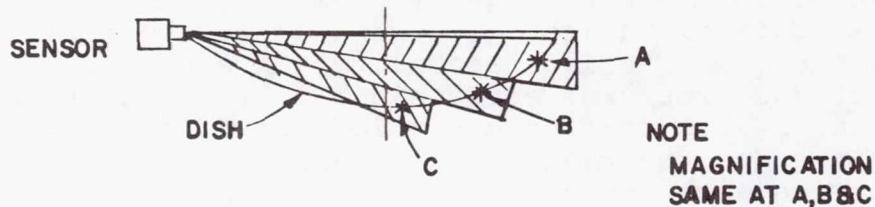


FIGURE 3

OPTICAL CONCEPT FOR MULTIPLE AZIMUTH AND ELEVATION FIELDS OF VIEW

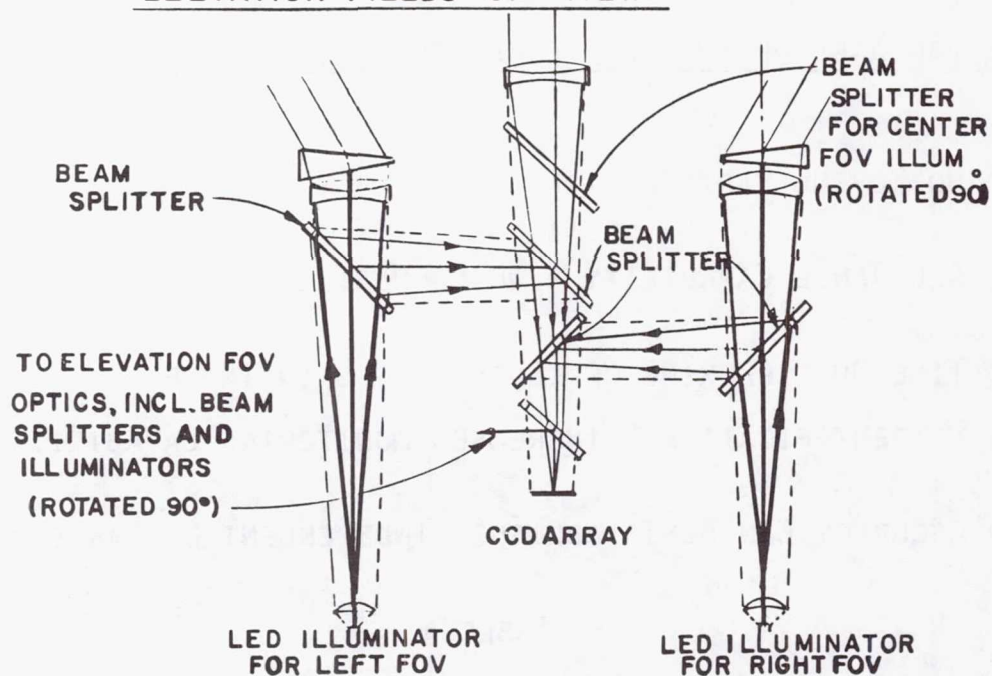


FIGURE 4

SUMMARY OF TYPICAL LSS SENSOR SYSTEM PARAMETERS

Table 5 below summarizes typical LSS sensor parameters as they evolved from system studies and actual design and test of a brassboard sensor. The parameter values are for one sensor component of a system which could include several optical heads depending on the geometry of the monitoring problem and required system performance parameters.

- O TWO PACKAGE CONFIGURATION - OPTICAL HEAD AND ELECTRONICS
- O SIZE AND WEIGHT - OPTICAL HEAD - 23 CM X 28 CM X 13 CM - 4KG
ELECTRONICS - 23 CM X 23 CM X 10 CM - 3KG
- O POWER REQUIREMENTS - APPROXIMATELY 35 WATTS
- O RETROREFLECTORS - CORNER CUBES
- O RANGING CAPABILITY - 4 METERS TO 100+ METERS
- O POSITION MEASUREMENT ACCURACY - ± 0.5 MM AT MAXIMUM RANGE
- O SENSING CAPABILITY - 40 OR MORE INDEPENDENT POINTS
- O RESPONSE TIME - 2-10 HZ
- O NO MOVING PARTS
- O FIELD OF VIEW - OPTICAL SYSTEM DESIGNED TO IMAGE ALL RETROREFLECTORS ONTO
DETECTOR ARRAY REGARDLESS OF ANGULAR POSITION OR RANGE
- O SYSTEM OUTPUT - TWO-AXIS POSITION OF EACH POINT IN DIGITAL FORMAT

TABLE 5

LSS SENSOR APPLICATIONS

We have developed conceptual configurations of position measuring systems for several typical LSS antennas. For a membrane mirror type antenna, where there are few rigid supporting members for the sensor, we provide additional monitoring sensors at the truss where the antenna feed is located, the desired reference point. As shown in Figure 5, four sensors, A, B, C, D, monitor membrane mirror points in the sectors and in turn are monitored by I and II. The sensors located at I and II are similar to those developed for single point monitoring for the Magsat Program (reference 1) and proposed for Orbiter bay measurement applications (reference 2). The Hoop-Column antenna of Figure 6 would employ sensors centrally located which look outward from the hub. A number of fields of view and LED illuminators would be employed in the no-moving-parts system. Depending on the location and number of points, from three to six optical heads would be required for full 360° angular coverage.

MEMBRANE MIRROR CONFIGURATION SENSING CONCEPT

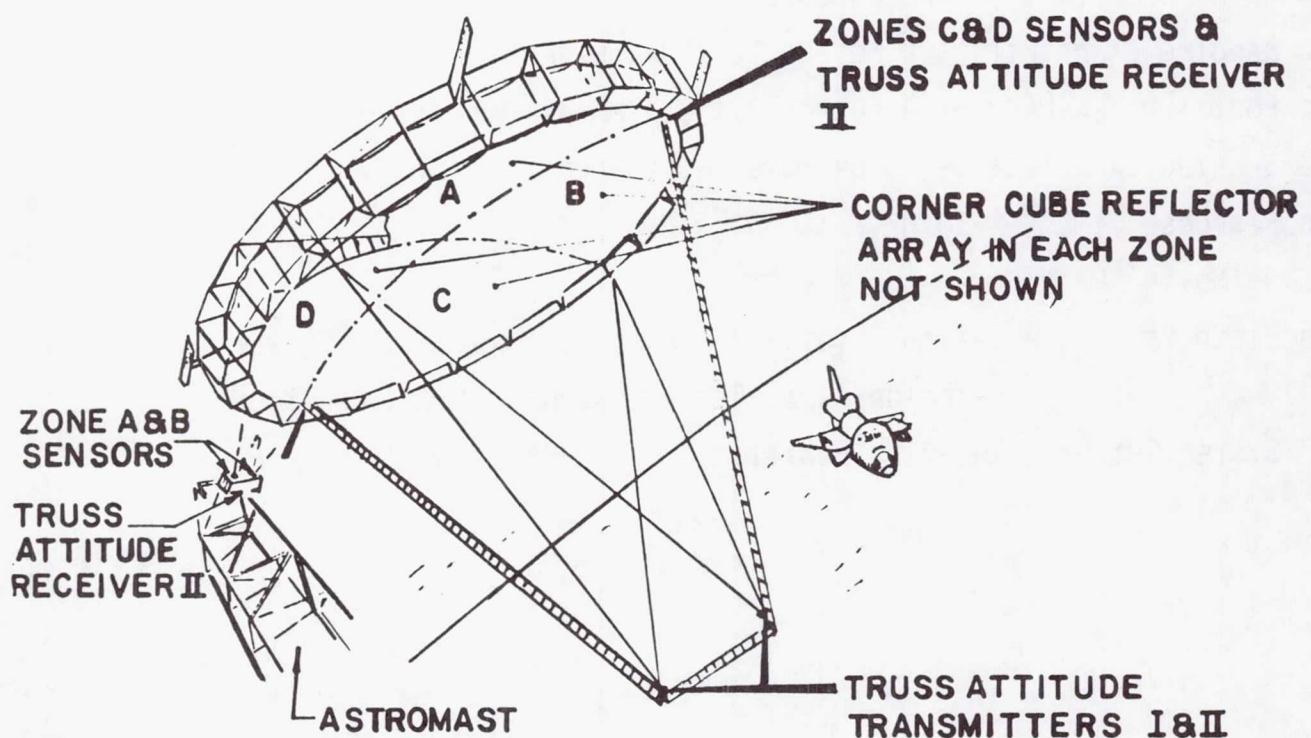


FIGURE 5

HOOP/COLUMN ANTENNA SHOWING MONITORING CONCEPT

MONITORING CORNER
CUBE REFLECTORS

TWO AXIS POSITION
MEASURING SENSOR(S) ON
FIXED MOUNT

MESH

TELESCOPING
COLUMN

HOOP

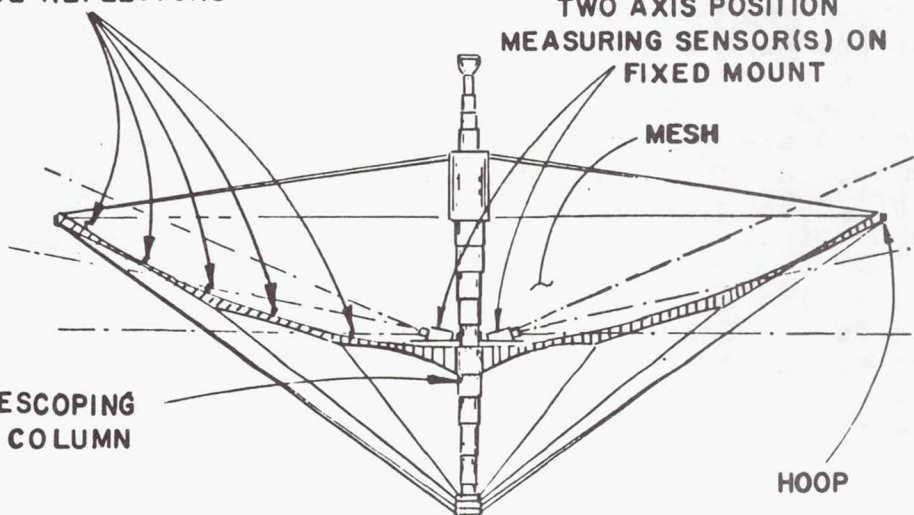


FIGURE 6

DEPLOYABLE ANTENNA- MEASUREMENT CONFIGURATION

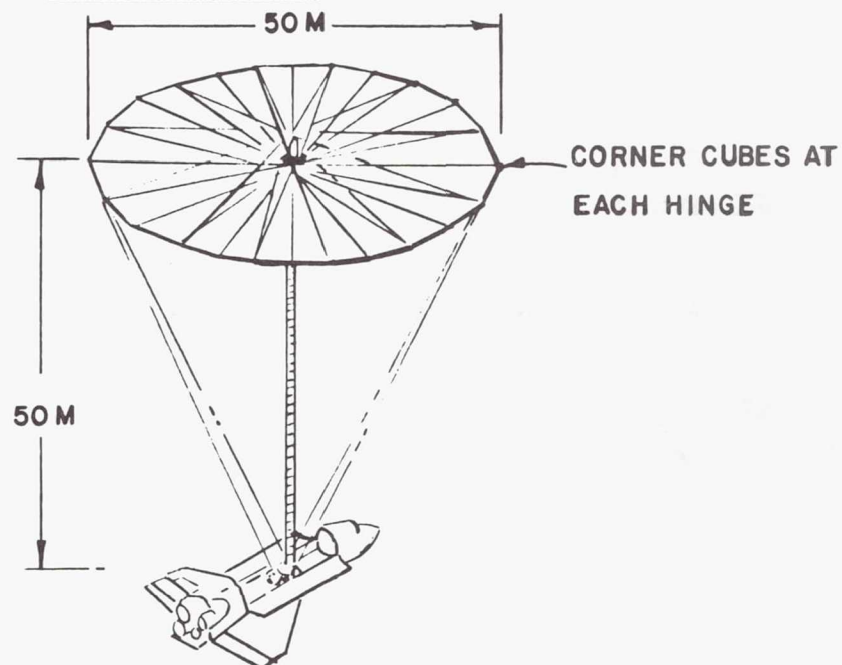


FIGURE 7

LSS SENSOR APPLICATIONS

Figures 7 and 8 are another application for a space-deployed antenna where the major points of monitoring interest are located on its rim. A single sensor is used to monitor 32 points simultaneously. This is accomplished by the sensor CCD array viewing upwards and being reflected outward to the rim corner cubes by an image polyhedron reflector. At the same time, a single LED located above the polyhedron illuminates the corner cubes by being reflected by another polyhedron and then combined with the CCD viewing rays. Additional sensors and viewing stations are located at the base of the mast to provide position data from corner cubes on the under portion of the antenna rim. The resulting information can be processed to yield three-axis position data for each point.

These examples illustrate the use of the conceptual sensor with several practical space antenna systems. For each example, a custom optical system was configured to image all viewed points on a single CCD area detector. However, aside from the optical system and software, no changes were required in the electronics and data processing hardware.

OPTICAL SCHEMATIC DIAGRAM

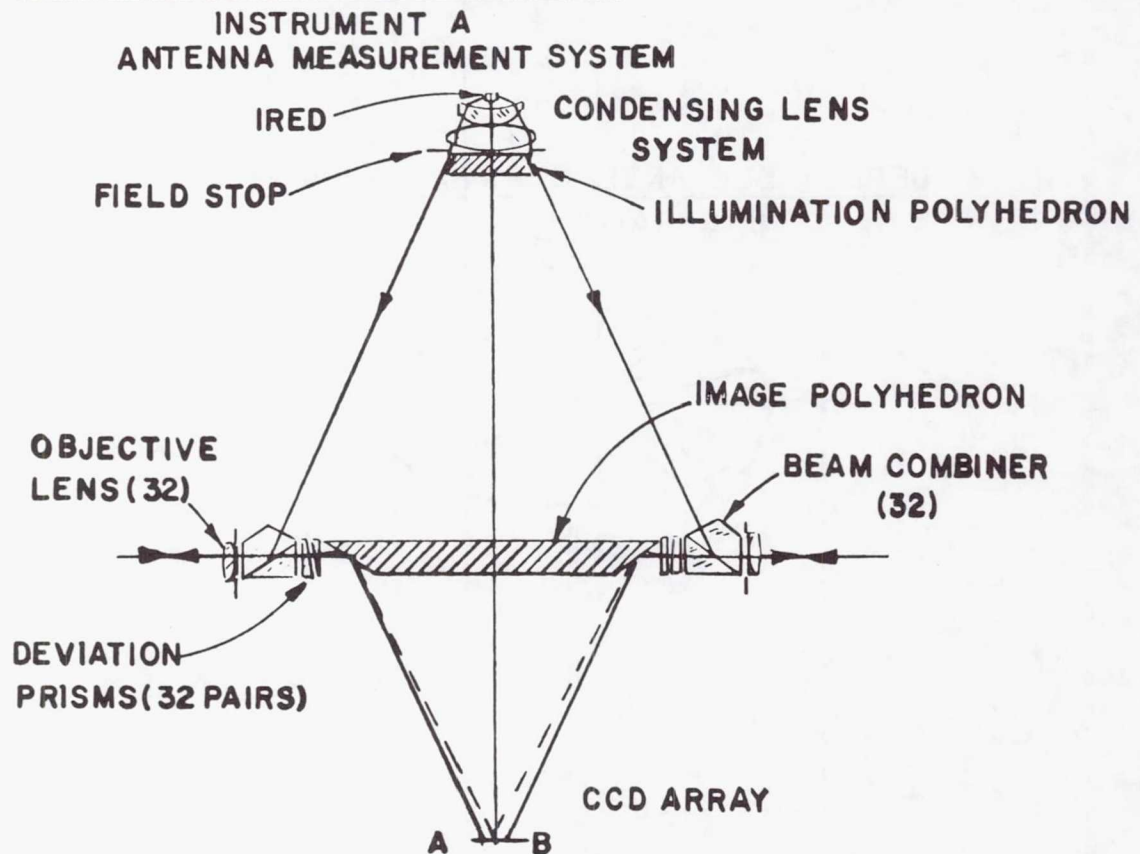


FIGURE 8

BARNES BRASSBOARD MODEL SENSOR

The Barnes brassboard position sensor was designed to verify the engineering concepts preliminary to the design of a qualified flight model. An initial design approach employing linear CCD arrays was fabricated and tested, but its obvious shortcomings in handling large numbers of monitoring points were soon recognized. The present CCD area detector sensor design appears to be very satisfactory and still provides room for performance growth as the capabilities of the CCD and related technologies mature. The major component blocks of the brassboard sensor are shown in Figure 9 and include a keyboard/printer for addressing the system and printing out results, a monitor for displaying the LSS targets and x, y positions, a computer for performing the algorithm and coordinate computations and an optical head and electronics box. In general, the functions of a final design sensor system have been conceptually implemented in the brassboard hardware and software. Various tests, including the simulation of the SEPS orbital experiment shown in Figure 10, have been conducted to date to verify operational performance of the system. In all respects, accuracy, operational range, real time performance, and other important parameters, brassboard performance, close to that of a final design sensor, met or exceeded planned objectives (see Table 6).



FIGURE 9 BRASSBOARD MODEL COMPONENT PARTS



FIGURE 10 LABORATORY SIMULATION OF SEPS ORBITAL EXPERIMENT

BARNES IRAD POSITION SENSOR PROGRAM

- o SAME CONCEPT AS PROPOSED FLIGHT HARDWARE
- o USES COMMERCIALY AVAILABLE COMPONENT BLOCKS
- o LABORATORY TEST MODEL DEMONSTRATES:

RANGE CAPABILITY - 50+ METERS

DYNAMIC TRACKING - AT 10HZ RATE (FOR SINGLE POINTS)

ACCURACY - APPROXIMATELY $\pm \frac{1}{2}$ MM

MULTIPLE POINT CAPABILITY - TRACKS AND PROCESSES MORE THAN
10 POINTS AT A TIME

TABLE 6

REFERENCES

1. Collyer, Wardham P.; Schenkel, Frederick W.: A Three Axis Angular Monitoring System for the Magsat Mission, SPIE Technical Conference (San Diego, California), July 1980.
2. Collyer, Wardham P.; Ward, Kenneth A.: Attitude Transfer by Electro-Optical Instrumentation for Shuttle Experiments, SPIE Technical Conference (Los Angeles, California), February 1981.

Page intentionally left blank

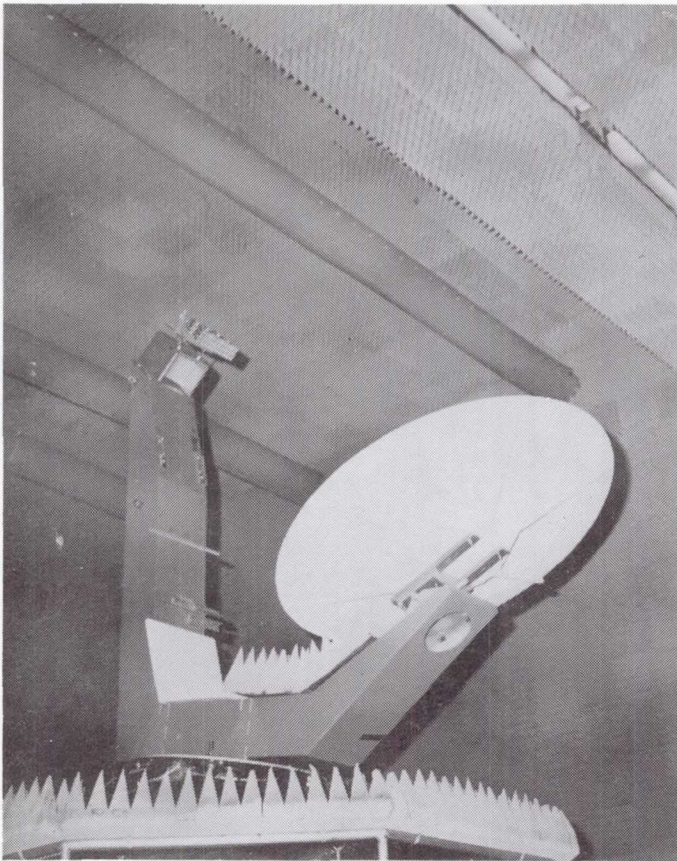
NEAR-FIELD TESTING OF
LaRC MULTIPLE-BEAM ANTENNA

G. J. Lang
Martin Marietta Denver Aerospace
Denver, Colorado

Large Space Systems Technology - 1981
Third Annual Technology Review
November 16-20, 1981

NEAR-FIELD ANTENNA MEASUREMENTS--AN ALTERNATIVE TO FAR-FIELD RANGES

Antenna patterns are conventionally measured directly in the far-field, at a distance where the field is approximately a plane wave. Alternatively, if both phase and gain are measured in a plane in front of the antenna, the far-field patterns can be computed by a Fourier transformation. For widebeam antennas, cylindrical or spherical sampling of the near-field surfaces are superior but have the disadvantage of increased transformation complexity. The Martin Marietta Denver Aerospace Near-Field Test Laboratory (NFTL) currently uses planar scanning with cylindrical capability to be available in 1982.¹ The Langley Research Center (LaRC) multiple-beam antenna is shown in figure 1 mounted in the NFTL. One of four probes available to sample the near-field is located in the slot in the upper right side of the photograph. Sampling is typically at intervals of a half wavelength or less to avoid aliasing. After each probe scan, the antenna is stepped to the right and the scan repeated until a square data grid is filled. For a small antenna at low frequencies, a grid of 65 thousand data points is typical with over 4 million points for a large antenna at 18 GHz.



- BOTH AMPLITUDE AND PHASE
OF FIELD MEASURED BY
SCANNING PLANE NEAR
ANTENNA
- FAR-FIELD PATTERNS
COMPUTED USING
FFT TECHNIQUES

Figure 1

WHY TEST ANTENNAS IN NEAR-FIELD?

Acquisition and processing of these large near-field data sets are obviously complex. Advantages of near-field measurements are outlined in figure 2. To obtain an approximately spherical wavefront, i.e., no more than 22.5 degrees phase error at the edge of reflector of diameter, D , requires a far-field range length of at least $2D^2/\lambda$, where λ is the wavelength. For example, a 15-m antenna at 18 GHz would require a range of at least 27 km (16.8 mi). Even when such long ranges are available, the interference from ground reflections, aggravated by the long range, can cause serious errors. Fragile structures intended for space use must be protected from weather. Radomes used for this protection can distort the fields and modify the measured patterns. In near-field measurements, the propagation path usually does not traverse a radome. RF signals from far-field tests can produce unacceptable interference with other users in the vicinity or vice versa. Near-field facilities located within shielded enclosures eliminate this problem. Therefore, most of the serious shortcomings of far-field measurements can be alleviated using near-field techniques. In addition, near-field data can be used as a direct diagnostic of antenna performance before the integration by the aperture which can make it difficult to isolate the cause of far-field pattern anomalies.

- IN FAR-FIELD, SPHERICAL WAVE APPROXIMATELY PLANAR FOR
 $R \geq 2D^2/\lambda$
- FOR 15-m ANTENNA AT 18 GHz, $R \geq 27$ km
- GROUND REFLECTION CAN CAUSE LARGE ERRORS IN FAR FIELD
- LONG RANGES AGGRAVATE PROBLEM
- FRAGILE SPACE STRUCTURES PROTECTED FROM ENVIRONMENT IN NEAR-FIELD RANGES
- RADOMES USED IN FAR-FIELD RANGES CAN DISTORT PATTERNS
- SHIELDED ENCLOSURE ELIMINATES RF INTERFERENCE - BOTH WAYS
- DIRECT PERFORMANCE DIAGNOSTICS FROM NEAR-FIELD DATA - NOT SUBMERGED IN INTEGRATION BY APERTURE

Figure 2

MARTIN MARIETTA NEAR-FIELD TEST LABORATORY (NFTL)

Many near-field facilities exist, but the NFTL shown in figure 3, is the only one that can handle antenna diameters up to 16.5 m (54 ft). Planes up to 23.5 x 23.5 m (77 ft) can be scanned with measurements made in quadrants, and then combined with software. The heavy-duty rotory table and 51-ft height to the probes combine to allow testing of large antennas even when mounted on spacecraft. Measurements can be made with full accuracy from 1 to 18 GHz with a gradual decrease in accuracy as the RF absorber effectiveness degrades from 1 to 0.1 GHz. Sampled data from up to four probes spaced at 10-ft. intervals is multiplexed to allow rapid scan of large planes. Mechanization is currently underway to implement simultaneous orthogonal linear polarization measurement capability.

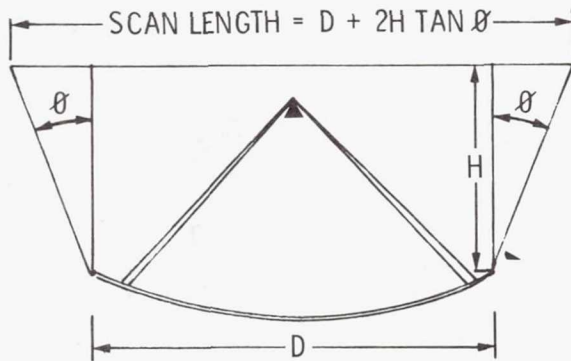


- ACCOMMODATES REFLECTOR DIAMETERS UP TO 16.5m (54 ft)
- SCANS PLANES UP TO 32.5m x 23.5m (77ft) MEASURED IN QUADRANTS
- FREQUENCY RANGE OF 1 TO 18 GHz
- ELECTRONICS OPERATE DOWN TO 0.1 GHz
- RF ABSORBER EFFECTIVENESS DEGRADES GRADUALLY BELOW 1 GHz
- UP TO FOUR PROBES SPACED AT 10-ft INTERVALS MULTIPLEXED FOR RAPID SCAN

Figure 3

NEAR-FIELD TESTING OF LARGE ANTENNAS IS A CHALLENGE

Although near-field testing solves many of the problems encountered in far-field measurements, a new set of challenges surface. Figure 4 shows that the scan plane must be larger than the antenna diameter by a distance determined from the angle-of-interest off boresight in the far field and the height of the scan above the reflector. The design challenge is in achieving a large-scan plane that is flat to within, typically, ± 0.004 in. as required for high frequency measurements. Accuracy of phase and amplitude measurements over a wide dynamic range must be in the order of 0.5 degrees and 0.1 dB/20 dB. Reflections from the facility must be lower than the sidelobes of interest. As previously noted, the field is sampled at half-wavelength or shorter intervals which typically produce over one-to-four million data points per frequency per polarization. This large amount of data must be processed into far-field patterns in near real time to preclude a large data reduction backlog during a long testing program. Also, if the data is not processed rapidly, faulty measurements could continue for an extended period before detection.



- SCAN PLANE IS LARGER THAN REFLECTOR DIAMETER BY ANGLE OF INTEREST OFF BORESIGHT

- AT HIGH FREQUENCIES (TYP 18 GHz), SCAN PLANE MUST BE FLAT IN ORDER OF $\pm 0.1\text{mm}$ (± 0.004 in.)
- INSTRUMENTATION ERROR MUST BE $< 0.5^\circ$ AND 0.1 dB/20 dB OF DYNAMIC RANGE
- REFLECTIONS FROM FACILITY MUST BE LOWER THAN SIDE LOBES OF INTEREST
- NEAR-FIELD SAMPLED AT HALF-WAVELENGTH INTERVALS OR LESS
- CAN GENERATE OVER 10^6 SAMPLE POINTS FOR FFT PROCESSING

Figure 4

PRIMARY COMPONENTS OF THE NFTL

The primary elements of the NFTL are shown in figure 5. An HP 1000 computer controls the mechanical scanning and data sampling with inputs through the data acquisition console. Probe position within the scan plane (X & Y axes) is monitored using lasers. A continuous scan motion along the Y-axis is used with probes sampled on-the-fly. Note, the rf source is always connected to the test article so that high power multiplexing of the probes is not required. This precludes making measurements through unilateral elements such as preamplifiers. Signals from the probes are translated to the 2-4 GHz band for transmission to a console mounted receiver and then translated to 100 kHz for amplitude and phase measurement. After analog-to-digital conversion, the data are transferred into a 10^9 -byte disc storage. A second HP 1000 computer and hardwired array processor under the control of a separate operator console, allows for data processing during acquisition. With the hardwired processor, the fast Fourier transformation (FFT) operations can be accomplished with a small computer in a time comparable to that of a large machine such as a CDC CYBER. Hard copy plotting options such as polar and rectangular principal plane patterns, contour plots, and 3-D plots of both phase and amplitude are available.

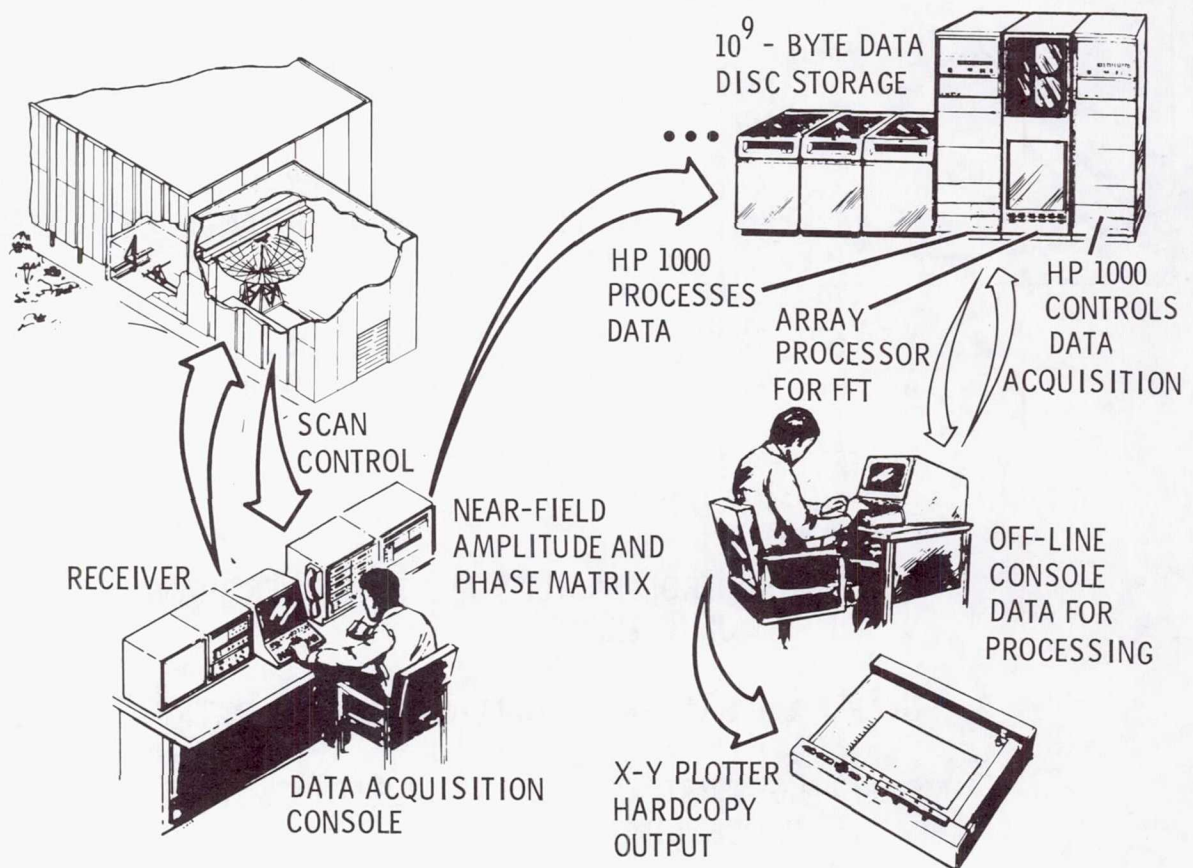
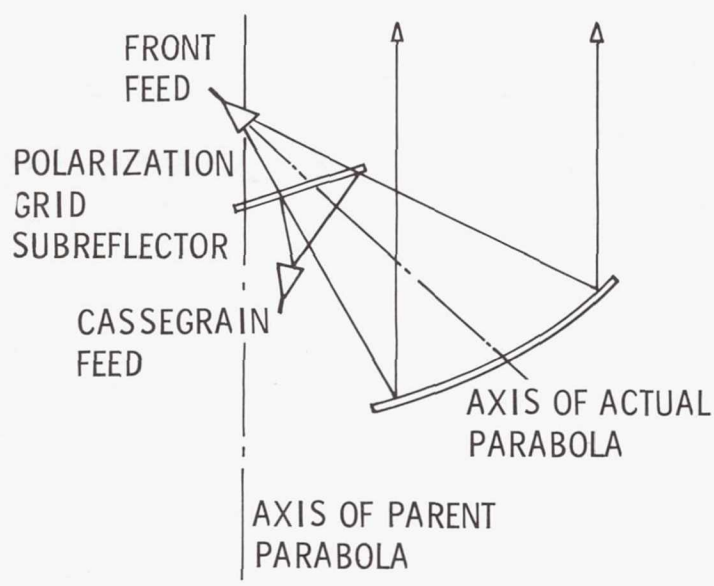


Figure 5

LaRC MULTIPLE-BEAM ANTENNA

Under contract to LaRC, TRW developed an offset-fed antenna that generates multiple beams using both focal point and cassegrain feed locations as shown in figure 6.2 Seventeen beams covering CONUS plus Alaska and Hawaii can be obtained with two antennas. The cassegrain subreflector is a polarization grid parallel to the polarization of the cassegrain feeds and orthogonal to the polarization of those at the focal-fed location. The 2-m offset-fed reflector is one-third the diameter of the parent parabola. This reflector is figured for a long focal length. F/D of the actual parabola, not the parent parabola, is 1.26. The downlink band covers 11.7 to 12.2 GHz and the uplink band spans 14.0 to 14.5 GHz. One nine-horn cluster feed is used for each beam. With the cluster feed amplitude weighting shown, sidelobe levels of the antenna pattern can be achieved that are 5 dB lower than with state-of-the-art corrugated horns.²



- 2m (6.5 ft) OFFSET FED APERTURE
- F/D OF ACTUAL PARABOLA IS 1.26
- 17 BEAMS FROM 2 ANTENNAS USING FRONT AND CASSEGRAIN-FEED LOCATIONS
- DOWNLINK BAND 11.7 TO 12.2 GHz
UPLINK BAND 14.0 TO 14.5 GHz

LOW SIDE LOBE FEED
USES POWER WEIGHTED ARRAY

0.16	0.4	0.16
0.4	1.0	0.4
0.16	0.4	0.16

Figure 6

ANTENNA AND SINGLE-BEAM FEED

Cascaded septum power dividers with the outside arms supplying 40 percent of the level of the center arm are used to supply the required power distribution. The power dividers and array of 3.7-cm square horns are shown in figure 7. Three of these horn clusters are also shown at the focal-fed location on the strongback with the reflector positioned with a tilt table and translation bars. These horns generate elliptical beams boresighted on California, New Mexico, and Tennessee. The photograph was taken before installation of the polarization grid on the mounting flats below the feeds.

Pattern measurements with this configuration have been made on TRW's 2-mi far-field range at San Juan Capistrano. Reflected signal levels on this range are at least 45 dB below the direct signal.² Upper-bound error analyses indicate that near-field measurements could be in error as much as -5 to +3 dB at the -40 dB side-lobe level. Measurements made on the low sidelobe antenna on a quality range provide the baseline for evaluating the conservatism in these upper bounds.

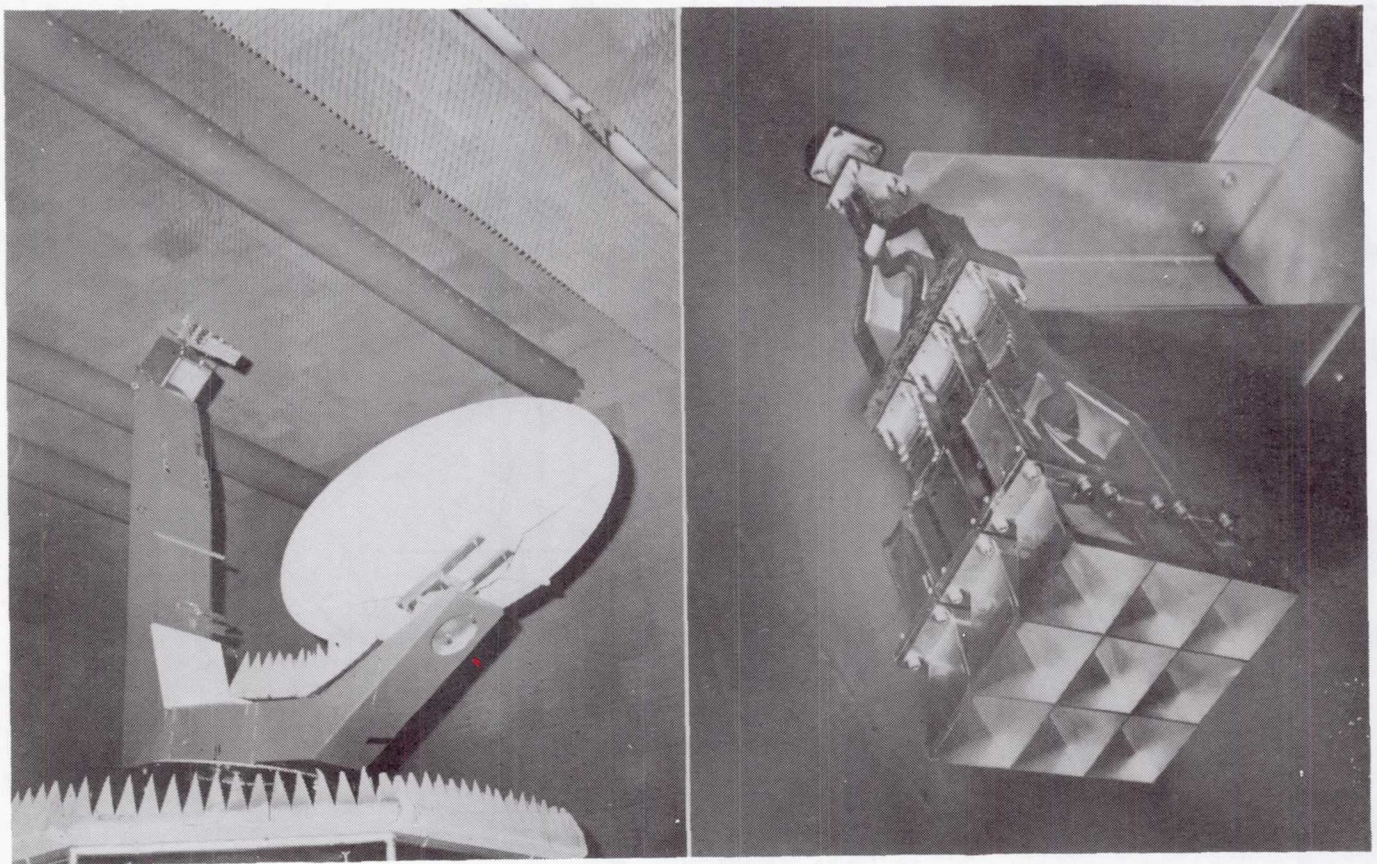


Figure 7

NEAR-FIELD SYMMETRIC PLANE PATTERN PRIOR TO ALIGNMENTS

The multibeam antenna arrived at NFTL without the testing tools required for alignment in the configuration used by TRW. While waiting for these tools, the antenna was assembled without alignment or focusing and installed on the support tower in the near-field facility. Measurements were made that are typical of those experienced during antenna development. The near-field pattern through the center of the reflector in the symmetric plane, i.e., perpendicular to the plane of the strongback is shown in figure 8. With the 2-m (78 in.) reflector diameter noted, phase varies rapidly outside the aperture. Within the aperture, the parabolic phase shape indicates some defocusing. Distortions in the amplitude pattern near the peak indicate the possibility of reflections.

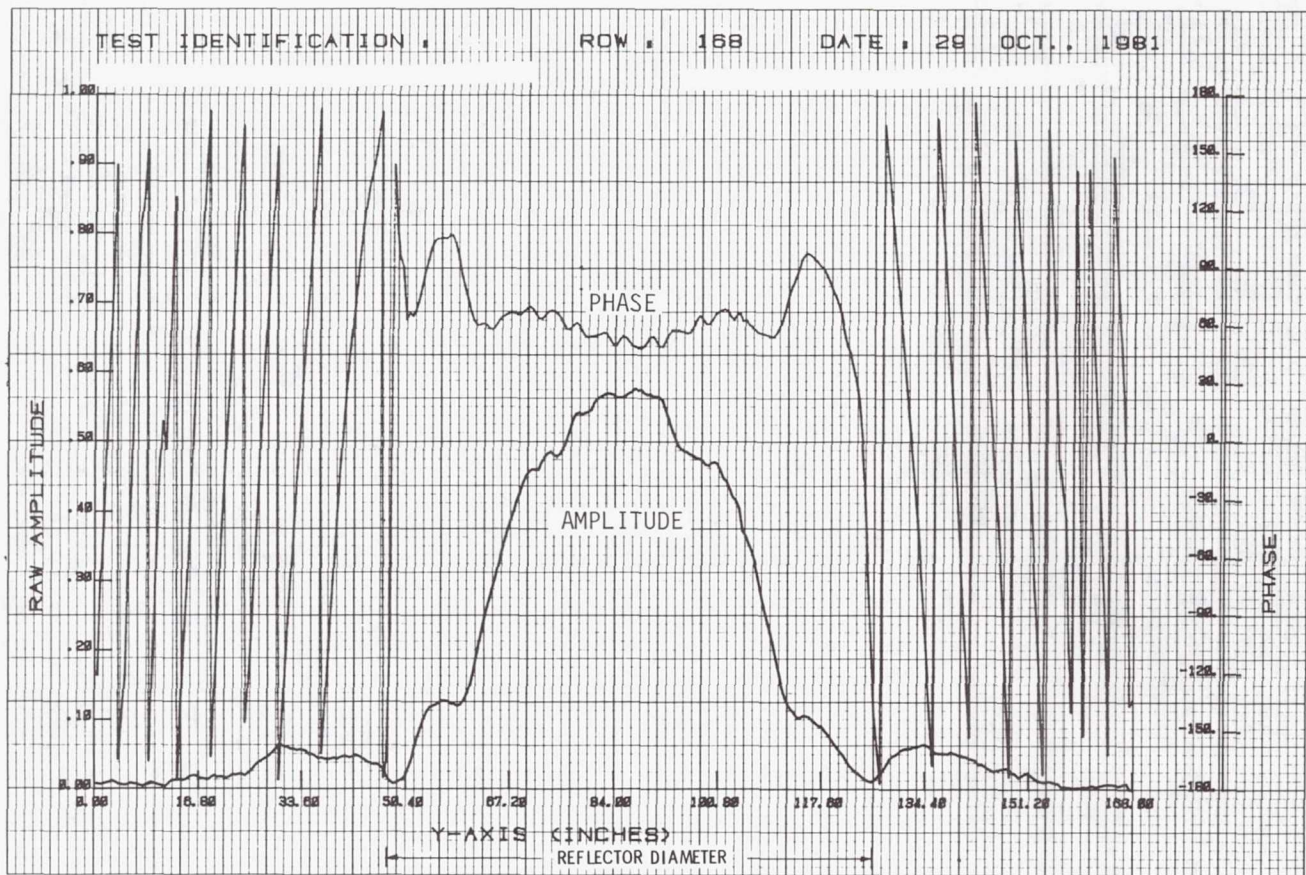


Figure 8

FAR-FIELD SYMMETRIC PLANE PATTERN PRIOR TO ALIGNMENTS

The far-field amplitude pattern through the peak is shown in figure 9. During the FFT processing from near- to far-field patterns, row and columns are interchanged. This interchange is noted in the test identification block on the plots. Except for the inflection points at the 33-36 dB level, there are no sidelobes greater than -39 dB. When focused, these first sidelobes should not merge into the mainlobe. Sharp nulls greater than 80 dB below the peak are indicative of the large dynamic range achievable with the near-field technique.

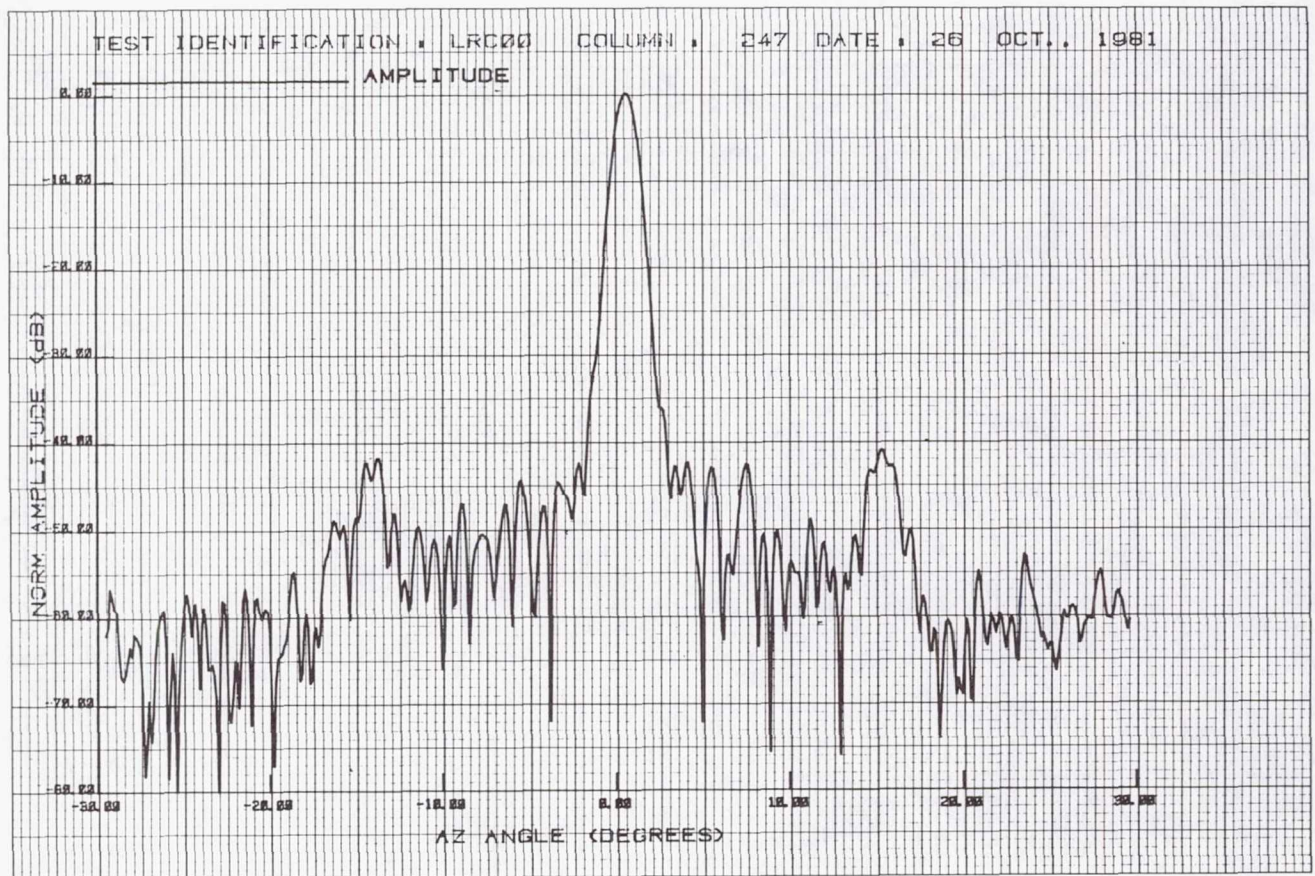


Figure 9

NEAR-FIELD ASYMMETRICAL PLANE PATTERN PRIOR TO ADJUSTMENTS

The large near-field phase variation in the plane of the strongback, shown in figure 10, indicates significant beam tilt in the far-field. However, the linear slope indicates that the gain loss caused by phase taper should be small. Near-field amplitude variations in the plane of the strongback exhibit a large periodic variation. As subsequently verified, this interference pattern results from energy reflected from the strongback. Such large amplitude reflections can be expected to produce a sidelobe enhancement at an angle off-boresight of $57.3 \lambda/W$ where W/λ is the number of wavelengths per period of ripple. With a 1-in. wavelength, the ripple period is 2.8 wavelengths, which infers a sidelobe peak at 20.5 degrees off-boresight. This indicates the need to plot the far-field patterns to a larger angle off-boresight than might normally be used.

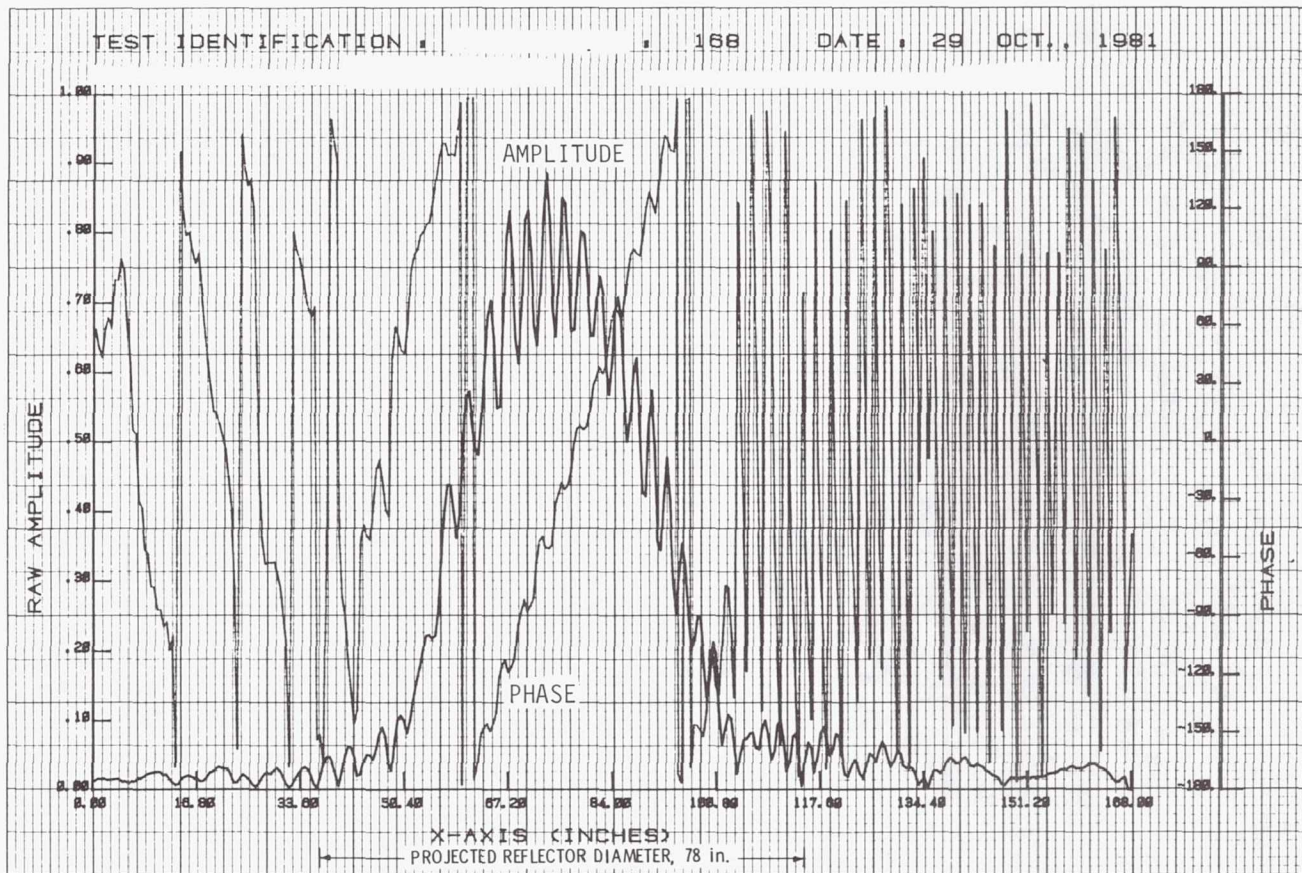


Figure 10

FAR-FIELD ASYMMETRICAL PLANE PATTERN PRIOR TO ADJUSTMENTS

The far-field sidelobe enhancement in the asymmetrical plane pattern is located in the region predicted by near-field data as shown in figure 11. Close-in sidelobes in this plane are higher than in the symmetric plane. This results primarily from the design requirement to make an elliptic beam shape adequate to cover the midlatitude states. The major axis of this ellipse is in the asymmetrical plane.

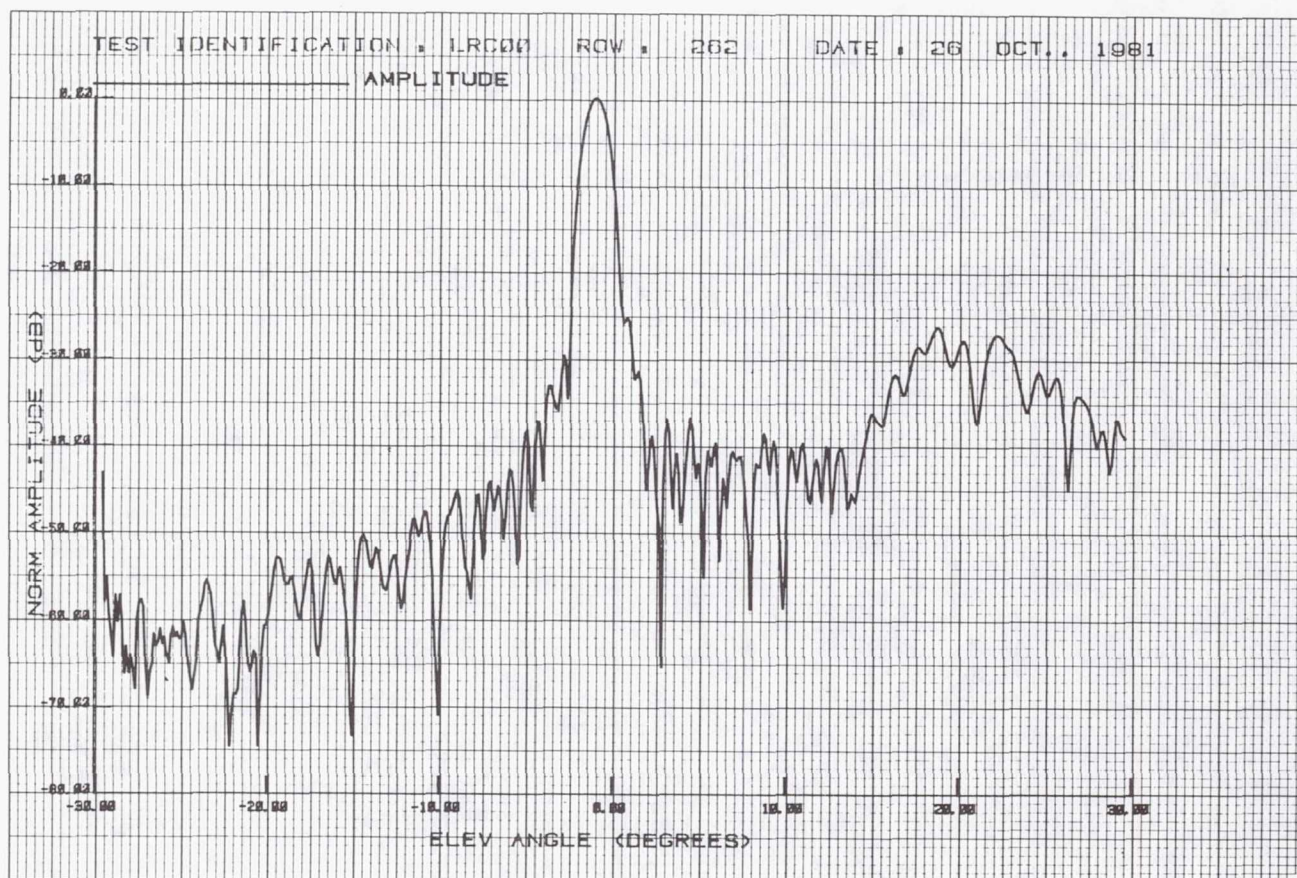


Figure 11

ADJUSTMENT OF ANTENNA CONFIGURATIONS

Alignment procedures noted in figure 12 were begun after test tooling was received from TRW. First, the reflector was positioned using a large contoured template rotated about the axis of the parent parabola. The correct pointing angle for the feed was set using a cruciform tool mounted on a rod positioned along this same axis. Next, an attempt was made to position the feed at the focal point, which was precluded by insufficient length of adjustment slots. It was determined that spacers were used to position the antenna closer to the reflector in earlier tests. These spacers were not supplied with the antenna. Near-field measurements showed that with the large F/D of 1.26, the patterns were relatively insensitive to feed position over a limited range along the axis of the actual parabola. Measurements made by TRW were 0.68 in. behind the focal point along the axis of the actual parabola. Without adding spacers or enlarging the adjustment slots, the closest position achievable was 1 in. behind the focal point. Near-field measurements indicated that this additional 0.32-in. defocusing would produce a negligible difference as long as there was no lateral offset from the axis of the actual parabola.

The rf absorber was placed on the strongback to reduce the reflected field components as shown in figure 7. Finally, the axis of the parent parabola was tilted 0.2 degrees to obtain an improved alignment with respect to the local vertical reference for the near-field facility.

- REFLECTOR AND FEED ALIGNED USING TEMPLATES
- PARENT PARABOLA AXIS ALIGNED TO VERTICAL
- FEED POSITIONED ON AXIS OF ACTUAL PARABOLA
1 IN. BEHIND FOCAL POINT
- RF ABSORBER PLACED ON STRONGBACK

Figure 12

NEAR-FIELD ASYMMETRICAL PLANE PATTERN AFTER ADJUSTMENTS

A dramatic change in the near-field pattern in the plane of the strongback is shown in figure 13. Ripples resulting from reflections are insignificant after installation of the rf absorber. Within the -20 dB level, only 53 in. of the 78-in. projected reflector diameter are illuminated. For this under-illuminated case, the far-field beamwidth is not determined by the reflector diameter but by the width where the illumination becomes insignificant. Far-field 3-dB beamwidth can be estimated using the expression $BW = 68 \lambda/D'$, where D'/λ is the smaller number of wavelengths across the reflector or the -20-dB illumination width. With alignment and minor lateral defocusing, the illumination pattern indicates the superior performance expected for the low sidelobe cluster feed. The small negative-phase slope across the aperture could be removed by moving the feed laterally with respect to the axis of the actual parabola. However, this minor refocusing was not implemented because the objective was to duplicate the performance as measured by TRW not to obtain the best focus.

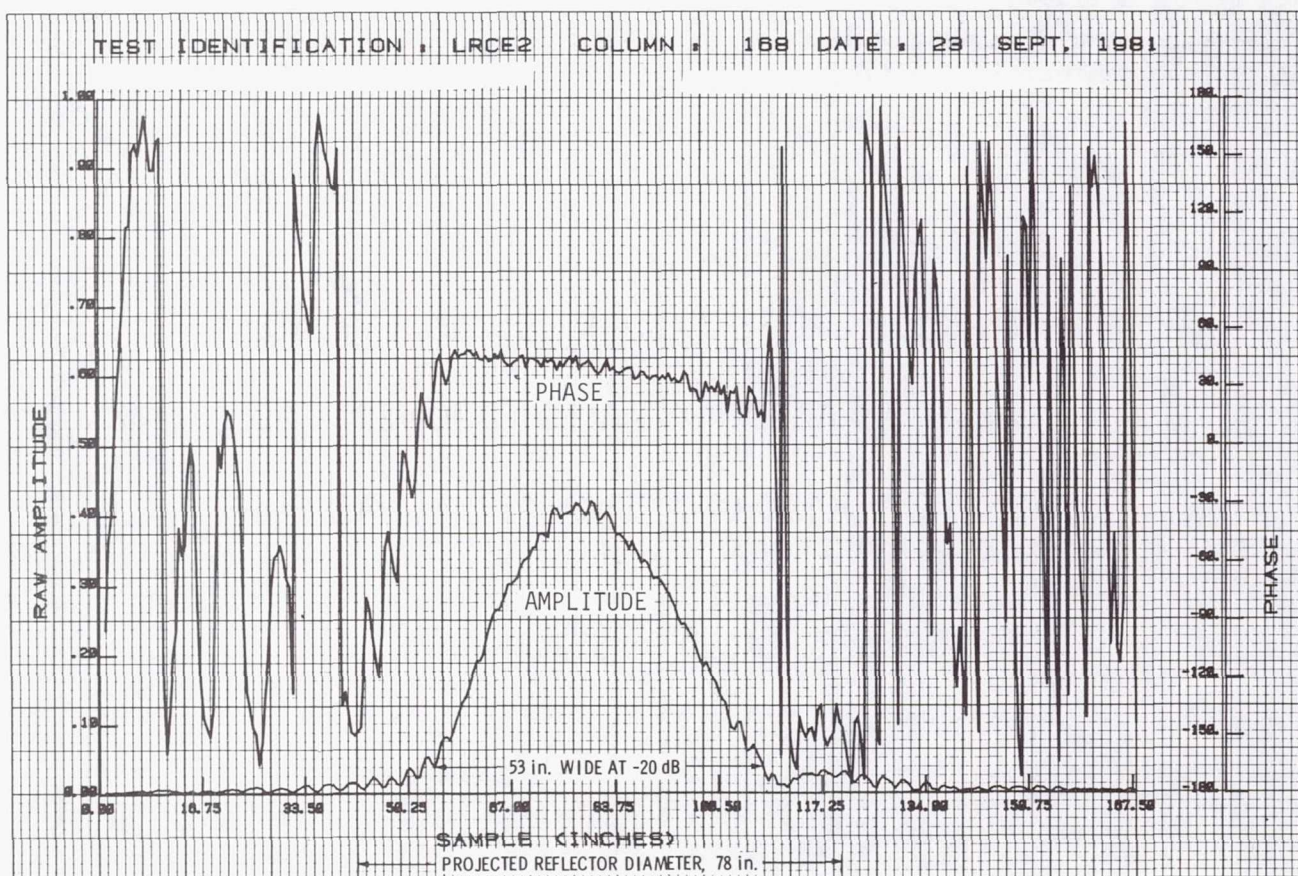


Figure 13

FAR-FIELD ASYMMETRICAL PLANE PATTERN AFTER ADJUSTMENTS

Improvements in the far-field asymmetrical plane pattern with adjustments is shown in figure 14. The sidelobes drop rapidly on both sides of the pattern. Data plotted over a wide angle indicates that the sidelobe enhancement in the 20-degree region disappeared when the ripple in the illumination pattern was eliminated. With focusing and alignment improvements the first sidelobes became well defined. The overall pattern was also much more symmetrical than before these adjustments.

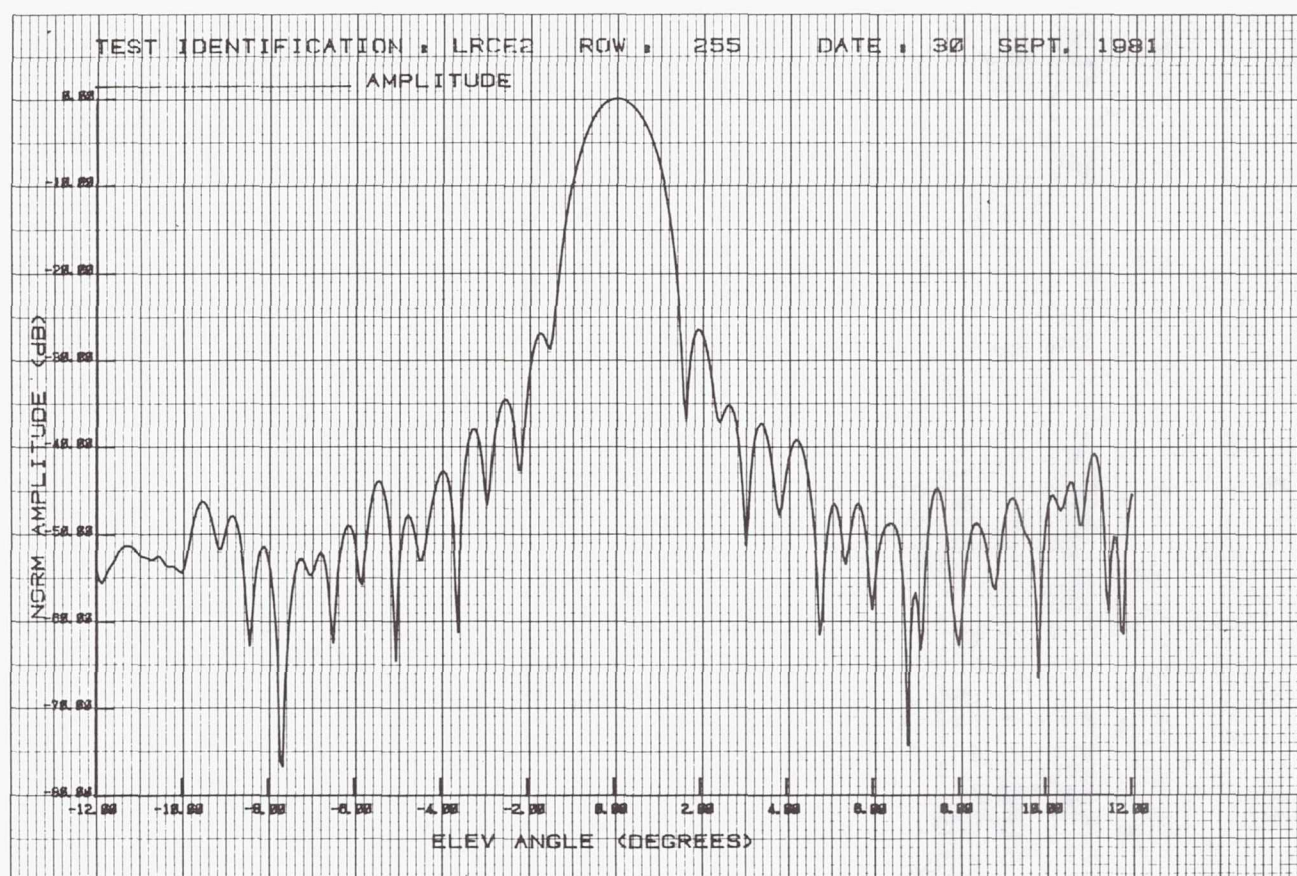


Figure 14

INITIAL COMPARISON OF NEAR- AND FAR-FIELD PLANE MEASUREMENTS

Data measured on the near-field range was scaled to the format recorded at TRW's Capistrano facility. An overlay of these plots is shown in figure 15. Mainbeam shapes are identical and first sidelobes similar but the further-out sidelobes have much larger amplitude in the far-field measurements. Thorough review of test configuration differences revealed two potential contributors--the far-field range had a 20-mil nylon environmental-protection screen known to produce a 3-dB sidelobe enhancement and these measurements were made with the polarization grid subreflector installed. Inquiry into the effects of the subreflector indicated that its use was not necessary when attempting to duplicate the TRW measurement conditions because the subreflector was believed to be transparent to orthogonally polarized fields.

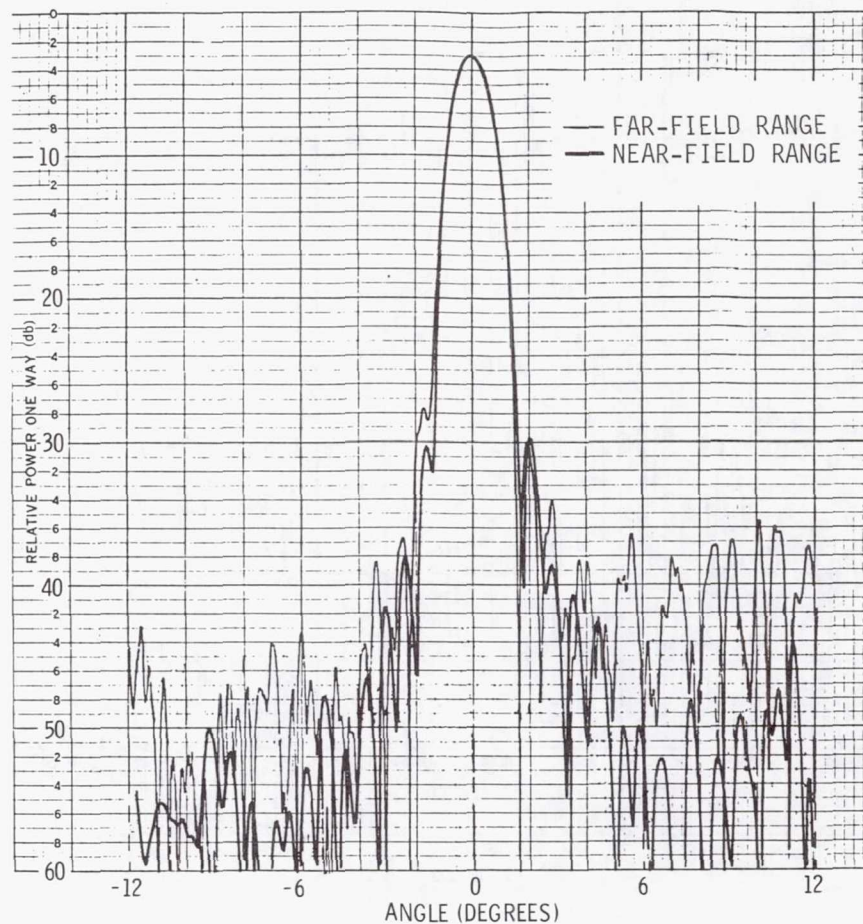


Figure 15

FAR-FIELD CONTOUR PLOT

Far-field beam contours at -3, -10, -20, -30, and -40 dB levels are shown in figure 16. The elliptic beam shape is apparent. Sidelobes in the symmetric plane (azimuth axis) are much lower than in the asymmetric plane. Measurements made by TRW indicated this low sidelobe performance can be achieved in all directions when using feeds designed for circular patterns. The extremely low sidelobe levels achievable with cluster feeds used with offset reflectors is impressive--only small regions extending above -40 dB can be expected to peak only to -37 or -38 dB.

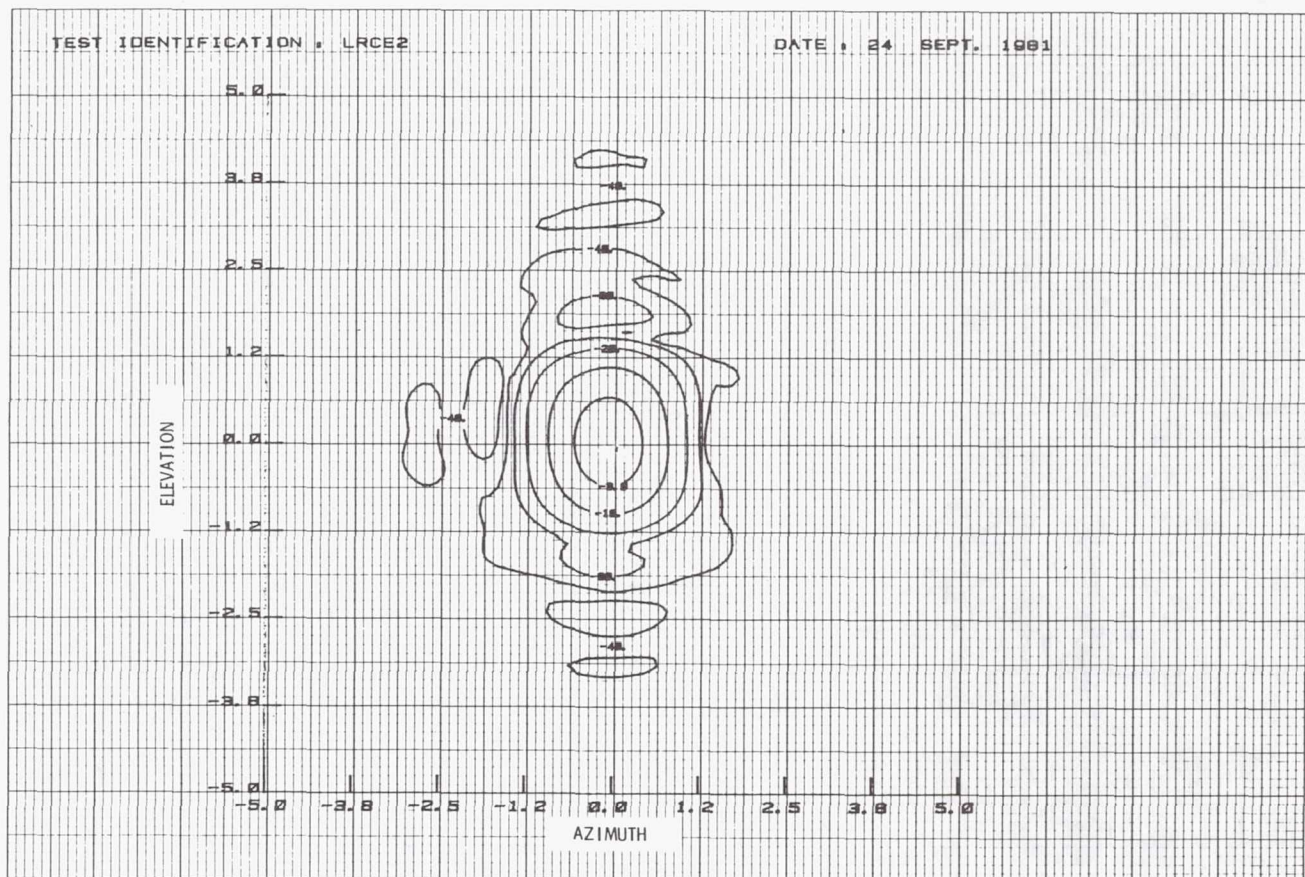


Figure 16

EFFECT OF POLARIZATION GRID SUBREFLECTOR

Near-field measurements made with the polarization grid subreflector installed as indicated on the assembly drawing supplied with the antenna showed a distorted illumination pattern. Study of a photograph of the antenna with subreflector installed indicated that an alternate set of mounting holes in the subreflector support structure was used. In this alternate location, the plexiglas mounting material was moved away from the feed axis and less field was refracted into the reflector. The resulting pattern is shown in figure 17. In the region of 6 to 8 degrees off boresight, peak sidelobe levels with the subreflector installed are in-the-order of 10 dB higher than without it and in most of the other regions there is some enhancement.

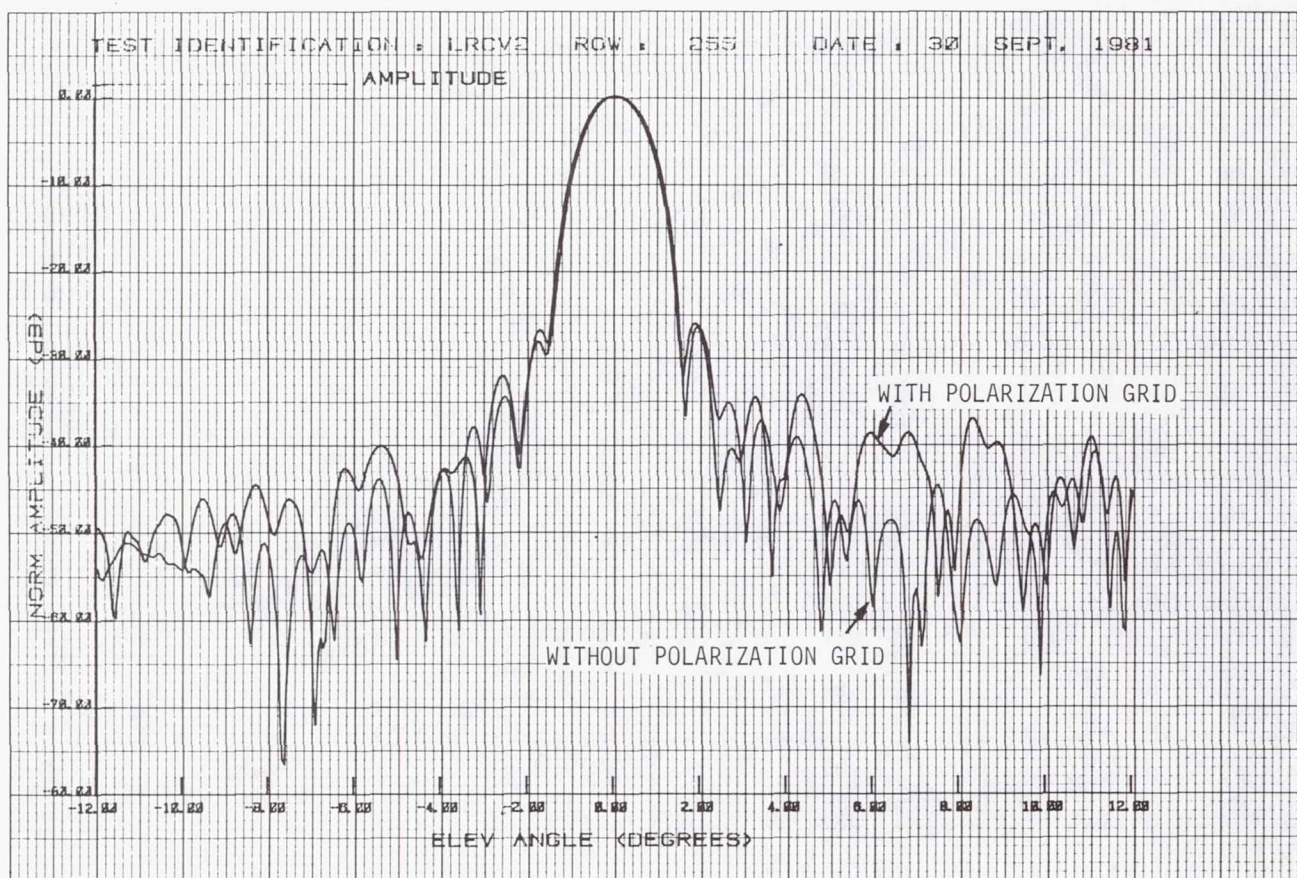


Figure 17

FAR-FIELD 3-D PLOT WITH POLARIZATION GRID SUBREFLECTOR

The 3-dimensional field representation in figure 18 shows a synoptic view of the far-field pattern with the polarization grid in place. Superposition of contour lines makes this display useful for quantitative interpretation. The "water-level" is set at -45 dB in this case with the lowest level contour at -30 dB. Except for the small region adjacent to the mainbeam along the elevation axis, all sidelobes shown fall within this 15-dB range.

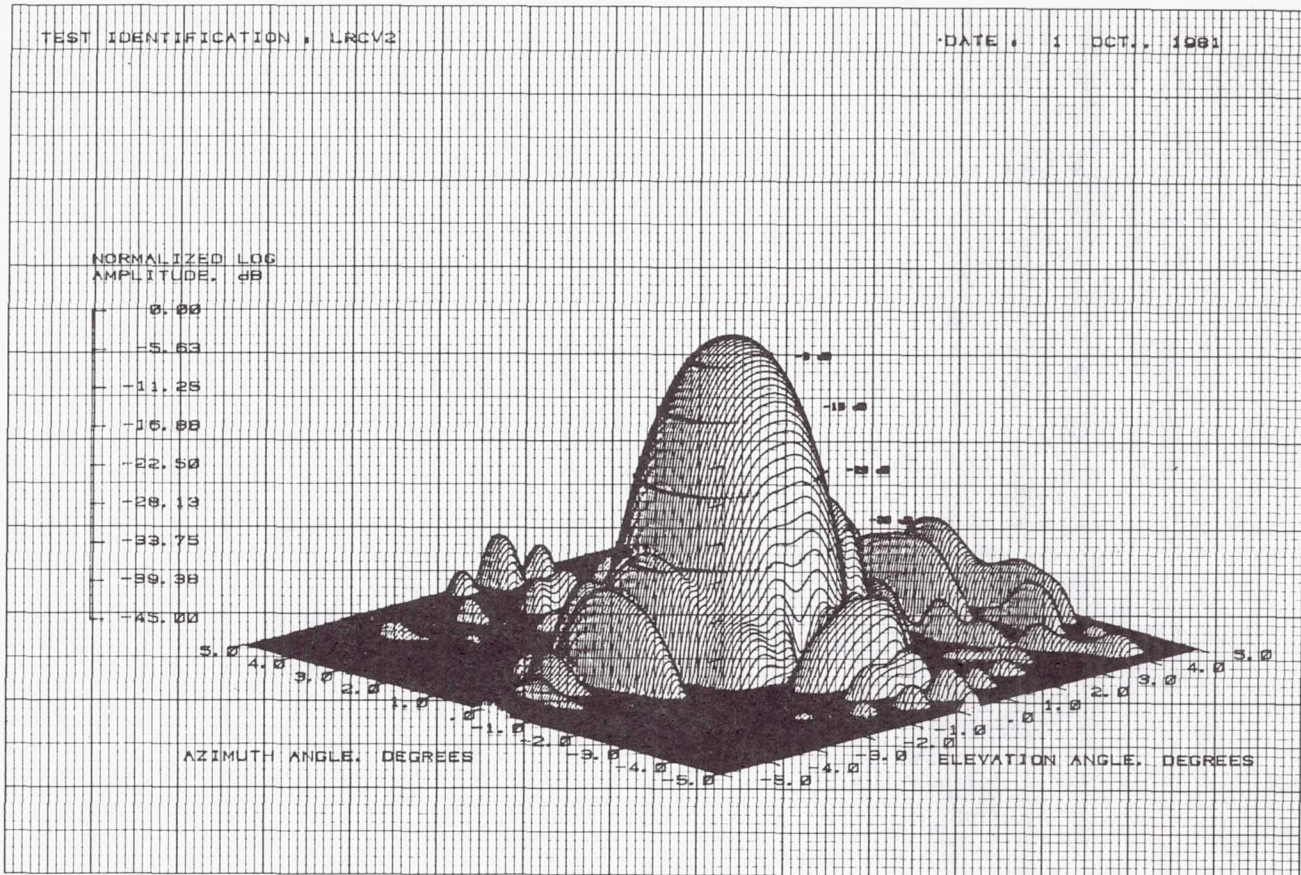


Figure 18

OVERLAY OF ASYMMETRICAL PLANE PLOTS MEASURED
ON NEAR- AND FAR-FIELD RANGES

Comparison of asymmetrical plane plots made on near- and far-field ranges with the polarization grid subreflector installed is shown in figure 19. Far-field range data remains higher than that measured in the NFTL, but the difference in most regions is consistent with the sidelobe enhancement produced by the environmental-protection screen used at the Capistrano range. The sidelobe peaking at 10 degrees off boresight is farther out than the major peak noted in NFTL data taken before repositioning the polarization grid support structure. But, there might still be some intermediate mounting position that could account for part of the difference in sidelobe levels.

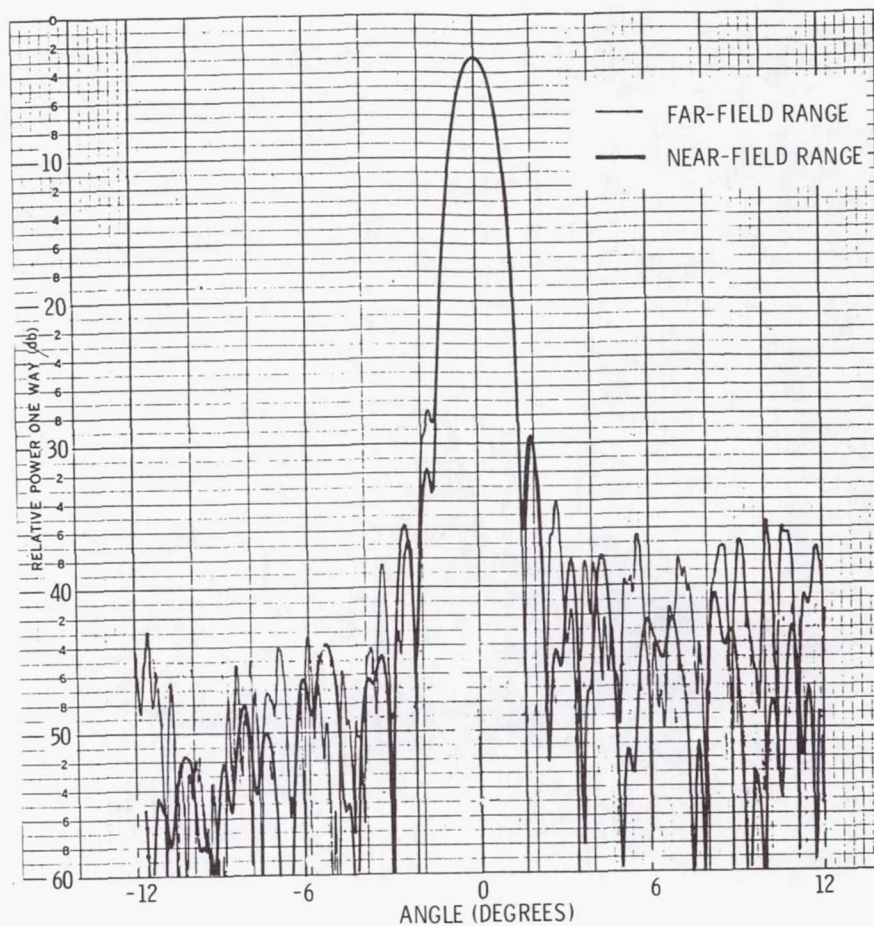


Figure 19

OVERLAY OF SYMMETRICAL PLANE PLOTS MEASURED ON NEAR- AND FAR-FIELD RANGES

In the symmetrical plane plots of figure 20, the average sidelobe level measured on the Capistrano range is higher than those measured in NFTL by 3 dB close-in and 9 dB at 10 degrees off boresight. Experience indicates that few error sources in near-field measurements produce a reduction in the average sidelobe level. One potential factor that could decrease this level is the use of field probes with insufficient beamwidth for the near-field scan geometry described in conjunction with figure 4. Probes used for these multibeam antenna measurements have a 1-dB beamwidth of +20 degrees in the E-plane that increases to +36 degrees in the H-plane. Therefore, variations in probe gain do not contribute to near-field error measurements within the +12 degree ranges shown. For applications in which planar near-field scans are used for widebeam measurements, probe compensation techniques can be applied. Accurate measurements have been demonstrated up to +80 degrees using this technique at NFTL.

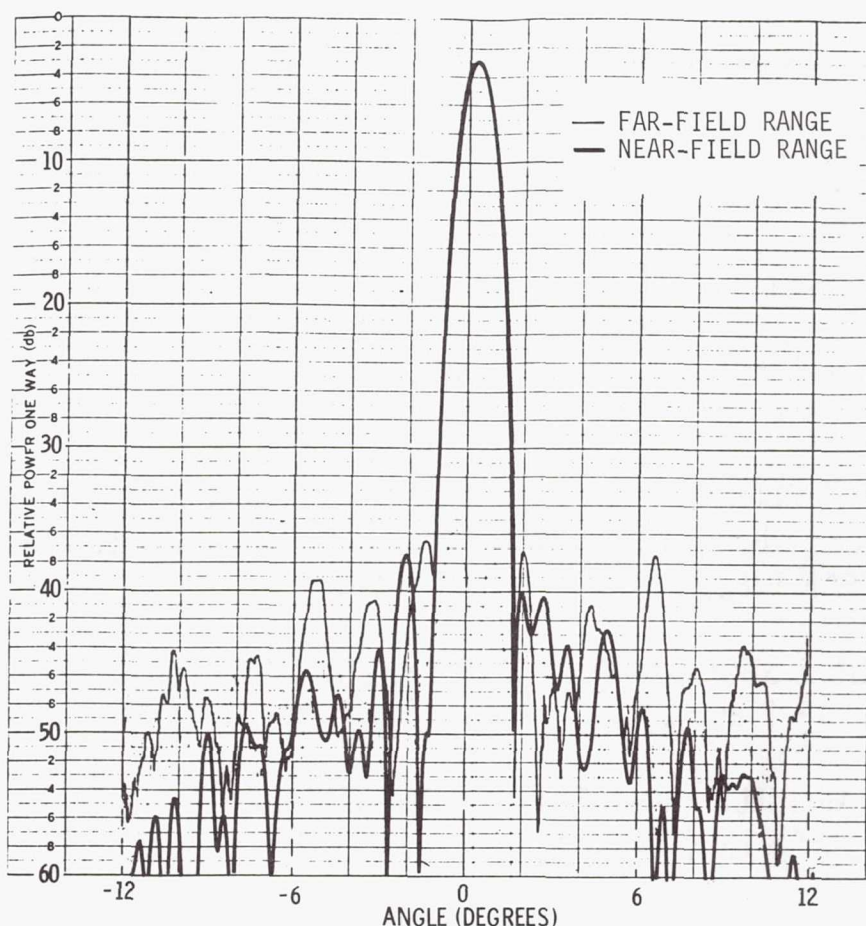


Figure 20

NEAR-FIELD TESTING WORKS

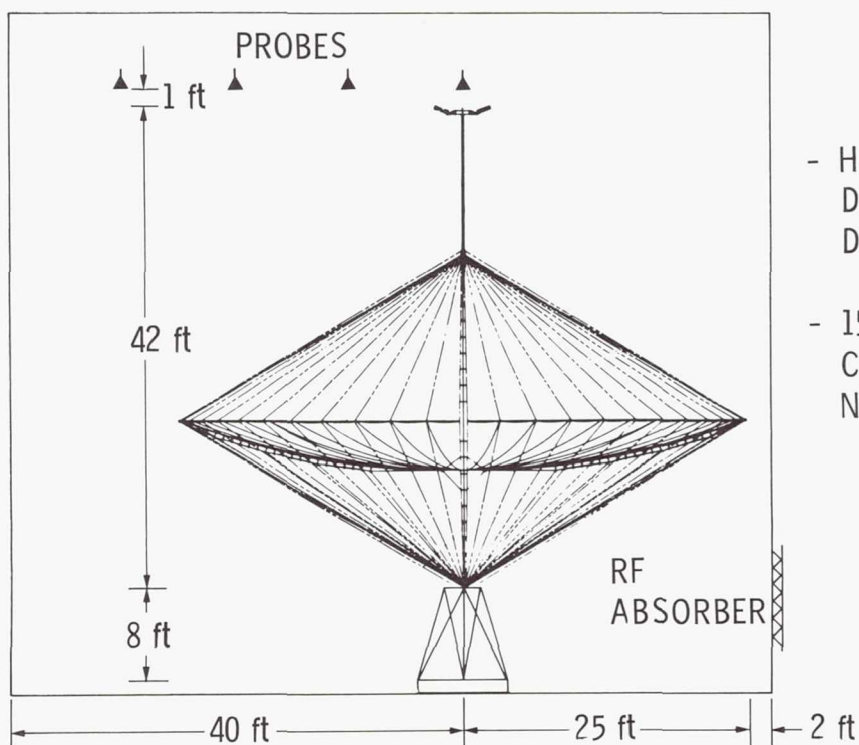
Applications of near-field data shown in figure 21 were used during the measurement sequence for the multibeam antenna. Near-field data were used before processing to far-field data to rapidly estimate beam tilt, 3-dB beamwidth, peak gain, and the location of sidelobe peaks. This capability is useful for efficient setup and alignment. Near-field data were also used to help position the rf absorber on the strongback to reduce reflections. For example, sidelobe levels measured in the NFTL showed pattern variations lower than the limits set by upper-bound analysis. Near-field measurements also indicated that the enhanced sidelobe levels, resulting from the effects of the polarization grid, were observed on the 20-mil nylon screen needed for environmental protection at the far-field range. The NFTL is now operating and can test antennas up to 54 ft in diameter.

- NEAR-FIELD DATA CAN BE DIRECTLY USED TO RAPIDLY ESTIMATE
 - BEAM TILT
 - 3-dB BEAMWIDTH
 - PEAK GAIN
 - SIDE LOBE PEAKS
- PATTERN LEVELS IN SIDE LOBE REGION ARE MORE ACCURATE THAN INDICATED BY UPPER-BOUND ANALYSIS
- NEAR-FIELD MEASUREMENTS SHOWED POLARIZATION - GRID EFFECTS OBSCURED BY ENVIRONMENTAL CURTAIN NEEDED FOR FAR-FIELD RANGE
- TROUBLE SHOOTING AND DEVELOPMENT AIDED BY NEAR-FIELD DATA
- A NEAR-FIELD FACILITY FOR TESTING LARGE ANTENNAS IS NOW OPERATIONAL

Figure 21

A FUTURE APPLICATION

A program at LaRC is currently supporting technological development of large hoop-column deployable antennas.^{3,4} This development activity is being accomplished by the Harris Corporation in Melbourne, Florida.⁵ A 15-m scale model of a 100-m hoop-column antenna should be available for near-field testing in 1984. Figure 22 shows that the NFTL can easily accommodate this 50-ft diameter by 42-ft high configuration. Using the maximum size scanning capability will allow data collection for sidelobes out to ± 23 degrees off boresight. Measurements at both C and Ku bands are consistent with the existing range instrumentation and routinely achieved scan-plane mechanical tolerances. Dedicated computer and mass data storage coupled with flexible software will support rapid data processing and produce displays in the varied formats described in this paper.



- HARRIS CORP IS CURRENTLY DEVELOPING HOOP/COLUMN DEPLOYABLE ANTENNA FOR LaRC
- 15-m MODEL OF 100-m CONCEPT CAN BE ACCOMMODATED BY NFTL FOR TESTING UP TO 18 GHz

Figure 22

REFERENCES

1. McKinney, J. F. and Osborn, J. D.: Test of Large Aperture Antennas Using Near-Field Techniques. Proceedings of the Sixth Aerospace Testing Seminar, Institute of Environmental Sciences and Aerospace Corp., Los Angeles, California, March 1981.
2. Chen, C. C. and Franklin, C. F.: Ku-Band Multiple Beam Antenna. TRW, Redondo Beach, California, December 1980, NASA Contract Report 154364.
3. Campbell, T. G.: Hoop/Column Antenna Technology Development Summary. Large Space Systems Technology - 1980. Volume I - Systems Technology, NASA CP-2168, 1981, pp. 357-364
4. Campbell, T. G.: Summary of Antenna Technology Development at the Langley Research Center. Large Space Systems Technology - 1981, NASA CP-2215, Pt. 2, 1982, pp. 491-501.
5. Sullivan, M. R.: Maypole (Hoop/Column) Concept Development Program. Large Space Systems Technology - 1981, NASA CP-2215, Pt. 2, 1982, pp. 503-550.

PROGRESS REPORT
ON THE
ELECTROSTATIC MEMBRANE ANTENNA CONCEPT TESTING

J. W. Goslee
NASA Langley Research Center
Hampton, Virginia

Large Space Systems Technology - 1981
Third Annual Technical Review
November 16-19, 1981

In past years LaRC has tested the electrostatic concept both in small sizes and in the present 16-foot diameter size in order to evaluate the concept and determine its feasibility for future antenna applications. The concept being tested is shown on the left side of Figure 1 and illustrates how the individual power supplies are connected to concentric electrodes which are located in back of the plastic membrane, which is the reflective surface. The right side shows a typical 0.3-mil Kapton test membrane with the electrostatic force applied, creating a concave reflective surface.

NASA ELECTROSTATIC MEMBRANE REFLECTOR, 1/20th SCALE

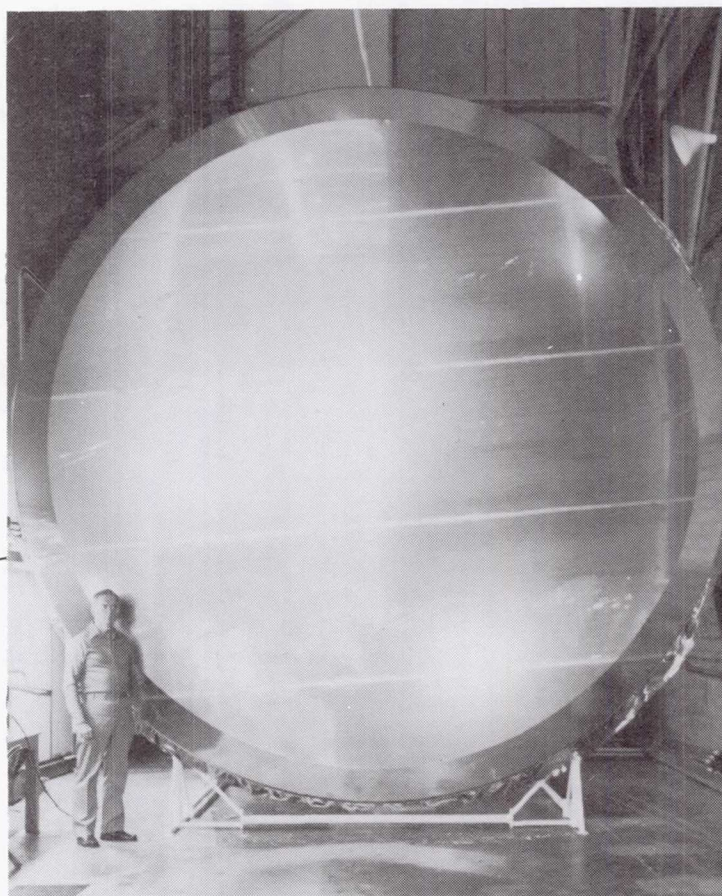
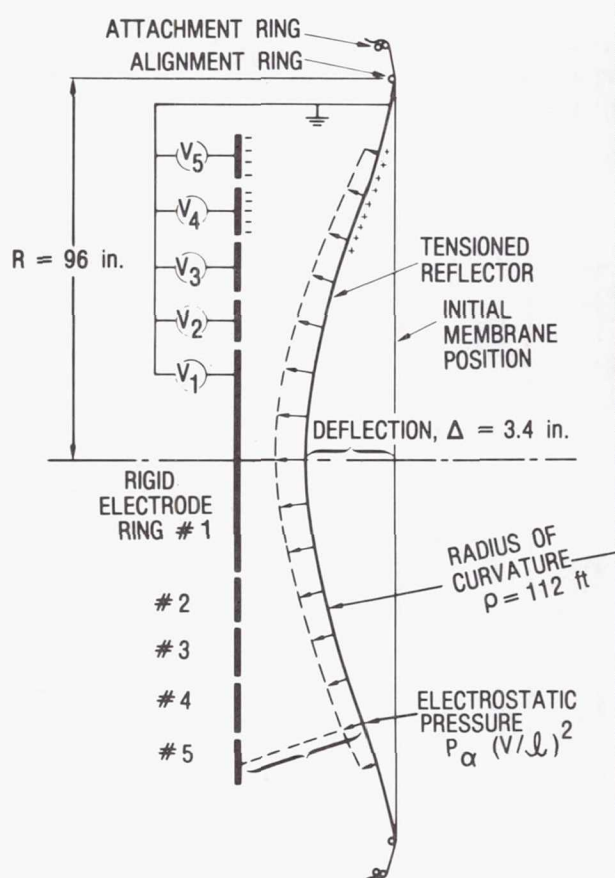


Figure 1

Testing was conducted during the latter part of 1980 and the first half of 1981, and 13 sets of data were secured using different membranes, different voltage combinations, and different measurement techniques. Contour plots were made showing the error between the perfect spherical surface and the measured surface. The view on the left in Figure 2 shows a contour plot of one of the early tests. Several deficiencies were seen in this plot; the ring supporting the membrane was not flat, the back electrode was not parallel to the membrane ring, and the diameter of the back electrode did not extend far enough to influence the perimeter of the membrane.

Some of these deficiencies were changed; the membrane ring was adjusted to be more flat and the back electrode was adjusted to be more parallel to the plane of the membrane ring. The view on the right of Figure 2 shows the residual error from a later test in the series.

MEMBRANE SURFACE IMPROVEMENTS DURING 1980-1981 TESTING

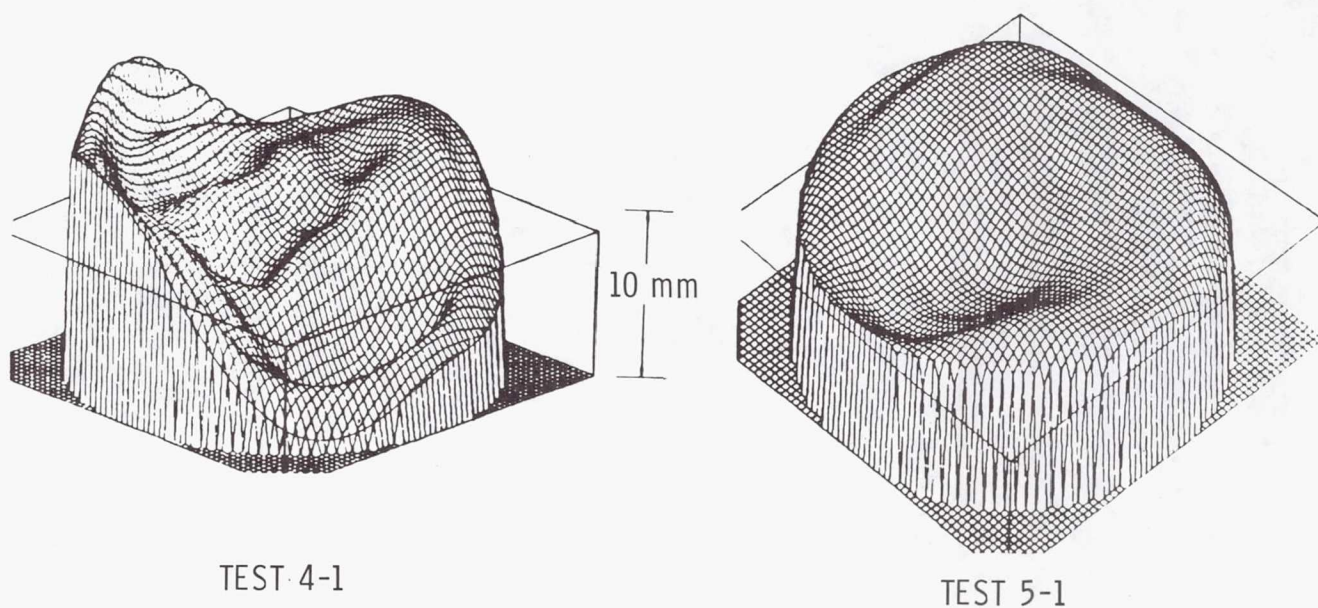


Figure 2

Another problem that was seen during the testing was the voltage spill-over between the electrode areas. It was felt that the electrode configuration would have to be changed to correct this condition.

During the latter part of FY 81, modifications were made to the back electrode to increase its versatility as well as correct some of the deficiencies that were seen during the testing. The electrode was made 10 inches larger overall to increase the effective control area and reduce the bulge that was seen around the perimeter of the membrane on the previous figure. The face of the electrode was covered with 5-mil Mylar and the control area separation was increased to 3 inches to decrease the tendency for voltage to spill over from electrode to electrode. The pattern of control areas was changed to provide more flexibility in testing to be done in FY 82. The modification shown in Figure 3(a) shows the five concentric rings with 3-inch separation between the control areas.

MODIFIED BACK ELECTRODE WITH 5 CONTROL AREAS

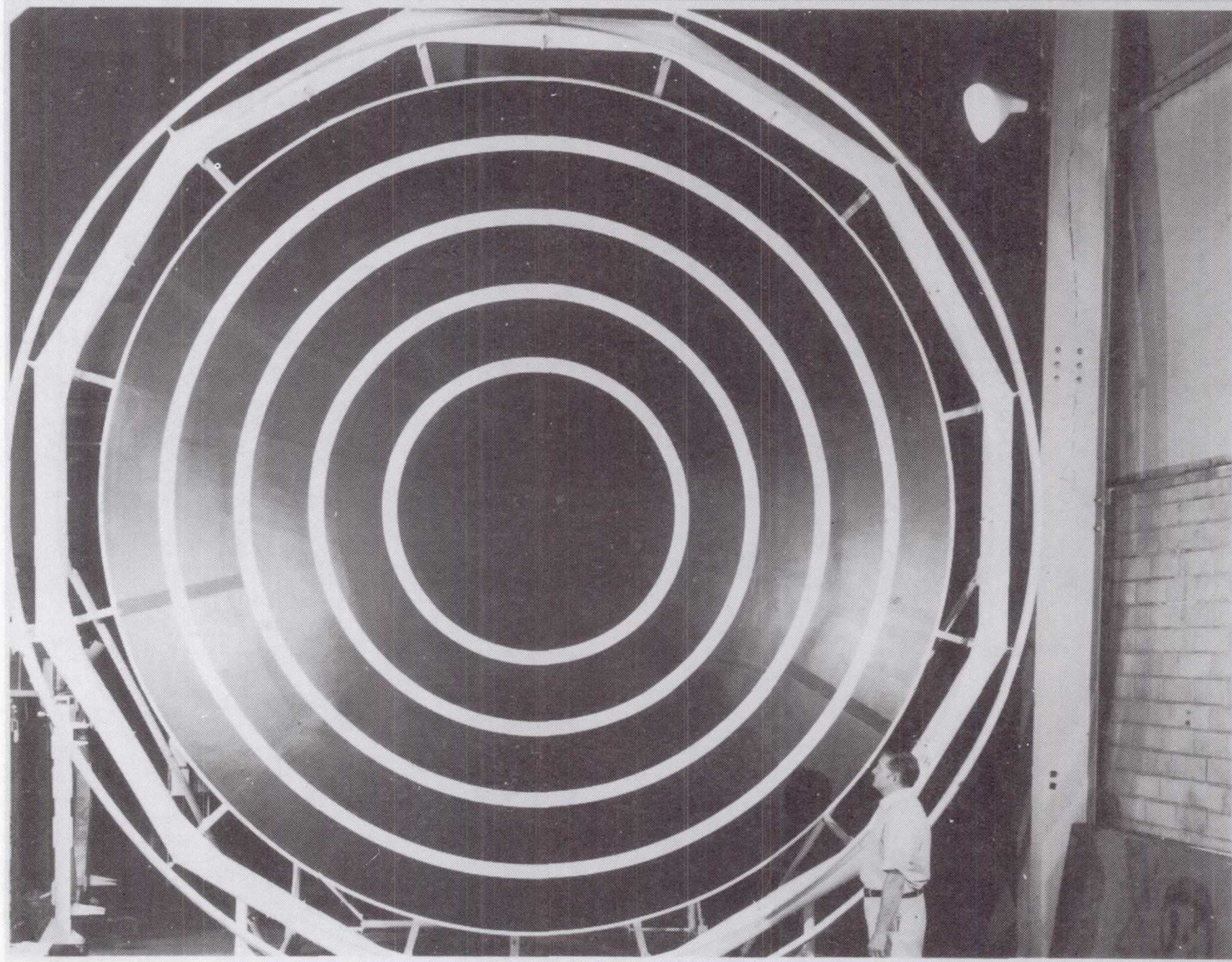


Figure 3(a)

The modification shown in Figure 3(b) has three concentric electrode areas. The General Research Corporation has developed a program for use with the HP-85 calculator which will permit an optimum set of voltages to be derived through a matrix operation after an initial set of voltages is applied.

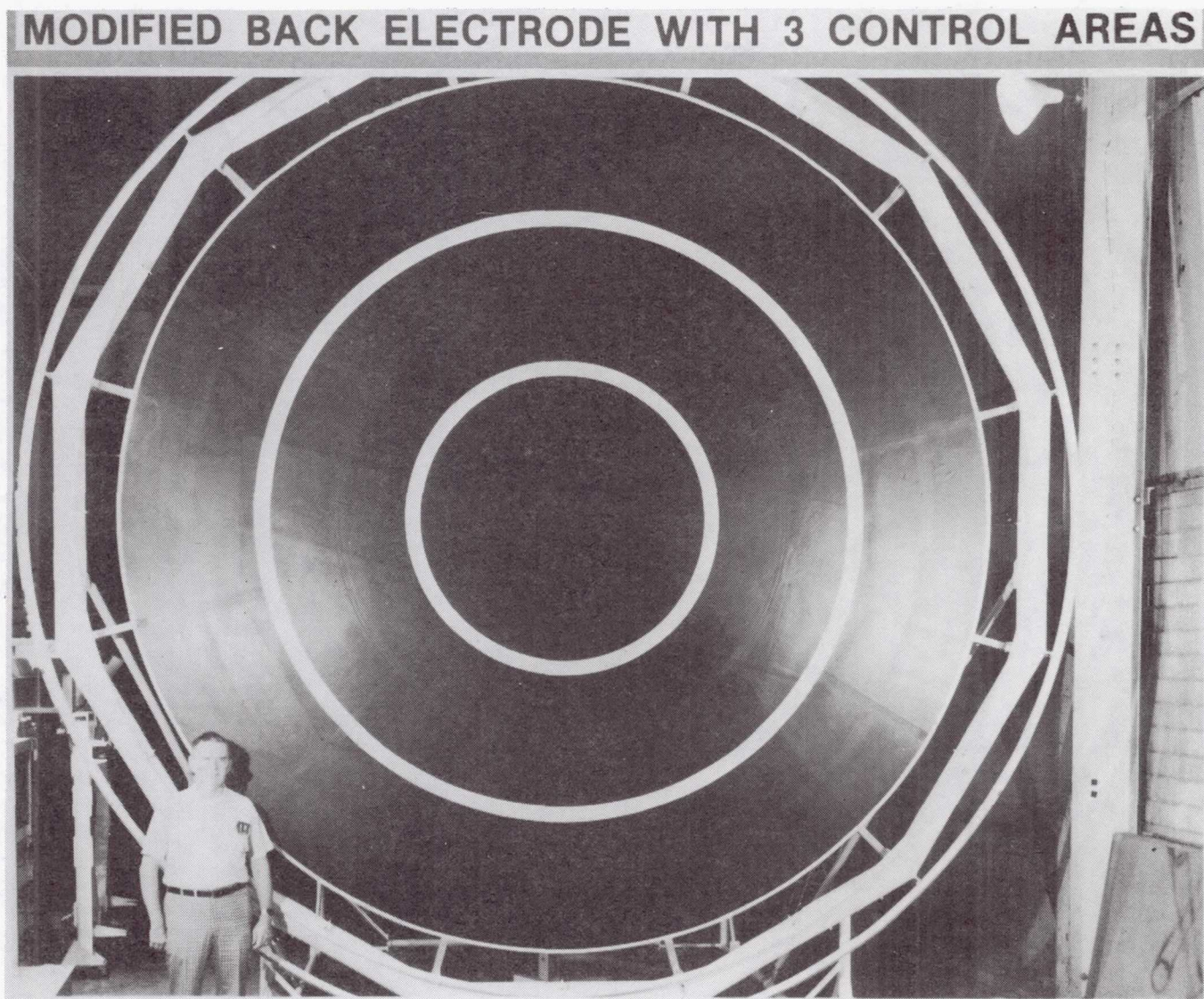


Figure 3(b)

The modification shown in Figure 3(c) shows 10 control areas which will have separate power supplies and will be used to demonstrate control capability around the outer edges of the membrane as well as deflection in the center.

MODIFIED BACK ELECTRODE WITH 10 CONTROL AREAS

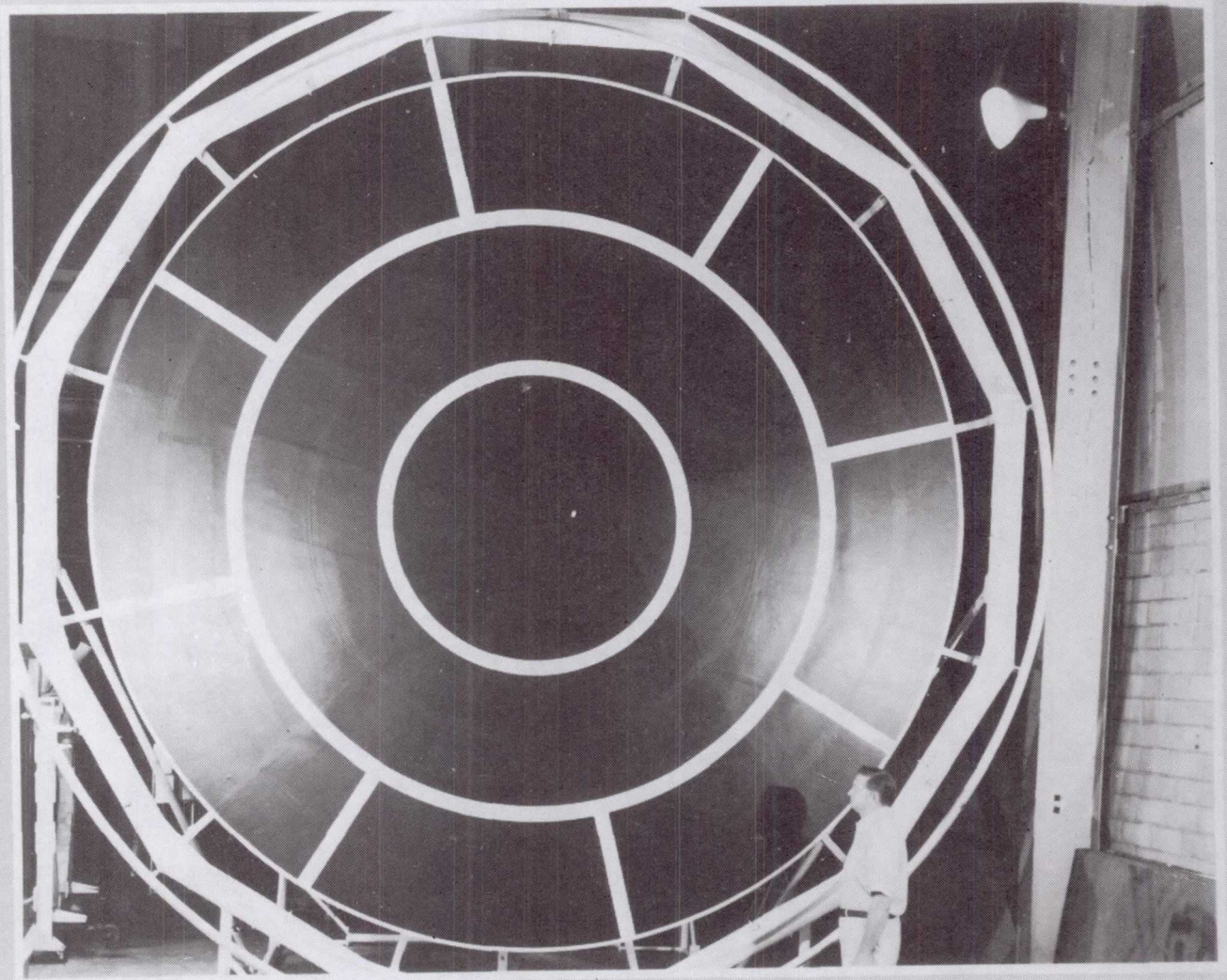


Figure 3(c)

While the testing with the modified electrodes is proceeding, a flexible back electrode will be designed and fabricated for testing later in 1982. The flexible back electrode will be made to adapt to the existing test fixture. Figure 4 shows a conceptual view of how a flexible back electrode and support structure could be made to fit the existing test fixture.

FUTURE FLEXIBLE BACK ELECTRODE AND SUPPORT STRUCTURE

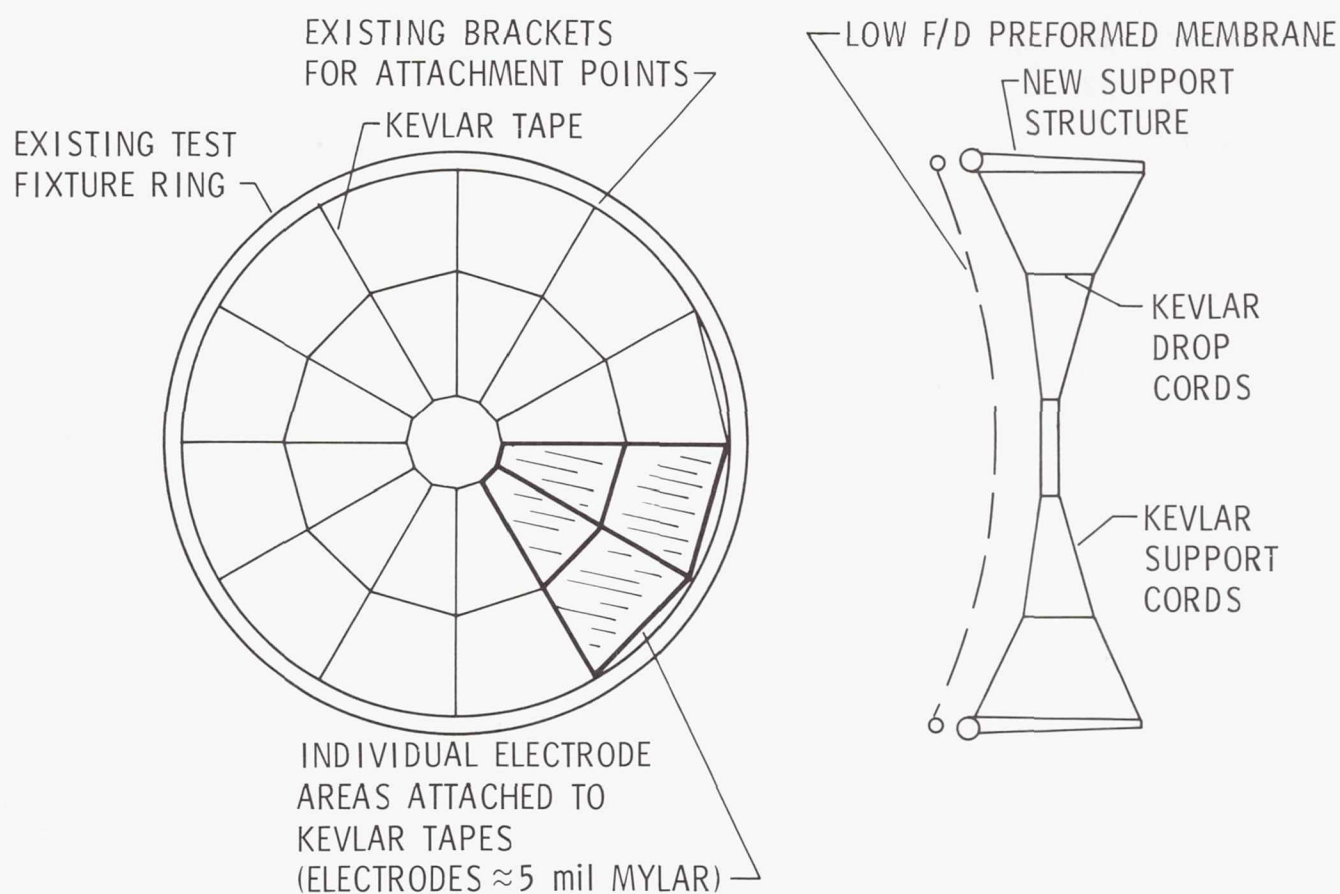


Figure 4

Page intentionally left blank

CONCEPTUAL DESIGN OF ELECTROSTATIC ANTENNA

J. V. Coyner
Martin Marietta Denver Aerospace
Denver, Colorado

Large Space Systems Technology - 1981
Third Annual Technical Review
November 16-19, 1981

CONTRACT INFORMATION

Radiometer antennas of the 100-meter diameter class can be placed into near-Earth orbit with one Shuttle flight. This study explored and developed certain conceptual designs and associated technologies for deployable antennas of this size. The study was divided into three tasks.

The first task was dedicated to the design of an electrostatically suspended and controlled membrane mirror and to the performance of the necessary analysis to develop conceptual designs for the supporting structure. The scope included evaluating three leading structural concepts, selecting two, and proceeding with the design and analysis of the integrated spacecraft including STS cargo bay stowage and deployment. An antenna performance evaluation was performed as a measure of the quality of the membrane/spacecraft when used as a radiometer in the 1 GHz to 5 GHz region.

The objective of Task II was to provide several related LSS structural dynamics models differing by their stiffness property (and therefore, lowest modal frequencies); then, to take these dynamic models, and develop control systems designs whose complexity varies inversely with increasing modal frequency regimes.

The objective of Task III was to expand and improve Langley Research Center's (LaRC) interactive computer-aided-design software.

- Customer: NASA-Langley Research Center
Mr. U. M. Lovelace
- Contract Number: NAS1-16447
- Period of Performance: 23 September 1980 to 8 December 1981
- Program Manager: Mr. A. L. Brook

Figure 1

MISSIONS

The ASSA program is a technology study, not a radiometer design. However, in an attempt to achieve realistic results, a mission was selected. The mission is a scaled-down version of the spherical dish radiometer, described on page 15 of "Focus Mission Scenario for Communications, Radiometer and Radio Astronomy . . . LSST Technology Requirements Definition" by T. G. Campbell and J. DiBattista; NASA LaRC. The geometry was scaled to give a 100-meter aperture using 50-m spots generated by beams on a line feed of 23-m length, 100-meter focal length. The 650-km circular orbit altitude was preserved although the 1-km resolution (at 1.08 GHz) could not be achieved. An efficient beam pattern was attained, however, by interlacing feed horn outputs. The mission characteristics are listed in Figure 2.

Purpose of Mission Selection:

- To Provide a Basis for Deriving Requirements and Assessing Performance

Mission Selected:

- 100-m Diameter Spherical Dish Radiometer
- Line Feed; F/D = 2 per Beam
- 650 km Circular Orbit Inclined 60 deg
- 10-yr Lifetime; 3-yr Reservice
- Single STS Launch
- 20 deg of Slew in 1/2 Orbit
- 1-km Resolution

Modification:

- For Task II, to Highlight Controls and Structures Interaction:
 - A Slew Rate of 45 deg in 5 min Was Introduced (Settling at ± 0.05 deg)
 - 170-m Diameter Antenna Was Assumed

Figure 2

100-m DIAMETER, 28 BAY COMPRESSION HOOP WITH ECMM

Large, lightweight reflector antennas in Earth orbit are the key to realizing many applications to IR and radiometric sensors. Many of these applications call for reflector diameters of 10 to 200 meters and rms surface qualities of 0.1 to 1000 μm . A concept of achieving such a high surface quality in a reflector that is inherently lightweight and compact has been studied over the last few years. The concept is that of using electrostatic forces to tension a thin, conducting membrane and maintain it in a precision antenna shape. This electrostatically controlled membrane mirror (ECMM) is an adaptive structure which maintains surface quality despite errors in construction, irregularities of materials, solar heating, and on-board disturbances.

The electrostatic controlled membrane mirror (ECMM) has been designed for a high-performance NASA radiometer mission. Its spherical surface is designed to have a ratio of aperture diameter to rms surface quality of approximately 10^5 ; e.g., a membrane of 100-meter diameter is to have a surface accurate to 1 millimeter. The high surface quality is achieved by tensioning the membrane to 5% of its yield stress by electrostatic pressure. An electric field strength of about 2.7 kV/cm is applied between the precision membrane that forms the reflector and an irregular membrane that forms a control-electrode surface. The pressure developed on the membrane reflector is 0.34 N/m^2 . The perimeter of the membrane is restrained by a rigid support structure automatically deployed from the Space Shuttle. The ECMM reduces the complexity of support structures by reducing the number of repeating elements. Closed-loop shape control is used to maintain the surface precision in the presence of disturbances. The control-electrode surface is segmented into approximately 220 electrically isolated panels. The reflector surface is constantly scanned by optical techniques to provide the inputs needed to maintain surface precision. As the membrane deviates from its required position, the figure sensor generates an error signal which a processor then translates into voltage changes, resulting in pressure correction. The control algorithms, on-board microprocessor, and optical sensor are current state of the art. A section view through the membrane surface is shown in Figure 3.

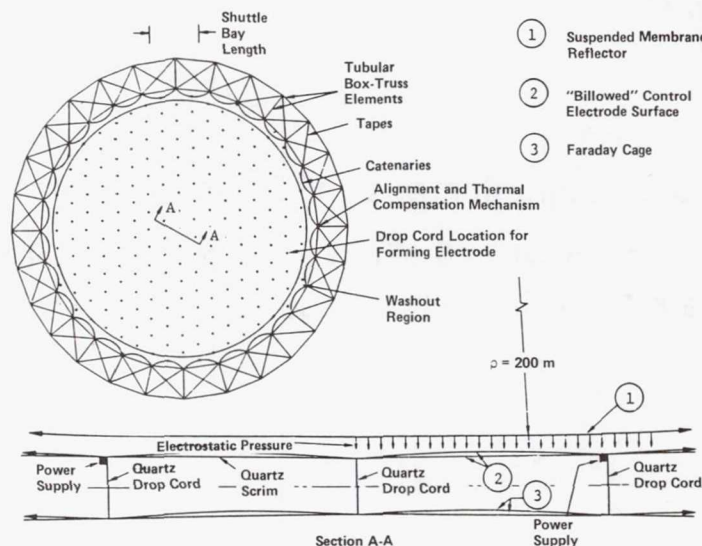


Figure 3

BOX-TRUSS RING (PLAN VIEW)

The reflector support structure comprises 28 epoxy/graphite box-truss cubes joined together to form a structural ring. A typical box-truss cube measures 11.56 m across the inside face, 13.46 m across the outside face, 8.5 m wide and 14 m high. A 4.6-meter graphite/epoxy prototype box is shown in Figure 6. Lying in the plane of each cube face and extending from each corner is a telescoping tape. These tapes are secured to a flat plate called a crossover fitting. When a cube is deployed, the crossover fitting is located at the center of each cube face. The tapes lying in the top and bottom planes of the cube unwind from spools instead of telescoping and connecting to crossover fittings. All tapes are pretensioned and serve to stabilize the deployed cube. For ease of stowage, the eight horizontal members, called surface tubes, are hinged in the center. Each surface tube hinge employs an over center latch that locks it into position when deployed. The four 14-m long, nonfolding, vertical tubes are attached to the corner fittings. At each corner where the surface tubes, the tapes, and the vertical tube intersect is a corner fitting.

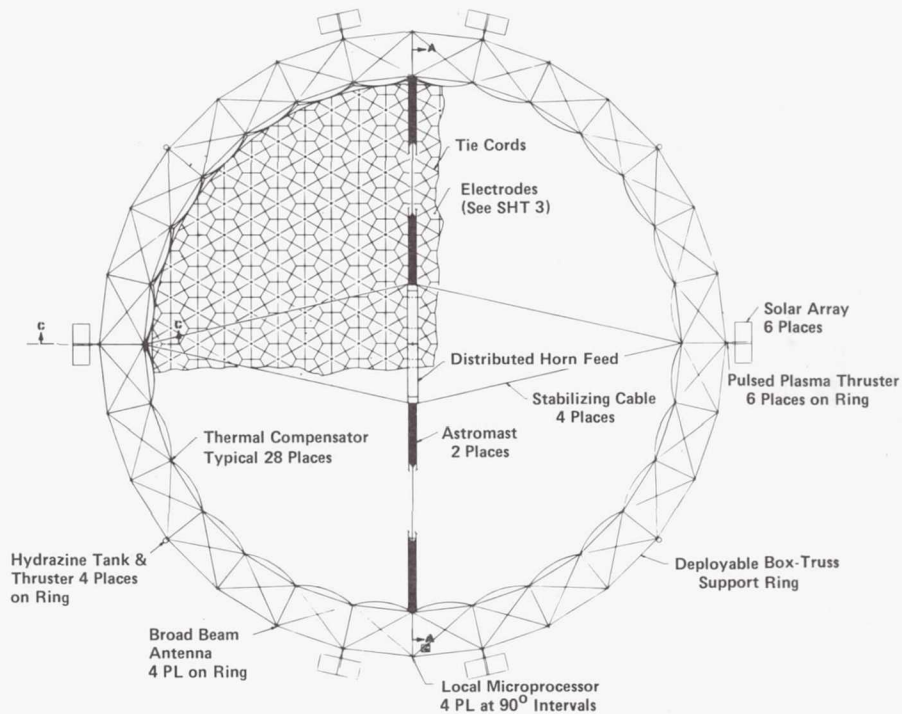


Figure 4

BOX-TRUSS RING (SECTION A-A)

Two pulsed plasma thrusters are stowed inside the feed along with a figure sensor, microprocessor, radiometer electronics, signal conditioning and control unit, attitude control system, and command and data handling system. The feed is suspended from the box-truss ring by two continuous-longeron lattice masts. Two sets of epoxy/graphite cords serve to stabilize the feed. The lattice masts constructed from graphite/epoxy, stow to a length that is approximately 2 percent of their deployed length. The masts use their own stored strain energy for deployment. A lanyard connected to a motor positioned at the back end of each canister controls the rate at which each mast will deploy.

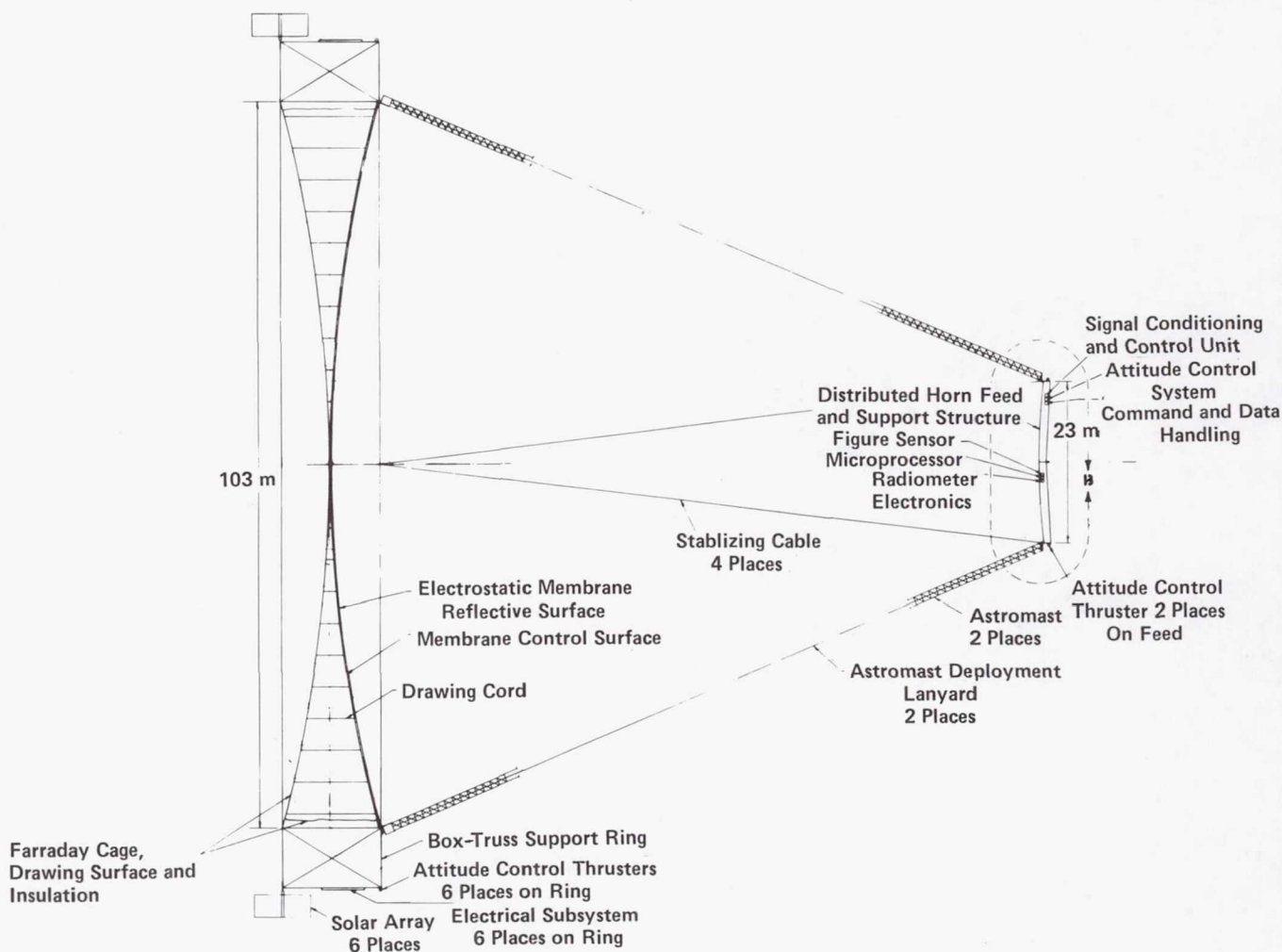


Figure 5

BOX-TRUSS CUBE (STOWED)

Martin Marietta has fabricated, and successfully deployed a 4.6-m cube, constructed entirely of graphite/epoxy, except for springs and pins. This cube weighs 27 kg. A flight-weight version would weigh approximately 20 kg. In the stowed configuration, the parallel structural members are compactly arranged and positively restrained. The length of the stowed structure (which is the deployed truss depth) can be varied for effective payload allocations. Note the packing of the corner fittings that closeout the structure to provide lateral and axial support.

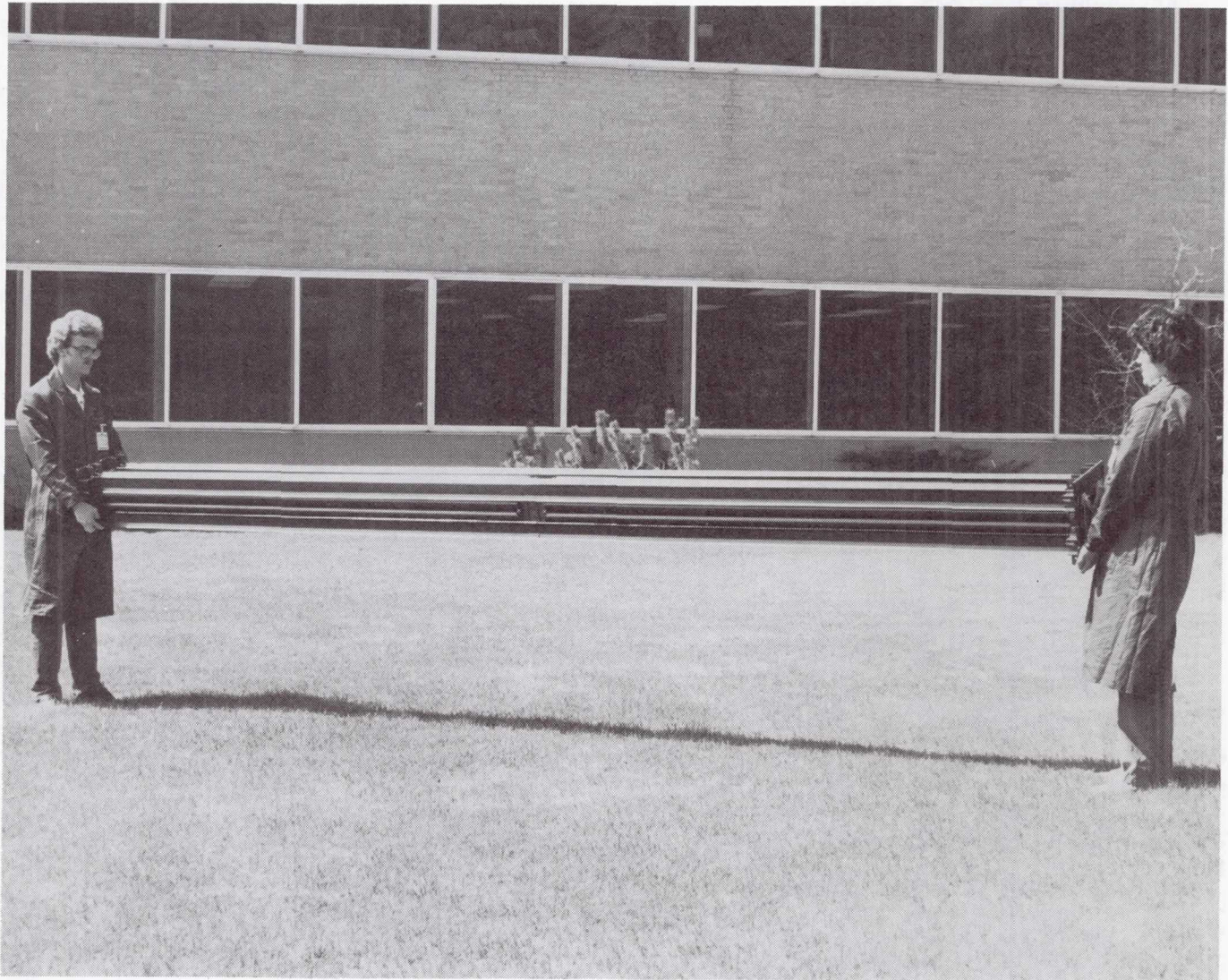


Figure 6(a)

BOX-TRUSS CUBE (DEPLOYED)

The deployable truss structure is based upon a box-shaped element used as a building block for large repetitive structures. One set of opposed frame sides are hinged in the center, pin-jointed at each end, and fold toward each other for storage; the adjacent sides are rigid. The hinge mechanism contains springs and an overcenter latch mechanism that drives the deploying frame and provides an impulse at completion of deployment to apply tension to diagonal members and, if present, an antenna surface. The diagonal members are telescoping elements that stabilize and shape the deployed structure. The truss structure consists of a number of deployable cubes sharing common corner fittings so that no on-orbit assembly is required. Deployment takes place in a sequence of steps that can be monitored and controlled by astronauts on the Shuttle Orbiter's aft flight deck. The sequential nature of the deployment process dissipates the deployment energy in an incremental manner, thereby reducing the possibility of producing structural failure in the deploying truss.

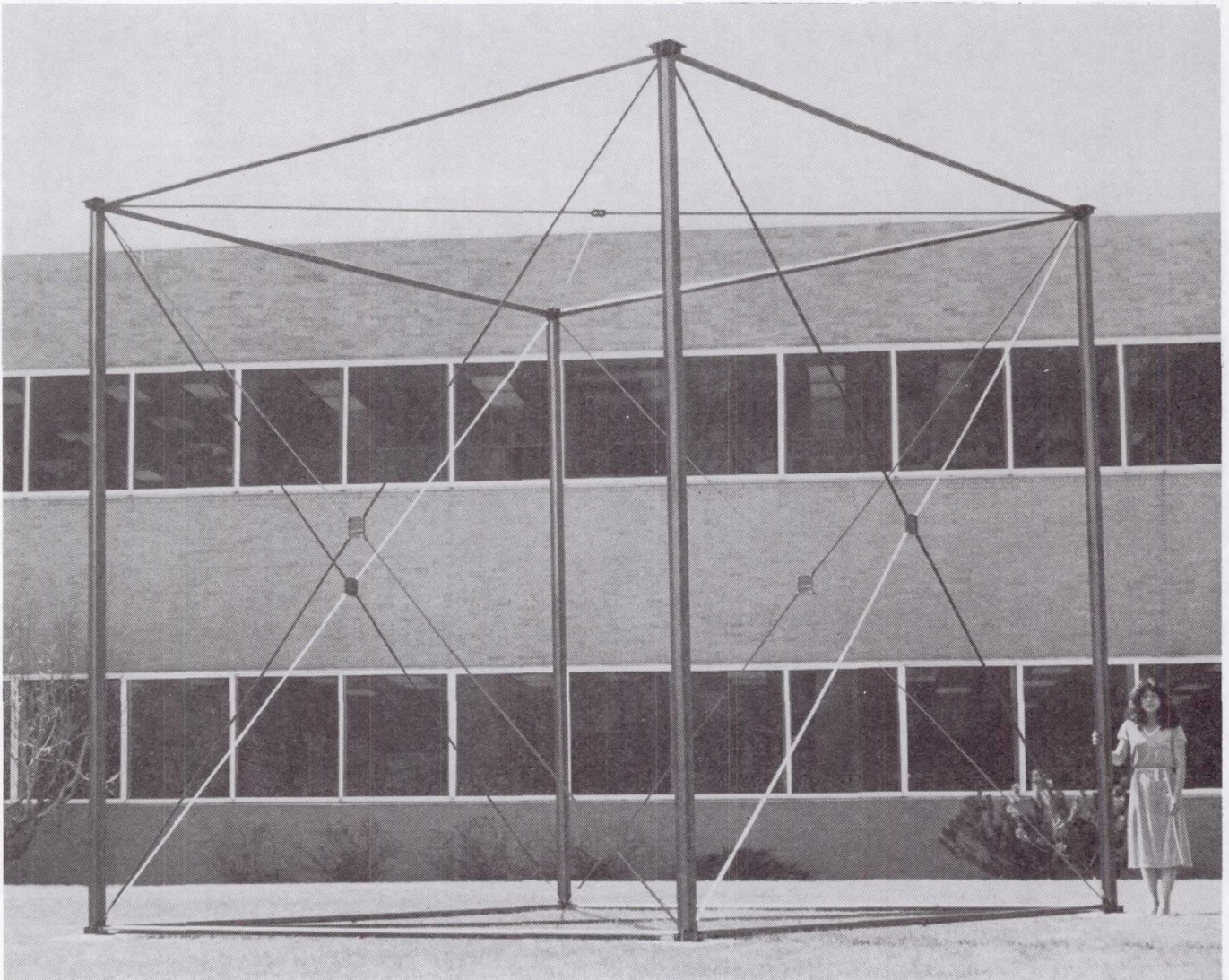


Figure 6(b)

FEED ASSEMBLY

A honeycomb epoxy/graphite structure houses the feed horns (Figure 7). A total of 302 individual horns are mounted inside the feed structure. To facilitate stowage, the feed structure is hinged in the middle. An overcenter latch locks the feed into position once it is withdrawn from the stowed package.

The reflector, as discussed earlier, has a diameter of 100 m. It has a spherical surface with a radius of curvature equaling 200 meters. The focal region where the feeds are located is on a concentric sphere at a radius of curvature of 100 meters, giving a focal length of 100 m. Each feed illuminates a spot on the reflector of 50 meters in diameter, which partially overlaps the spots of nearby feeds. Considering just this spot, the antenna has an effective f/D of 2.0.

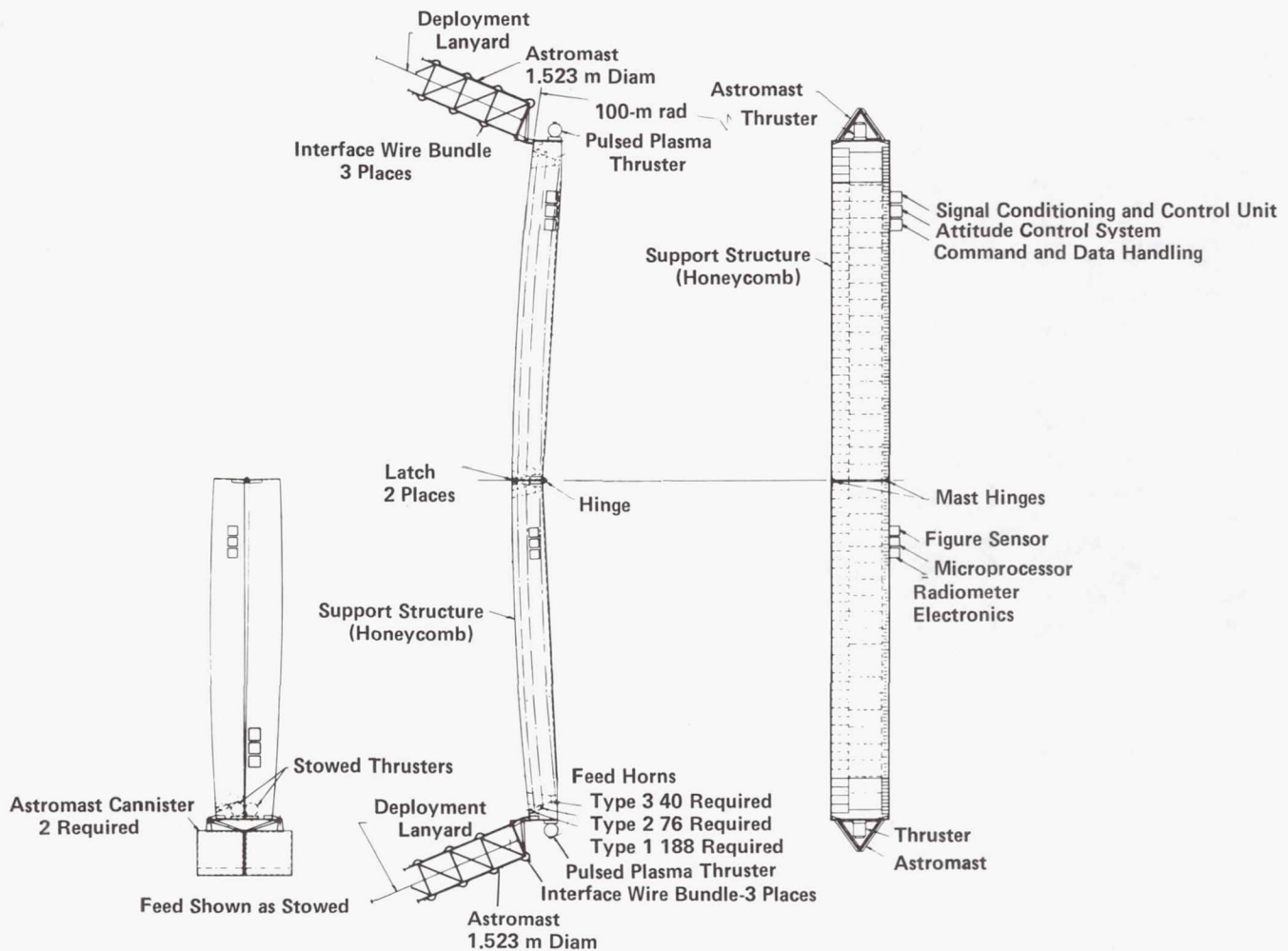


Figure 7

STOWED CONFIGURATION

The satellite stows into a cylindrical form measuring 3.9 meters in diameter by 14.2 meters in length (Figure 8). A rigid shell is formed from the stowed vertical and surface tube members of the box-truss ring. Symmetrically arranged about this shell exterior are the hydrazine tanks with their thrusters, the solar arrays, the battery packs and the pulsed plasma thrusters. Attached to the interior surface of the shell is the electrostatic membrane. This membrane runs the full length of the shell, surrounding the feed support structure and mast canisters. The mast canisters are also attached to the box-truss ring. During deployment, this attachment will act as a pivot. For maximum strength and stiffness, all satellite subsystems attach to either the cube corner fittings or the vertical tubes of the box truss ring.

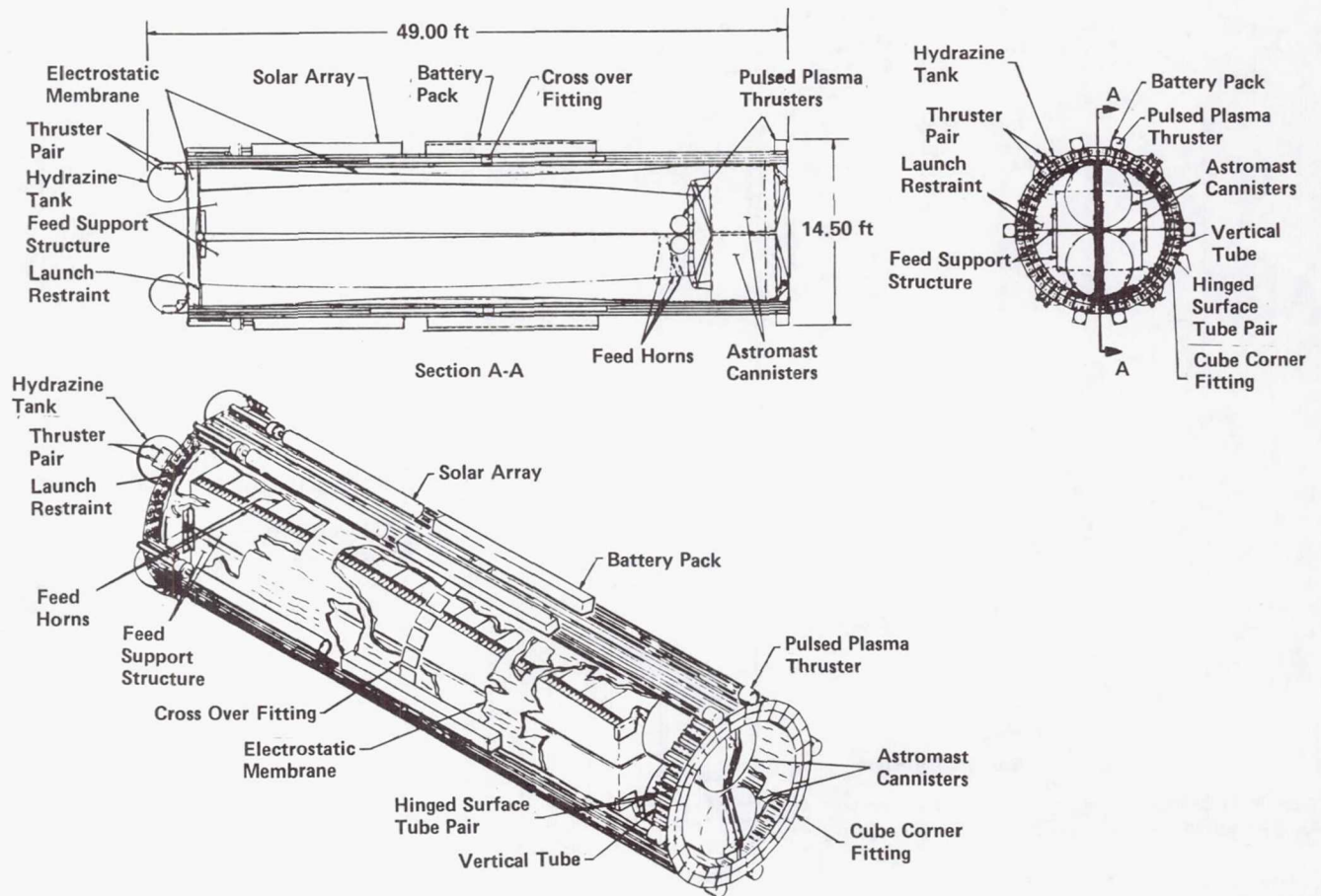


Figure 8

SOLAR ARRAY, ELECTRICAL SUBSYSTEMS AND PULSED PLASMA MOUNTING

The purpose of the integrated modular power subsystem is to provide a compact, easily assembled and serviced unit that will be integrated to a structural member of a spacecraft structure. The power subsystem was developed for a radiometer spacecraft shown in Figure 4. The integrated power modules were distributed around the ring to provide distributed and redundant power systems for the spacecraft and the electrostatically controlled membrane mirror. Figures 4 and 5 present the deployed spacecraft and show the location of the deployed power modules. Figure 8 presents the stowed spacecraft configured to use the Shuttle Orbiter efficiently. As can be seen in Figure 8, the integrated power modules packaged efficiently along side the stowed box-truss ring.

The battery package was reconfigured to package linearly along the structural member. Power is then distributed to the spacecraft through an electrical connection at the end of the structural member.

Each solar array and its associated battery pack and control electronics is permanently mounted to the same vertical members on the external ring of the spacecraft ring structure. The decision to mount the solar arrays to the rim structure rather than the feed was for the following reasons:

- 1) The aperture blockage of 1400 sq ft caused by mounting the arrays on the feed cannot be tolerated
- 2) Arrays mounted on the feed would be occulted by the radiometer during certain portions of certain orbits
- 3) Power-consuming subsystems are predominantly on the spacecraft ring structure (about 78 percent)
- 4) Large concentrations of mass such as the battery packs should be located as close as possible to the spacecraft center of gravity, which is closer to the ring
- 5) Consideration was also given to spacecraft torqueing due to drag coefficients resulting from solar arrays mounted at the feed

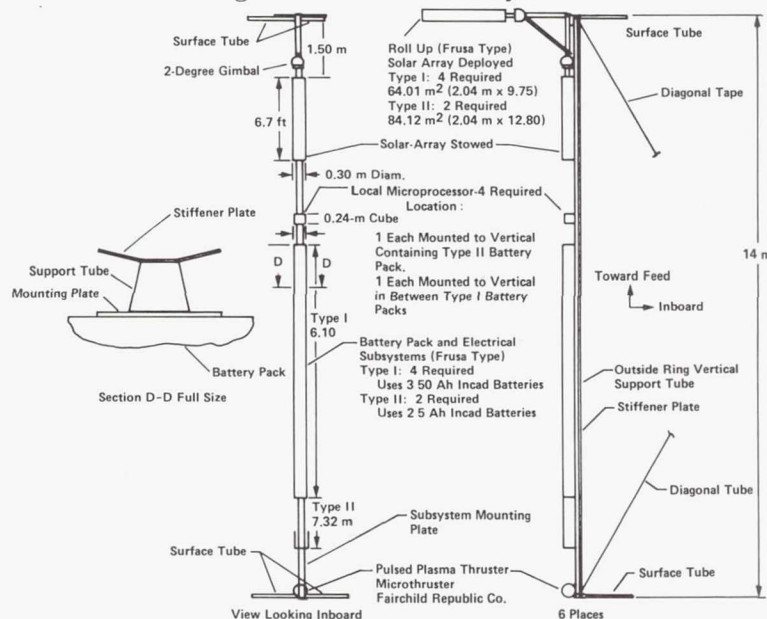


Figure 9

PARAMETERS OF REFLECTOR PREFORMING

The electrostatic membrane is a tension structure. Its smoothness and stiffness are related directly to the internal membrane stress. The preferred membrane stress level is an involved subject. Through repeated studies and testing, a consensus has developed on the operating stress level. The principal factors are the following:

- 1) Materials and manufacturing flaws must be ameliorated
- 2) Thermal strains must be controlled
- 3) Micro-creep must be minimized
- 4) Tear propagation from holes or slits must not occur

The membrane reflector undergoes large deflections but only moderate strains. Figure 10 is a schematic of the membrane reflector. The initial untensioned and tensioned shapes are both spherical. The center enlargement shows a typical membrane separation and deflection. Basic design variables are ΔZ , the membrane centerline deflection, and the gap between the taut reflector and the control electrode. The stress in the taut reflector is proportional to ΔZ . The position stability of the membrane is proportional to the ratio of gap/ ΔZ . The perimeter constraint is very important in membrane mechanics. In subsequent discussions on membrane thermal compensations, the fixed-rim state will be replaced with an adjustable rim, which alters the stress state.

The baseline membrane was not designed to a minimal voltage. The gap between membrane reflector and control electrode was increased from 0.1 m to 0.2 m, which doubled the nominal operating voltage. The larger gap allows more tolerant electrode designs. Allowable irregularities in the control electrode surface increase dramatically as the gap is increased. This subject will be discussed in detail later in this section. The nominal centerline voltage for the baseline is 58 kV. This voltage is imparted to all electrodes; however, the average gap increases as a function of radius which effectively reduces the pressure near the edge.

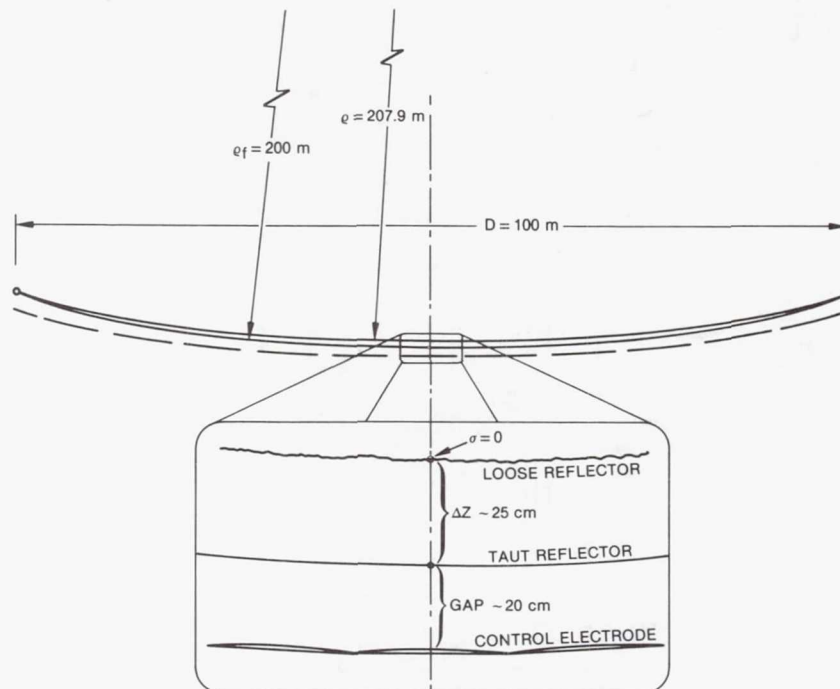


Figure 10

CONTROL ELECTRODE SMOOTHNESS

Figure 11 schematically illustrates a membrane electrode layout. In the arrangement, the membrane electrode surface is "contoured" by inelastic quartz drop cords. Because of the very low thermal expansion coefficient, quartz is also inlaid in the membrane electrode surface. The polymer membrane surface has a much larger thermal expansion coefficient than quartz. In orbit, the membrane electrode shape changes with temperature. As the temperature decreases from 300 K to 200 K, the amplitude decreases as the electrode surface contracts. For a peak-to-peak irregularity of ± 8 cm, a drop cord separation of no more than 4.5 m is recommended. The reflector's surface roughness would be less than 1.0 mm (rms). The drop cord separation could be substantially larger if the electrode surface was formed with flat "facets" between the quartz cords. Starting with flat facets at $T = 300$ K would produce a very taut electrode surface at $T = 200$ K.

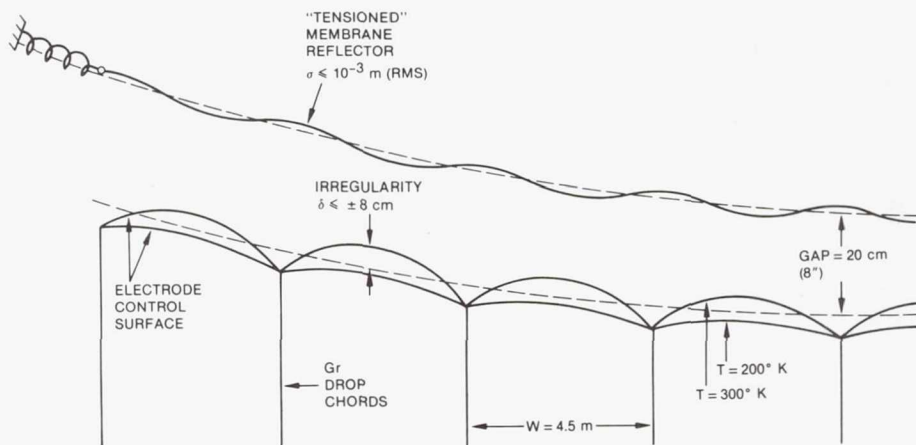


Figure 11

ELECTRODE SIZE VS SURFACE QUALITY

The curve of Figure 12 shows that 1-mm peak-to-peak surface quality can be attained with 6-meter-wide circular ring electrodes, and 1-cm peak-to-peak surface quality can be attained with 14-meter-wide electrodes.

Note that the above numbers are for peak-to-peak surface accuracy. The rms surface quality is better than the peak-to-peak value by a factor of $1/2 \sqrt{2} \approx 0.35$. Thus the attainable rms surface quality is considerably better than the preceding peak-to-peak figures for the same size electrodes. However, this analysis has only considered errors due to electrode size, when in fact other error sources do exist. It is reasonable at this point to assume 1-mm and 1-cm rms surface qualities are attainable with the above electrode sizes in the presence of all error sources.

The conclusions are that to attain a 1-mm rms surface quality, 220 6-m x 6-m (36 m^2) electrodes are required, and to attain a 1-cm rms surface quality, 40 14-m x 14-m (196 m^2) electrodes are required. Contiguous electrodes should be used (hexagons or segmented circular rings) so not to waste any available electrode area and thus keep electrode voltages to a minimum.

- INFLUENCE CURVE ADDITION ERRORS
- PEAK-TO-PEAK AND RMS VALUES

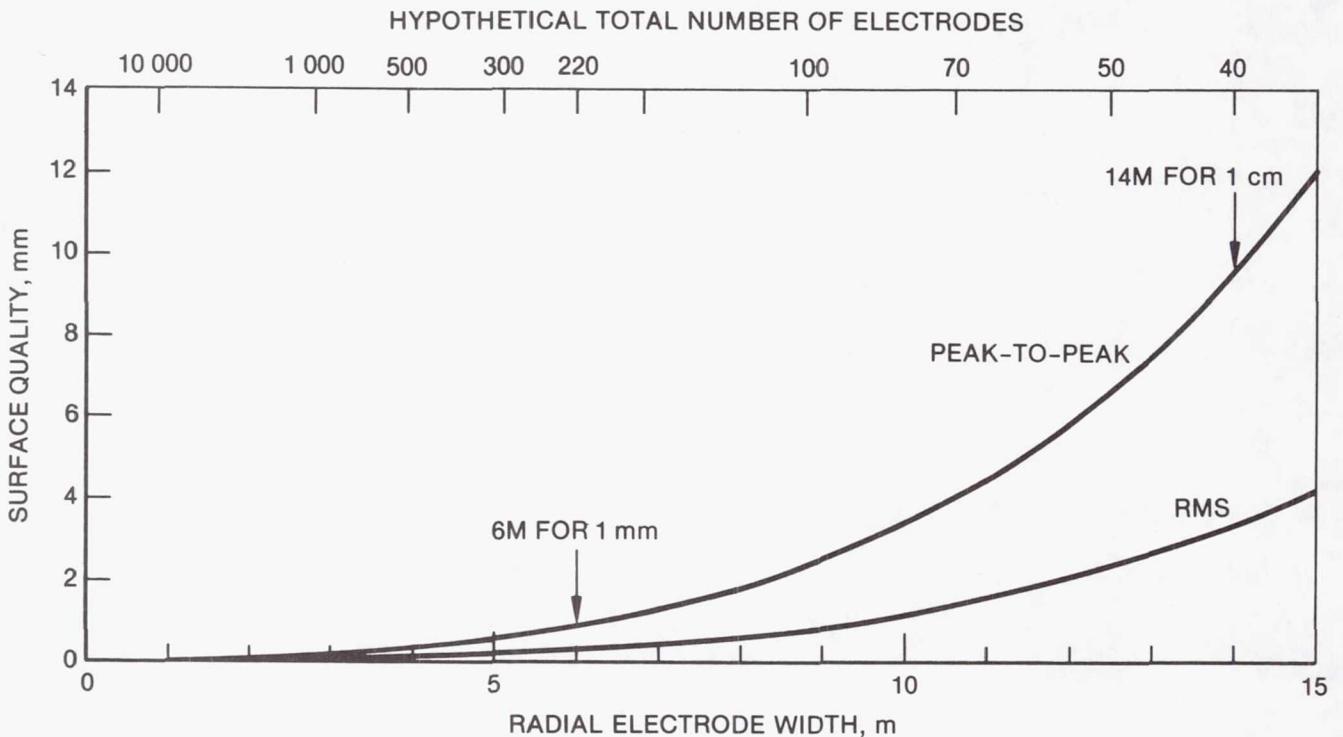


Figure 12

SHAPE CONTROL

Thermal variations are the primary disturbance, driving the complexity of the entire control loop. Measurement rate and voltage update rate must be specified early in the design process, because they are major factors in designing both the figure sensor and the central processor. To use the "quasi-steady-state" matrix multiplication concept for control, at least one measurement must be provided for each electrode. For the case of 1-mm rms surface quality, this requires 220 measurements every 20 s. For the case of 1-cm rms surface quality, the requirement is 40 measurements every minute. These measurement rates, and one set of voltage updates with each set of measurements, are enough to maintain the surface quality during the near-steady-state thermal conditions. However, during rapid temperature variations the temperature change rate of 6 K/s would cause membrane movement of ≈ 8 mm/s without any voltage corrections. Thus during these periods, much more rapid voltage updates are required, i.e., 20 updates per second for the 1-mm case and 2 updates per second for the 1-cm case. Measurement sensors that could supply 220 measurements to the required accuracy each 0.05 s are not available, nor are microprocessors that could perform the matrix operations that quickly. A solution to this problem is to use a much smaller number of measurement points during periods of rapid temperature changes, and omit the matrix calculations but simply scale up all voltages according to position changes of the center of the membrane (a much faster calculation).

The changes in strain under orbital conditions are significant but manageable. The thermal strain is $\epsilon_T = \alpha \Delta T$ where for $\alpha = 2 \times 10^{-5}/\text{K}$ (the thermal expansion coefficient) and $\Delta T = 100$ K (the temperature change), $\epsilon_T = 0.002$. The membrane reflector's radius changes by about $\Delta r = r \epsilon_T = 0.1$ m (4 inches) during each orbit. These strains are approximately 1.3 times larger than the electrostatically developed strain of the baseline. The addition of a perimeter thermal compensation device can prevent the development of large stresses from these introduced strains.

- **220 ELECTRODES FOR 1 MM RMS SURFACE QUALITY**

- 40 ELECTRODES FOR 1 CM RMS SURFACE QUALITY**

- **0.3 MM ALLOWABLE RESIDUAL CONTROLLER ERROR FOR 1 MM RMS CASE**

- 3.0 MM ALLOWABLE RESIDUAL CONTROLLER ERROR FOR 1 CM RMS CASE**

- **THERMAL VARIATIONS**

- **LOW RATE $\dot{T} \leq 0.02$ K/SEC 90% OF TIME**

- **HIGH RATE $\dot{T} \leq 6$ K/SEC 10% OF TIME**

- **ΔZ DUE TO THERMAL VARIATIONS WITHOUT VOLTAGE ADJUSTMENTS (SOFT SPRING PERIMETER COMPENSATION)**

- **LOW RATE $\Delta \dot{Z} \leq 0.03$ MM/SEC 90% OF TIME**

- **HIGH RATE $\Delta \dot{Z} \leq 8$ MM/SEC 10% OF TIME**

Figure 13

CONTROL SCHEMATIC

The membrane reflector's shape is maintained by independent control of the voltage on discrete electrodes. The high-voltage supplies are regulated by an on-board processor. A surface-monitoring sensor measures the location of discrete points on the membrane reflector from a reference. This figure sensor is an important item for the ECMM. There must be at least one sensed point for each control electrode. Obviously, the desired reflector rms smoothness dictates the sensor's position accuracy. Its update rate is determined by the mission requirements. A single high-rate sensor could scan multiple points. Off-the-shelf sensors that meet the mission requirements are not available today. However, there are several commercial absolute-ranging devices that could, with small improvements, meet the mission goals. Special laboratory bread-board interferometers could provide significant capability. Substantial voltage changes are required for shape adjustments. Hence, a separate voltage supply is prescribed for each control electrode. Each voltage supply is very small and light (about 0.25 kg) because very little power is required.

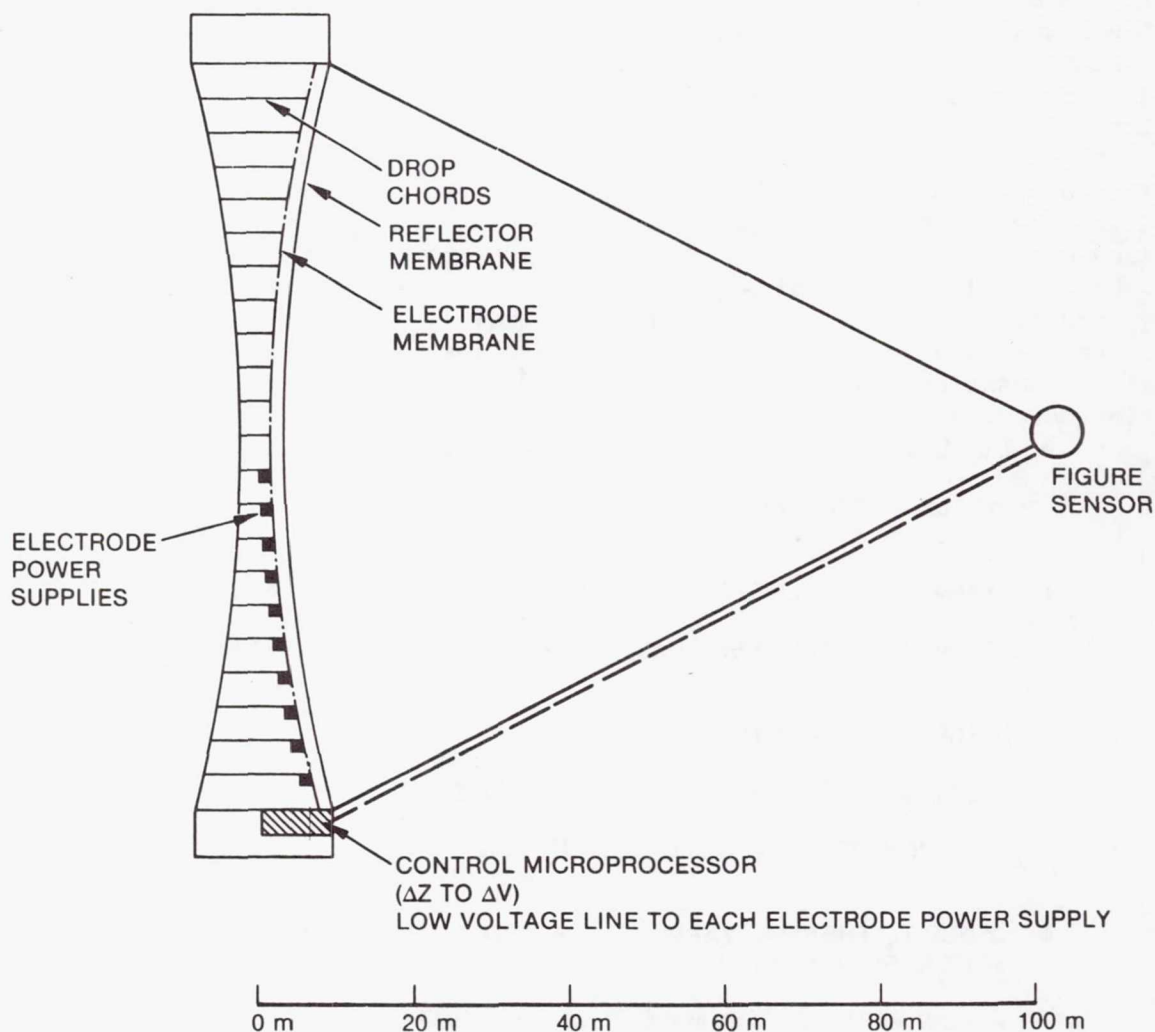


Figure 14

CONTROL SUMMARY

A control system for the ECMM must maintain the reflector surface within desired tolerances in the presence of various external disturbances and inherent system variations. Examples of external disturbances are temperature variations, solar pressure, and pointing control torques. System variations include membrane attachment ring out-of-roundness, electrode position offset, and nonhomogeneous membrane material. Minimizing control system complexity is very desirable, thus minimizing engineering problems and cost. Complex, realtime closed-loop control systems, which include a form of modal control and modern state-space control, have been previously considered in conceptual studies. These high-complexity control types were necessary due to very stringent surface quality requirements and a severe external disturbance spectrum. The 100-m ECMM design has less stringent surface quality requirements, and the external disturbance spectrum is not as severe as in the previous work. A less complex "quasi-steady-state" control system is able to perform all the required functions of the 100-m ECMM. This technique is workable due to the fact that the ECMM experiences long periods (tens of minutes, 80 percent of each orbit) in near steady-state conditions. These conditions include the spacecraft in eclipse, and the spacecraft in full sun, with the sun shining on the electrode support membrane and not on the reflector membrane. In these conditions, errors such as support rim out-of-roundness, electrode position errors, and the like are nearly steady, and a "quasi-steady-state" closed-loop control system will be used to maintain surface quality tolerances. The most stressing situation on the control system occurs when the spacecraft goes into or out of eclipse, leading to rapid temperature variations and large changes in required electrode voltages. The "quasi-steady-state" control system will function properly under nonsteady-state conditions provided membrane natural mode frequencies are not excited by electrode voltage changes, and provided the measurement and voltage update rate is high enough to keep the reflector surface within tolerances. Excitation of the membrane natural modes can be prevented by separation of electrode control frequencies and membrane mode frequencies.

- **LOW RATE CONTROL USED OVER MOST OF THE ORBIT**
 - **CONTROL IS STRAIGHTFORWARD**
- **SHADOWING EFFECTS REQUIRE A HIGH CONTROL RATE**
 - **MORE ANALYSIS REQUIRED**
- **CONTROL MICROPROCESSORS AND ELECTRODE POWER SUPPLIES ARE SOA**

Figure 15

Page intentionally left blank

ANTENNA SUBSYSTEM REQUIREMENTS

R. E. Freeland
Jet Propulsion Laboratory
Pasadena, California

Large Space Systems Technology - 1981
Third Annual Technical Review
November 16-19, 1981

REVIEW OBJECTIVES

At the request of NASA Headquarters, an in-depth review of the hoop/column and offset wrap-rib antenna technology development programs was conducted at the Langley Research Center during February 1981. The objectives of the review are shown below.

- EXAMINE THE DEVELOPMENT LOGIC FOR THE GROUNDBASED LSST HOOP/COLUMN AND OFFSET WRAP-RIB ANTENNA TECHNOLOGY DEVELOPMENT PROGRAMS
- IDENTIFY ADDITIONAL WORK THAT NEEDS TO BE UNDERTAKEN TO BRING CONCEPT DEVELOPMENTS TO A SYSTEM LEVEL TECHNOLOGY READINESS STATE

LSST ANTENNA PROGRAM REVIEW COMMITTEE

The antenna program review material was prepared and presented by the two LSST antenna concept development program managers and their respective contractors (R. E. Freeland of JPL and the Lockheed Company for the offset wrap-rib antenna, and T. G. Campbell of LaRC and The Harris Corporation for the hoop/column antenna). Each LSST antenna concept development program manager reviewed the base program and identified additional technical tasks required to bring the specific concept developments to a system level technology readiness state. The review committee consisted of intercenter technical experts that collectively represented a systems capability. The review committee, which is shown below, evaluated the material presented and made specific recommendations as to how the subject concept developments should be implemented.

CHAIRMEN: H. T. WRIGHT, DIRECTOR FOR PROJECTS

H. K. CLARK, ASSISTANT DIRECTOR FOR SYSTEMS ENGINEERING AND OPERATIONS

MEMBERSHIP:

SYSTEM AND REQUIREMENTS:

W. R. HOOK (LaRC)

MECHANICAL SYSTEMS:

J. R. RAMLER (LaRC)

R. T. WINGATE (LaRC)

THERMAL:

M. J. LONG (LaRC)

STRUCTURES:

N. D. WATSON (LaRC)

C. E. LIFER (JPL)

MATERIALS:

M. M. MIKULAS (LaRC)

CONTROLS:

D. R. TENNEY (LaRC)

S. SZIRMAY (JPL)

RF SYSTEMS:

J. D. SHAUGHNESSY (LaRC)

SYSTEM DYNAMICS:

W. F. CROSWELL (LaRC)

E. W. TRAVIS (FSFC)

G. C. HORNER (LaRC)

INSTRUMENTATION:

L. V. TAYLOR (LaRC)

FLIGHT TEST AND SHUTTLE OPERATIONS:

E. C. HAMILTON (MSFC)

LSST ANTENNA REVIEW COMMITTEE RECOMMENDATIONS AND STATUS

After three days of review and in-depth discussions relative to the base program for both concepts and the additional technical tasks needed to bring the antenna developments to a more systems oriented approach, the committee recommended and prioritized additional activities that should be integrated with the existing base programs. The recommendations that were considered mandatory by the committee and their status are given below.

RECOMMENDATIONS

- CONTINUE DEVELOPMENT OF BOTH PROGRAMS BUT ORIENT TO A SYSTEMS APPROACH
- CONDUCT TWO STRAWMAN SYSTEM CONFIGURATION STUDIES
 - MOBILE COMMUNICATIONS
 - RADIOMETER

APPROACH FOR STRAWMAN STUDIES

- DEVELOP SET OF STRAWMAN SYSTEM REQUIREMENTS
- CONDUCT RF FEED DEFINITION STUDIES
- CONDUCT DYNAMICS/CONTROL DEFINITION STUDIES
- DEVELOP SPACECRAFT CONFIGURATION
- DEFINE SUBSYSTEM INTERFACES AND CONSTRAINTS
- INVESTIGATE LONG DURATION AND GROUND STORAGE ENVIRONMENTAL EFFECTS ON COMPOSITE MATERIALS
- CONDUCT LARGE ANTENNA COMPONENT STRUCTURAL TESTING
- IDENTIFY NEED FOR FLIGHT VALIDATION TESTS

STATUS

UNDER WAY

UNDER WAY

UNDER WAY

COMPLETE / COMPLETE

UNDER WAY/PLANNED

UNDER WAY/PLANNED

UNDER WAY/PLANNED

UNDER WAY/PLANNED

PLANNED

PLANNED

PLANNED

CONFIGURATION DEVELOPMENT OF THE
LAND MOBILE SATELLITE SYSTEM (LMSS) SPACECRAFT

C. T. Golden, J. A. Lackey, and E. E. Spear
Boeing Aerospace Company
Seattle, Washington

Large Space Systems Technology - 1981
Third Annual Technical Review
November 16-19, 1981

AGENDA

This figure presents the outline of the topics discussed in this paper.

- CONTRACT OVERVIEW
- WRAP RIB LMSS
 - CONFIGURATION
 - PACKAGING
 - SUBSYSTEM REQUIREMENTS
- HOOP COLUMN LMSS
 - CONFIGURATION
 - PACKAGING
 - SUBSYSTEM REQUIREMENTS
- CONCLUSIONS TO DATE

LSST/LMSS SYSTEM STUDY OVERVIEW

Boeing was selected by the JPL LSST Antenna Organization to provide configurations and system/subsystem requirements for large deployable antennas. Initially the study was to combine the NASA focused missions and the LSST generic large antennas to develop a system design and subsystem requirements. Early in the study it became evident that the focus missions and the generic antennas would not generate the desired data at a meaningful level of detail. The Land Mobile Satellite System was selected as the mission requirements baseline and two antenna system designs (wrap rib and hoop column) adapted to satisfy the mission requirements.

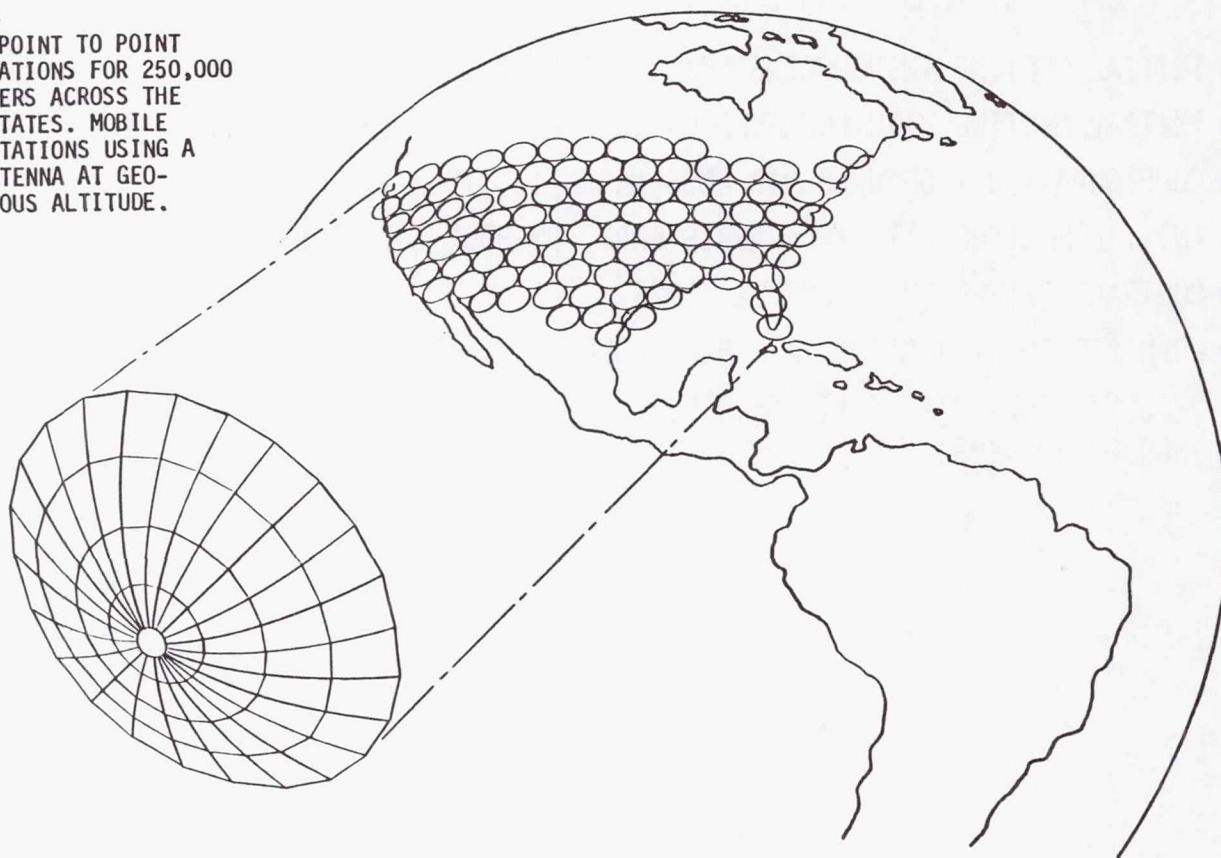
- CONTRACT AWARD: JULY 22, 1980
"A STUDY OF SUBSYSTEM INTERFACES OF DEPLOYABLE ANTENNAS FOR THE LARGE SPACE SYSTEMS TECHNOLOGY (LSST) PROGRAM"
- INITIAL MEETING INTRODUCING LMSS SEPTEMBER 15, 1980
- INITIAL MEETING WITH LOCKHEED ON WRAP RIB LMSS FEBRUARY 24, 1981
- CONFIGURATION 1 OF WRAP RIB LMSS MARCH 18, 1981
- INITIAL MEETING WITH THE HARRIS CORP. ON HOOP COLUMN LMSS MAY 18, 1981
- CONTRACT EXTENSION: JUNE 22, 1981
- WRAP RIB CONFIGURATION 4A & HOOP COLUMN CONFIGURATION 2 COMPLETE AUG. 17, 1981
- PRESENT STUDY STATUS AT LSST THIRD ANNUAL REVIEW, LARC, NOVEMBER 16 THROUGH 19, 1981

LAND MOBILE SATELLITE SYSTEM (LMSS)

The LMSS is a concept to provide point to point communication capability through a satellite on geosynchronous orbit to mobile receivers. Applications typically would be in dispatch and communication with cars and trucks (commercial, municipal, emergency, etc.). Ground based systems are limited by tall buildings, terrain, and other interference factors. By using a sophisticated relay satellite in space, the mobile ground stations can remain small, light, and relatively inexpensive and still provide high quality communications. The up and down link to the mobile units will use UHF frequencies while the fixed ground link will use telephone lines to a base station, and up and down links to the satellite will be at S-band. The system being proposed will serve 250,000 subscribers in the mid-1990 time period.

LMSS

PROVIDE POINT TO POINT
COMMUNICATIONS FOR 250,000
SUBSCRIBERS ACROSS THE
UNITED STATES. MOBILE
GROUND STATIONS USING A
RELAY ANTENNA AT GEO-
SYNCHRONOUS ALTITUDE.



LMSS CONFIGURATION STUDY
MISSION REQUIREMENTS

The LMSS mission requirements are listed on this chart. The requirements are at the mission level and are not intended to dictate design solutions. Note that the f/d of the antenna is not specified. For the study the two previously developed LSST antenna concepts (the wrap rib and hoop column) were iterated considering these requirements to develop viable system designs of the LMSS. Other concepts may work (a trade study ruled out cassegranian systems) but the study was limited to the selected two.

- FREQUENCY -- 821 → 831 & 2650 → 2690 MHz UPLINK
866 → 876 & 2550 → 2590 MHz DOWNLINK
- BEAM TO BEAM ISOLATION -- 25 dB GOAL
- BEAMWIDTH -- 0.4 → 0.5° NOMINALLY
- NUMBER OF USERS -- 250,000 NOMINALLY
- USER DISTRIBUTION -- POPULATION DENSITY RELATED (WITH VOX)
- COVERAGE -- CONUS
- POLARIZATION -- CIRCULAR
- POINTING -- (ABSOLUTE $\pm 0.10^\circ$, STABILITY $\pm 0.03^\circ$)
- ORBIT -- GEOSYNC AT 110° WEST LONG
- LAUNCH YEAR, 1995; SINGLE SHUTTLE LAUNCH; LIFETIME, 10 YEARS
- COMPATIBLE WITH ATT CELLULAR SYSTEM
- MOBILE G/T -- -20 → -25 dB
- BASE STATION G/T -- 11 dB

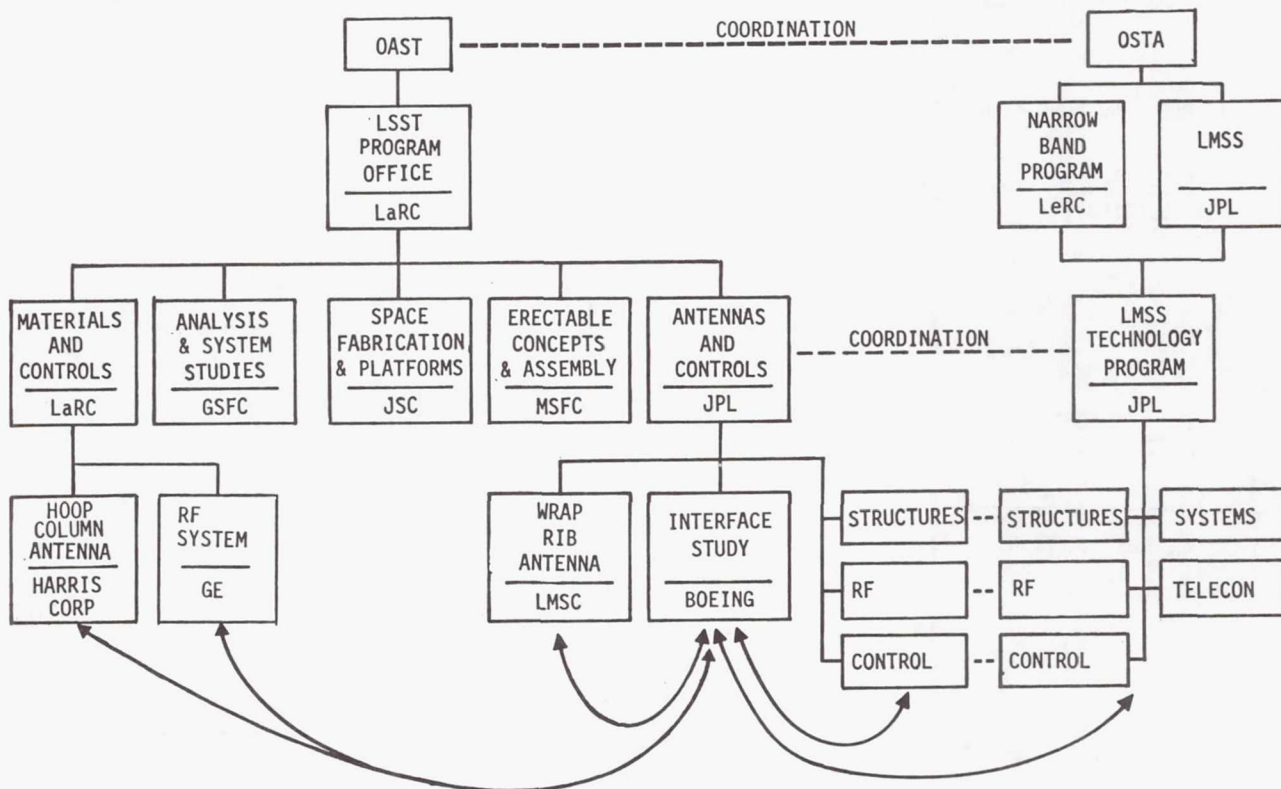
LMSS CONFIGURATION STUDY
ADDITIONAL REQUIREMENTS

The participants decided that there should be some commonality in subsystem requirements. The mission requirements cover most of these and the ones cited below complete them. Although the requirements are the same, the design that implements them need not be. Differences such as the single aperture vs. the quad aperture are expected throughout the subsystem designs.

DEPLOYMENT	AT GEO SYNC (NO RESTOW CAPABILITY)
POWER	10 KW BEGINNING OF LIFE
ATTITUDE CONTROL	STATION KEEPING PROPULSION 300 ISP
MESH CONTOUR	12 MM
RF FEED	POWER AMPLIFIER EFFICIENCY 50%

LSST/LMSS STUDY PARTICIPANTS

The LSST organization, LMSS organization and some of their subcontractors are shown. Boeing's role is to collect the data generated by the responsible design or analysis group to synthesize the system configuration. The major wrap rib contributors are: Lockheed for the boom, deployment, and reflector; and JPL for the RF system design, controls and structure. These latter three groups consist of individuals that are either supporting the LSST work, LMSS work or in some cases both. The major hoop column contributors are: The Harris Corporation for the structure and reflector; General Electric for the RF system design; and JPL for the structural analysis and controls subsystem definition. Through memos, telecons, action items, and coordination meetings, Boeing has orchestrated a series of iterations that will result in a point design for each antenna reflector concept to perform the LMSS mission.



LMSS WRAP RIB CANDIDATE CONFIGURATIONS

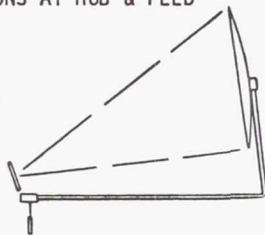
In the initial development of the system design, trades were performed to select the overall configuration. This chart summarizes candidate configurations and the selected baseline.

A driving consideration is the provision of control of the relative positions of the feed and the reflector. Candidate 3 was an early concept with all control devices at the feed area. However, the boom was found to be too flexible to meet reflector pointing stability requirements. Candidate 4 features the control devices in a midboom bus. This results in some, but not enough, boom stiffening but the cabling from the bus to the feed could not practically be stowed within the collapsed boom and RF lines would be unacceptably long. Candidate 2, the cassegranian system, has all the disadvantages of Candidate 4. In addition, the extreme reflector offset makes the boom flexibility problem worse and the complexity of an added subreflector does not improve the RF performance.

The selected configuration, Candidate 1, features control devices at both the feed and reflector hub areas to maintain feed/reflector alignment. Boom stiffness is then no longer critical so the boom can be smaller, thus reducing weight and more easily meeting the launch packaging envelope constraints. The bus with the electrical power equipment is in the most efficient location adjacent to the UHF and S-band feeds.

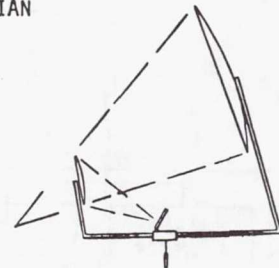
1. BUS FUNCTIONS AT HUB & FEED

SELECTED



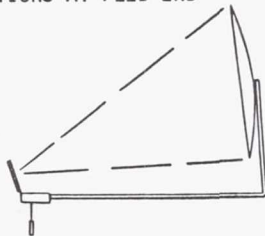
BEST FOR CONTROL OF FEED/REFLECTOR
RELATIVE POSITIONS

2. CASSEGRANIAN



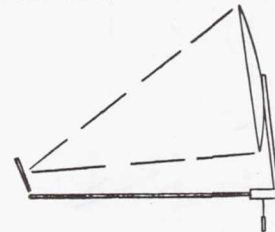
HEAVIEST, MOST COSTLY, & MOST
COMPLEX MECHANICALLY
NO SIGNIFICANT PERFORMANCE
ADVANTAGE

3. ALL BUS FUNCTIONS AT FEED END



POOR FOR CONTROL WITH
REFLECTOR ON LONG, FLEXIBLE
BOOM

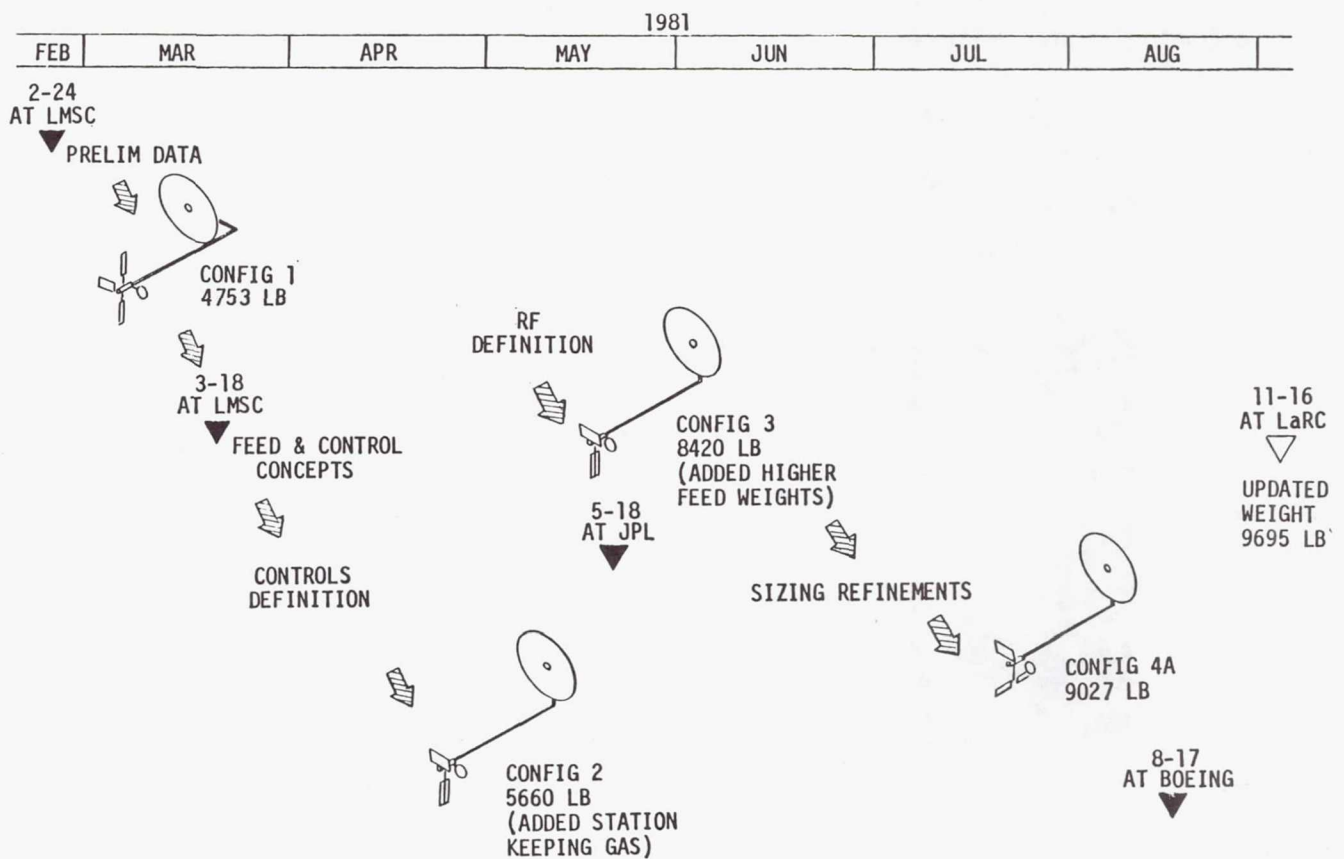
4. MIDBOOM BUS LOCATION



NO PRACTICAL WAY TO GET POWER
& S-BAND CABLING TO FEED

LMSS WRAP RIB BOEING STUDY HISTORY

Shown below is the history of the study and its four major configurations. As shown, the overall geometry has remained fairly constant, but the weight has essentially doubled and the other mass properties increased accordingly.

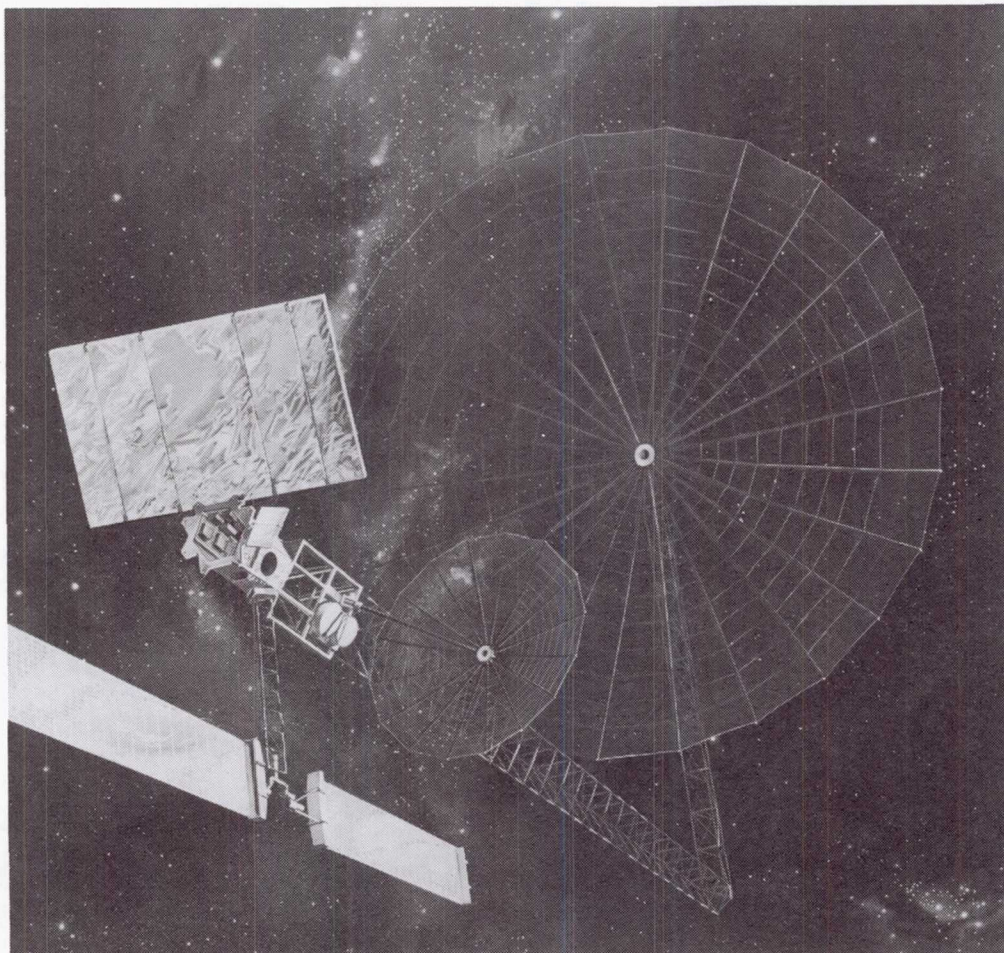


LAND MOBILE SATELLITE SYSTEM SPACECRAFT

55 METER OFFSET WRAP RIB CONCEPT

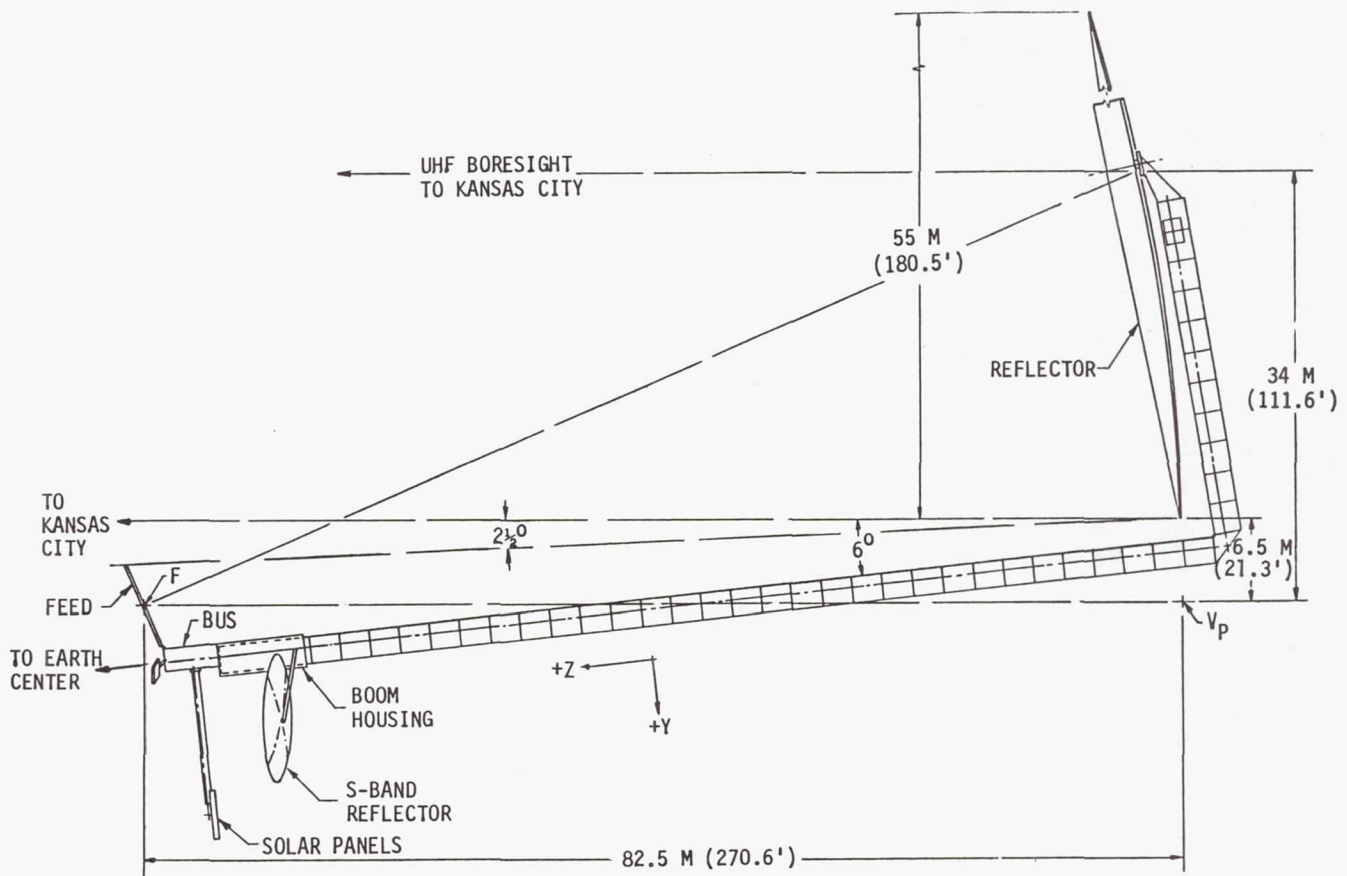
This is a preliminary configuration of an offset wrap rib reflector spacecraft capable of relaying radio messages to land mobile units throughout the Continental United States. It is intended to service units such as ambulances, police cars, taxis -- in essence all radio dispatched vehicles. Its position in geosynchronous orbit avoids present radio interferences caused by tall buildings, hills, and other factors. It is one of numerous concepts for extending current space technology made feasible by the Space Shuttle. The spacecraft is sized for a single Shuttle launch and a 10-year life beginning in the mid-1990's.

The long boom points at the earth's center, which is up and to the left. The shorter, vertical boom at the right points up to the north supporting the antenna reflector. The large panel at the left is the ultra-high-frequency feed. It and the 55 meter diameter wire mesh reflector are angled to point at the center of the United States near Kansas City. Multiple beams emanating from the feed panel are arranged to cover all contiguous 48 states with a potential in the design for communication with Alaska, Hawaii and parts of Canada.



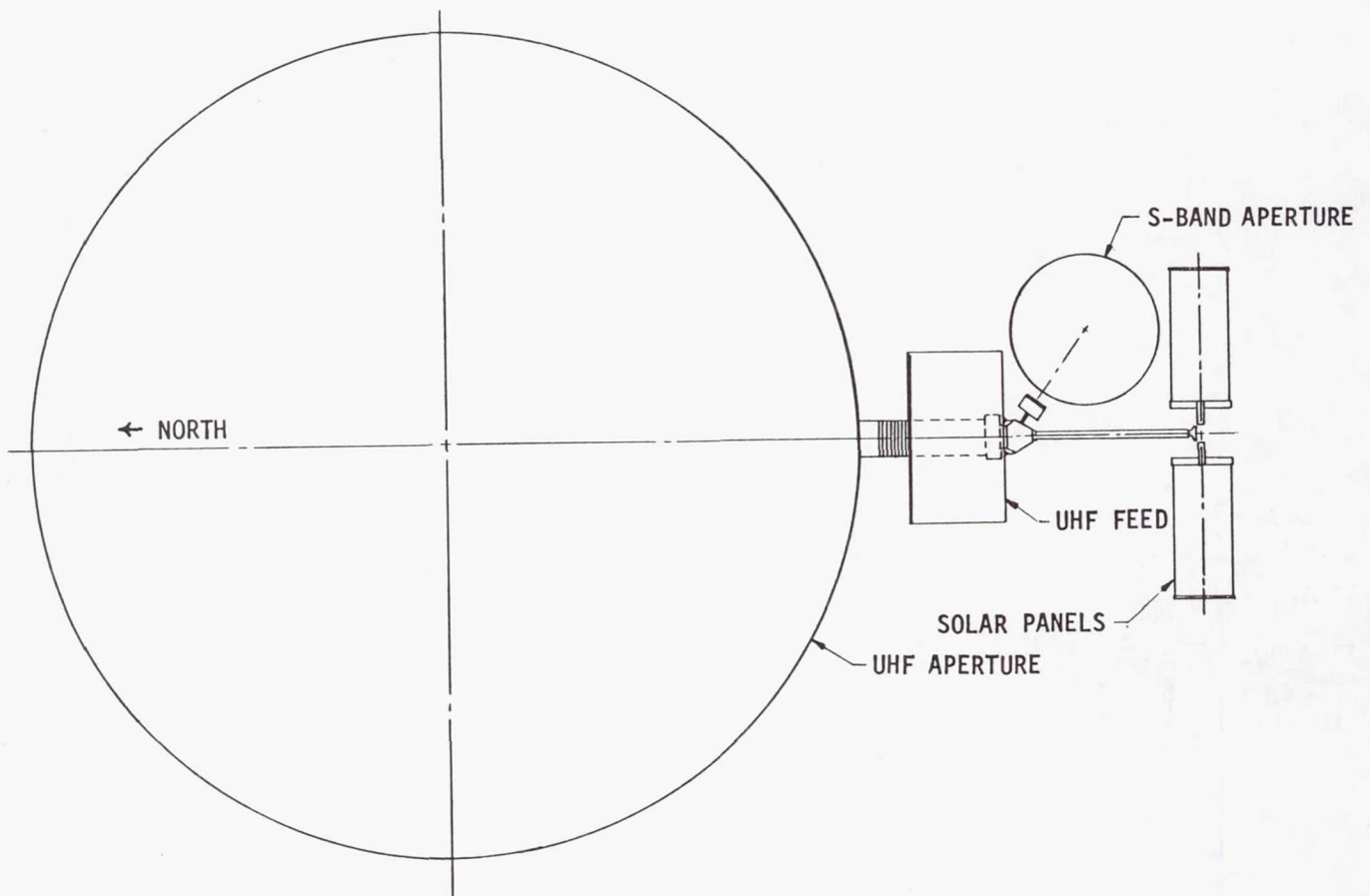
LMSS WRAP RIB SPACECRAFT

The LMSS spacecraft will be positioned on orbit at 110° West longitude with the main boom pointed at the earth's center (equator). The antenna bore sight is raised 6° above the boom to point to the latitude of Kansas City. The 1° pointing correction to the east (to point to Kansas City) is not being considered at this time, but will be included in any final design.



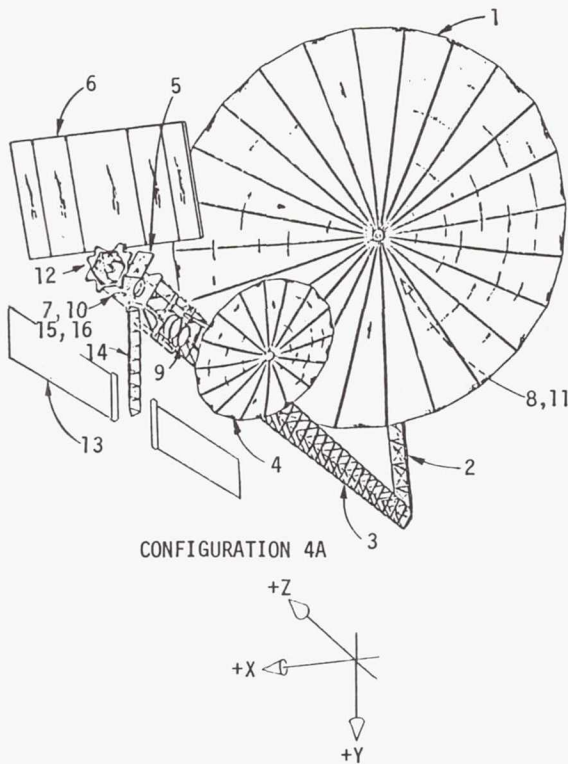
LMSS WRAP RIB
VIEW FROM EARTH

The wrap rib LMSS as viewed from earth (equator) is shown rotated 90° . The N-S axis of the spacecraft runs in the long direction of view with the UHF reflector to the top (North). The clearances between apertures (UHF & S-Band) with respect to the UHF feed and solar panels are shown. The solar panels rotate about the N-S axis.



LMSS WRAP RIB WEIGHT STATEMENT

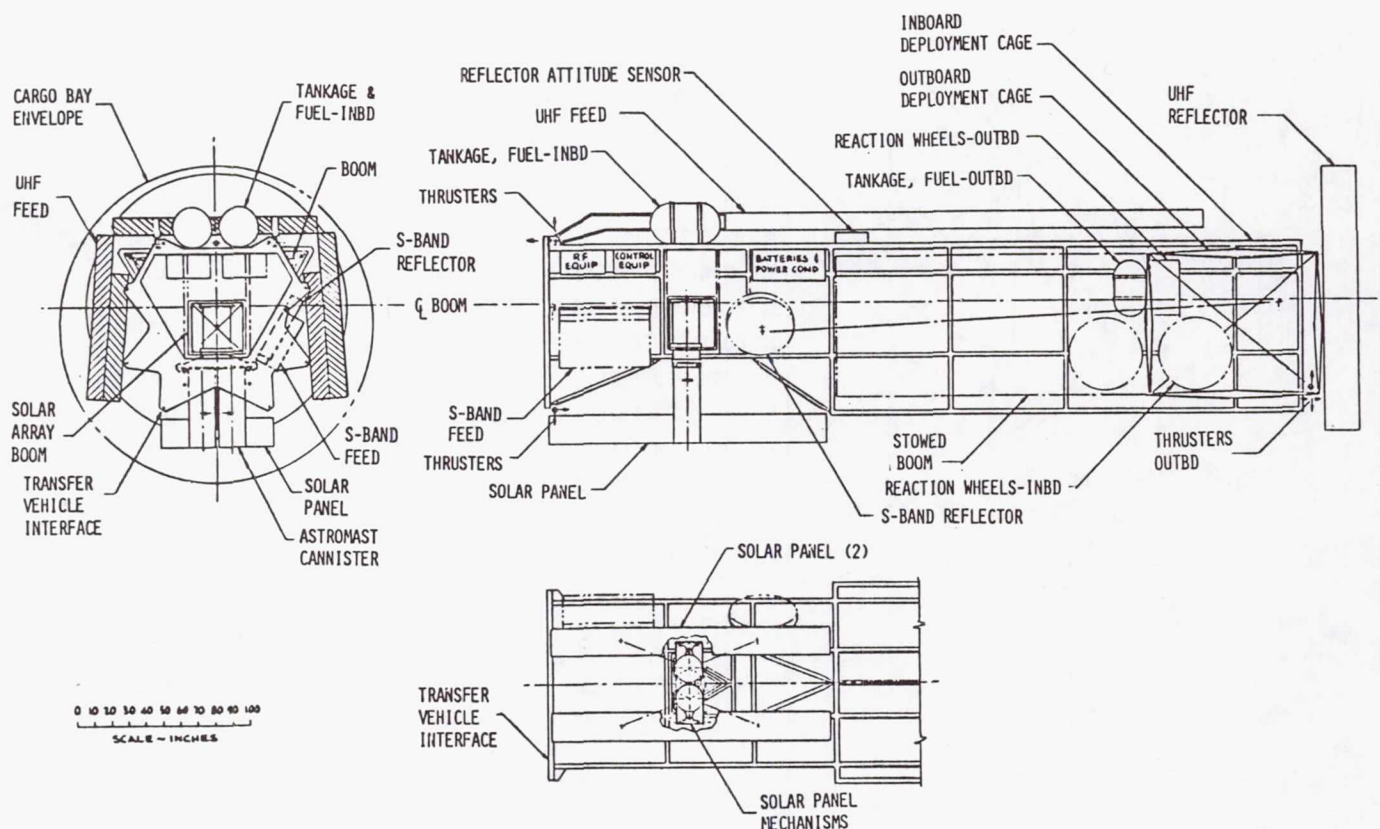
The weight statement for the latest wrap rib LMSS configuration is shown below. It should be noted that the weights are not grouped by subsystem, but by location. This was done purposely to implement mass properties determination. A subsystem weights breakdown will be made to reflect subsystem requirements.



ITEM	WEIGHT	
	KGS	LBS
1. UHF REFLECTOR & BOOM ATTACH	336	740
2. UHF BOOM-OUTBD & CABLE	41	90
3. UHF BOOM-INBD & CABLE	95	210
4. S-BAND BOOM & REFLECTOR	68	151
5. S-BAND FEED	78	171
6. UHF FEED	1166	2571
7. RF ELECTRONICS IN BUS	227	500
8. REACTION WHEELS & SENSORS - OUTBD	40	88
9. REACTION WHEELS - INBD	256	565
10. CONTROL EQUIP & SENSORS - BUS		
11. TANKAGE, FUEL, & THRUSTERS - OUTBD	200	442
12. TANKAGE, FUEL, & THRUSTERS - INBD	758	1671
13. SOLAR PANELS	166	367
14. SOLAR PANEL MAST & MECH	50	110
15. BATTERIES & POWER COND	131	288
16. BUS STRUCT, CABLING, T/C, & CAGE	386	850
SUBTOTAL	3998	8814
GROWTH	400	881
TOTAL	4398	9695

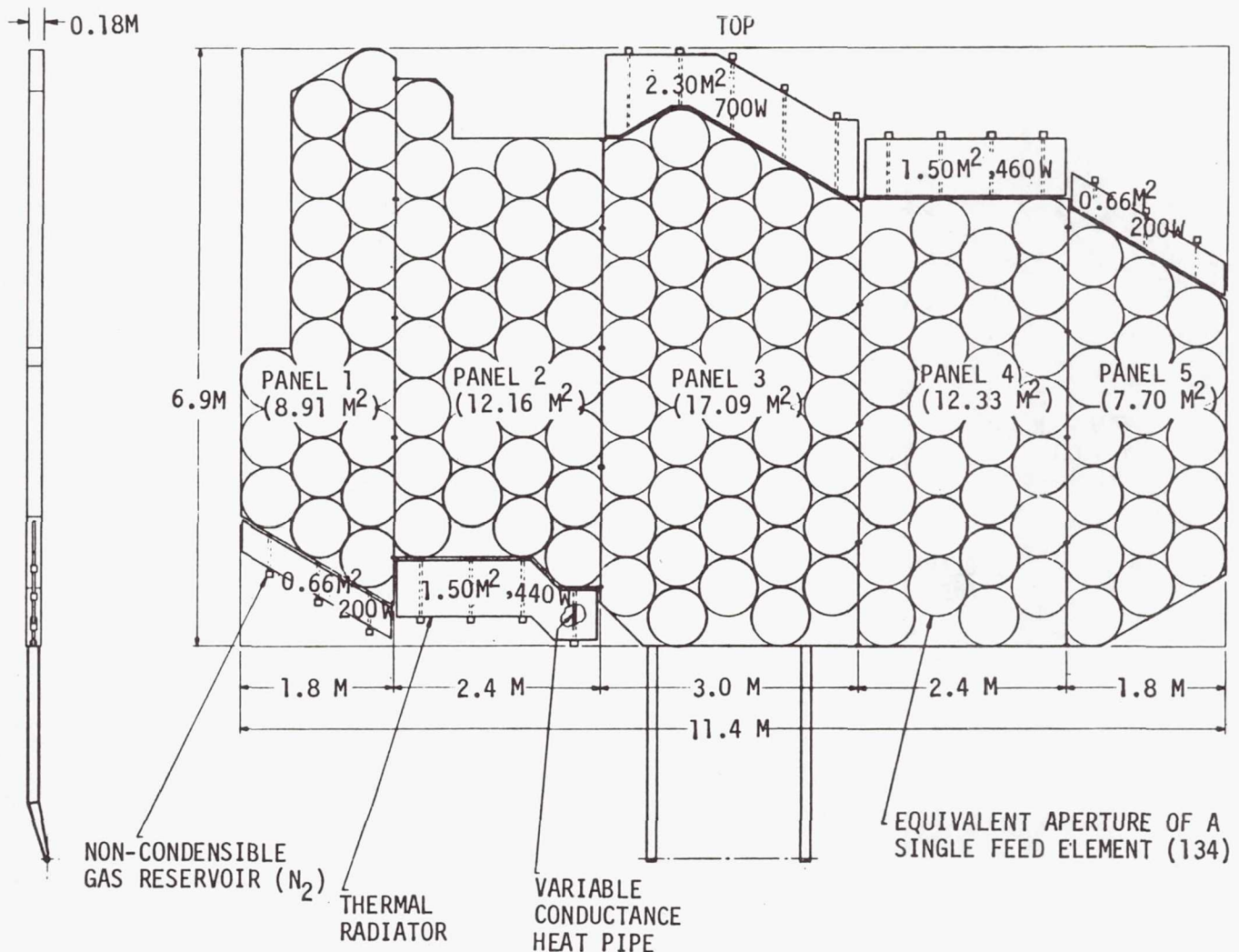
LMSS WRAP RIB LAUNCH CONFIGURATION

The launch configuration is constrained by the 4.6 m (180") diameter dynamic envelope within the shuttle cargo bay and the length of bay available after installing an appropriate sized orbit transfer stage. The prime configuration driver with respect to stowing the spacecraft in the Shuttle is the UHF feed. The feed must be folded in 5 sections (thus complicating the feed structure and RF circuitry) and extends over 80% of the length. This required that the boom cross section be reduced from the maximum "packagable" size of 3 m (120") to 2.4 m (95"). As shown in the side view, the spacecraft bus (feed end) is attached to the transfer vehicle and the LMSS cantilevered from the interface. The secondary attitude control equipment is shown mounted in the deployment cage adjacent to the UHF reflector.



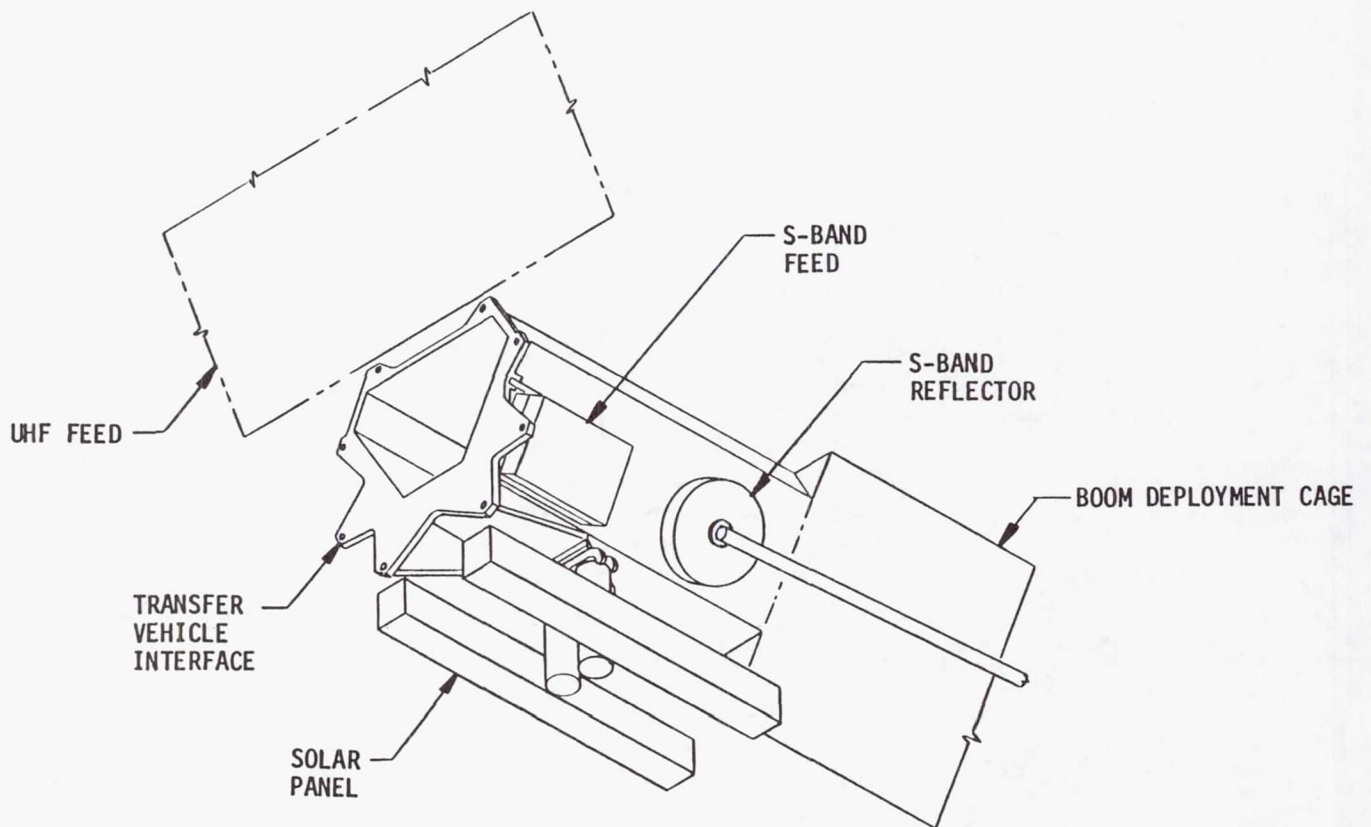
LMSS WRAP RIB FEED GEOMETRY

The face of the feed viewing the 55 meter reflector is shown. There are 134 individual planar arrays (87 to cover CONUS and 47 around the periphery to provide the required RF beam isolation). The feed is 6.9M x 11.4M x .018M and weighs 1212 KG (2667 lbs.). In addition to the planar feeds, each feed segment has a passive thermal radiator attached to dissipate heat produced by the high power amplifiers (about 2000 W total). The actual area required is only the planar arrays and radiators. To facilitate the structural design and mechanism implementation 5 rectangular segments may be used. Within the thickness of the feed are the ground planes, beam forming network, and electronics (duplexer, high power amplifier, low noise amplifier, thermal control heat pipes, etc.).



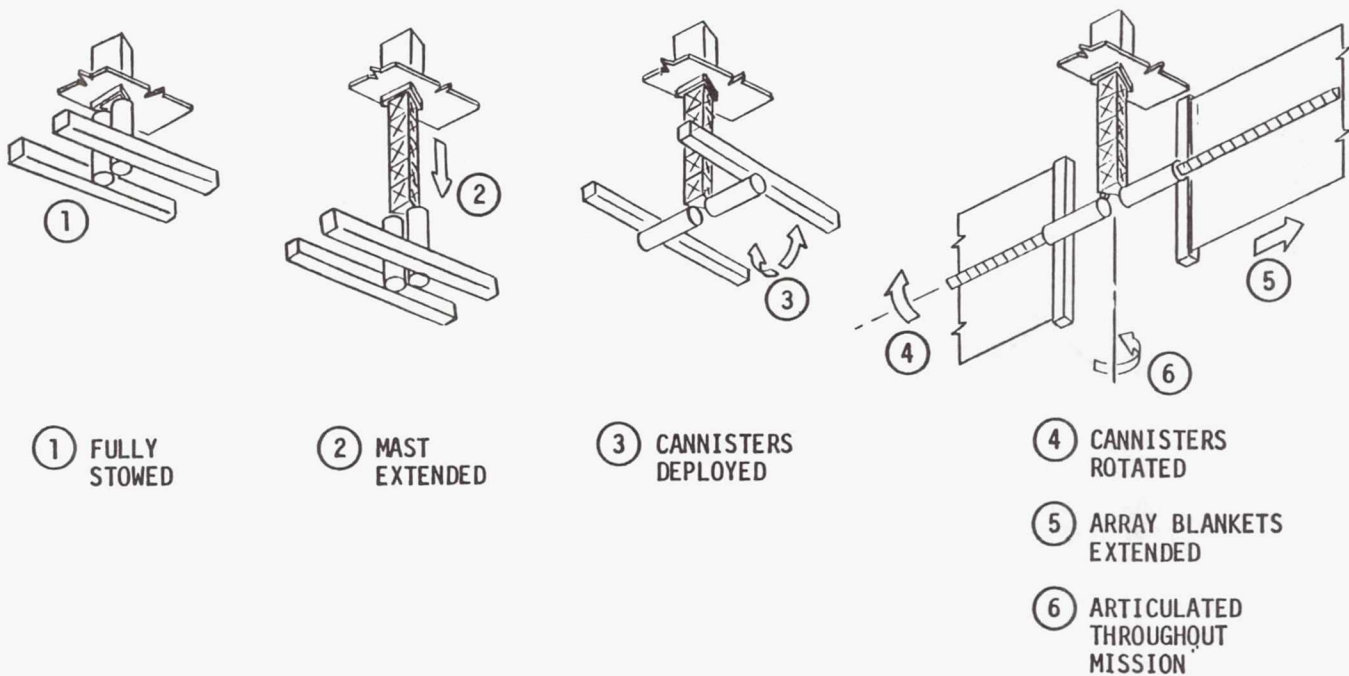
LMSS WRAP RIB
APPENDAGE STOWAGE

Shown is an isometric of the stowed spacecraft configuration adjacent to the Orbit Transfer Vehicle. The stowed position of the solar panel and the S-band feed and antenna are shown.



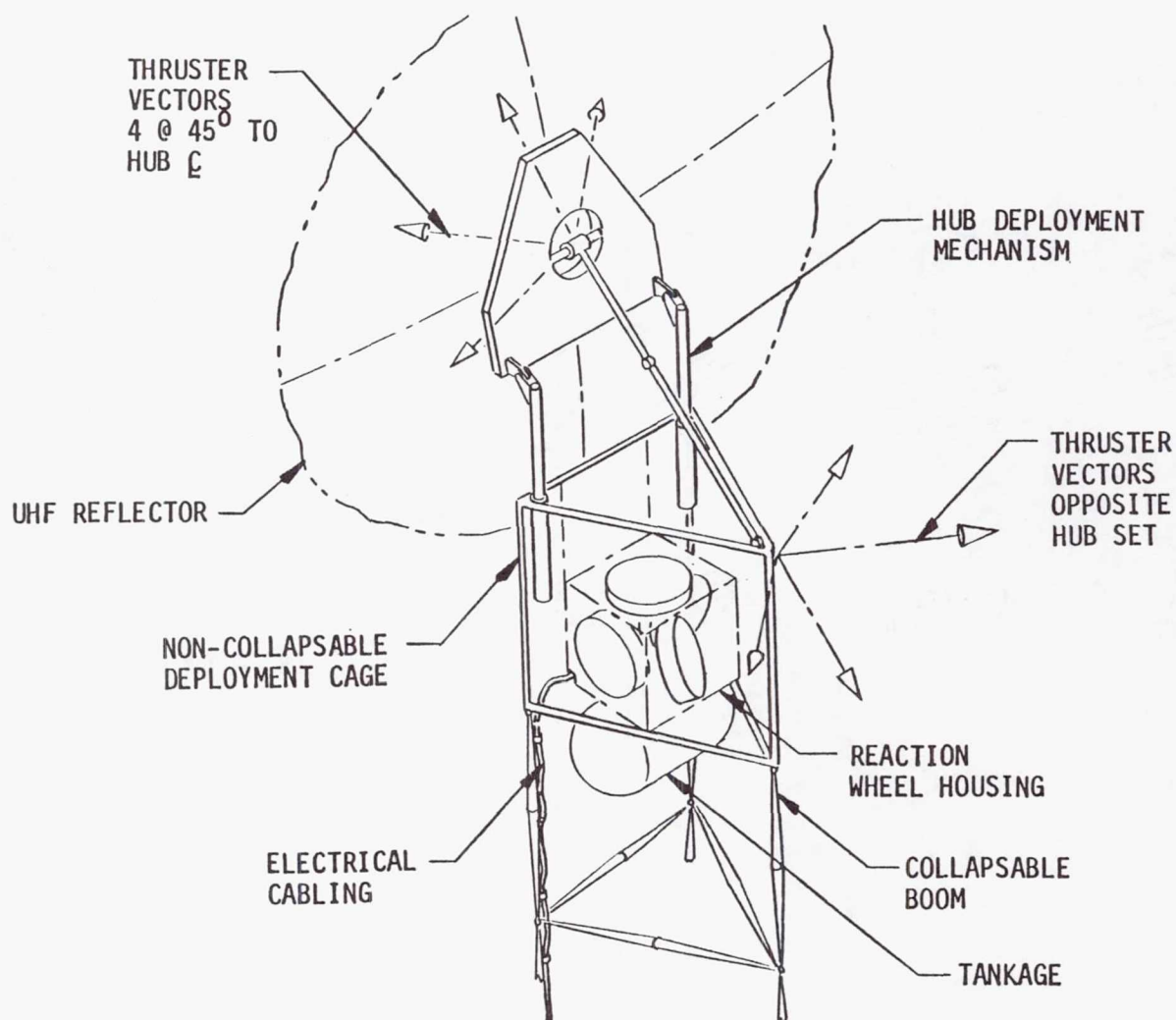
LMSS WRAP RIB
SOLAR PANEL DEPLOYMENT

Shown is the proposed solar panel deployment. A time line for this in the overall deployment sequence has not been established. It appears to be an independent event that can be sequenced at the most desirable time. The deployed solar panels will require "unwinding" once a day to preclude cable twisting. The solar panels must be rotated around the X axis to deploy. It may be desirable to articulate them about the X axis during the mission to keep them normal to the sun line. This should be decided in a future design trade.



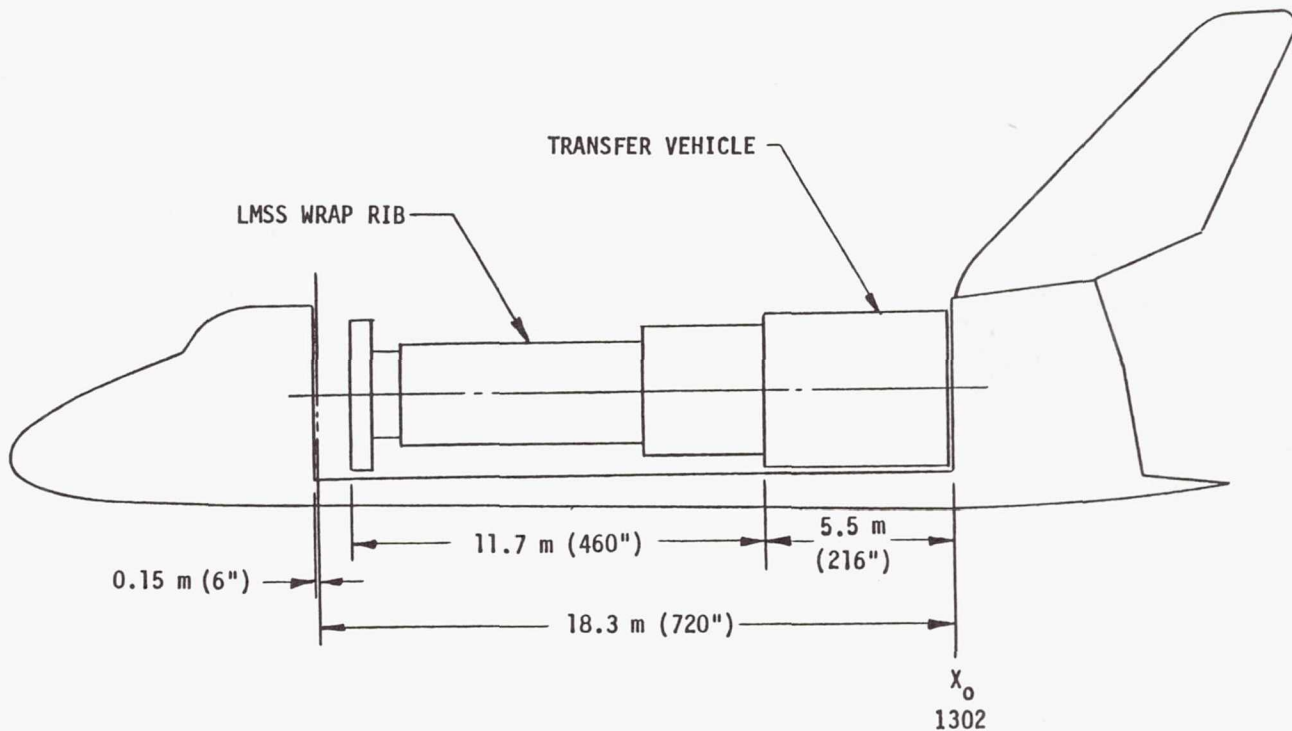
LMSS WRAP RIB REFLECTOR HUB AREA

The configuration of the LMSS adjacent to the reflector hub is shown on this chart. Pointing control of the deployed UHF reflector is not shown but may be required. The secondary attitude control equipment is located as shown. The requirement for attitude control functions at the hub also require that power and command cabling be run along the boom from the spacecraft bus (feed end). This has been examined and appears feasible.



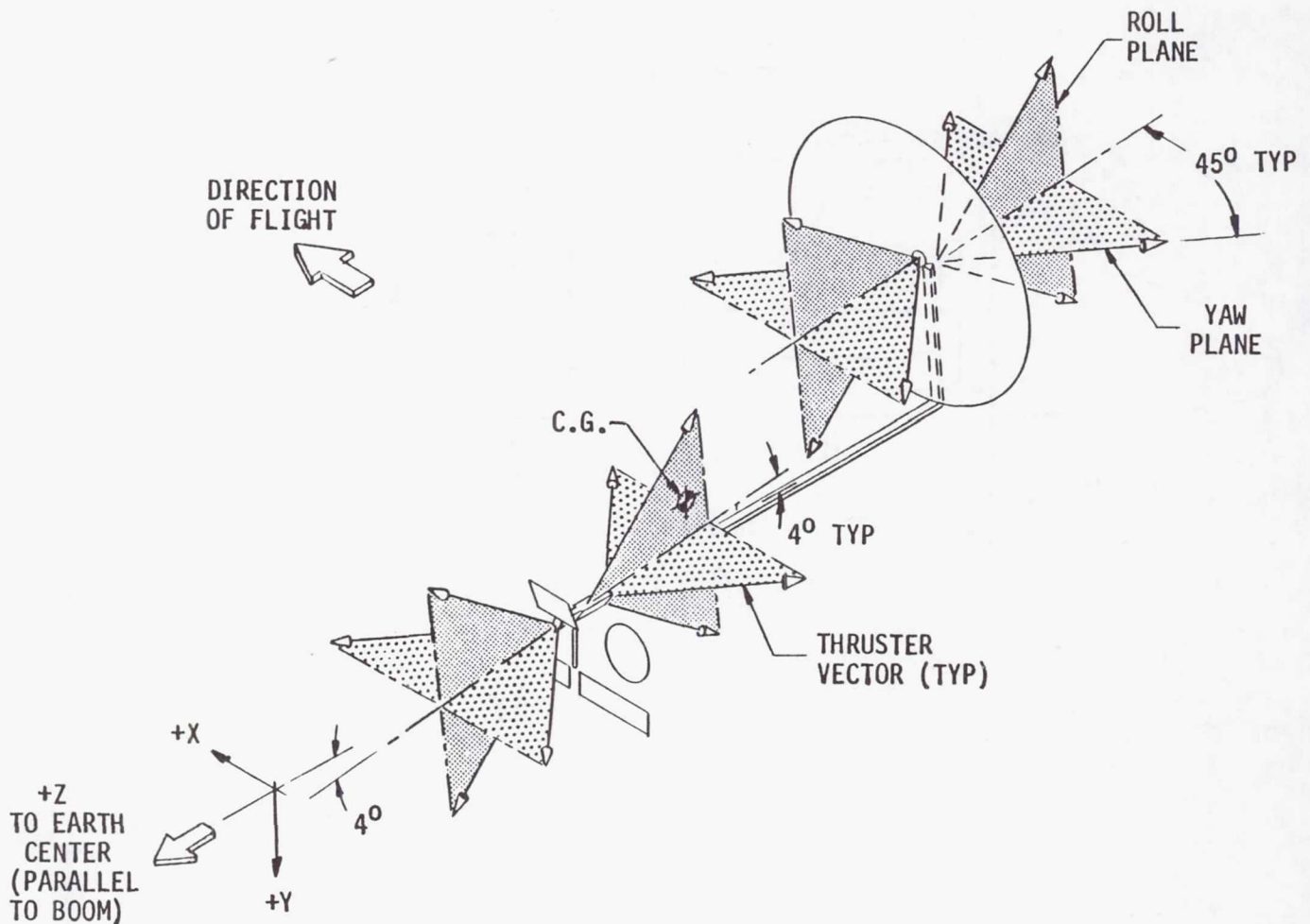
LMSS WRAP RIB
IN CARGO BAY

The overall stowage of the wrap rib LMSS is shown. The stowed length of 11.7 m (460") fits easily within the cargo bay. Assuming a 4082 kg (9,000 lb.) capacity transfer vehicle requires 5.5 m (216") there is a 1.1 m (44") clearance. In addition, there is a potential of shortening the wrap rib LMSS by an additional 1 m (40") to 1.1 m (44") by reducing the large diameter (center) of the longitudinal struts from 0.1 m (4") to .08 m (3"). Thus a transfer vehicle length of up to 7.6 m (300") can be accommodated. If the current weight of the spacecraft cannot be reduced a larger orbit transfer vehicle (OTV) will be required. Depending upon what size OTV is available or planned, this may be a problem.



LMSS WRAP RIB PROPOSED THRUSTER LOCATIONS

The proposed thruster locations are shown. To have the thrusters in the usual orientation (along primary axes) results in thruster plume and thrust impingement on most radiating and structural members. It was decided that a 30° half-cone should describe the plume and we would use a 45° centerline clearance. Rigid adherence to this results in canting the thrusters at the spacecraft bus (feed area) 4° in the Y plane to clear the feed. (This may be changed during detail design.) During deployment (stowed package configuration separated from the transfer vehicle) two sets of thrusters are operable: (1) the +Z set of 4 thrusters as shown; and (2) the set of 4 thrusters from the center of the 55 m reflector which will be pointed in the -Z direction at the -Z end of the stowed package. In this positioning roll control is questionable, and additional thrusters may be required for the initial deployment events. If canting the thrusters as shown results in a significant increase in the weight of station keeping propellant, thrusters may have to be placed on deployable booms. This will have a serious impact on the packaging concept. A design trade needs to be conducted in conjunction with the attitude control subsystem definition.



LMSS WRAP RIB
SUBSYSTEM REQUIREMENTS

In the purest sense the following subsystems may be closer to hardware groupings. Each is so inner related it is hard to split them up to discuss a "subsystem" (i.e. structure). The UHF feed weighs more than many of today's spacecraft and has structure, mechanisms, thermal control and cabling as well as its RF hardware, but we will call it a subsystem. In addition, we'll address structure (bus, boom and reflector), attitude control and electrical power (solar panels, batteries and power conditioning). Other subsystems are not as well defined or as critical to the system design at this time, and will not be covered.

WRAP RIB SUBSYSTEM REQUIREMENTS

UHF RF FEED

Below are the major subsystem requirements influencing the feed definition at this time. Considerable technology development will be required to define many items (radiating elements and beam forming network). Until a better understanding of how the feed design will be implemented is attained, detail requirements at the subsystem level will not be identified. Interfaces and sizing (dimensions and weight) were required for this study and the necessary data was developed.

- CONUS COVERAGE
- FREQUENCY: UPLINK 821 → 831 MHz DOWNLINK 866 → 876 MHz
- BEAM WIDTH 0.44°
- BEAM TO BEAM ISOLATION 25 dB
- 7 FREQUENCY SINGLE CIRCULAR POLARIZATION PLAN
- AMPLIFIER EFFICIENCY 50% (HEAT DISSIPATION 2000 W)
- HARD POINT ATTACHMENT REQUIRED DURING BOOST
- FLATNESS 0.5 CM RMS (INCLUDING HINGE LINE EFFECTS)
- COMPATIBLE WITH ATT CELLULAR SYSTEM
- WEIGHT 3071 LBS (INCLUDES BUS MOUNTED ELECTRONICS)

WRAP RIB SUBSYSTEM REQUIREMENTS

STRUCTURE

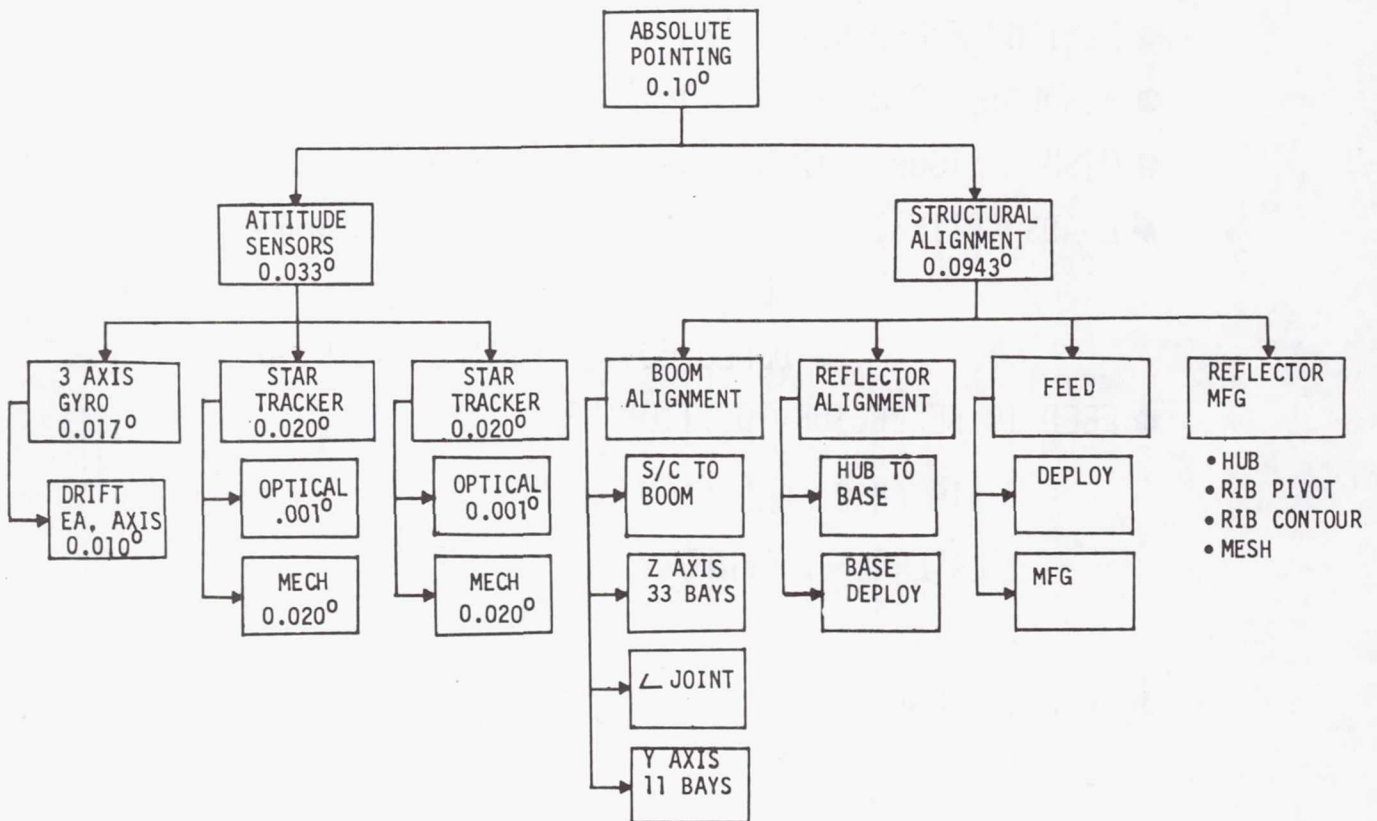
The wrap rib structural elements consist of the bus, boom and reflector. The major interfacing and sizing requirements are shown below. Because of the nature of the concept the usual approach of specifying a structural stiffness high enough to minimize response/exciting problems can't be used. The expected first mode frequency will be less than 1 Hz and the challenge is to design and control this type structure to satisfy the system/mission requirements.

- MINIMUM FREQUENCY: TBD
- ABSOLUTE POINTING: 0.0887°
- MESH CONTOUR: 12 MM RMS (INCLUDES DYNAMIC EFFECTS)
- LOADS CRITERIA: STOWED - SHUTTLE LAUNCH
DEPLOYMENT - DYNAMICS
DEPLOYED - STATION KEEPING
- FEED TO REFLECTOR POSITIONING
 - DISTANCE (DESPACE)
 - LATERAL (DECENTER)
 - TILT
- WEIGHT: 1690 LBS

} TBD

LMSS WRAP RIB SUBSYSTEM REQUIREMENTS ABSOLUTE POINTING ERROR BUDGET

The error budget to provide 0.10° absolute pointing is shown. The allocation to attitude control sensor mounting is 0.033° leaving 0.094° for structural elements. Considering the boom and reflector only the allocation is 0.090° (removing structural alignment of the feed). The significant element within this is the requirement that the ends of each boom segment be parallel within 0.010° . Usual manufacturing tolerance for optically aligned structures of this type is 0.02° . Requiring reducing the tolerance by a factor of 2 will be difficult to realize and may require ground demonstration or adjustment on orbit.



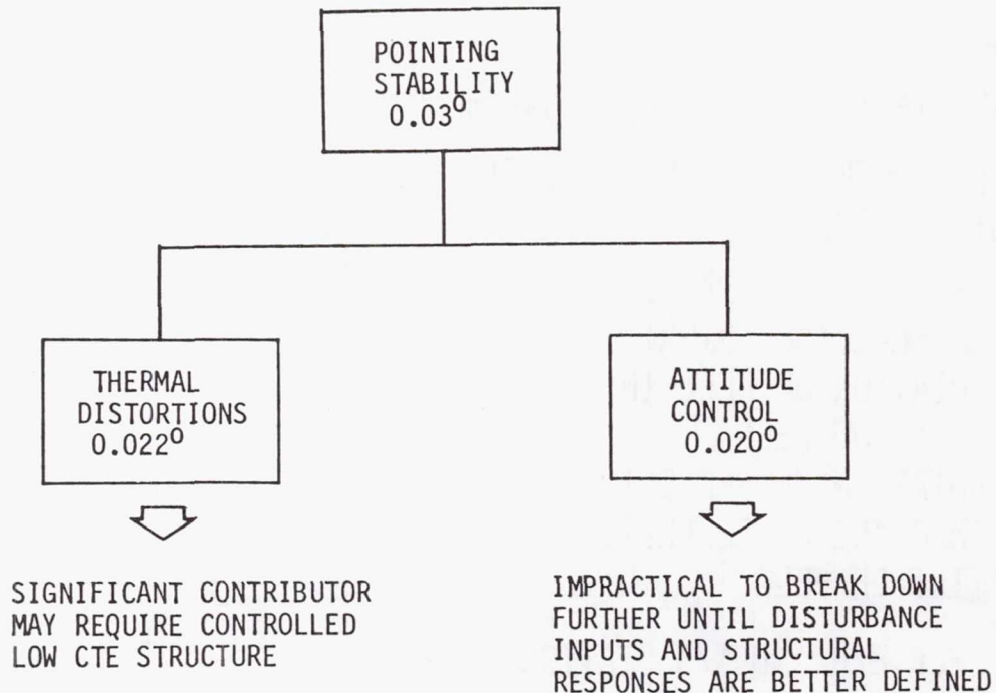
WRAP RIB SUBSYSTEM REQUIREMENTS
ATTITUDE CONTROL

The significant requirement on the attitude control subsystem is the continuous pointing stability of 0.03° coupled with the low structural frequency (probably <0.5 Hz) and the requirement for 10 years of North/South station keeping. Before more definitive subsystem requirements and design solutions can be developed, the structural response characteristics and disturbance inputs must be defined. The attitude control analysis essentially runs one iteration behind the design process since they need all the geometry, mass properties and structural data to initiate their work. The attitude control analysis of this configuration is in work and will be reported separately.

- 10 YEAR LIFE
 - POINTING STABILITY OF 0.02° CONTINUOUS
 - LOCATION OF CENTER OF FEED RELATIVE TO CENTER OF REFLECTOR DURING ANY 10 MINUTE PERIOD
 - DISTANCE (DESPACE)
 - LATERAL (DECENTER)
 - ROTATION OF FEED IN PLANE OF FEED
 - ROTATION OF REFLECTOR IN PLANE OF REFLECTOR
 - TILT OF FEED
- } TBD
- PROVIDE FOR E/W AND N/S STATION KEEPING
 - SUBSYSTEM WEIGHT 2766 LBS

POINTING STABILITY ERROR BUDGET
LMSS WRAP RIB AND HOOP COLUMN

The pointing stability requirements have been arbitrarily divided between thermal distortions and the ability of the attitude control subsystem to accommodate the structural characteristics of the spacecraft. These values are guidelines to see what significant constraints they may impose as well as establish a basis for future trades. A preliminary assessment of the thermal distortions indicates that they may be significant enough to perhaps require low coefficient of expansion (near zero CTE) graphite for construction of the structure in both configurations.



WRAP RIB SUBSYSTEM REQUIREMENTS

ELECTRICAL POWER

The electrical subsystem is a typical state of the art design with the exception of the requirement of accommodating shadowing. Extremely long masts/booms would be required to keep the solar panels constantly in the sun. This results in significant solar pressure, weight, cost, complexity and packaging problems. Therefore the solar panels must be designed (1) to perform in a "soft" shadow condition (sun through the mesh) reducing the solar energy about 5% and (2) to survive full or "hard" shadow impingement from structural/mechanism members for short durations. A detail design analysis will be required.

SOLAR PANELS

- 10 YEAR LIFE, 10 KW BOL
- 5% SOFT SHADOWING (SUNLIGHT THROUGH THE MESH)
- HARD SHADOWS 4" WIDE (STRUCTURAL MEMBERS)
- SOLAR PANEL MAST AND MECHANISMS 110 LBS
- VOLTAGE 28 VDC \pm ?
- SOLAR PANEL WEIGHT 367 LBS

BATTERIES

- 10 YEAR LIFE
- 50% SYSTEM MAX DUTY CYCLE DURING ECLIPSE - 30 MIN.
- 80% DEPTH OF DISCHARGE
- MAY BE USED TO SUPPLEMENT SEVERE SHADOWING PERIODS
- WEIGHT 288 LBS (BATTERIES AND POWER CONDITIONING)

LMSS HOOP COLUMN CANDIDATE CONFIGURATIONS

In the initial development of the system design, trades were performed to select the overall configuration. This chart summarizes candidate configurations and the selected baseline.

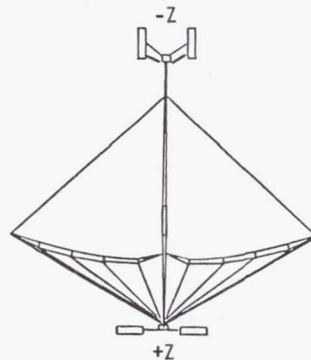
A driving consideration is the packaging of electrical cabling routed between the ends of the column. Any such cabling would be 87 meters long deployed, but would have to be collapsed for launch into a volume 7.3 meters long by 0.5 meter diameter. The cabling required for Candidate 2 could not be so packaged. Cabling to each of 88 UHF feed elements, the S-band feed elements, reaction wheels, thrusters, and various electronics would constitute an impossibly large volume of wiring, and RF runs would be excessively long. Candidate 3 lessens the electrical cable stowage problem, but results in an unacceptable solar array location. Candidate 4 features raw power cabling routed from the +Z array to power conditioning equipment at the -Z end (either midboom or extreme end). Again, the cable stowage problem is lessened but is still a concern as are line losses and extra cabling weight. Candidate 4 might yet be a viable alternative depending on detailed electrical and packaging analyses and possible advances in cable technology.

The selected configuration, Candidate 1, features independent power units one at either end. The primary power is at the -Z end to provide short electrical and RF runs to the UHF and S-band feeds. A smaller power unit at the +Z end supplies the +Z control equipment and may supplement some raw power to the -Z ends. This is the most efficient arrangement in terms of packaging and total weight and has no inherent RF performance penalties, the -Z solar panels being located in dead areas between the RF beams.

1. TWO INDEPENDENT BUSES

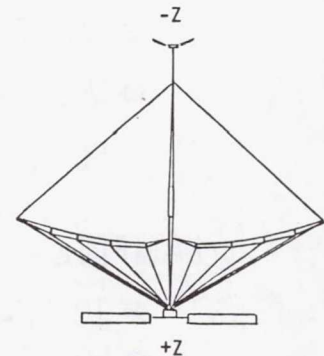
SELECTED

ALLOWS SHORT POWER LINES TO FEEDS & TO CONTROL EQUIP AT BOTH ENDS



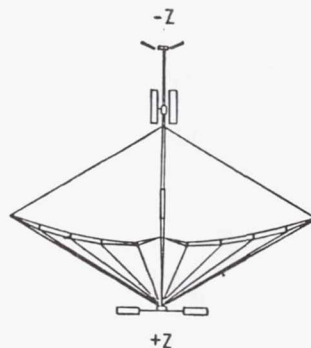
2. MAIN BUS AT +Z END

INADEQUATE STOWAGE VOLUME FOR POWER LINES TO FEEDS & CONTROL EQUIP AT -Z END



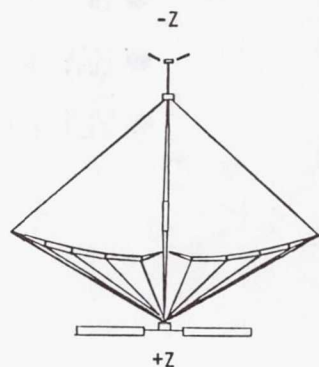
3. MID-BOOM SOLAR ARRAY

MID-BOOM ARRAY SHORTENS POWER LINES BUT WOULD BLOCK RF BEAMS



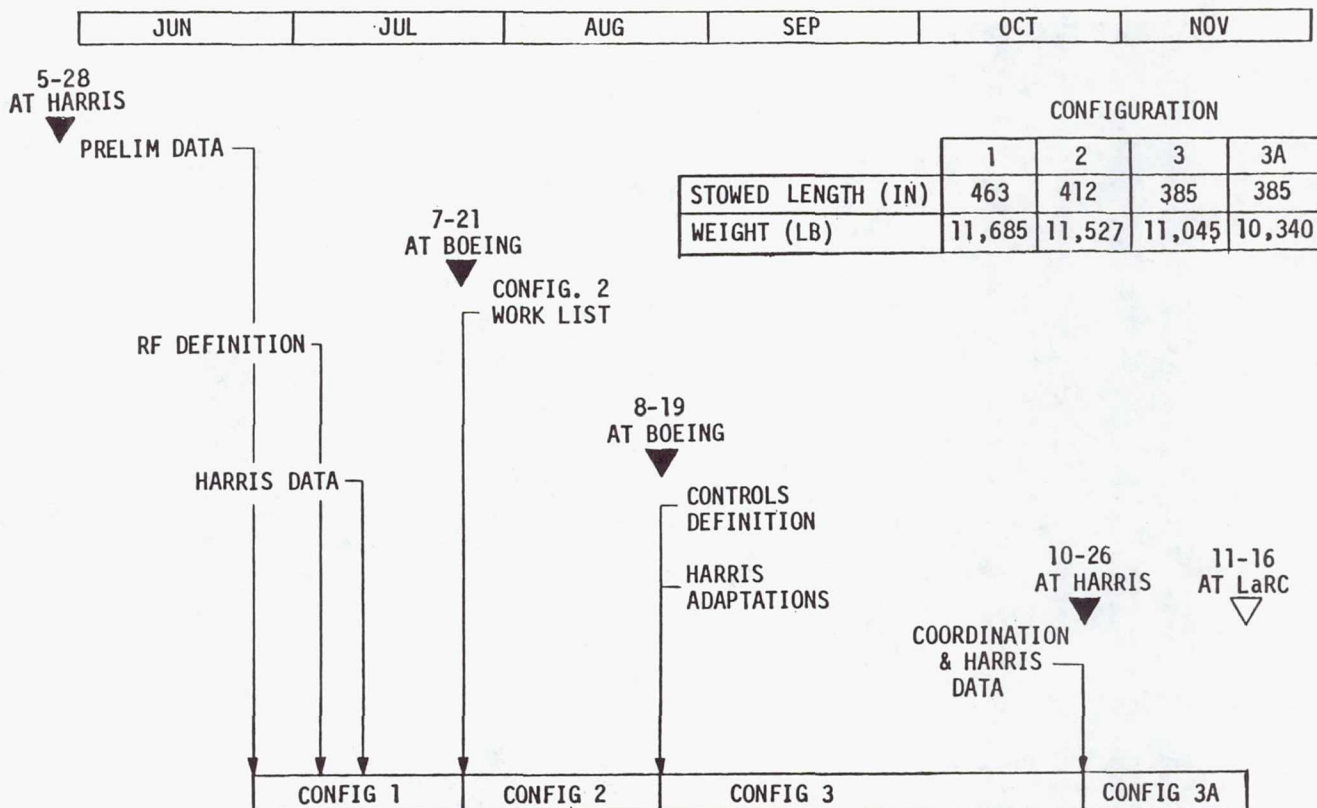
4. BATTERIES & POWER COND IN MID-BOOM BUS

VARIATION OF NO. 2 TO SHORTEN CABLING. PACKAGING MORE DIFFICULT THAN NO. 1



LMSS HOOP COLUMN BOEING STUDY HISTORY

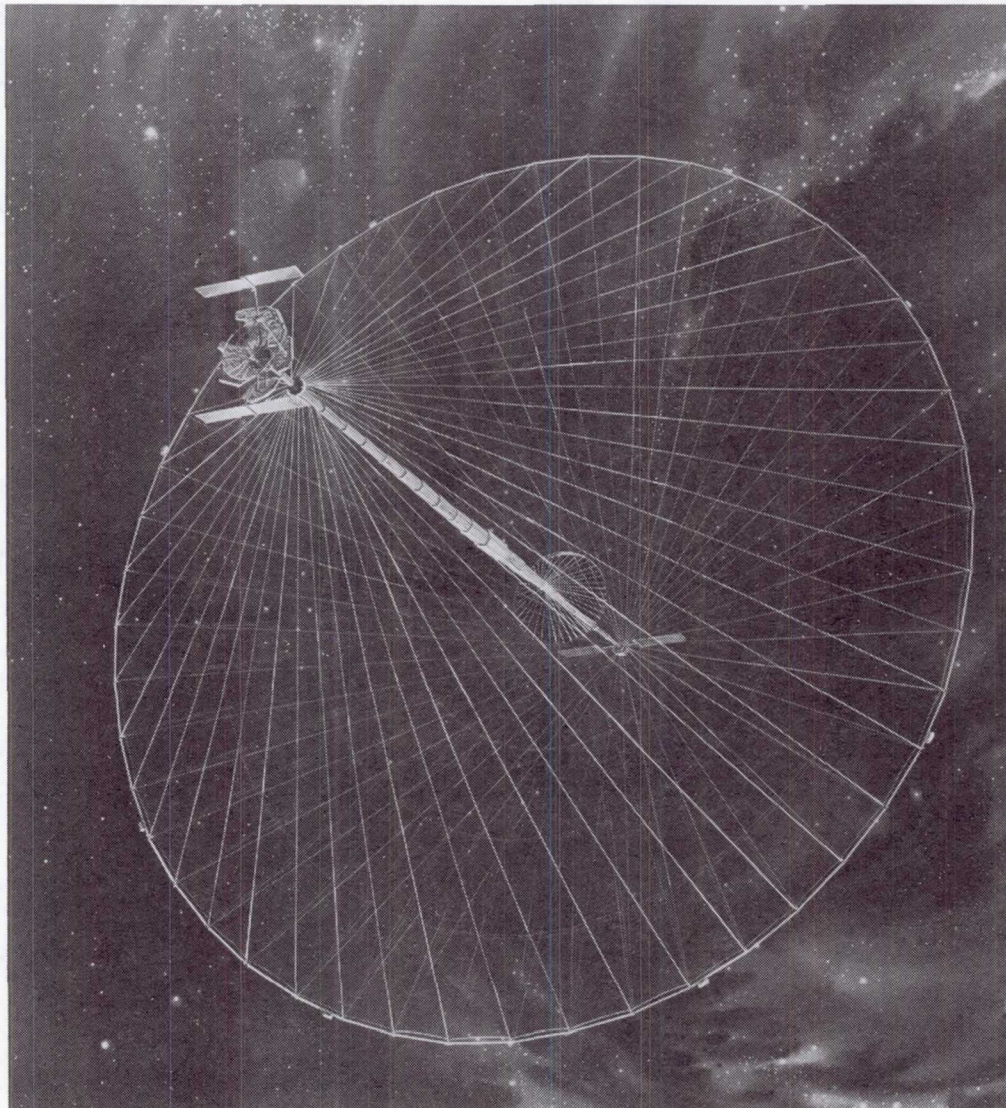
The history of the hoop column design effort is shown. To date the trend has been to improve the design, shorten the stowed length and reduce the weight with each revised configuration. The stowed length and weight are now within the range of the larger proposed 1995 transfer vehicles.



LAND MOBILE SATELLITE SYSTEM SPACECRAFT 120 METER HOOP COLUMN CONCEPT

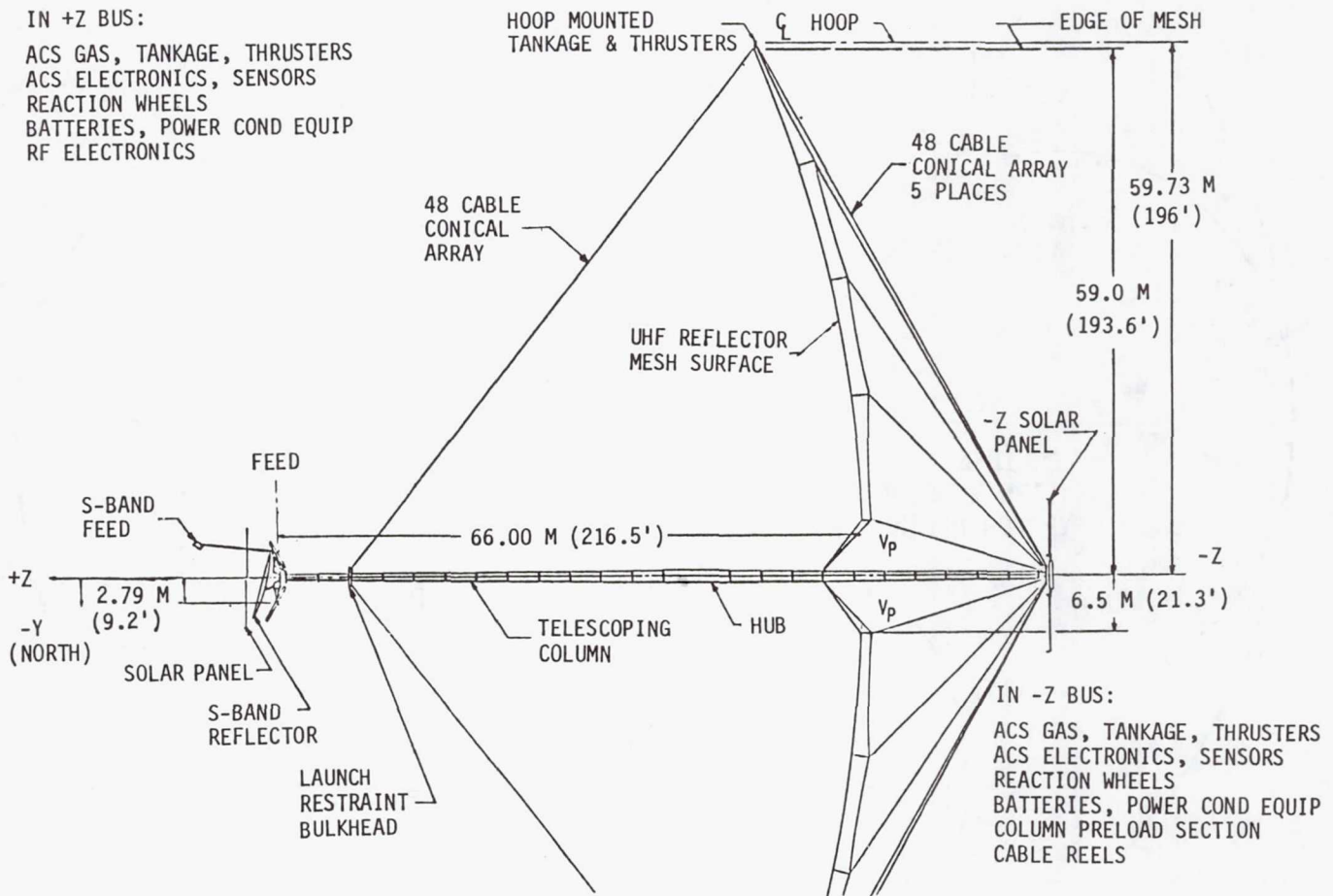
This is a preliminary concept of a quad aperture reflector spacecraft capable of relaying radio messages to land mobile units throughout the United States. It is intended to service units such as ambulances, police cars, taxis -- in essence any radio dispatched vehicles. Its position in geosynchronous orbit avoids present radio interferences caused by tall buildings, hills, and other factors. It is one of numerous concepts for extending current space technology made feasible by the Space Shuttle. The spacecraft is sized for a single Shuttle launch and a 10-year life beginning in the mid-1990's.

The central column points at the center of the United States near Kansas City. Each of the four feed panels at the upper left projects a multiple beam pattern onto its assigned quadrant on the large, molybdenum-mesh reflector. There are uplink and downlink feeds for both the eastern and western halves of the country. The radio beams are arranged to cover all contiguous 48 states with a potential in the design for communication with Alaska, Hawaii, and parts of Canada.



LMSS HOOP COLUMN SPACECRAFT

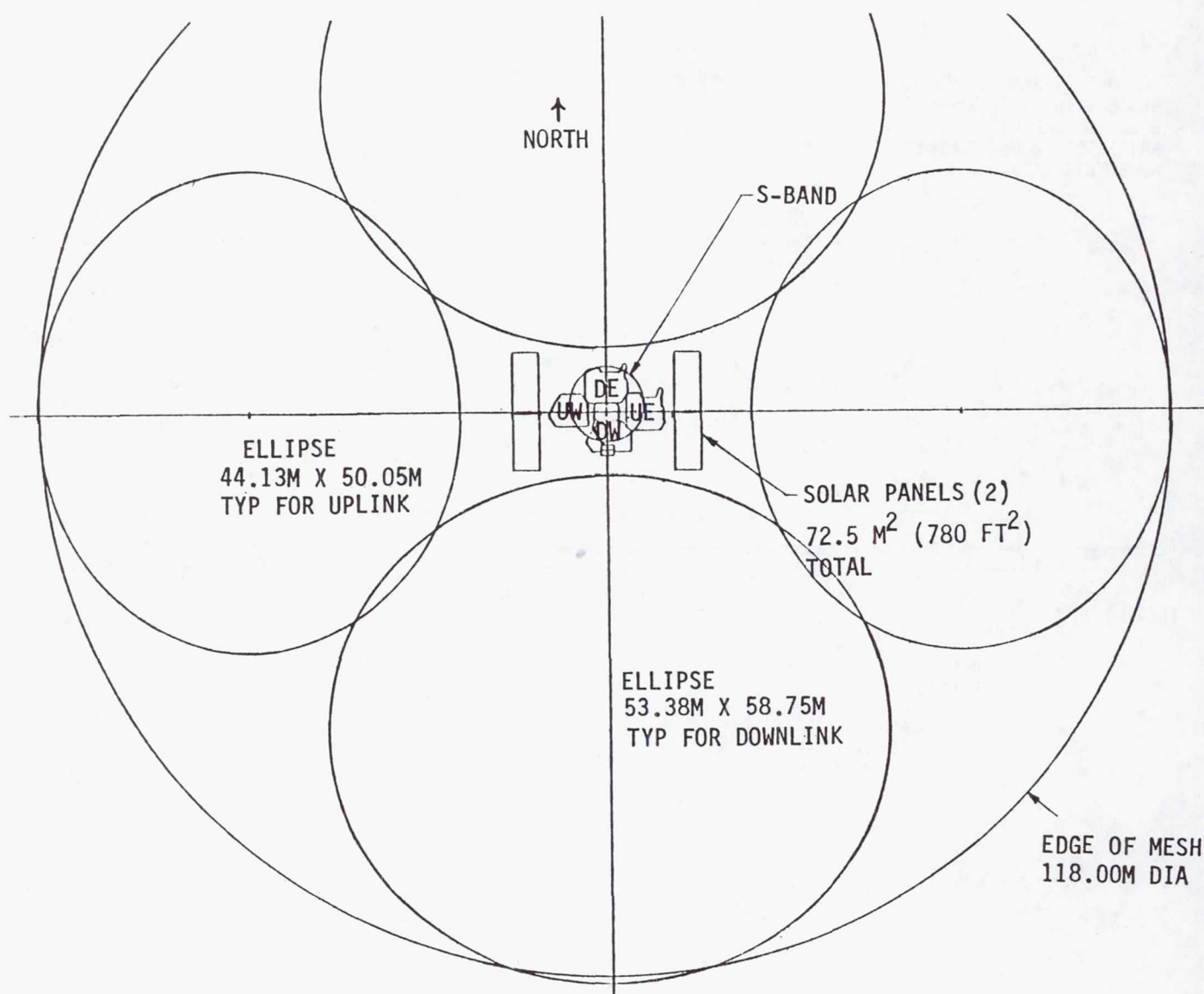
This sectional side view through the hoop column N-S plane shows the overall size of the spacecraft. The reflector is about 120 meters in diameter, and the column including S-band feed and -Z bus is 97 m.



LMSS HOOP COLUMN

QUAD APERTURES

A view of the quad aperture hoop column is shown looking from the earth at the UHF reflector. The four slightly elliptical spots are the antenna apertures. The two larger ones in the N-S plane (vertical) are the downlink for the eastern and western halves of the United States. The slightly smaller apertures in the E-W plane (horizontal) are for uplink communications. The solar panels, feeds (4), and S-band antenna are clustered in the center. This particular configuration requires solar panel articulation about both axes. If the pattern were rotated 90° , single axis articulation of the solar panels would be adequate. An analysis on the impact on RF performance has been made and the rotation is practical.



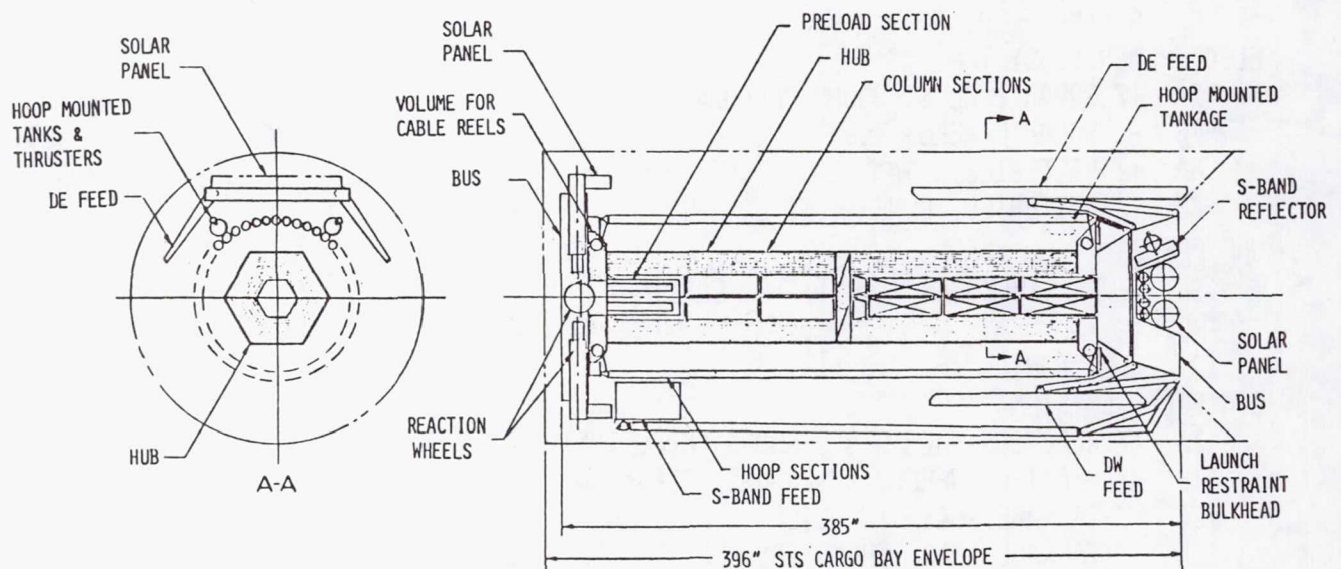
LMSS HOOP COLUMN
WEIGHT STATEMENT

The weight statement for the latest hoop column LMSS configuration is shown below.

	WEIGHT	
	KG	LBS
HOOP, COLUMN, REFLECTOR STRUCTURE TOTAL	(992)	(2188)
1 COLUMN & CABLES	608	1340
2 HOOP	285	628
3 REFLECTOR	99	220
INSULATION	(71)	(156)
4A MLI, +Z BUS	16	35
4B MLI, -Z BUS	10	23
4C MLI, HOOP	19	41
4D MISC.	26	57
S-BAND ASSY.	(175)	(385)
5 S-BAND REFLECTOR & BOOM	59	130
6 S-BAND FEED, BOOM, COAXES	116	255
ELEC. POWER SUBSYSTEM	(364)	(802)
7A +Z SOLAR PANELS, BOOMS, MECHANISMS	154	340
7B -Z SOLAR PANELS, BOOMS, MECHANISMS	76	167
8A +Z BATTERIES, POWER COND EQUIP.	96	212
8B -Z BATTERIES, POWER COND EQUIP.	38	83
UHF FEEDS	(977)	(2153)
9 FEEDS (INCLUDES STRUCT, TC, CABLING)	977	2153
TELEMETRY	(93)	(207)
10 ELECTRONICS	93	207
CONTROL SUBSYSTEM	(1308)	(2885)
11A +Z REACTION WHEELS & SENSORS, ELECTRONICS	216	476
11B -Z REACTION WHEELS & SENSORS, ELECTRONICS	56	124
12A +Z TANKAGE, GAS, THRUSTERS	563	1241
12B -Z TANKAGE, GAS, THRUSTERS	390	859
12C HOOP MOUNTED TANKAGE, GAS, THRUSTERS	96	212
BUS STRUCTURE	(195)	(430)
13A +Z BUS STRUCTURE	127	280
13B -Z BUS STRUCTURE	68	150
ELEC. CABLING (EXCEPT RF) & MISC.	(88)	(194)
14 CABLING (IN BUSSES & COLUMN)	68	150
15 MISC. (INSTRUMENTATION, OPTICAL ALIGNMENT)	20	44
	<hr/>	<hr/>
SUBTOTAL	4263	9400
GROWTH	426	940
	<hr/>	<hr/>
TOTAL	4689	10,340

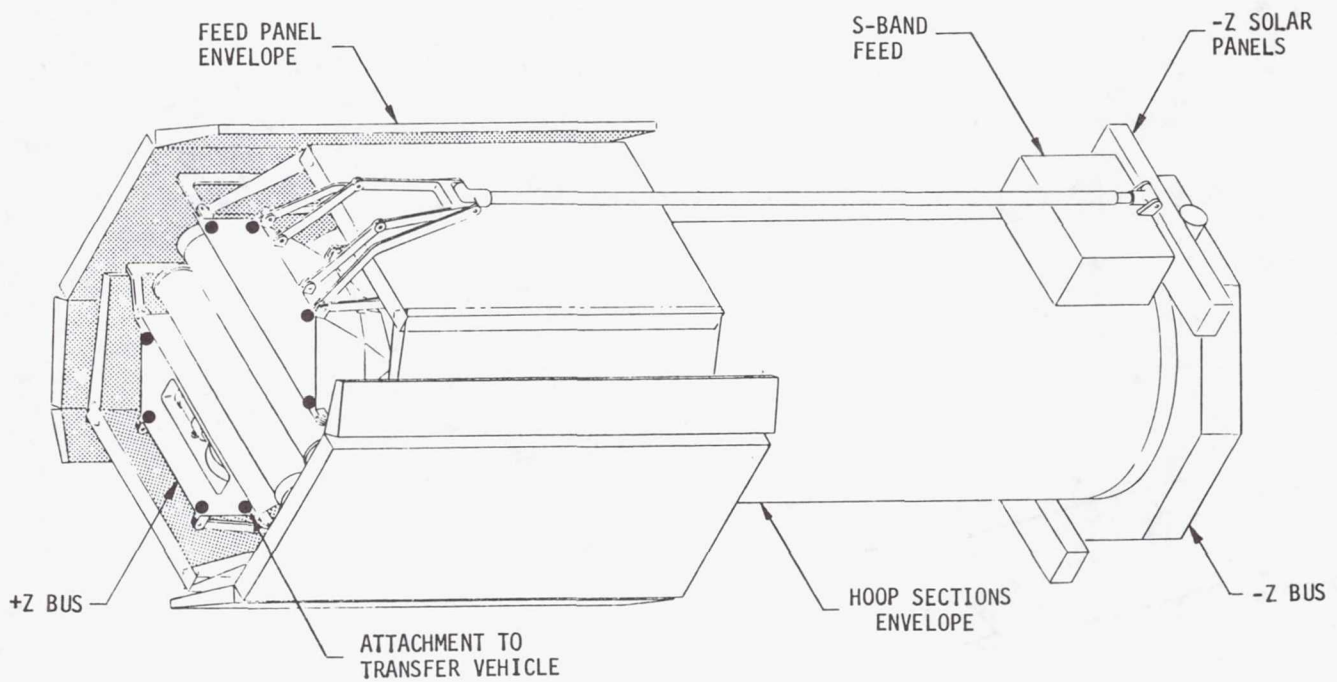
LMSS HOOP COLUMN LAUNCH CONFIGURATION

The stowed configuration is constrained by the 4.6 m (180") diameter of the cargo bay and the length available after installing an appropriate sized orbit transfer stage. There are three configuration drivers with respect to the hoop column launch configuration: (1) diameter required to stow the 4 feed arrays; (2) the length required for the hoop column members plus the +Z and -Z busses; and (3) the length required for the S-band feed boom. At this time all fit, but the margin or potential for growth or reducing the size of the launch configuration is slight. Assuming the 5443 kg (12,000 lb.) capability transfer stage has a length of 8.2 m (324"), there is only 0.3 m (11") clearance in the length of the shuttle cargo bay.



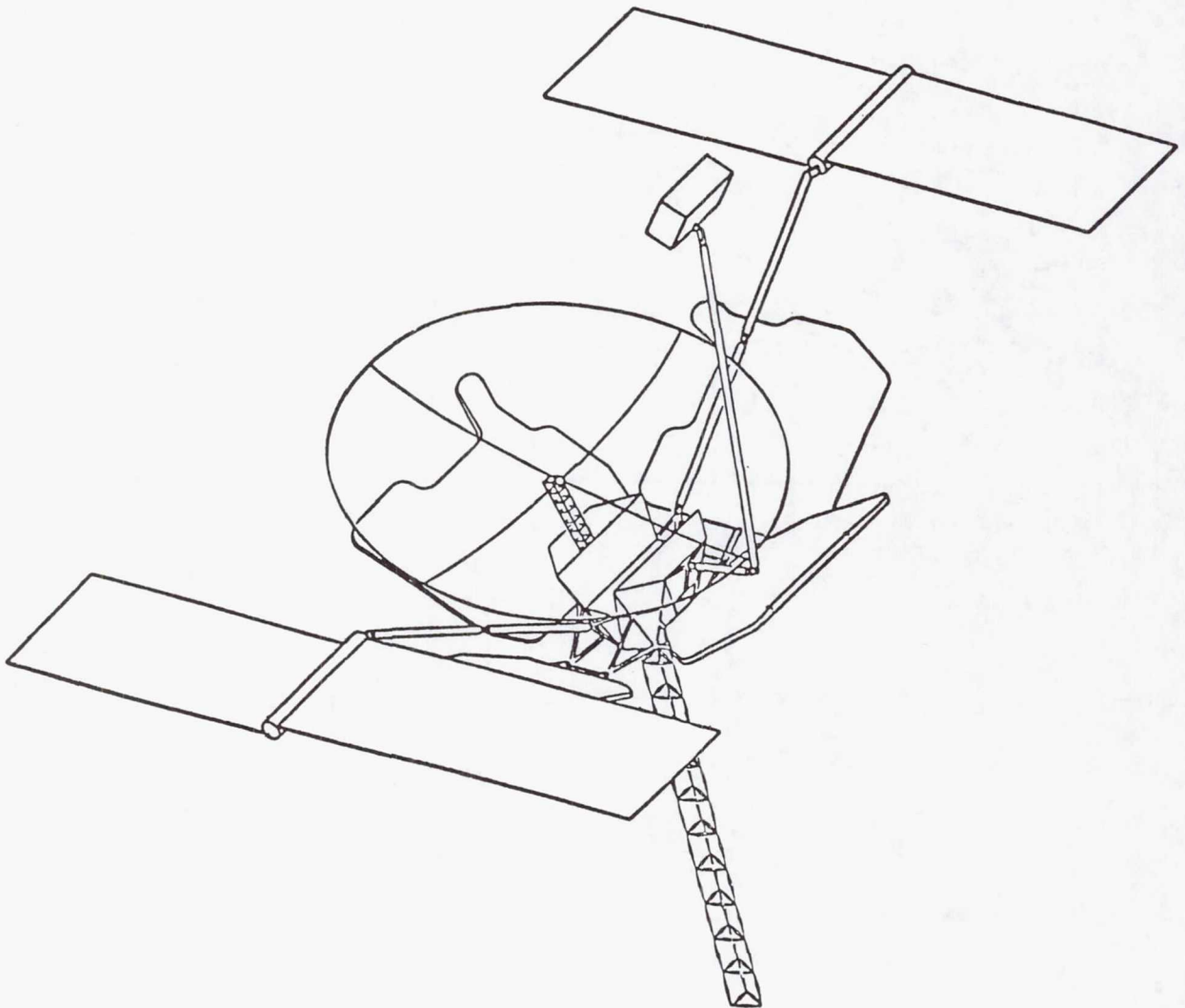
LMSS HOOP COLUMN
LAUNCH CONFIGURATION

This chart shows an isometric of the stowed hoop column. The attachment to the transfer vehicle is at the +Z bus.



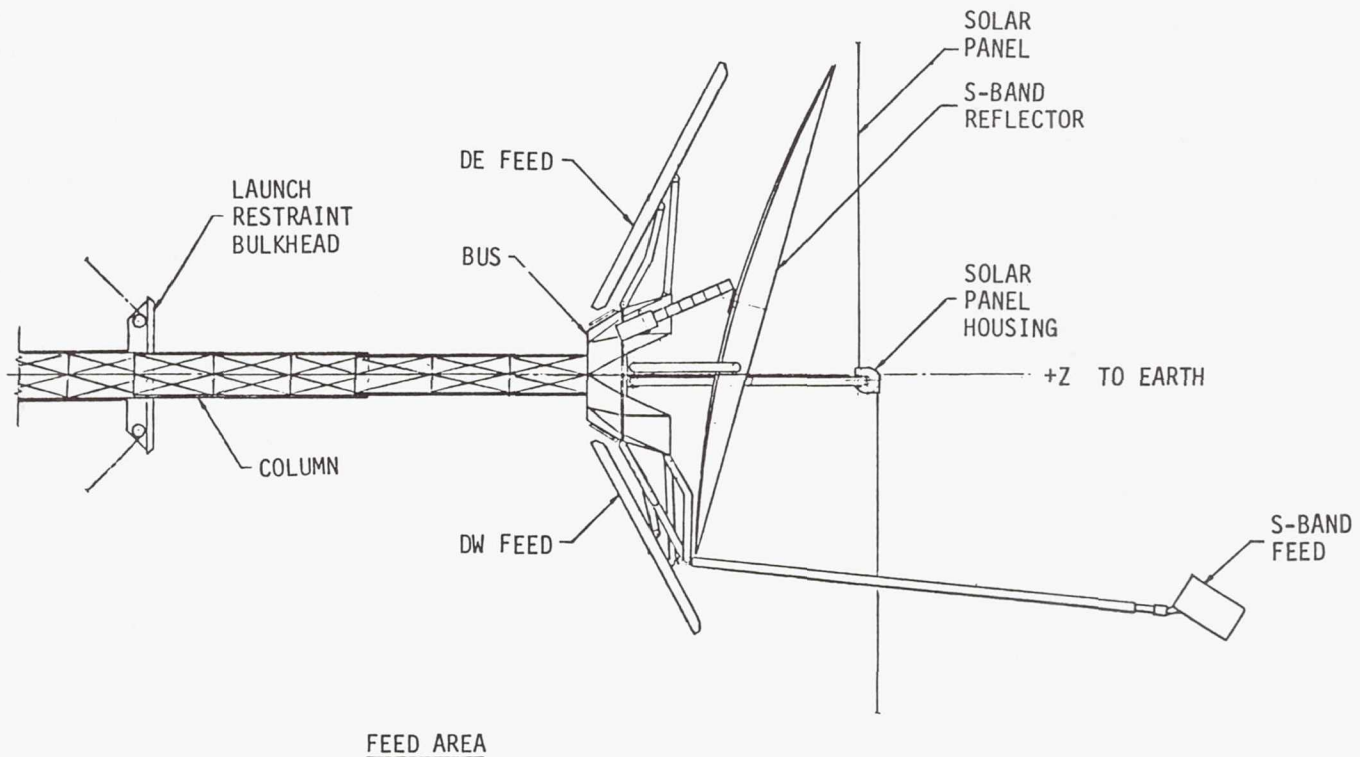
LMSS HOOP COLUMN
FEED AREA

This chart shows the deployed elements at the feed end (+Z bus) of the column. The subsequent charts in this series show cross sections in the N-S and E-W planes of the feed and then a view of the feeds and other appendages looking toward earth.



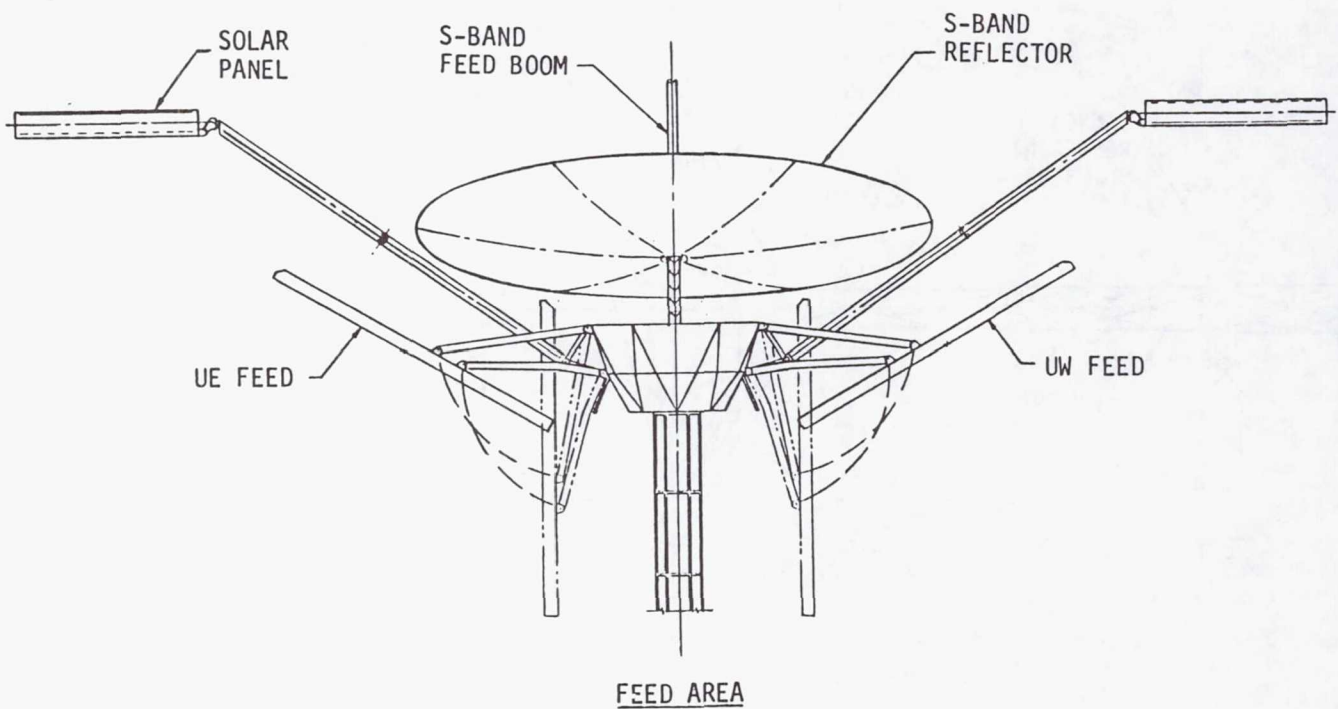
LMSS HOOP COLUMN NORTH-SOUTH PLANE

Shown is a view of the feed area. It should be noted that the bus (+Z end) is mounted on an extension of the column and not a separate deployable mast. The launch restraint bulkhead is attached to the third column section and carries the hoop positioning cables. The entire column is now deployable without depending on the compression load developed by the hoop support cabling. As shown the S-band antenna and feed are positioned directly in front (earth pointing) of the UHF feed arrays and do not contribute to any aperture blockage. The solar panels are mounted to the East and West of the column over non-aperture areas of the reflector.



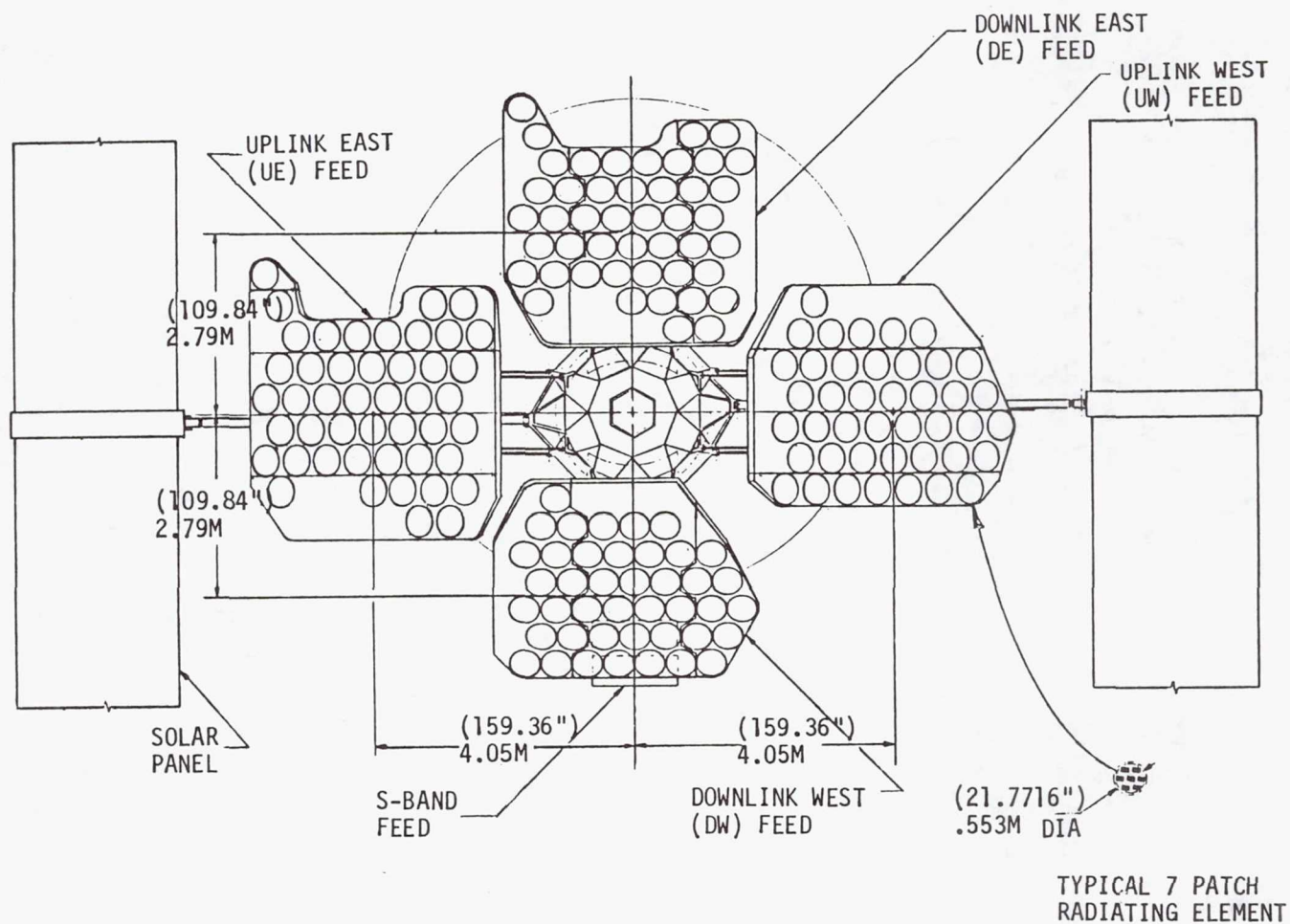
LMSS HOOP COLUMN
EAST-WEST PLANE

Shown is a view of the hoop column feed area (+Z feed) in the East-West plane. As in the previous chart the S-band antenna and feed are nested in front of the 4 feeds. The solar panels are on deployable booms that position them outboard of the feeds over an area of the reflector that is not used as part of an aperture. In this configuration the solar panels must be articulated in two axes to maintain sun pointing.



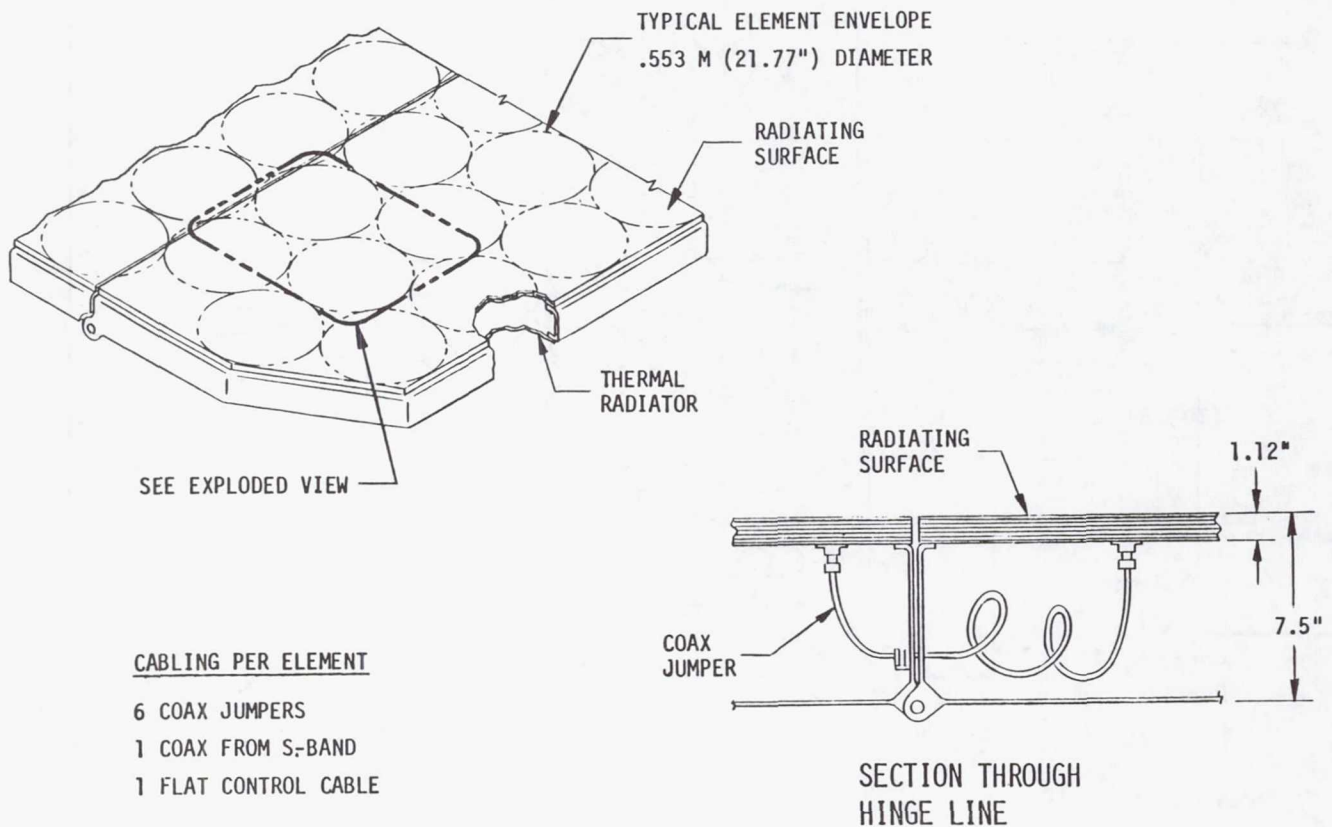
LMSS HOOP COLUMN
FEED AREA - VIEW TOWARD EARTH

Shown are the feed, S-band and solar panels viewed from the column center line looking toward earth (Kansas City, MO.).



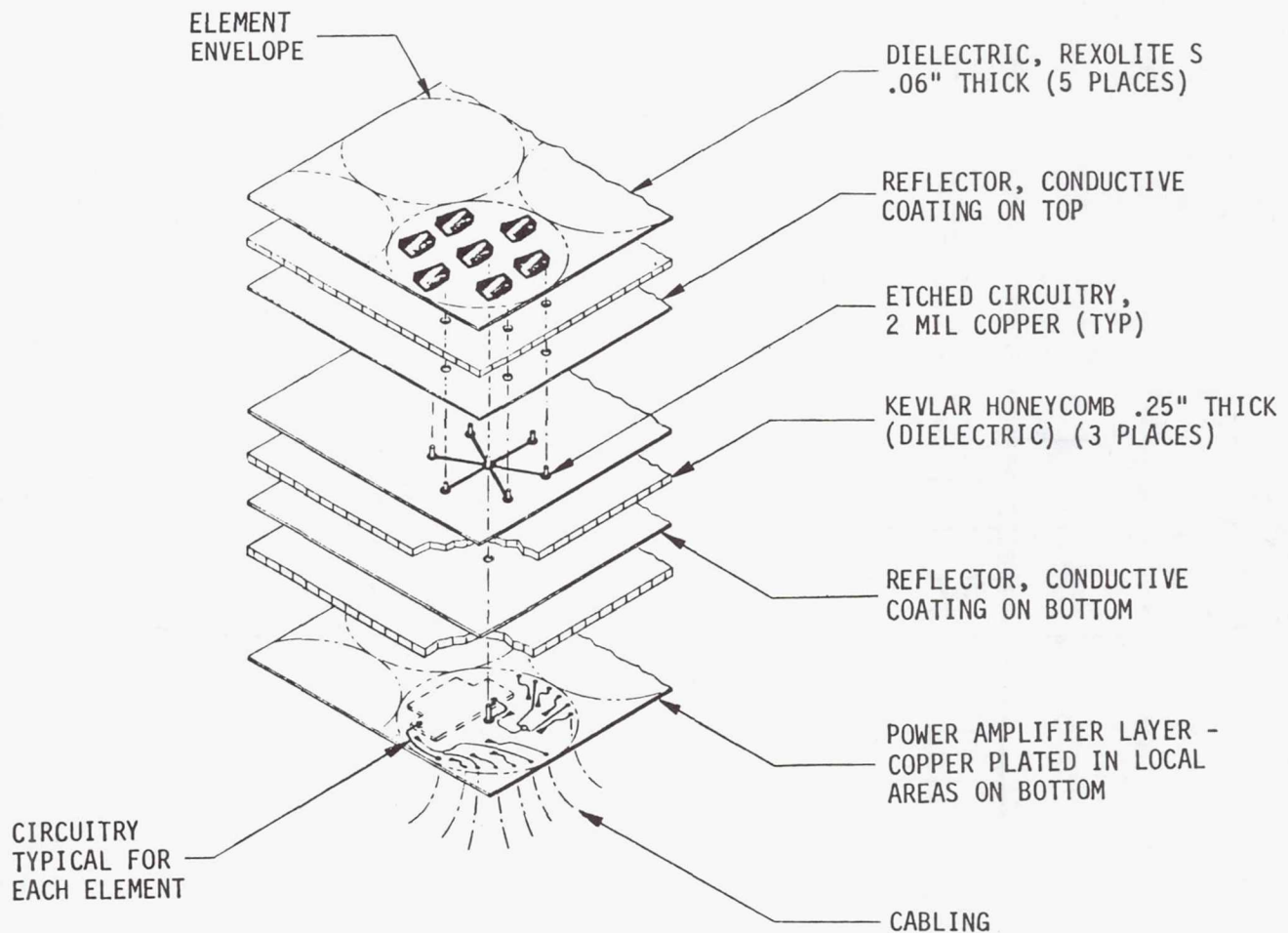
LMSS HOOP COLUMN UHF FEED ASSEMBLY

A portion of two adjacent hinged feed subpanels is shown. Each subpanel includes a 2.8 cm (1.12") thick stackup of dielectric sheets which support etched circuitry as shown on the following chart. The stackup is mounted on backup structure which provides the required stiffness and stability. A thermal radiator plate boxes in the structure and adds to the stiffness. The enclosed volume, about 15.9 cm (6¼") thick, is occupied by thermal transfer devices and, as shown in the section view, by coax loops.



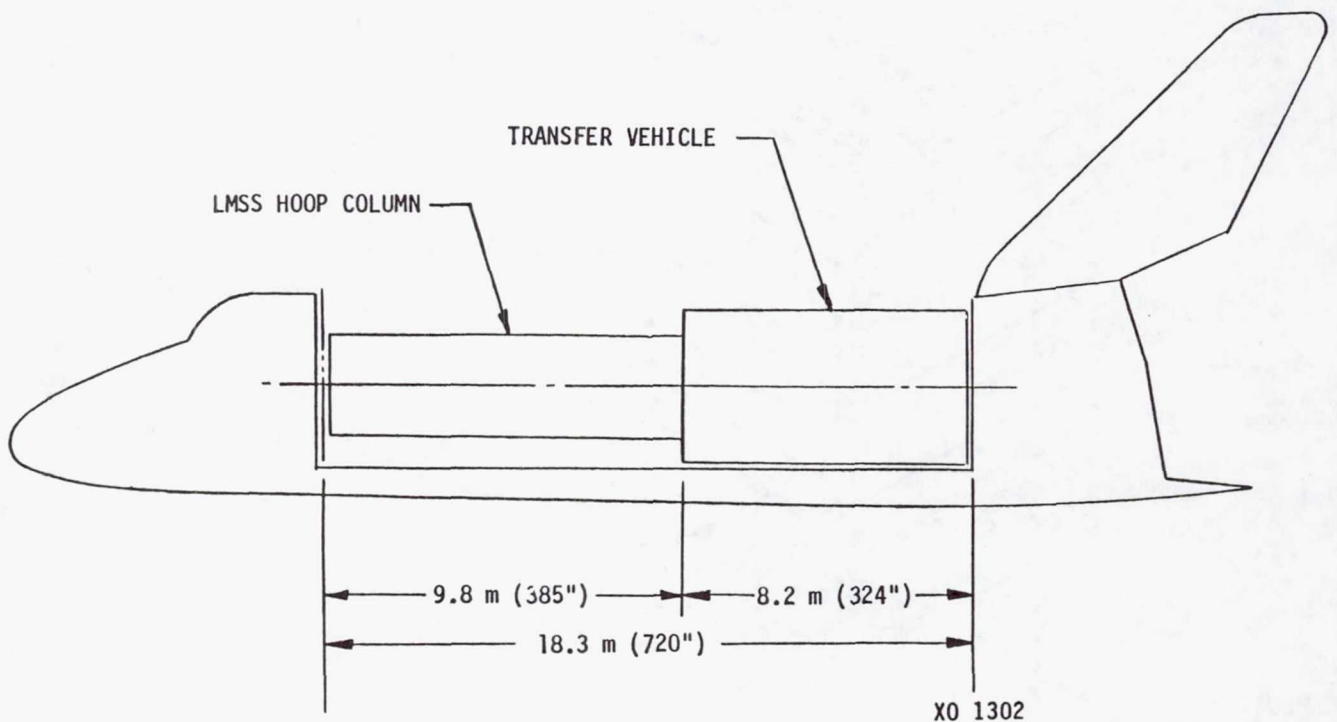
LMSS HOOP COLUMN UHF FEED
EXPLODED VIEW - 2.8 cm (1.12") STACKUP

The working portion of one feed element is shown. The eight layers are bonded together to make the entire stackup. The baseline seven patch design is shown. A four patch design is also being considered.



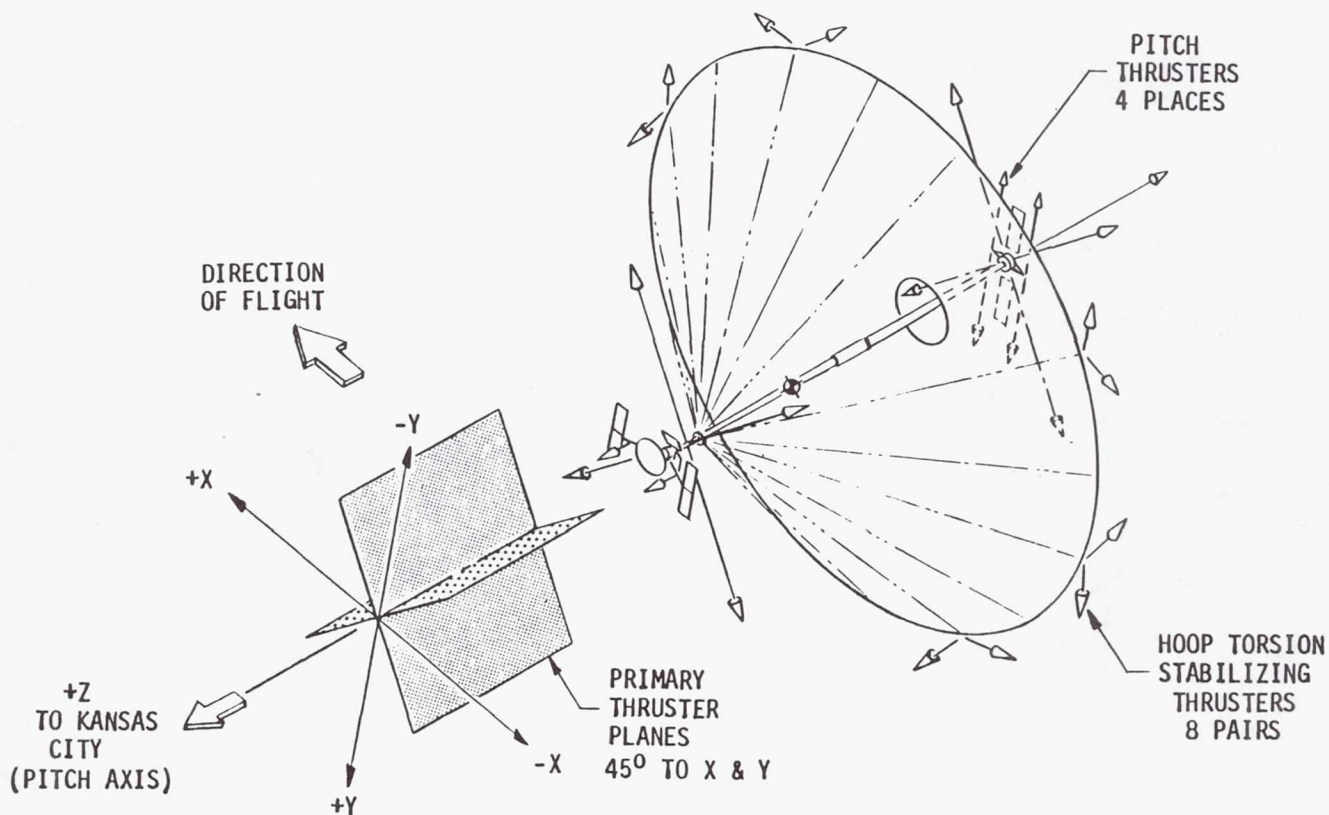
LMSS HOOP COLUMN
IN CARGO BAY

The hoop column LMSS/transfer stage vehicle comes within 0.3 m (11") of filling the STS cargo bay length. This is based on using a 5543 kg (12,000 lb.) capability transfer stage that is 8.2 m (324") long (does not presently exist). Again the availability/capability of a transfer stage in the 1990's is critical to being able to perform the LMSS mission.



LMSS HOOP COLUMN PROPOSED THRUSTER LOCATIONS

The proposed location for attitude control thrusters is shown. The hoop column configuration is essentially symmetrical along the column axis with the CG displaced slightly in the +Z direction. Due to its geometry, there are fewer problems with respect to plume impingement on adjacent members. An area of concern is pitch (direction of flight) control of the UHF reflector. The tension ties to the hoop in the form of the quartz and graphite epoxy cables do not provide any appreciable torsional stiffness. At this time the Controls Group (JPL) and the Hoop Column Designers (The Harris Corp.) are examining placing 8 pairs of thrusters on the periphery of the hoop to provide control capability of the reflector. As in the case with the wrap rib the thruster placement must be iterated with the attitude control subsystem design to assure an integrated design.



LMSS HOOP COLUMN SUBSYSTEM REQUIREMENTS

In the purest sense the following subsystems may be closer to hardware groupings. Each is so inner related it is hard to split them up to discuss a "subsystem" (i.e. structure). The UHF feed weighs more than many of today's spacecraft and has structure, mechanisms, thermal control and cabling as well as its RF hardware, but we'll call it a subsystem. In addition we'll address structure (busses, column, hoop, cable and mesh), attitude control and electrical power (solar panels, batteries, and power conditioning). Other subsystems are not as well defined or as critical to the system design at this time and will not be covered.

HOOP COLUMN SUBSYSTEM REQUIREMENTS
UHF RF SUBSYSTEM (FEED)

Below are the major subsystem requirements influencing the feed definition at this time. Considerable technology development will be required to define many items (radiating elements and beam forming network). Until a better understanding of how the feed design will be implemented is attained, detail requirements at the subsystem level will not be identified. Interfaces and sizing (dimensions and weight) were required for this study and the necessary data was developed.

- CONUS COVERAGE
- FREQUENCY: UPLINK 821 → 831 MHz, DOWNLINK 866 → 876 MHz
- BEAM TO BEAM ISOLATION - 25 dB
- 4 FREQUENCY - TWO POLARIZATION PLAN
- AMPLIFIER EFFICIENCY 50% (HEAT DISSIPATION 2000 W)
- HARD POINT ATTACHMENT REQUIRED DURING BOOST
- FLATNESS 0.5CM RMS (INCLUDING HINGE LINE EFFECTS)
- BEAM WIDTH 0.44°
- COMPATIBLE WITH ATT CELLULAR SYSTEM
- WEIGHT 2653 LBS (INCLUDES SUBMOUNTED ELECTRONICS)

HOOP COLUMN SUBSYSTEM REQUIREMENTS

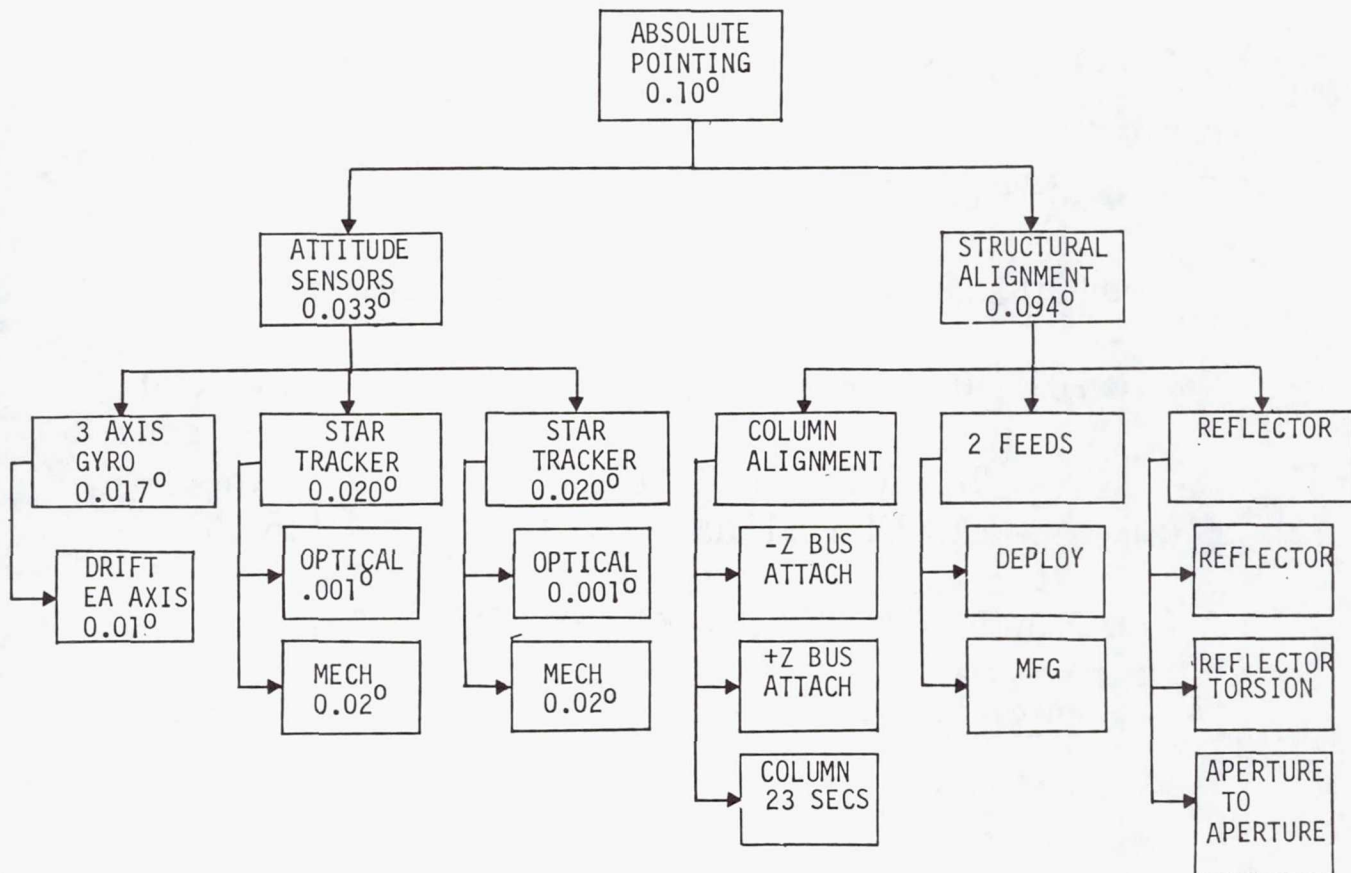
STRUCTURE

The hoop column structural elements consist of the bus, boom and reflector. The major interfacing and sizing requirements are shown below. Because of the nature of the concept the usual approach of specifying a structural stiffness high enough to minimize response/exciting problems can't be used. The expected first mode frequency will be less than 1 Hz and the challenge is to design and control this type structure to satisfy the system/mission requirements.

- MINIMUM FREQUENCY: TBD
- ABSOLUTE POINTING: 0.085°
- MESH CONTOUR: 12 MM RMS (INCLUDING DYNAMIC EFFECTS)
- LOADS CRITERIA: STOWED - SHUTTLE LAUNCH
DEPLOYMENT - DYNAMICS
DEPLOYED - STATION KEEPING
- FEED TO REFLECTOR POSITIONING DURING ANY 10 MIN. PERIOD
 - DESPACE (DISTANCE) ± 10 CM
 - DECENTER (LATERAL) ± 6.6 CM
 - TILT (FEED ONLY) $\pm 0.3^{\circ}$
- WEIGHT: 2618 LBS

LMSS HOOP COLUMN
ABSOLUTE POINTING ERROR BUDGET

The error budget to provide 0.10° absolute pointing is shown. The allocation to attitude control sensor mounting is 0.033° , leaving 0.094° for structural elements. Considering the boom and reflector only the allocation is 0.085° (removing structural alignment of the feed). The significant element within this is the requirement that the ends of each column segment be parallel within 0.015° . Usual manufacturing tolerance for optically aligned structures of this type is 0.02° . Reducing the tolerance will be difficult to realize and may require ground demonstration or adjustment on orbit.



HOOP COLUMN SUBSYSTEM REQUIREMENTS

ATTITUDE CONTROL

The significant requirements on the attitude control subsystem are the continuous pointing stability of 0.03° coupled with the low structural frequency (probably <0.5 Hz) and the requirement for 10 years of North/South station keeping. Before more definitive subsystem requirements and design solutions can be developed, the structural response characteristics and disturbance inputs must be defined. The attitude control analysis essentially runs one iteration behind the design process since they need all the geometry, mass properties and structural data to initiate their work. The attitude control analysis of this configuration is in work and will be reported separately.

- 10 YEAR LIFE
- POINTING STABILITY OF 0.02° CONTINUOUS
- POSITION OF FEED RELATIVE TO REFLECTOR DURING CALL

DISTANCE FEED TO REFLECTOR	± 10 CM
LATERAL POSITION	± 6.6 CM

- PROVIDE FOR BOTH E/W AND N/S STATION KEEPING
- SUBSYSTEM WEIGHT 2885 LBS

HOOP COLUMN SUBSYSTEM REQUIREMENTS

ELECTRICAL POWER

The electrical subsystem is a typical state of the art design with the exception of the requirement of accommodating shadowing. Extremely long masts/booms would be required to keep the solar panels constantly in the sun. This results in significant solar pressure torques, weight, cost, complexity and packaging problems. Therefore the solar panels must be designed: (1) to perform in a "soft" shadow condition (sun through the mesh) reducing the solar energy about 5%; and (2) to survive full or "hard" shadow impingement from structural/mechanism members for short durations. A detail design analysis will be required.

SOLAR PANELS

- 10 YEAR LIFE, 10 KW BOL
- 5% SOFT SHADOWING (SUNLIGHT THROUGH THE MESH)
- HARD SHADOWS 4" WIDE (STRUCTURAL MEMBERS)
- SOLAR PANEL WEIGHT: +Z BUS 340 LBS (INCLUDES MAST AND DRIVE)
 -Z BUS 167 LBS (INCLUDES MAST AND DRIVE)
- VOLTAGE 28 VDC \pm ?

BATTERIES

- 10 YEAR LIFE
- 50% SYSTEM MAX DUTY CYCLE DURING ECLIPSE - 30 MIN.
- 80% DEPTH OF DISCHARGE
- MAY BE USED TO SUPPLEMENT SEVERE SHADOWING PERIODS
- WEIGHT: +Z BUS 212 LBS (BATTERIES AND POWER CONDITIONING)
 -Z BUS 83 LBS (BATTERIES AND POWER CONDITIONING)

LSST/LMSS CONFIGURATION STUDY
CONCLUSIONS TO DATE

The conclusions to date on the LSST/LMSS configuration study are presented below. One additional point (perhaps not a conclusion) should be added. The cooperation and support of all the participants has been excellent. Without the exhibited team cooperation among all the companies and agencies the study may well have floundered and accomplished little if anything.

- BOTH ANTENNA CONCEPTS CAN BE CONFIGURED TO SUPPORT THE LMSS MISSION AS POSTULATED
- SIGNIFICANT REQUIREMENTS/DESIGN DEVELOPMENT HAS BEEN COMPLETED
- ADDITIONAL WORK SHOULD BE ACCOMPLISHED IN THE AREAS OF:
 - FEED DESIGN
 - ATTITUDE CONTROL SUBSYSTEM DESIGN
 - THERMAL DISTORTION ANALYSIS
 - MASS PROPERTIES DEFINITION
 - SYSTEM/SUBSYSTEM DEFINITION

CONFIGURATION DEVELOPMENT OF THE
LAND MOBILE SATELLITE SYSTEM (LMSS) SPACECRAFT

CONCLUSIONS

C. T. Golden, J. A. Lackey, and E. E. Spear
Boeing Aerospace Company
Seattle, Washington

Large Space Systems Technology - 1981
Third Annual Technical Review
November 16-19, 1981

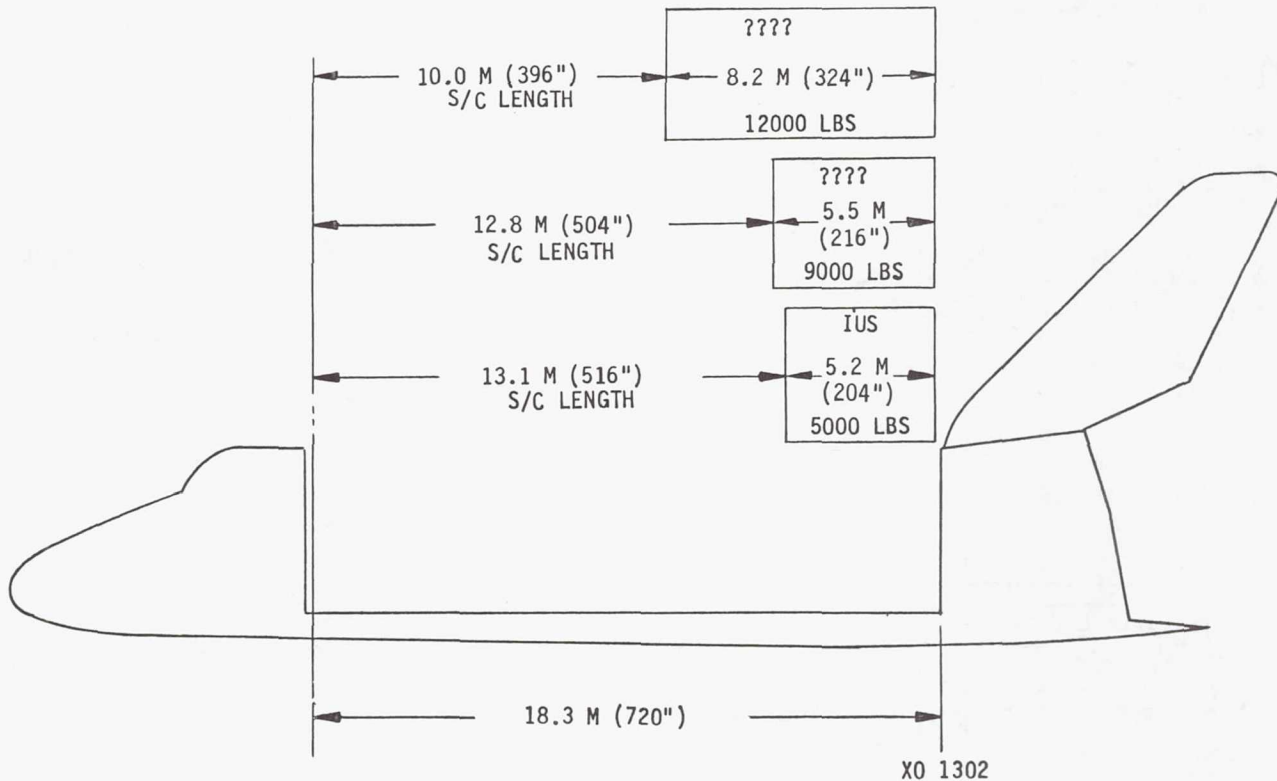
LSST ANTENNA DEVELOPMENT CONCLUSIONS

We feel the study results indicate that both antenna designs are feasible to support an LSST/LMSS mission. They may or may not be practical depending upon the availability of a transfer vehicle with adequate capability. Two development problems exist. The feeds proposed for both designs have yet to be built and proven. Some RF component breadboard testing is proposed in 1982. Since the viability of the program using large space structures depends on the UHF RF system, the importance of this development work cannot be emphasized too much. The second development area is the total aspect of attitude control of a structure as big and soft as those proposed. Pointing, stability, station keeping, weight and the 10-year life all contribute to the technical complexity of this attitude control subsystem. We feel at least one more design iteration is needed to improve (1) mass properties definition, (2) structural models, and (3) attitude control subsystem definition.

- AN LSST/LMSS MISSION CAN BE SUPPORTED BY BOTH CONFIGURATIONS
- THREE AREAS REQUIRING DEVELOPMENT ARE:
 - AVAILABILITY/CAPABILITY OF AN ORBIT TRANSFER VEHICLE
 - UHF FEED TECHNOLOGY
 - ATTITUDE CONTROL ANALYSIS & DESIGN
- TECHNICAL PROBLEMS
 - ABSOLUTE POINTING OF 0.10° IS QUESTIONABLE WITHOUT GROUND TEST OR ON ORBIT ADJUSTMENT
 - POINTING STABILITY OF 0.03° IS QUESTIONABLE CONSIDERING THERMAL DISTORTIONS AND DYNAMIC DISTURBANCES
- ADDITIONAL CONFIGURATION DESIGN ITERATIONS ARE NECESSARY

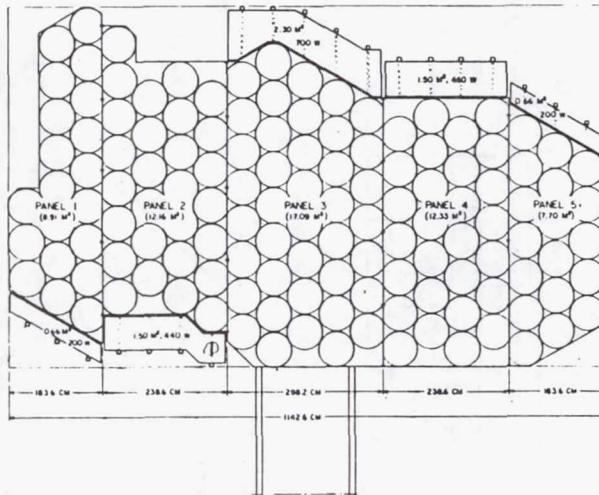
STOWAGE VOLUME SPACECRAFT AND TRANSFER VEHICLE

The IUS with its 2273 kg (5000 lb.) capability to geosync cannot support either of the proposed LMSS spacecraft missions. At this time we do not know of any firm plans for increased capability stages in the 1990 time frame (really rather near term). If the LMSS is to be flown in today's configuration, a transfer vehicle of 4545 kg (10,000 lb.) capability with a length less than 7.62 m (300 in.) is required for the wrap rib and a 5000 kg (11,000 lbs.) capability with a length less than 8.5 m (335 in.) is required for the hoop column.



FEED ASSEMBLY TECHNOLOGY DEVELOPMENT AREAS

The proposed feed for the wrap rib LMSS is shown, but the technology development required applies to the hoop column feed and partially to the S-band feeds for both. There is a high degree of confidence that the concepts proposed and the work accomplished will lead to viable design solutions. But the criticality of the feed size, weight, hinging, packaging and performance with respect to the total system cannot be overstated. If the LMSS is going to work in this size configuration, the feed concepts must be developed and verified early.

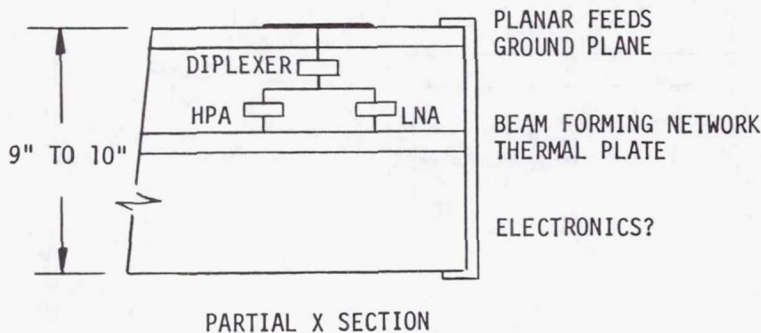


● RF DESIGN

- FREQUENCY/POLARIZATION PLAN
- RADIATING ELEMENTS
- BEAM FORMING NETWORK (BFN)

● STRUCTURAL/MECHANICAL DESIGN

- DEPLOYMENT
- HINGE LINES
 - COAXIAL CABLE RUNS
 - BFN
- WEIGHT
- THERMAL CONTROL



CONTROL SUBSYSTEM

The attitude control subsystem for both configurations is based on today's technology but involves a rather sophisticated application. The pointing stability requirement of 0.02° (0.022° for thermal distortions to make 0.03°) combined with the comparatively low structural frequency and large size results in a need to control both ends of the configuration. The requirement for absolute pointing of 0.10° requires tight if not impractical structural alignment of feeds, booms and reflectors. This may lead to a requirement for on orbit spatial sensing and adjustment capability. A control concept has been proposed and supporting analysis must be completed to verify the design solution.

- IDENTIFIED THE NEED FOR TWO POINT CONTROL (SPACECRAFT AND WRAP RIB HUB OR SPACECRAFT AND OPPOSITE END OF COLUMN)
- GROUND TEST NOT PRACTICAL, SO FABRICATION & ASSEMBLY CRITICAL IN OBTAINING ABSOLUTE POINTING OF $< 0.10^\circ$
- MAY NEED TO SENSE AND ADJUST CRITICAL SPATIAL PARAMETERS ON ORBIT
- MUST CONTROL SPACECRAFT FROM PLACEMENT ON ORBIT THROUGH DEPLOYMENT AND OPERATIONAL LIFE (ORDERS OF MAGNITUDE CHANGE IN INERTIA PROPERTIES)
- LOCATION AND ORIENTATION OF THRUSTERS CRITICAL WITH RESPECT TO GAS IMPINGEMENT ON MESH AND STRUCTURAL ELEMENTS

TRADES AND ANALYSIS THAT SHOULD BE CONDUCTED

The effort to date can best be characterized as a preliminary system design. Technology developments were assessed, configuration drivers were studied and supporting subsystems identified and described. Each iteration led to better descriptions and more definitive requirements. At this time we are confident that both antenna concepts can be developed into a spacecraft that can satisfy the LMSS mission requirements. At this time we are less sure about several details; these should be subject to further study. The mass properties are a mixture of weights of similar things, guesses, and conservative estimates. Since this is part of a most critical interface with the transfer vehicle, they should be further refined. The RF concept for both feeds seems viable, but the mechanical design of the feed with respect to hinging, cabling, structures and mechanisms is too preliminary. The attitude control subsystem is a sophisticated application of today's technology with less than a full appreciation of what that degree of sophistication fully means in weight, power, performance, etc. The studies cited below would all have a significant input to further definition of Large Space Systems Technology development and the practicality of an LSST/LMSS in the 1990's.

- SUBSYSTEM PRELIMINARY DESIGN ITERATION
- MASS PROPERTIES UPDATE BOTH CONFIGURATIONS
- THRUSTER POINTING VS. DEPLOYABLE BOOMS
- STRUCTURAL MODEL UPDATE
- PRELIMINARY MECHANICAL DESIGN OF THE FEEDS
- ATTITUDE CONTROL SUBSYSTEM UPDATE
- THERMAL DISTORTION ANALYSIS
- RF TOLERANCE ANALYSIS
- FEASIBILITY OF UPDATING ABSOLUTE POINTING FROM GROUND
- FEASIBILITY AND CONCEPT FOR ON ORBIT POINTING AND STABILITY CONTROL
- FEASIBILITY AND BENEFITS OF PARTIAL ZERO "G" DEPLOYMENT DEMONSTRATIONS

LIST IS ESSENTIALLY PRIORITIZED
TOP TO BOTTOM

LAND MOBILE SATELLITE SYSTEM (LMSS)

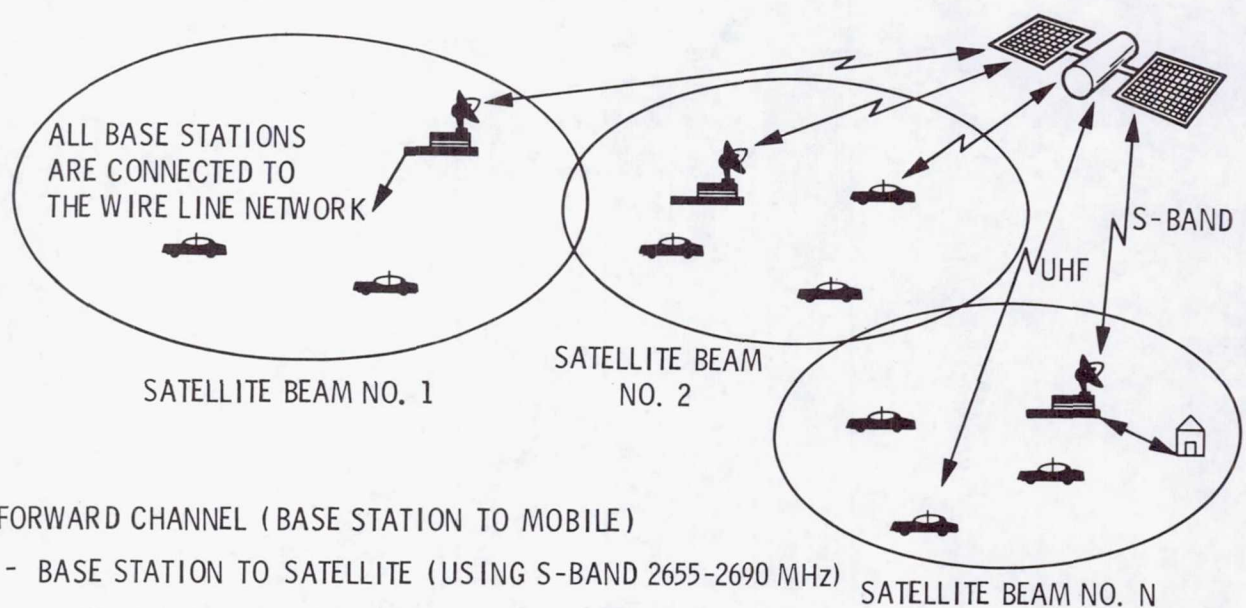
Single Aperture System Design

W. J. Weber, III
Jet Propulsion Laboratory

Large Space Systems Technology - 1981
Third Annual Technical Review
November 16 - 19, 1981

LMSS SYSTEM ARCHITECTURE

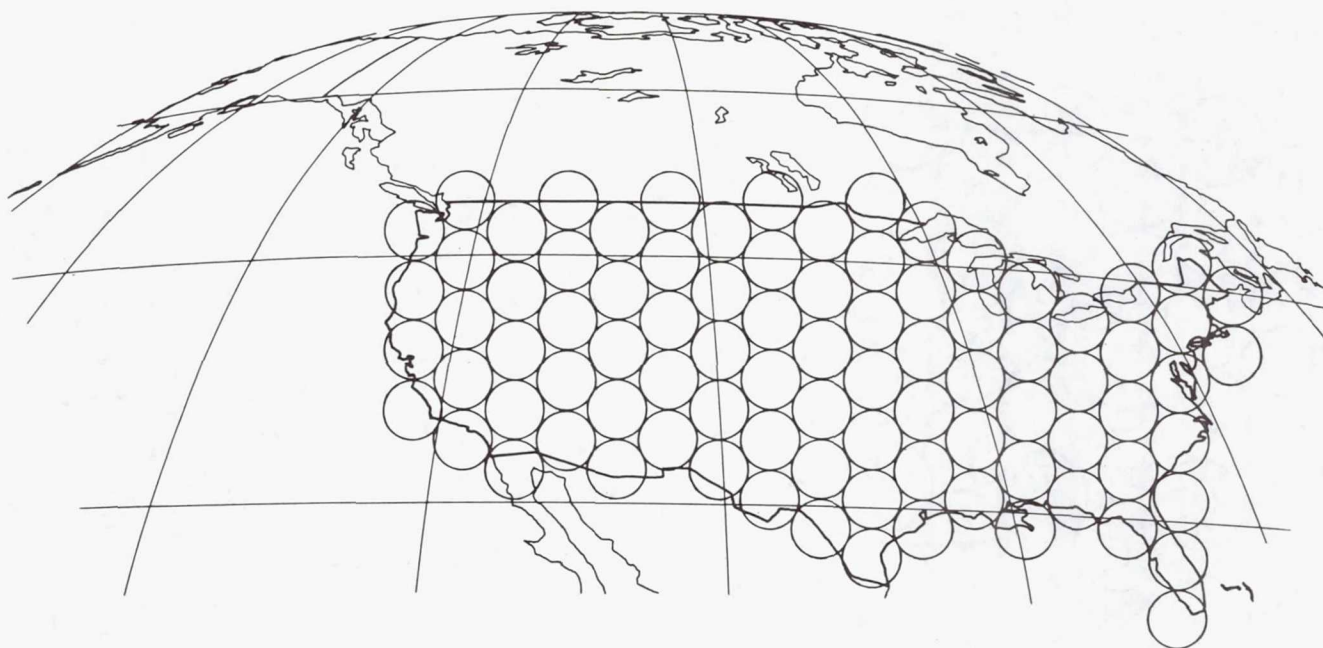
The satellite in the land mobile satellite system (LMSS) acts as a "repeater in the sky". Voice signals from simple mobile transceivers are transmitted to the satellite at UHF. These signals are received by the satellite's large multiple beam antenna, are translated in frequency by a satellite transponder to an S-band frequency, and then retransmitted through the satellite's smaller S-band antenna to the base station located closest to the mobile vehicle. The base station completes the telephone connection by routing the signals into the regular telephone network. The voice signals in the other direction (to the mobile vehicle) follow the same path in reverse, that is, from the telephone network to the base station, to the satellite at S-band, and finally back to the mobile at UHF. Communications between two mobile units served by the satellite system requires a "double-hop", that is, from one mobile through the satellite to the base station and then back through the satellite to the other mobile.



- FORWARD CHANNEL (BASE STATION TO MOBILE)
 - BASE STATION TO SATELLITE (USING S-BAND 2655-2690 MHz)
 - SATELLITE TO MOBILE (USING UHF 866-876 MHz)
- REVERSE CHANNEL (MOBILE TO BASE STATION)
 - MOBILE TO SATELLITE (USING UHF 821-831 MHz)
 - SATELLITE TO BASE STATION (USING S-BAND 2550-2585 MHz)

UHF BEAM LAYOUT

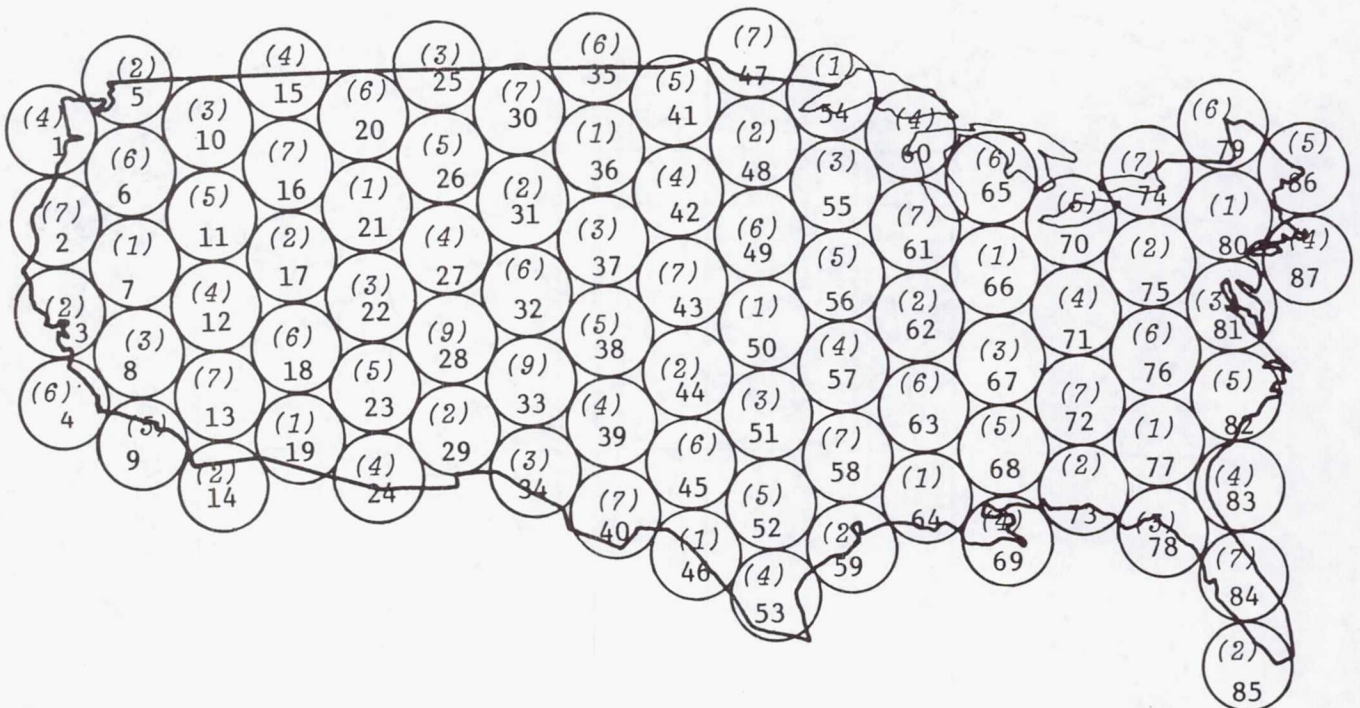
The large size of the UHF antenna on the satellite provides two advantages with respect to the LMSS system design. First of all, it provides tremendous gain for both transmitting and receiving at the satellite. This enables very simple, low power equipment in the mobile vehicle. In fact, the mobile equipment will be nearly identical to the equipment now being developed for the new cellular mobile radiotelephone systems. The second advantage of the large antenna is that beams produced by it have narrow beamwidths. This means that with multiple antenna feeds a large number of beams can be produced. Thus, a given number of frequency channels can be reused many times due to the geographic separation of the beams. This frequency reuse implies a corresponding increase in the capacity of the system and a larger number of potential customers. The UHF antenna for this study was selected to have an aperture of 55 meters. This implies a beamwidth of roughly 0.45 degree and requires 87 beams to cover the contiguous 48 states (CONUS) as shown. Depending on assumptions about frequency allocation, signal bandwidth, and other factors, this system can serve hundreds of thousands of mobile subscribers located anywhere in CONUS.



FREQUENCY PLAN FOR UHF BEAMS

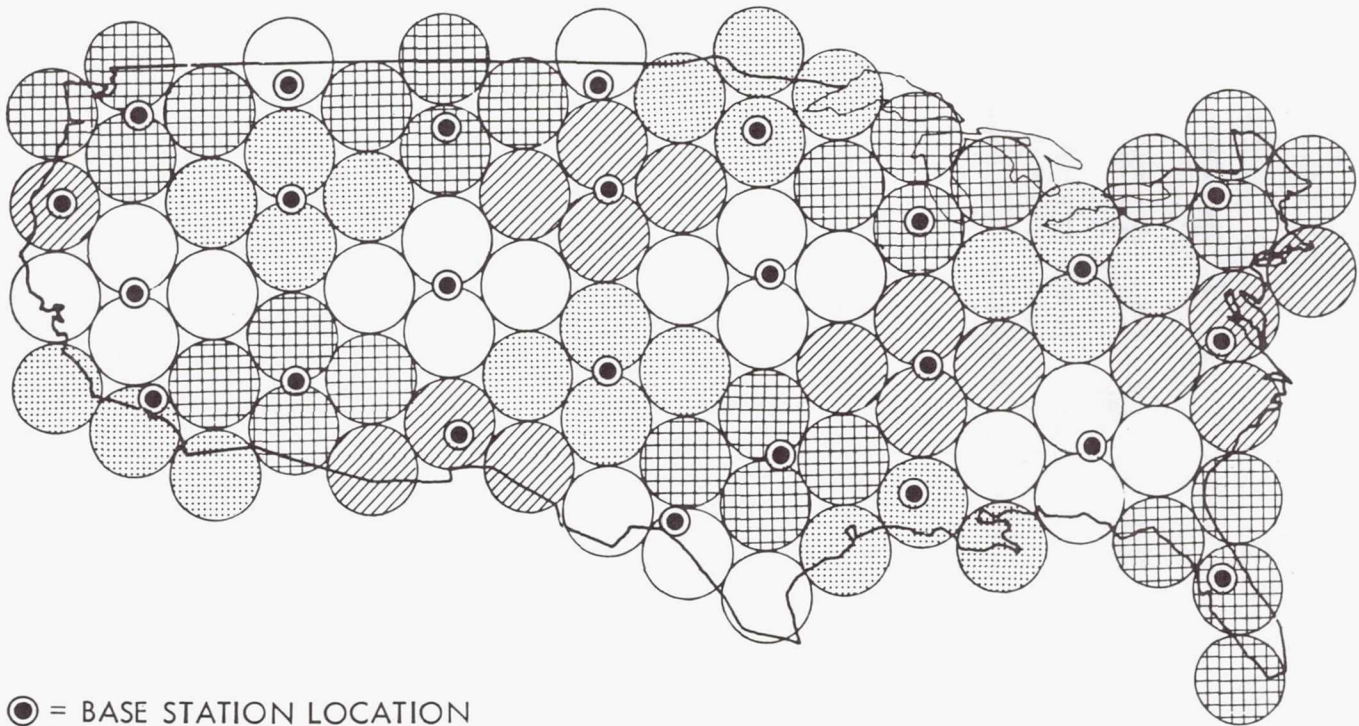
The diagram shows the UHF beams numbered from 1 to 87. The number in parentheses represents the frequency sub-band assigned to each beam. Thus, each beam with the number (4) means that the same frequencies are reused within each of these beams. The multiple beam antenna must be designed in such a way that the beams using the same frequencies do not substantially interfere with each other. Interference is reduced in two ways. The first is the geographical separation of the beam footprints. This can be accomplished by increasing the number of frequency sub-bands. However, this also reduces the effective frequency reuse and hence the capacity of the system. The second method for reducing interbeam interference is to reduce the individual beam sidelobes. Low sidelobe control is a function of many interrelated antenna design parameters and techniques. The number of frequency sub-bands chosen for this study was seven. This is a compromise between the desire for high frequency reuse and what is a practical and achievable antenna design relative to sidelobe control. The diagram below shows beam 71 and all the co-frequency beams of frequency sub-band (4) which interfere with it. The ring of co-frequency beams closest to beam 71 will dominate the co-channel interference received in beam 71.

Another frequency plan seriously considered for this study consisted of 4 frequency sub-bands with the addition of dual polarization. This plan provides greater system capacity; however, the satellite antenna feed design problems are much more significant. Future development work will determine the viability of this concept.



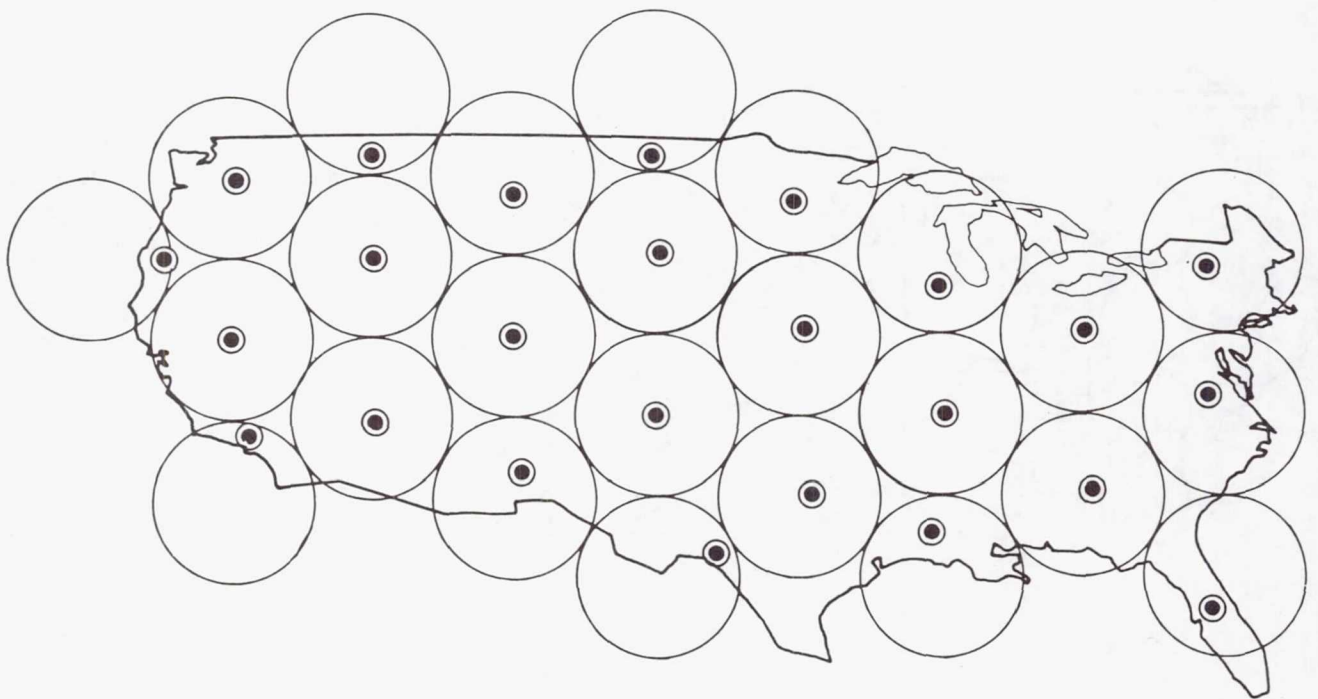
UHF BEAM AND BASE STATION RELATIONSHIP

The number of base stations is a function of the economics of the system design. A great number of base stations reduces the number of long distance telephone charges between the base station and the party at the fixed location. However, these base stations are expensive. Having few base stations reduces the initial capital expenditure but implies a greater number of long distance charges to the user. For this study one base station provides service for four UHF beams as shown in the coverage pattern. This requires a total of 25 base stations for CONUS coverage.



S-BAND BACKHAUL BEAM LAYOUT

Because the bandwidth available at S-band is restricted to 35 MHz for the uplinks, it is necessary to employ frequency reuse to provide an effective increase in bandwidth through the use of a multiple beam antenna. The diagram shows the beam footprints from a 10 meter S-band satellite antenna providing coverage to the 25 base stations. The beamwidth of the individual beams is 0.9 degree and a frequency reuse pattern of 4 sub-bands is employed.



● = BASE STATION LOCATIONS

IMPLICATIONS OF INTERBEAM ISOLATION REQUIREMENT

As discussed in the frequency reuse plan, low interference between co-frequency beams is primarily a function of the sidelobe control of the beams. One factor influencing the sidelobe levels is the edge taper of the feed pattern as it illuminates the main aperture. Low sidelobe control requires a high degree of edge taper. The high edge taper in effect implies a feed element with a narrow beamwidth and a resultant high gain. This means that to produce such feed patterns a relatively large feed element must be employed.

STRINGENT BEAM ISOLATION REQUIREMENT



LOW SIDELOBES



HIGH EDGE TAPER



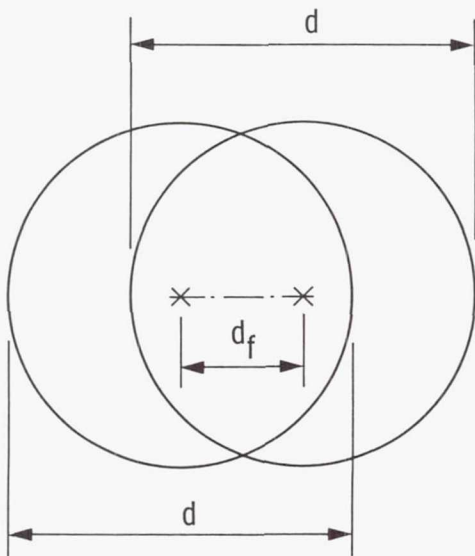
HIGH GAIN FEED ELEMENTS



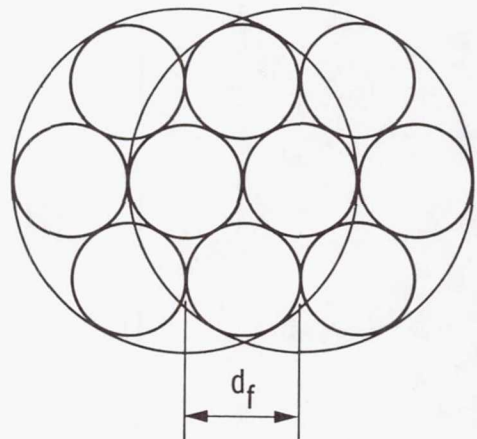
FEED WITH LARGE APERTURE

NEED FOR CLUSTER FEED

The requirement for large feed elements to produce low sidelobes presents an additional feed design problem. In order to produce beams with 3 dB footprints which are contiguous in the coverage area, the large feed elements on the satellite must physically overlap as shown in the left diagram. To resolve this physical impossibility, each feed element can be decomposed into 7 smaller elements. The adjacent beam's feed can be formed by 7 similar feed elements; however, it is necessary to share some of the elements with adjacent beams as shown in the right diagram. Thus, each beam's feed is composed of 7 feed elements and each of these individual feed elements can be associated with as many as 7 beams.



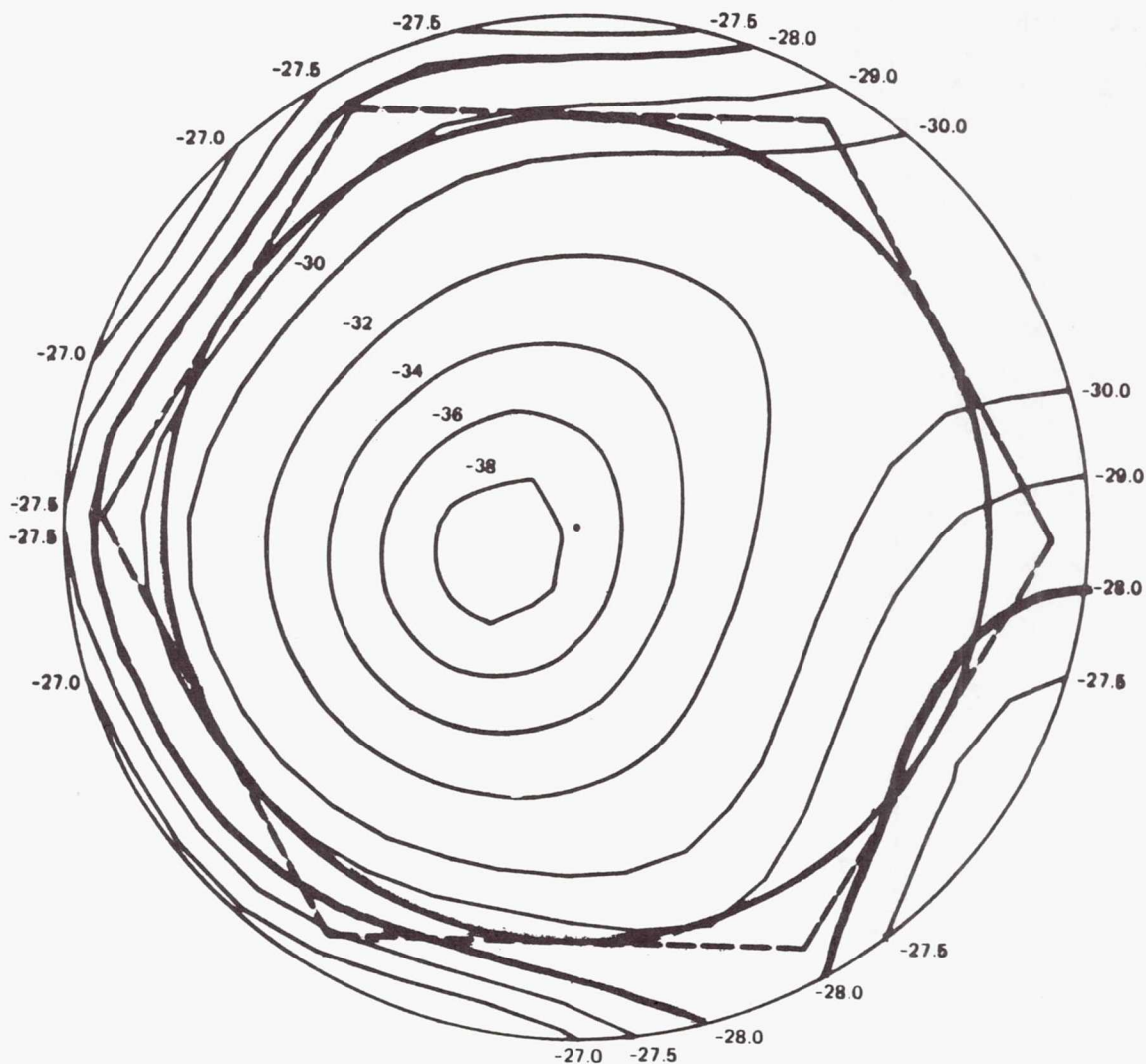
TWO OVERLAPPING SINGLE FEEDS
(PHYSICALLY IMPOSSIBLE)



TWO OVERLAPPING 7 ELEMENT CLUSTER FEEDS
(4 COMMON ELEMENTS)

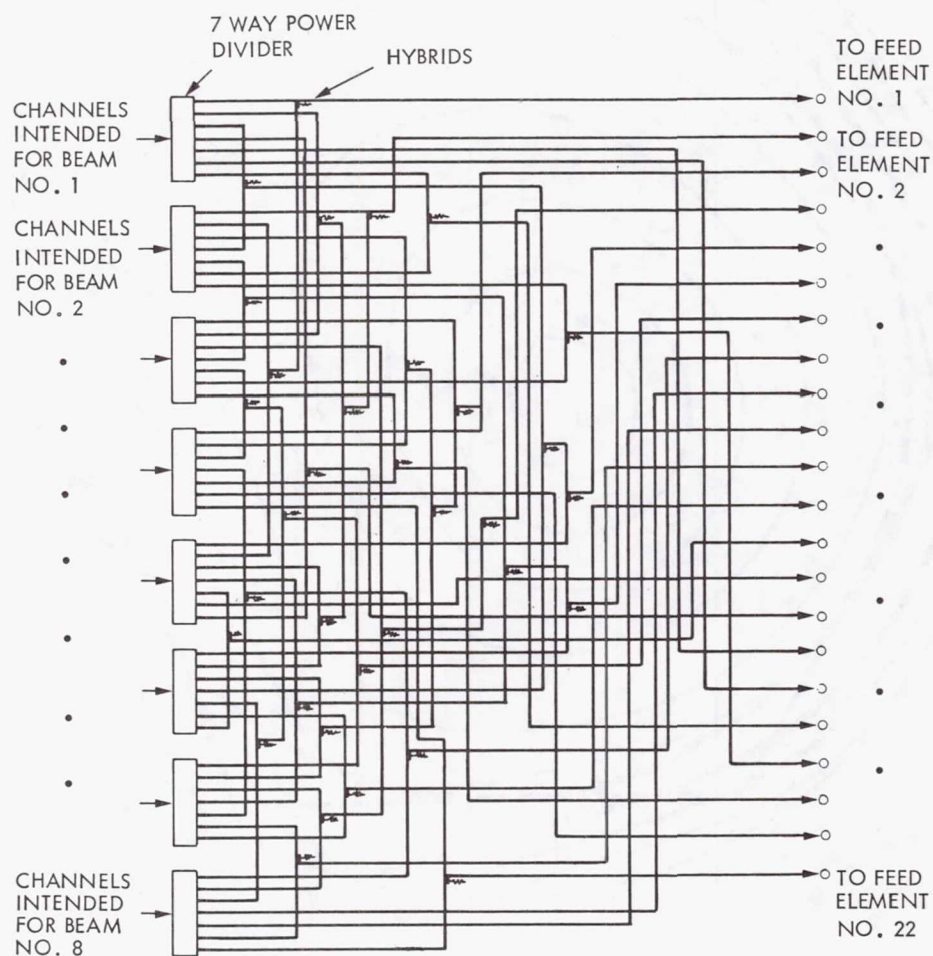
BEAM ISOLATION PERFORMANCE

The real measure of the multiple beam antenna's performance is the beam isolation level. Beam isolation represents the total amount of interference which can be expected from the summation of all interfering co-frequency beams. (This is not merely a gain plot of one interfering beam.) The figure below shows the beam isolation contours for the footprint of beam No. 71. This beam is one of the beams most affected by co-channel interference because the interfering beams have higher sidelobes due to their large scan angle off boresight. Most of the interference comes from the first ring of interfering beams which as previously shown includes beams 57, 60, 69, 83, and 87. For the antenna system design used in this study, the worst case isolation within beam 71 is roughly -28 dB which is well within the requirement of -25 dB.



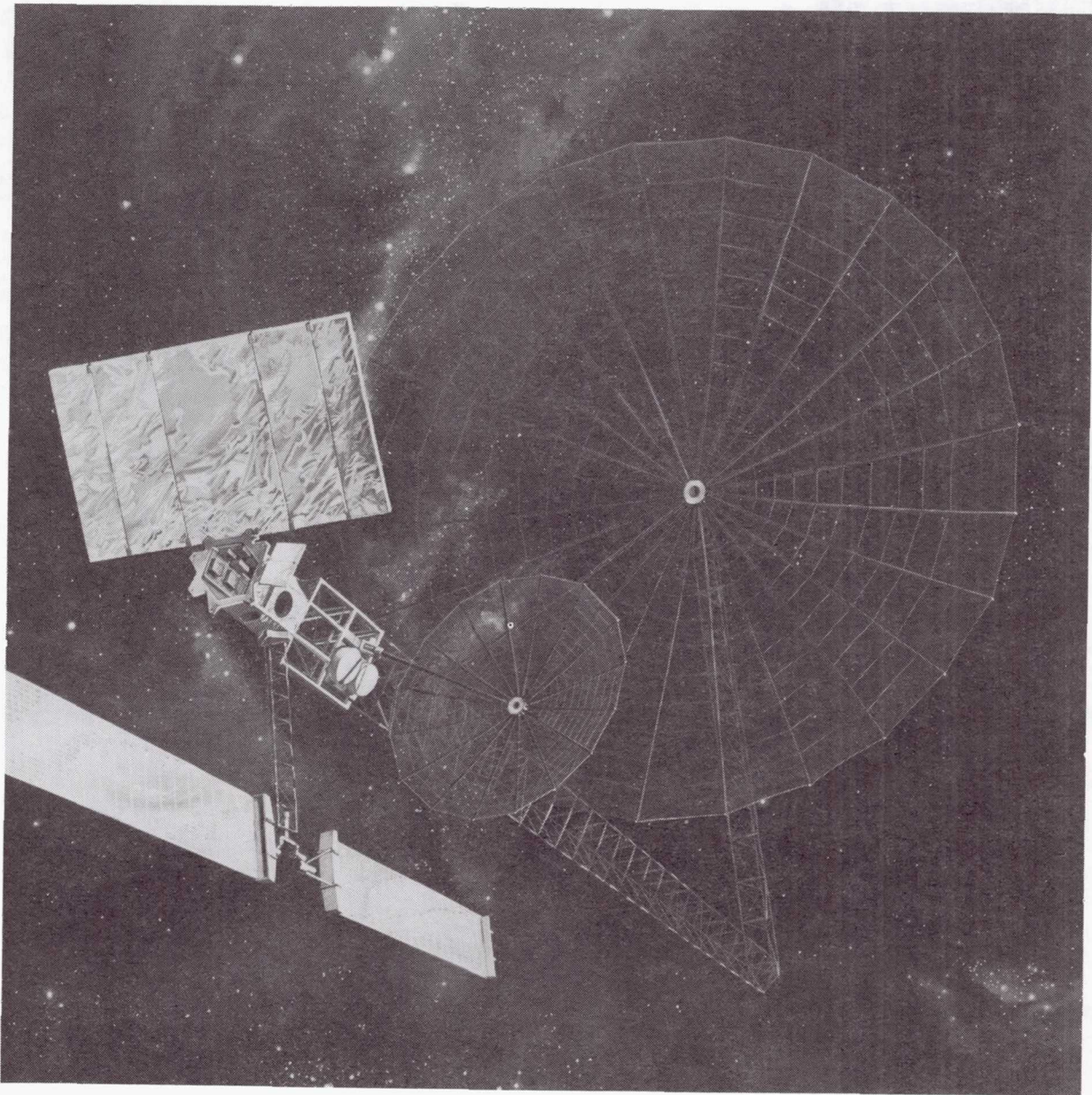
BEAM FORMING NETWORK SCHEMATIC

The beam forming network (BFN) distributes the signals for each beam to the appropriate feed elements. It is composed of power dividers, combiners, and the necessary interconnection circuitry. The example shown below is the entire BFN for an eight beam feed system. In this case the signals for the eight beams are distributed to 22 feed elements. Each signal is distributed to exactly 7 elements. Because of the small number of beams, (i.e. 8) the largest number of signals distributed to a given feed element is five, as is the case for feed element No. 2 which receives signals associated with beams 1, 2, 3, 5, and 6. In the 87 beam case used in this study a total of 134 feed elements is required. Many of these elements are associated with 7 beams. The BFN in this case consists of 87 7-way power dividers and a large number of two-way combiners. Because a signal for a particular feed element can go through as many as three two-way combiners, each with as much as 3 dB in signal loss, it is necessary to locate the RF power amplifiers after the BFN. Thus, a total of 134 amplifiers, one for each feed element, is required.



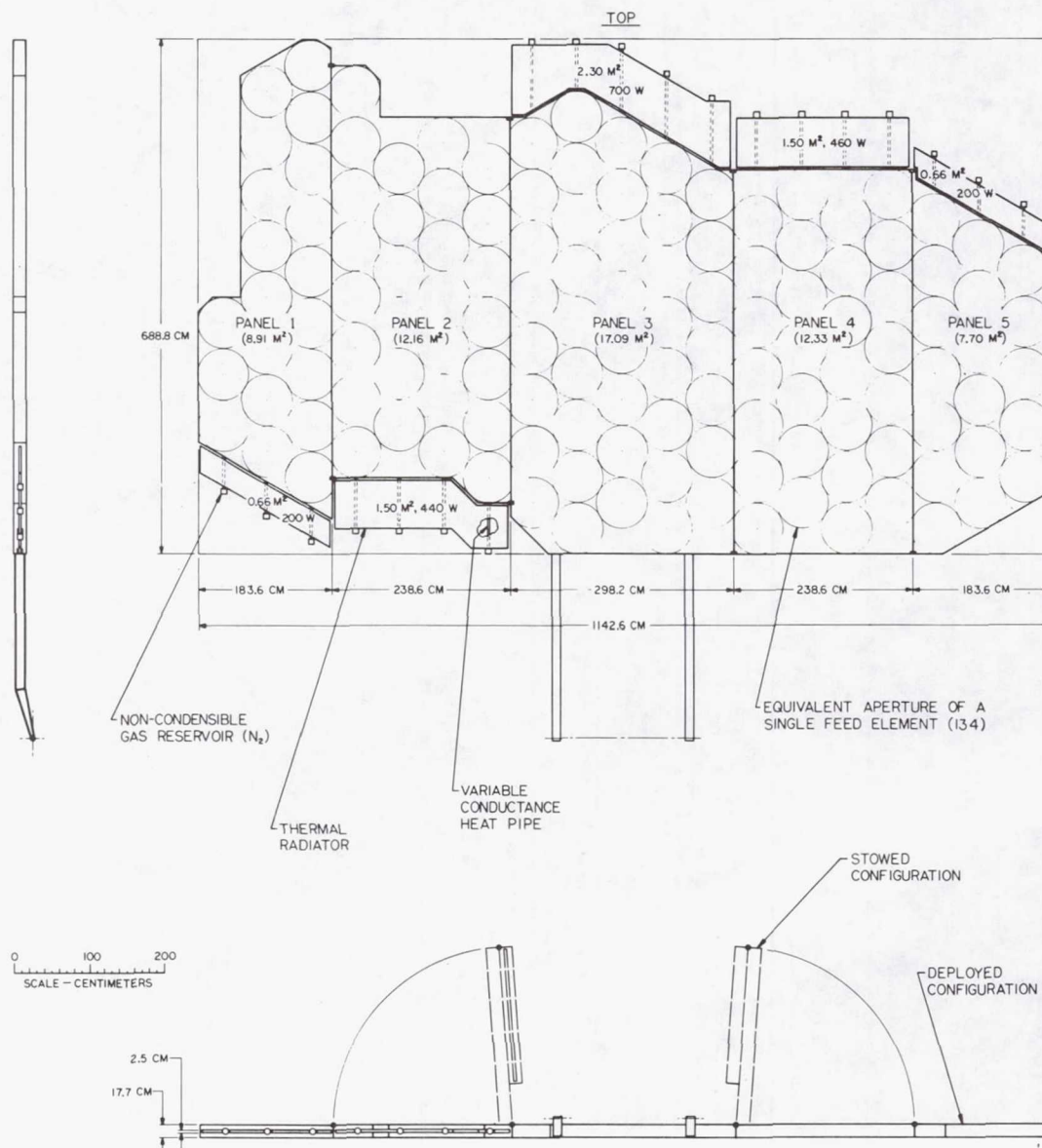
LMSS SPACECRAFT

The configuration as shown includes the single aperture 55-meter UHF antenna. The shorter vertical boom is approximately 35 meters and the longer boom, pointing to the Earth's center, is about 85 meters. The large panel in the upper left is the UHF planar feed array and is approximately 70 square meters in area. The 10-meter S-band backhaul antenna is shown in the center of the picture and its multi-beam feed is located on the right side of the spacecraft bus.



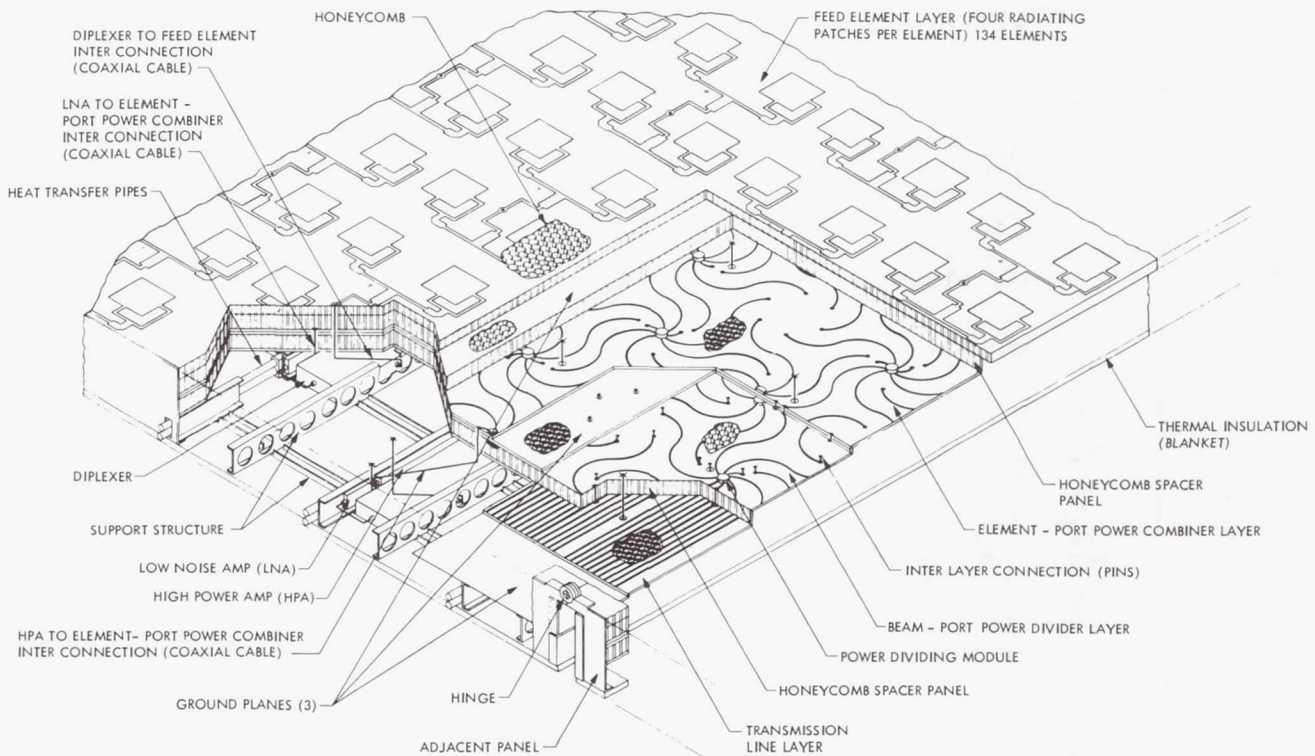
UHF FEED ARRAY ASSEMBLY

The UHF feed array assembly is located at the focal point of the MSAT UHF reflector. As shown, the assembly is 6.9 m by 11.4 m. A structure of this size will not fit within the Shuttle payload envelope and therefore must be folded into 5 sections. The assembly thickness must be less than 25 cm. The figure shows the manner in which the feed assembly is deployed and how it is folded in the stowed condition. The circles schematically show the location of the 134 feed elements. Thermal radiators are shown at the ends of each panel and are used to dissipate the excess heat from power amplifiers located in the feed assembly structure.



FEED PANEL ASSEMBLY CONCEPTUAL DESIGN

The feed array assembly includes the following major subassemblies: the feed elements; the beam forming network; the RF electronics, including the power amplifiers, low noise amplifiers, and duplexers; the thermal control system; and the structure. The top layer of the assembly contains the feed elements with each feed element consisting of a four patch sub-array. The feed layer consists of foil patches supported by a fiberglass skin which in turn is separated from a ground plane by 1.8 cm thick honeycomb. Next, there is a 2.5 cm thick honeycomb isolating layer separating the feed layer from the beam forming network (BFN). The BFN consists of two back-to-back microstrip boards each constructed of 0.32 cm thick honeycomb dielectric and covered with 0.013 cm thick fiberglass printed circuit board skins. Another 2.5 cm thick honeycomb isolating layer separates the beam forming network and the transmission line layer. The transmission line layer, also made of printed circuit board and honeycomb, connects the individual beam ports on the BFN to cables at the lower edge of the feed array assembly which in turn connect to the bus-located electronics. A series of channels run parallel to the panel rings to provide additional structure and support for the RF electronics. Mounted between the channels are the power amplifiers, low noise amplifiers, and duplexers. The amplifiers are connected via a heat sink to heat transfer pipes which run along the channels and transport the waste heat to remote radiators located at either end of each feed assembly panel. The last layer consists of a thermal blanket that covers the backside of the feed array assembly.



FEED ASSEMBLY WEIGHT BREAKDOWN

ITEM	WEIGHT Kg
Radiating Elements	113
R.F. Electronics	305
Power Amplifiers	122
Low Noise Amplifiers	31
Diplexers	152
Beam Forming Network	244
Cables	120
R.F.	61
D.C.	59
Thermal Control Hardware	232
Heat Radiators	72
Heat Transfer Pipes	69
Heat Sink Flanges	91
Structure	156
Total	1170

QUAD APERTURE RF DEFINITION

P. Foldes
General Electric Company
Space Systems Division
Valley Forge, PA

Large Space Systems Technology - 1981
Third Annual Technical Review
November 16-19, 1981

REQUIREMENTS FOR LAND MOBILE SATELLITE SYSTEM (LMSS)

In order to provide a better focus for the development effort of large space structures a number of early mission applications have been identified. Among these the Land Mobile Satellite System (LMSS) represented the most pressing requirement; thus it was selected as a point design for the 1981 LSST development effort.

Table 1 summarizes the main assumptions for the requirements of the overall communication system and its launch vehicle. It is stipulated that the system must serve a total of appr. 250,000 mobile telephone channel users within the 48 states and the space segment for this overall capacity must be placed into operation by a single STS flight. Due to the volume and weight of the spacecraft which can meet such a requirement no present LEO to GEO transportation system is available, but it appears that this part of the mission is technically feasible by some derivative of a wide-body Centaur vehicle.

OVERALL SYSTEM

START OF OPERATION
LIFETIME
MAXIMUM USER CAPACITY (NOMINAL)
BLOCKING PROBABILITY
DISTRIBUTION OF USERS
 INITIAL
 EVENTUAL
COMPATIBILITY WITH ATT CELLULAR SYSTEM
 INITIAL
 EVENTUAL
ECLIPSE CAPABILITY
TRANSPONDER TYPE
ORBIT
NOMINAL SLANT RANGE
POLARIZATION
COVERAGE AREA
POINTING ACCURACY

1995
10 YEARS
250000
p = .02

UNIFORM (WITHOUT VOX)
POPULATION DENSITY RELATED (WITH VOX)

YES
NOT WITH PRESENT CELLULAR SYSTEM
20%
NONSWITCHING (BENTPIPE)
GEO SYNCH. 110° LONG
R = 36800 KM
CP
US 48 STATES
.03° PEAK

LAUNCH VEHICLE

EARTH TO LEO
LEO TO GEO

STS
TBD*

*POTENTIAL VEHICLE MAY PROVIDE FOLLOWING GEO PAYLOAD
LIMITS: 6350 KG/9.75 M TO 4082 KG/12.76 M.

Table 1

FREQUENCY ASSIGNMENTS FOR LMSS

The frequency assignments for the system (Table 2) utilize the UHF band for the mobile user to satellite up and downlinks and S-band for the satellite to fixed base station up and downlinks. The fixed users and the base stations are connected via the existing telephone network. It is assumed that one 10-MHz band each is available for the UHF up and downlink, and these bands are not shared with other communication systems. For S-band, 4 times larger bandwidth is assumed. The communication format is compatible with ATT's contemplated cellular system. The satellite based mobile communication system is providing a service for those residual (remote) mobile users who cannot be served economically by the land based cellular system.

MOBILE TO SATELLITE	821 - 831 MHz
SATELLITE TO BASE STATION	2550 - 2590 MHz
BASE STATION TO SATELLITE	2650 - 2690 MHz
SATELLITE TO MOBILE	866 - 876 MHz
MAX. AUDIO FREQUENCY	$B_A = 3.4 \text{ KHz}$
IF NOISE BANDWIDTH	$B_{IF} = 25 \text{ KHz}$
CARRIER SEPARATION	$B_O = 30 \text{ KHz}$
ALLOCATION BAND SUBDIVISION	$K = 4$
UHF BANDWIDTH PER BEAM	$B_{BU} = 2.5 \text{ MHz}$
S-BAND BANDWIDTH PER BEAM	$B_{BS} = 10 \text{ MHz}$
UHF CHANNELS PER BEAM	$M_U = B_{BU}/B_O = 83$
UHF VOICE CHANNELS PER BEAM	$V_U = 81$
UHF SIGNALING CHANNELS PER BEAM	$S_U = 2$
S-BAND CHANNELS PER BEAM	$M_S = 332$
S-BAND VOICE CHANNELS PER BEAM	$V_S = 324$
S-BAND SIGNALING CHANNELS PER BEAM	$S_S = 8$
CHANNEL DESIGNATIONS, UHF	
SET 1	1,5,...329
SET 2	2,6,...330
SET 3	3,7,...331
SET 4	4,8,...332

Table 2

BEAM TOPOLOGY AND EIRP CHARACTERISTICS FOR THE LMSS SYSTEM

Table 3 displays the basic characteristics of the beam topologies and EIRP G/T requirements. In order to provide the necessary user number capability, 91 UHF component beams (cells) were selected to cover the 48 states. This results in $\alpha_u = .423^\circ$ cell size. The corresponding S-band cell number is 23 with $\alpha_s = 1^\circ$ cell size. In order to provide adequate isolation between cells using the same frequency and polarization the overall 10 MHz UHF allocation bandwidth is divided into four 2.5-MHz-wide subbands. Both polarizations are used for these subbands creating a total of 8 independent, practically "orthogonal" subbands. The topology plan is selected in such a way that 2 "empty" cells are between identically polarized cells and 1 "empty" cell between oppositely polarized cells using the same subfrequency band. Such a plan provides $U_0 = 243,607$ telephone channels, assuming that the users are uniformly distributed. The number of useful channels decreases to 106,943 for population density distributed user configuration.

CELL SIZE, UHF
 CELL SIZE, S-BAND
 NUMBER OF CELLS, UHF
 NUMBER OF CELLS, S-BAND
 TOTAL NUMBER OF CHANNELS
 TOTAL NUMBER OF VOICE CHANNELS
 USER PER CHANNEL FOR $V_U = 81$
 USERS PER BEAM
 USERS IN TOTAL SYSTEM
 UNIFORM DISTRIBUTION
 POPULATION DENSITY RELATED DISTRIBUTION
 TYPICAL EW CELL WIDTH
 TYPICAL CELL AREA
 AREA PER USER (UNIFORM DISTRIBUTION)
 AVERAGE DISTANCE BETWEEN USERS
 NO. OF EW CELLS (UHF)
 NO. OF NS CELLS (UHF)

$\alpha_U = .423^\circ$
 $\alpha_S = 1^\circ$
 $N_U = 91$
 $N_S = 23$
 $T_C = N_U M_U = 7553$
 $T_V = 7371$
 33.05
 $U = 2677$
 $U_0 = U N_U = 243607$
 $U_M = .439 U_0 = 106943$
 $D_C = 272 \text{ KM}$
 $A_C = 82000 \text{ KM}^2$
 $A_U = 30.6 \text{ KM}^2$
 $L_U = 5.53 \text{ KM}$
 15.5
 7.8

	UHF		S-BAND	
	UP	DOWN	UP	DOWN
f (MHz)	821	866	2650	2550
λ (M)	.3654	.3464	.1132	.1176
GROUND EIRP DB	12		20.6	
GROUND G/T DB	-24.5			16.2
SPACE EIRP DB	42.3	(AT CONTOUR)		20 (AT PEAK)
SPACE G/T DB	22.2		8.8	

Table 3

FRONT END CHARACTERISTICS OF THE LMSS IN UHF BAND

Table 4 summarizes some of the electrical and mechanical characteristics for the spacecraft and ground terminal UHF equipment. For the spacecraft antenna implementation a hoop-column type of structure is assumed in a so-called "quad aperture" configuration. For this concept an essentially axially symmetrical overall antenna structure is retained. At the same time the central blockage associated with the bulky feed aperture necessary for multibeam operation is eliminated. The feed blockage elimination is achieved by utilizing part of the 4 quadrants of the potentially available overall reflector surface. For this configuration the necessary overall structural diameter is a little more than twice the diameter of an individual subaperture. However, the availability of 4 subapertures may be utilized for a number of system simplifications or performance enhancements.

For the present design separate subapertures are used for the up and down-link, which eliminates the need for receive/transmit duplexers. Additionally, the eastern and western parts of the country are served by separate subapertures, which reduces the scan requirement of the component beams.

UHF DOWNLINK, SPACECRAFT	HOOP COLUMN, QUAD. APERTURES
ANTENNA TYPE	$D_o = 118 \text{ M}$
OVERALL DIAMETER	$D_{av}^d = 53 \text{ M}$
SUBAPERTURE DIA, AVERAGE	55 M/51 M
SUBAPERTURE MAJOR/MINOR AXES	$Q = .111 D_{av}^d$
OFFSET	$F = 66 \text{ M}$
FOCAL LENGTH	$D = .553 \text{ M}$
FEED DIA.	EAST/WEST
SUBAPERTURE UTILIZATION	$\theta_M/\alpha_V \approx 3.5$
MAX. SCAN	$G_{MO} = 51.3 \text{ DB}$
LOSS LESS PEAK GAIN FOR MAX. SCAN	$\Delta G = -5 \text{ DB}$
CONTOUR GAIN DIFFERENTIAL	$\alpha_L = .2 \text{ DB}$
CIRCUIT LOSS	$G = 46.1 \text{ DB}$
MINIMUM GAIN	$P_{TU} = -4 \text{ DBW} = .4 \text{ W}$
TRANSMIT POWER PER VOICE CHANNEL	$P_{TUB} = 33.2 \text{ W}$
TRANSMIT POWER PER BEAM	$P_U = 3021 \text{ W}$
TOTAL TRANSMIT POWER	$\eta = 25\%$
TRANSMITTER EFFICIENCY	$P_{OU} = 12085 \text{ W}$
DC POWER FOR TRANSMITTERS	$I = 25 \text{ DB}$
BEAM ISOLATION	$IM = 25 \text{ DB}$
INTERMODULATION	RCP OR LCP
POLARIZATION	.5 DB
AXIAL RATIO	
UHF DOWNLINK, EARTH STATION	CROSSED DIPOLE OVER GROUND PLATE
ANTENNA TYPE	(QTY 2 FOR DIVERSITY)
POLARIZATION	SELECTABLE RCP OR LCP
AXIAL RATIO	< 5 DB
ANTENNA RECEIVE AREA	$A_R = .015 \text{ M}^2 = -18 \text{ DB/M}^2$
RECEIVER NOISE TEMPERATURE	$T_R = 26.5 \text{ DB/ K}$
(WITH 2 LOW NOISE FRONT END)	
G/T	- 24.5 DB/ K

Table 4

FRONT END CHARACTERISTICS OF THE LMSS IN S-BAND

Table 5 displays the front end characteristics of the S-band subsystem. A relatively small 7.7-m offset-fed paraboloid antenna is selected for this subsystem in order to simplify its deployment and allow its mounting behind the UHF feed.

S-BAND, DOWNLINK, SPACECRAFT

ANTENNA TYPE

OFFSET FED SUBAPERTURE COMMON FOR
E/W AND UP/DOWN. MOUNTED ON BACK
OF UHF FEED.

ANTENNA DIA.
FOCAL LENGTH
MAX. ANTENNA GAIN
MIN. ANTENNA GAIN

DS = 7.7 M
F = 7.7 M
G_{SM} = 42.8 DB
G_{SM} = 39.3 DB

S-BAND, DOWNLINK, EARTH STATION

ANTENNA TYPE
ANTENNA DIA.
ANTENNA GAIN
SYSTEM NOISE TEMPERATURE
G/T

SYMMETRICAL CASSEGRAIN
4.5 M
44 DB
150°K = 21.8 DB/'K
22.2 DB/'K

Table 5

BEAM TOPOLOGY PLAN FOR UNIFORM USER DENSITY DISTRIBUTION

Figure 1 shows the beam topology plan for uniform user distribution. The actually developed conceptual design for the feed is for the uniform distribution, but the East-West subdivision and the panelization of the feed required for launch packaging takes the potential density distribution boundary lines into account. Within the overall feed topology plan the numbers in the cells show the subfrequency band (r-f channel) numbers assigned for a cell. The uncircled and circled numbers exhibit orthogonal polarizations. Eight cells, e.g. 1, 2, 3, 4, ①, ②, ③, ④ form a "grand cell" (shown by heavy boundary) which can be repeated indefinitely. Note that in the exhibited ground cell, the cell carrying subchannel ① has 4 adjacent ① cells. These are 2 "empty" cells away (empty insofar as channel ① is concerned). All other cells marked by ① are even further away.

The feed array elements (subarrays) corresponding to this topology plan have a similar layout. When such a feed is divided along an approximately N-S line (shown by heavy boundary) into 2 assemblies, then the boundary-located feed providing coverage ① generally must utilize more than one radiating element for control of its sidelobes into the other No. ① cells. For this purpose the "East" feed generally has to be extended beyond its West boundary and the "West" feed beyond its East boundary.

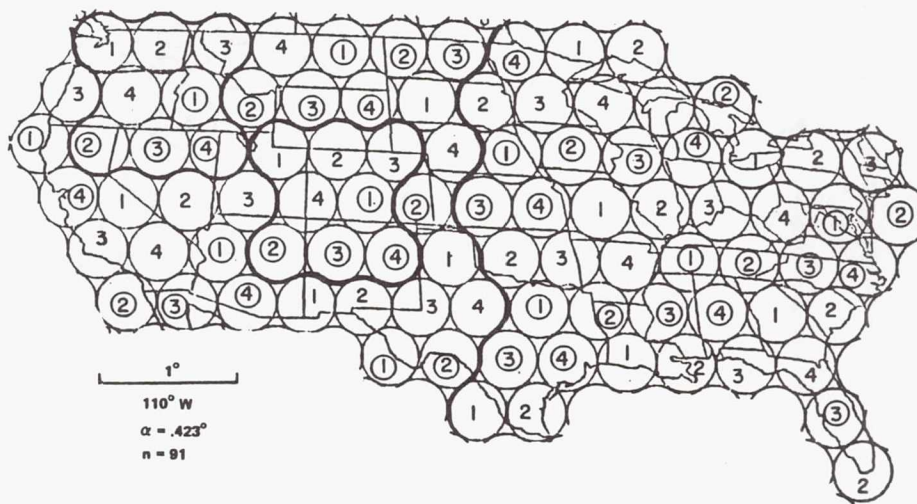


Figure 1

BEAM TOPOLOGY PLAN FOR NONUNIFORM USER DENSITY DISTRIBUTION

Figure 2 shows a simplification of the plan displayed in Figure 1. This plan takes into account that the users are not distributed uniformly over the area of the 48 states. The simplification results in 40 available beams and a reduction of user capacity to 43.9% of the original. When this plan is combined with the use of Voice Operated Transmitters (VOX) approximately 71.6% of the original users (uniform user distribution, no VOX) can be accommodated.

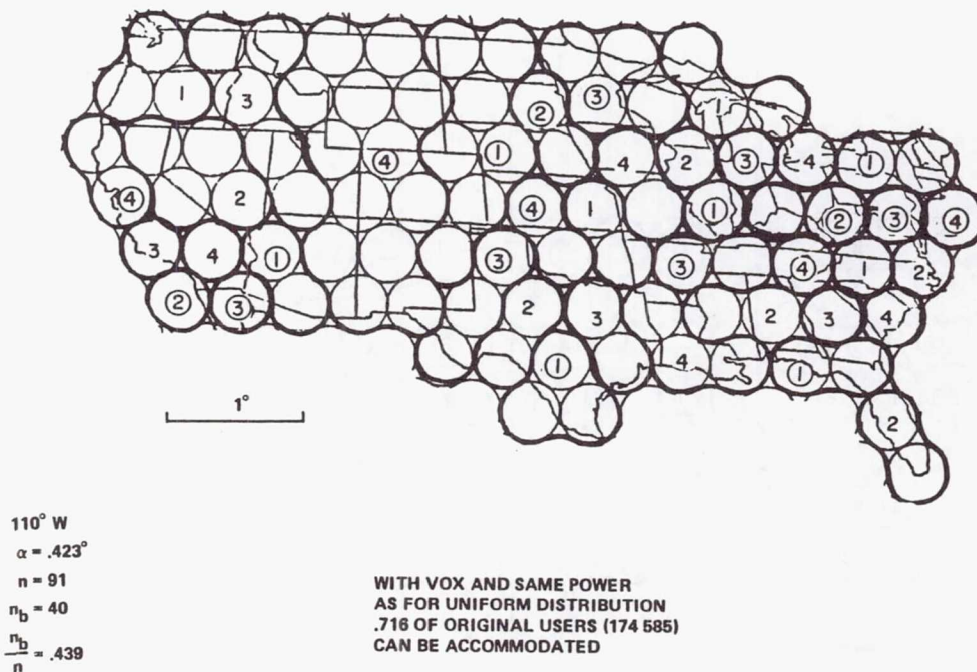


Figure 2

EXTENSION OF THE BEAM TOPOLOGY PLAN OVER THE NORTH AMERICAN CONTINENT

Figure 3 shows the extension of the beam topology plan exhibited in Figure 1 to cover the North American continent. The overall plan provides 91 singlet beams covering the US and 31 beams each for Canada and Mexico. The plan allows 7 element feeds for the formation of all US cells and for those Canadian and Mexican cells which are marked by a dot. The 7 element feed configuration assures the capability for ideal sidelobe control for the beams associated with the corresponding cells. When the feed array associated with US coverage is extended beyond the indicated heavy boundary by at least 5 (half width) radiating elements for the cells marked by Δ the sidelobe level is controllable by 4 auxiliary beams for those Canadian and Mexican cells which are marked by +. This allows at least 25 dB beam isolation anywhere within the North American continent using the above beam topology plan.

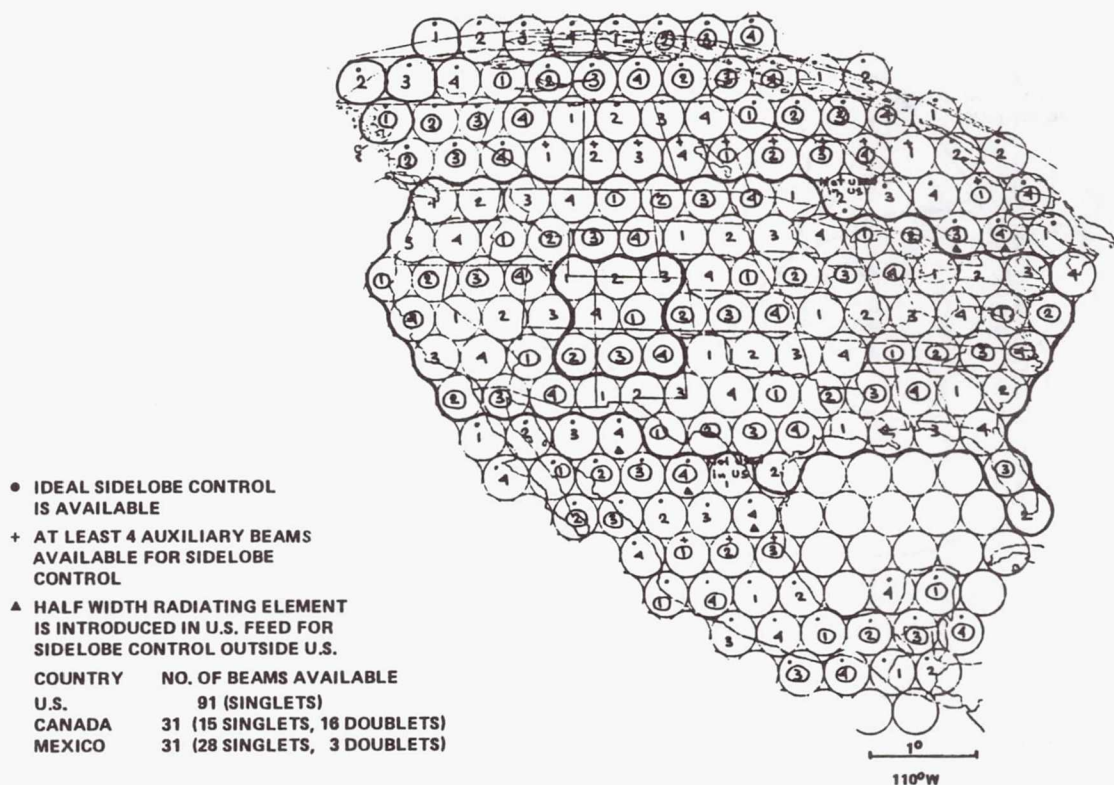


Figure 3

FRONT VIEW OF THE QUAD ANTENNA APERTURE
(E-W SIDE SOLAR ARRAY IMPLEMENTATION)

Figure 4 exhibits the front view geometry of a quad antenna, which is compatible with the system requirement and the beam topology plan discussed earlier. The plan shows that the nominal downlink aperture is 53.4 m while the nominal uplink aperture is 47 m for the UHF antenna. The larger downlink aperture provides about 3 dB larger antenna gain for the downlink than for the uplink, thus minimizing the r-f transmit power requirement for a given EIRP. The uplink antenna diameter is still compatible with the beam isolation requirement. At the same time the geometry allows the use of solar arrays on the East and West sides of the feed system.

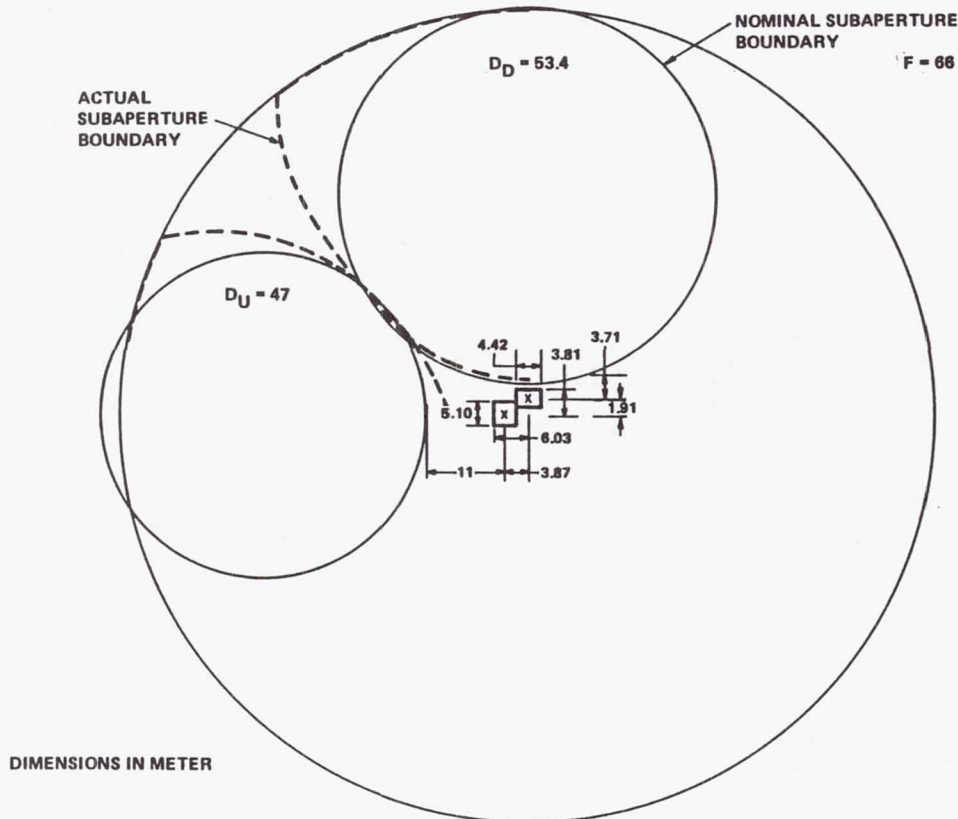


Figure 4

OPTICS GEOMETRY IN THE N-S PLANE, N SIDE OF THE UHF DOWNLINK ANTENNA
(E-W SIDE SOLAR ARRAY IMPLEMENTATION)

Figure 5 shows the reflector and feed profiles of the UHF downlink antenna.

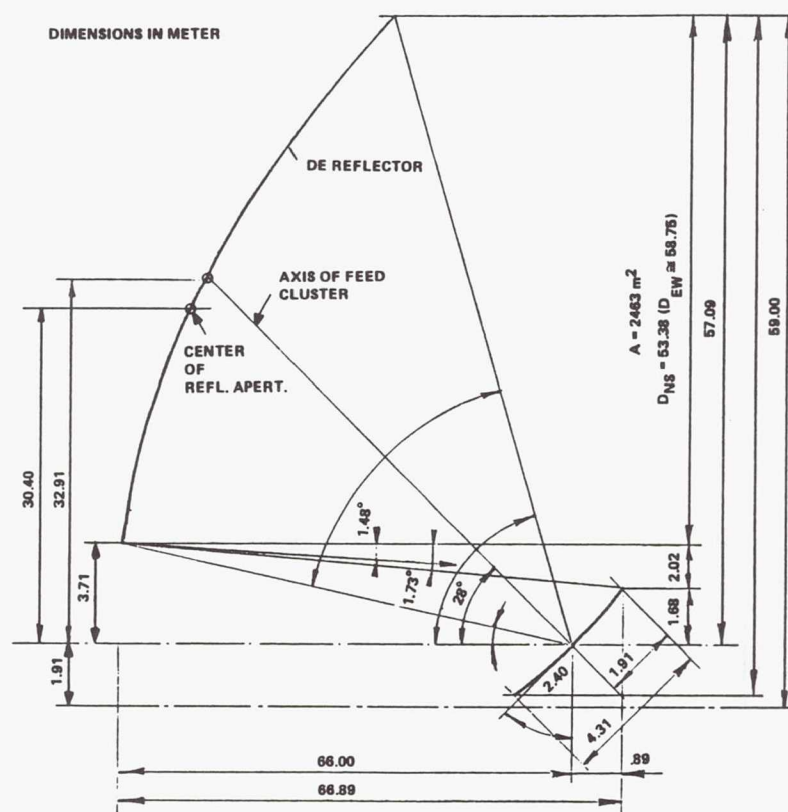


Figure 5

OPTICS GEOMETRY IN THE E-W PLANE, E SIDE OF THE UHF UPLINK ANTENNA
(E-W SIDE SOLAR ARRAY IMPLEMENTATION)

Figure 6 shows the reflector and feed profiles of the UHF uplink antenna.

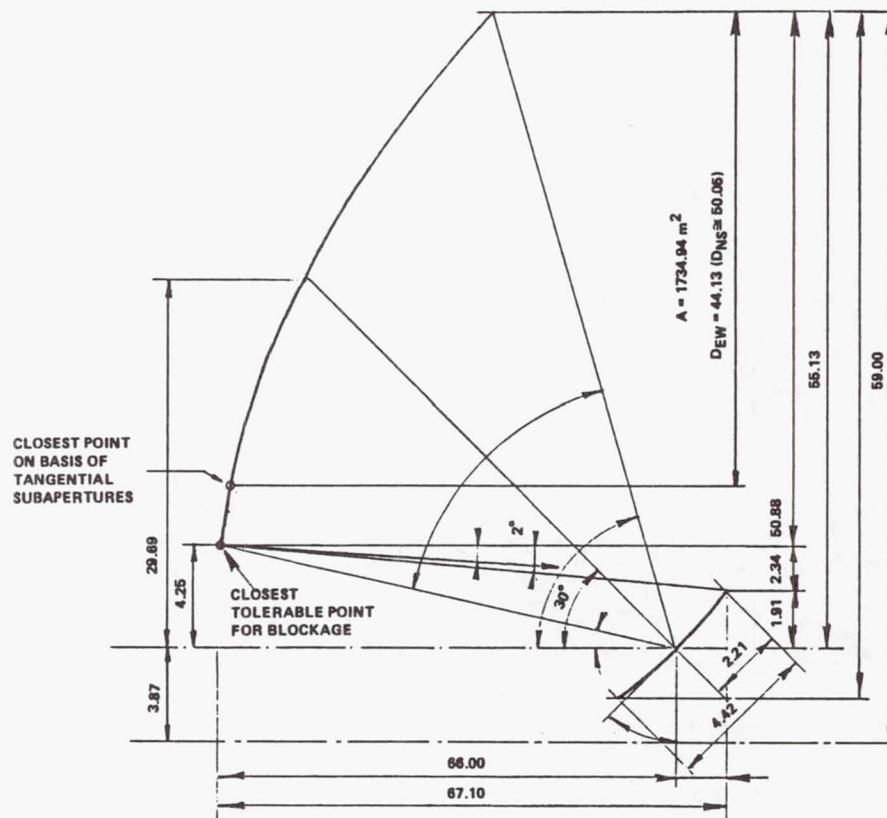
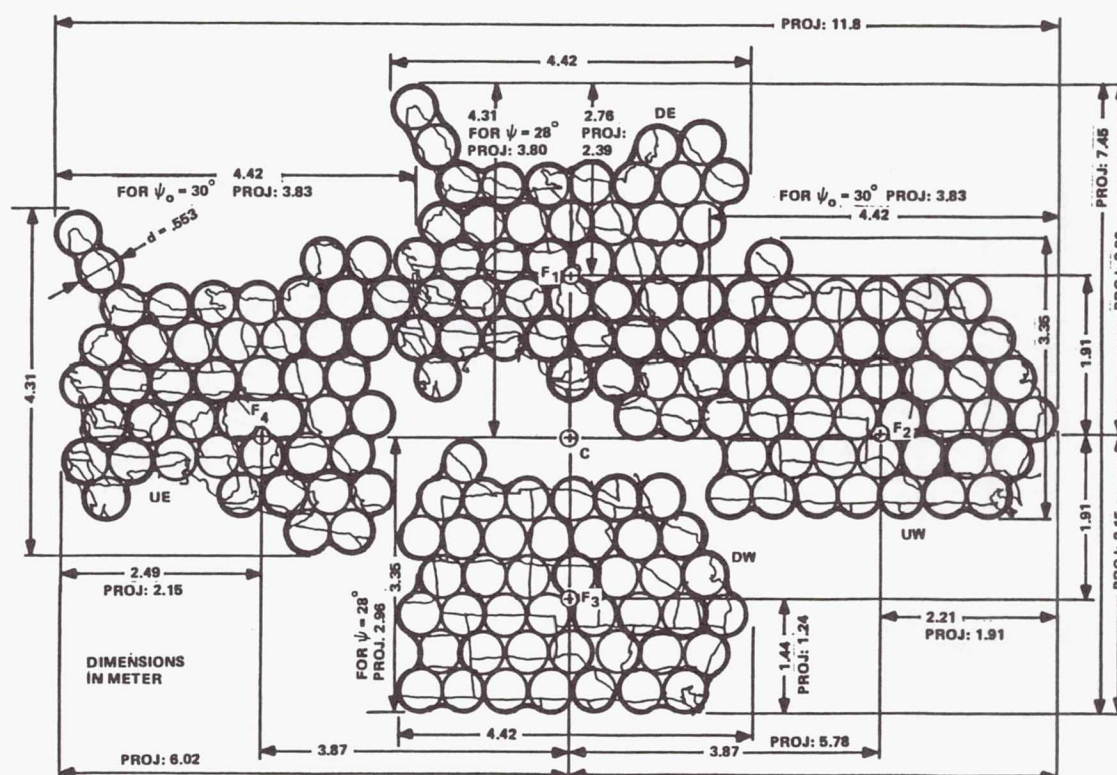


Figure 6

GEOMETRY OF THE FEED LAYOUT

Figure 7 displays the feed array geometry necessary for the optics shown in Figures 4 - 6. The sidelobe controlling "half width" radiating elements along the East-West dividing lines of the feed array and along the North and South border are not shown on this figure. After the 4 feeds are deployed into their operational position their projected envelope to the aperture plane is within an 11.8 m x 6.95 m rectangle. The F_1 , F_2 , F_3 and F_4 points indicate the location of the focal points of the subapertures of the quad antenna.



DIMENSIONS WITH "PROJ" PREFIX SHOW PROJECTED DIMENSIONS OF FEED PANELS TO PLANE ORTHOGONAL TO AXIS OF COLUMN.

Figure 7

UHF FEED CONFIGURATION

Figure 8 shows one possible physical implementation of the feed defined by the geometry in Figure 7. Each of the feed arrays is divided into 2 or 3 feed panels which can be folded for the Shuttle stowed configuration. During launch the plane of these panels is parallel to the axis of the Shuttle. In the operational position the panels are unfolded and tilted to 28° or 30° relative to the aperture plane of the overall quad antenna. The feed systems utilize printed radiating elements (subarrays), printed power dividers and monolithic transmit and receive r-f electronics. All these are implemented inside the feed panels. The beamforming network (BFN) utilizes flexible coaxial cables for the low power connections in the system, which allows the unfolding of the panels during deployment.

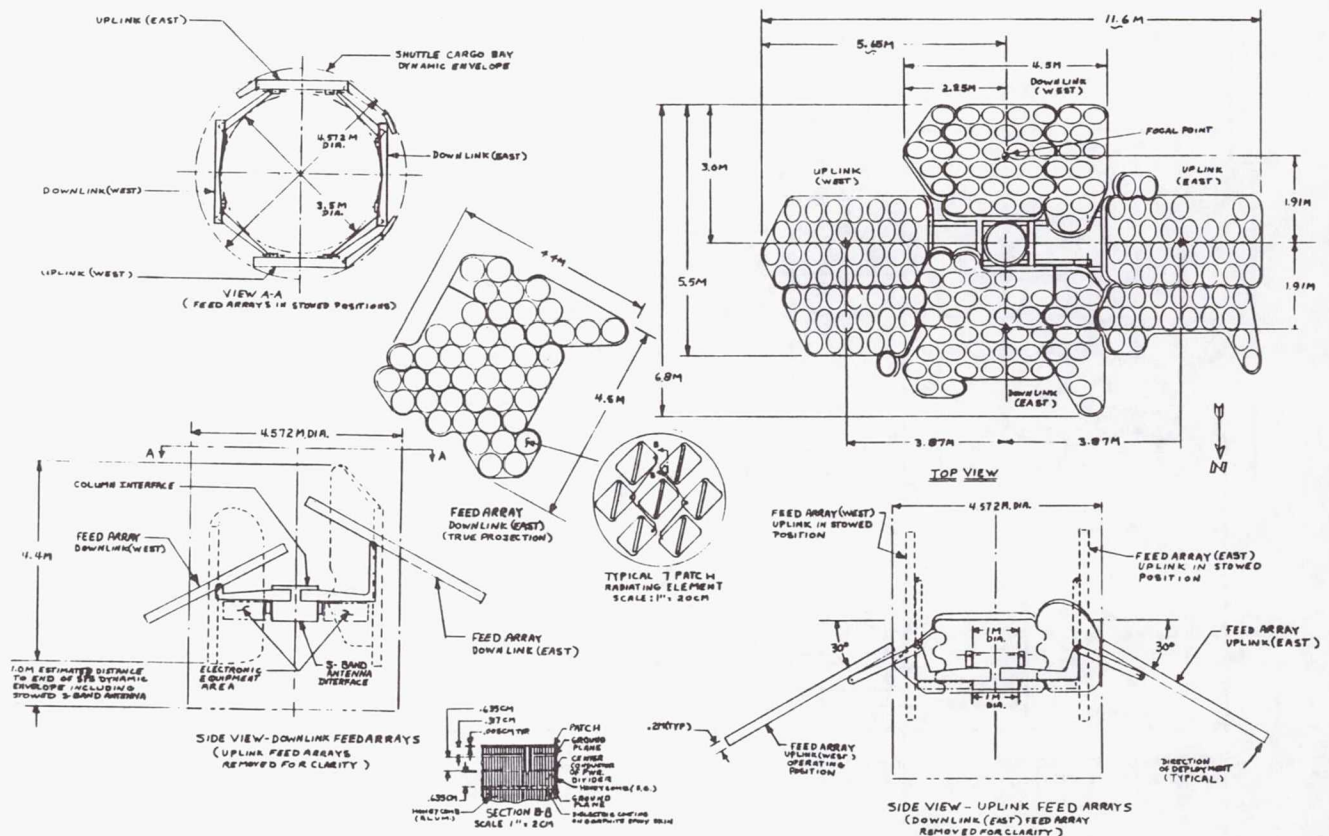


Figure 8

SINGLET GAIN CONTOUR FOR THE UNSCANNED SINGLET BEAM GENERATED
BY A TE_{11} MODE EXCITED CIRCULAR W.G. FEED

Figure 9 exhibits the basic downlink radiation characteristics of a singlet beam of the quad antenna, realized by a single radiating element of appr. $1-1/2\lambda$ in diameter and excited by the TE_{11} mode.

Configuration		DOWNLINK ANT
Geometry	D, in	2323 X 2087
	F/D	F = 2598 in
	Q, in	268
	d, in	21
	α , deg	0.423
	n	1
Beam		FOCUSED
Polarization	MAIN	CIRCULAR
Longitude, deg.		110 W
Antenna Axis	EW	
Pointing, Deg.	NS	
	EW Bias	
Frequency, GHz		0.856
Max. Gain, db		52.0

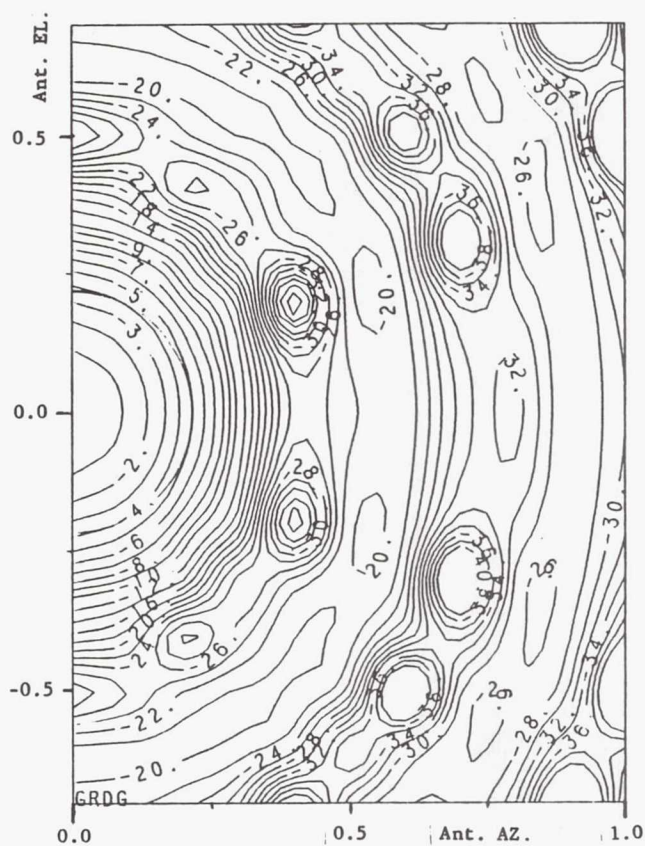


Figure 9

SINGLET BEAM CONTOUR IN MAXIMALLY SCANNED POSITION

Figure 10 shows the beam in the maximum necessary scanned position. For this case center of the beam is at Boston and the sidelobe level in the nearest applicable interfered cell (marked by dotted line) is -24 dB. Since the level of the main beam at the boundary of a cell is appr. -4 dB for this condition the adjacent beam isolation is only 20 dB, which is not adequate.

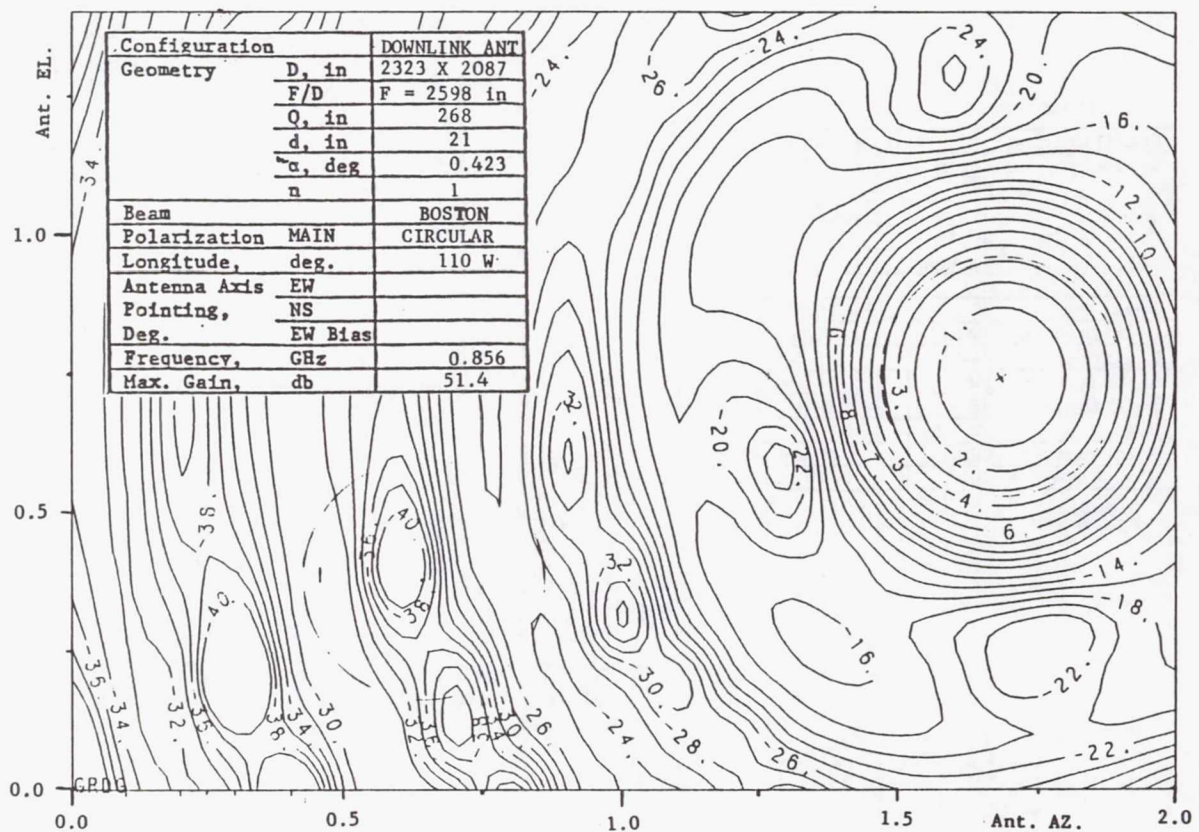


Figure 10

MAXIMALLY SCANNED SINGLET BEAM CONTOUR GENERATED BY A 7 ELEMENT SUBARRAY

Figure 11 indicates the gain contours if the radiating element is implemented by a 7 element subarray instead of the TE₁₁ type of w.g. mode field distribution used for Figure 9. It can be seen that the gain contours are nearly identical to the previously calculated ones and the adjacent beam isolation is still only 20.5 dB.

It can be concluded from these calculations that a single $1-1/2\lambda$ diameter radiating element, whether it is a single radiator or a subarray, is not capable of producing beams with 25 dB beam isolation with the selected optics geometry and beam topology.

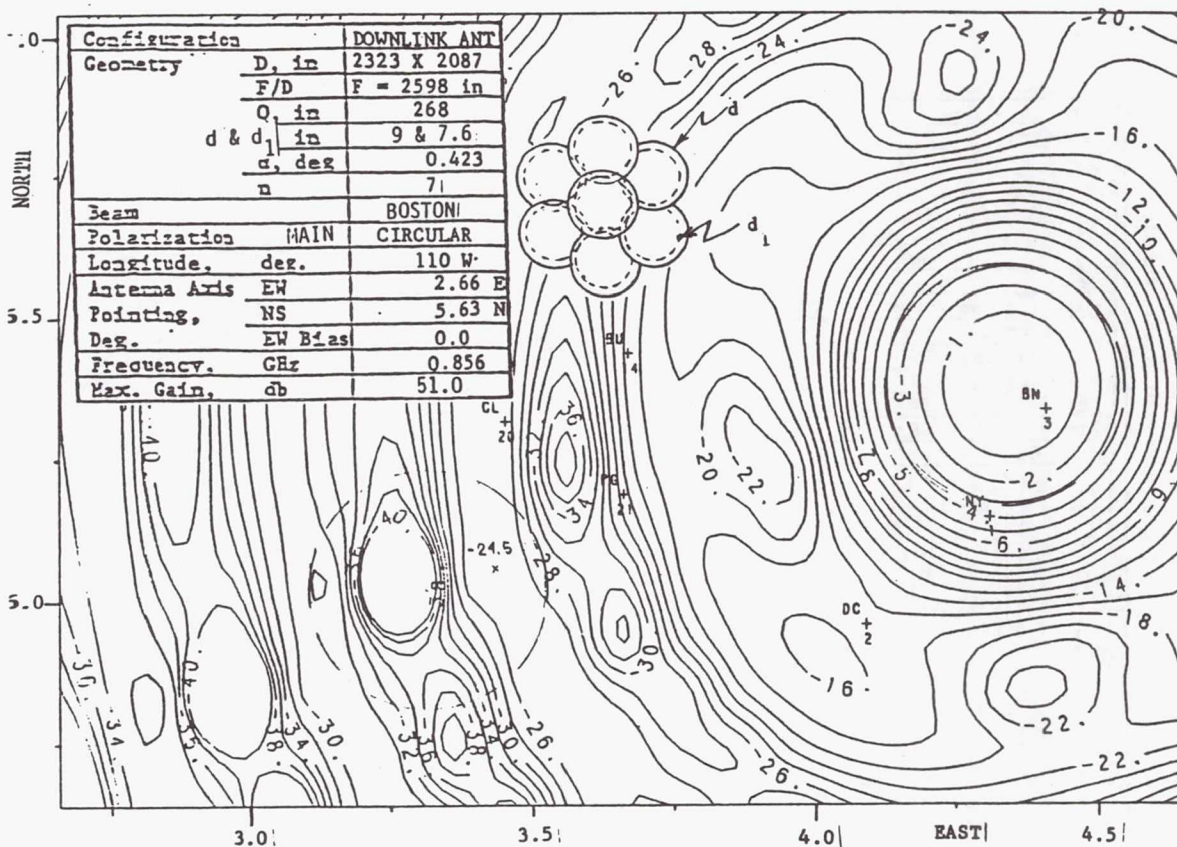


Figure 11

SIDELOBE CONTROL ACHIEVABLE BY A DOUBLET FEED

Figure 12 indicates downlink gain contours of a possible feed configuration which is approximately compatible with the 25 db beam isolation requirement, selected geometry, and beam topology plan. The configuration uses a so-called "doublet" feed, consisting of 2 radiating elements (1 main and 1 auxiliary) with 1 and 0.1 unit power excitation. The sidelobe level of the "Boston" beam is -32 dB in the nearest interfered cell. Since 3 additional nearby interferers might produce sidelobes in this cell it is possible that they will result in a total -26 dB level. The main beam at cell contour is -3 dB for this condition; thus the resultant C/I ratio may be 23 dB. With optimization of the excitation levels of the elements in the doublet, the maximum sidelobes of the interfering signals in the interfered cell will not occur at the same angle. For this case the C/I can be further improved.

The beam topology plan shown in Figure 1 indicates that any beam can create major interference at least in 4 nearby cells. Thus the sidelobe control principle shown in Figure 12 needs generally 4 auxiliary radiating elements, yielding a 5 element feed cluster for the generation of each pencil beam.

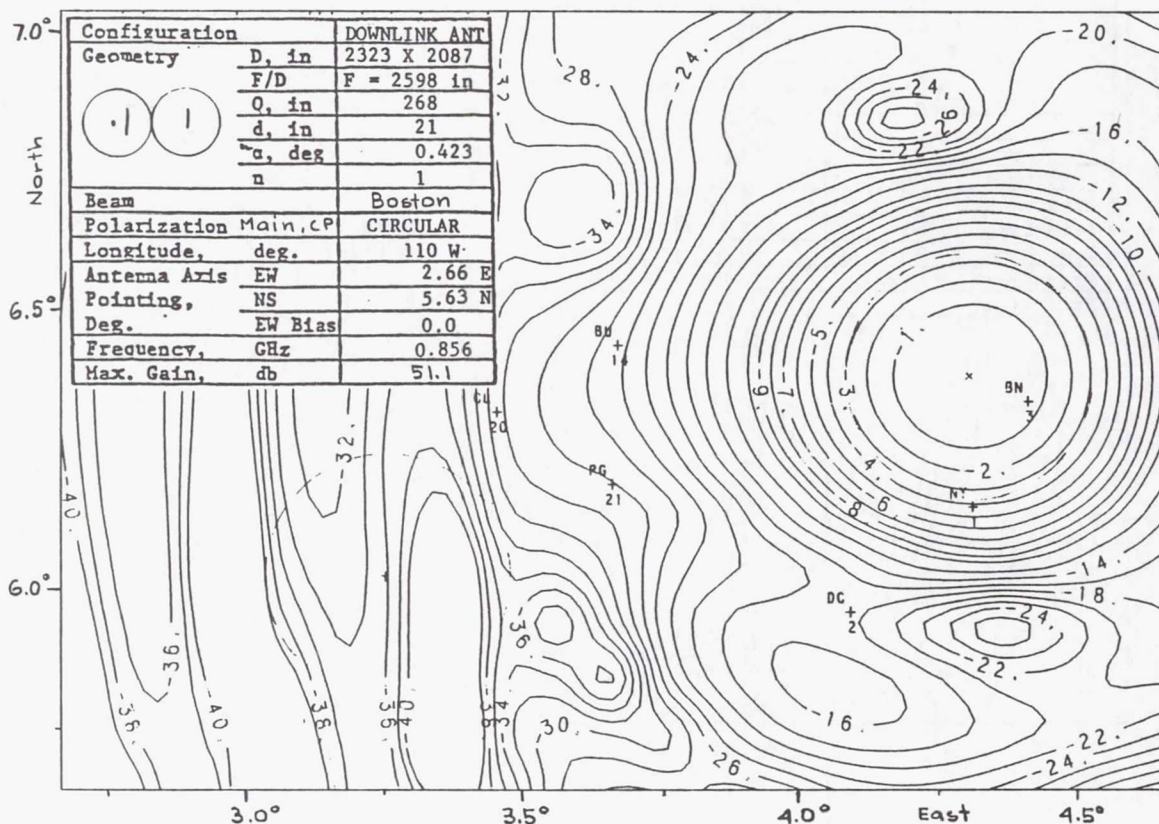


Figure 12

SIDELOBE CONTROL WITH A 7 ELEMENT FEED

A further improvement of sidelobe level can be obtained if the auxiliary elements are increased to 6. In this case the resulting feed is hexagonally symmetrical and consists of 7 elements. The gain contours are exhibited in Figure 13 for 0 dB center and -10 dB outer element excitation. The peak gain is reduced from 51.4 dB (with single element feed) to 50 dB but the edge gain is still 48 dB and the sidelobe level is -38 dB down in the interfered cell. This results in 36 dB adjacent beam isolation. The resultant C/I of the complete system is still nearly 36 dB because the peaks of the interfering sidelobes from the different adjacent beams occur at different angles.

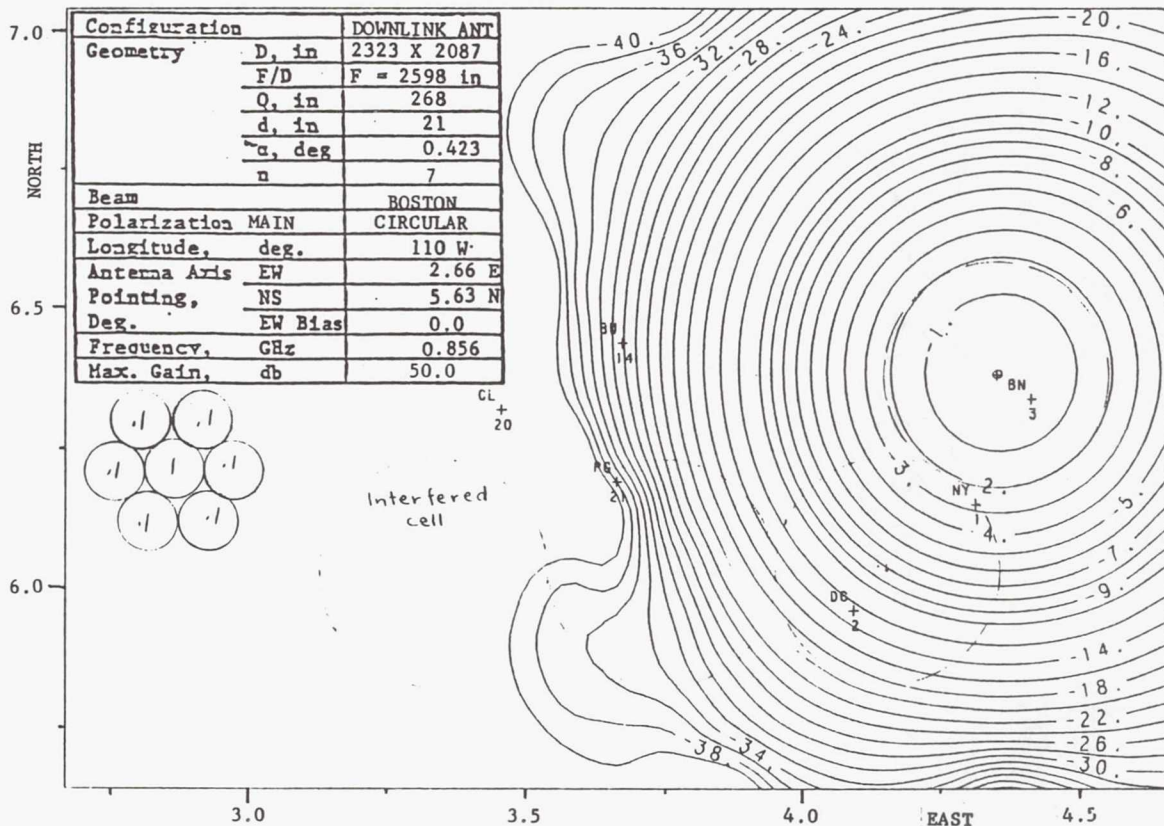


Figure 13

FRONT VIEW OF THE QUAD ANTENNA
(N-S SIDE SOLAR ARRAY IMPLEMENTATION)

Figure 14 shows a quad antenna geometry in which the uplink subapertures are in the N-S plane and the downlink subapertures in the E-W plane. This configuration reduces the total available aperture area for the downlink antennas, but provides an alternative in which the solar arrays can be on the North and South sides of the feed array; thus they need only a single axis drive.

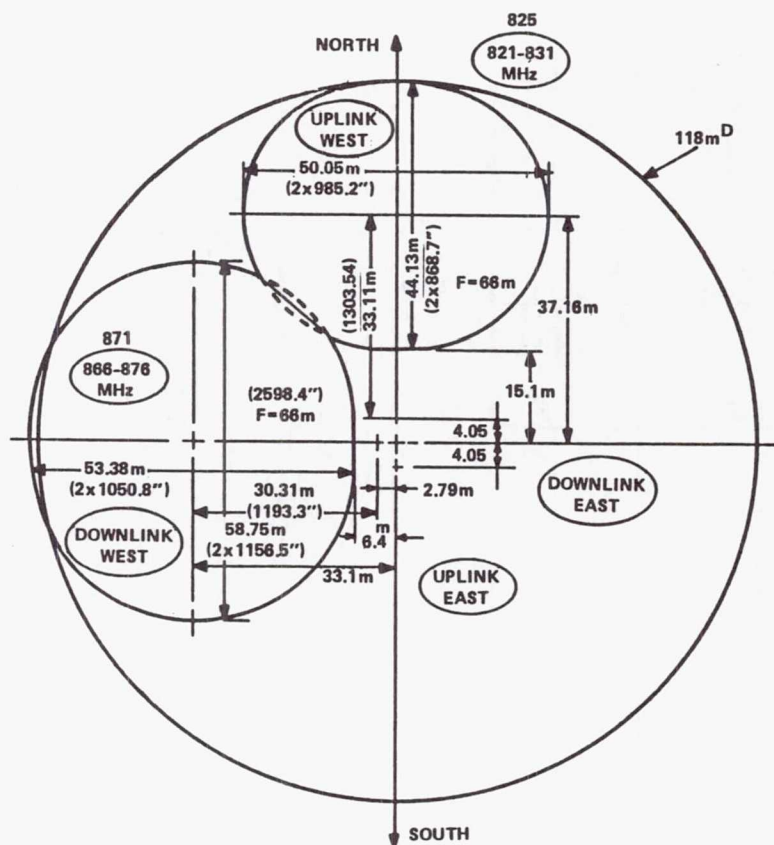


Figure 14

DOWNLINK OPTICS GEOMETRY IN N-S PLANE
FOR N-S SIDE SOLAR ARRAY IMPLEMENTATION

Figure 15 shows the reflector and feed profile in the N-S plane for the implementation when the solar array is on the North and South sides of the feed array.

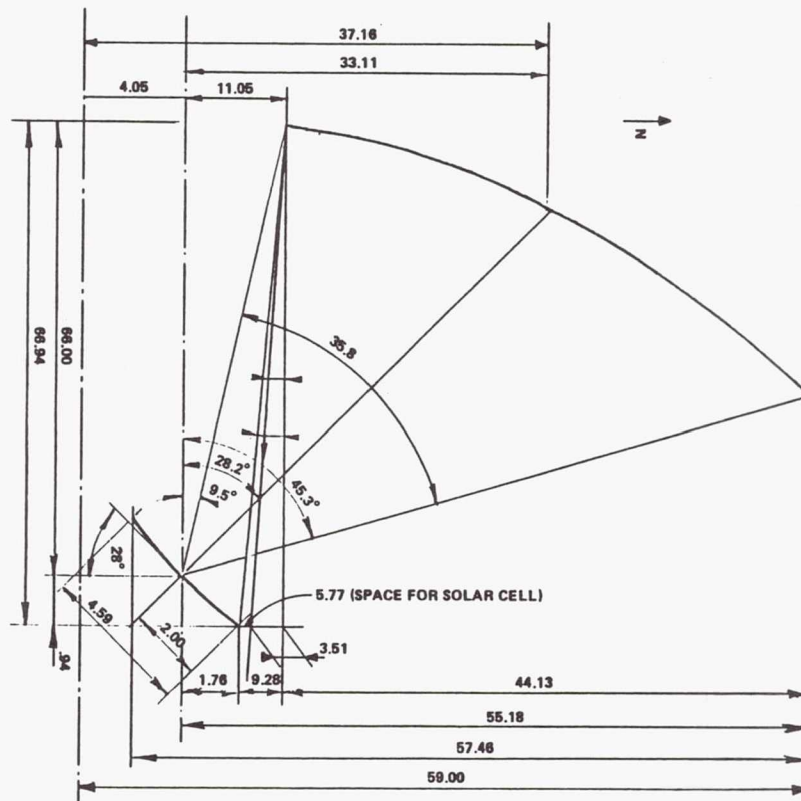


Figure 15

Figure 16 displays the feed geometries for the N-S plane solar array implementation. The layouts include the allowance for half width radiating element extensions of the arrays for the discussed sidelobe control.



SINGLET GAIN CONTOUR FOR THE MAXIMALLY SCANNED BEAM, UHF UPLINK

Figure 17 shows the uplink gain contours for the maximally scanned beam for the configuration with N-S plane implemented solar arrays. For the singlet implementation the sidelobe level is -24 dB in the interfered cell.

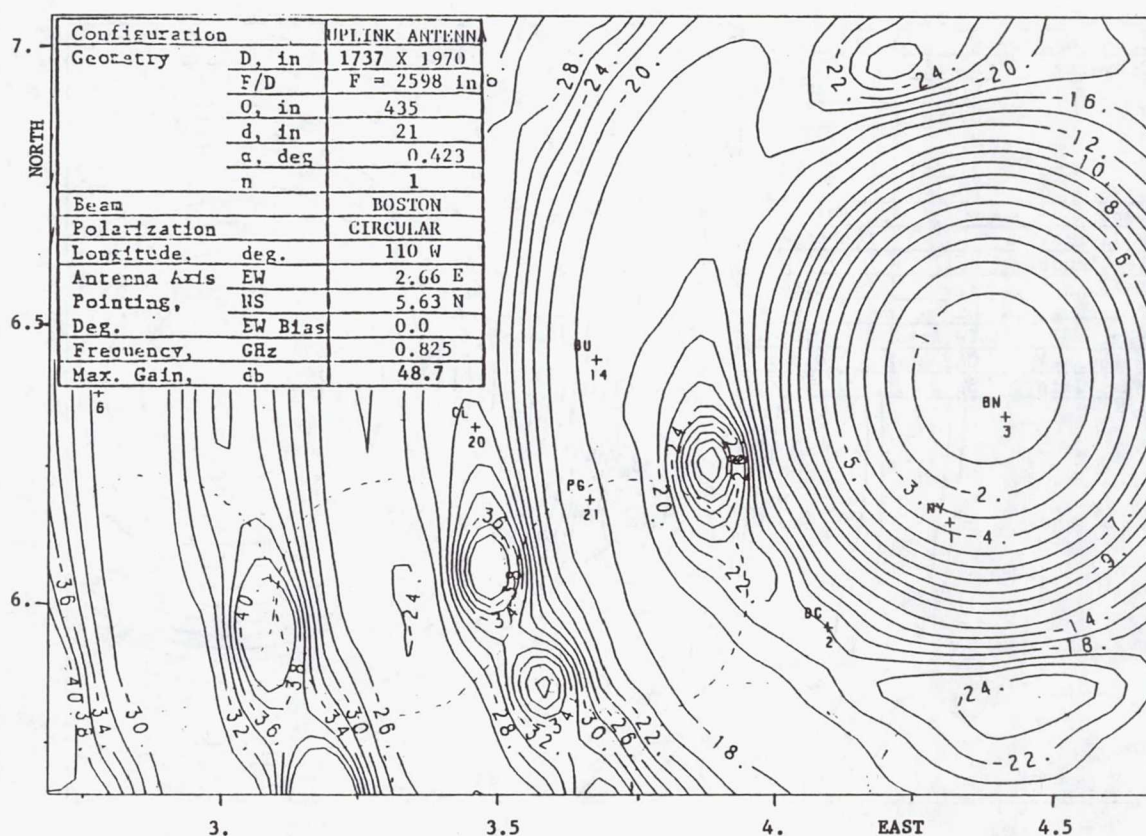


Figure 17

7 ELEMENT FEED CLUSTER GAIN CONTOUR FOR THE MAXIMALLY
SCANNED BEAM, UHF UPLINK

Figure 18 shows that for the 7 element cluster feed the sidelobe level is -32 dB. It can be seen that the combined effects of the 90° rotation of the quad antenna, the smaller subaperture diameter, and the lower frequency cause a 6-dB deterioration relative to the corresponding sidelobe level of the down-link antenna (Figure 13). However, the resultant sidelobe level from 4 nearby interfering sources is still -30 dB yielding C/I = 28 dB, which meets the specification.

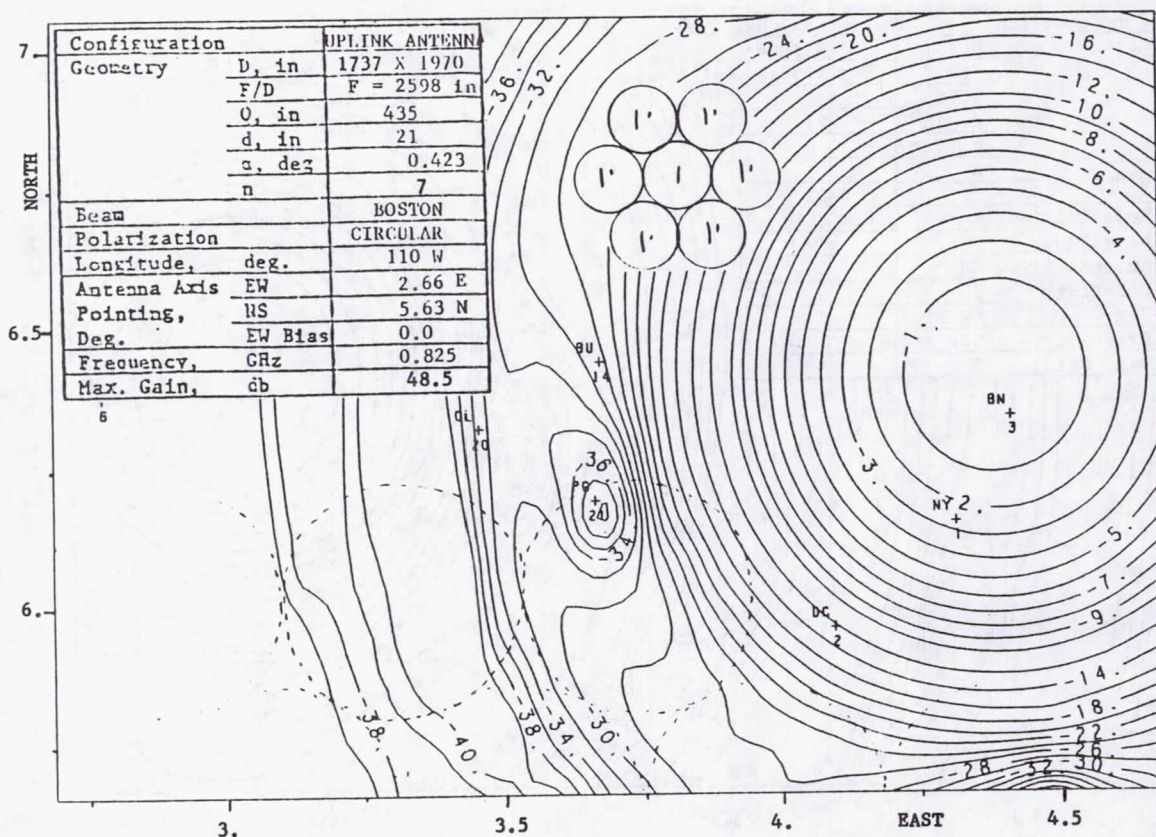


Figure 18

GAIN CONTOURS FOR NONSTANDARD 7 ELEMENT CLUSTERS CONFIGURED FOR COVERAGE BOUNDARY APPLICATION

Figure 19 exhibits the effect of the diameter reduction of 2 of the 6 auxiliary elements in the 7 element cluster. Such elements are desirable for coverage boundary located feeds in order to achieve the necessary side-lobe control outside the coverage area without significant increase in overall feed panel size. The reduced elements have half the standard $1-1/2\lambda$ diameter but this is compensated for by higher power excitation. The calculated gain contour differs very little from the gain contour of the standard element (Figure 18) and still yields appr. 28 dB resultant C/I.

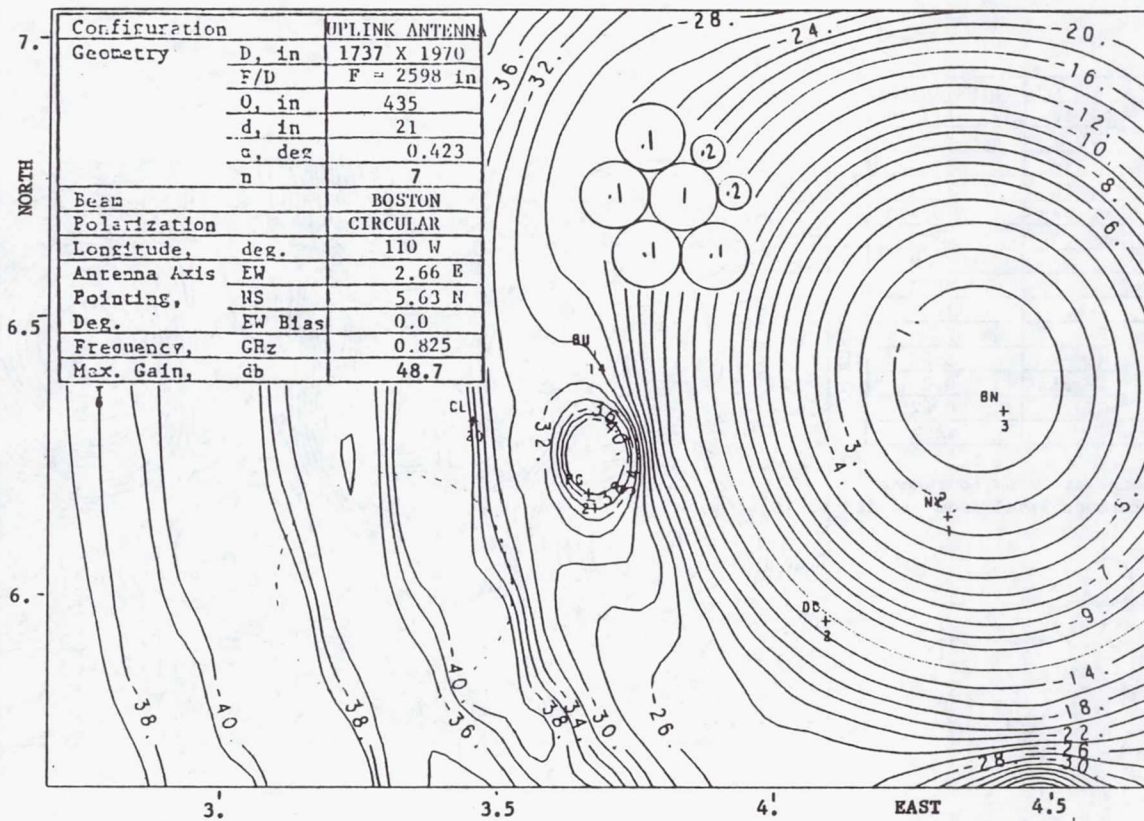


Figure 19

USE OF 5 ELEMENT FEED CLUSTER REQUIRING ONLY SINGLE POLARIZED RADIATING ELEMENTS

With the selected beam topology plan the implementation of the 7 element feed clusters requires that each radiating element in the feed (generally) has dual polarization capability. The reason for this is that they must act simultaneously as main and auxiliary radiator (for different coverage cells) and these could be oppositely polarized. If only max. 4 auxiliary radiating elements are needed for any beam then it is possible to select their corresponding radiating elements in the overall feed array so that only single polarized elements are necessary.

Figure 20 shows such a configuration. The center interfered cell receives sidelobe power from the adjacent identical frequency and polarization beams. Each of these main beams carries 1 unit of power. The selected auxiliary horns carry either 10 dB or 20 dB lower power level and their location is selected so that they are compatible with single polarized radiating elements. In the center interfered cell, the sidelobe level is -16 dB without the auxiliary horns. This improves to -26 dB with the selected excitation. The resultant C/I = 24 dB is somewhat marginal, but it must be noted that no great effort was devoted to optimize the excitations. The values of the achieved C/I indicate the feasibility of the concept.

Configuration		UPLINK ANTENNA
Geometry	D, in	1737 X 1970
	F/D	F = 2598 in
	Q, in	435
	d, in	21
	α , deg	0.423
	n	8
Beam		BOSTON
Polarization		CIRCULAR
Longitude, deg.		110 W
Antenna Axis	EW	2.66 E
Pointing, NS		5.63 N
Deg. EW Bias		0.0
Frequency, GHz		0.825
Max. Gain, db		48.7

4 Auxiliary horns are used to reduce central interference level from -16 dB to -26 dB.

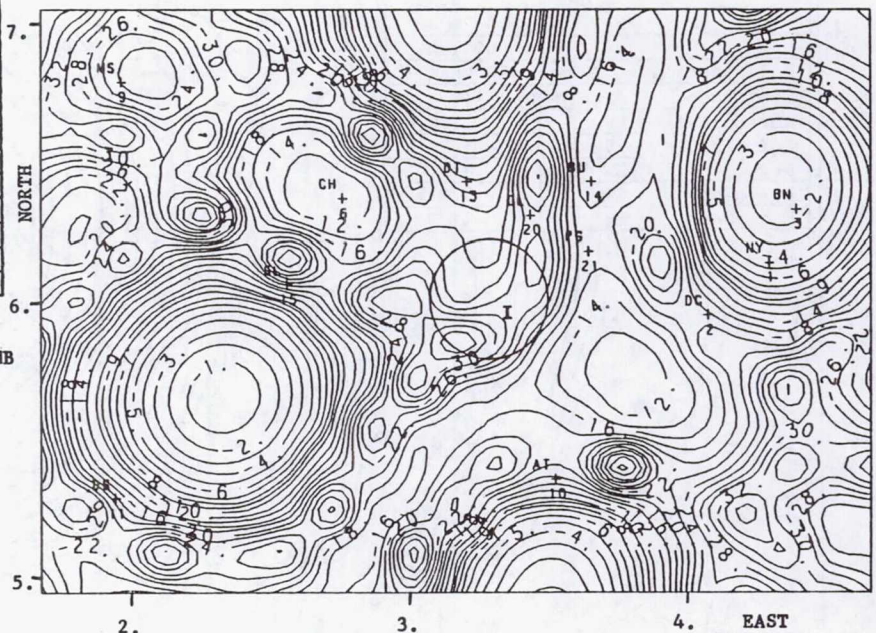
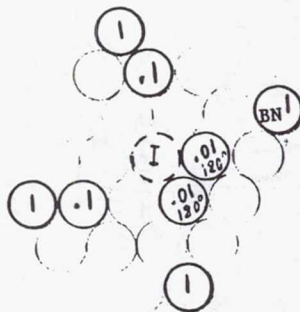


Figure 20

EXAMPLE FOR SINGLE POLARIZED 4 ELEMENT SUBARRAY RADIATING ELEMENT IMPLEMENTATION

Figure 21 shows a 4 element subarray in which each element is a somewhat irregularly shaped printed patch with a diagonal slot array. The geometry results in relatively wide frequency band circular polarization within the required appr. 36° full cone angle toward the reflecting surface of the subaperture. The combining network for the 4 patches is on the same substrate as the patches and the geometry is selected in such a way that their radiation is part of the overall circular polarization design.

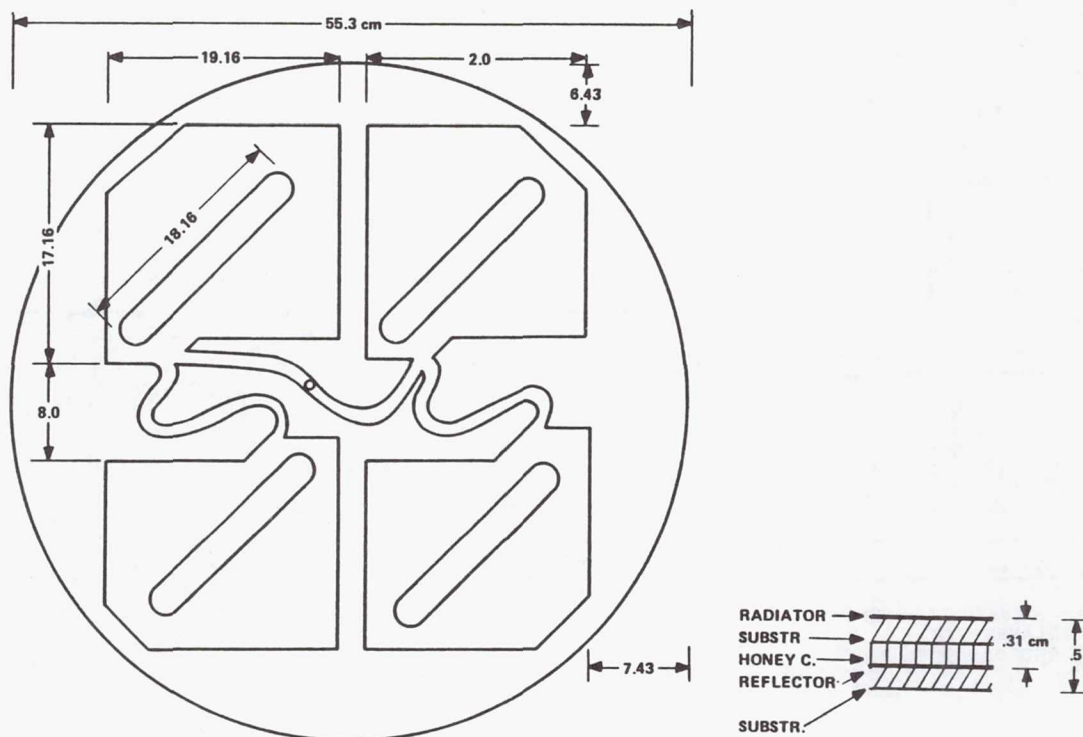


Figure 21

EXAMPLE FOR DUAL POLARIZED, 4 ELEMENT SUBARRAY RADIATING ELEMENT IMPLEMENTATION

Figure 22 shows a 4 element subarray capable of dual circular polarization. In this case the RCP power divider can be implemented on the periphery of the 4 element patch configuration but the LCP power divider requires another printed circuit layer.

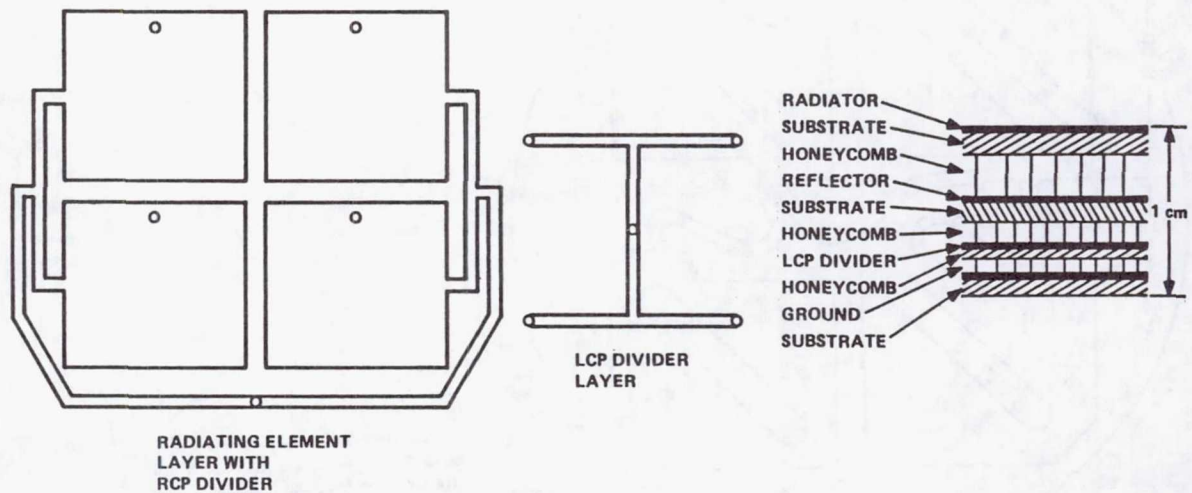


Figure 22

EXAMPLE FOR SINGLE POLARIZED 7 ELEMENT SUBARRAY RADIATING ELEMENT IMPLEMENTATION

Figure 23 exhibits a 7 element subarray. The shape of the patches is similar to the ones shown on Figure 21 but due to the closeness of the patches the power divider has to be implemented on a separate printed circuit layer. (Two such extra layers are required if dual polarization is necessary.)

It can be seen that the 7 element subarray implementation is much more complicated than for the 4 element subarray and it needs at least 2 layers. However, it can be excited in a tapered manner (center element at 0 dB, outer elements at appr. -6 dB level) which results in more symmetrical radiation patterns and smaller coupling between subarrays.

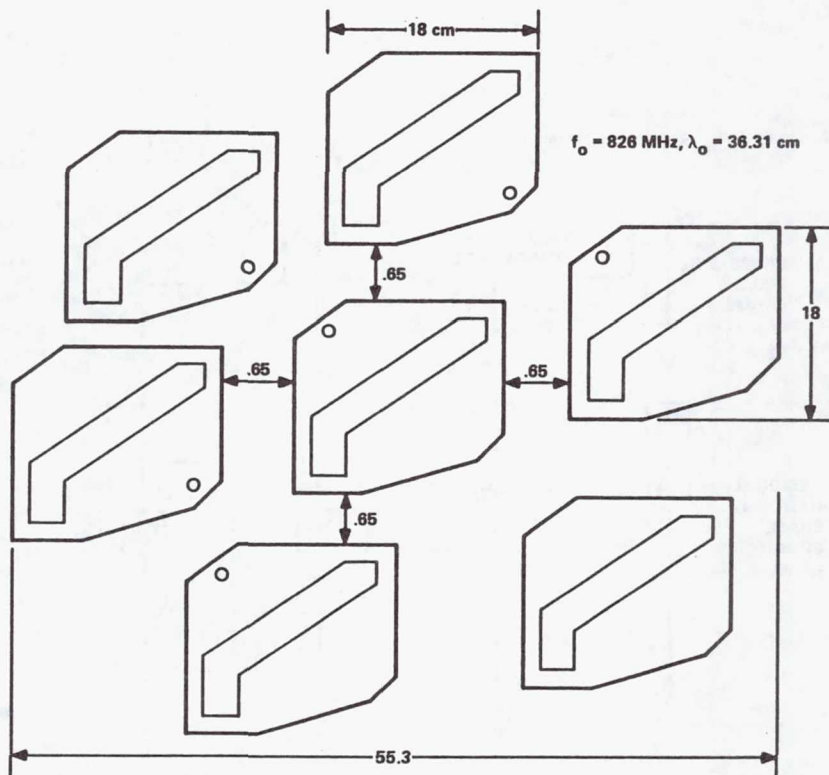


Figure 23

DIFFERENTIAL PHASE ERROR INTRODUCED BY RANDOM PA PHASE ERRORS

The beamforming network necessary to form multiple element (5 ~ 7) feed clusters cannot be separated from the PA circuit layout design. The power for a given auxiliary radiating element must be coupled out from the signal path leading to the main radiating element. This coupling path can be implemented either in the input circuit, before the PA (Figure 24a), or in the output circuit, after the PA (Figure 24b). In either case the coupled out signal must be further amplified in order that the total loss in the high power circuit is kept at a minimum. Since the sidelobe cancellation is based on the maintenance of the phases between the main and auxiliary radiating elements it is important that the effect of PA phase drifts is minimized. A common phase drift of the 2 involved PA's does not cause a change in the sidelobe cancellation. However, for the residual random (independent) phase errors associated with the individual PA's the scheme shown in Figure 24b has smaller maximum phase error between cancelling radiated fields.

From an implementation point of view the two schemes differ very little in practice; thus only the Figure 24b type of scheme will be discussed further.

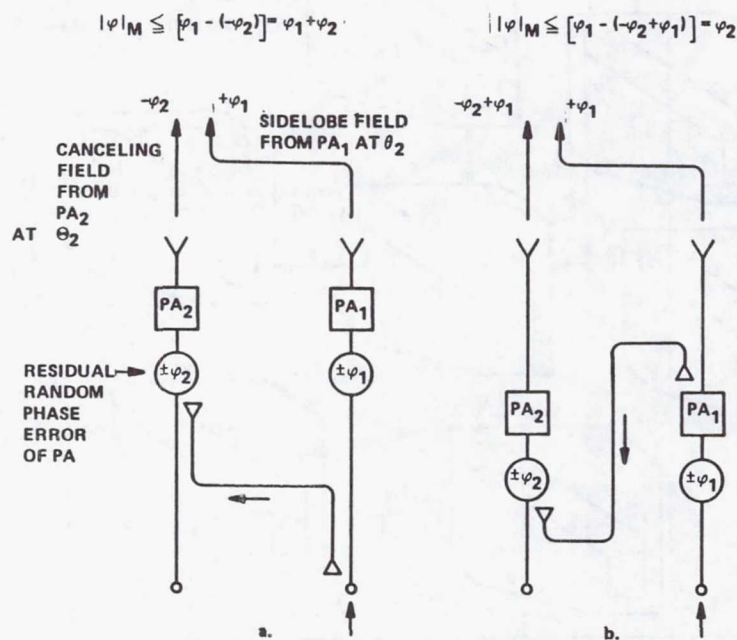


Figure 24

BFN USING DUAL POLARIZED RADIATING ELEMENTS

Figure 25 shows the BFN - PA circuit implementations for dual polarized radiating elements using 7 element overall feed clusters. Note that two PA's (one at 0 dB, one at appr. -10 dB level) are needed for each radiating element.

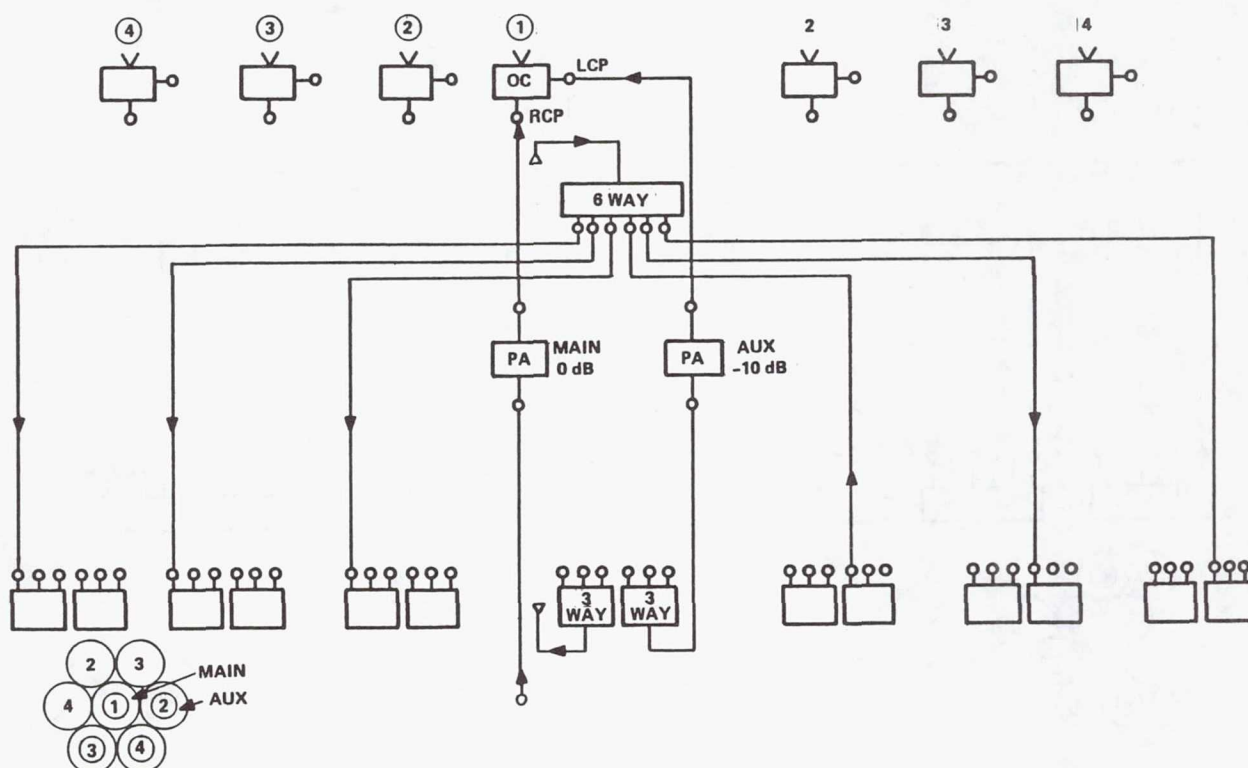


Figure 25

BFN USING SINGLE POLARIZED RADIATING ELEMENTS

Figure 26 displays the block diagram of the BFN-PA circuit using single polarized radiators.

In this case only 1 PA is needed per radiator (subarray).

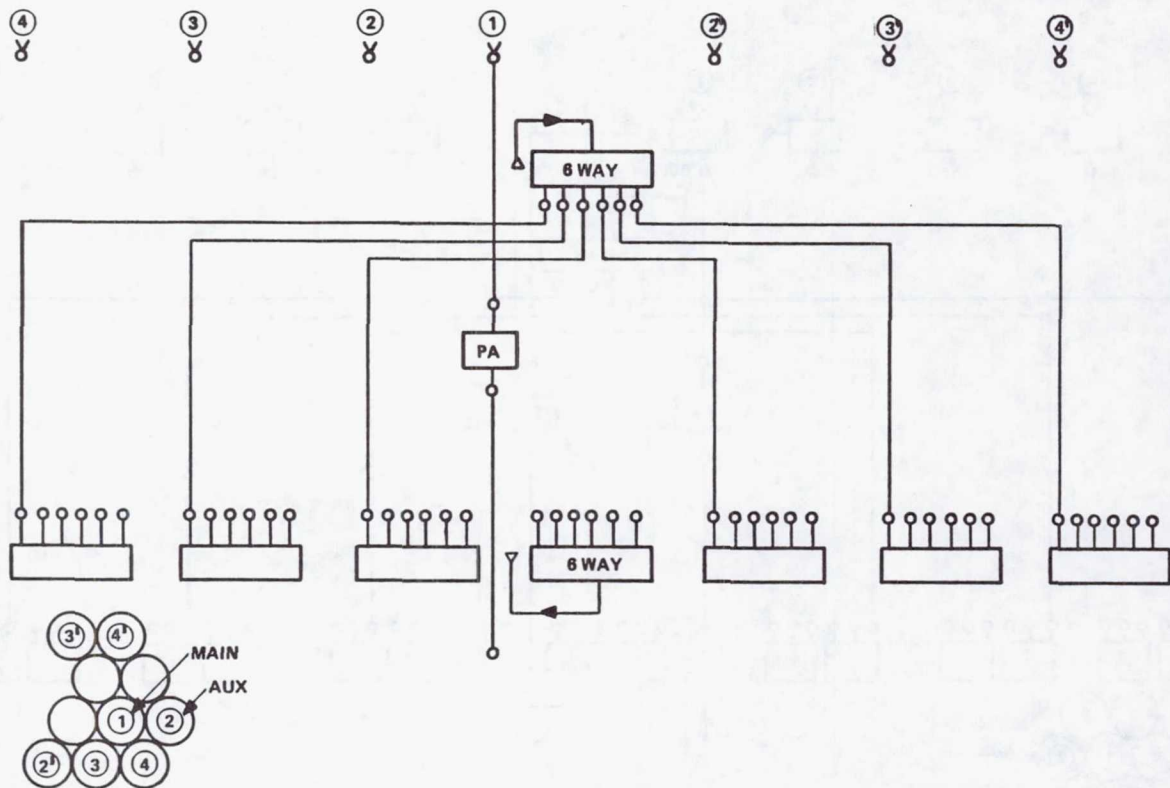


Figure 26

CONCEPTUAL LAYOUT OF BFN-PA CIRCUIT FOR DUAL AND SINGLE POLARIZED RADIATING ELEMENT

Figures 27a and 27b shows the physical implementation of the circuits described in Figures 25 and 26. The Figure 27a configuration contains 2 PA's, a 6-way and two 3-way dividers in 1 substrate. (For easier PA design the circuits may be separated into two layers.) The circuit board has 7 input and 7 output connectors (1 main and 6 auxiliary in each case). The main input terminal is fed from the S-band downconverter via a coaxial cable. The auxiliary input terminals are fed from the auxiliary output terminals of the other transmit modules via coaxial cables. The main output terminal is connected by an internal plug to the input terminal of the radiating element subarray.

Figure 27b shows the PA configuration for the single polarized case. Here more board space is available for the PA and two identical 6-way dividers are provided, one at the input and one at the output of the PA. The terminal connections are similar to the ones described Figure 27a.

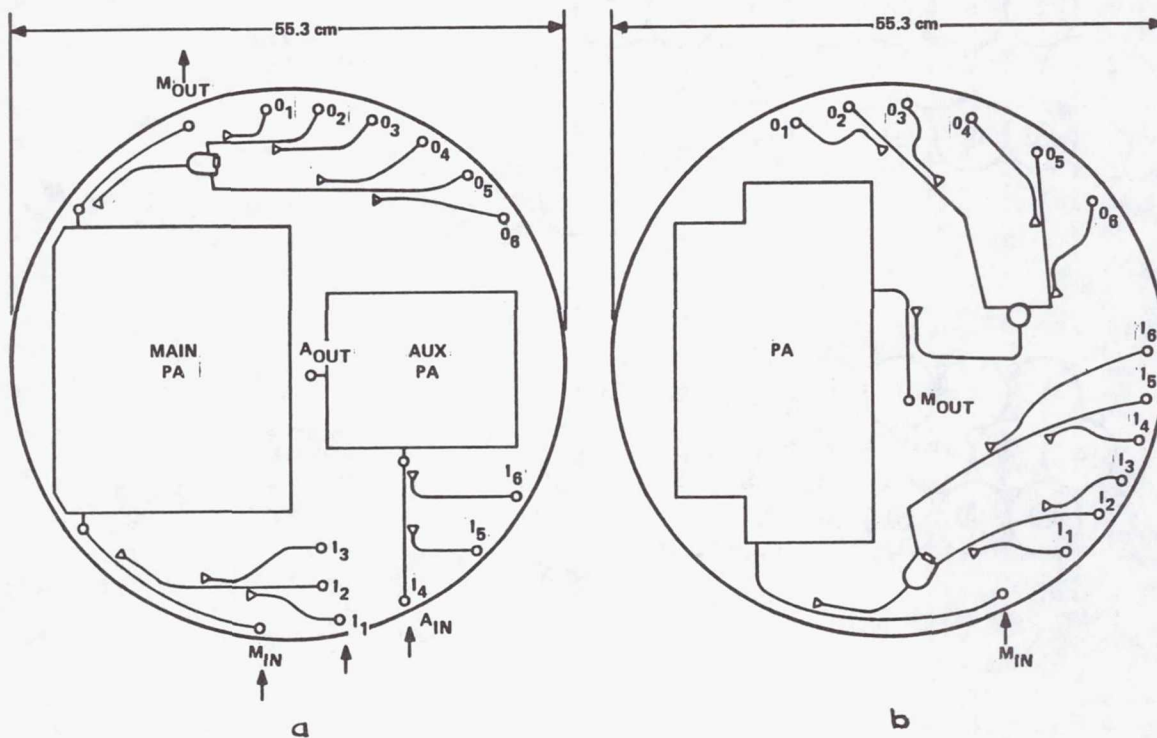
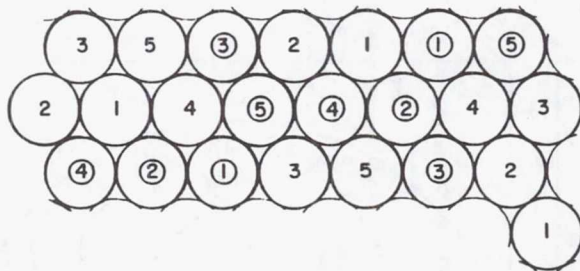


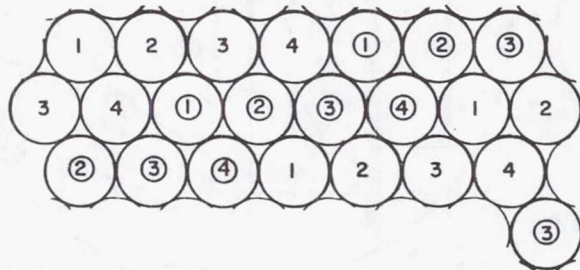
Figure 27

S-BAND BEAM TOPOLOGY ALTERNATIVES

Figure 28a shows a 4 frequency and Figure 28b a 5 frequency beam topology plan using 22 beams. They allow 2 or 3 empty cells between coverages respectively.



4 FREQUENCY PLAN,
2 EMPTY CELLS
n = 22

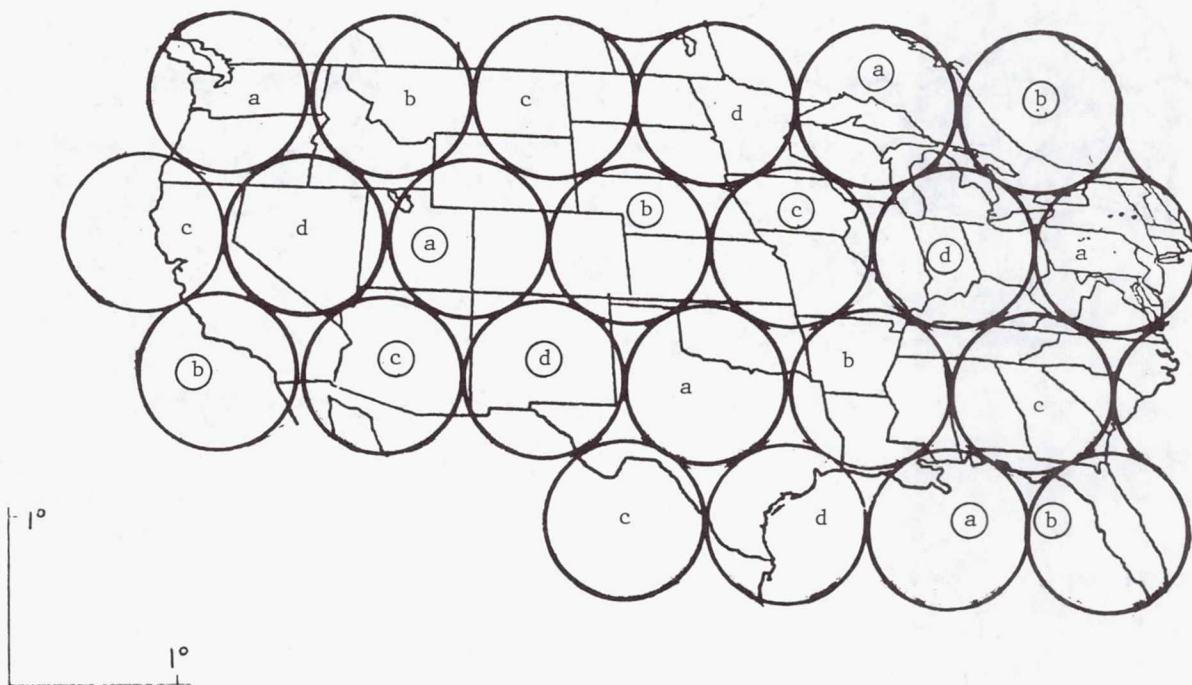


5 FREQUENCY PLAN,
3 EMPTY CELLS
n = 22

Figure 28

SELECTED S-BAND BEAM TOPOLOGY PLAN

Figure 29 shows the selected S-band beam topology plan using 23 beams, $\alpha = 1^\circ$ cell sizes and a 4 frequency, dual polarization configuration.

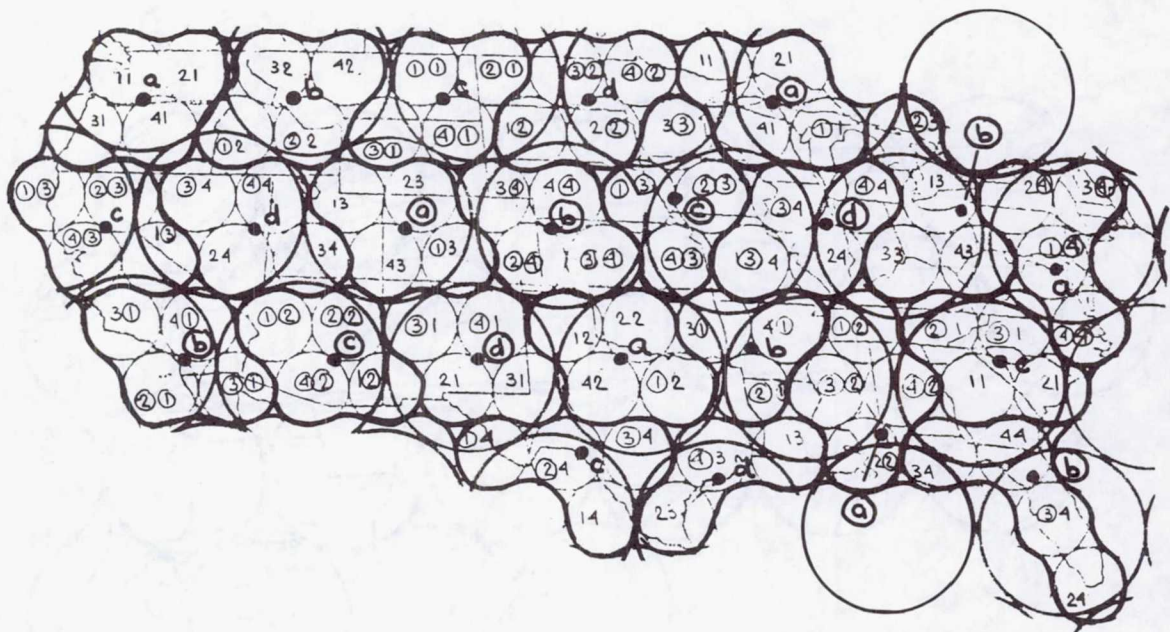


SYNCHRONOUS VIEW AT -110.00 DEGREES LONGITUDE

Figure 29

LOCATION OF S-BAND BASE STATIONS

Figure 30 displays the superimposed UHF and S-band beam topology plans and the location of the S-band base stations (marked by heavy dots). The plan assures an average base station to fixed user distance of appr. 180 km and a maximum distance of appr. 375 km. The maximum distance can be reduced by about a factor of 2 at the expense of adding 3 more base stations and retaining the same spacecraft antenna diameter.



110° W LONG

$\alpha_{\text{UHF}} = .423^\circ$

$n_{\text{UHF}} = 90$

$\alpha_s = 1^\circ$

$n_s = 23$

$r_{\text{av}} \sim 180 \text{ km}$

$r_M \sim 375 \text{ km}$

Figure 30

GEOMETRY OF THE S-BAND ANTENNA

Figure 31 shows the profile of the reflector and feed of the S-band antenna. Waveguide type polarizer and horn are assumed for the radiating element.

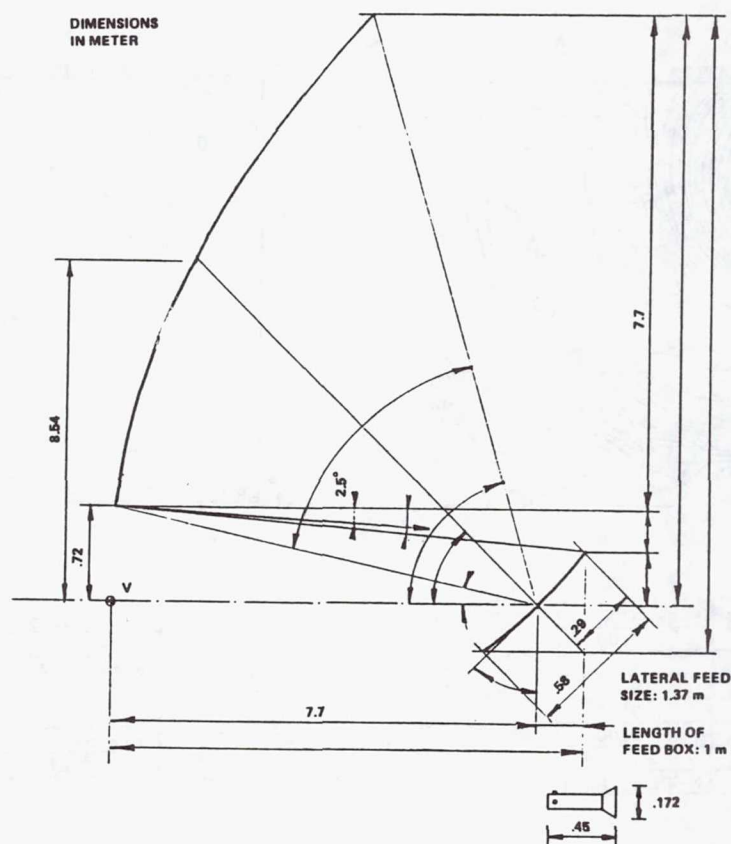


Figure 31

GAIN CONTOUR OF THE S-BAND ANTENNA FOR A MAXIMALLY SCANNED SINGLET

Figure 32 shows the gain contour of the maximally scanned singlet beam using a TE₁₁ mode excited circular aperture radiating element. Note that the sidelobe level is -24 dB and C/I is 21 dB in the applicable nearest interfered cell.

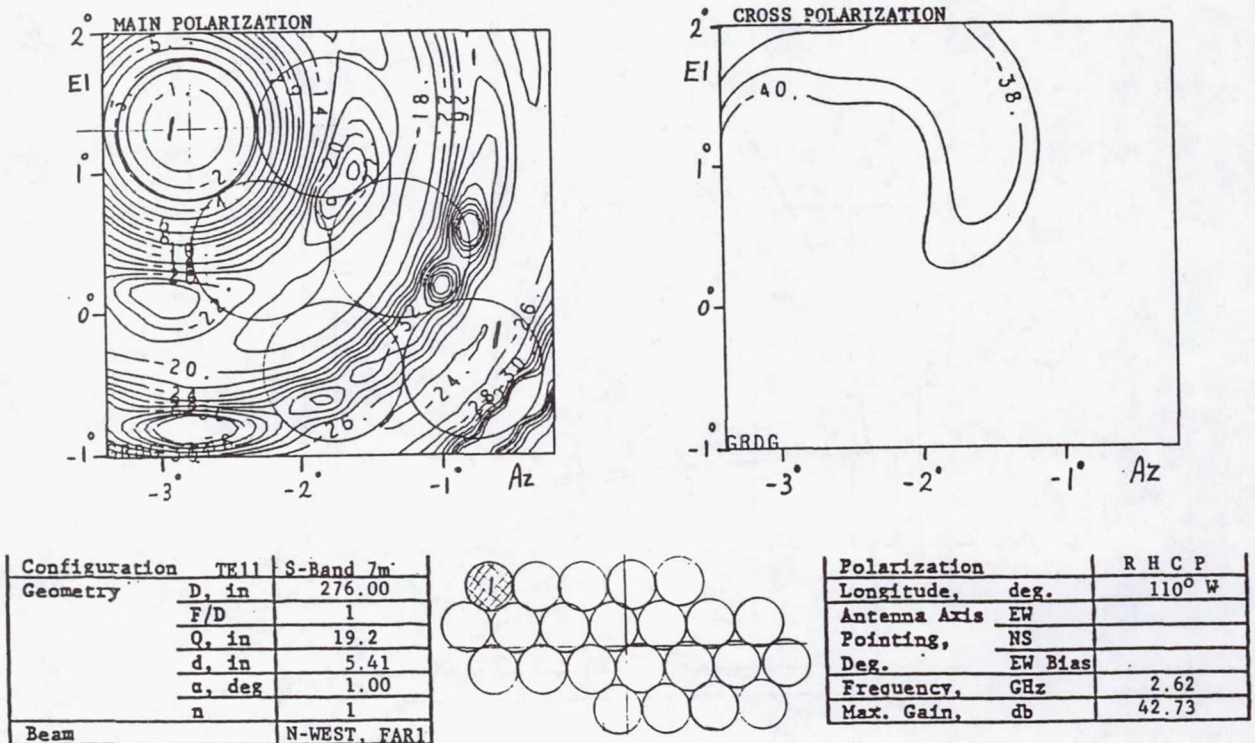


Figure 32

GAIN CONTOUR OF THE S-BAND ANTENNA FOR A 7 ELEMENT FEED CLUSTER

Figure 33 displays the gain contour achieved by the use of a 7 element cluster. The maximum gain is .73 dB less than with a single element but the sidelobe level is -35 dB and C/I is 33 dB in the interfered adjacent cell. The resultant C/I for the complete system is better than 27 dB.

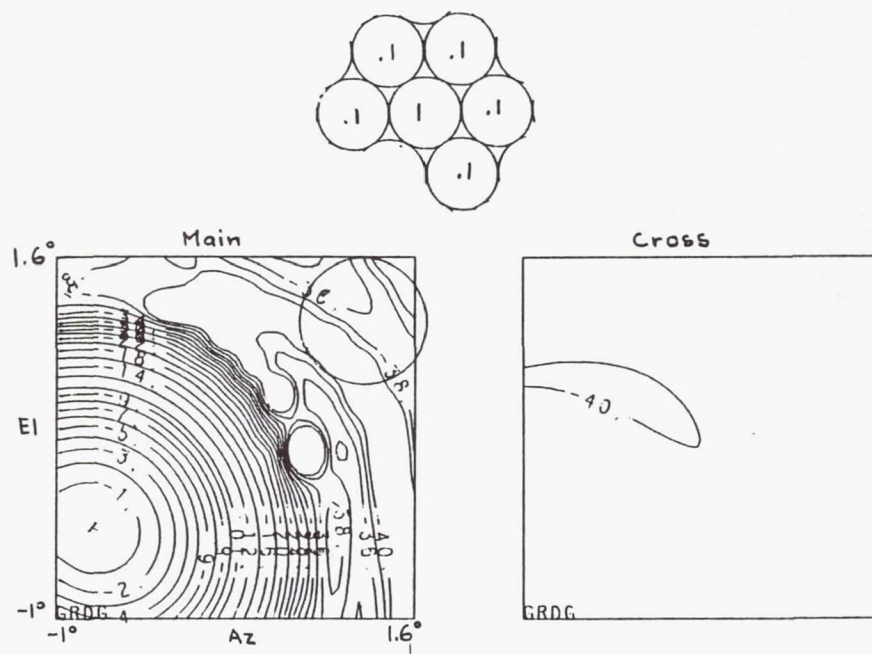


Figure 33

CONCLUSIONS

- A single STS packaged 118 m diameter hoop column antenna is capable of providing service for appr. 250,000 mobile users.
- The selected quad aperture configuration is able to provide at least 25 dB C/I without cable blockage, column scatter, coupling between quad apertures, and tolerance effects.
- A feed can be designed which uses single polarized radiating elements while the overall system employs dual polarization.
- The quad aperture concept can eliminate the use of diplexers and their associated losses.
- The critical technology issues in the RF area include the design of the radiating elements, BFN, monolithic power amplifiers and receiver front end, tolerance control and packaging of the feed.

ATTITUDE CONTROL SUBSYSTEM STUDY
FOR THE
LAND MOBILE SATELLITE SYSTEM SPACECRAFT

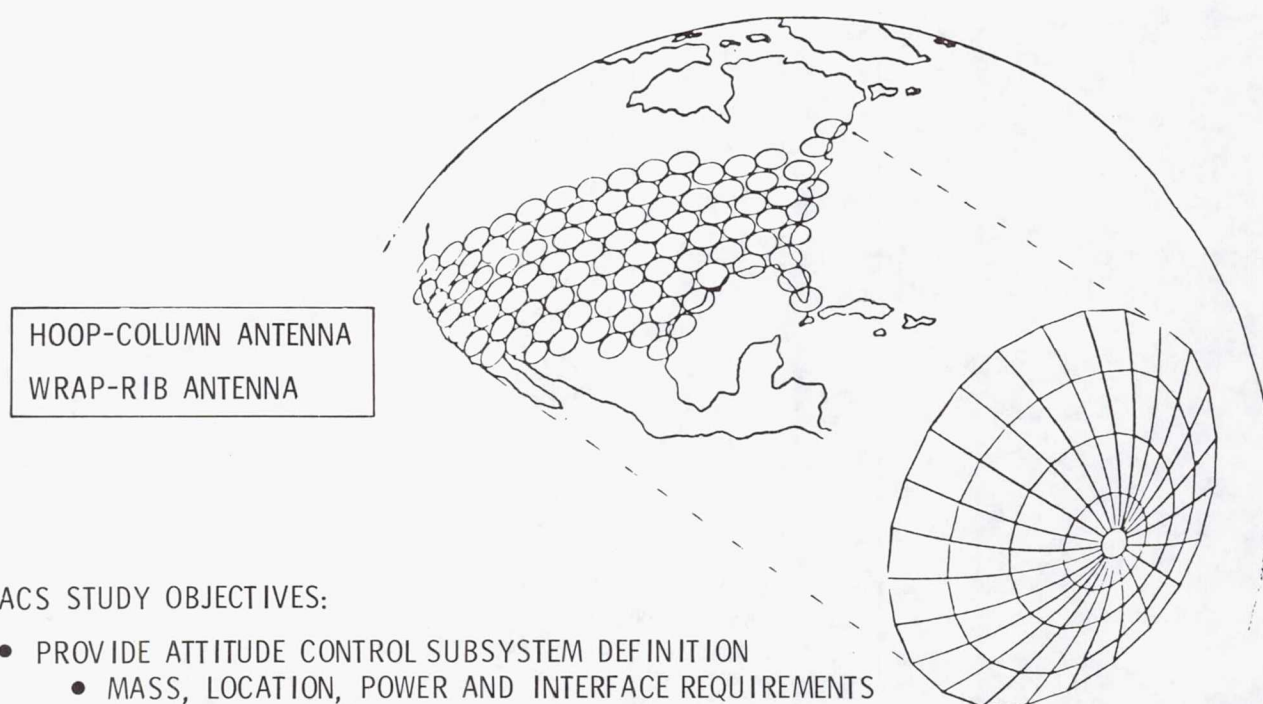
A.F. Tolivar
Jet Propulsion Laboratory
Pasadena, California

Large Space Systems Technology - 1981
Third Annual Technical Review
November 16-19, 1981

LMSS ATTITUDE CONTROL SUBSYSTEM STUDY OVERVIEW

The Land Mobile Satellite System (LMSS) is a multi-beam communications mission intended to provide telephone service to mobile users across the continental United States. This mission calls for a mid 1990's single Shuttle launch of a large reflector antenna at geosynchronous altitude. Two candidate LMSS configurations are under study. One involves a 55m Wrap-Rib design. The other involves a 122m diameter Hoop-Column design. Technology readiness is to be demonstrated by 1987.

The purpose of this Attitude Control Subsystem (ACS) study is to apply the generic LSST antenna control technology to the specific requirements of the LMSS mission and to define suitable attitude control subsystem designs for both LMSS configurations. The generic antenna control technology on which these designs are based was reported on by Yu-Hwan Lin in his paper entitled "Control of Large Space Antennas: Wrap-Rib--Hoop/Column" (see section on Controls). A further purpose of the study is to identify the technology developments required to establish technology readiness by 1987.



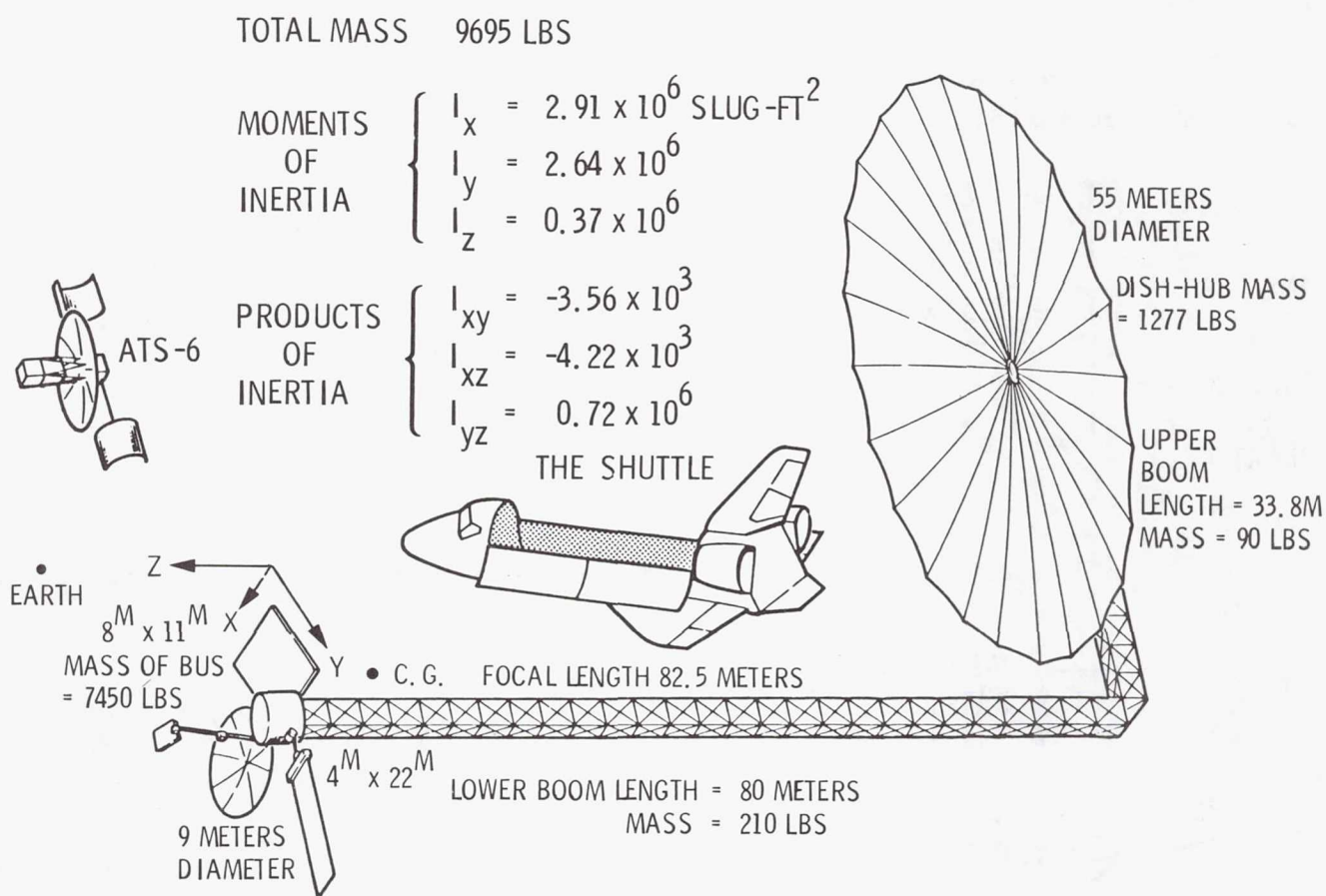
ACS STUDY OBJECTIVES:

- PROVIDE ATTITUDE CONTROL SUBSYSTEM DEFINITION
 - MASS, LOCATION, POWER AND INTERFACE REQUIREMENTS
- ASSESS ACS TECHNOLOGY DEVELOPMENT REQUIREMENTS
 - TECHNOLOGY READINESS BEFORE 1990

WRAP-RIB LMSS

CONFIGURATION AND MASS PROPERTIES

The Wrap-Rib LMSS consists of a 55m diameter dish, a massive feed array and a long L-shaped boom connecting the two. The long boom section is about 80m long and the short section measures about 33 meters. Total system mass is about 4400 kg (9700 lb), 80% of which is concentrated at the bus area, with the remaining 20% contributed by the reflector and the hub. Moments of inertia are large; note a very large cross product of inertia, a result of the inherent inbalance of the offset-feed configuration. The axis of least inertia is approximately along an imaginary straight line connecting the bus and the hub. This results in a 16° offset between the local vertical (Z-axis) and the axis of least inertia.



HOOP-COLUMN LMSS

CONFIGURATION AND MASS PROPERTIES

The Hoop-Column LMSS consists of the following fundamental elements: a 122 meter diameter hoop and an 88m telescoping mast. The hoop is held by cords extending from it to the mast (much like the spokes of a bicycle wheel). The antenna reflector mesh is held stretched and properly formed by the hoop and by a number of catenary cords and ties properly tensioned by means of control cables. Four massive feeds are located at one end (+Z) of the column. Spacecraft buses and solar panels are provided at both ends (+Z, -Z) of the column.

Total system mass is about 4690 kg (10,340 lb), half of which is concentrated at the +Z bus. The remaining mass is, roughly, equally distributed among the column, the hoop and the -Z bus. Moments of inertia are large. Cross products of inertia are negligible because of the inherent symmetry.

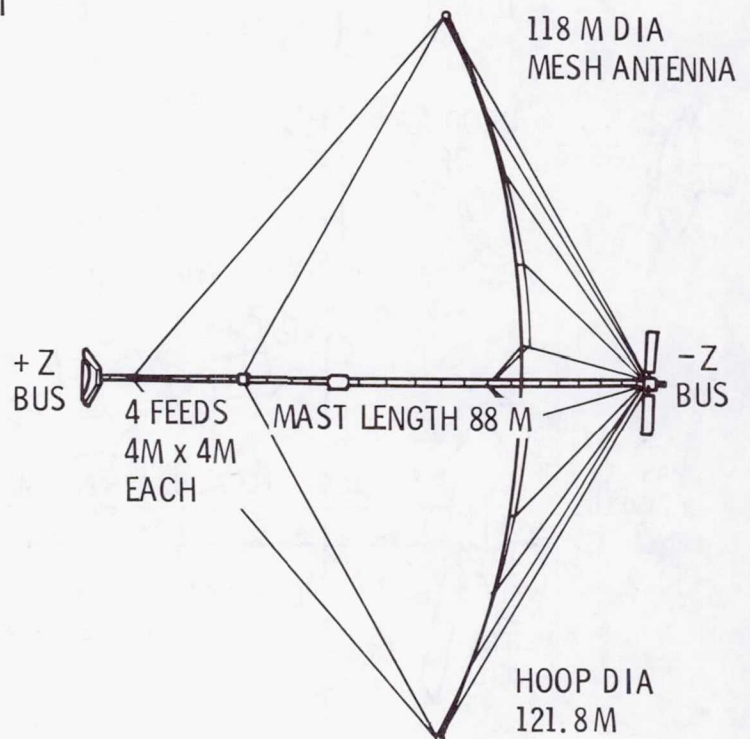
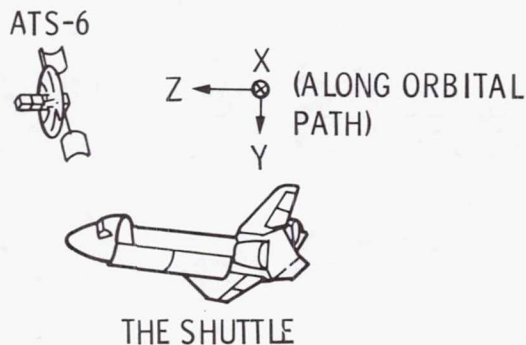
TOTAL MASS 10,340 LBS

MOMENTS OF INERTIA

$$\begin{cases} I_x = 5.89 \times 10^6 \text{ SLUG-FT}^2 \\ I_y = 5.89 \times 10^6 \\ I_z = 1.52 \times 10^6 \end{cases}$$

PRODUCTS OF INERTIA

$$I_{xy} = I_{yz} = I_{yz} = 0$$



MISSION PHASES

For attitude control purposes the mission is partitioned into four major phases: Phase I for launch into synchronous orbit; Phase II for separation, deployment, and acquisition of local vertical and celestial references; Phase III for system checkout, updating, and performance testing; and Phase IV, the operational cruise phase. The ACS operations during these phases are discussed in the following paragraphs.

During Phase I LMSS is first carried by the Shuttle to lower earth orbit (LEO) and subsequently transferred into geosynchronous orbit (GEO) by the Orbit Transfer Vehicle (OTV). All control functions during this period are provided by the Shuttle and OTV Guidance and Control (G&C) systems. Throughout this phase the LMSS ACS is typically powered on but functionally disabled. Immediately prior to separation the ACS is initialized and initial attitude information is handed off to the ACS from the OTV G&C system.

Phase II covers the separation, deployment, and acquisition of local vertical. Various alternate scenarios are possible during this phase (for example, deployment can be performed after separation, or before it, while LMSS is still attached to the OTV). Several choices are also possible as to the order of the various deployment activities. For the purposes of our design we have made the following assumptions:

- i) The deployment sequence consists of four principal events: boom extension, reflector unfurling, solar panel deployment, and feed deployment (not necessarily in that order). Complete deployment can take anywhere from about 1-2 hours to 12 hours or more if sequence is ground assisted with ground analysis and verification of intermediate deployment states.

PHASE	APPROX. DURATION
I. LAUNCH INTO SYNCHRONOUS ORBIT	24 - 48 HRS
II. SEPARATION, DEPLOYMENT AND ACQUISITION OF LOCAL VERTICAL AND CELESTIAL REFERENCES	6 - 24 HRS
III. SYSTEM CHECKOUT, UPDATING AND PERFORMANCE TESTING	1 - 3 MONTHS
IV. OPERATIONAL CRUISE	10 YEARS

- ALL CONTROL FUNCTIONS DURING PHASE I ARE PERFORMED BY THE LAUNCH VEHICLE OR THE ORBIT TRANSFER VEHICLE
- LMSS ACS MUST PROVIDE CONTROLS DURING PHASES II, III, AND IV

MISSION PHASES - Continued

- ii) It is desirable to deploy the solar panels as early as convenient in the sequence and to point them to the sun.
- iii) Once the LMSS is deployed, it is undesirable to perform extensive search maneuvers to locate the earth and the sun and to reorient the spacecraft to the correct pointing. Such search maneuvers typically involve several 360° search turns. Because of the very large inertia of the deployed LMSS, such turns would require considerable time (several hours).

The following scenario can be postulated for Phase II: it will be assumed that prior to separation the OTV will orient the LMSS to the desired initial orientation (+Z axis along local vertical, +Y axis due south). The LMSS gyro package will be initialized to this orientation just prior to separation.

The separation event is normally commanded by activating pyrotechnic latches which when released allow a set of spring loaded mechanisms to push apart the two bodies. As a result of the separation forces, residual tip off rates are invariably imparted to the bodies. In the case of LMSS such angular rates could be in the order of $1^{\circ}/s$. A separation time of 0.3 seconds would be typical (this is the time it would take for the spring mechanisms to extend completely. During this brief period of time, the gyros are on but the ACS thrusters are briefly inhibited. About 1 second after separation the thrusters are enabled and will begin to fire to null out the separation rates, to stabilize the LMSS about the desired initial orientation, and to impart to it the required $15^{\circ}/hr$. orbital rate.

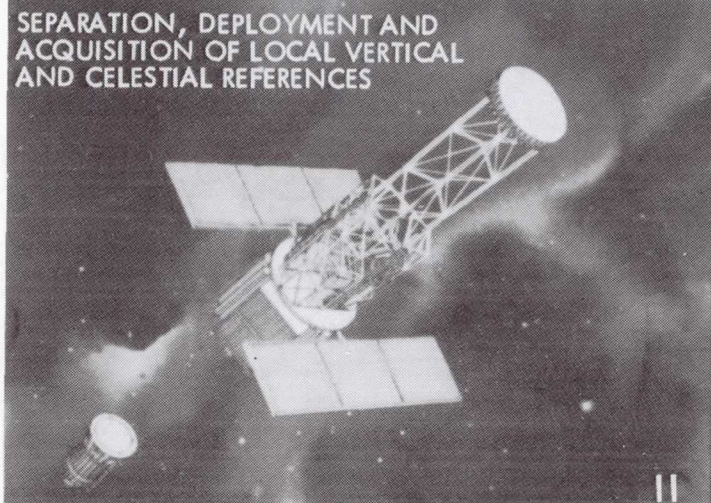
Once the LMSS has been stabilized following the separation event, deployment can begin with the initial extension of the boom, followed by deployment of the solar array and sun acquisition. This will be followed by deployment of the 2 reflectors and their feeds. During these events, the deploying antenna is maintained correctly pointed to the ground and the sun by means of ephemeris data, gyro and earth sensor outputs, and solar panel sun sensor data. Precise pointing during this phase is not important; the main objective is to complete the separation and deployment events in the "acquired" mode, i.e., with the earth and the sun in the field-of-view of the optical sensors.

Phase III is a period of 30 to 90 days during which extensive system evaluation calibration and checkout take place. An optical sensor is used during this phase to measure the static linear and angular alignment errors of the deployed feed and reflector and their relation with respect to the ACS control reference frame. The same optical sensor is also used during this phase to perform the in-orbit dynamic characterization of the system (systems identification). Such in orbit testing of the system (which is needed because of the impossibility of ground testing such a large structure) will yield the mode shape and frequency data required to update the control system flight software to achieve the desired precise pointing and stabilization of the antenna. It is envisioned that this will be an iterative process requiring significant ground support.

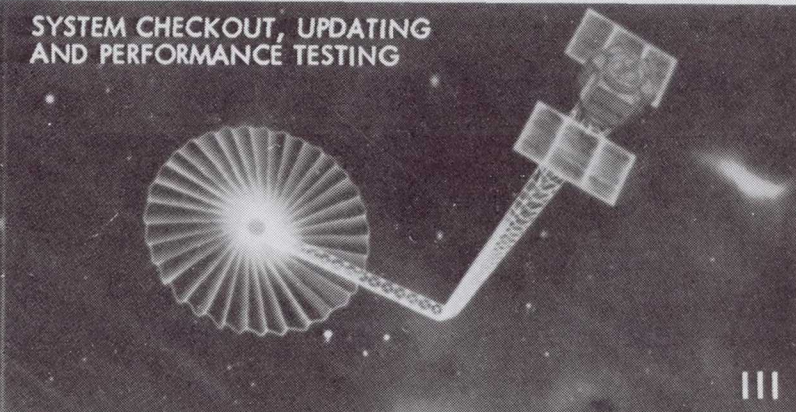
The 10 year operational phase (Phase IV) begins after the system has been thoroughly checked out, calibrated, and the required performance levels have been achieved. During Phase IV the ACS will maintain precision pointing of the antenna to the desired ground target for the duration of the mission. Stationkeeping operations will be carried out periodically without interruption of service of degradation of pointing.

WRAP-RIB LMSS MISSION PHASES

MISSION PHASES



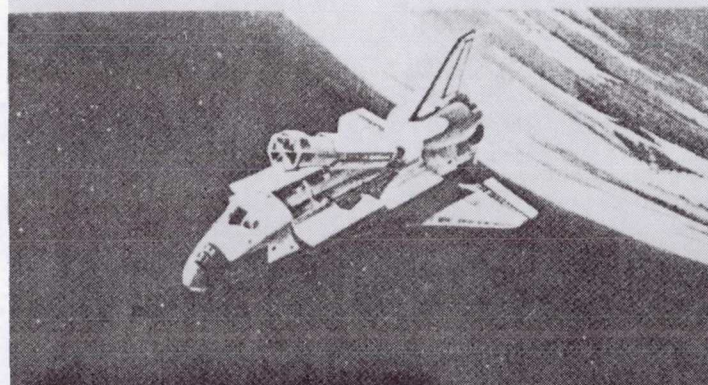
SYSTEM CHECKOUT, UPDATING AND PERFORMANCE TESTING



OPERATIONAL CRUISE

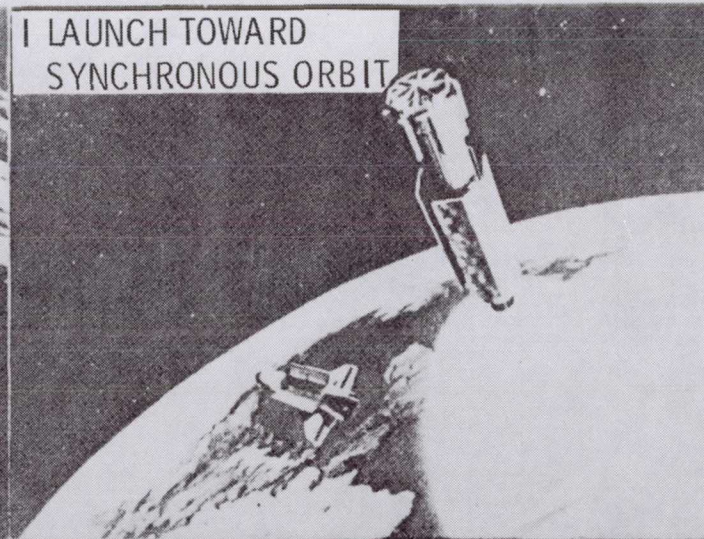
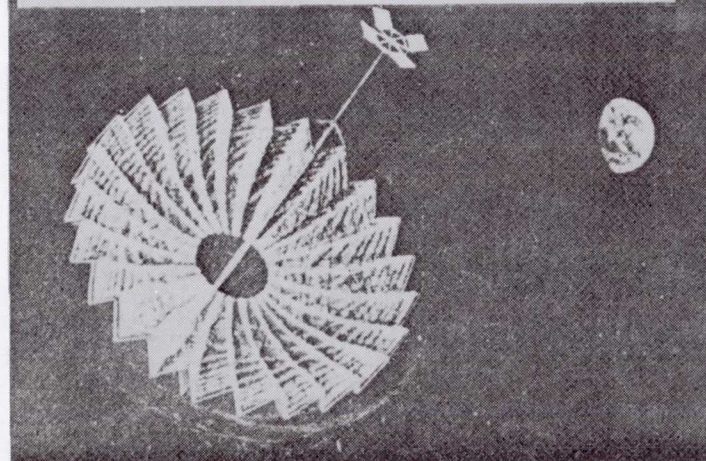


HOOP/COLUMN LMSS MISSION PHASES

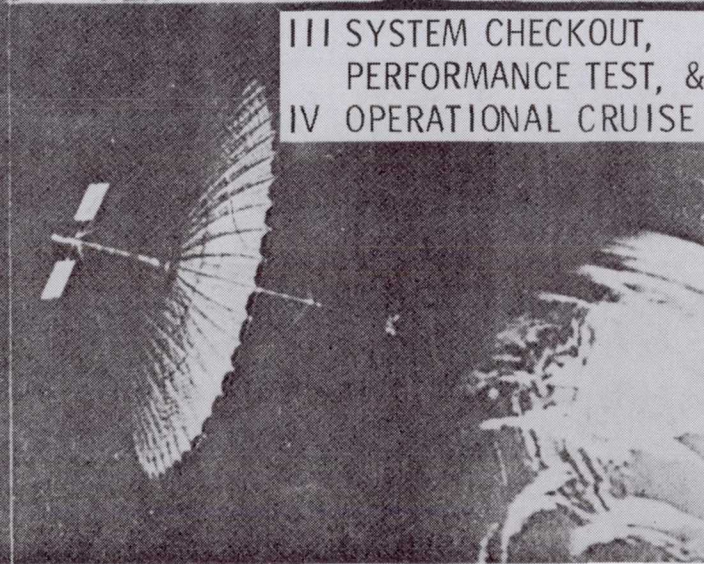


SHUTTLE DELIVERY
TO LOW ORBIT

II SEPARATION, DEPLOYMENT AND
ACQ LOCAL VERTICAL AND
CELESTIAL REFS



I LAUNCH TOWARD
SYNCHRONOUS ORBIT



III SYSTEM CHECKOUT,
PERFORMANCE TEST, &
IV OPERATIONAL CRUISE

FUNCTIONAL REQUIREMENTS

The LMSS Control subsystem functional requirements are given below. Accuracy requirements are given in the following page. Note that the ACS performs two fundamental functions during the operational phase: i) the attitude control function and, ii) the autopilot function, during which it commands the stationkeeping thrusters to achieve the desired ΔV while maintaining correct pointing. Also note a need for a high degree of autonomy and a long 10 year lifetime requirement.

- REDUCE SEPARATION RATES, RETAIN CONTROL DURING DEPLOYMENT, AND ACQUIRE REFERENCES (PHASE II)
- PROVIDE SOLAR ARRAY POINTING TO THE SUN (II, III, IV)
- PROVIDE THE CORRECT ANTENNA POINTING DURING MISSION PHASES FOLLOWING ACQUISITION OF REFERENCES (III, IV)
- AUTOMATICALLY REACQUIRE REFERENCES IN THE EVENT THEY ARE LOST
- MAINTAIN THE PROPER DISH SURFACE ACCURACY AND THE RELATIVE FEED/DISH POSITION AND ORIENTATION (IV)
- COMMAND PROPULSION AND CONTROL HARDWARE DURING STATION KEEPING TO MAINTAIN EARTH POINTING AND ACHIEVE DESIRED ΔV (IV)
- PROVIDE CONTINUOUS CONTROL FOR 10 YEAR OPERATION

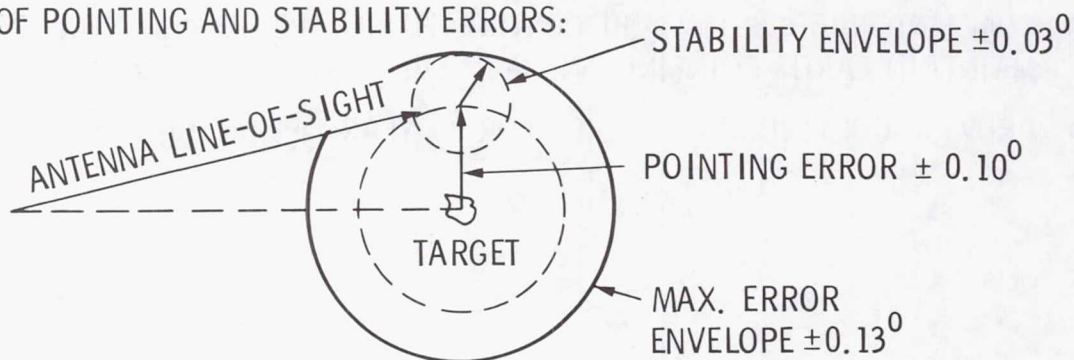
LMSS ACCURACY REQUIREMENTS

In order for the LMSS to provide adequate communication service, system accuracy requirements must be satisfied as shown below (and discussed in the paper by C. T. Golden, et al.).

The Attitude Control Subsystem accuracy requirements have been set, as shown below, at a fraction of the total system accuracy requirement.

	SYSTEM	CONTROL
POINTING* (AFTER CALIBRATION/ COMPENSATION FOR THERMAL OFFSETS, ETC.)	$\pm 0.10^0$	$\pm 0.03^0$
STABILITY*	$\pm 0.03^0$	$\pm 0.02^0$
DISH SURFACE ACCURACY, RMS	12 MM	6 MM
SOLAR ARRAY POINTING	$\pm 1^0$	$\pm 1^0$

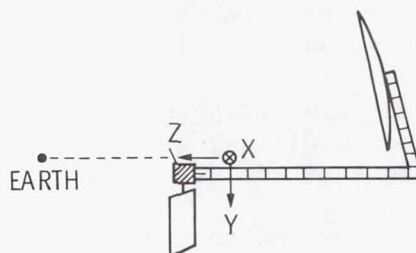
* ILLUSTRATION OF POINTING AND STABILITY ERRORS:



ENVIRONMENTAL DISTURBANCES — WRAP-RIB

- GRAVITY GRADIENT TORQUES
 - CONSTANT TORQUE OF 1.14×10^{-2} FT-LB (ABOUT X-AXIS) DUE TO 16° ANGLE BETWEEN AXIS OF MIN. INERTIA AND LOCAL VERTICAL (DAILY MOMENTUM = 984 FT-LB-SEC)
- DYNAMIC BALANCING TORQUES
 - VEHICLE NOT BALANCED ABOUT ITS SPIN AXIS (1 REV/DAY) WHICH IS ALSO 16° OFF FROM AXIS OF MAX. INERTIA
 - A CONSTANT TORQUE OF 3.79×10^{-3} FT-LB (ABOUT X-AXIS) REQUIRED TO MAINTAIN SUCH A SPIN (DAILY MOMENTUM = 328 FT-LB-SEC)
- SOLAR PRESSURE TORQUES
 - CYCLIC WITH ONE DAY PERIOD
 - DISH DOMINATING

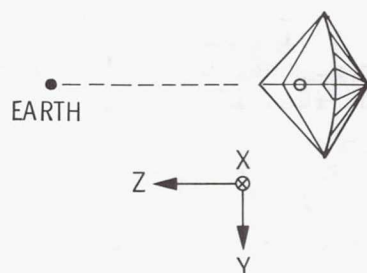
	X-AXIS	Y-AXIS	Z-AXIS
TORQUE RANGE (FT-LB) $\times 10^2$	± 1.28	± 2.75	± 0.628
PEAK-TO-PEAK MOMENTUM (FT-LB-SEC)	288	653	151



ENVIRONMENTAL DISTURBANCES — HOOP/COLUMN

- GRAVITY GRADIENT TORQUES
 - CONSTANT TORQUE OF 0.72×10^{-2} FT-LB (ABOUT X-AXIS) DUE TO 6° OFFSET BETWEEN AXIS OF MINIMUM INERTIA AND LOCAL VERTICAL (DAILY MOMENTUM = 622 FT-LB-SEC)
- DYNAMIC BALANCING TORQUES
 - VEHICLE NOT BALANCED ABOUT ITS SPIN AXIS (1 REV/DAY) WHICH IS ALSO 6° OFF OF AXIS OF MAX INERTIA
 - A CONSTANT TORQUE OF 0.24×10^{-2} FT-LB (ABOUT X-AXIS) REQUIRED TO MAINTAIN SUCH A SPIN (DAILY MOMENTUM = 207 FT-LB-SEC)
- SOLAR PRESSURE TORQUES
 - CYCLIC WITH ONE DAY PERIOD
 - DISH DOMINATING

	X-AXIS	Y-AXIS	Z-AXIS
TORQUE RANGE (FT-LB) $\times 10^2$	± 0.224	± 1.83	± 0.004
DAILY MOMENTUM (FT-LB-SEC)	28	548	1



ACS DESIGN CONCEPT

In addition to the requirements for maintaining precise attitude pointing and stability of a large flexible structure in an environment of large disturbances, a number of other key drivers led to the selection of the LMSS orbital control system. The system has to accommodate stationkeeping updates while maintaining operation and be able to provide a 10 year useful orbit life with high reliability. The designs presented in what follows represent integrated designs capable of performing all required functions during the various mission phases, including both the attitude control and autopilot functions.

The ACS designs presented here for the Wrap-Rib and the Hoop-Column configurations represent fundamentally similar ACS design philosophy and technology. These systems are based on the "type 3" control systems which Y.H. Lin described and analyzed in the paper referenced earlier. Fundamentally, both systems make use of distributed sensing and control to stabilize and point the antennas. The minor differences between the two systems are due to the basic differences in configuration, mass, and dynamic characteristics.

Primary attitude control in both systems is placed at the +Z (feed) bus and is controlled to 0.01° using a high bandwidth gyro based control loop which is nested within an attitude determination and gyro drift correction loop using star trackers.

The reflector and the remainder of the structure is then stabilized and controlled with respect to the feed bus to an equivalent 0.01° by means of

- i) Optical dish sensor located at the feed which monitors the motion of the reflector with respect to the feed.
- ii) Six degree-of-freedom control actuators to provide forces and torques at two ends of the structure:
 - at feed and hub for the Wrap-Rib configuration
 - at feed and -Z bus for the Hoop-Column configuration

(Hoop-Column also uses 1 DOF Hoop mounted thrusters to achieve hoop stabilization and proper antenna torsional control). Six DOF actuators include 3 small fine pointing reaction wheels (20 N-m-s) and 3 attitude control and station-keeping jets (0.2 - 0.9 N thrust) at each location.
- iii) A second gyro package at the -Z bus is also used for stabilization in the Hoop-Column configuration.

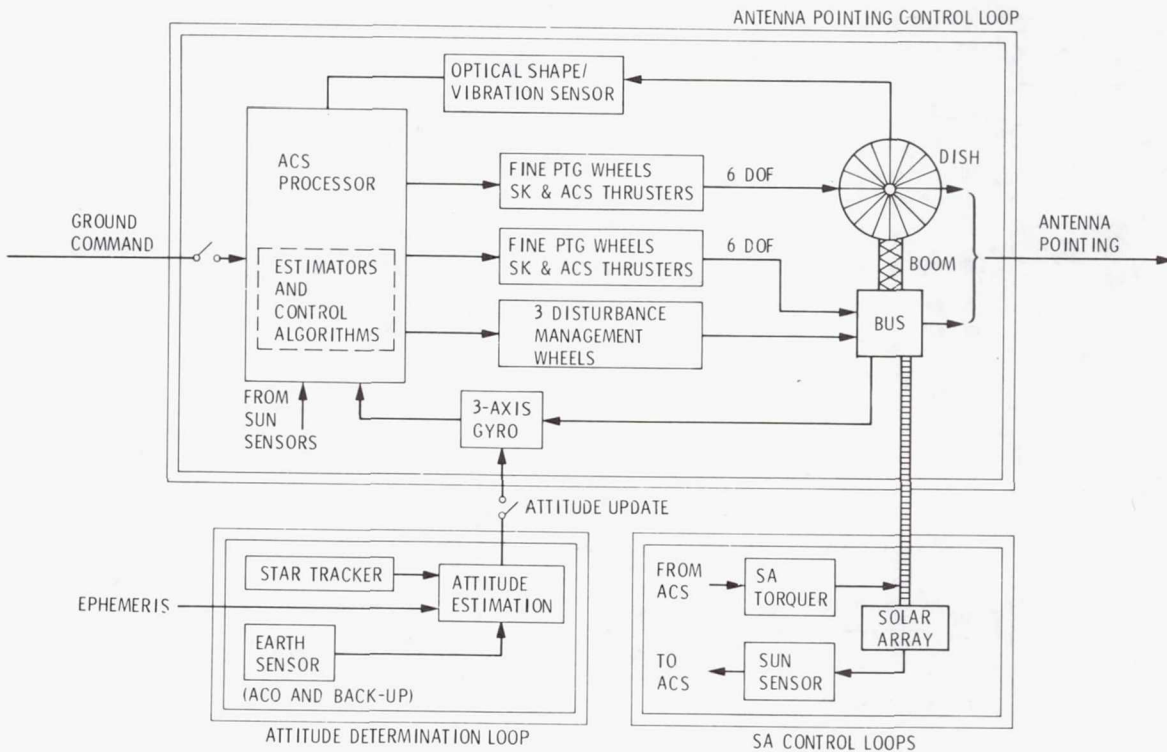
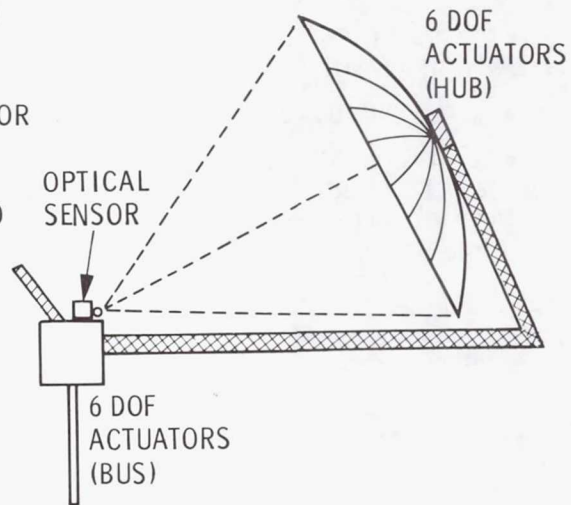
The optical sensors are also used during Phase III to carry out the necessary alignment checkout and to perform the dynamic measurement required for in-orbit systems identification.

ACS DESIGN CONCEPT — WRAP-RIB

- PRIMARY ATTITUDE CONTROL OF BUS TO 0.01° USES HIGH BW GYRO BASED CONTROL LOOP NESTED WITHIN AN ATTITUDE DETERMINATION AND GYRO DRIFT CORRECTION LOOP USING STAR TRACKERS

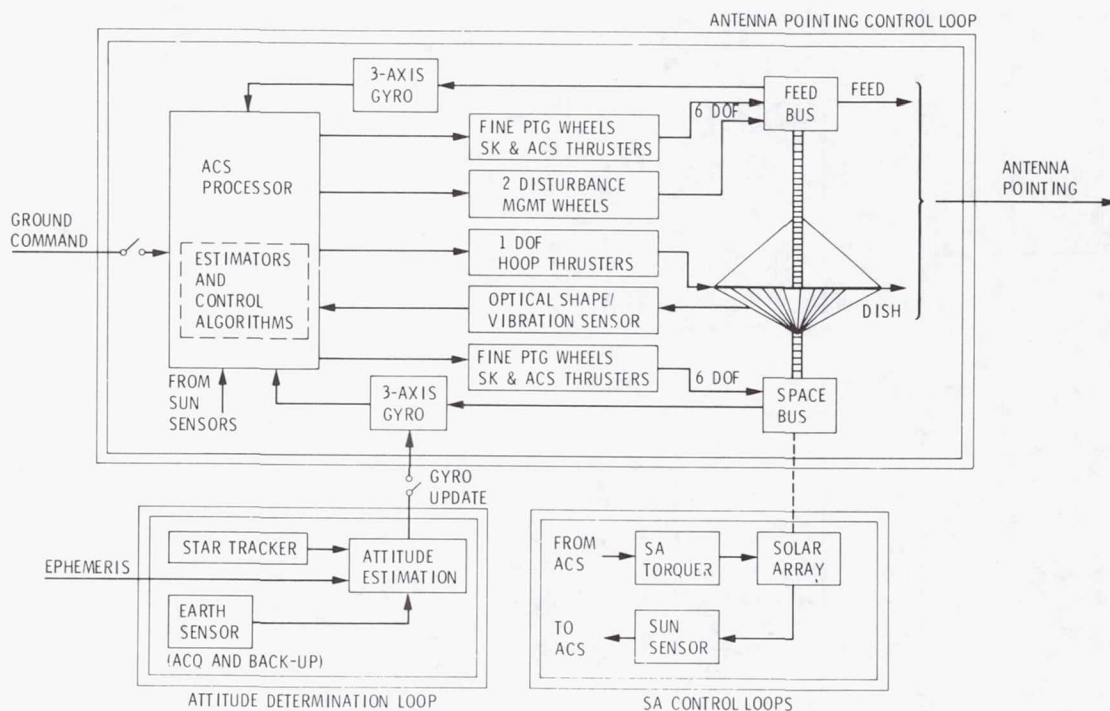
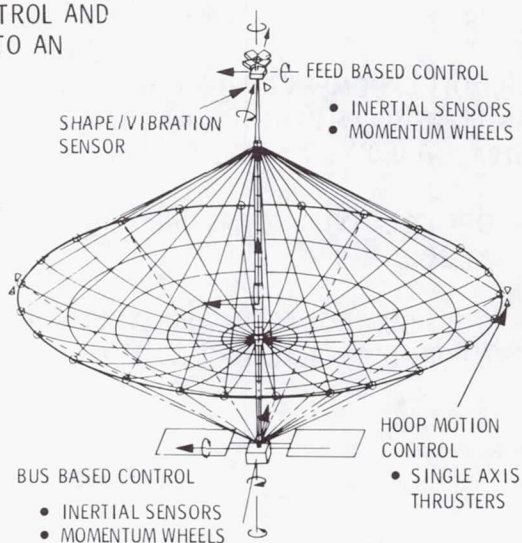
- DISH MOTION COMPENSATION CONTROL AND BOOM STABILIZATION WITH RESPECT TO BUS TO AN EQUIVALENT 0.01° BY MEANS OF:

- OPTICAL DISH SHAPE/VIBRATION SENSOR AT BUS, AND
- 6 DOF CONTROL ACTUATORS AT BUS AND 6 DOF CONTROL ACTUATORS AT HUB



ACS DESIGN CONCEPT — HOOP/COLUMN

- PRIMARY ATTITUDE CONTROL OF FEED BUS TO 0.01° USES HIGH BW GYRO BASED CONTROL LOOP NESTED WITHIN AN ATTITUDE DETERMINATION AND GYRO DRIFT CORRECTION LOOP USING STAR TRACKERS
- REFLECTOR/HOOP MOTION COMPENSATION CONTROL AND STABILIZATION WITH RESPECT TO FEED HELD TO AN EQUIVALENT 0.01° BY MEANS OF:
 - OPTICAL DISH SHAPE AND HOOP POSITION SENSORS AT FEED
 - SPACE BUS GYRO PACKAGE
 - 6 DOF CONTROL ACTUATORS AT FEED, 6 DOF CONTROL ACTUATORS AT SPACE BUS, AND 1 DOF HOOP THRUSTERS



ACS DESIGN CONCEPT (continued)

In addition to the small fine pointing wheels, 3 larger wheels are provided for disturbance management. The wheels are sized to allow 100% management of cyclic solar pressure torques, and partial management of gravity gradient and balancing torques with 4 momentum dumpings per day. This approach was selected in a trade study which was performed to compare a gas jet only system vs. a gas jets and wheels system. Selection criteria included performance, reliability, and weight.

Thrusters at both ends of the structure are pulse modulated to keep net average thrust through the S/C center of mass during stationkeeping operations. Thrusters are also used for all turn maneuvers required for reacquisition.

The thrusters are also used in Phase II for primary control during initial separation rate reduction and coarse pointing during deployment. Configuration must allow use of thrusters while structure is deploying.

- DISTURBANCE TORQUE MANAGEMENT PROVIDED BY REACTION WHEELS WHICH ARE SIZED FOR:
 - 1) DUMPING EVERY 6 HOURS THE ACCUMULATED MOMENTUM DUE TO ONE-SIDED TORQUES, I.E. GRAVITY GRADIENT AND DYNAMIC BALANCING TORQUES
 - 2) 100% WHEEL MANAGEMENT OF DAILY CYCLIC SOLAR PRESSURE TORQUES
- THRUSTERS AT BOTH ENDS OF STRUCTURE USED TO KEEP NET THRUST THROUGH VEHICLE C.G. DURING STATION KEEPING
- THRUSTER CONTROL PROVIDES COARSE POINTING ($1^0 - 5^0$) DURING SEPARATION, DEPLOYMENT AND ACQUISITION (THRUSTERS MUST BE AVAILABLE IMMEDIATELY AFTER SEPARATION)
- THRUSTER CONTROL PROVIDES TORQUES FOR REACQUISITIONS
- ARTICULATION OF EACH SOLAR PANEL PROVIDED BY 1 DOF ACTUATOR DRIVES AND CONTROLLED BY SUN SENSORS

ACS EQUIPMENT LIST
WRAP-RIB AND HOOP-COLUMN

The following two charts tabulate the control equipment list needed to implement the ACS designs just described. The tables identify each component and list its physical characteristics (mass, dimensions), power and mounting requirements, as well as a brief description of its design heritage, estimated lifetime, and other pertinent comments.

For the most part all the required components are either under development, presently available, or would require reasonable refinements of presently available technology. Perhaps the most critical exception to this is the optical shape and vibration sensor. A potential solution to this gap is the SHAPES 3-D sensor (described in the paper presented by J. M. McLauchlan in the session on Controls).

EQUIPMENT, NUMBER*	UNIT MASS KG (LB)	UNIT AVG/PEAK POWER WATTS	DIMENSION PER UNIT CM (IN.)	DESIGN HERITAGE	LOCATION*		ESTIMATED UNIT LIFETIME YEARS	COMMENTS
					+Z	-Z		
FINE POINTING WHEELS 8 8	10 (22)	5/70	15 x 35 DIAM. (6 x 14 DIAM.)	STD BALL BEARING OR MAGNETIC BEARING DESIGNS	4 4	4 4	10	1 WHEEL PER AXIS PLUS ONE SKEWED SPARE AT EACH OF 2 LOCATIONS, 20 N-MS PER WHEEL. MASS, POWER AND SIZE BASED ON CURRENT BALL BEARING WHEEL TECHNOLOGY
3-AXIS FIBER OPTICS INERTIAL REFERENCE UNIT 1 2	11 (24.2)	20/20	25 x 25 x 25 (9.9 x 9.9 x 9.9)	OAST SINGLE-AXIS FORS SENSOR	1 1	0 1	10	FIBER OPTICS ROTATION SENSOR (FORS). SINGLE- AXIS LONG-LIFE GYRO PRESENTLY IN BREAD BOARD STATUS
2-AXIS CCD STAR TRACKER 2 2	5.5 (12.2)	10/10	13 x 18 x 32 (5 x 7 x 12)	OAST PROTOTYPE STELLAR TRACKER	2 2	0 0	10	8° x 8° FIXED HEAD STAR TRACKER; 5 SEC ACCURACY, PRESENTLY IN ENGINEER- ING MODEL STATUS (NO ADVANCED DEVELOPMENT FUNDED). EXTRA UNIT IS FOR BACK-UP
2-AXIS EARTH SENSOR 2 2	2.54 (5.6)	3.2/3.2	14 x 12.25 x 11 (5.7 x 5.0 x 4.5)	LANDSAT AND QUANTIC MOD. IV R	2 2	0 0	7	QUANTIC MODEL 5100; DESIGNED FOR DSCS III; ACCURACY AT 0.042° (3σ); EARTH ACQUISITION ATTITUDE RANGE ± 17°
2-AXIS SUN SENSOR 2 3	0.52 (1)	1/1	15 x 15 x 8.9 (6 x 6 x 3.5)	ATS-6	2 2	0 1	7	ANALOG, 180° SOLID ANGLE
OPTICAL SHAPE AND VIBRATION SENSOR 1 1	20 (44)	100/100	25.4 x 35.6 x 76.2 (10 x 14 x 30)	NEW	1 1	0 0	10	CHARACTERISTICS BASED ON SENSOR CONCEPT FOR SPATIAL HIGH ACCURACY POSITION ENCODING SENSOR (SHAPES) MOUNTED AT BUS, OPTICAL- LY STARES AT DISH

* TOP NUMBER FOR WRAP-RIB DESIGN, BOTTOM NUMBER FOR HOOP/COLUMN DESIGN

ACS EQUIPMENT LIST

WRAP-RIB AND HOOP-COLUMN - Continued

The digital computer shown is based on ATAC-16S technology and an estimated processing requirement of 286,000 instructions per second.

One solar array actuator is required to articulate the Wrap-Rib configuration single solar panel. Two actuators are needed to articulate the 2 sets of solar arrays used in the Hoop-Column configuration.

The table also shows the characteristics of the large disturbance management wheels and a tabulation of the attitude control propellant requirements.

EQUIPMENT, NUMBER*	UNIT MASS KG (LB)	UNIT AVG/PEAK POWER WATTS	DIMENSION PER UNIT CM (IN.)	DESIGN HERITAGE	LOCATION*		ESTIMATED UNIT LIFETIME YEARS	COMMENTS
					+Z	-Z		
DIGITAL COMPUTER (2) $\frac{2}{2}$	25 (55)	40/40	16.8 x 29.5 x 22.9 (6.6 x 11.6 x 9)	GALILEO	$\frac{2}{2}$	$\frac{0}{0}$	20	EACH UNIT CONSISTS OF 2 ATAC-16S PROCESSORS, 2 RAMS, 2 I/O'S AND 2 DMA'S EXTRA UNIT IS FOR BACK-UP AND IS POWERED ALL TIME
1 DOF SOLAR ARRAY ACTUATOR $\frac{1}{1}$	5 (11)	2/19	27 x 11.0 DIAM (10.6 x 4.3 DIAM)	TBD	$\frac{1}{0}$	$\frac{0}{1}$	10	STEPPING MOTOR AND GEAR TRAIN
2 DOF SOLAR ARRAY ACTUATOR $\frac{0}{2}$	10 (22)	5/20	50 x 20 DIA (20 x 8 DIA)	TBD	$\frac{0}{2}$	$\frac{0}{0}$	10	
DISTURBANCE MANAGEMENT WHEELS-WRAP RIB (3) X-AXIS (472 FT-LB-SEC) Y-AXIS (327 FT-LB-SEC) Z-AXIS (76 FT-LB-SEC) DISTURBANCE MANAGEMENT WHEELS-HOOP/COLUMN (2) X-AXIS (214 FT-LB-SEC) Y-AXIS (137 FT-LB-SEC)	37.1 (82) 32.6 (72) 18.6 (41) 27.3 (60) 30.0 (66)	5/100 5/100 5/70 5/100 5/100	TBD TBD	STD BALL BEARING OR MAGNETIC BEARING DESIGNS	1 1 1 1 1	0 0 0 0 0	10	UNIT MASS, POWER AND SIZE ESTIMATED BASED ON AVAILABLE BALL BEARING WHEEL HARDWARE
ACS PROPELLANT-WRAP RIB AT +Z AT -Z ACS PROPELLANT HOOP-COLUMN AT +Z AT -Z AT HOOP	1 1 1 1 1 1 8 46.8 (103) 46.8 (103) 12 (26.4)	N/A N/A	TBD TBD	N/A N/A	1 0 1 0 0	0 1 0 1 1		MONOPROPELLANT HYDRAZINE WITH SPECIFIC IMPULSE OF 120 SEC. IN PULSE MODE, 220 SEC. FOR STEADY STATE. MASS INCLUDES ACS PROPELLANT REQUIREMENTS FOR COMBATING GRAVITY GRADIENT AND DYNAMIC BALANCING TORQUES, BUT EXCLUDES PLUMBING, THRUSTER HARDWARE & ALL STATION KEEPING PROPELLANT

ACS WEIGHT AND POWER SUMMARY

The ACS subsystems for the 55m Wrap-Rib and 122m Hoop-Column configurations are summarized in the chart below. Both systems weigh about 1270 kg (2800 lbs), including a 600 m/s stationkeeping propellant, and require about 270 watts average power. Of that weight, 22% corresponds to ACS electronics, sensors and actuators, with the remaining 78% taken up by propellant and associated plumbing and tankage (14% for attitude control, 64% for stationkeeping).

	WRAP-RIB	HOOP / COLUMN
ELECTRONICS, SENSORS, ACTUATORS	615 lbs	600 lbs
ACS PROPELLANT	394 lbs	417 lbs
STATION KEEPING PROPELLANT AND ASSOCIATED HARDWARE	1757 lbs	1867 lbs
TOTAL WEIGHT	2766 lbs	2884 lbs
AVERAGE POWER	261 W	281 W

LMSS ACS DEFINITION STUDY SUMMARY

- DEFINED CONTROL SYSTEM CONCEPTUAL DESIGNS FOR BOTH ANTENNAS
 - DESIGNS BASED ON EXTRAPOLATION OF STATE OF THE ART IN CONTROL ANALYSIS AND HARDWARE PLUS LATEST ADVANCES IN LSS CONTROL TECHNOLOGY
 - MORE WORK IS REQUIRED TO DEVELOP CONCEPT AND TO DEMONSTRATE FEASIBILITY AND LEVEL OF CONTROL PERFORMANCE
- REQUIRED TECHNOLOGY DEVELOPMENTS FOR TECHNOLOGY READINESS ARE CONSIDERABLE - THOUGH ACHIEVABLE BY 1987:
 - NEW DESIGN AND ANALYSIS TECHNIQUES TO DEAL WITH HIGH DIMENSIONAL DYNAMICS, INEVITABLE MODEL AND PARAMETER ERRORS, AND THE NEED FOR CONTROL SYSTEM ROBUSTNESS, AND IN-ORBIT SYSTEM ID
 - DEVELOPMENT AND DEMONSTRATION OF FEED/REFLECTOR MOTION SENSING AND CONTROL
 - ADVANCED HARDWARE - LONG LIFE, HIGH PERFORMANCE SENSORS AND ACTUATORS
 - FIBER OPTICS GYRO
 - CCD BASED STAR TRACKERS
 - OPTICAL SHAPE/VIBRATION SENSOR

Page intentionally left blank

STRUCTURAL ASSEMBLY DEMONSTRATION EXPERIMENT

Jack W. Stokes
National Aeronautics and Space Administration
George C. Marshall Space Flight Center
Marshall Space Flight Center, Alabama

Large Space Systems Technology - 1981
Third Annual Technical Review
November 16-19, 1981

FOREWORD

As an outgrowth of the activity performed in developing a Large Space Systems Assembly Analysis, a flight experiment is being proposed. The necessity of such an experiment stems from the desire to more closely define and quantify those parameters operating upon and contributing to assembly data for the Assembly Analysis cost algorithm.

We would like to acknowledge the valuable assistance and support that has been received in the conception of the Structural Assembly Demonstration Experiment. Appreciation is extended to the Massachusetts Institute of Technology, Space Systems Laboratory for their effort in defining the experiment goals; to the Vought Corporation for its effort in providing assistance in hardware design; to the Essex Corporation in its assistance in documentation development and underwater simulation expertise, and to the Marshall Space Flight Center, Science and Engineering Directorate for its design development of the various experiment considerations, both structural and thermal.

BACKGROUND

The major thrust of our activity over the past several years has been in the development of a Large Space Systems (LSS) Assembly Analysis (ref. 1). Data has been collected for the resultant cost algorithm via paper analysis and operational simulations (ref. 2). However, the need has arisen to correlate neutral buoyancy, or underwater operational simulations data with that of on-orbit assembly, in order to verify and to predict LSS assembly times and techniques (see fig. 1).

Several informal discussions with personnel from NASA Office of Aeronautics and Space Technology (OAST) and Massachusetts Institute of Technology (MIT) resulted in an established experiment requirement. A formal presentation was then made to the Space Systems and Technology Advisory Committee (SSTAC) in order to obtain experiment guidance.

Once the need for a comparative demonstration was established, trade studies were made to define the objectives, simulation modes, and type of test structure required to meet the objectives.

An effort is presently underway to define an experiment proposal and experiment program plan in order to receive formal experiment approval for the Structural Assembly Demonstration Experiment (SADE). Thermal, structural, and dynamic considerations have been included in the experiment concept. Data for SADE will be collected from activity both underwater and on-orbit under as near identical circumstances as possible. A major guideline for SADE is to keep costs at a minimum.

- **NEED: PREDICT ORBITAL LSS ASSEMBLY OPERATIONS DEFINITION FROM MAN/SYSTEM SIMULATIONS. VALIDITY OF PREDICTIONS NEEDS CONFIRMATION.**
- **TRADE STUDIES TO DETERMINE BASELINE SIMULATION MODES AND TYPE OF TEST STRUCTURE**
- **INFORMAL DISCUSSIONS/PRESENTATIONS:**
 - 2ND ANN. LSS TECH REV.
 - OAST/DICK CARLISLE
 - SSTAC - 3RD ANN. LSS TECH REV.
 - 2ND OAST PITCH
- **INFORMAL NASA/UNIVERSITY/INDUSTRY PARTICIPATION AGREEMENT**
- **EXPERIMENT DEFINITION**
- **SSTAC/AUGMENTATION CONSIDERATIONS - THERMAL & STRUCTURAL**
- **FLIGHT EXPERIMENT PROPOSAL (IN WORK - DUE DECEMBER 1981)**

Figure 1

SADE BASELINE OBJECTIVES/CHARACTERISTICS

The experiment is of an operational variety, designed to assess crew capability in LSS assembly.

The six SADE objectives (figure 2) include: (a) the establishment of a quantitative correlation between LSS neutral buoyancy simulation and on-orbit assembly operations in order to enhance the validity of those assembly simulations; (b) the quantitative study of the capabilities and mechanics of human assembly in an Extravehicular Activity (EVA) environment; (c) the further corroboration of the LSS Assembly Analysis cost algorithm through the obtainment of hard data base information; (d) the verification of LSS assembly techniques and timelines, as well as the identification of crew imposed loads and assembly aid requirements and concepts; (e) verification of a Launch/Assembly Platform (LAP) structure concept for other LSS missions; and (f) lastly, to advance thermal control concepts through a flexible heat pipe.

OBJECTIVES:

- TO ESTABLISH A QUANTITATIVE CORRELATION BETWEEN EARTH-BASE ASSEMBLY SIMULATIONS AND ON-ORBIT OPERATIONS. ENHANCE VALIDITY OF NEUTRAL BUOYANCY SIMULATIONS.
- TO QUANTITATIVELY STUDY THE CAPABILITIES AND MECHANICS OF HUMAN ASSEMBLY IN EVA
- TO FURTHER CORROBORATE THE ASSEMBLY COST ALGORITHM AND TO PROVIDE "HARD" DATA BASE INFORMATION
- TO VERIFY ASSEMBLY TECHNIQUES AND TIMELINES, CREW IMPOSED LOADS, AND CREW AND ASSEMBLY AIDS FOR LARGE SPACE STRUCTURES/SYSTEMS
- TO VERIFY A LAUNCH/ASSEMBLY PLATFORM CONCEPT FOR ADVANCED MISSIONS
- ADVANCE THERMAL CONTROL CONCEPTS

Figure 2

SADE BASELINE OBJECTIVES/CHARACTERISTICS (Continued)

Characteristics of the SADE (figure 3) are as follows.

The SADE structure will remain attached to the Shuttle via the LAP. The only interface planned with the Shuttle is a structural one, except as safety and integration requirements dictate. Data will be collected via on-board video recorders and pallet-mounted instrumentation recorders activated by EVA personnel. Assembly and stowage will be strictly manual via EVA, with Remote Manipulator System (RMS) assistance.

A major characteristic of the experiment is the similarity between the ground test portion of the experiment and the orbital operations portion. The same test procedures and, hopefully, test subjects will be incorporated to operate extremely similar hardware. Variations in hardware include flotation modifications to the deployable cells as well as water-compatible interconnect module struts and thermal hardware mockups.

Finally, the SADE structure, scheduled to be returned at the end of the mission, will be available for additional flights, as required.

CHARACTERISTICS

- SHUTTLE ATTACHED
- NO INTERFACES OTHER THAN MECHANICAL. DATA RECORDED/RETRIEVED W/O ACTIVE INTERFACE
- ERECTABLE/RESTOWABLE VIA EVA & RMS
- IDENTICAL FLIGHT & NEUTRAL BUOYANCY HARDWARE
(EXCEPTION: FLOTATION TUBES, THERMAL EXPERIMENT MOCKUPS)
- IDENTICAL FLIGHT/GROUND BASE TEST PROCEDURES & TEST SUBJECTS
- REUSABLE

Figure 3

SADE CONFIGURATION TRADES

Based upon the identified requirements, a comprehensive set of trade studies was conducted in order to identify the structure which could best meet the requirements. Several types of structures were evaluated against the need for low-cost hardware reflecting current state-of-the-art design (figure 4). Erectable structures were considered those of which the various elements are manufactured on the ground, packaged for flight, and brought to orbit by the Shuttle. Once on orbit, assembly would occur via EVA activities.

Fabricated structures are those which are assembled as erectables, but are actually fabricated on-orbit from stock material by employing some type of fabricating machine.

Deployable structures generally are considered to be structures assembled on the ground, packaged to reduce volume, and, once on-orbit, deployed through either internal or external mechanisms to full volume.

The SADE approach concentrates on both erectable and deployable assembly, as both techniques are of current interest to the aerospace community for near-term structures/systems. The particular structure was selected because it had already passed through a configuration development phase, and was judged by the related design personnel as being prototyped for flight. The structure had withstood 18 underwater deployment trials at MSFC via the RMS and two pressure-suited test subjects.




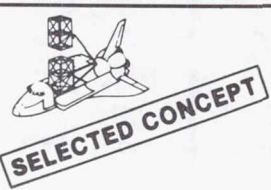
ERECTABLE STRUCTURE	ADVANTAGES	DISADVANTAGES
	<ul style="list-style-type: none"> • REQUIRES EVA ASSEMBLY • PRESENTS MORE TASK SEQUENCE DATA • EASILY STOWED - MORE "PIGGYBACK" DATA • VARIABLE CONFIGURATION • SINGLE ELEMENT FAILURES REPLACEABLE WITH SPARES 	<ul style="list-style-type: none"> • NOT DEVELOPED HARDWARE • NOT EARLY APPLICATION CANDIDATE • ASSEMBLY TOLERANCES PROHIBIT UNAIDED RMS OPERATIONS • NO STRUCTURAL CHECKOUT PRIOR TO FLIGHT
FABRICATED STRUCTURE	<ul style="list-style-type: none"> • POTENTIAL FOR RMS/EVA WORK COMBINATION WITH SPECIAL RMS END EFFECTOR 	<ul style="list-style-type: none"> • "BEAM MACHINE" DEVELOPMENT SCHEDULES • WEIGHT & MASS OF MACHINE • DIFFICULT TO SHARE PAYLOADS • LOGISTICS BURDEN • NO STRUCTURAL CHECKOUT PRIOR TO FLIGHT
		
DEPLOYABLE STRUCTURE	<ul style="list-style-type: none"> • DEVELOPED HARDWARE • COMPACT STOWAGE, "MISSION SHARABLE" • PERMITS RMS/EVA OPERATIONS IN COMBINATION • PREFLIGHT STRUCTURE CHECKOUT 	<ul style="list-style-type: none"> • LIMITED CREW DIRECT INVOLVEMENT
		
DEPLOYABLE/ERECTABLE HYBRID STRUCTURE	<ul style="list-style-type: none"> • DEVELOPED HARDWARE • COMPACT STOWAGE, "MISSION SHARABLE" • PERMITS RMS EVALUATION • EXCELLENT CREW INVOLVEMENT FOR GROUND/FLIGHT COMPARISON 	<ul style="list-style-type: none"> • NO SIGNIFICANT DISADVANTAGES
	<div style="border: 1px solid black; border-radius: 50%; padding: 10px; text-align: center;"> <p>i.e. LOOKS AT A RANGE OF LIKELY CONSTRUCTION TECHNIQUES</p> </div>	

Figure 4

SADE MILESTONES

Figure 5 represents the flow of events in the development of the concept for SADE. As the need for neutral buoyancy operations validation became apparent, the SADE approach was conceived. As previously stated, various concepts were considered until the current structure was baselined in January 1981. This concept was presented to the SSTAC in June 1981, at which time it was strongly suggested that a more complex, augmented experiment was in order. As a result, augmentation of thermal, structural, and dynamics and control investigations was considered. The dynamics and control study effort was not incorporated, however, when it was concluded that a much longer basic structure was required in order to obtain valid data. Such a structure would have violated the groundrule of using developed hardware and driven the costs up significantly.

Therefore, the current experiment package includes the 15 m (50 ft.) deployable structure attached to an advanced concept launch/assembly platform, and supporting a thermal heat pipe experiment package.

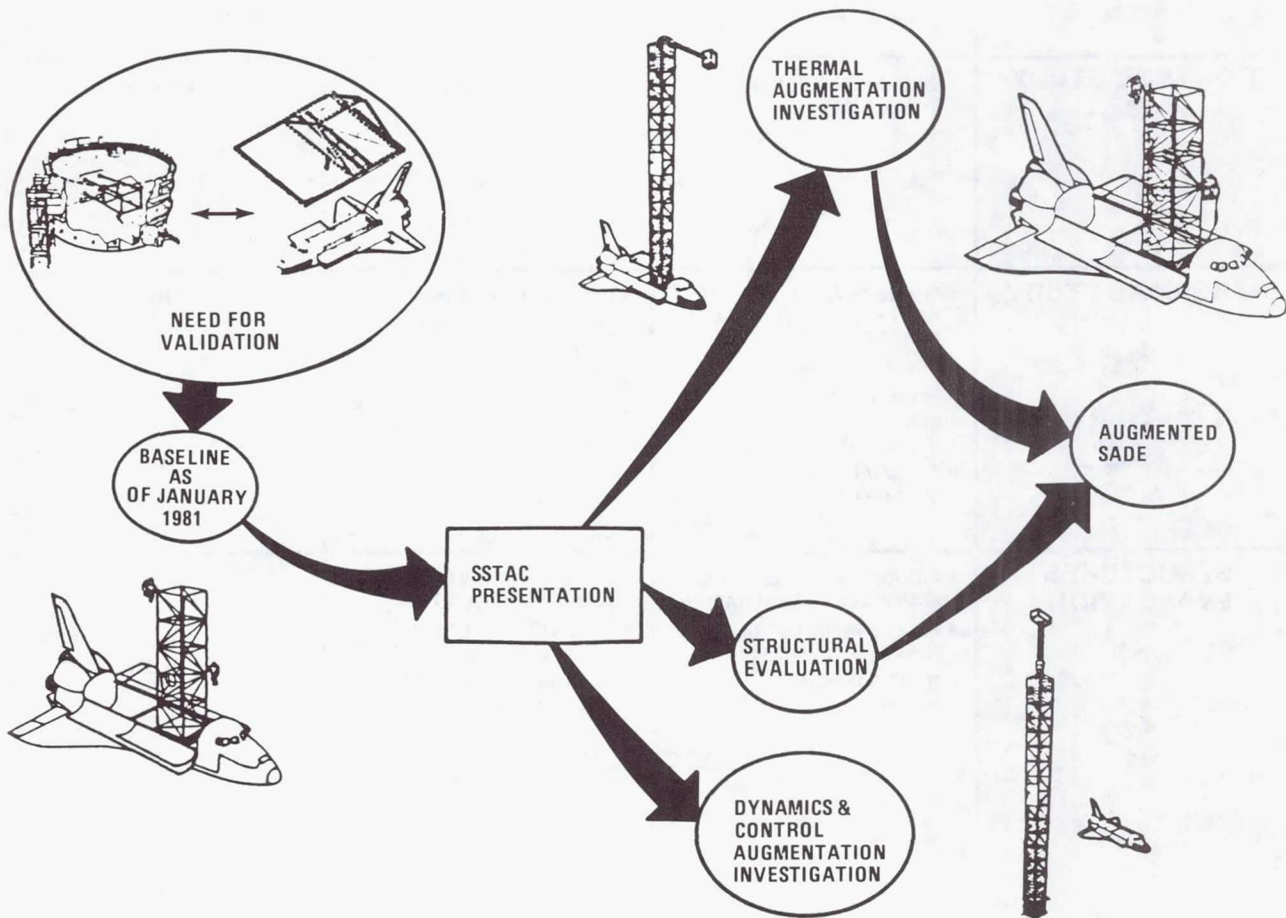

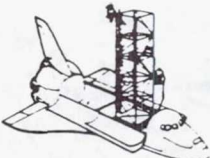



Figure 5

SADE AUGMENTATION CONSIDERATIONS

The augmentation trades are depicted in figure 6 below. The objectives and characteristics of each are stated, as are the disadvantages relating to the SADE groundrules. It should be noted that no real disadvantages could be determined for the thermal and structures proposals; however, they were included in the baseline concept. The thermal objectives are now considered to be part of the baseline SADE objectives. Hence, the thermal portion of the study will not be treated as an augmentation.

DYNAMICS STUDY	OBJECTIVES	CHARACTERISTICS	DISADVANTAGES
	<ul style="list-style-type: none"> • DYNAMIC CHARACTERISTICS OF "FREE-FREE" STRUCTURE • FURTHER USE OF LSS TEST MEASUREMENT EQUIPMENT • BASE FOR SMALL, LOW-FREQUENCY BOOMS 	<ul style="list-style-type: none"> • LOW FREQUENCY (≤ 1 Hz), EVENLY SPACED MODES • FREE-FREE MODE 	<ul style="list-style-type: none"> • RF LINK REQUIRED • ATTITUDE CONTROL REQUIRED • NON-RETRIEVABLE • FREE-FLYING • LARGE/COSTLY
CONTROL STUDY	<ul style="list-style-type: none"> • DISTRIBUTED CONTROL EVALUATION 	(SAME AS ABOVE)	(SAME AS ABOVE)
	<ul style="list-style-type: none"> • TRANSVERSE FLAT PLATE HEAT PIPE FOR THERMAL CONTROL • THERMAL SURVEY OF STRUCTURE • REALISTIC CREW INSTALLATION TASKS • THERMAL COATING EVALUATION 	<ul style="list-style-type: none"> • DEVELOPED CONCEPT • EASILY INTEGRATED INTO STRUCTURE • COMPACT • COMPATIBLE WITH SHUTTLE-ATTACHED OPERATIONS 	NONE
	<ul style="list-style-type: none"> • ADVANCED SASP LAUNCH/ ASSY FIXTURE EVALUATION • ACCELERATION/STRAIN SURVEY OF STRUCTURE • JOINT DAMPING CHARACTERISTICS 	<ul style="list-style-type: none"> • SIMILAR TO ADVANCED SASP LAUNCH/ASSY FIXTURE • CREW ACTIVITIES SIMILAR • STRUCTURE ERECTION TECHNIQUE SIMILAR TO ADVANCED SASP 	NONE

INCORPORATED

INCORPORATED

Figure 6

THERMAL EXPERIMENT

Objectives for the thermal portion of the SADE are listed below in figure 7, and include the assembly and verification of a heat pipe experiment, as well as refurbishing its radiator.

The hardware includes a 15 m to 18 m (50 ft. to 60 ft.) long two section heat pipe with radiator and heat source. A special coupling will attach the heat pipe sections together. The radiator coating technique has yet to be defined, but both tape and electrostatic painting are being considered.

● OBJECTIVE

- DEMONSTRATE ASSEMBLY AND PERFORMANCE OF A LARGE CONSTRUCTABLE HEAT PIPE THERMAL CONTROL SYSTEM.
- DEMONSTRATE THE CAPABILITY TO CHANGE/REFURBISH THERMAL CONTROL COATINGS ON ORBIT.

● EXPERIMENT DESCRIPTION

- DEMONSTRATE UTILIZATION, CONSTRUCTABILITY AND PERFORMANCE OF HIGH PERFORMANCE HEAT PIPES TO TRANSFER HEAT LOADS OVER LONG DISTANCES. FOR PROPOSED ORBITING, SPACE PLATFORMS, ANTENNA SYSTEMS AND LARGE MANNED SPACE STATIONS WITH CYCLIC THERMAL DISTORTIONS, RESULTING IN MECHANICAL LOADS.
- HARDWARE - A 50'-60', TWO-SECTION HEAT PIPE WITH NOMINAL HEAT SOURCE AT ONE END; HEAT REJECTING RADIATOR. PIPE ATTACHED TO EXTERIOR STRUCTURE OF SADE, OVER ITS ENTIRE LENGTH. A "U" SHAPED PIPE OR COUPLING JOINT USED TO JOIN TWO 25 - 30 FT HEAT PIPES.
- RADIATOR DESIGNED SUCH THAT A COATING EXPERIMENT COULD BE PERFORMED BY CHANGING THE COATING AND HENCE THE THERMAL PROPERTIES OF THE RADIATOR.

Figure 7

SADE EXPERIMENT DESCRIPTION

One major objective of SADE is to develop a comparative technique between neutral buoyancy and on-orbit operations. Hence, operational activities will occur both underwater and in space. Employing hardware already available from a previous conceptual test (ref. 3), simulations will be performed in the Marshall Space Flight Center Neutral Buoyancy Simulator. The assembly procedure will be developed and refined in this phase. Hardware definition will be accomplished. Following development activities, crew training and baseline simulations will be conducted.

Flight hardware will be fabricated and integrated into the assigned Shuttle mission. The trained crew will perform assembly, utility integration, thermal experiment operations, and restowing of the experiment equipment. Once the hardware has been returned to the ground, the data will be analyzed. If required, additional neutral buoyancy operations may be performed.

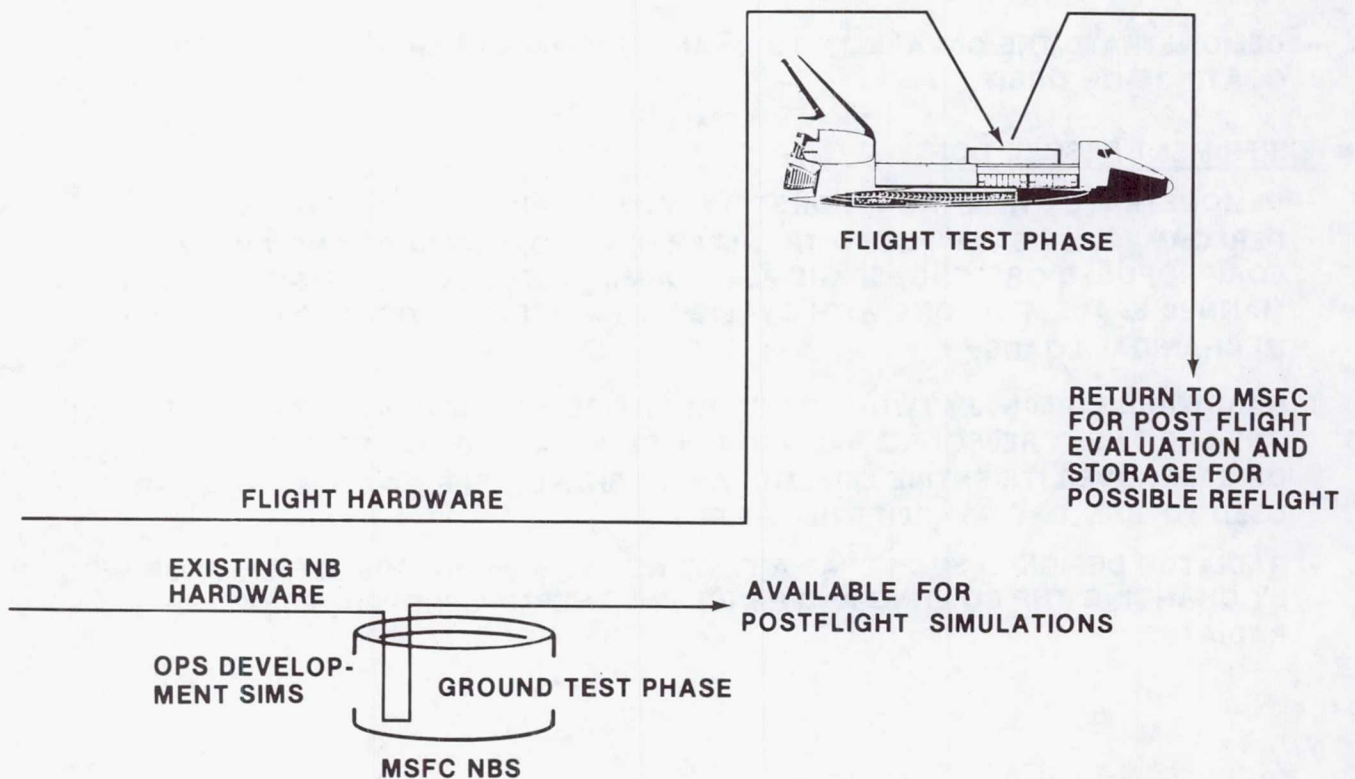


Figure 8

SADE HARDWARE DESCRIPTION

Figure 9 depicts the SADE deployable structure stowed on the LAP, which in turn is attached to an OFT or Spacelab "dumb" pallet. The structure folds into a 3 by 6 by 1 meter (10 by 20 by 3 feet) package.

Figure 10 depicts how the structure will appear when assembled. The center cell represents the erectable cell, while the remaining upper and lower cells represent the two respective modules.

SADE STOWED STRUCTURE

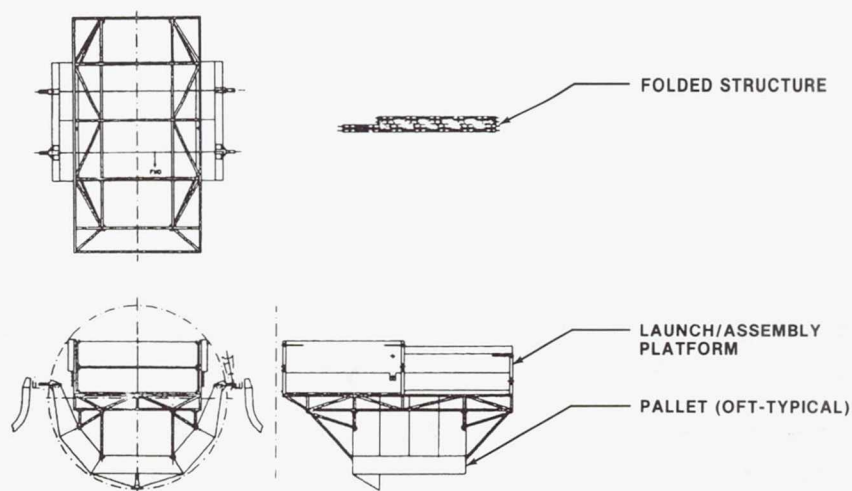


Figure 9

SADE DEPLOYED STRUCTURE

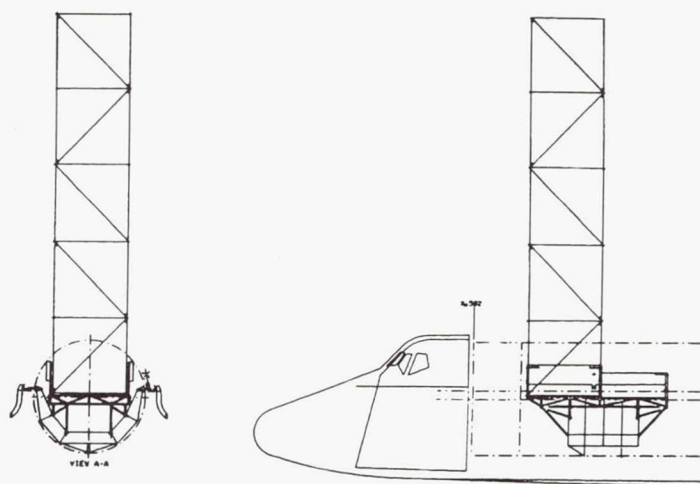


Figure 10

SADE TEST SEQUENCE

The typical SADE operations sequence to be performed both in the NBS and on-orbit is described below in figure 11 and depicted in figure 12. Three separate EVA's are planned, the first to occur early in the mission, the second mid-mission, and the third on the last mission day. The mid-mission EVA is dedicated to the thermal experiment and will require the two crewmen to activate the instrumentation system and to recoat the heat pipe radiator. The recoating technique has yet to be defined.

The last EVA, to stow the experiment, will be a reversal of the assembly sequence.

- **SIMULATIONS OPERATION TO BE CONDUCTED IN THE MSFC NEUTRAL BUOYANCY SIMULATOR & ON-ORBIT INCLUDE THE FOLLOWING:**
 - A. CREW TRANSLATION FROM EVA AIRLOCK TO SADE DEPLOYMENT WORK AREA**
 - B. CREW RELEASE OF ALL MANUALLY OPERATED LATCHES AND RESTRAINT DEVICES**
 - C. DEPLOYMENT OF FOLDED CELLS USING EVA CREW, THE RMS, AND THE MMU**
 - D. EVA ASSEMBLY OF THE ERECTABLE INTERCONNECT MODULE**
 - E. EVA ATTACHMENT OF HEAT PIPE, RADIATORS, SENSORS, CABLES, MODULES OR OTHER DEVICES NOT PERMANENTLY ATTACHED TO STRUCTURE**
 - F. FOLDING, DISASSEMBLY AND STOWAGE OF THE STRUCTURE AND ANY ATTACHED HARDWARE.**
- **3 EVA'S - ASSEMBLY, THERMAL EVALUATION/RECOATING DISASSEMBLY**

Figure 11

SADE ASSEMBLY SEQUENCE

Figure 12 illustrates the procedure for unstowing and assembling the SADE structure. The last cartoon depicts the installation of the thermal hardware and the attachment of instrumentation cabling to the various structure elements.

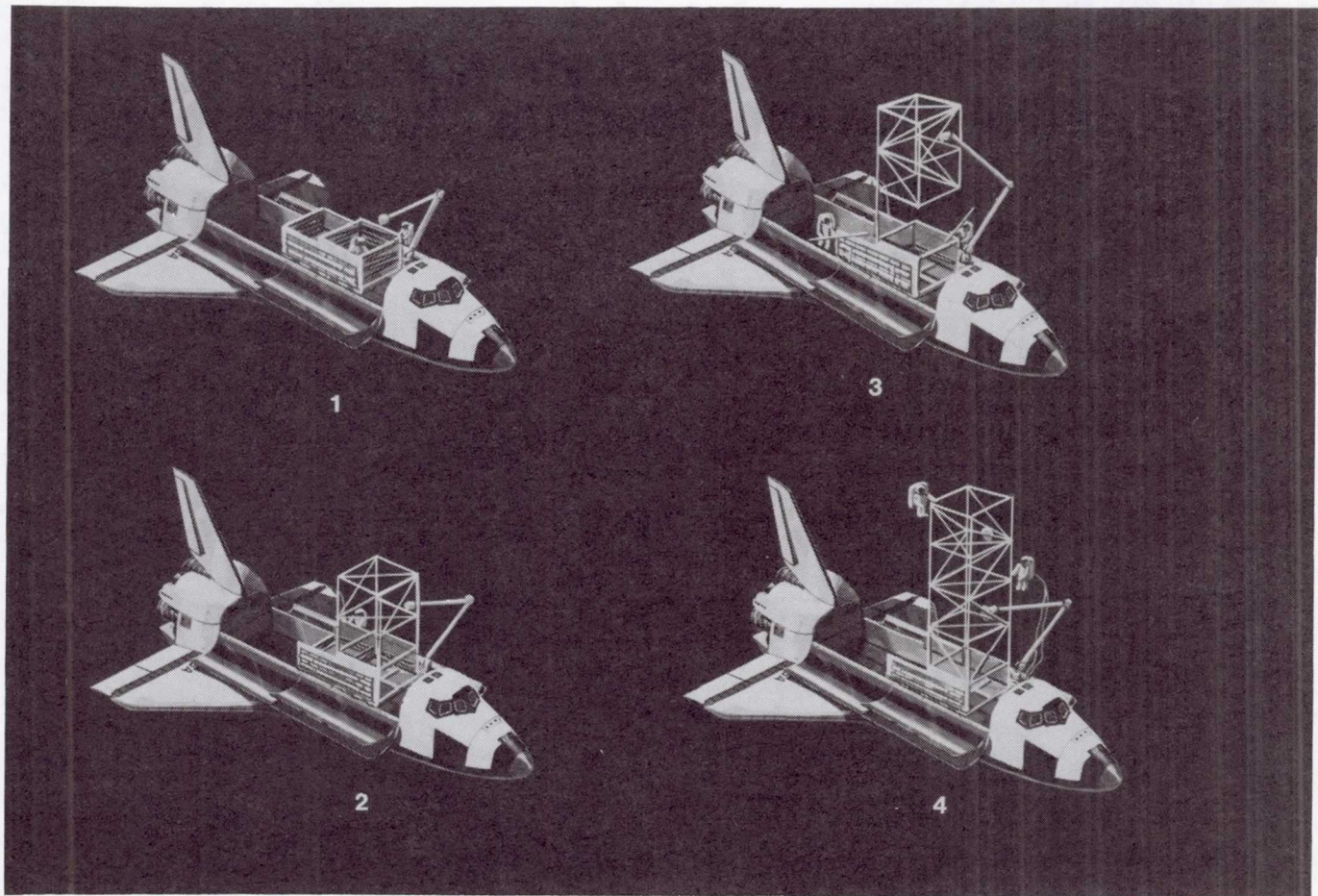


Figure 12

SADE TIME ESTIMATES

As previously stated, the structure selected for the SADE had previously been employed for a neutral buoyancy test addressing deployable/erectable structures. Data from the test sequence, conducted at MSFC during September 1980, is depicted in Table 1 below, and should give some rough indication of expected assembly times for SADE operations. These times are typical of LSS assembly sequences in a neutral buoyancy environment, but, based on experience, appear to be low for orbital assembly. The goal of SADE is to determine what realistic assembly times actually are for on-orbit activities.

Note that the interconnect installation and deployment data are unrealistic for SADE, as a different interconnect technique was baselined in the previous neutral buoyancy test (ref. 2).

TYPICAL DETAILED TIMELINE (BASED UPON PREVIOUS NEUTRAL BUOYANCY TESTS)

RANGE AND MEAN TIME TO PERFORM REPRESENTATIVE TASKS
INVOLVED IN ERECTING LARGE SPACE STRUCTURES
CONSERVATIVE TOTAL ESTIMATED TIME (MEAN - 22 MIN., 34 SEC.
DATA DERIVED FROM NB-37, ERECTABLE/DEPLOYABLE STRUCTURES TEST

<u>TASK DESCRIPTION</u>	<u>(T = SEC) RANGE</u>	<u>(T = SEC) MEAN</u>	<u>TASK REPLICATIONS (N)</u>
1. RMS ORIENT & GRASP TARGET USING OPPOSED JAW EFFECTOR & FROM VARIOUS AND UNCONTROLLED START LOCATIONS	29-252	128	27
2. EVA LOCK UP ALL FOUR DROGUES	58-198	105	11
3. DEPLOY CELLS A MODULE 1, CELL 1	80-192	135	5
B MODULE 1, CELL 2	81-126	96	5
C MODULE 2, CELL 1	124-318	207	6
D MODULE 2, CELL 2	92-135	127	6
4. INSTALL INTERCONNECTS & DEPLOY	72	72	1
5. EVA UNLOCK DIAGONAL WING LOCKS IN PREPARATION TO STOW	14-57	28	9
6. COLLAPSE CELLS FOR STOWAGE: CELL 2 (FIRST CELL COLLAPSED)	28-130	65	4
CELL 1 (SECOND CELL COLLAPSED)	28-178	109	4
7. EVA TRANSLATE 3 M OF A CELL	7-19	12 (X5 = 60)	24
8. EVA TRANSLATE A CELL DIAGONAL	12-24	18 (X4 = 72)	4
9. EVA TRANSLATE ALONG FRAME (~ 3 m)	11-18	15 (X10 = 150)	8
TOTAL	636-1719	1117 (1354)	

(NOTE: NO DATA AVAILABLE FOR ATTACHMENT OF SENSORS OR THERMAL HARDWARE, OR UNSTOWING/RESTOWING INTERCONNECT ELEMENTS.)

Table 1

EXPERIMENT DESIGN SEQUENCE

The flow chart (fig. 13) presents the development technique envisioned for SADE. As the design objectives, approach, and methods become fully defined, the data requirements, based upon experiment and Shuttle needs, will be determined. A data analysis plan will be developed, as will anticipated experiment results. Test hardware will be finalized, and flight qualification testing will be performed. Underwater activities will include development simulations, training simulations, and baseline simulations. Flight data will be collected, followed by additional underwater simulations, if required. A complete data analysis will be performed and results published.

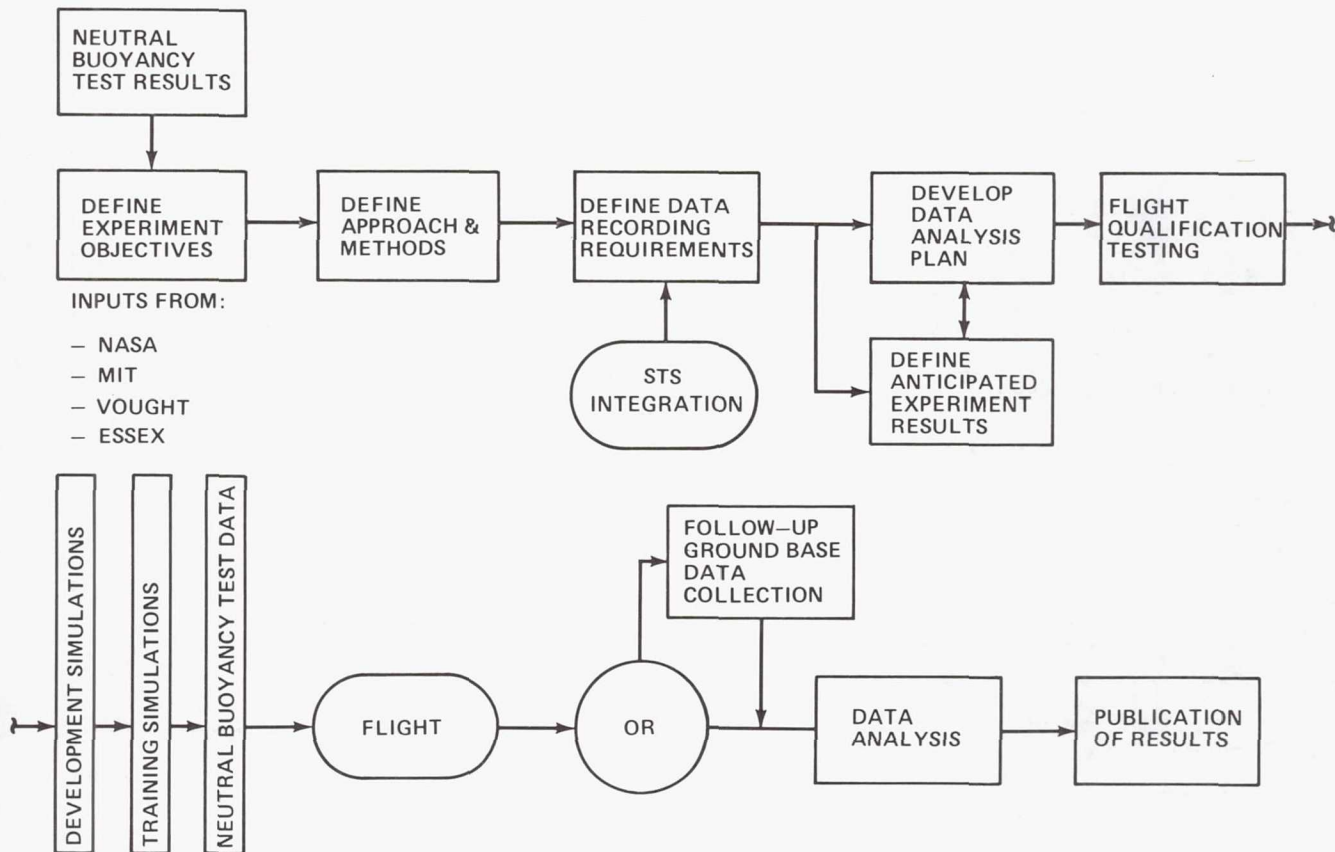


Figure 13

SADE SCHEDULE

Figure 14 depicts the chronological flow of the experiment design sequence. Experiment definition is well along. Experiment integration is now beginning. Hardware will be available in late 1985, for a flight opportunity, probably sometime in 1987.

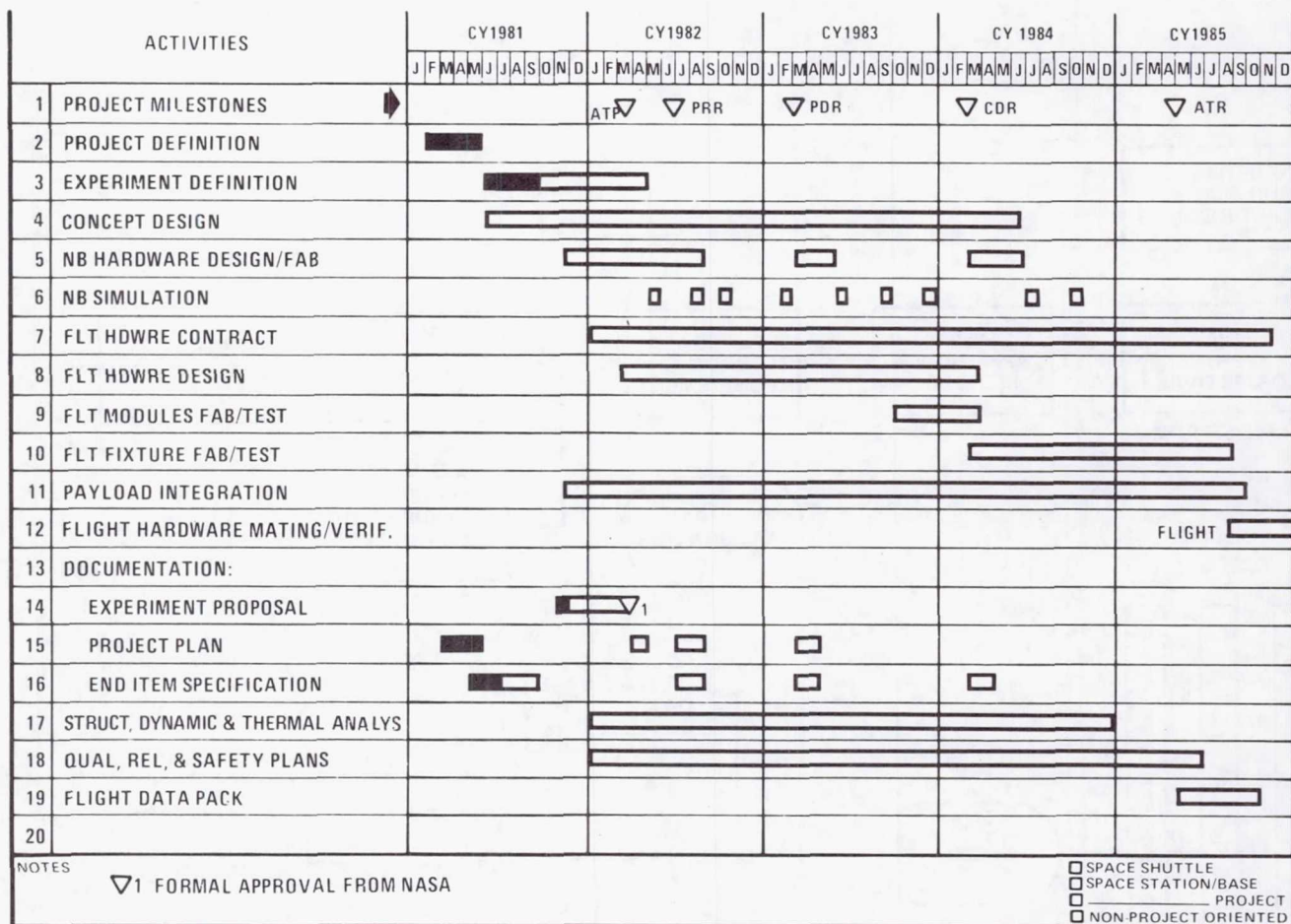


Figure 14

SYMBOLS AND ABBREVIATIONS

EVA	Extravehicular Activity
LAP	Launch/Assembly Platform
LSS	Large Space Systems
MSFC	Marshall Space Flight Center
MIT	Massachusetts Institute of Technology
NBS	Neutral Buoyancy Simulator
OAST	Office of Aeronautics and Space Technology
RMS	Remote Manipulator System
SADE	Structural Assembly Demonstration Experiment
SSTAC	Space Systems and Technology Advisory Committee

REFERENCES

1. Watters, Harry H. and Stokes, Jack W.: Construction in Space - Toward a Fresh Definition of the Man/Machine Relation. *Astronautics and Aeronautics*, vol. 17, no. 5, May 1979, pp. 42-63
2. Stokes, J. W. and Watters, H. H.: Space Assembly Methodology. Large Space Systems Technology - 1980. Volume I - Systems Technology. NASA CP-2168, 1981, pp. 199-215.
3. Stokes, J. W.; Engler, E. E.; and Agan, W. E.: Neutral Buoyancy Test Results of a Deployable Space Beam. Second AIAA Conference on Large Space Platforms (San Diego, CA), February 1981. Paper No. AIAA-81-0437

STRUCTURAL ASSEMBLY DEMONSTRATION EXPERIMENT (SADE)

EXPERIMENT DESIGN

D. L. Akin and M. L. Bowden
M.I.T. Space Systems Laboratory
Cambridge, Massachusetts

Large Space Systems Technology - 1981
Third Annual Technical Review
November 16-19, 1981

SADE Experiment Design

Operating as a contractor to the Marshall Space Flight Center, the Space Systems Laboratory of the Massachusetts Institute of Technology is responsible for the design and analysis of the experimental studies which make up the Structural Assembly Demonstration Experiment (SADE). The following paper summarizes the presentation given by Dr. D. L. Akin and M. L. Bowden at the Third Annual Technical Review of Large Space Systems Technology, 1981. This was given in conjunction with the presentation "Structural Assembly Demonstration Experiment (SADE)", by H. Watters and J. Stokes of NASA Marshall Space Flight Center. The SADE concept is to erect a hybrid deployed/assembled structure as an early space experiment in large space structures technology.

SADE Objectives

The basic objectives can be broken down into four generic areas.

Simulation Correlation: By performing assembly tasks both in space and in neutral buoyancy simulation, a mathematical basis will be found for the validity conditions of neutral buoyancy, thus enhancing the utility of water as a medium for simulation of weightlessness.

Human Factors: A data base will be established describing the capabilities and limitations of EVA crewmembers, including effects of such things as hardware size and crew restraints.

Structural Data: Experience of the M.I.T. Space Systems Lab in neutral buoyancy simulation of large space structures assembly indicates that the assembly procedure may create the largest loads that a structure will experience during its lifetime. Data obtained from the SADE experiment will help establish an accurate loading model to aid designers of future space structures.

Thermal Data: The size of the proposed SADE structure presents an opportunity for auxiliary experiments. With the SADE structure as a support, a large heat pipe will be tested for efficiency in space, free from the thermally restrictive environment of the payload bay.

SIMULATION CORRELATION

HUMAN FACTORS

STRUCTURAL DATA

THERMAL DATA

Task Correlation

The primary objective of the SADE program is to correlate actual EVA experience with identical task performance in a neutral buoyancy simulator. Neutral buoyancy is the only method possible on earth for simulation of structural assembly activities in space, due to the size of the elements and the time necessary for assembly. This chart relates the data collection and analysis methods to be used in this section of the study.

- METHODS:
- VIDEO TAPE STRUCTURAL ASSEMBLY OPERATIONS USING CCTV CAMERAS MOUNTED ON FORWARD STARBOARD AND AFT PORT CARGO BAY BULKHEADS.
 - POST-FLIGHT TIME AND MOTION STUDIES OF EVA OPERATIONS BASED ON VIDEO TAPES, TIME LAPSE MOVIE (1 FPS, WIDE ANGLE LENS, STARBOARD WINDOW AFT FLIGHT DECK), AND INTERMITTENT MOVIE FOOTAGE BY EVA CREW MEMBERS.
 - COMPARISON BASED ON TASK TIMES (EXAMPLE TASKS: TRANSLATION, ALIGNMENT, CONNECTION) AND SUBTASK TIMES (EXAMPLE SUBTASKS: UNSTOW INTERCONNECT BEAM #3) TO PREVIOUS NEUTRAL BUOYANCY TESTS PERFORMED WITH SAME CREW MEMBERS AND SAME TIME LINES.
 - POSSIBILITY OF POST-FLIGHT NEUTRAL BUOYANCY SIMULATIONS FOR ADDITIONAL COMPARISON DATA BASE.

Results of Task Correlation

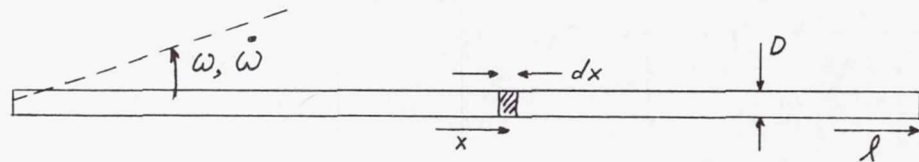
The result of primary importance from this section of the SADE experiment is the establishment of a quantitative correlation between earth-based assembly simulations and on-orbit operations. This will result in a set of correlation factors applicable to similar tasks performed in the future; these factors will allow the experiment designer to do mission planning with confidence in the applicability of neutral buoyancy simulation results to actual EVA operations. In addition, the effects of water drag on subject motion will be studied by direct comparisons of neutral buoyancy and EVA experience.

- RESULTS:
- QUANTITATIVE CORRELATION OF TASK TIMES IN NB SIMULATION WITH ACTUAL TASKS IN SPACE,
 - DEVIATION OF INDIVIDUAL SUB-TASK TIMES FROM TASK AVERAGES IN BOTH NB AND SPACE, INDICATING RELIABILITY OF DATA,
 - QUALITATIVE INVESTIGATION OF UNDERWATER SIMULATION VALIDITY BASED ON SIMULTANEOUS TASK REVIEW (SPLIT-SCREEN VIDEO TAPES OF SAME SUB-TASK, FROM SAME CAMERA POSITION COMPARING CREW MEMBER BODY REACTIONS UNDERWATER TO THOSE IN SPACE),

Dynamic Model Correlation

The preceding correlation technique applies to identical tasks: that is, the structural elements used in simulations underwater are high fidelity flight configuration mockups, except for modifications necessary to insure neutral buoyancy. The difference in dynamics between space and underwater for such hardware can best be illustrated by a long cylindrical beam rotating at an angular velocity ω and an acceleration of $\dot{\omega}$. As can be seen below, the inertia force scales as the cube of the length, while the drag force is dependent on both the fourth power of the length, and the square of the angular velocity. The net effect is that the total torque which must be applied for rotation underwater is the sum of the inertial and viscous torques, and, as a result, handling a beam underwater requires greater effort than in space.

FOR A NEUTRALLY BUOYANT, DISTRIBUTED MASS BEAM:



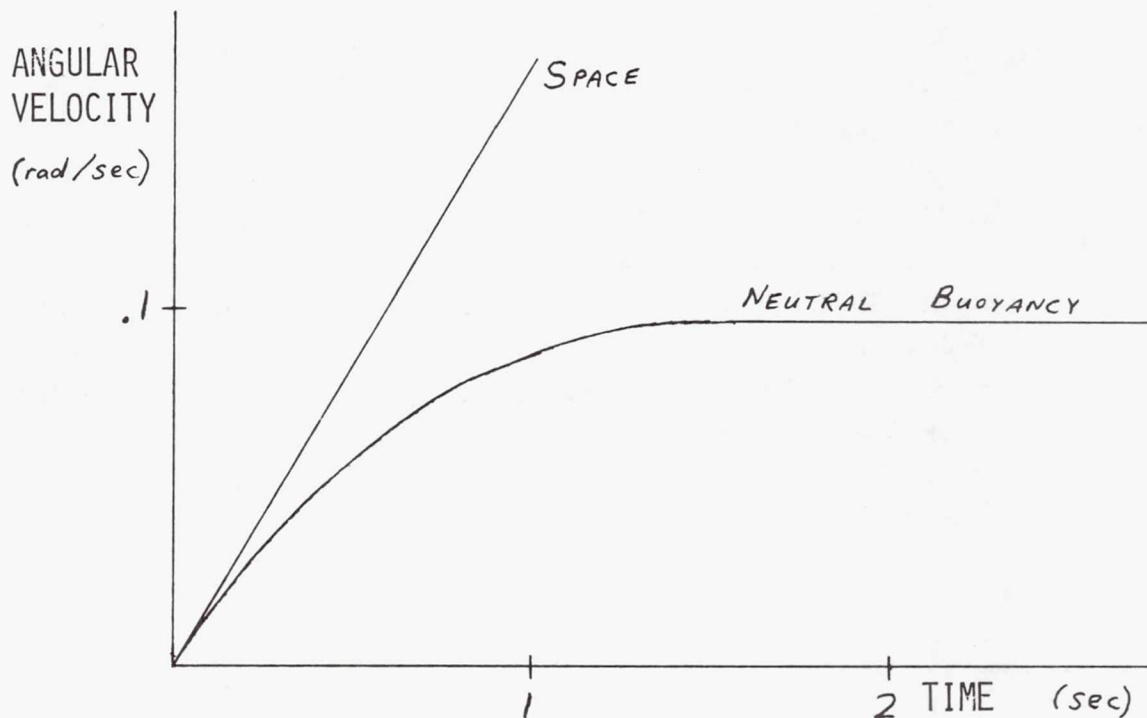
$$\text{TORQUE DUE TO: } \left\{ \begin{array}{l} \text{INERTIA: } \int_0^l \frac{\rho}{4} \dot{\omega} D^2 x^2 dx \\ \text{DRAG: } \int_0^l c_D \frac{\rho}{2} \omega^2 D x^3 dx \end{array} \right.$$

$$\tau = \underbrace{\frac{\rho}{12} D^2 l^3 \dot{\omega}}_{\text{INERTIAL}} + \underbrace{\frac{\rho}{8} c_D D l^4 \omega^2}_{\text{VISCOUS}}$$

Dynamics Example

In order to demonstrate the effect of the preceeding equations, exact solutions have been found for the differential equations, and the results are plotted here for a typical beam, such as a component of the SADE interconnect cell. As can be seen, the angular velocity increases rapidly and linearly at a constant applied torque, as would be expected in the absence of other forces. The same beam underwater, on the other hand, reaches terminal velocity within 2 seconds, and will not accelerate unless additional torque is applied. The significant discrepancy between the two curves emphasizes the inaccuracy in dynamics when flight configuration hardware is used for neutral buoyancy tests.

INTERCONNECT DIAGONAL
STAINLESS STEEL BEAM
7.5 N M TORQUE APPLIED



Dynamic Model Correlation

In order to reduce the error evident in the previous graph, it has been proposed to design neutral buoyancy hardware based on an "effective moment of inertia", which is composed of both inertial and drag terms. Within a range of assumed rotation velocities and accelerations, such a dynamically scaled component would require approximately the same total effort to rotate through a given angle in a given amount of time as the actual component in space. Under these conditions, neutral buoyancy simulations should directly correspond to the on-orbit timelines for medium-critical tasks such as alignment. In order to achieve this dynamic scaling, the component size and mass must be significantly reduced from the flight configuration: the reduction in inertia is compensated for by drag effects.

- METHODS:
- DYNAMICALLY SCALED INTERCONNECT HARDWARE
 - MINIMIZE DRAG, VIRTUAL MASS.
 - DESIGNED SO THAT EFFORT REQUIRED TO ALIGN BEAM UNDER-WATER ("EFFECTIVE MOMENT OF INERTIA") IS EQUAL TO EFFORT REQUIRED FOR THE SAME ALIGNMENT TASK IN SPACE.
 - PRIMARY TRAINING AND DATA BASE COLLECTION WILL USE FLIGHT CONFIGURATION HARDWARE TO PROVIDE PROCEDURES TRAINING AND DIRECT TASK CORRELATION BACKGROUND.
 - DATA RETURN FROM FLIGHT IS AMPLIFIED BY SIMPLE ADDITIONAL TASKS.
 - BEAM ROTATION PERPENDICULAR TO CAMERA ALLOWS MEASUREMENT OF ANGULAR RATES.
 - DIFFERENT MOMENTS OF INERTIA OF INTERCONNECT BEAMS PROVIDE ADDITIONAL DATA.

SADE Structural Component Characteristics

Since the SADE project represents a unique opportunity to get a correlation data base for comparing component dynamics underwater and in space, it is important to maximize data return. For this reason, the eight individual elements of the interconnect structure have been designed to provide four discrete levels of moment of inertia. Design details of the interconnect beams are presented below, along with similar details for the elements of the deployable modules.

		RADIUS	THICKNESS	LENGTH	MASS	MOMENT OF INERTIA
DEPLOYED MODULE	LONGITUDINALS	3.175	0.089	300	1.438	4.31
	LATERAL/ VERTICALS	1.588	0.159	300	1.285	3.85
	DIAGONALS	1.588	0.159	424	1.816	10.88
INTERCONNECT	LIGHT LONGITUDINAL	1.905	0.089	300	0.844	2.53
	LIGHT DIAGONAL	1.905	0.089	424	1.193	7.15
	HEAVY LONGITUDINAL	1.905	0.635	300	14.907	44.72
	HEAVY DIAGONAL	1.905	0.635	424	21.069	126.25
UNITS		cm	cm	cm	kg	kg m ²

Results of Dynamic Model Correlation

At the completion of this effort, a validated mathematical model of component dynamics in both space and water will exist. By using this model, a researcher can design a set of hardware, representing a dynamic analogue of the flight hardware. Simulations performed using this dynamic hardware underwater should give a close estimate of actual timelines for assembling flight hardware in space.

This technique should not be viewed as negating the importance of the direct task correlation data obtained using identical hardware underwater and in space. Correlation of neutral buoyancy results using flight configuration hardware will remain vitally important, as procedures development and crew training will demand high fidelity hardware. Rather, this scaling technique should be considered a useful tool for the neutral buoyancy researcher. By using dynamically scaled components, for example, a structure much too large to fit into a neutral buoyancy facility in flight configuration can still be tested underwater to arrive at procedures and timelines estimates, thus increasing the utility of existing simulator facilities.

- RESULTS:
- A VALIDATED MATHEMATICAL MODEL OF STRUCTURAL COMPONENT DYNAMICS IN SPACE AND IN NEUTRAL BUOYANCY SIMULATION.
 - CAPABILITY TO DESIGN A NEUTRAL BUOYANCY STRUCTURE MOCKUP WHICH WILL FEEL (IN TERMS OF EXPENDED EFFORT) SIMILAR TO THE DESIRED FLIGHT DESIGN.
 - EXPANSION OF THE USEFULNESS OF NEUTRAL BUOYANCY, AS STRUCTURES UNDERWATER SIMULATE MUCH LARGER STRUCTURES IN SPACE.

Human Factors Hardware

The second generic area covered by the research objectives of SADE is that of human factors. This includes studies such as the effects of mass and moment of inertia, connector design, the requirements and role of body restraints, and integrated use of the manned maneuvering unit (MMU) and the shuttle Remote Manipulator System (RMS). Much of this data will be collected during the assembly of the interconnect structure, which is a set of eight beams connecting the two two-cell deployable modules. This chart lists the characteristics of the structural elements for this cell.

- STRUCTURAL CONNECTORS
- LIGHT LONGITUDINAL MEMBERS (2) (LL)
 - 3M LONG, ALUMINUM
 - .8 KG
- LIGHT DIAGONAL MEMBERS (2) (LD)
 - 4.2 M LONG, ALUMINUM
 - 1.2 KG
- HEAVY LONGITUDINAL MEMBERS (2) (HL)
 - 3 M LONG, STAINLESS STEEL
 - 14.9 KG
- HEAVY DIAGONAL MEMBERS (2) (HD)
 - 4.2 M LONG, STAINLESS STEEL
 - 21.1 KG

Structural Connector Characteristics

In order to evaluate connector design, different structural connectors will be mounted on the eight individual beams of the interconnect cell. Relative details of the five connectors chosen are shown in this figure. "Angular tolerance" relates to the required accuracy of the alignment before mating connector parts meet. The actual connection procedure is somewhat arbitrarily broken down into three segments: "capture" (whether or not the connections are coupled upon initial contact, "rigidizing" (regarding the existence or not of a discrete operation required to rigidize the joints), and "latching" (whether or not a discrete step is required for the final locking). Since the SADE structure must also be disassembled for stowage prior to entry, note is taken of whether or not a release tool is required for releasing the connection. It is desirable in this study to have a wide assortment of connector types in the experiment; this particular selection adequately spans the range of characteristics, while eliminating the need for new joint development.

		MSFC BALL & SOCKET	LARC SNAP UNION	MIT CONNECTOR	VOUGHT CLEVIS COUPLER	VOUGHT AUTOLOCK COUPLER
ANGULAR TOLERANCE	HIGH	●			●	●
	LOW		●	●		
CAPTURE	YES	●	●		●	●
	NO			●		
RIGIDIZING	YES	●				
	NO		●	●	●	●
LATCHING	YES			●		
	NO	●	●		●	●
RELEASE TOOL	YES	●	●			
	NO			●	●	●

Assembly Crew Assignments

As currently envisioned, four crew members will be associated with conducting the SADE experiment. Two will be the EVA test subjects, with considerable prior experience in neutral buoyancy. Another crew member will operate the manipulator arm and follow EVA activities with shuttle closed circuit television (CCTV) cameras during periods when the RMS is not operating. The fourth crew member will serve as the test director, reading checklists to the EVA crew, and additionally will assist in CCTV operations and serve as interior documentary photographer with hand-held still and movie cameras. It is recognized that the work load for the crew on the aft flight deck will probably be higher than that of the EVA crew, in number if not in difficulty of tasks.

ASSEMBLY CREW ASSIGNMENTS

- Two EVA CREW MEMBERS
 - ONE WITH MANNED MANEUVERING UNIT (SUBJECT A)
 - ONE UNAIDED (SUBJECT B)
- ONE RMS OPERATOR (PORT STATION, AFT FLIGHT DECK)
 - ALSO PRIMARY VIDEO/CCTV OPERATOR
- ONE TEST DIRECTOR (STARBOARD STATION, AFT FLIGHT DECK)
 - ALSO SECONDARY VIDEO/CCTV OPERATORS
 - ALSO DOCUMENTARY PHOTOGRAPHER (STILLS/MOVIES)

Assembly Procedure

As part of the planning procedure for the SADE experiment, a "strawman" assembly procedure was decided upon. That procedure, which is being recommended for initial neutral buoyancy tests by the M.I.T. study team, is presented over the next three pages as representative of a typical assembly procedure outline. While it is felt that this particular procedure is near-optimal in terms of data collected, it has not yet passed through safety review, and should not be misconstrued as an approved baseline.

The procedures listing begins with the start of the assembly tasks, and does not include standard EVA procedures, such as egress, MMU donning, and so forth. Of special note here is step 2, in which the subject in foot restraints faces a camera on the forward bulkhead (standard CCTV and/or aft flight deck movie cameras) and rotates the beam in a plane perpendicular to the line of sight of the camera. Starting with the beam parallel to the orbiter y-axis, it is rotated to a stop parallel to the z-axis, then accelerated and decelerated through another 90 degrees. The beam is then rotated back to its initial position, without the intermediate stop, and then placed into the structure. While this may seem to be a "mindless" experiment, it is actually critical to some of the human factors testing. By finding beam position as a function of time, estimates of human control laws and torquing capabilities can be made. This data will be of prime importance for determining the optimum role of humans in future space operations.

TASK	DATA OBTAINED ON
(1) UNSTOW TWO ELEMENTS OF INTERCONNECT CELL (LL, LD)	EVA OPERATIONS
(2) ROTATE EACH ELEMENT THROUGH 90° AND 180° IN FRONT OF CAMERA	HUMAN CONTROL LAWS & TORQUE LEVELS EFFECT OF MASS AND MOMENT OF INERTIA (WITH FOOT RESTRAINTS)
(3) INSTALL INTERCONNECT ELEMENTS ON FOLDED MODULE 1	ASSEMBLY IN FOOT RESTRAINTS CONNECTOR DESIGN
(4) REPEAT STEPS (1), (2), AND (3) FOR TWO MORE ELEMENTS OF INTERCONNECT CELL (HL, HD)	(AS LISTED ABOVE)
(5) ENGAGE GRAPPLE FIXTURE ON MODULE 1 WITH RMS	RMS OPERATIONS
(6) RELEASE MODULE 1 LAUNCH RESTRAINTS	EVA OPERATIONS
(7) DEPLOY MODULE 1 (CELLS 1 AND 2) WITH RMS	RMS DEPLOYMENT CAPABILITY

Assembly Procedure

The primary thrust of this section of the assembly procedure is to test the capabilities of an unrestrained test subject. Both subjects are required to translate, either hand over hand along the structure or with MMU, while carrying a structural element, and then install this element at the top of the deployed module. The same motion is performed with the beams before they are connected, so that the subject's ability to control his body position can be evaluated. Each subject will be required to do this exercise twice, once with a light beam and once with a heavy beam, so that the effect of mass and moment of inertia on assembly dynamics and human control laws can again be evaluated.

TASK	DATA OBTAINED
(8) UNSTOW 2 MORE ELEMENTS OF INTERCONNECT CELL (LL, LD)	EVA OPERATIONS
(9) SUBJECT B TRANSLATES ALONG MODULE 1 WITH LL ELEMENT	MANUAL TRANSLATION WITH HARDWARE ASSEMBLY LOADS
(10) SUBJECT A MOVES TO WORKSITE AT TOP OF MODULE 1 WITH LD	MMU TRANSLATION WITH HARDWARE
(11) SUBJECTS ROTATE ELEMENTS THROUGH 90° AND 180° IN FRONT OF CAMERAS	HUMAN CONTROL LAWS & TORQUE LEVELS EFFECTS OF MASS & MOMENT OF INERTIA (WITHOUT FOOT RESTRAINTS)
(12) CONNECT ELEMENTS TO TOP OF MODULE 1	ASSEMBLY WITHOUT BODY RESTRAINTS ASSEMBLY LOADS
(13) SUBJECTS TRANSLATE BACK TO LAUNCH ASSEMBLY PLATFORM	UNENCUMBERED MANUAL TRANSLATION UNENCUMBERED MMU TRANSLATION ASSEMBLY LOADS
(14) - (19) REPEAT STEPS (8) THROUGH (13) WITH REMAINING 2 ELEMENTS OF INTERCONNECT CELL (HA AND HL)	(AS LISTED ABOVE)

Assembly Procedure

This section of the assembly procedure is especially notable because it briefly tests the whole gamut of space assembly techniques:

- fully manual operations - as test subject B deploys the first cell of the deployable module (step 23)
- augmented manual operations - as test subject A, using the MMU for power, deploys the second cell of the deployable module (step 24)
- teleoperator operations - as the RMS is used to rotate module 1 and position it accurately above module 2 (step 26)

TASK	DATA OBTAINED
(20) SUBJECTS RELEASE MODULE 1 HOLDDOWNS	EVA OPERATIONS
(21) RMS MOVES MODULE 1 AND INTERCONNECT CELL UP, AFT, AND OUTBOARD PORT	MANIPULATION OF HIGH MOMENT OF INERTIA, LIGHTWEIGHT STRUCTURE WITH RMS
(22) RELEASE MODULE 2 LAUNCH RESTRAINTS	EVA OPERATIONS
(23) SUBJECT B DEPLOYS MODULE 2, CELL 1, MANUALLY	USE OF UNAIDED EVA FOR DEPLOYMENT
(24) SUBJECT A DEPLOYS MODULE 2, CELL 2, USING MMU	USE OF MMU FOR DEPLOYMENT
(25) SUBJECT B TRANSLATES TO TOP OF MODULE 2	UNENCUMBERED MANUAL TRANSLATION
(26) RMS ROTATES MODULE 1 180° AND BRINGS IT INTO POSITION OVER MODULE 2	MANIPULATION OF HIGH MOMENT OF INERTIA WITH RMS
(27) ATTACH INTERCONNECT CELL TO MODULE 2 WITH RMS GUIDED BY EVA CREW	INTEGRATED RMS/EVA ASSEMBLY OPERATIONS

Structural Element Vibration Analysis

Before data recording requirements can be reasonably discussed, some estimates are necessary as to the data sampling rates for structural loading data. In this table, the five most significant vibrational modes (3 cantilever, 2 free-free) of the individual structural elements have been found. Although the natural frequencies of the three types of elements found in the deployable modules have been included for completeness, they tend to respond at structural rather than element frequencies, and the quantities of primary interest are those pertaining to the four types of interconnect beams. The free-free modes are those likely to be excited during transportation of the beams to the work site: cantilever modes are found during the interconnect structural assembly procedure. If the first cantilever mode is the only one of interest, waveform reconstruction can be accomplished using a sampling rate of the order of 10-15 Hz, except for the light longitudinal beam, which would require 20-30 Hz. If the first free-free mode is also taken into account, sampling requirements would increase to 100 Hz, and the second cantilever mode would also be covered. Since this would have to triple (300 Hz) in order to include the second free-free and third cantilever modes, the design sample rate for this criteria will be considered to be 100 Hz, incorporating only the first three structural modes.

DEPLOYED MODULE		1 ST CANTILEVER	2 ND CANTILEVER	3 RD CANTILEVER	1 ST FREE-FREE	2 ND FREE-FREE
	LONG.	2.798	17.539	49.114	17.818	49.101
	LAT./ VERT.	1.325	8.307	23.261	8.439	23.255
	DIAG.	0.664	4.164	11.661	4.231	11.658
INTERCONNECT	LT. LONG.	1.673	10.488	29.370	10.655	29.362
	LT. DIAG.	0.840	5.266	14.747	5.350	14.743
	HVY. LONG.	0.854	5.354	14.993	5.439	14.989
	HVY. DIAG.	0.429	2.688	7.528	2.731	7.526

Data Recorder Options

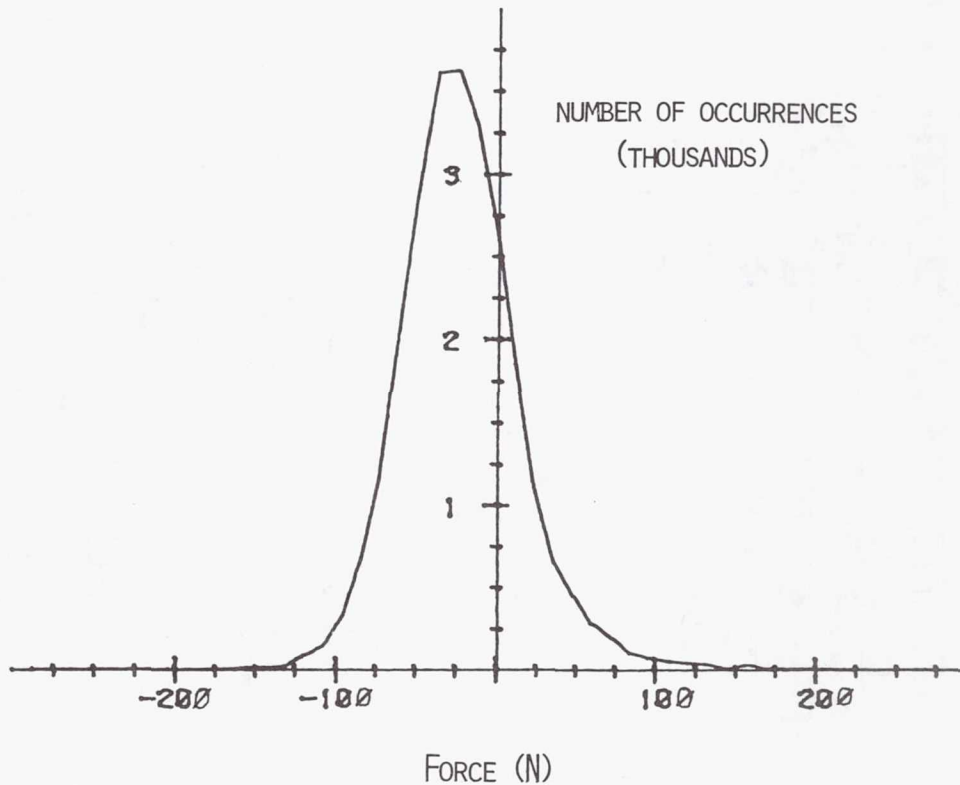
Two options exist for flight data recorders: a data system developed by NASA Langley for experiments on the long duration exposure facility (LDEF), and a solid-state recorder under development by M.I.T. The LDEF Experiment Power Data System has the advantage of being an "off-the-shelf" unit, and thus represents the lower technological risk. It is a central unit, which would be mounted on the SADE Launch Assembly Platform (LAP), and record signals brought in through wires from sensors distributed around the structure. The disadvantage of this, of course, is that no connections exist to sensors in the top module or interconnect cell until after the structure is complete and wires can be run to those areas. While the wiring integration is a worthwhile human factors task in itself, this would prevent the acquisition of assembly loads on most of the structure. The M.I.T. Solid-State Self Contained Recorder (SSSCR) must be flight qualified, but represents the other extreme of a separate recorder for each data signal, distributed around the structure. The use of many such dedicated sensor/recorder packages insures that most of the data is returned, even if some of the units fail.

- LDEF EXPERIMENT POWER DATA SYSTEM
 - CENTRAL RECORDING OF DISTRIBUTED SENSORS
 - 14 MB OF STORAGE
 - DEVELOPED TECHNOLOGY

- SOLID-STATE SELF CONTAINED RECORDER
 - UNDER DEVELOPMENT BY MIT SSL
 - DEDICATED SENSOR/RECORDER PACKAGE
 - HIGHLY REDUNDANT

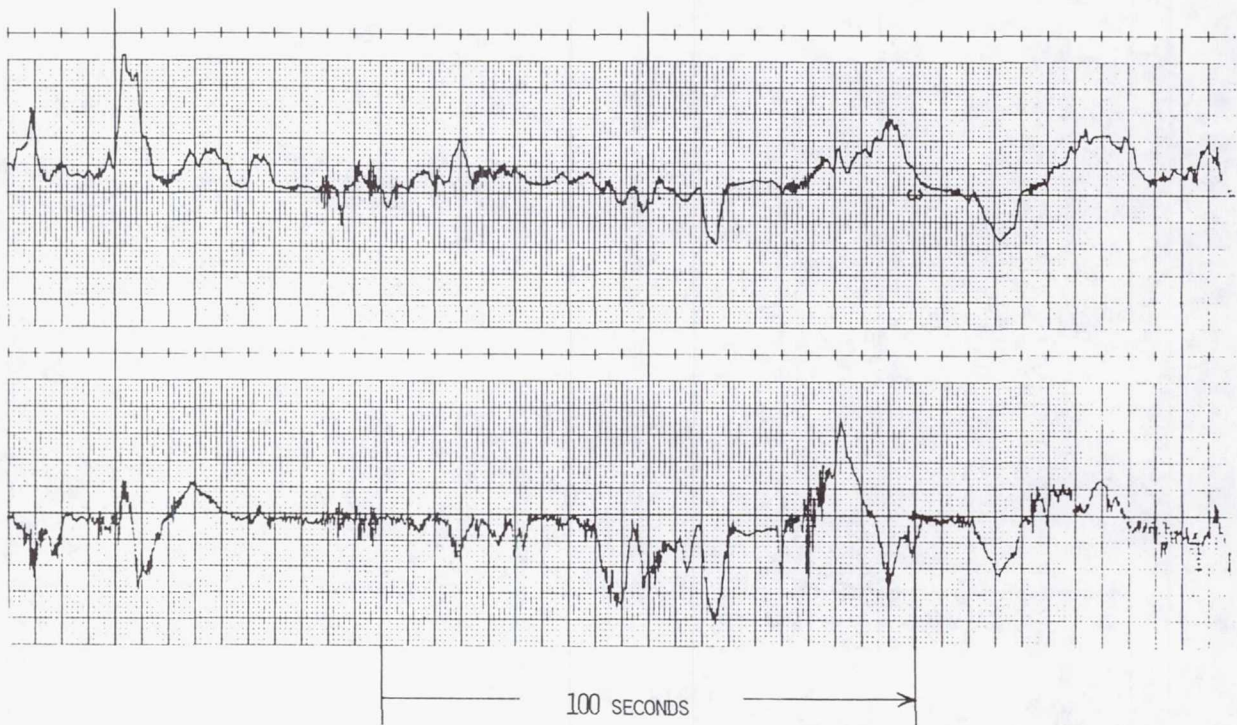
Sample Strain Gauge Results

This graph illustrates the distribution of load levels on a structural element during a neutral buoyancy assembly procedure. The number of times a given load level (positive for tension; negative for compression) occurred in the beam during the assembly is plotted against that load level. Thus, one can see, for example, that the beam was in compression during most of the assembly, but the highest loads, which were quite infrequent, were tension loads. This is probably not true in general, of course, but it does illustrate the type of information one can obtain from a recording of the strain levels in a beam.



Sample Strain Gauge Data

This sample of strain gauge data (obtained during assembly of a neutral buoyancy structure) illustrates some of the characteristics that are expected for the data obtained from the SADE experiment. The major peaks appear to be broad enough that even a fairly low sampling rate for the data recording instruments (such as 10 Hz) will be sufficient to pick up the peak loads during assembly. Further analysis of data obtained during early neutral buoyancy tests indicate that for purely manual assembly, the peak loads that a test subject can apply to the structure will be on the order of 300-400 N (tension or compression) and 80-100 Nm (bending moment).



Details of the M.I.T. SSSCR

Activated by an EVA crew member prior to releasing a structural element from the launch restraints, the Solid-State Self Contained Recorder is designed to take readings from colocated strain gauges, convert the strain readings into force and moment applied to the beam, and convert this continuous (analog) signal into the desired form for recording into solid state memory. The unit will be left attached to the structure throughout the flight.

The strain gauge readings are taken from 3 gauges placed at 90° intervals around the beam. The gauges are excited with an AC voltage, and the three strain readings are used to find force and principal moments applied to the beam. This is accomplished through a phase shifting technique, which resolves the magnitude of the moment vector in the complex plane. The data conversion options available include direct wave-form conversion, storing the peak loads which occurred during a set time interval, noting when the loads exceed a preset limit and storing the time of that event, or performing a fast Fourier transform of the waveform, and storing the Fourier coefficients. All of these options will be used, but only one option may be used per recorder. The memory section consists of integrated circuits (programmable read-only memory) which store the information in the form of 8-bit words for post-flight transcription and data reduction.

- STRAIN→STRESS RESOLVER
 - 3 LONGITUDINAL STRAIN GAUGES AT 90° FROM BEAM AXIS
 - AC GAUGE EXCITATION WITH PHASE SHIFTING
 - DIRECT ANALOG OUTPUT OF FORCE AND MOMENTS
- DATA CONVERSION OPTIONS
 - DIRECT (WAVE-FORM STORAGE)
 - PEAK LOADS DURING TIME INTERVAL
 - TIME OF THRESHOLD PASSAGE
 - FAST FOURIER TRANSFORM
- MEMORY
 - SOLID STATE (PROM)
 - SIZE OF MEMORY TAILORED TO REQUIREMENTS

Recorder Allocations

The particular assignment of recorder type to each application is a function of the previously listed characteristics of each system. The LDEF EPDS is the recorder of choice for the thermal experiments, and is in fact well suited to this experiment, as the sensor connections can be made during installation of the heat pipe experiment. This is a welcome addition to the EVA tasks list, and will allow additional information on EVA operations. The EPDS is also applicable to structural information return for the lower module, which always remains attached to the cargo bay. This will augment the information return on the design of the deployable modules, as the effect of preinstalled wiring can be verified. Detailed analysis of the type and number of sensors for this unit await a decision on whether or not dedicated EPDS systems will be used for the thermal and structural experiments, or whether a single recorder will be shared by the two areas.

The M.I.T. SSSCR is well suited to the beams of the interconnect structure and the upper deployed module, as they may be activated prior to component use. Stress readings will then be taken during the assembly procedure, which is one of the prime objectives of the structural experiment. Each interconnect beam will be equipped with two SSSCR units: one will measure peak loads for a design data base, and the other will measure stress waveforms for dynamics and damping studies. Details of unit emplacement on the top deployed module await a detailed investigation of the structural clearances available in the folded configuration.

- LDEF EPDS
 - THERMAL EXPERIMENT
 - MODULE 2 STRUCTURAL MEASUREMENTS
 - DETAILS AWAIT THERMAL REQUIREMENTS
- MIT SSSCR
 - INTERCONNECT CELL
 - 2/BEAM (PEAK LOADS AND WAVEFORMS)
 - MODULE 1
 - USAGE AND PLACEMENT DEPENDENT ON STOWAGE CLEARANCES

SOLAR ARRAY FLIGHT EXPERIMENT (SAFE)

R. W. Schock
Marshall Space Flight Center
Huntsville, Alabama

Large Space Systems Technology - 1981
Third Annual Technical Review
November 16-19, 1981

INTRODUCTION

The solar array flight experiment (SAFE) consists of four experiments on two different flights. The first experiment, termed the baseline, has a basic purpose - to demonstrate the flight readiness of lightweight solar array technology for solar electric propulsion and other payload power applications. The early availability of this experiment and its basic large space structure characteristics make it a logical candidate to demonstrate other disciplines critical to large space structures. These demonstrations form the basis for three other solar array experiments, two in remote sensing and one in control. All of these experiments will be briefly reviewed in this paper.

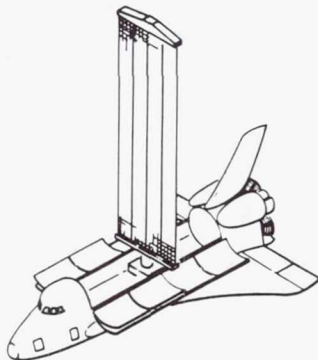
The characteristics of the solar array which are generically similar to large space structures are:

1. Large size
2. Mechanical complexity of its extendable/retractable ABL mast
3. The inability to dynamic test in earth atmosphere and one g, due to size, air damping dominance on the blanket, and structural instability in one g
4. Low natural frequencies

The specific characteristics of the solar array are shown below and illustrate the applicability to large space structures.

SOLAR ARRAY CHARACTERISTICS

- ARRAY WT - 225 Kg
- BLANKET - 132 Kg
- MAST - 40 Kg
- CONTAINER - 40 Kg
- COVER ASSY - 14 Kg
- FREQUENCY - .033 - .4 HZ
- ARRAY LENGTH - 3101 CM
- ARRAY WIDTH - 400 CM
- MAX. ALLOWABLE BM ~ 120.9 N-m



RESPONSE ANALYSIS - VRCS

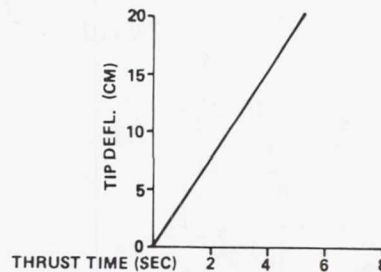
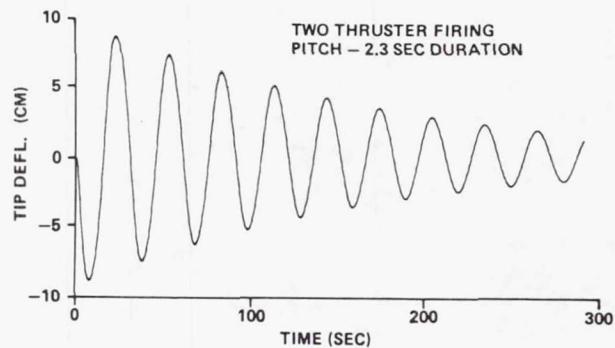


Figure 1

BASELINE SOLAR ARRAY FLIGHT EXPERIMENT

Development of solar array technology which supports solar electric propulsion began in 1973. The major thrust of the technology program was the overall demonstration of availability of technology by the fabrication and testing of a full scale (4 x 32 m) solar array wing.

Even though ground evaluation of technology could not find any deficiencies which would prevent its utilization in space, it was realized that due to the lightweight nature of the design, its operational capability could only be fully proven in space. For this reason, NASA decided to fly a full scale 66 W/kg solar array wing as an experiment on one of the early Shuttle flights. The wing, built for development testing, was refurbished and the necessary peripheral hardware (operational control and data acquisition) added to develop the wing into a flight experiment. Experiment objectives are:

1. Demonstrate array capability to deploy and retract in the space environment.
2. Demonstrate array structural integrity for Shuttle launch and reentry
3. Measure and observe extended array dynamic behavior
4. Correlate observed thermal and electrical performance with predicted performance.
5. Qualify flexible fold solar array technology for use on Shuttle payloads.

The solar array wing design has 84 flexible solar cell panels which are accordion folded into or out of a solar array blanket containment box when the solar array wing retracts or extends. These panels are joined together by hinges located along the long dimension of the panel. A coilable continuous longeron extension mast, located behind the blanket, is used to provide the motion which deploys and stows the blanket. The mast which is 32 m long (extended) and 37.3 cm in diameter is coiled into a canister which is 1.52 m x 40.6 cm when the blanket is retracted. The array preload provides compressional force upon the stowed solar array blanket to protect the solar cell assemblies against vibration during launch or reentry operations of Shuttle. The experiment is presently being developed by LMSC for MSFC with a planned launch in mid-1983. The following figure illustrates the on-orbit flight operations.

ON-ORBIT FLIGHT OPERATIONS

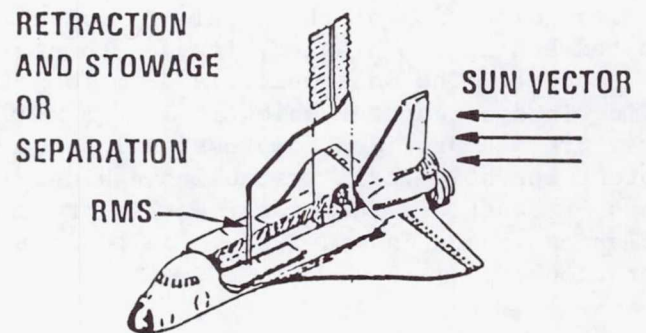
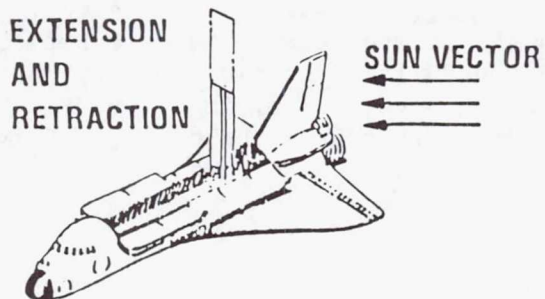
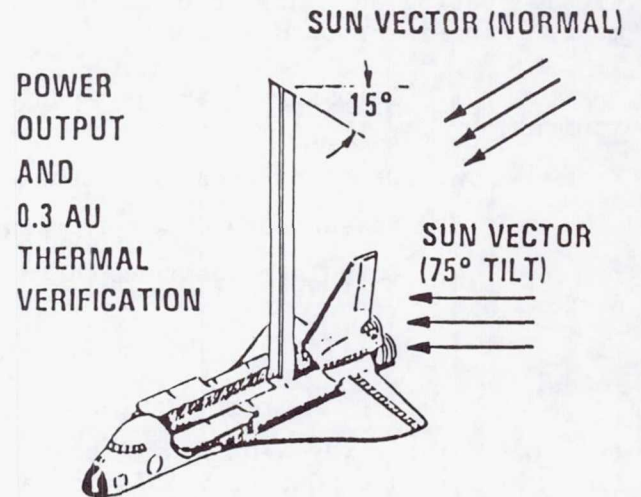
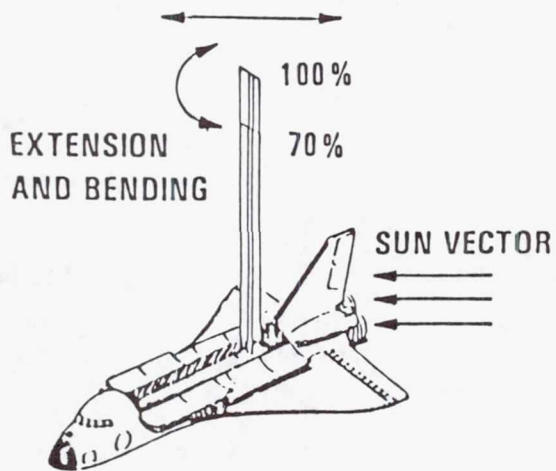


Figure 2

SAFE DYNAMICS AUGMENTATION

The basic objectives of the solar array dynamics experiment are:

1. Demonstrate the technology readiness of an on-orbit remote sensing dynamic data processing and recording system for use in large space structure response measurements.
2. Process remotely sensed data to obtain solar array dynamic characteristics for correlation with analysis and ground test and application to response control techniques.

To accomplish these objectives, two remote sensing systems are being developed. The first, an adaptation of a multi-field star tracker, is being developed by MSFC. The second, a photogrammetric technique, is being developed by LaRC. The star tracker technique is illustrated below. The emitter, positioned at the base of the solar array, illuminates the array of retroreflectors. The retroreflectors return the emitted energy to the receiver. The receiver focuses the reflector images on a solid state sensor. A scanner samples the sensor and feeds reflector image positions to a microprocessor. The microprocessor computes the dynamic array displacement from the initial or rest position and provides a digital output through a data conditioner to a digital tape recorder. The recorded data is stored and returned for ground processing.

Ground processing will define the dynamic characteristics of the array, such as frequencies, mode shapes, and damping. These characteristics will be used to verify math models, provide test defined inputs for control software, and provide zero g correlation to one g ground test data.

SOLAR ARRAY FLIGHT EXPERIMENT

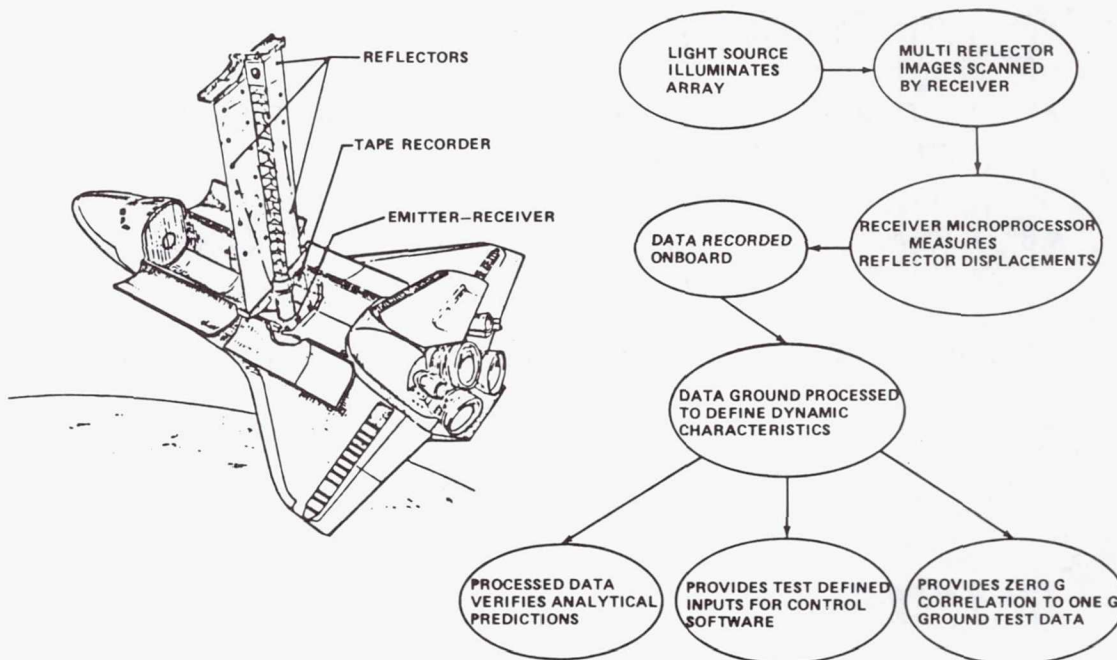


Figure 3

SAFE DYNAMICS AUGMENTATION
GROUND TEST

To provide early verification of the remote sensing data processing concept, a laboratory test is planned for the second and third quarters of FY 83. The ground test approach is illustrated below. In the first series of tests, light emitting diodes and accelerometers will be mounted on a 16 m, space fabrication-type beam. The beam will be loaded to approximate the natural frequencies of solar array, excited by low frequency shakers, and both the LED information and the accelerometers will be processed to assess compatibility of results.

A second test will be run six months later with a brassboard of the illuminator/receiver, flight-type reflective elements, and the same complement of accelerometers. This test will verify the remote sensing flight concept.

● GROUND TEST PROGRAM APPROACH

● REMOTE SENSING PROOF OF CONCEPT TESTS

- 16M SPACE BEAM EXCITED BY SINE, RANDOM AND IMPULSE
- LED EMITTERS AND ACCELEROMETERS ON BEAM
- LED EMITTER DATA ACQUIRED AND PROCESSED BY SENSOR TO PROVIDE REAL TIME DISPLACEMENT
- BOTH REMOTE SENSED AND HARDWIRE ACCELERATION DATA RECORDED AND PROCESSED TO PROVIDE DYNAMIC CHARACTERISTICS
- SUPPLEMENTAL ON-LINE REAL TIME PROCESSING WILL BE INVESTIGATED

Figure 4

SAFE PHOTOGRAMMETRIC EXPERIMENT

Four orbiter CCTV cameras at standard bulkhead locations will be used to obtain stereo video observations of a pattern of targets on the solar array. The video observations will be stored on tape for post-flight analysis. Photogrammetric triangulation analysis will be employed to produce a time history of the displacement of each target observed. Appropriate system identification techniques will then be employed to describe the dynamic modal and frequency responses exhibited by the solar array during the flight tests for both structural dynamics and control dynamics purposes.

PERSPECTIVE VIEW OF SENSOR MOUNTED FOR MONITORING POINTS ALONG A 16 METER TEST BEAM

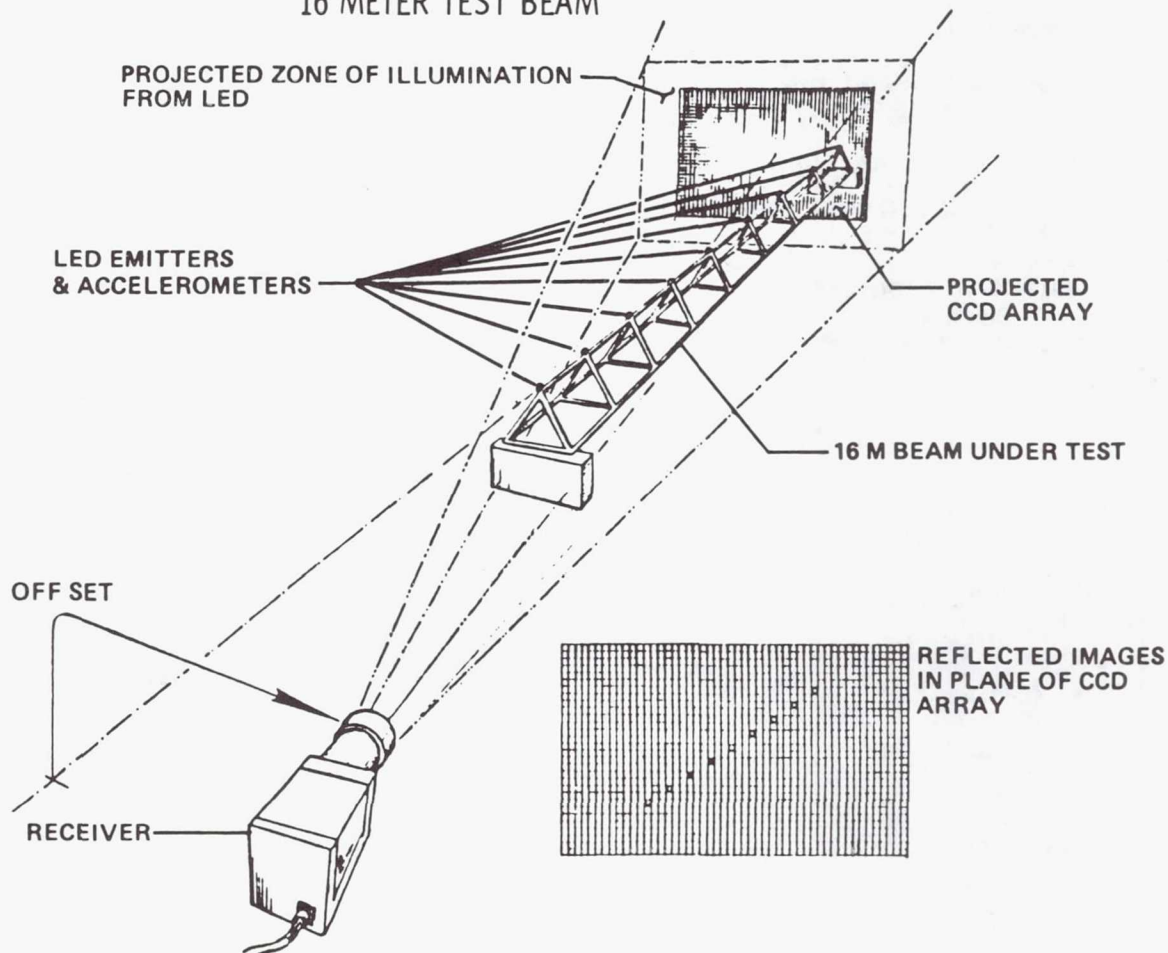


Figure 5

PHOTOGRAMMETRIC APPROACH DYNAMIC EXPERIMENT

SUMMARY

- SAME CONFIG & EXCITATION AS BASELINE FLIGHT TEST
- 4 CCTV CAMERAS VIEWING BLANKET
- DISPLACEMENT DATA RECORDED ON VIDEO TAPE
- GROUND PROCESSED TO OBTAIN DYNAMIC CHARACTERISTICS

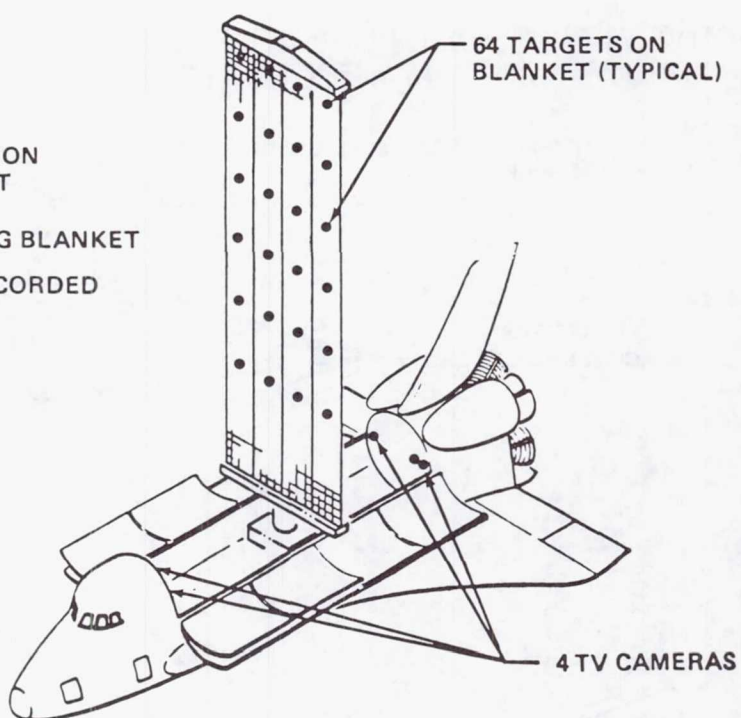


Figure 6

SAFE CONTROL AUGMENTATION

The objectives of the SAFE control augmentation are to demonstrate centralized control, distributed sensor control, and disturbance isolation control for this large space structure. The control problem can be delineated by observing the modal descriptions of a space structure which is

$$F = \{f_1, f_2, \dots\}$$

where f_i 's are modal frequencies, $|f_i - f_{i+1}| < \Delta$, and Δ depends upon the particular space structure. For previous space structures, such as Saturn V and Skylab, the fundamental frequency, f_1 , was large enough so that adequate response could be obtained by choosing a controller frequency, f_c , less than f_1 . This is not the case for this flight experiment because the fundamental frequency, f_1 , is 0.0353 Hz. If the control frequency is less than 0.0353 Hz, the response performance is poor. So the control problem is to imbed a control frequency, f_c , in this modal description so that the system is stable and has good response performance. Since the Δ max for this experiment is 0.062 Hz, this constraint provides an additional challenge to the control designer, i.e., to imbed a control frequency, f_c , in

$$\{f_1, f_2, \dots, f_i, f_c, f_{i+1}, \dots\}$$

when $|f_i - f_{i+1}| \leq 0.062 \text{ Hz}$

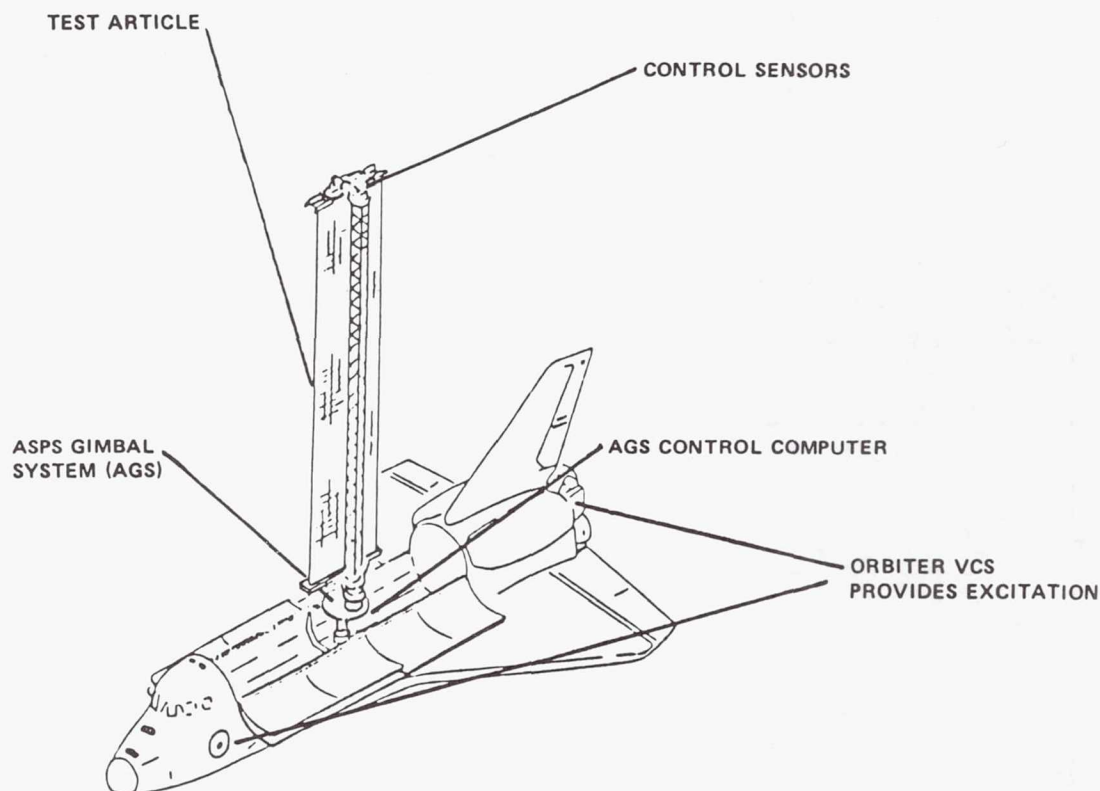


Figure 7

SAFE CONTROL AUGMENTATION

To effect the centralized control objectives of this flight experiment, the three AGS rate gyro's and the three AGS torquers are used to specify a centralized control frequency in the structure's nested modes. The three AGS rate gyro's, the three SAFE rate gyro's and the three AGS torquers are necessary to demonstrate the distributed sensor control. All the control components in the block diagram, illustrated below, are used to implement the disturbance isolation control.

For the centralized control, the three AGS rate gyro signals are fed into the NASA standard #2 computer. The computer contains the control equations that determine what torque is necessary to achieve stability and response performance. This torque is applied to the structure by the AGS gimbal system.

The distributed sensor control equations use the signals from the three AGS rate gyro's and the three SAFE rate gyro's, which are displaced from the AGS rate gyro's, to determine the necessary control torque. This control torque is applied to the structure through the AGS gimbal torques. The displaced sensor provides additional control degrees of freedom which should demonstrate an improvement in response performance.

The disturbance isolation control uses the three AGS rate gyro signals, the three SAFE rate gyro signals, and the three base accelerometers to determine torques which will reduce SAFE experiment loads caused by orbiter disturbances, i.e., isolates the SAFE experiment from the orbiter's dynamics.

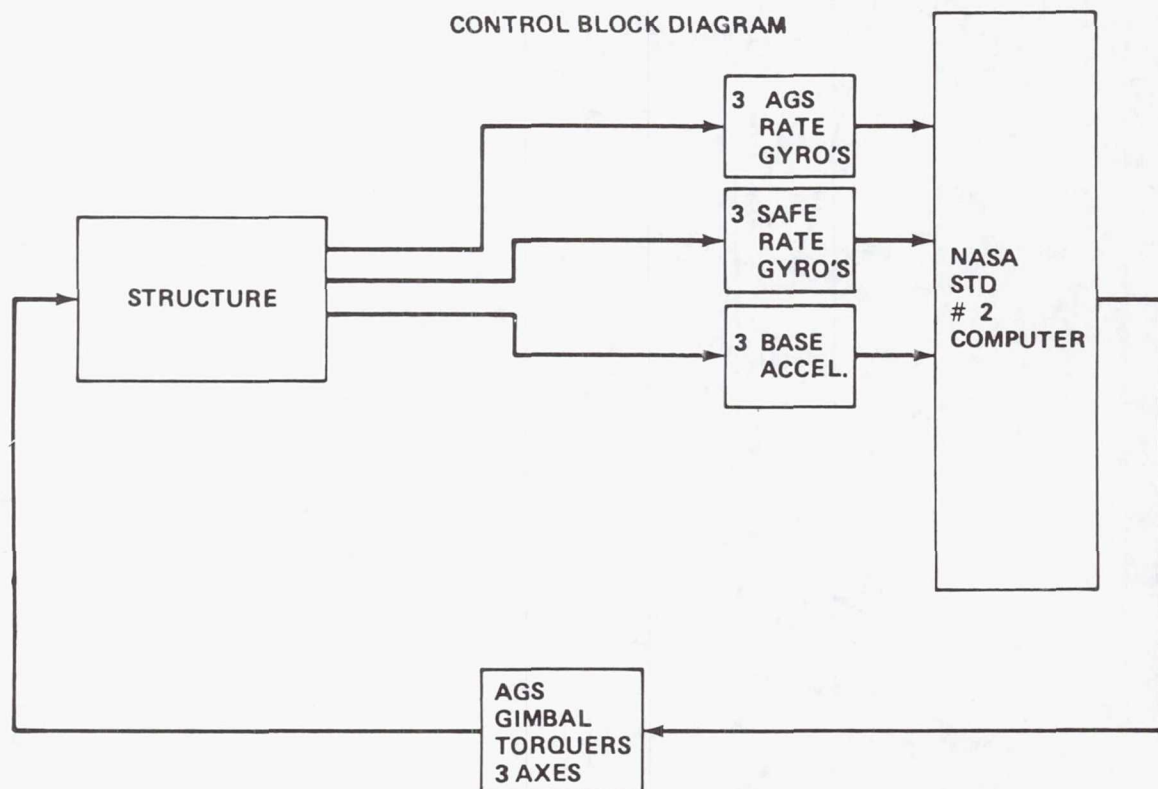


Figure 8

SOLAR ARRAY FLIGHT EXPERIMENT

The baseline solar array flight experiment will be delivered and ready for flight in mid-CY 82. Since the photogrammetric experiment uses the orbiter CCTV and data recording equipment, no developmental schedule is required. The star tracker remote sensing concept and the control experiment require either hardware or software development and their development schedules are shown below.

Successful completion of the two flight experiment programs will yield a flight qualified, light weight solar array concept, verification of two dynamic remote sensing concepts, flight qualified dynamic remote sensor hardware, and a control and pointing concept flight demonstration and verification. All results are directly applicable to future needs in the large space structure program.

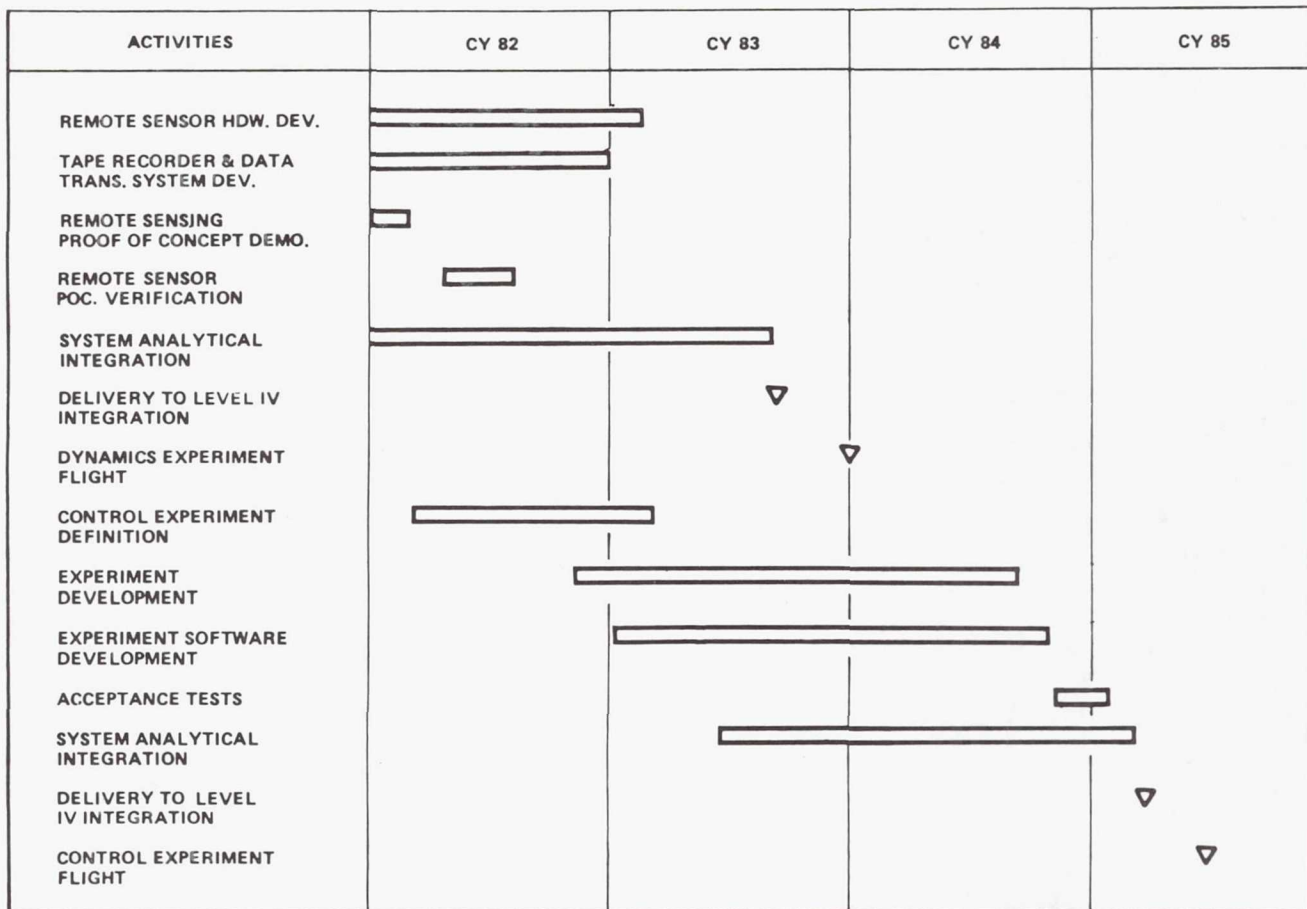


Figure 9

Page intentionally left blank

LARGE SPACE STRUCTURES SHUTTLE
FLIGHT EXPERIMENT

Lyle M. Jenkins
NASA Johnson Space Center
Houston, Texas

Large Space Systems Technology - 1981
Third Annual Technical Review
November 16-19, 1981

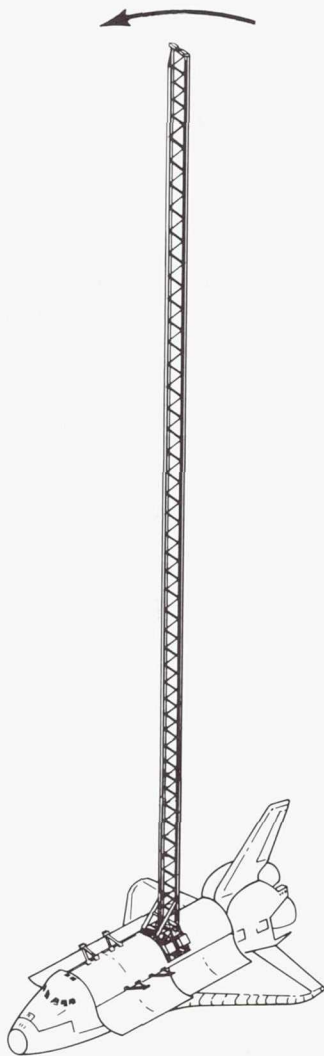
SPACE CONSTRUCTION EXPERIMENT OBJECTIVES

A number of diverse objectives are incorporated in a single flight experiment concept. The Space Shuttle system has inherent capabilities that are applicable to the construction of large space systems. If the ability to construct with deployable structures is to be used, the Orbiter DAP must be able to control the structure during buildup. Large deployable structures are essential to the development of large space systems. They must be understood in terms of system identification and modal damping. The simple linear structure should permit evaluation in flight and correlation with ground tests and simulations. This linear structure may be applicable to the feed mast of a large antenna. It also may be possible to incorporate elements of LSS control systems in anticipation of a more complex experiment such as a free-flyer.

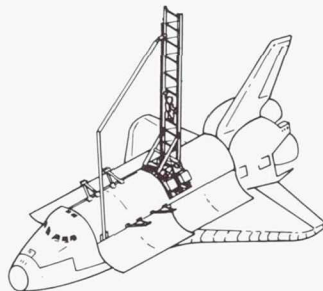
- DEVELOP AND DEMONSTRATE SHUTTLE CONSTRUCTION CAPABILITIES
- EVALUATE DIGITAL AUTOPILOT CONTROL WITH ATTACHED STRUCTURE
- OBTAIN DYNAMICS DATA ON A LARGE DEPLOYABLE STRUCTURE
- EVALUATE ANTENNA FEED MAST TEST ARTICLE
- DEVELOP FLIGHT CONTROL TECHNOLOGY FOR LARGE STRUCTURE

EXPERIMENT ACTIVITIES

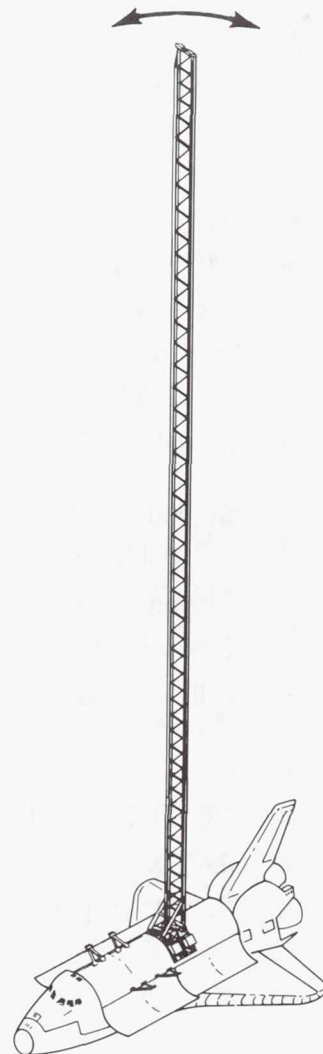
The basic experiment concept involves three classes of activity in the process of meeting the experiment objectives. A single element deployed from the cargo bay of the Orbiter can evaluate construction operations during buildup of the experiment configuration. Control during Orbiter maneuvers will evaluate the performance of the Orbiter DAP. Dynamics excitation of the structure identifies system characteristics for correlation with ground test and simulations.



CONTROL



CONSTRUCTION
OPERATIONS



STRUCTURAL
DYNAMICS

GENERAL DYNAMICS-CONVAIR TASKS

The major portion of experiment definition activity has been at Convair. The final report for the initial part of the study was recently distributed. Draper Labs is analyzing the response of the Orbiter DAP to the experiment configuration. Recently, coordination between JSC and LaRC was begun to expand experiment requirements relative to structure/control system interactions with emphasis on large antennas.

The Part I study configuration will provide a starting point for evaluation of the new requirements being generated. The design will be revised to reflect applicable requirements. The Part II mid-term review is currently planned for mid-December.

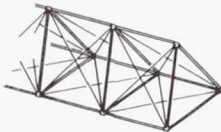
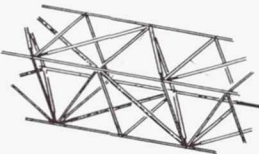
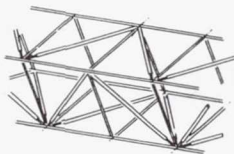
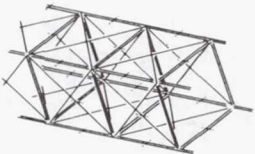
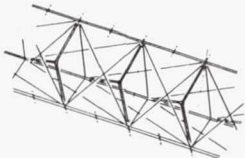
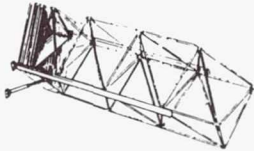
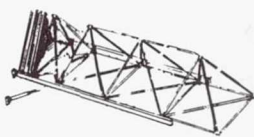


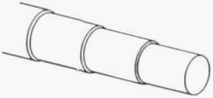
- PART I:
 - TRADES AND CONCEPTS - DEPLOYABLE STRUCTURE, DAMPING, EVA/RMS OPERATIONS, SUITCASE EXPERIMENTS, RESTORAGE AND RETURN, EXPERIMENT CONFIGURATION.
 - PRELIMINARY DESIGN AND ANALYSIS.
 - TEST PLAN.
 - PROGRAM PLAN.
- PART II:
 - PAYLOAD INTEGRATION AND TEST PLANNING - FLIGHT ASSIGNMENT, SHUTTLE INTERFACES, TIMELINES, GROUND OPS, FLIGHT SAFETY.
 - ANTENNA FEED MAST EXPERIMENT - EVALUATE REQUIREMENTS, REVISE DESIGN.
 - FLIGHT CONTROL ANALYSIS - EVALUATE INTERACTIONS WITH SHUTTLE.
 - GROUND TESTS AND SIMULATIONS.
- STATUS:
 - PART I REPORT DISTRIBUTED.
 - PART II MID-TERM IN DECEMBER.
 - COORDINATION WITH LaRC ON ANTENNA STRUCTURE REQUIREMENTS.
 - CONTROL INTERACTION EVALUATION AT DRAPER LABS.

CANDIDATE BEAM CONCEPTS

A review of available data on deployable structures and large space systems (LSS) technology, plus Convair's in-house activities in the design and development of space structures, led to selection of ten representative LSS structural beam elements as candidates to be evaluated for applicability to the Space Construction Experiment.

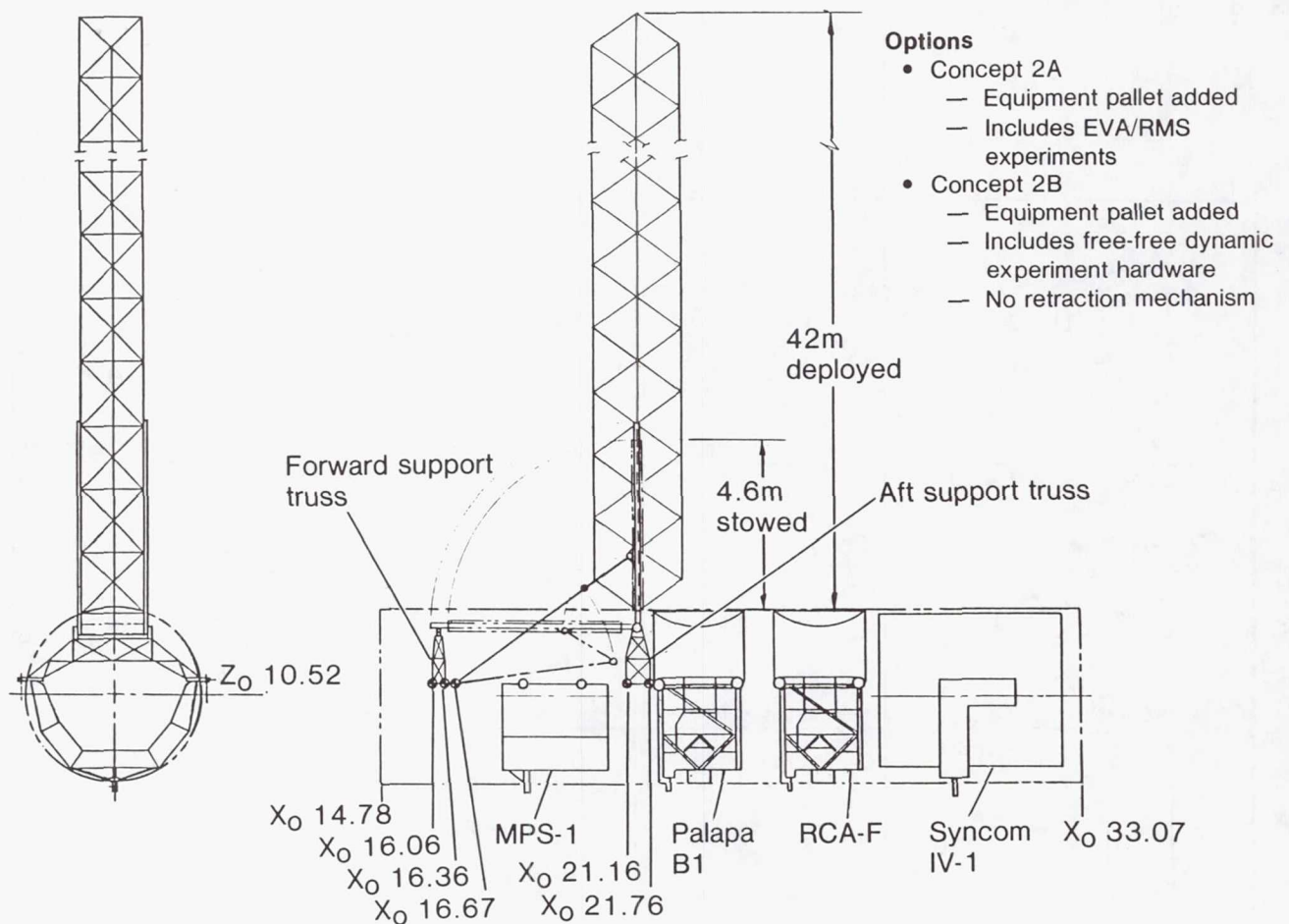
To provide a basis of commonality by which to compare the various candidates, an arbitrary configuration was created for each. These configurations were sized to the maximum folded envelope that could be carried within the Orbiter payload bay. All structures were assumed to have the same material properties in primary structural elements. All primary structural elements, except cables and tapes, were assumed to have the same slenderness ratio of 250. This value was selected as probably the maximum that would be used for large space structures applications.

After consideration of good and bad points for candidate beams, the Convair diamond truss was selected for further definition as the experiment structural element.

<div style="text-align: right;">1</div>  <p style="text-align: center;">Astromast</p>	<div style="text-align: right;">2a</div>  <p style="text-align: center;">Box beam - single fold</p>	<div style="text-align: right;">2b</div>  <p style="text-align: center;">Box beam - double fold</p>	<div style="text-align: right;">2c</div>  <p style="text-align: center;">Box beam - braced</p>
<div style="text-align: right;">3</div>  <p style="text-align: center;">'Y' frame beam</p>	<div style="text-align: right;">4a</div>  <p style="text-align: center;">Diamond beam</p>	<div style="text-align: right;">4b</div>  <p style="text-align: center;">Half-diamond triangle beam</p>	<div style="text-align: right;">5</div>  <p style="text-align: center;">Tetra-beam</p>
<div style="text-align: right;">6</div>  <p style="text-align: center;">Delta beam</p>	<div style="text-align: right;">7</div>  <p style="text-align: center;">Tele-mast</p>	<p>Common basis for comparison</p> <ul style="list-style-type: none"> • All concepts sized to fill payload bay of orbiter • Primary structural material - graphite/epoxy • Slenderness ratio (L/P) of all structural elements = 250 	

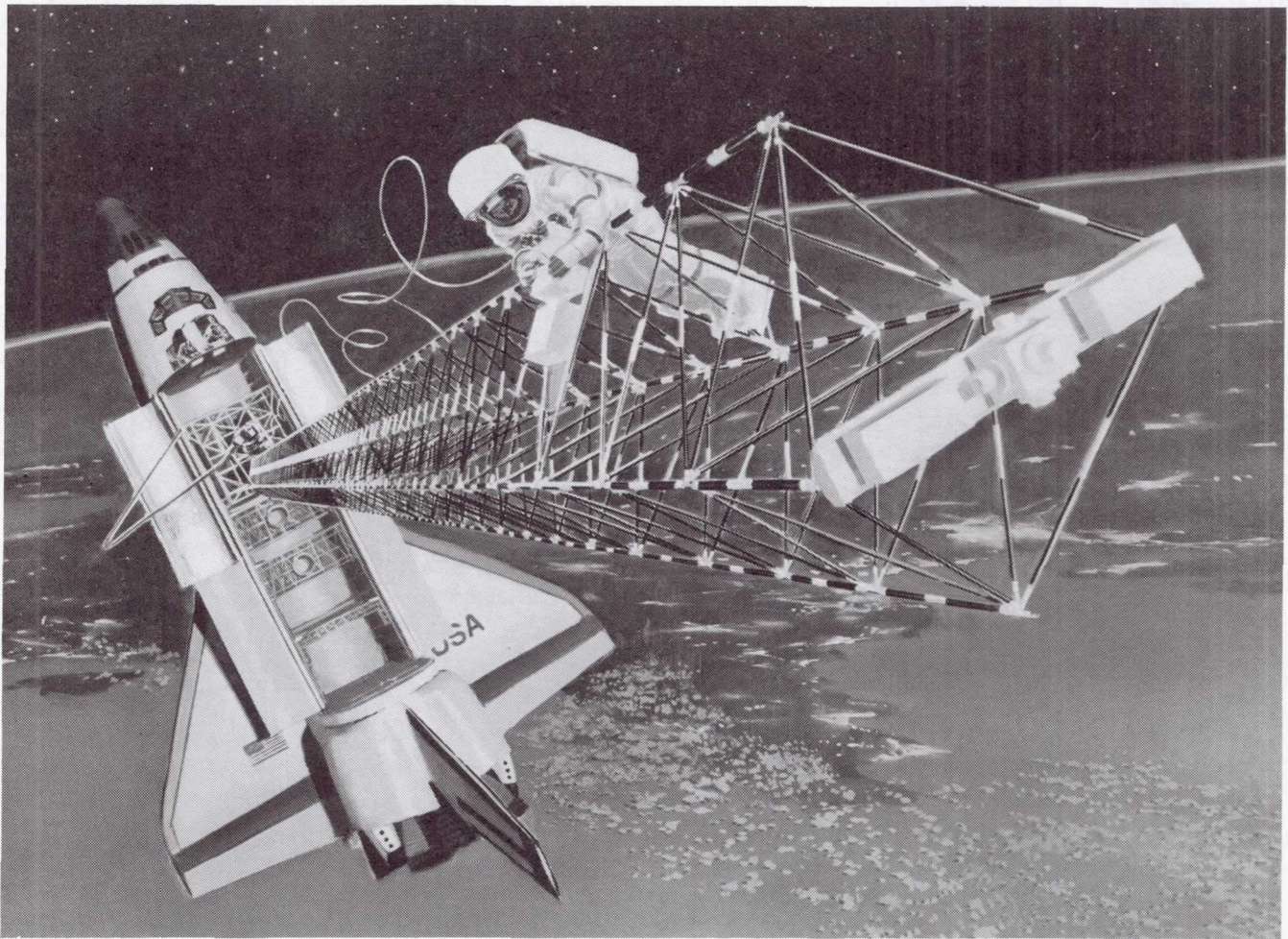
EXPERIMENT CONCEPT

The deployable beam concept was incorporated into several configurations. The principal criterion was compatibility with early flight payload manifests. The general approach was to occupy space above pallets which have no requirement to look out of the bay, such as materials processing experiments. A special support structure is used to bridge between the longerons.



EXPERIMENT CONCEPT ILLUSTRATION

The artist's concept of an experiment configuration illustrates several aspects of a baseline configuration. It also raises some probable issues such as the length of EVA tether, solo EVA, and attitude other than gravity gradient. The structure shown is the Convair diamond truss, a damping augmentation package, and tip masses are shown. The astronaut is installing an instrumentation module.



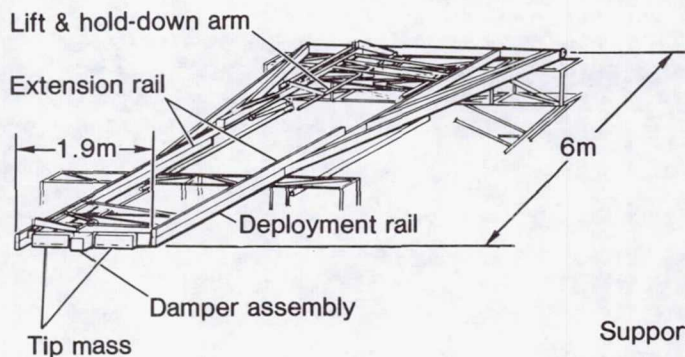
BASIC EXPERIMENT GENERAL ARRANGEMENT AND PERFORMANCE SUMMARY

The study trades and concepts evaluation resulted in the selection of a deployable tetrahedral truss supported by a truss-type support structure. The basic experiment shares space in the forward section of the payload bay with an MPS experimental pallet on a flight accompanied by deployed satellite payloads.

The 50.1 m truss assembly is stowed in its deployment rail in a short, flat packaging envelope. The initial deployment sequence is performed using the RMS to accomplish the unlatch and rotation. Following initial deployment, two motor-driven deploy/retract carriages deploy the tetrahedral truss one bay at a time. The deployment rails provide moment reaction support of the truss structure at all times. This sequence may be stopped or reversed at any stage of deployment. For retraction the carriages act to automatically unlock or trip the hinges in a truss bay and fold it to a folded position. The deployment rails are braced, as shown, to react to pitch and roll moments. This configuration will provide the starting point for the consideration of new requirements relative to large antenna development.

BASIC EXPERIMENT GENERAL ARRANGEMENT & PERFORMANCE SUMMARY

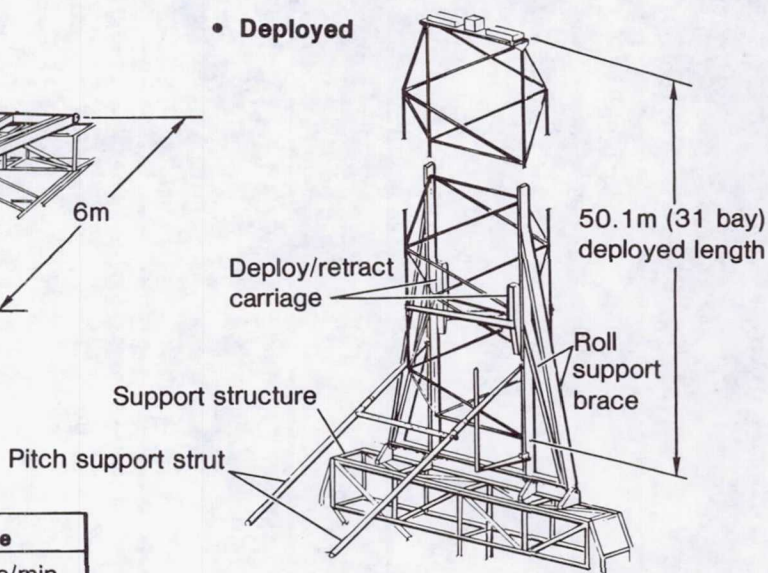
• Stowed



• Performance characteristics

Item	Value
Deployment/retraction rate	3 bays/min
Deploy/retract drive speed	0.3m/sec
Power (peak)	500w
Damping ratio (active)	0, 1%, 2%
Tip mass	400 kg

• Deployed



SELECTED EVA/RMS OPERATIONS SUMMARY

Our recommendations for flight experiments/tests to thoroughly augment ground experiments and simulations from our assessment analysis are shown on this chart for RMS operations and EVA operations with RMS.

Experiments recommended to be included in the basic deployable structures tests and ones suitable for suitcase experiments are identified. It turns out that the deployable truss from the basic experiment is needed to most efficiently perform the RMS and EVA with RMS experiments. Also, these experiments/tests should be performed together rather than individually as suitcase experiments on separate flights in order to obtain the best results. They are interrelated with each other and the most use should be obtained from the EVA time to be cost effective.

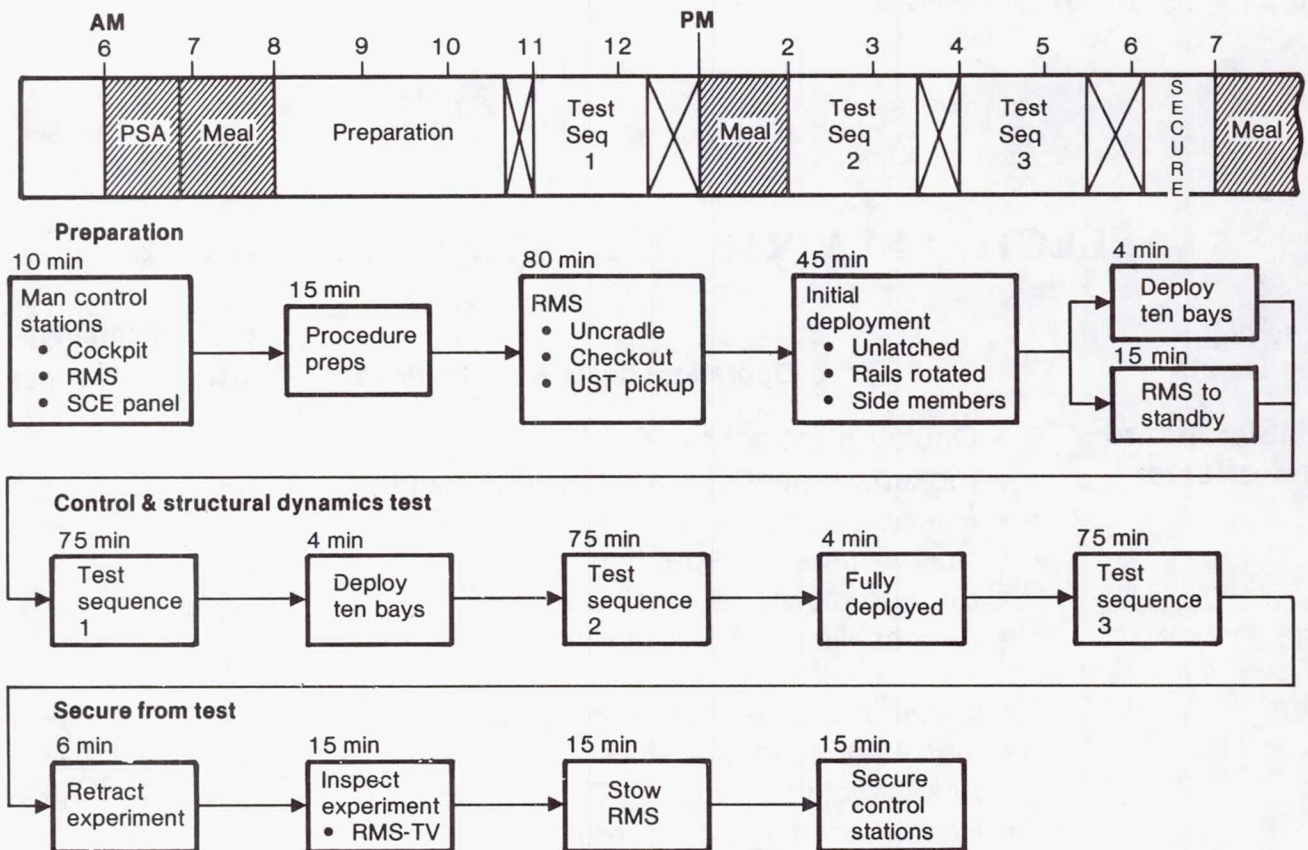
Tasks that benefit the performance of the basic flight experiment will require ground training and simulation. Correlation between ground and flight will improve the ability to predict timelines and capabilities.

SELECTED EVA/RMS OPERATIONS SUMMARY

Early flight experiments	Operations/tests & evaluations	Applicability	
		Basic	Suitcase
RMS/standard end effector	• Deploy & retract truss	✓	
	• Pickups & handoffs (special end piece)	✓	✓
	• Position & attach modules	✓	✓
	• Surveillance & inspection	✓	
	• Engage/maneuver/position truss	✓	✓
	• Assess illumination/visibility	✓	
EVA	• Install structural elements/rigging	✓	✓
	• Install subsystem elements	✓	✓
	• Assess joints, couplings, connectors	✓	✓
	• Repair/maintenance operations	✓	
	• Assess portable work aids/fixtures	✓	✓
	• Assess illumination/visibility	✓	
	• Assess RMS effectiveness	✓	✓
	• Inspection/verification/checkout	✓	

FLIGHT TEST OPERATIONS SEQUENCE AND TIMELINES - DAY 1

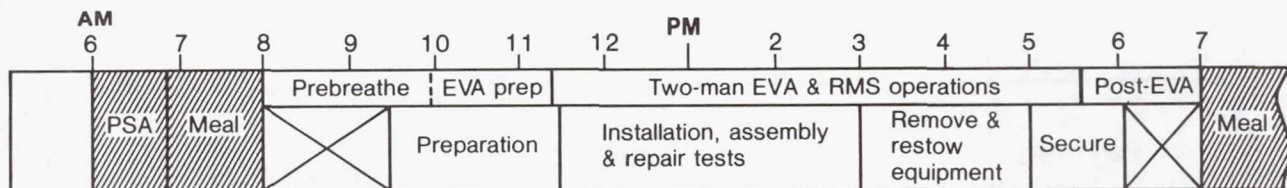
The flight test operations sequence and timelines for the first day of the experiment are shown on the chart below. The first day's activities will include a series of controls and dynamics tests primarily aimed at verifying or defining the limits and characteristics of the Orbiter DAP. The major test sequences are described.



CONSTRUCTION OPERATIONS TEST SEQUENCE AND TIMELINES - DAY 2

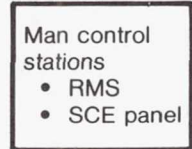
The construction operations test sequence will be conducted on the second day of the experiment. This test sequence includes several selected assembly and installation tasks which require manual and EVA assisted operations as selected in Task 1 of the study.

As seen from the timeline, the actual amount of time available to perform construction operations is limited by the preparation, removal and restowage and securing time.

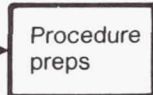


Preparation

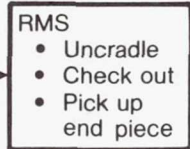
10 min



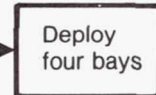
15 min



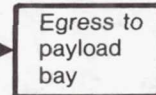
80 min



2 min



10 min

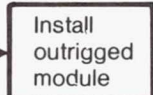


EVA/RMS operations

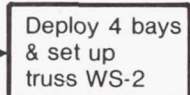
20 min



65 min



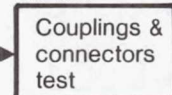
10 min



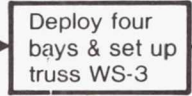
55 min



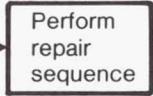
25 min



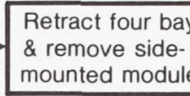
10 min



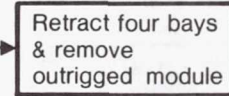
25 min



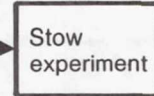
40 min



40 min

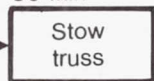


20 min

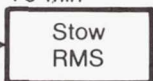


Secure from test

30 min



15 min



15 min



FLEXIBLE PAYLOAD COMPARISION

In an attempt to better understand the flexible payload/DAP interactions, data was assembled on other payloads simulated at Draper Labs. Since the deployed/stowed inertia ratio is indicative of an effective mass associated with the flexibility, it is significant to note that the only payload that showed signs of having a DAP problem had one of the lowest ratios. However, that payload, RMS-PEP, did have the lowest bending frequency.

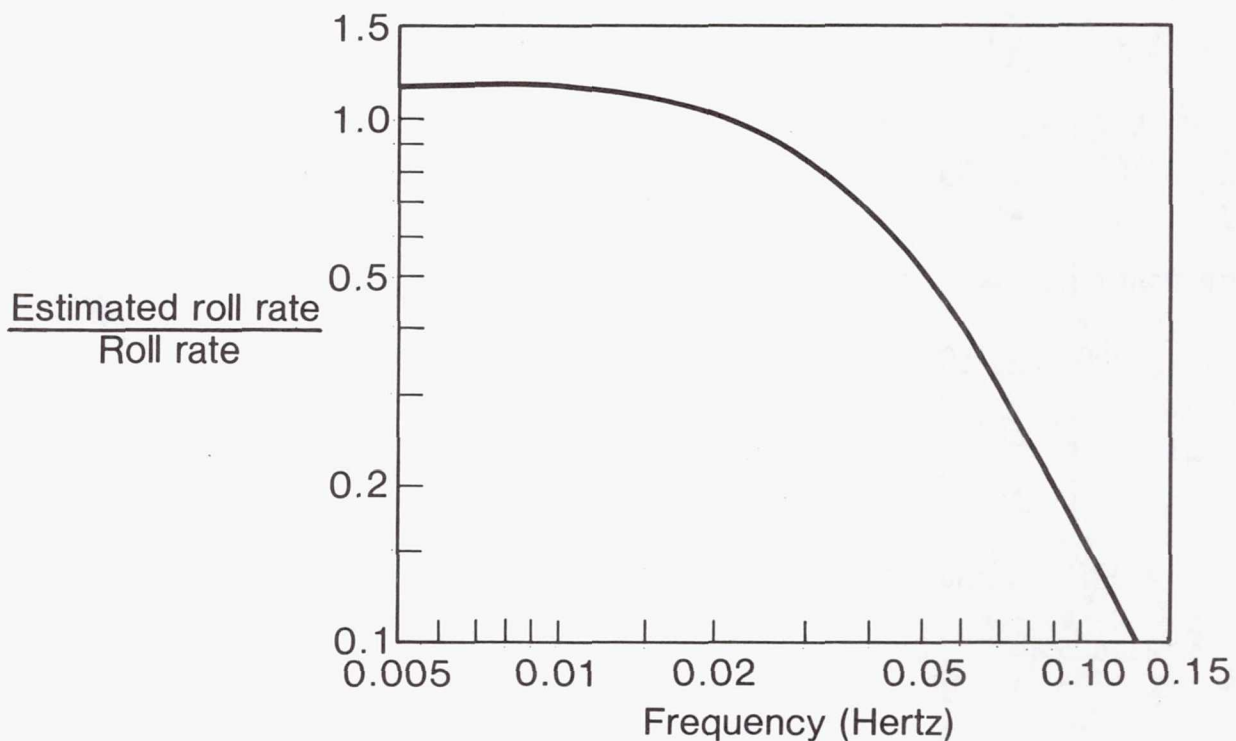
It would appear that there was some frequency-sensitive element in the system that attenuated the structure-induced oscillations of the Orbiter before they reached the jet logic.

Payload	Lowest frequency (Hertz)	$\frac{\text{Deployed } I_{xx}}{\text{Stowed } I_{xx}}$
RMS-PEP	0.052	1.19
Space telescope	0.566	1.20
IUS/TDRS	0.127	1.18
IUS/Galileo	0.16	1.36
IUS/DoD1	0.097	1.25
Beam, 100m, 100 kg	0.14	2.00

Only the RMS-PEP displayed a significant increase in propellant consumption (21 %)

STATE ESTIMATOR FILTER CHARACTERISTICS

The DAP State Estimator was identified to be the frequency-sensitive element in the DAP that was attenuating the beam-induced oscillations. The filter characteristic shown is for the default filter gains, those gains which the computer uses unless other values are specified. The 0.05 Hz oscillations of the RMS-PEP were cut in half by the filter and this relatively low mass payload still caused a moderate increase in propellant consumption. Heavier payloads with a bending frequency of 0.05 Hz or less may critically interact with the control system. Of course, the filter could be changed so that it started cutting off at a still lower frequency, but while this would eliminate flexibility problems there could be other problems caused by the rate information being too old by the time it reaches the phase plane logic. It is clear that if the experimental structure is to evaluate the proven limits of the DAP, the first bending frequencies will have to be lowered.



CONTROL SYSTEM EXPERIMENT REQUIREMENTS

Initial evaluations of the Orbiter Digital Autopilot (DAP) indicated a greater capability than anticipated. Changes to the combined LSS/Orbiter inertia, modal frequency of the LSS, rate limits, attitude dead band and Orbiter maneuvers will be evaluated to challenge the limits of the DAP. The potential interactions between the control system and the experiment structure are abnormal consumption of RCS propellant, oscillations of the LSS which are not stable and tend to diverge, divergent oscillations of the Orbiter/LSS combination or excessive cycling of commands to the RCS jets. Because the periods of oscillation are long for the combinations of interest there will be sufficient time to monitor the operation and take action to preclude hazardous conditions.

- COMBINATIONS OF LSS/ORBITER INERTIA, LSS MODAL FREQUENCY, RATE LIMITS, DEAD BAND, AND ORBITER MANEUVERS TO EVALUATE INTERACTIONS.
- INTERACTIONS
 - RCS FUEL CONSUMPTION
 - DIVERGENT OSCILLATIONS OF THE LSS
 - DIVERGENT VEHICLE OSCILLATIONS
 - JET COMMAND OSCILLATIONS

DYNAMIC TESTING

The first test listed has been limited to roll maneuvers since that axis, with its smaller moment of inertia, is influenced much more by flexible structure than either pitch or yaw. Random noise modal surveys have been chosen since they are significantly more efficient time-wise than other techniques. However, one sinusoidal excitation and free decay test has been included so as to provide data on amplitude sensitive behavior. One dynamic issue which has not been shown is the effect of outriggers or offset feed provisions on the end of the beam. Noting that any structure is dynamically modeled by mass properties and modes, the preliminary conclusion is that the added structure does not present a different dynamic problem; the incremental moment of inertia contributions are small and the first bending mode would not be significantly different in the critical roll axis. This conclusion can be checked by preparing beam and outrigger structural dynamic data at Convair and evaluating the dynamic behavior on the CSDL simulations.

Issues

1. Effect of test structure flexibility & vibration on orbiter & DAP
2. Effect of orbiter-induced dynamics on test structure
3. Minimum modal damping ratios
4. Dynamic modeling accuracy, especially for higher modes

Tests

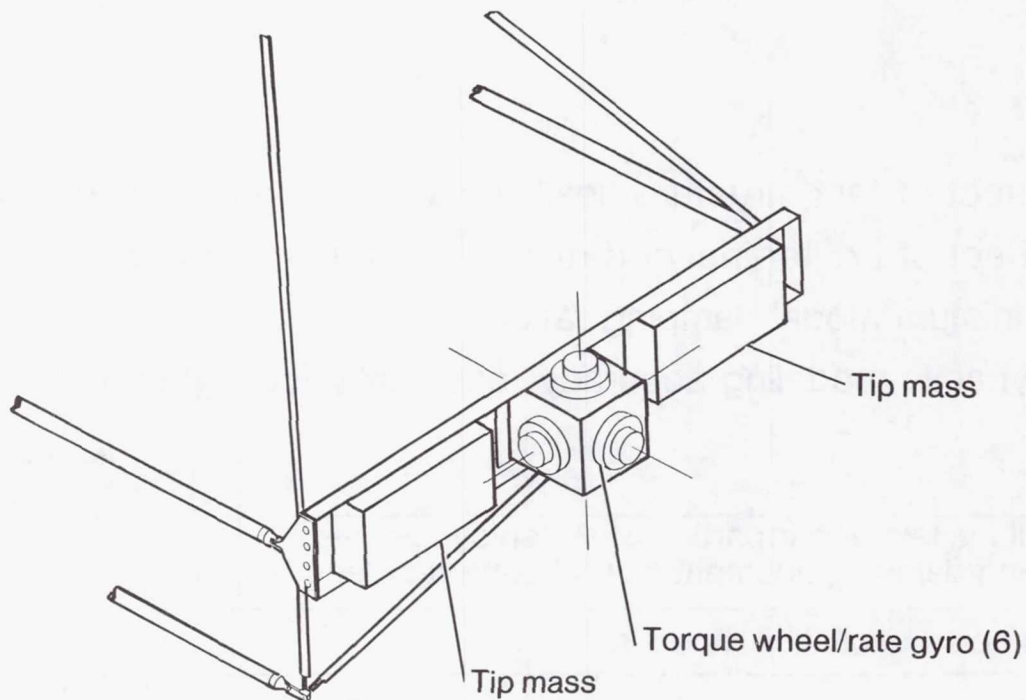
	Issues			
	1	2	3	4
Small roll maneuvers at partial & full deployment — decreasing damping augmentation at each test length	✓	✓		
Random noise excitation modal surveys	✓		✓	✓
Sinusoidal excitation & free decay of higher mode	✓		✓	✓

Instrumentation & excitation

- Strain gages at base (orbiter-structure interaction)
- Distributed accelerometers (mode shapes & damping)
- Rate gyros from damper sets (lower mode data)
- Excitation by torque wheels from damper sets

RECOMMENDED DAMPING AUGMENTATION APPROACH

By using two torque wheel damper sets per axis with each set providing 1% damping to the first bending mode, it is possible to select 2% damping (both sets operating), 1% damping (one set operating), or zero added damping with both sets off. Sizing the maximum torque of the wheels is not especially critical since they still provide damping in saturation but not as much as when they are operating in the linear range. The installation shown includes provision for variable tip masses by pumping fluid into closed cylinders. Thus between partial deployment and partial tip mass, the extreme condition can be approached in fine increments.



- Multiple torque wheel/rate gyro damper sets
- Each set adds 1% damping to first bending mode
- Preliminary sizing criteria: Max torque of 4.0 Nm as set by a 40m beam & a 0.05 deg/sec "step" change in orbiter body rate

SUMMARY

It appears practical to challenge the Orbiter DAP with a large, attached structure. The definition of this capability is a fundamental step in the development of nearly all large space systems currently under consideration. Experiment features may be incorporated that apply to control systems for large space systems such as modal damping devices. In a relatively simple deployable structure, the correlation of flight test results with ground test and analysis should provide a basis for extrapolation to more complex structures. Initial experiment concepts will provide a starting point for the examination of antenna feed mast requirements with the objective changing the design to produce a representative test article. Correlation of construction operations with ground simulations will provide for better task and timeline definition. EVA needs to be a direct benefit to the conduct of the experiment. Early consideration of safety issues is a precaution against defining an unacceptable experiment concept. Integration of many objectives seems feasible and is generally perceived as the only way to justify a relatively expensive experiment.

- SHUTTLE CONTROL OF ATTACHED STRUCTURE CAN BE EXERCISED IN THE EXPERIMENT.
- LSS CONTROL TECHNOLOGY (ACTIVE DAMPING),
- SIMPLE DEPLOYABLE STRUCTURE TO PROVIDE GROUND TEST CORRELATION (SYSTEM IDENTIFICATION),
- EVALUATION OF DEPLOYABLE STRUCTURE AS ANTENNA FEED MAST,
- CORRELATE BENEFICIAL EVA OPERATIONS WITH GROUND SIMULATIONS,
- FLIGHT SAFETY EVALUATION IN WORK,
- INTEGRATION OF MULTIPLE OBJECTIVES IN A SINGLE TEST IS FEASIBLE.

1. Report No. NASA CP-2215, Part 2		2. Government Accession No.		3. Recipient's Catalog No.	
4. Title and Subtitle LARGE SPACE SYSTEMS TECHNOLOGY - 1981				5. Report Date March 1982	
				6. Performing Organization Code 506-62-43-05	
7. Author(s) William J. Boyer, compiler				8. Performing Organization Report No. L-15096	
				10. Work Unit No.	
9. Performing Organization Name and Address NASA Langley Research Center Hampton, VA 23665				11. Contract or Grant No.	
				13. Type of Report and Period Covered Conference Publication	
12. Sponsoring Agency Name and Address National Aeronautics and Space Administration Washington, DC 20546				14. Sponsoring Agency Code	
15. Supplementary Notes					
16. Abstract This document is a compilation of the papers presented at the Third Annual Large Space Systems Technology (LSST) Review at the Langley Research Center. The research was supported in Fiscal Year 1981 by the LSST Program Office and the Materials and Structures Section, Research and Technology Division, of the Office of Aeronautics and Space Technology. The review provided government, university, and industry personnel with an opportunity to exchange information, to assess the present status of technology development in large space systems, and to plan the development of new technology for large space systems. These papers were divided into four major areas of interest: (1) technology pertinent to large antenna systems, (2) technology related to the control of large space systems, (3) basic technology concerning structures, materials, and analyses, and (4) flight technology experiments. Part 1 contains information on program status; structures, materials, and analyses; and control of large space systems. Part 2 covers large antenna systems and flight technology experiments. Design studies, structural testing results, and theoretical applications are presented with accompanying validation data. These research studies represent state-of-the-art technology that is necessary for the development of large space systems. A total systems approach including structures, analyses, controls, and antennas is presented as a cohesive, programmatic plan for large space systems.					
17. Key Words (Suggested by Author(s)) Large space systems Large antenna systems Structures, materials, and analyses Flight technology experiments			18. Distribution Statement Unclassified - Unlimited Subject Category 15		
19. Security Classif. (of this report) Unclassified	20. Security Classif. (of this page) Unclassified	21. No. of Pages 497	22. Price A21		